# PHYSICS OF FAST AND INTERMEDIATE REACTORS

# I

Proceedings of a Seminar, Vienna, 3-11 August 1961

INTERNATIONAL ATOMIC ENERGY AGENCY · VIENNA 1962

PHYSICS OF FAST AND INTERMEDIATE REACTORS

VOL. I

The following States are Members of the International Atomic Energy Agency:

AFGHANISTAN
ALBANIA
ARGENTINA
AUSTRALIA
AUSTRIA
BELGIUM
BRAZIL
BULGARIA
BURMA
BYELORUSSIAN SOVIET SOCIALIST REPUBLIC
CAMBODIA
CANADA
CEYLON
CHILE
CHINA
COLOMBIA
CONGO (LÉOPOLDVILLE)
CUBA
CZECHOSLOVAK SOCIALIST REPUBLIC
DENMARK
DOMINICAN REPUBLIC
ECUADOR
EL SALVADOR
ETHIOPIA
FINLAND
FRANCE
FEDERAL REPUBLIC OF GERMANY
GHANA
GREECE
GUATEMALA
HAITI
HOLY SEE
HONDURAS
HUNGARY
ICELAND
INDIA
INDONESIA
IRAN
IRAQ
ISRAEL
ITALY
JAPAN
REPUBLIC OF KOREA
LEBANON
LUXEMBOURG
MALI
MEXICO
MONACO
MOROCCO
NETHERLANDS
NEW ZEALAND
NICARAGUA
NORWAY
PAKISTAN
PARAGUAY
PERU
PHILIPPINES
POLAND
PORTUGAL
ROMANIA
SENEGAL
SOUTH AFRICA
SPAIN
SUDAN
SWEDEN
SWITZERLAND
THAILAND
TUNISIA
TURKEY
UKRAINIAN SOVIET SOCIALIST REPUBLIC
UNION OF SOVIET SOCIALIST REPUBLICS
UNITED ARAB REPUBLIC
UNITED KINGDOM OF GREAT BRITAIN AND NORTHERN IRELAND
UNITED STATES OF AMERICA
VENEZUELA
VIET-NAM
YUGOSLAVIA

The Agency's Statute was approved on 26 October 1956 at an international conference held at United Nations headquarters, New York, and the Agency came into being when the Statute entered into force on 29 July 1957. The first session of the General Conference was held in Vienna, Austria, the permanent seat of the Agency, in October, 1957.

The main objective of the Agency is "to accelerate and enlarge the contribution of atomic energy to peace, health and prosperity throughout the world".

Printed in Austria by Globus, Druck- und Verlagsanstalt, Vienna
March 1962

PROCEEDINGS SERIES

# PHYSICS OF FAST AND INTERMEDIATE REACTORS

## I

PROCEEDINGS OF THE SEMINAR
ON THE PHYSICS OF FAST AND INTERMEDIATE REACTORS
SPONSORED BY
THE INTERNATIONAL ATOMIC ENERGY AGENCY
AND HELD IN VIENNA, 3 — 11 AUGUST 1961

INTERNATIONAL ATOMIC ENERGY AGENCY
VIENNA 1962

PHYSICS OF FAST AND INTERMEDIATE REACTORS, IAEA, VIENNA, 1962
STI/PUB/49

# FOREWORD

It is generally agreed that the ultimate economic advantage of power produced by nuclear fission over that produced by conventional sources depends on the ability of a certain type of reactor to breed precious nuclear fuel out of the plentiful but not readily fissionable isotope of uranium. This fact is mainly responsible for the importance attached to the development of fast power reactors, but many other interesting properties of unmoderated or weakly moderated reactor systems have also been brought to light by reactor physicists.

In August 1961 the Agency organized in Vienna a Seminar on the Physics of Fast and Intermediate Reactors, at which all the topics relating to this important branch of reactor science were discussed. The main feature of this meeting was extensive discussion of the 66 written contributions, which set the stage for a wide exchange of experience and ideas throughout 13 half-day sessions. The Seminar was attended by 132 scientists from 22 Member States and two international organizations.

It is hoped that these Proceedings of the Seminar, which include both the papers presented and a record of the discussions, will be useful as a reference work both to research workers in the field and to newcomers to it for many years to come. The Agency's thanks are due to all the participating scientists for their written or oral contributions and especially to those among them who, as session chairmen, led the discussions and contributed greatly to the success of the meeting.

March 1962

Scientific Secretary
Seminar on the Physics of Fast
and Intermediate Reactors

## *EDITORIAL NOTE*

*The papers and discussions incorporated in proceedings published by the International Atomic Energy Agency are checked for scientific accuracy by the Agency's experts in the subjects concerned and edited by the Agency's editorial staff to the extent considered necessary for the reader's assistance. The views expressed and the general style adopted remain, however, the responsibility of the named authors or participants.*

*The units and symbols employed are to the fullest practicable extent those standardized or recommended by the competent international scientific bodies.*

*The affiliations of authors are those given at the time of nomination.*

*The use in these Proceedings of particular designations of countries or territories does not imply any judgement by the Agency as to the legal status of such countries or territories, of their authorities and institutions or of the delimitation of their boundaries.*

# CONTENTS OF VOLUME I

INTRODUCTION

I. NEUTRON PHYSICS

I.1. DATA REQUIREMENTS

Nuclear data requirements for fast and intermediate reactor calculations . . . . 3
*J. J. Schmidt*

Requirements for fast-neutron data and the fast-neutron cross-section measuring programme in the United Kingdom . . . . . 21
*A. T. G. Ferguson and R. Batchelor*

I.2. CROSS-SECTION REQUIREMENTS

A critical summary of microscopic fast-neutron interactions with reactor structural, fissile and fertile materials . . . . . 29
*A. B. Smith*

Mesures de sections efficaces intéressant les réacteurs rapides . . . . . 55
*F. Cheynier, R. Joly, J. R. Leroy, A. Michaudon et P. Ribon*

Измерение параметров резонансной структуры сечений, влияющих на распространение быстрых нейтронов в средах . . . . . 65
*М. Н. Николаев, В. В. Филиппов и И. И. Бондаренко*

Angular distributions of fast neutrons scattered by Al, Si, P, S and Zn . . . . 75
*K. Tsukada, S. Tanaka, M. Maruyama and Y. Tomita*

Neutron inelastic scattering by sodium-23 . . . . . 87
*J. H. Towle and W. B. Gilboy*

Neutron capture cross-section for energies above a few hundred electron-volts . 95
*J. H. Neiler*

Measurements of $\alpha$ for $U^{233}$, $U^{235}$ and $U^{239}$ for monoenergetic neutrons . . . . . 111
*J. C. Hopkins and B. C. Diven*

Effective resonance absorption integrals for zirconium and niobium . . . . . 119
*E. Hellstrand, G. Lindahl and G. Lundgren*

I.3. FISSION PROPERTIES

Experimental studies of fission properties utilized in reactor design . . . . . 125
*D. Butler, S. Cox, J. Meadows, J. Roberts, A. Smith and J. Whalen*

The number of prompt neutrons from $U^{235}$-fission over the range 0.04 MeV to 3 MeV . . . . . 139
*A. Moat, D. S. Mather and P. Fieldhouse*

Numbers of prompt neutrons per fission for $U^{233}$, $U^{235}$, $Pu^{239}$ and $Cf^{252}$ . . . . 149
*B. C. Diven and J. C. Hopkins*

An absolute measurement of $\bar{\nu}$ of californium-252 . . . . . 155
*I. Asplund, H. Condé and N. Starfelt*

I.4. NUCLEAR THEORY

Statistical model in nuclear reactions . . . . . 165
*E. Erba, U. Facchini and E. Menichella Saetta*

Calculation of fast-neutron reaction cross-sections . . . . . 171
*P. A. Moldauer*

Neutron fission-product cross-sections . . . . . 179
*V. Benzi and A. M. Saruis*

I.5. MULTI-GROUP CROSS-SECTIONS

Group cross-sections for fast reactors . . . . . 189
*P. F. Zweifel and G. L. Ball*

A punched-card library of neutron cross-sections and its use in the mechanized preparation of group cross-sections for use in Monte Carlo, Carlson $S_n$ and other multi-group neutronics calculations on high-speed computers . . . . . 207
*K. Parker*

An accurate treatment of resonance scattering in light elements in fast reactors 231
*H. Hummel and A. Rago*

## II. INTEGRAL EXPERIMENTS

### II.1. CRITICAL EXPERIMENTS

Integral experiments on fast systems of plutonium, uranium and thorium . . . 253
*J. J. McEnhill and J. W. Weale*
Critical experiments and nuclear calculations — LAMPRE-I . . . . . 263
*M. E. Battat*
Experimental results on large dilute fast critical systems with metallic and ceramic fuels . . . . . 271
*J. K. Long, A, R. Baker, W. Gemmel, W. P. Keeney, R. L. McVean and F. W. Thalgett*
The epithermal critical experiments . . . . . 287
*H. A. Morewitz and S. G. Carpenter*
Design and construction of the Argonne fast critical facility (ZPR-VI) . . . . 295
*W. Y. Kato and L. R. Dates*
Description de l'assemblage critique RACHEL . . . . . 313
*P. Bourgeois, C. Clair, R. Comte et J. J. Long*
Propriétés neutroniques de l'assemblage critique RACHEL . . . . . 321
*C. Clair*
Экспериментальные исследования некоторых физических особенностей промежуточных реакторов с бериллиевым замедлителем . . . . . 327
*А. И. Лейпунский, В. А. Кузнецов, Г. Я. Артюхов, А. И. Могильнер, Ю. А. Прохоров, В. М. Стелковский, Л. А. Чернов*

### II.2. OTHER INTEGRAL EXPERIMENTS

Etude du flux de neutrons à l'équilibre dans l'uranium naturel . . . . . 347
*J. L. Campan, P. P. Clauzon et C. P. Zaleski*
Fast-neutron spectra by threshold-detector activation . . . . . 377
*O. W. Dietrich and J. Thomas*
Propagation à longue distance de flux de neutrons dans les réacteurs à neutron rapides . . . . . 387
*A. Kania, R. Pasquet, P. Pépin, J. Rastoin et M. Solanes*
Распространение нейтронов в никелевом экране реактора на быстрых нейтронах . 403
*М. Н. Николаев, В. И. Голубев, А. А. Абагян и М. Ю. Орлов*

### II.3. THEORETICAL CORRELATIONS

Integral physics data for fast-reactor design . . . . . 415
*W. B. Loewenstein and D. Meneghetti*
The correlation of integral experiments and high-energy cross-sections . . . . 435
*J. Chernick, H. C. Honeck, P. Michael, S. O. Moore and G. Srikantiah*
Status of computational and experimental correlations for Los Alamos fast-neutron critical assemblies . . . . . 445
*G. E. Hansen*
Recent advances and problems in theoretical analyses of ZPR-III fast critical assemblies . . . . . 457
*D. Meneghetti*

# INTRODUCTION

During the Seminar, sixty-five papers were orally presented, and seven more were accepted for publication in the Proceedings. In order that these Proceedings might be in the hands of their users at an early date, the method of presentation of the papers and of the extensive session discussions had to be somewhat different from the one usually followed. The complete record of the sessions will be found at the end of Volume III.

The order in which the papers are presented here is not in all cases that of their presentation during the Seminar. Changes have been made where it was considered that these would enhance the usefulness of these volumes as reference books. The subject grouping adopted is given below.

Volume I

I. *Neutron Physics*

- I.1. Data requirements
- I.2. Cross-section measurements
- I.3. Fission properties
- I.4. Nuclear theory
- I.5. Multi-group cross-sections

II. *Integral Experiments*

- II.1. Critical experiments
- II.2. Other integral experiments
- II.3. Theoretical correlations

Volume II

III. *Reactor Theory*

- III.1. Calculation methods
- III.2. Effects of cross-section errors
- III.3. Reactivity effects
- III.4. Long-term effects
- III.5. Reactor concept studies

Volume III

IV. *Reactor Dynamics*

- IV.1. Kinetics
- IV.2. Stability
- IV.3. Doppler effect
- IV.4. Safety problems

V. *Physics of Specific Reactors*

# I. NEUTRON PHYSICS

## 1. DATA REQUIREMENTS

# NUCLEAR DATA REQUIREMENTS FOR FAST AND INTERMEDIATE REACTOR CALCULATIONS

J. J. SCHMIDT
KERNFORSCHUNGSZENTRUM, KARLSRUHE,
FEDERAL REPUBLIC OF GERMANY

**Abstract — Résumé — Аннотация — Resumen**

**Nuclear data requirements for fast- and intermediate-reactor calculations.** During 1960/61, some work has been done at Karlsruhe in the compilation of reliable nuclear data for fast- and intermediate-reactor calculations. Materials included thus far are He, $O^{16}$, $Na^{23}$, Cr, Fe, Ni, Mo, $U^{235}$, $U^{238}$ and $Pu^{239}$.

For fast- and intermediate-reactor optimization studies, reliable theoretical prediction of space-dependent neutron energy spectra, critical masses, breeding ratios, burn-up, Doppler coefficients and related subjects, the author was interested in much more detailed microscopic cross-section data—concerning mainly neutron absorption and fission—than are needed, for example, for the evaluation of few-group constants in the conventional multi-group diffusion theory.

In spite of much progress in the experimental determination and theoretical interpretation of nuclear data, many inconsistencies in the experimental results of different authors and laboratories and large gaps in experimental nuclear-data work still remain. This paper discusses a great number of these gaps and inconsistencies in respect of the above-mentioned nuclei.

**Constantes nucléaires requises pour les calculs de réacteurs à neutrons rapides et à neutrons intermédiaires.** En 1960/61, des travaux ont été exécutés à Karlsruhe en vue de réunir des données nucléaires sûres pour les calculs de réacteurs à neutrons rapides et à neutrons intermédiaires. Les matières étudiées jusqu'à présent sont: He, $^{16}O$, $^{23}Na$, Cr, Fe, Ni, Mo, $^{235}U$, $^{238}U$ et $^{239}Pu$.

Pour l'établissement des conditions optima concernant les réacteurs à neutrons rapides et à neutrons intermédiaires, pour calculer avec précision la distribution spatiale des flux de neutrons, les masses critiques, les taux de surgénération, la combustion, les coefficients Doppler et les éléments connexes, l'auteur avait besoin de données beaucoup plus détaillées sur les sections efficaces microscopiques — notamment en ce qui concerne l'absorption et la fission des neutrons — que, par exemple, pour l'évaluation des constantes fondées sur l'emploi de quelques groupes dans la théorie classique de la diffusion à plusieurs groupes.

En dépit de grands progrès dans la détermination expérimentale et l'interprétation théorique des données nucléaires, on constate encore des contradictions dans les résultats des expériences de divers auteurs et laboratoires, et il existe toujours de graves lacunes dans les travaux sur les données nucléaires. L'auteur traite d'un grand nombre de ces lacunes et contradictions en ce qui concerne les éléments mentionnés plus haut.

**Требования в отношении ядерных данных для расчетов реакторов на быстрых и промежуточных нейтронах.** В течение 1960/61 годов в Карлсруэ была проведена некоторая работа по компиляции надежных ядерных данных для расчетов реакторов на быстрых и промежуточных нейтронах. К материалам, которые пока вошли в компиляцию, относятся гелий, кислород-16, натрий-23, хром, железо, никель, молибден, уран-235, уран-238 и плутоний-239.

Для осуществления успешных исследований реакторов на быстрых и промежуточных нейтронах, для надежного теоретического предсказания пространственной зависимости спектров нейтронной энергии, критических масс, коэффициентов воспроизводства, выгорания, коэффициентов Допплера и относящихся к ним проблем автор данного доклада

заинтересован в получении более подробных данных о микроскопических поперечных сечениях, касающихся главным образом поглощения и деления нейтронов, чем требуется, например, для оценки констант небольшего количества групп в обычной многогрупповой теории диффузии.

Несмотря на значительный прогресс в экспериментальном определении и теоретическом толковании ядерных данных, по-прежнему имеют место многочисленные расхождения в экспериментальных результатах различных авторов и лабораторий и большие пробелы в экспериментальной работе по получению ядерных данных. В настоящем докладе рассматривается целый ряд этих пробелов и расхождений, касающихся ядер вышеупомянутых материалов.

**Datos nucleares necesarios para los cálculos de reactores rápidos e intermedios.** En los años 1960 y 1961 se ha estado trabajando en Karlsruhe en la compilación de datos nucleares fidedignos que se utilizan en los cálculos de reactores de neutrones rápidos e intermedios. Los elementos estudiados hasta el presente comprenden: He, $^{16}O$, $^{23}Na$, Cr, Fe, Ni, Mo, $^{235}U$, $^{238}U$ y $^{239}Pu$.

Para establecer los parámetros óptimos de los reactores rápidos e intermedios, y para poder predecir teóricamente con suficiente precisión los espectros de las energías neutrónicas en función del espacio, las masas críticas, las razones de reproducción, el grado de combustión, los coeficientes Doppler, etc., se requieren datos mucho más detallados sobre las secciones eficaces microscópicas —especialmente sobre la absorción neutrónica y la fisión— que, por ejemplo, para evaluar las constantes de algunos grupos en la teoría clásica de difusión de grupos múltiples.

A pesar de los notables progresos realizados en la determinación experimental y en la interpretación teórica de los datos nucleares, siguen existiendo todavía muchas discrepancias entre los resultados experimentales dados a conocer por distintos autores y laboratorios; asimismo, subsisten grandes lagunas en los datos nucleares. En la memoria se examina toda una serie de esas lagunas y contradicciones en relación con los núclidos mencionados más arriba.

## Introduction

A crucial point in the physical design of fast and intermediate reactors is the exact knowledge of the nuclear data of the fissionable, breeding, structural and cooling materials involved. Design parameters such as space-dependent neutron energy spectra, reactor material composition, critical masses and radii, breeding ratios, burn-up, and Doppler-coefficients are more or less strongly affected by the energy-dependence of the neutron cross-sections of the reactor materials chosen. The fast-reactor theory [1, 2] has been developed sufficiently to allow accurate prediction of these design parameters, provided that the nuclear data involved in the theory are accurately known.

As to the Karlsruhe fast power-breeder reactor project, two principal possibilities of cooling are considered. The first is the almost classical one, i.e. Na-cooling, the other one, He-cooling, being somewhat unusual in connection with fast power-breeder reactors. Principal investigations have shown that He-cooling is sufficient to meet the requirements of a fast power-breeder cooling material. Large-scale experiments for He-cooling are being prepared. For optimization studies regarding these two principal types of oxide power-breeder reactor, we have made a compilation of all neutron nuclear data in respect of He, $O^{16}$, $Na^{23}$, Cr, Fe, Ni, Mo, $U^{235}$, $U^{238}$ and $Pu^{239}$, in the energy region between 1 eV and 10 MeV. We have taken account of all available pertinent literature. A report about this work, including extensive microscopic cross-section tables, graphs, and a detailed description of the compilation procedures used, is in preparation and will soon be published as an external Karlsruhe report.

Unfortunately, in spite of much progress in the experimental determination and theoretical interpretation of nuclear data since the 1958 Geneva Conference, many inconsistencies in the experimental results of different authors and laboratories and gaps in experimental nuclear data work still remain. In the following sections I should like to discuss some striking discrepancies and gaps in the nuclear data of the above-mentioned nuclei.

The consideration of these and other discrepancies and gaps has led us to the decision to install a pulsed 3-MeV Van de Graaff for nuclear-data measurements at Karlsruhe.

## 1. Inelastic neutron scattering

In regard to inelastic neutron scattering, which is mainly responsible for the neutron-energy distributions in unmoderated reactors, large gaps still remain to be filled.

To begin with, let me quote briefly the present status as to inelastic scattering in $O^{16}$, $Na^{23}$, $U^{235}$, $U^{238}$ and $Pu^{239}$. By use of the time-of-flight method, CRANBERG and LEVIN [3—5] at LASL (the Los Alamos Scientific Laboratory) measured inelastic excitation cross-sections of $U^{235}$, $U^{238}$, and $Pu^{239}$ at 550, 980 and 2000 keV, and for some $U^{238}$-levels also at 1500 and 1893 keV. SMITH [6] at ANL (Argonne National Laboratory) measured the inelastic excitation cross-sections of the two lowest levels of $U^{238}$ at 44 and 146 keV from about 0.5 to 1.5 MeV. The gamma-ray detection method has successfully been applied to the lowest levels of many nuclei, e.g. by HALL and BONNER [7] at the Rice Institute to excitation cross-sections of some $O^{16}$-levels below 9.8 MeV, by FREEMAN and co-workers [8] at Harwell, and LIND and DAY [9] at LASL to the inelastic excitation of Na-levels up to about 3 MeV. In particular, the work of Cranberg, whose results have been confirmed by the measurements of Smith [6], has clearly shown the superiority in resolution of the pulsed time-of-flight method in comparison to the earlier spherical shell transmission measurements with threshold detectors [10—12].

Unfortunately, the range of applicability of the gamma-ray detection method and, as Cranberg discusses in detail in his recent paper [5], the reliability of the pulsed time-of-flight method are restricted to regions of low-lying and well-separated target excitation levels, say, to a few MeV at the most, the upper energy-limit depending on the size of the target nuclei. Above this limit the excited nuclear levels get so close to each other that they cannot be separated any more by the methods just mentioned. As to the time-of-flight technique applied to the heaviest nuclei, it also becomes difficult at higher neutron incident energies to discriminate between elastic scattering and inelastic scattering leading to low-lying excitation levels. Therefore, above a few MeV only measurements of the total inelastic scattering cross-section or of the non-elastic cross-section may be made; experimental information as to non-elastic cross-sections in the higher MeV-region remains rather scarce. This is particularly true of the U- and Pu-isotopes: for example, above 2 MeV nothing is known experimentally about the inelastic scattering of common fissionable isotopes such as $U^{235}$ and $Pu^{239}$; for $U^{238}$ only four not sufficiently reliable $\sigma_x$-measurements at 2.5, 4, 6 and 7 MeV [13, 14] have been made; between about 4 and 10 MeV no $\sigma_{n,n'}$ or $\sigma_x$-measurements are available for Na; for Cr and Mo similar gaps in the inelastic scattering data in the higher MeV-region exist.

Some of these gaps and experimental impossibilities have been filled up efficiently by theoretical calculations: for single-level excitation cross-sections by

means of the statistical HAUSER-FESHBACH theory [24] and, for example, for the cross-section of compound nucleus formation, by application of the optical model with improved nuclear potentials in adapting theoretical parameters to the few experimental results. To quote only some work concerning the heaviest nuclei, such semi-empirical Hauser-Feshbach calculations as those done by DRESNER [15, 23] for $U^{238}$; RAE, MARGOLIS and TROUBETZKOY [16] for $U^{235}$; and MOLDAUER [17] for $U^{235}$, $U^{238}$ and $Pu^{239}$, partly in addition to the measurements, furnished useful results with regard to excitation cross-sections for some individual low-lying levels or groups of levels of the above-mentioned nuclei, useful mainly in those energy regions where it is very difficult to do measurements. This is particularly true of the energy-dependence of the excitation cross-sections pertaining to the lowest excited states of $U^{235}$ and $Pu^{239}$ below about 100 keV.

Above about 7 MeV, according to the work of BJORKLUND and FERNBACH [18—20], the optical model of the nucleus with nuclear surface-absorption and inclusion of a spin-orbit coupling term of the Thomas-type in the nuclear potential is able to reproduce reasonably well the few experimentally determined non-elastic cross-sections. Adapting the theoretical parameters to the few measured cross-section values permits fairly good prediction, within the limits of about $\pm 10\%$, of unknown non-elastic cross-sections of the same nucleus or by nuclear systematics of the neighbouring nuclei, which in the case of isotopes without magic neutron number are nearly identical with the compound nucleus formation cross-sections [21, 22].

Therefore, mainly with regard to the already-mentioned nuclei, an intermediate energy range between about 2 and 7 MeV remains, where neither enough measurements nor reliable theoretical predictions exist. According to this lack of data, and because neutron-energy distributions in fast reactors are still rather sensitive to inelastic slowing-down from these energies, and for better insight into the range of applicability and further improvement of the optical model, there is great need for measuring the total inelastic scattering cross-section at more points between 2 and about 10 MeV. Also, with regard to calculations of fast-reactor neutron-spectra, further determination of nuclear excitation levels and

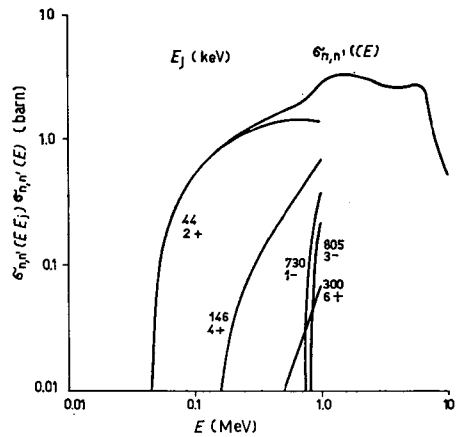


Fig. 1
Inelastic excitation cross-sections and total inelastic scattering cross-section of $U^{238}$ between threshold and 10 MeV.

inelastic excitation cross-sections, and the assignment of spins and parities to these and other already known levels are particularly needed for the heavy nuclei such as $U^{235}$, $U^{238}$ and $Pu^{239}$ below about 2 MeV, and for the medium-weight and lighter nuclei such as Na, Cr, Ni and Mo below about 3 to 5 MeV.

Fig. 1 shows the inelastic scattering cross-section of $U^{238}$. Combined are the excitation cross-sections for levels up to 1 MeV as calculated by Dresner [15, 23] and the available experimental and theoretical information about non-elastic cross-sections in the higher MeV region [13, 14, 31].

With regard to neutron-energy spectra in fast reactors it is also important to know the energy distributions of neutrons inelastically scattered in the higher MeV region, where it is impossible to distinguish between different single levels on account of the small level-distance. I should like to mention here only some of the main features. The results of the theory of nuclear evaporation [25—29] show rather good agreement with the experimentally determined spectra of inelastically scattered neutrons. Unfortunately, there are also gaps and inaccuracies in this experimental work. To quote only some of the main gaps: for the fissionable isotopes $U^{235}$ and $Pu^{239}$ no results of measurements of inelastically scattered neutron-spectra have as yet been reported; for $U^{238}$ only three such spectra have been measured and nuclear temperatures assigned: at 2.45 MeV by Cranberg [3], and at 2.5 and 3.5 MeV by FETISOV [30] (see also [31]). Similar gaps exist for Fe (only one preliminary temperature value has been reported [32, 33]), Cr, Ni and Mo. For a proper adjustment of nuclear temperatures so as to apply successfully the evaporation theory to the spectra of inelastically scattered neutrons, it would be interesting to measure inelastically scattered neutron distributions at several energies: for the heavy elements, mainly $U^{235}$ and $Pu^{239}$, and also $U^{238}$, above 2 MeV; for medium-weight structural nuclei, such as Cr, Ni, Fe and Mo, above 3—5 MeV; and finally for Na, above about 4 MeV.

## 2. Neutron absorption

In fast and epithermal breeder-reactor design, an exact knowledge of the energy-dependence of neutron-absorption cross-sections, such as $\sigma_\gamma$, $\sigma_p$, is required for:

(*a*) Liquid-metal coolants, such as Na, in order to determine exactly the cooling-circuit activation for the purpose of shield-design;

(*b*) Breeding and fissionable materials, such as $U^{235}$, $U^{238}$, and $Pu^{239}$, for reliable evaluation of critical reactor dimensions, critical masses of fissionable material, and breeding ratios;

(*c*) Structural materials, such as Fe, Ni, Cr and Mo, for judging suitably the influence of parasitic neutron-absorption on critical masses and on reactor neutron economy; and

(*d*) Fission products, for judging the long-term reactivity behaviour in reactors with high burn-up.

Between 1 and 10 MeV only very few measurements of neutron radiative capture cross-sections have been made. Also, in this energy region, at least for medium-weight structural nuclei, the neutron-absorption by the (n, p) process is considerably higher than by radiative capture: there are still gaps to be filled by further measurements, particularly for $Ni^{58}$ between the threshold at 0.39 MeV [34] and 1 MeV, and also between 3.6 MeV and about 10 MeV. Among the naturally occurring isotopes of the three neighbouring elements Fe, Ni and Cr, $Ni^{58}$—which, with an isotopic fraction of 67.76%, is the most abundant

of the stable Ni-isotopes—has the lowest threshold and the highest probability of occurrence of the (n, p) process. To quote an example for the influence of the $Ni^{58}$ (n, p) process on critical masses, the replacement of stainless steel (only about 8% Ni) by inconel (about 77% Ni) as structural material enlarges the critical masses of highly enriched fast reactors with hard neutron-energy spectra.

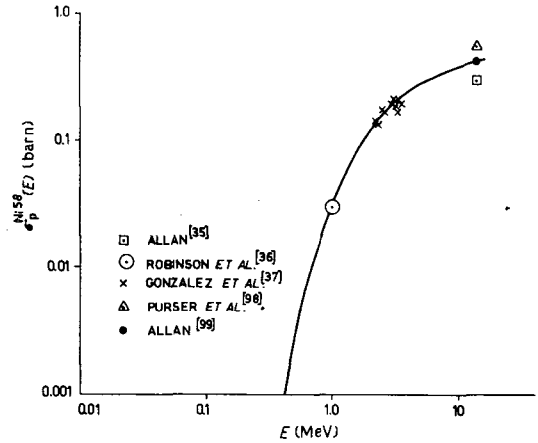


Fig. 2
$\sigma_p$ ($Ni^{58}$) from threshold to about 15 MeV.

Fig. 2 shows the energy-dependence of $\sigma_p$ ($Ni^{58}$) between threshold and about 15 MeV obtained by extrapolation from available measurements [35—37, 98, 99]. Fortunately, the bulk of the neutrons in a true fast power-breeder reactor have, in general, energies below 1 MeV; furthermore, one can, with regard to the radiative capture cross-sections of many nuclei, theoretically predict with rather good reliability a $1/E$-behaviour above 1 MeV by combining results of the statistical theory of nuclear reactions with the few existing measurements [17, 38]. Finally, above 1 MeV neutron-absorption by any of the mentioned absorption processes, mainly in the fissionable and fertile isotopes, is much less probable than inelastic scattering or fission, and thus does not influence fast-reactor neutron economy very much.

The most important energy region of fast breeder neutrons ranges from about 1 keV to 1 MeV [1, 2]. Between about 25 keV and 1 MeV there are now many $\sigma_{n\gamma}$-measurements [39–50]. Unfortunately, for the same element the results from different measurements occasionally differ greatly, perhaps in some cases due to systematic errors in different experimental methods or, which seems to be more probable, those introduced by the use of different standard values. A typical example pertaining to this latter situation is that for molybdenum: one has two series of $\sigma_{n\gamma}$ $(E)$-measurements between about 100 keV and 1 MeV, one repeated several times with nearly equal results by Diven [41], the other one made by Staviskii and Shapar [47], both differing consistently by about 50 to 100% at all energies in this region. Fig. 3 shows the experimental results for the radiative capture cross-section of molybdenum in the energy range between 1 keV and 1 MeV together with two curves, showing the energy-dependence of the radiative capture cross-section as assumed by Okrent *et al.* [17]

(dashed curve) and by ourselves (dash-dotted curve). The experimental points shown up to 6 keV are fast-chopper data obtained by BLOCK and SLAUGHTER [54]; at 30 and 65 keV, data by GIBBONS *et al.* [55]. are plotted; between 50 and 1000 keV the Russian data [47] are shown above the most recent Diven

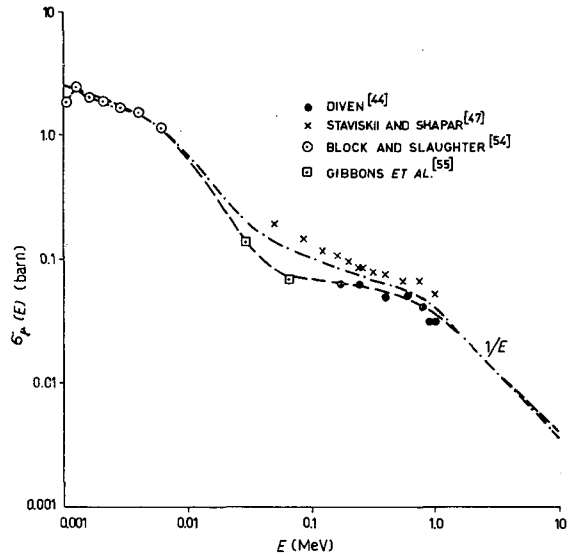


Fig. 3
Radiative capture cross-section of molybdenum between 1 keV and 10 MeV. The dashed curve and the dash-dotted curve refer respectively, to the energy-dependences assumed by Okrent *et al.* [17] and the author.

results [41]. The energy-dependence of the capture cross-section appears to be well established up to about 10 keV. Okrent *et al.* [17] drew a smooth curve through the data by Block, Gibbons, and Diven nearly without consideration of the Russian data, and arrived at an energy-dependence of the capture cross-section, which, from the viewpoint of nuclear reaction theory, can be rather well understood; the curve thus obtained shows the expected appearance of p-wave neutrons above several keV, of d- and f-wave neutrons above some 100 keV. Our own curve differs from that of Okrent *et al.* [17] essentially only in the energy region between 30 and about 1000 keV. There we have chosen a variation midway between the Diven and the Russian data, because we could not clearly decide whether the Russian standard-value of $97 \pm 16$ mb for $\sigma_\gamma^{Mo}$ at about 200 keV is really too high or not. Some question remains as to the capture group-constants of molybdenum given by Okrent *et al.* in [17]; we do not understand the discrepancy between these group-constants and the energy-dependence of the Mo-capture cross-section assumed by the same authors and reproduced in Fig. 3 of this paper.

As for $U^{238}$, the energy-dependence of the capture cross-section has been well established between about 3 and 250 keV by Duke University [51], Los Alamos [39], Harwell [39], and ORNL [52] measurements and by theoretical fitting with reaction theory by, among others, BILPUCH *et al.* [51], with some assumptions as to the p-wave strength-functions for neutron elastic-scattering

and absorption. Between 0.25 and 1 MeV the most recent $\sigma_\gamma$ $(E)$-measurements by Diven [41] are much higher than the corresponding curve in [39], which combines many earlier consistent measurements, the largest discrepancy of about 50% occurring at 1 MeV. Fig. 4 shows the capture cross-section of

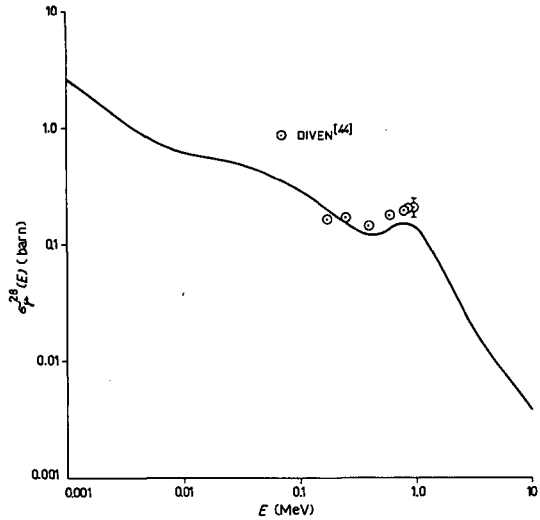


Fig. 4
Radiative capture cross-section of $U^{238}$ between 1 keV and 10 MeV.

$U^{238}$ as a function of the neutron incident energy between 1 keV and 10 MeV, together with the discrepancies mentioned between the former BNL-curve [39] and the new Diven data [41]. Such partially unexplained discrepancies in regard

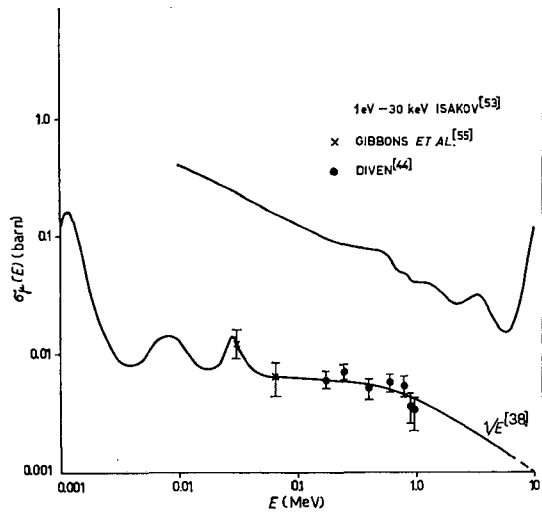


Fig. 5
Radiative capture cross-section of iron between 1 eV and 10 MeV.

to the neutron-absorption by structural and fertile materials may produce strong discrepancies in the theoretical prediction of critical masses and breeding ratios.

For many nuclides, such as Ni, Cr, etc., no $\sigma_\gamma$ $(E)$-measurements exist below about 25 keV, mainly because of the lack of measuring devices with sufficiently good energy-resolution. Recently the capture cross-section of iron from about thermal energies up to about 30 keV has been measured by ISAKOV *et al.* [53] by use of a spectrometer employing the neutron slowing-down time in lead [56]. Fig. 5 shows the radiative capture cross-section of iron between 1 eV and 10 MeV. Very recently a new powerful method for capture cross-section measurements in the higher eV and low keV energy region has been developed by Rae and Moxon at Harwell; it consists in the use of thin plastic scintillators and a graphite gamma-ray-to-electron converter for gamma-ray detection. Furthermore fast-chopper measurements of Block and Slaughter [54] above several hundred electron-volts are now available for several nuclides, e.g. molybdenum, as previously mentioned. Because, for example, in a fast oxide breeder with a rather degraded neutron-energy spectrum, a rather high percentage of neutrons still have energies below 25 keV, compared to breeders using metallic fuel, and because the radiative capture cross-sections generally increase strongly towards lower neutron energies, further $\sigma_\gamma$ $(E)$-measurements between about 100 eV and 25 keV, particularly for heavy and medium-weight structural materials of interest, would be desirable. In addition, it would be helpful for $\sigma_\gamma$ $(E)$-calculations with Breit-Wigner or reaction theory to know the $\Gamma_\gamma$'s of some resonances, particularly for medium-weight structural nuclei, such as Cr and Ni, where the level-distance is rather large compared to that in heavy structural materials.

### 3. $\alpha_{49}$ $(E)$ and $\alpha_{25}$ $(E)$

In the foregoing section I have discussed some of the main needs and discrepancies with regard to the fast-neutron absorption of structural and fertile materials. Since for the fissionable isotopes $\alpha = \sigma_\gamma/\sigma_f$ is the main interesting quantity from the point of view of fast-reactor physics—and not so much $\sigma_\gamma$ alone—I shall discuss the energy-dependence of $\alpha$ for $Pu^{239}$ and $U^{235}$ in a separate section.

Together with a knowledge of the space-dependent neutron-energy spectra in fast and intermediate reactors, the quantity $\alpha$ is an important measure of the fission quality of the fissionable material used: it influences strongly physical design parameters of the reactor systems considered, such as critical masses, breeding ratios, and the speed of the build-up of higher isotopes. For reliable prediction of these and other quantities an exact knowledge of the energy-dependence of $\alpha$ between about 100 eV and several MeV is required. I might mention here that the energy-dependence of the $Pu^{239}$ and $U^{235}$ fission cross-sections, at least in the continuum region, is well established, and that therefore inaccuracies in the quantity $\alpha$ correspond mainly to inaccuracies in the capture cross-section.

$\alpha_{49}$ $(E)$. To begin with $Pu^{239}$, as regards $\alpha_{49}$ in the energy region between 100 eV and 10 MeV, SAMPSON and MOLINO [60], combining strongly discrepant earlier results [58, 60, 64], suggested an average $\alpha_{49}$ $(E)$-curve, which is roughly consistent with integral EBR-I $\overline{\alpha}_{49}$-measurements [61]. Fig. 6 shows the experimental points that have been previously reported, together with the dashed

Sampson-Molino curve [60], and the most recent data measured by DIVEN [62]. The former data below about 30 keV and the new Diven data above 30 keV have been combined in a "presently proposed" curve, which is the unbroken line shown. Okrent *et al.* [17] adopt essentially the curve of Sampson and Molino

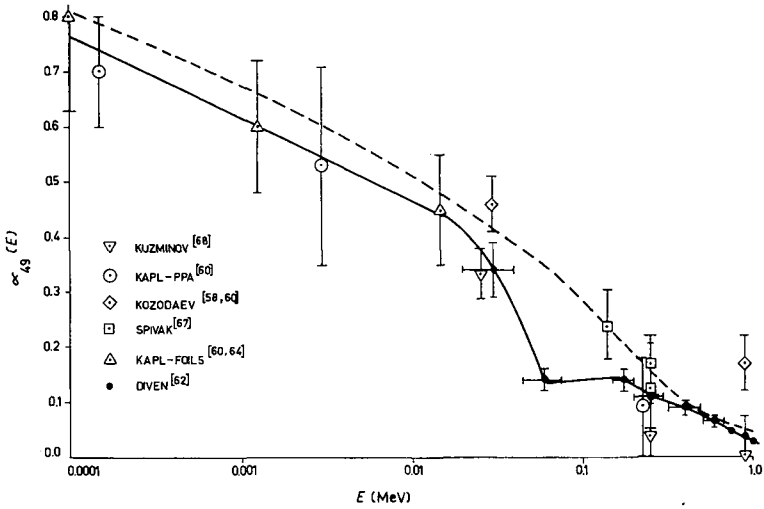


Fig. 6
$\alpha_{49}$ $(E)$ between 100 eV and 1 MeV.

with some reservations in stating that by using newer inelastic scattering data and other cross-sections now available, the fit to the integral EBR-I $\bar{\alpha}$-data in the outer blanket is even worse than that obtained by Sampson and Molino. Here I wish mainly to discuss the discrepancy between the curve of Sampson and Molino and the most recent Diven data. A particularly strong decrease in $\alpha_{49}$ between 30 and about 60 keV is seen, corresponding to a strong decrease in the capture cross-section because of the only very smooth variation of the fission cross-section at these energies. Perhaps this strong decrease could be explained by strong inelastic-scattering competition due to excitation of the $Pu^{239}$ rotational levels at 8 and 57 keV, and other, perhaps vibrational, not yet known inelastic excitation levels between these two levels. Between 30 and about 250 keV the data by Diven are much lower than those of the Sampson-Molino curve, the strongest discrepancy by a factor of 2.3 occurring around 60 keV near the maximum of the neutron-energy spectra in a typical fast oxide power-breeder. This decrease of $\alpha$ would result in a decrease of the $Pu^{239}$ radiative capture cross-section hitherto assumed and would perhaps permit a better fitting to the EBR-I $\bar{\alpha}$-data; for the fitting points are, with the higher capture cross-section of the Sampson-Molino curve used, higher than the measured values at all EBR-I space-points, particularly in the outer blanket, which is more affected by degraded neutrons than by high-speed ones. Therefore particularly in the outer blanket the new Diven data (on the "presently proposed" curve) should come closer to the integral $\bar{\alpha}$-measurements.

$\alpha_{25}$ $(E)$. The present state of knowledge about $\alpha_{25}$ $(E)$ is summarized in Fig. 7. By combining all available former experimental and theoretical results [16,

63–65, 67–68], it is possible to draw through these points the smooth dotted curve shown up to about 1 MeV. The first difficulty, which has been discussed in great detail by Okrent *et al.* [17], arises if one tries to get into agreement this set of discrete $\alpha_{25}$ $(E)$-values with the results of the integral EBR-I $\bar{\alpha}_{25}$-measurements [61]. The dash-dotted curve shows the energy-dependence of $\alpha$

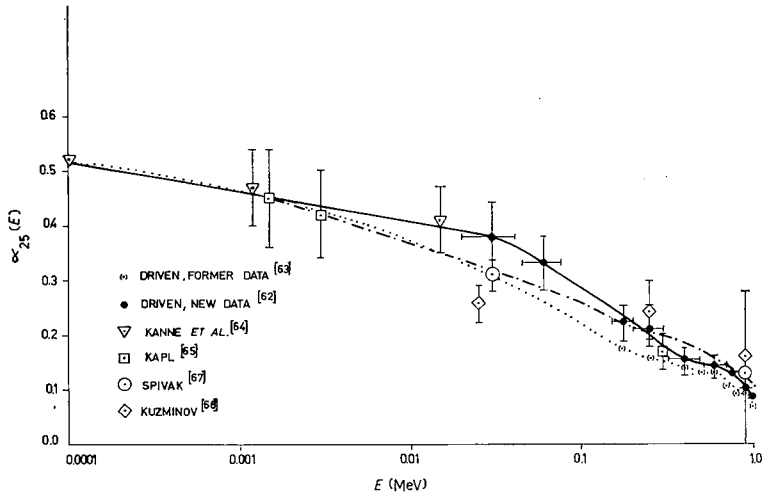


Fig. 7
$\alpha_{25}$ $(E)$ between 100 eV and 1 MeV.

as finally adopted by Okrent *et al.* [17] by going far above the upper limits of the former Diven data, for fitting the EBR-I $\bar{\alpha}_{25}$-data. Even this curve furnishes in all reactor zones lower $\bar{\alpha}$ data than those obtained by the EBR-I measurements. The most recent experimental $\alpha_{25}$ $(E)$-results obtained by Diven [62] indicated in the figure are very much higher than the upper limits of his former data [63], at least in the energy region below about 300 keV. By combining these new Diven values leading to somewhat higher capture cross-sections with the previous data below 30 keV we hope to achieve better agreement between integral EBR-I and the discrete $\alpha_{25}$ $(E)$-measurements. Thus I show in the same figure a "presently proposed" solid curve for the energy-dependence of $\alpha_{25}$.

## 4. Resonance region and parameters

In fast and intermediate reactors the resonance region of neutron cross-sections is intimately related to the problems of inherent reactor safety during prompt power excursions. This is mainly true of the reactivity temperature coefficient due to Doppler broadening of the resonances, that being the only reactivity coefficient immediately available in sudden neutron flux and power changes. In order to evaluate reliably the sign and magnitude of the Doppler coefficient, an exact knowledge of as many as possible of the resonance parameters of fissionable, breeding, and structural nuclei involved in fast and intermediate reactors is indispensable. The effects of the gaps and discrepancies in the experiments and, therefore, of the discrepancies in the theoretical interpretation of

nuclear parameters of the resonance region on calculated Doppler coefficients may best be elucidated by listing the values, published by different authors at different times, of that homogeneous mixture of $U^{235}$ and $U^{238}$ for which the Doppler coefficient changes from positive to negative. If we introduce the abbreviation: Vol. fraction of $U^{238}$/Vol. fraction of $U^{235} = y$, then the following $y$-values have been published up to now:

| | |
|---|---|
| $y = 1.87$ | GOERTZEL *et al.* [69, 70] |
| $y = 0.79$ | LANE *et al.* [71] |
| $y = 1.03$ | BETHE [72] |
| $y = 0.675$ | LUK'JANOV *et al.* [73]. |

Let us exclude for the moment the value by Goertzel as being determined only for a neutron incident energy of about 100 keV—this energy is only an upper limit of the whole energy region contributing to the Doppler coefficient—far above the three other values, in which all interesting energies in the resonance and continuum region have been taken into account. Then a discrepancy in the other values of about 20–30% remains. This discrepancy is only to a small extent due to certain differences in the theoretical methods used, but it rather reflects the great inaccuracies in the experimental data and their theoretical interpretation concerning the resonance parameters and the distribution laws of neutron and fission widths.

As to the experimental needs, especially with regard to a reliable theoretical prediction of Doppler coefficients, I shall mention only the main features.

To begin with the neutron half-widths and the level-spacings, here the distribution laws are well established today, i.e. for the neutron widths a Porter-Thomas distribution with a number of degrees of freedom equal to the number of open neutron entrance channels for given $l$ and $J$, and a Wigner-distribution for the level-spacings. Also the $(2J+1)$-dependence of level density is well established, at least for low target nucleus spins. Thus we can restrict our discussion to the more complex problems connected with the radiation and fission half-widths.

The number of known radiation half-widths although steadily increasing is still relatively small: for example, out of 13 resonances of molybdenum isotopes between 45 and 700 eV, only two greatly differing $\Gamma_\gamma$'s[74]; out of 18 resonances of $Pu^{239}$ between 7.83 and 52.6 eV, only 9 $\Gamma_\gamma$'s [75]; out of 28 resonances of $U^{235}$ between 1.14 and 19.3 eV, only 10 $\overline{\Gamma}_\gamma$'s [76]. The $\overline{\Gamma}_\gamma$ determined from these data, which form generally the basis for determining other resonance parameters, such as the fission-widths, are at least inaccurate, within the limits of $\pm 20\%$ or more, these inaccuracies thus affecting the fission widths. Fortunately in agreement with the theoretical expectation that due to the existence of many exit channels the radiation widths of different resonances of the same isotope follow a distribution law of the $\chi^2$-type with many degrees of freedom [77], the magnitude of the few known $\Gamma_\gamma$'s does not change very much from resonance to resonance of the same isotope. But, as these average radiation widths are generally evaluated only by a few single $\Gamma_\gamma$'s measured, these averages may change with the increasing number of measured radiation-widths. To quote only one example: recently MICHAUDON *et al.* at Saclay [78] made radiation-width measurements for $U^{235}$-resonances between about 11 and 19 eV; from these results it appears that the average radiation-width for $U^{235}$-resonances assumed up to now [76], i.e. 35 MeV, is too small by about 15%, a fact which

could perhaps be explained by the assumption of somewhat different average radiation-widths for the two different s-wave spin states of $U^{235}$.

Furthermore, with regard to the $U^{238}$ nucleus, some theoretical and experimental arguments [51, 79, 81] point out that the average radiation-widths for s- and p-wave resonances should be different. This would mean also a difference with respect to the two different $l=1$ spin states, which is rather difficult to understand in comparison with a good number of other nuclei, where such a difference could not yet be observed. As to the arguments mentioned above in favour of such a difference for $U^{238}$: with the assumption that s- and p-wave strength-functions for neutron-absorption differ by a factor of 2.6, in addition to an estimate for the p-wave neutron strength-function, Bilpuch *et al.* [51] got a good fit with reaction theory to their own and other measurements of the $U^{238}$ capture cross-section in the higher keV region, without, however, taking into account competition by inelastic scattering to the first rotational excitation levels at 44 and 146 keV. Furthermore, an upper limit of about 60 MeV has been preliminarily measured for the radiation-width of the resonance at 10.2 eV [81], which is claimed to be a p-wave resonance, although with low probability; this rather high value has to be compared with $\overline{\Gamma}^{28}_{\gamma l=0} \approx 25$ MeV [82, 96]. For the tentatively assigned $l=1$ resonances, Rosen [82] assumed simply $\overline{\Gamma}^{28}_{\gamma l=1} = \overline{\Gamma}^{28}_{\gamma l=0}$. To decide reliably whether there is a real difference in $\overline{\Gamma}^{28}_{\gamma}$ for different spin states and/or neutron angular momenta, it would be desirable to have measurements for some clearly assigned $U^{238}$ p-wave resonances.

Finally, it is generally assumed that $\overline{\Gamma}_{\gamma}$ is independent of the compound nucleus spin $J$, without experimental proof, particularly in the case of fissionable isotopes such as $Pu^{239}$ and $U^{235}$ with old half-integer values of the target spin $I$. However, because of the rather high value of the target spin of these nuclei, it is very difficult to decide experimentally between the two different spin states connected with s-wave neutrons. Therefore it is concluded that for better justification of the assumption of the $J$-independence of the average capture-width $\overline{\Gamma}_{\gamma}$ and for better knowledge of these averages, at least for s- and p-wave resonances, the knowledge of many more resonances with different $l$- and $J$-values would be desirable.

As to the fission-widths, I have already mentioned the inaccuracy introduced by the inaccuracy in the assumed average radiation-width. In the following lines I restrict myself to a discussion of $Pu^{239}$-resonances; very similar arguments hold then for $U^{235}$.

In the case of $Pu^{239}$, the fission-widths $\Gamma_f$ are given only for the resonances up to 52.6 eV [13, 75, 84] with inaccuracies as high as $\pm 25\%$ and with large discrepancies between experimental results of different authors [13]. As for the resonances at 10.9, 15.5, 17.6 and 22.2 eV, the determination of resonance parameters by area analysis of the transmission dips on the one hand, and by measurements of $\eta/\nu$ the other, resulted in discrepant values $\Gamma_f/\Gamma_f+\Gamma_\gamma$ [75]. Furthermore, the $\eta/\nu$-measurements [75, 84] pointed out a strong asymmetry of these resonances. This asymmetry could be explained either by (*a*) interference between several resonances of equal $l$ and $J$ and could then, with certain simplifying assumptions as to the number of exit channels in capture and fission, be described by the Wigner-Eisenbud formalism, which has been applied successfully to the first few resonances of $U^{233}$ [85, 86], $U^{235}$ [87–89] and $Pu^{241}$ [90], or by (*b*) the unresolved overlapping of several closely spaced resonances [75].

Therefore in some cases a reinvestigation of resonances with better experimental resolution and with more elaborate theoretical interpretation taking account of interference effects, rather than with the most often used one-level Breit-Wigner formula, seems desirable. Nothing at all is known about the $Pu^{239}$-resonance parameters of the numerous levels between 52.6 and, say, 1 keV. In any case, it seems to be easier to measure $Pu^{239}$- than $U^{235}$-resonances and to distinguish different spin states, because the level-distance per spin state is several times larger, and the target spin $I$ much smaller, in $Pu^{239}$ compared to $U^{235}$.

As a direct consequence of this incomplete knowledge of the fission-widths, the statistical distribution law for the $\Gamma_f$'s, the number of degrees of freedom in fission and, consequently, the average fission-widths $\bar{\Gamma}_f$ can be determined only with great inaccuracy: different distribution laws nearly equally justified by the few experimental results lead to strongly different $\bar{\Gamma}_f$ [91, 92].

Thus, when different $\bar{\Gamma}_f$-values according to different $\Gamma_f$-distributions are used, the reaction theory, which has to be applied to the region of unresolved resonances for the determination of effective cross-sections, leads to different results for the Doppler coefficients in the keV energy range, which in fast and intermediate reactors contributes much to the energy integral of the Doppler coefficient [71—72, 93].

In view of the above arguments, the value of the further thorough investigation of the resonance region, going on in many laboratories, particularly of the main fissionable isotopes such as $Pu^{239}$ and $U^{235}$, is greatly acknowledged.

## 5. List of nuclear-data requirements for some fissionable and fertile isotopes

Finally, with regard to the main fissionable and fertile isotopes, I should like to summarize my discussion of gaps and discrepancies in experimental and theoretical nuclear-data work in a list containing only those requirements which I consider particularly important from the point of view of fast and intermediate

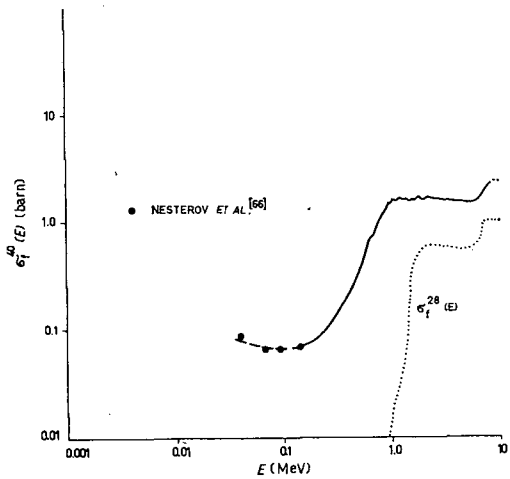


Fig. 8
Fission cross-section of $Pu^{240}$ between 40 keV and about 10 MeV.

TABLE I

**NUCLEAR DATA REQUIREMENTS FOR SOME FISSIONABLE AND FERTILE ISOTOPES**

| Element | Quantity | Energy | Comments |
|---|---|---|---|
| $U^{235}$ | $\sigma_T(E)$ | 100 eV—10 keV | Re-measurement with improved accuracy needed. |
| | $\Gamma_f, \Gamma_\gamma$ | 10 eV— 1 keV | In spite of much excellent work (see for instance [94] and references indicated there) more information about capture and fission resonance parameters is needed (see Section 4 of this paper). |
| | $\alpha(E)$ | 10 eV—10 keV | In addition to the results reported in [65] measurements are particularly needed in the resonance region, where $\alpha$ and $\eta$ vary strongly due to the mutual interference of the fission resonances (see Section 4). |
| | $\sigma_{n,n'}(E)$ $\sigma_{n,n'}(E, E')$; $T$ | 2—10 MeV | No measurements have been reported up to now. |
| | $\sigma_{n,n}(E, \theta)$ | 2—10 MeV | Measurements so far reported [5, 95] cover only some energies between 0.5 and 2 MeV. |
| U nat. | $\sigma_T(E)$ | ~2—10 keV | In this energy region $\sigma_T$ of natural uranium has been measured with bad resolution [39]. |
| $U^{238}$ | $l, J, \Gamma_\gamma$ ($l=1$) | Resonances between 6.68 and ~2000 eV | Reliable $l$-assignments for the levels in the indicated energy range are needed for exact determination of the strength functions. The strength function values found by Rosen [82] and by Lynn *et al.* [96] differ by 13%, whereas the Lynn-value is rather consistent with the Brookhaven result [97]. $J$ and $\Gamma_\gamma$-assignments for several p-wave resonances desired. |
| | $\sigma_\gamma(E)$ | 250 keV—1 MeV | Diven [41] obtained consistently higher values than are reported in [39]. |
| | $\sigma_{n,n'}(E)$ | ~2—10 MeV | Only four not sufficiently reliable $\sigma_X$-measurements at 2.5, 4, 6, 7 MeV are reported in [13, 14]. |
| | $\sigma_{n,n'}(E, E')$; $T$ | ~2—10 MeV | Only three determinations of the energy spectrum of inelastically scattered neutrons and nuclear temperature assignments at 2.45 MeV [3], at 2.5 and 3.5 MeV [30] have as yet been made (see also [31]). |
| | $\sigma_{n,n}(E, \theta)$ | 3—10 MeV | Only below 3 MeV a few measurements are reported in literature [5, 95]. *Cont. p. 18* |

TABLE I, cont.

| Element | Quantity | Energie | Comments |
|---|---|---|---|
| $Pu^{239}$ | $\sigma_T(E)$ | 90 eV—10 keV | Re-measurement with much greater accuracy needed. |
| | $\alpha(E)$ | 60 eV—10 keV | Nearly no measurements up to now (see [65]). |
| | $\Gamma_f, \Gamma_\gamma$ | Resonances between ~60 eV and ~1 keV | $\Gamma_f, \Gamma_\gamma$-values so far reported (see for example [75, 76, 80, 84] cover only resonances below about 60 eV (see also Section 4). |
| | $\sigma_f(E)$ | 1—10 keV | Re-measurement with greater accuracy needed. |
| | $\sigma_{n,n'}(E)$ | ~2—10 MeV | No measurements have been reported up to now. |
| | $\sigma_{n,n'}(E, E'); T$ | ~2—10 MeV | No measurements have been reported up to now. |
| | $\sigma_{n,n}(E, \theta)$ | ~2—10 MeV | Measurements so far reported [5, 95] cover only energies in the region between 0.5 and 2 MeV. |
| $Pu^{240}$ | $\sigma_T(E)$ | 50 eV—10 MeV | No measurements have as yet been made. |
| | $\sigma_f(E)$ | 10—40 keV | Measurements in the resonance region [83] indicate some appreciable sub-threshold fission. The measurements so far reported [39, 66] cover the energy region between 0.04 and 8 MeV; they are shown in Fig. 8. |
| | $\sigma_\gamma(E)$ | 1 keV—1 MeV | No measurements have as yet been made. |
| | $\bar{\nu}_p(E)$ | 0.1—10 MeV | No discrete experimental data are as yet available, except for some discrepant reactor spectra averages. |
| | $\sigma_{n,n'}(E)$ | Threshold–10 MeV | No measurements have as yet been made. |
| | $\sigma_{n,n'}(E, E'); T$ | Threshold–10 MeV | No measurements have as yet been made. |

reactor physics; it is emphasized, however, that this is by no means a complete list of what is really needed. In the fourth column only short comments are given; the reader is referred to the foregoing detailed discussions. It should be briefly mentioned in addition to the table contents that there is a rather large scatter in the existing data and also a general lack of data in the region between 5 and about 14 MeV concerning the number of prompt fission neutrons of the main fissionable and fertile nuclei. In Fig. 8 the fission cross-section of $Pu^{240}$ is shown as compiled by the completed measurements available at present [39, 66]. The curve has some upward trend around 40 keV and does not show a real threshold. Also, preliminary measurements in the resonance region made by LEONARD *et al.* [83] indicate some appreciable sub-threshold fission in $Pu^{240}$. Thus, in a fast reactor, one would expect some positive reactivity contribution due to fission of built-up $Pu^{240}$ nuclei, rising with increasing burn-up. In order to estimate this effect correctly, it would be useful to have some experimental points for $\alpha$ or for the fission cross-section of $Pu^{240}$ below about 40 keV.

Regarding the requirements for the other nuclei mentioned above, such as $O^{16}$, $Na^{23}$, and the structural materials, I refer to my forthcoming Karlsruhe report about fast- and intermediate-reactor cross-sections between 1 eV and 10 MeV, covering the whole resonance and continuum energy region pertinent to fast- and intermediate-reactor design.

## REFERENCES


[1] OKRENT, D., *et al.*, Proc. UN Int. Conf. PUAE **5** (1956) 347.
[2] OKRENT, D., and LOEWENSTEIN, W. B., Proc. 2nd UN Int. Conf. PUAE **12** (1958) 16.
[3] CRANBERG, L. and LEVIN, J. A., *Phys. Rev.* **103** (1956) 343.
[4] CRANBERG, L. and LEVIN, J. A., *Phys. Rev.* **109** (1958) 2063.
[5] CRANBERG, L., LA-2177 (1959).
[6] SMITH, A., WASH-1029 (1960).*
[7] HALL, D. B. and BONNER, T. W., *Nucl. Phys.* **14** (1959/60) 295.
[8] FREEMAN, J. M. and MONTAGUE, J. H., *Nucl. Phys.* **9** (1958/59) 181.
[9] LIND, D. A. and DAY, R. B., *Ann. Phys.* **12** (1961) 485.
[10] ALLEN, R. C., *Nucl. Sci. Engng* **2** (1957) 787.
[11] BATCHELOR, R., *Proc. phys. Soc.* (*Lond.*) **A 69** (1956) 214.
[12] BEYSTER, J. R., WALT, M. and SALMI, E. W., *Phys. Rev.* **104** (1956) 1319.
[13] HUGHES, D. J., Proc. 2nd UN Int. Conf. PUAE **16** (1958) 8.
[14] BEYSTER, J. R. *et al.*, LA-2099 (1957).
[15] DRESNER, L., ORNL-3016 (1960).
[16] RAE, E. R., MARGOLIS, B. and TROUBETZKOY, E. S., *Phys. Rev.* **112** (1958) 492.
[17] MOLDAUER, P. A., YIFTAH, S. and OKRENT, D., Fast Reactor Cross Sections, Oxford, Pergamon Press (1960).
[18] BJORKLUND, F. and FERNBACH, S., UCRL-4926-T (1957).
[19] BJORKLUND, F. and FERNBACH, S., UCRL-4927-T (1957).
[20] BJORKLUND, F. and FERNBACH, S., Proc. Int. Conf. on the Nuclear Optical Model, Florida State University, Tallahassee (1959).
[21] HOWERTON, R. J., UCRL-5351 (1958).
[22] HOWERTON, R. J., UCRL-5345 (1958).
[23] DRESNER, L., Internal Karlsruhe Report (to be published in *Nucl. Sci. Engng*).
[24] HAUSER, W. and FESHBACH, H., *Phys. Rev.* **87** (1952) 366.
[25] WEISSKOPF, V. F., *Phys. Rev.* **52** (1937) 295.
[26] WEISSKOPF, V. F. and EWING, D. H., *Phys. Rev.* **57** (1940) 472, 935.
[27] BLATT, J. M. and WEISSKOPF, V. F., Theoretical Nuclear Physics, John Wiley, New York (1952).
[28] NEWTON, T. D., *Canad. J. Phys.* **34** (1956) 806.
[29] LANG, J. M. B. and LE COUTEUR, K. J., *Proc. phys. Soc.* (*Lond.*) **A 67** (1954) 586.
[30] FETISOV, N. I., Soviet Research on the Lanthanide and Actinide Elements, 1949—1957, Part III, Nuclear Chemistry and Nuclear Properties.
[31] MANDEVILLE, C. E. and KAVANAGH, D. L., CWR-4028, (1958).
[32] THOMSON, CRANBERG, L. and SEAGONDOLLA R, L.W., WASH-1026 (1959)*.
[33] THOMSON and CRANBERG, L., WASH-1028 (1960).*
[34] Nuclear Data Sheets, National Academy of Sciences, National Research Council, Washington, D. C.
[35] ALLAN, D. L., *Proc. phys. Soc.* (*Lond.*) **A 70** (1957) 195.
[36] ROBINSON, B. L. and FINK, R. W., *Bull. Amer. phys. Soc.* **1** (1956) 40.
[37] GONZALEZ, L., RAPAPORT, J. and VAN LOEF, J. J., *Phys. Rev.* **120** (1960) 1319.
[38] TRALLI, N., APEX-467 (1958).
[39] HUGHES, D. J. and SCHWARTZ, R. B., BNL-325, 2nd ed. (1958).
[40] LANE, A. M. and LYNN, L. E., *Proc. phys. Soc.* (*Lond.*) **A 70** (1957) 557.
[41] DIVEN, B. C., Proc. 2 nd UN Int. Conf. PUAE **15** (1958) 60.
[42] DIVEN, B. C., TERRELL, J. and WALTER, WASH-1013 (1958).*
[43] GIBBONS, J. H., MACKLIN, R. L. and NEILER, J. H., WASH-1018 (1959).*
[44] TERRELL, J., ANL-6122 (1960).
[45] GIBBONS, J. H., *et al.* WASH-1026 (1959).*

[46] MACKLIN, R. L., Proc. 2nd UN Int. Conf. PUAE **15** (1958) 68.
[47] STAVISKII, Y. Y. and SHAPAR, A. B., AEC-tr-3946 (1960).
[48] LYON, W. S. and MACKLIN, R. L., *Phys. Rev.* **114** (1959) 1619.
[49] BAME, Jr. S. J. and CUBITT, R. L., *Phys. Rev.* **113** (1959) 256.
[50] LYNN, J. E., FIRK, F.W.K. and MOXON, H. C., *Nucl. Phys.* **5** (1958) 603.
[51] NEWSON, H. W. and BILPUCH, E. G., *Ann. Phys.* **10** (1960) 455.
[52] MACKLIN, R. L. *et al.*, ORNL-2910 (1960).
[53] ISAKOV, A. I., *et al.*, JETP-11 (1960) 712.
[54] BLOCK, R. C. and SLAUGHTER, G. C., ORNL-2910 (1960).
[55] GIBBONS, J. H., *et al.*, *Phys. Rev.* **122** (1961) 182.
[56] BERGMAN, A. A. *et al.*, Proc. UN Int. Conf. PUAE **4** (1956) 135.
[57] KALASHNIKOVA, V. I. *et al.*, *J. nucl. Energy* **5** 1957 (226).
[58] KOZODAEV, M. S., Proc. UN Int. Conf. PUAE **4** (1956) 295, 349.
[59] CODD, J., SHEPHERD, L. R. and TAIT, J. H., *Progr. nucl. Energy I*, **1** (1956) 251.
[60] SAMPSON, J. B. and MOLINO, D. F., KAPL-1793 (1957).
[61] KAFALAAS, P. *et al.*, *Nucl. Sci. Engng* **2** (1957) 657.
[62] SHER, R. and MOORE, S. BNL-653 (N-3) (1961).
[63] DIVEN, B. C., TERRELL, J. and HEMMENDINGER, A., *Phys. Rev.* **109** (1958) 144.
[64] KANNE, W. R. *et al.*, Proc. UN Int. Conf. PUAE **4** (1956) 315.
[65] Reactor Physics Constants, ANL-5800 (1958).
[66] NESTEROV, V. G. and SMIRENKIN, G. N., *Atomn. Energiya* **9** (1960).
[67] SPIVAK, P. E., *J. nucl. Energy* **4** (1957) 79.
[68] KUZMINOV, B. D. *et al.*, *Atomn. Energiya* **4** (1958).
[69] GOERTZEL, G. *et al.*, Proc. UN Int. Conf. PUAE **5** (1956) 472.
[70] FESHBACH, H., GOERTZEL, G. and YAMAUCHI, H., *Nucl. Sci. Engng* **1** (1956) 4.
[71] LANE, A. M., LYNN, J. E. and STORY, J. S., AERE-T/M-137 (1956).
[72] BETHE, H. A., APDA-119 (1957).
[73] LUK'JANOV, A. A. and ORLOV, V. V., *Atomn. Energiya* **10** 1961 262.
[74] HARVEY, J. A., *et al.*, *Phys. Rev.* **99** (1955) 10.
[75] BOLLINGER, L. M., COTÉ, R. E. and THOMAS, G. E., Proc. 2nd UN Int. Conf. PUAE **15** (1958) 127.
[76] HUGHES, D. J., MAGURNO, B. A. and BRUSSEL, M. K., BNL-325-suppl., 2nd ed. (1960).
[77] PORTER, C. E. and THOMAS, R. G., *Phys. Rev.* **104** (1956) 483.
[78] MICHAUDON, A., Private communication (to be published in *J. Phys. Radium*).
[79] CAMERON, A. G. W., TID-7547 (1957).
[80] VLADIMIRSKY, V. V. *et al.*, Proc. 2nd UN Int. Conf. PUAE **15** (1958) 309.
[81] BOLLINGER, L. M. *et al.*, WASH-1013 (1958).*
[82] ROSEN, J. L., CU-185 (1959).
[83] LEONARD, B. R. Jr. and ODEGAARDEN, R. H., WASH-1031 (1961).*
[84] FARLEY, F. J. M., *J. nucl. Energy* **3** (1956) 33.
[85] MOORE, M. S. and REICH, C. W., *Phys. Rev.* **118** (1960) 718.
[86] VOGT, E., *Phys. Rev.* **118** (1960) 724.
[87] REICH, C. W. and MOORE, M. S., *Phys. Rev.* **111** (1958) 929.
[88] VOGT, E., *Phys. Rev.* **112** (1958) 203.
[89] SHORE, F. J. and SAILOR, V. L., *Phys. Rev.* **112** (1958) 191.
[90] SIMPSON, O. D., MOORE, M. S. and SCHUMAN, R. P., WASH-1031 (1961).*
[91] OLEKSA, S., *J. nucl. Energy* **5** (1957) 16.
[92] BETHE, H. A., *Progr. nucl. Energy I* **1** (1956) 91.
[93] NICHOLSON, R. B., APDA-139 (1960).
[94] MICHAUDON, A. *et al.*, CEA-1093 (1959).
[95] HUGHES, D. J. and CARTER, R. S., BNL-400 (1956).
[96] LYNN, J. E., FIRK, F. W. K., and MOXON, M. C., TNCC (UK)-44 (1959).
[97] HUGHES, D. J. and PILCHER, V. E., *Phys. Rev.* **100** (1955) 1249.
[98] PURSER, K. H. and TITTERTON, E. W., *Austral. J. Phys.* **12** (1959) 103.
[99] ALLAN, D. L., *Nucl. Phys.* **24** (1961) 274.

* It is emphasized that the WASH reports are cited only for arguments given in the text. No WASH results are quoted in Figs. 1—8; the same reservations apply here that are indicated in the introduction to the WASH reports.

SM-18/23

# REQUIREMENTS FOR FAST-NEUTRON DATA AND THE FAST-NEUTRON CROSS-SECTION MEASURING PROGRAMME IN THE UNITED KINGDOM

A. T. G. FERGUSON
ATOMIC ENERGY RESEARCH ESTABLISHMENT, HARWELL,
AND
R. BATCHELOR
ATOMIC WEAPONS RESEARCH ESTABLISHMENT, ALDERMASTON,
UNITED KINGDOM

**Abstract — Résumé — Аннотация — Resumen**

**Requirements for fast-neutron data and the fast-neutron cross-section measuring programme in the United Kingdom.** The requirements for fast-neutron data arising from the fast-reactor and shielding programmes in the United Kingdom are surveyed, and methods of assessment of accuracy and energy range are discussed. From this survey it appears that the most urgent need is for: (*a*) fission cross-sections in the range below 150 keV; (*b*) an accurate knowledge of $\bar{\nu}$ as a function of neutron energy; and (*c*) inelastic neutron scattering cross-sections for neutrons of up to 5 MeV energy.

A brief account is given of the facilities available in the United Kingdom for making measurements of this nature. The experimental programmes current, and planned, to satisfy the above requirements are considered in some detail.

**Données sur les neutrons rapides dont le Royaume-Uni a besoin; programme britannique de mesures des sections efficaces pour les neutrons rapides.** L'auteur passe en revue les données sur les neutrons rapides dont le Royaume-Uni a besoin pour mener à bien ses programmes de réacteurs à neutrons rapides et de protection; il examine les méthodes utilisées pour évaluer les résultats et déterminer les gammes d'énergie. Il ressort de cette étude que les données dont on a le plus besoin sont: *a*) les sections efficaces de fission dans la gamme des énergies inférieures à 150 keV; *b*) une connaissance exacte de $\bar{\nu}$ en fonction de l'énergie des neutrons; *c*) les sections efficaces de diffusion inélastique pour les neutrons dont l'énergie ne dépasse pas 5 MeV.

L'auteur indique succinctement quels sont les moyens disponibles au Royaume-Uni pour faire des mesures de cette nature. Il donne ensuite des détails sur le programme des expériences en cours et des expériences prévues pour satisfaire aux besoins exposés ci-dessus.

**Потребности Соединенного Королевства в данных о быстрых нейтронах и его программа по измерению сечений быстрых нейтронов.** В докладе рассматриваются потребности Соединенного Королевства в данных о быстрых нейтронах, вытекающие из программы строительства реакторов на быстрых нейтронах и разработки их защиты, и обсуждаются методы определения точности данных и диапазона энергии. Из этого обзора вытекает, что наибольшая потребность испытывается в: *a*) сечениях деления в диапазоне ниже 150 кэв; *b*) точном знании $\bar{\nu}$ как функции энергии нейтронов; *c*) сечениях неупругого рассеяния нейтронов с энергией до 5 Мэв.

В докладе кратко описываются установки, имеющиеся в Соединенном Королевстве для измерений такого рода. Более подробно рассматриваются текущие и планируемые экспериментальные программы для удовлетворения вышеуказанных потребностей.

**Programa británico de medición de secciones eficaces para neutrones rápidos y datos necesarios.** Se examinan los datos relativos a los neutrones rápidos que el Reino Unido necesita para la ejecución de sus programas de reactores rápidos y de blindaje, y se discuten los procedimientos empleados para evaluar el grado de precisión y determinar la gama energética. De dicho estudio, se desprende que la información que con mayor urgencia se requiere es la relativa a: *a*) las secciones eficaces de fisión en la gama de energías inferiores a 150 keV; *b*) un conocimiento exacto de $\bar{\nu}$ en función de la energía neutrónica; *c*) las secciones eficaces de dispersión inelástica para neutrones de hasta 5 MeV.

El autor indica brevemente las instalaciones de que se dispone en el Reino Unido para efectuar mediciones de este tipo. Por otra parte, describe con bastante detalle los programas actuales y en proyecto, encaminados a satisfacer las mencionadas necesidades.

## Introduction

In the United Kingdom, there has been a continuing interest in fast reactors as an ultimate means of achieving cheap nuclear power. Zero-energy reactors ZEPHYR and ZEUS have been followed by the power reactor DFR. In parallel with this there has been a programme of neutron cross-section measurements whose intensity at any time has in general reflected the current rate of activity in the fast-reactor field. Between these two streams, viz. direct power reactor development and nuclear cross-section measurements, there have been a number of simple integral experiments which, by virtue of their simplicity, have been very fruitful in showing up discrepancies between nuclear data and integral properties.

The United Kingdom reactor programme is now entering a new phase in which much larger, more dilute, power reactors are being considered along with their zero-energy counterparts VERA and ZEBRA. The expansion in the use of multigroup calculations has placed great emphasis on the need for knowledge of the inelastic cross-sections for neutrons. In addition, there has been a considerable widening of the scope of international co-operation in the field of cross-section measurements. All these developments have led to considerable effort in the United Kingdom in setting out clearly and in some detail both the immediate and more long-term demands for neutron cross-sections in the fast-neutron field.

A considerable contribution to the United Kingdom cross-section request list comes from the demands of reactor shielding, a field in which computational developments have closely paralleled those used in fast reactors. The requirements for shielding frequently call for measurement of cross-sections at higher neutron energies and over a wider range of materials.

## The preparation of the United Kingdom request list

It is generally easy to decide qualitatively which cross-sections are needed for calculations. It is another matter to decide precisely on the energy range and accuracy of the cross-sections required, and weigh up the cost of the measurement in terms of money and demands on limited resources.

In the case of requests arising from proposed dilute fast reactors, the procedure adopted was to take a typical case, 1500 l in volume with a mixed U-Pu

carbide fuel containing large amounts of stainless steel, and calculate the effects on the reactivity and breeding ratio of small changes in the nuclear data. Setting arbitrary limits to the errors in $k_{\text{eff}}$ and breeding ratio, limits were derived for the acceptable limits of error in the nuclear cross-sections [1]. Such methods lead to a reasoned and consistent request list. Nevertheless, the experimental nuclear physicists were alarmed by a number of requests for data of high accuracy over energy ranges extending to energies up to 14 MeV. Experimentally, at the present time measurements in the neutron energy range 7—14 MeV present great difficulties. Investigation showed that these requests arose from the fact that the variational calculations had been made using only five energy groups, the uppermost extending from 1.3 to 14 MeV. Some further consideration by the reactor physicists has in most cases led to the energy range being subdivided, which greatly reduces the accuracy being demanded at the higher energies.

As a result of this co-operation between nuclear and reactor physicists in its preparation, the United Kingdom request list forms a sound basis for the experimental programme of cross-section measurements.

## The United Kingdom request list for fast-neutron data

The requests of highest priority for fast-neutron data are shown in Table I. The request of outstanding difficulty is undoubtedly that for $\bar{\nu}(E)$ to an ac-

TABLE I

**REQUESTS OF HIGHEST PRIORITY FOR FAST-NEUTRON DATA**

| Parameter | Element | Energy range (MeV) | Accuracy (%) |
|---|---|---|---|
| 1. Neutron scattering | | | |
| 1.1 $\sigma_{nn}(E, b)$ | Al | 0.01— 1 | 10 |
| | Fe | 0.01— 1 | |
| 1.2 $\sigma_{nn'}(E, E')'$ | Na | Thresh— 1 | 10 |
| | | 1— 5 | 5 |
| | | 5—10 | 20 |
| | Al | Thresh— 5 | 5 |
| | Fe | Thresh— 5 | 5 |
| | $U^{238}$ | Thresh— 1 | 10 |
| | | 1— 5 | 2 |
| | | 5—10 | |
| $\bar{\nu}(E)$ | $U^{235}$ | 0.001— 5 | 1 |
| | | 5—10 | 5 |
| | $Pu^{239}$ | 0.001— 5 | 1 |
| | | 5—10 | 4 |
| $\sigma_{n\gamma}$ | $U^{235}$ | 0.001— 5 | 2 |
| | | 5—10 | 10 |
| | $Pu^{239}$ | 0.001— 5 | 2 |
| | | 5—10 | 10 |
| | $U^{238}$ | Thresh— 5 | 2 |
| $\sigma_{n\gamma}$ | $U^{235}$ | 0.001— 5 | 5 |
| | $U^{238}$ | 0.001— 1 | 2 |
| | | 1— 5 | 10 |
| | $Pu^{239}$ | 0.001— 5 | 5 |

curacy of 1%, and reflects the importance of the "neutron sources" in reactor calculations. For similar reasons the fission cross-sections are important. Existing knowledge is almost adequate to meet these requests except in the energy region below 150 keV, where neutron flux measurement presents the major difficulty. In estimating both breeding ratio and critical mass, the capture cross-sections of the major components are important. Some of these, such as that of $U^{238}$, can be measured by activation using radiochemical techniques. In such cases, the accuracy demanded seems attainable with extreme care. In the remaining cases, it is necessary to estimate the intensity of the capture $\gamma$-rays. This technique has not yet reached the desired precision, though very intensive work on it is going on at Oak Ridge and Los Alamos in the United States and elsewhere. The other major field in which high precision is required is inelastic scattering. The increase in intensity of pulsed neutron sources which has resulted from recent technical development, with background reducing techniques such as pulse-shape discrimination, will greatly assist in obtaining high accuracy in scattering cross-sections.

## Facilities for fast-neutron measurements

Comparatively little work is done in the field of fast-neutron physics in the United Kingdom outside the laboratories of the UKAEA at Harwell and Aldermaston. The programmes of these two groups are co-ordinated by a joint working party. Where practicable, high-energy measurements are made at Aldermaston and low-energy measurements at Harwell, although it is recognized that it is not always easy to separate investigations in this way. For the more important data it is also necessary to duplicate the measurements, if possible, by different techniques.

*Aldermaston facilities*

1. A 6-MeV Van de Graaff. This has for some years had post acceleration pulsing. A duoplasmatron ion source and top terminal pulsing facility are at present being installed, which should increase the intensity of pulsed beam and reduce background.
2. A high-current 3-MeV horizontal Van de Graaff — not pulsed.
3. A 12-MeV tandem generator.

*Harwell facilities*

4. A 5-MeV electrostatic generator. This has a post acceleration pulsed beam.
5. A 3-MeV Van de Graaff with top terminal pulsing followed by post acceleration magnetic bunching to give a very high intensity pulsed source. This is in process of installation at this time.
6. A 500-keV Cockcroft-Walton set used as a high intensity source of 14-MeV neutrons.
7. A high-intensity 30-MeV electron linear accelerator. This provides a pulsed source of neutrons which permits certain cross-sections to be measured with good energy resolution up to neutron energies of 100 keV.
8. A 12-MeV tandem generator. At present this machine is not pulsed.

## The programme of fast-neutron data measurements

The cross-section measuring programme of the two laboratories is described below in broad terms. Such programmes are always subject to modification in the light not only of changing demands but also of measurements made at other laboratories and therefore no attempt is made to give very much detail.

*Neutron-scattering measurements* $\sigma_{n,n}(E, \theta)$ and $\sigma_{n,n'}(E, E')$

The post acceleration pulsing facility has recently been used for measurements up to 4-MeV neutron energy. Some measurements on sodium are described in detail by TOWLE and GILBOY [2]. With the top terminal pulsing facility, these measurements will be extended up to about 9 MeV, although the detailed planning of these measurements will not be made until some experience has been obtained with this new unit. At AERE, the 3-MeV pulsed Van de Graaff can be used to cover the lower energies up to 3 MeV and for the region between 4 and 6 MeV. For a detailed study of the inelastic processes as a function of energy, measurement of the associated $\gamma$-rays has many advantages. This technique will continue to be developed and applied at AERE. In order to assist these studies, it is proposed to look at the level schemes of the target nuclei using the reaction (p, p′, $\gamma$), using the AERE tandem generator.

*Measurements of* $\bar{\nu}(E)$

At Harwell, Colvin and Sowerby have been concentrating on obtaining a high-precision value of $\bar{\nu}$ for the fission of $U^{235}$ and other isotopes by thermal neutrons. This has been done using a large cubic array of graphite and $BF_3$ detectors as a fission-neutron detector. The efficiency of this device is measured by counting the corresponding protons and neutrons when deuterium in an ion chamber is disintegrated by monoenergetic $\gamma$-rays. The latter are obtained from (p, $\gamma$) reactions, a beam of protons from the Harwell 5-MeV electrostatic generator being focussed on to a target at the centre of the cube adjacent to the ion-chamber. The relative values of $\bar{\nu}$ (thermal) have been measured, and the calibration described above is almost completed.

At Aldermaston, Moat, Mather and Fieldhouse have been concentrating recently on measuring the variation of $\bar{\nu}$ with neutron energy. They have used a heavily shielded liquid scintillator in conjunction with the pulsed neutron source provided by the 6-MeV Van de Graaff [3].

*Fission cross-sections*

The main problems here concern the assaying of fission foils and the accurate measurement of neutron flux. At Aldermaston, White has started on a programme of measurements, mainly in the region 10 to 150 keV but with some spot points at higher energies. Semi-conductor counters are used to help in the assaying of foils. For the flux measurements, a hydrogen-filled proportional counter is used, and a counter based on the reaction $B^{10}$ (n, $\alpha$) is contemplated. Auxiliary measurements are planned to improve the accuracy of our knowledge of the cross-section of the latter reaction.

At Harwell, James will be making fission cross-section measurements on the electron linear accelerator up to an energy of about 30 keV. With a view to improving measurements of neutron flux at higher energies, a flux monitor, based on a thin hydrogenous radiator on a semiconductor detector, is being developed.

## Capture and reaction cross-sections

At Aldermaston, Perkin and Barry are equipped to measure cross-sections by activation techniques, and further measurements on $U^{238}$ and $Au^{197}$ are now in progress. These measurements are closely integrated with the fission cross-section measurements referred to above. Direct measurements of capture $\gamma$-rays are not planned at either establishment, in view of the extensive programmes in this field at other establishments and the limitations of staff at our own laboratories.

## REFERENCES

[1] MOORHEAD, T. P., *These proceedings*, vol. **II**, p. 111.
[2] TOWLE, J. H. and GILBOY, W. B., *These proceedings*, vol. **I**, p. 87.
[3] MOAT, A., MATHER, D. S. and FIELDHOUSE, P., *These proceedings*, vol. **I**, p. 139.

# I. 2. CROSS-SECTION REQUIREMENTS

SM—18/76

# A CRITICAL SUMMARY OF MICROSCOPIC FAST-NEUTRON INTERACTIONS WITH REACTOR STRUCTURAL, FISSILE AND FERTILE MATERIALS

A. B. SMITH

ARGONNE NATIONAL LABORATORY, ARGONNE, ILL.,
UNITED STATES OF AMERICA

**Abstract — Résumé — Аннотация — Resumen**

**A critical summary of microscopic fast-neutron interactions with reactor structural, fissile and fertile materials.** Prevailing knowledge of fast-neutron-induced reactions utilized in the nuclear design of reactor systems is reviewed. Principal emphasis is placed upon microscopic experimental methods, results and precisions. Fast-neutron scattering is considered in detail, including the results of experimental determinations of scattering from oxygen, iron, zirconium, niobium, tungsten, thorium and uranium. Representative results of experimental studies of fast-neutron capture and fast-neutron-induced fission are given. The measurements discussed not only provide results of considerable applied usefulness but are also examples of the application of advanced experimental nuclear techniques. Areas of limited, conflicting or non-existent experimental information are outlined. A prognosis of future knowledge of fast-neutron reactions is made, with emphasis on the fulfillment of reactor requirements for basic nuclear data.

**Aperçu critique des interactions microscopiques des neutrons rapides avec les matériaux de construction et les matières fissiles et fertiles utilisées dans les réacteurs.** L'auteur fait le point des connaissances sur les réactions provoquées par les neutrons rapides sur lesquelles on tend à fonder les projets de réacteurs. Il met en relief les méthodes, les résultats et la précision de mesures expérimentales à l'échelle microscopique. Il étudie en détail la diffusion des neutrons rapides, et donne les résultats de mesures expérimentales de diffusion dans l'oxygène, le fer, le zirconium, le niobium, le tungstène, le thorium et l'uranium. Il donne les résultats les plus significatifs d'études expérimentales sur la capture des neutrons rapides et sur la fission provoquée par des neutrons rapides. Les mesures étudiées, non seulement fournissent des renseignements d'une utilité pratique considérable, mais aussi constituent des exemples de l'application de techniques expérimentales nucléaires à la pointe du progrès. L'auteur indique les domaines où les données expérimentales sont limitées, contradictoires ou inexistantes. Il se livre à des pronostics sur le développement des connaissances expérimentales en matière de réactions provoquées par des neutrons rapides, en insistant sur les conditions que doivent remplir, dans les réacteurs, les données nucléaires fondamentales.

**Критический обзор микроскопического взаимодействия быстрых нейтронов с конструкционными, расщепляющимися и воспроизводящими реакторными материалами.** В докладе рассматривается применение широко распространенных знаний о реакциях, вызываемых быстрыми нейтронами в ядерных проектах реакторных систем. Основное значение придается микроскопическим экспериментальным методам, результатам и точности. Подробно рассматривается рассеяние быстрых нейтронов, включая результаты экспериментального определения рассеяния на кислороде, железе, цирконии, ниобии, вольфраме, тории и уране. Приводятся данные, полученные в результате экспериментальных исследований захвата быстрых нейтронов и деления, вызванного нейтронами. Измерения, приведенные в докладе, не только могут быть применены с большой пользой, но и сами являются примером применения передовой экспериментальной ядерной техники. Указываются

области, в которых экспериментальные данные либо недостаточны, либо противоречивы, либо вообще отсутствуют. Делается прогноз в отношении будущих знаний о реакциях на быстрых нейтронах и подчеркивается необходимость выполнения реакторных требований для получения основных ядерных данных.

**Resumen crítico de las interacciones microscópicas de los neutrones rápidos con los materiales estructurales fisionables y fértiles utilizados en los reactores.** El autor examina el estado actual de los conocimientos acerca de las reacciones inducidas por los neutrones rápidos que se utilizan en el proyecto de reactores nucleares. Estudia con particular atención los métodos experimentales microscópicos, sus resultados y la precisión de los mismos. Considera con detalle la dispersión de los neutrones rápidos, y da los resultados de mediciones experimentales de la dispersión en el caso del oxígeno, hierro, zirconio, niobio, wolframio, torio y uranio. Expone los resultados más significativos de los estudios experimentales de la captura de neutrones rápidos y de la fisión inducida por los mismos. Las mediciones estudiadas no sólo conducen a resultados de gran utilidad práctica, sino que sirven como ejemplos de la aplicación de las técnicas nucleares experimentales más modernas. El autor indica los terrenos en que la información experimental es limitada, contradictoria o inexistente. Por último, formula previsiones sobre el desarrollo de los conocimientos relativos a las reacciones de los neutrones rápidos, subrayando lo referente al cumplimiento de las condiciones necesarias para que el reactor proporcione datos nucleares básicos.

## Introduction

It is the objective of this paper to review critically the current experimental knowledge of the fast-neutron induced reactions upon which the nuclear design of fast reactive systems is based. The discussion is largely confined to microscopic neutron properties, and principle emphasis is placed upon experimental methods, results, and precisions. The reactions described in detail are chosen not only because of their very considerable applied usefulness but also because they represent outstanding examples of the application of advanced experimental techniques to the obtaining of basic fast-neutron data. An effort is made to project the current work into the future so as to estimate the nature and precision of the basic data that will soon become available to the reactor theorist. The discussion is divided into three sections: fast-neutron scattering, fast-neutron capture and fast-neutron induced fission. Principle consideration is given to the incident neutron energy interval 10 keV to 1.6 MeV. This region is extended when it is felt that the understanding of a particular reaction is improved by doing so.

## Fast-neutron scattering

### Experimental techniques and methods

Experimental studies of fast-neutron scattering are basically problems in fast-neutron spectroscopy. It is usually necessary to resolve elastically and inelastically scattered neutron groups. For this purpose various spectral sensitive devices have been employed [1]. These range from relatively crude biased recoil counters and threshold detectors to highly complex spectrometers. Recent rapid advances in high-speed electronic techniques have resulted in productive spectrometric systems based upon the measurement of the time of transit of the fast neutron over a flight path of the order of a meter [2]. So successful has this method

been that most of the early work carried out with other techniques has been superceded by these time-of-flight results.

Associated with the development of fast-timing and detection devices have been rapid improvements in the techniques for the production of very short and intense neutron bursts. A typical example of a fast-time-of-flight apparatus including the instrumentation necessary for producing an intense neutron burst is shown in Fig. 1*. A beam of charged particles is sent through a deflection

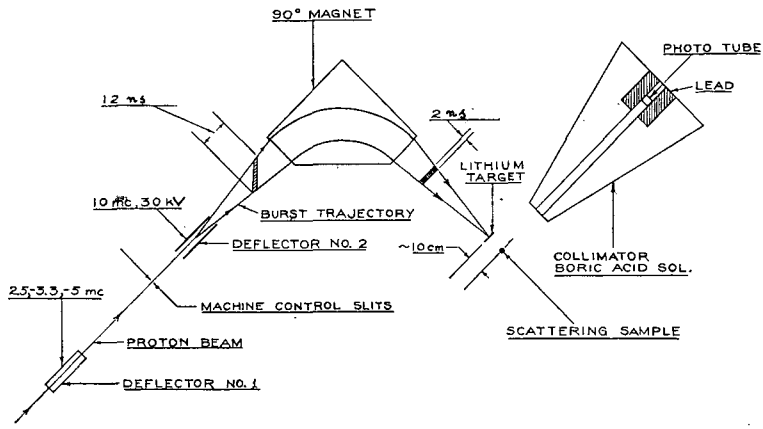


Fig. 1
A schematic diagram of a fast-time-of-flight apparatus including an electro-magnetic bunching system.

system in such a manner that the ions are swept across the entrance face of a large magnet. The sense of the sweep is arranged so that particles entering the magnet first in time follow longer trajectories, while those entering at progressively later times proceed along trajectories having correspondingly shorter paths. The particles are deflected by the magnet through 90° and focused at the target. By proper adjustment of the instrument parameters, ions entering the magnet at sequential times but with the same speed are made to arrive at the target simultaneously. The system thus focuses particles in both space and time. The particular apparatus described is capable of accepting an 11-ns input burst and producing a 1-ns pulse at the target. The peak pulse intensity is considerably greater than 1 mA and the duty cycle as high as 1%. The ion burst is converted at the target to a pulse of monoenergetic neutrons by means of the $Li^7$ (p, n) $Be^7$ reaction [3]. Some of these neutrons are scattered from the small sample down the well-shielded flight path to the neutron detector approximately 1 m distant. The measured time between the production of the neutron burst and the arrival at the detector of the scattered neutron is a measure of the neutron speed and thus energy.

Systems such as that described above are capable of 1-ns time resolution. However, practical considerations due to sample and detector size and to target thickness spread this optimum resolution to 2—3 ns. Under these conditions, the energy resolution of the instrument is ~4% at a 500-keV incident neutron

* The system described is that existing at the Argonne National Laboratory.

energy and a 1-m flight path. The resolution increases linearly with flight path and decreases approximately as the square root of the incident energy. It is thus possible to study in detail the scattering of 100- to 1000-keV neutrons from all nuclei but those having very closely spaced low-lying levels. In the results of experiments with such equipment, the theoretical reactor physicist can conceptually expect to have available basic scattering data, the energy resolution and precision of which usually exceed his ability to utilize it. In practice, the existence of the tools capable of making such measurements does not reduce the enormity of the task facing the experimental physicist. Indeed the measurements with greatly improved resolutions may actually lead to a more complex interpretation of the scattering processes as in the case of iron (see below).

## Scattering from the fertile materials $U^{238}$ and $Th^{232}$

The fertile materials $U^{238}$ and $Th^{232}$ are characterized by an even-even rotational nuclear structure [4, 38]. Early studies of fast-neutron scattering from them utilized recoil counters, reaction threshold detectors, and sphere-transmission techniques [39, 40, 32]. Results of these measurements were not unambiguous.

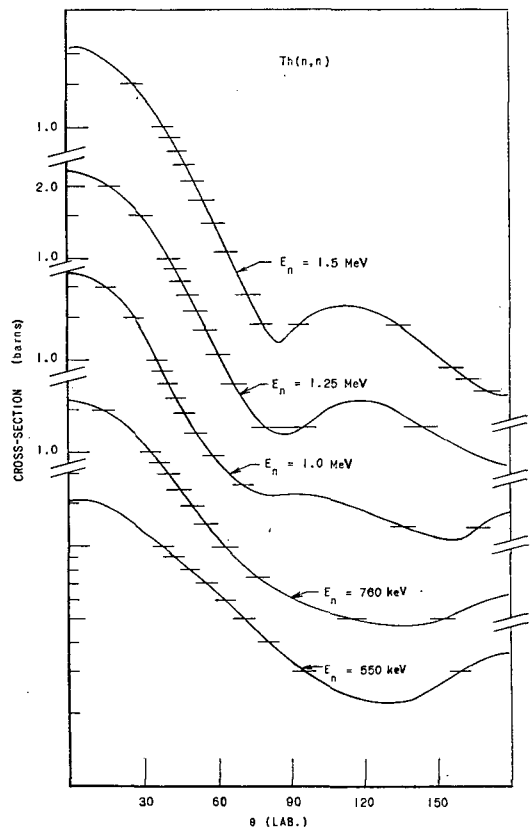


Fig. 2
The differential elastic scattering cross-section of thorium as a function of incident neutron energy.

More recent work has employed the fast-time-of-flight method described above. With this technique, it is possible to determine the pure elastic differential scattering cross-section. Results from such measurements of scattering from thorium are shown in Fig. 2 [33]. These angular distributions are in good agree-

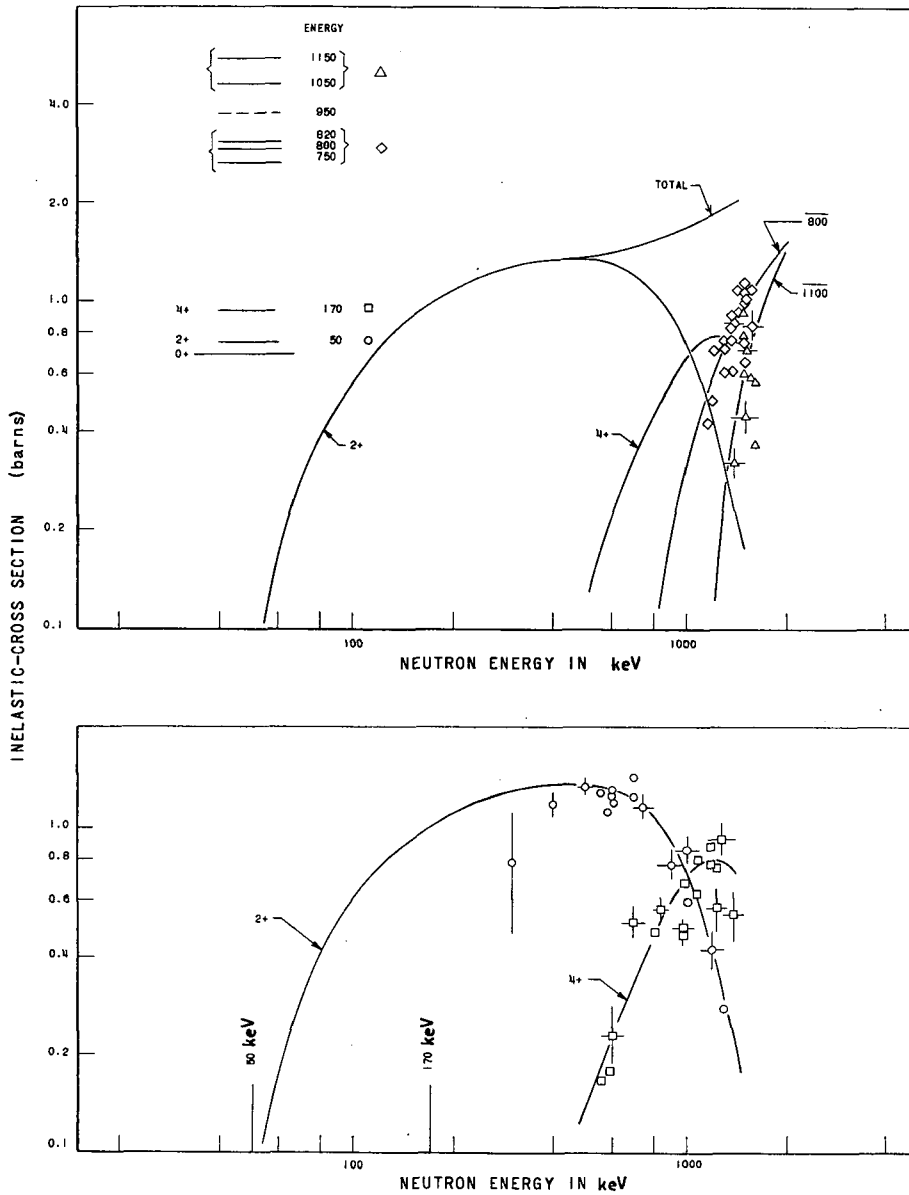


Fig. 3
The inelastic scattering cross-section for the excitation of specific residual nuclear levels in thorium.

ment with the known total scattering cross-section and, qualitatively, have the shapes predicted by the optical model. Similar studies of elastic scattering from $U^{238}$ have been carried out [42]. Unfortunately, most of these latter contain varying contributions from the more energetic inelastic neutron groups.

The inelastic scattering cross-section of thorium is graphically described in Fig. 3 [33]. In the upper part of the figure is shown that portion of the nuclear

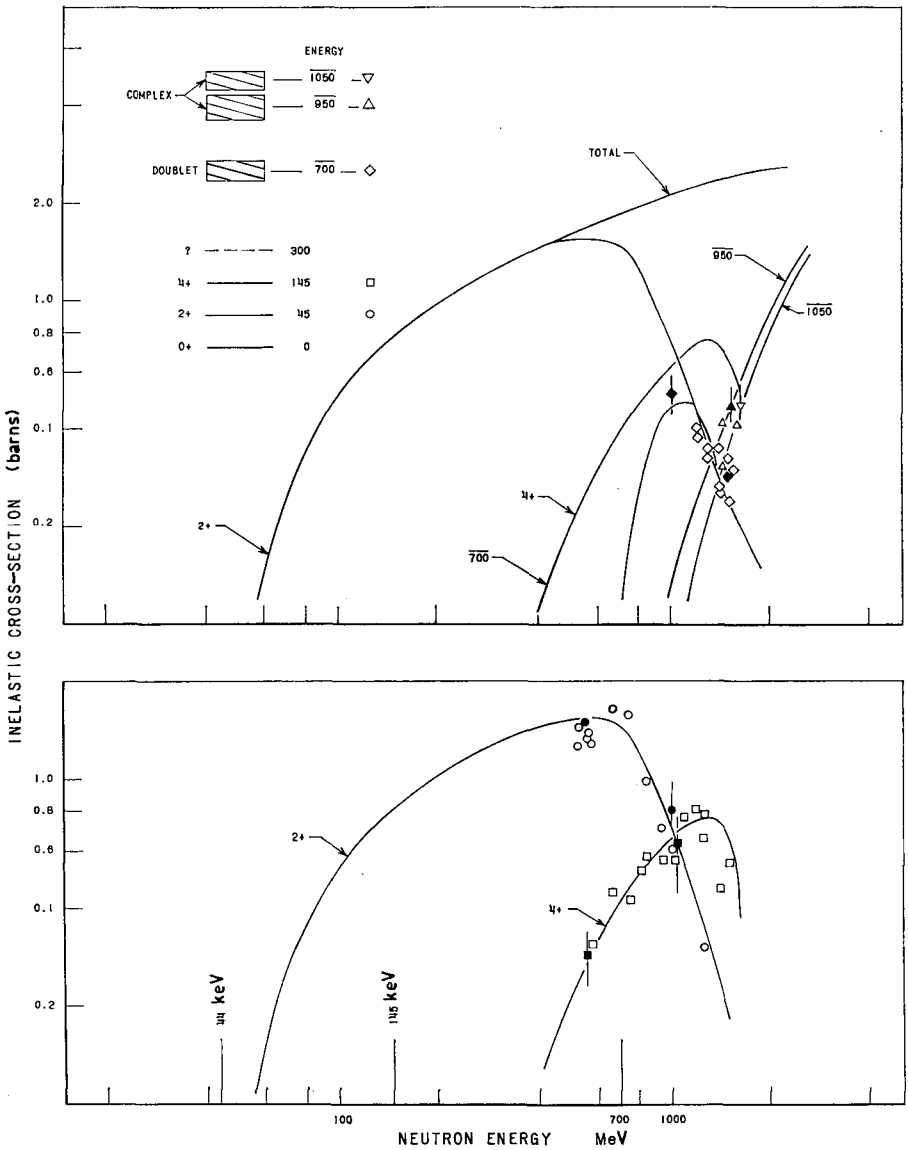


Fig. 4
The inelastic scattering cross-section for the excitation of specific nuclear levels in $U^{238}$. Solid points pertain to Ref. 42, open points to Ref. 13.

structure of thorium that contributes appreciably to the inelastic scattering of neutrons whose incident energy is below 1.6 MeV. From Coulomb excitation measurements other structure is known to be present, but scattering to any one of these additional levels at no time contributes more than 0.1 b to the total inelastic cross-section [4, 33]. The first, $2+$, level at 50 keV is the major factor in the scattering of the lower-energy incident neutrons. The angular distribution of inelastically scattered neutrons resulting in the excitation of this level is not isotopic but is symmetric about 90°. The cross-sections for inelastic scattering resulting in the excitation of nuclear levels at 50, 170, $\overline{800}$, and $\overline{1100}$ keV are given in Fig. 3. As shown in the level structure diagram, the "level" at $\overline{800}$ keV is actually composed of three components while the "level" at $\overline{1100}$ keV is at least a doublet. The solid curves in the figure representing the two lower-level excitation functions result from a fit of a Hauser-Feshbach type calculation to the experimental points [11, 12]. The curves representing the higher levels are of an empirical nature.

The results of studies of inelastic scattering from $U^{238}$ are summarized in Fig. 4 [42, 12, 13]. As in the case of thorium, the complex higher-energy-level structure has been combined so as to establish "average" levels at $\overline{700}$, $\overline{950}$, and $\overline{1050}$ keV. The two lowest levels follow the characteristic pattern of even-even nuclei in this region [4, 38]. The solid curves in Fig. 4 representing the excitation of the two lower levels are theoretical fits to the data [12, 13, 14]. The excitation of the higher energy levels is not well understood theoretically. As a result, the curves representing the excitation of the composite levels at $\overline{700}$, $\overline{950}$, and $\overline{1050}$ keV are empirical. The contribution to inelastic scattering of other known levels in $U^{238}$ is negligible. It should be noted that Fig. 4 shows the results of measurements by two independent workers. The agreement is good.

At incident neutron energies above 1.6 MeV, the combination of degenerating instrument resolution and the rapidly increasing density of the nuclear structure makes definitive measurements very difficult. Above several MeV, theorectical and experimental results based upon a statistical nuclear temperature can be used reliably [15, 16]. The intervening region is now, and will be, very difficult to reach with any degree of precision. Currently, there are few if any reliable scattering measurements below $\sim$300 keV. However, the techniques (see above) hold promise of considerable productivity in this lower-energy region. While theoretical calculations appear to be reasonably successful in explaining the inelastic scattering to low-lying nuclear levels, it is not evident that theory can quantitatively interpret inelastic scattering resulting in the excitation of the higher energy levels [14].

### Scattering from fissile nuclei

The even-odd fissile nuclei $U^{233}$, $U^{235}$, $Pu^{239}$, and $Pu^{241}$ have a complex nuclear structure comprised of a relatively high density of low-lying nuclear levels [39]. Some of these materials are very alpha-active, and all of them have fission cross-sections amounting to $\sim$20% of the total cross-section. These characteristics combine to make the experimental study of fast-neutron scattering from the fissile isotopes among the most difficult of fast-neutron problems.

Macroscopic methods, biased recoil detectors, and time-of-flight techniques have been employed to estimate the elastic and inelastic scattering cross-sections of $U^{235}$ and $Pu^{239}$ [40, 17]. Results of elastic scattering measurements obtained

at an incident neutron energy of 0.55 MeV are shown in Fig. 5 [17]. These particular distributions contain inelastically scattered neutrons whose energies are within approximately 90 keV of the incident beam energy. For comparison the angular distribution resulting from the scattering from $U^{238}$ under identical conditions is included in the figure. The similarity between the curves is not indicative of the results obtained at other incident energies.

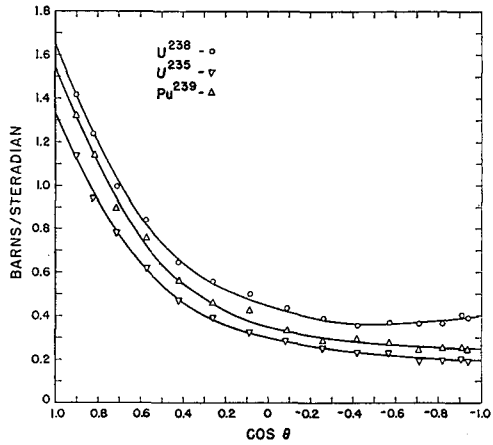


Fig. 5
The differential elastic scattering cross-section of $U^{235}$, $U^{238}$, and $Pu^{239}$ at 0.55 MeV including all neutrons within 90 KeV of the incident energy.

The results of time-of-flight determinations of the inelastic scattering of fast neutrons from $U^{235}$ and $Pu^{239}$ are summarized in Table I [17]. At incident energies of 0.55, 0.98, and 2.0 MeV, the cross-sections for the scattering of neutrons with various incremental energy losses are given. Within each energy increment

TABLE I

**NEUTRON SCATTERING FROM $U^{235}$ AND $Pu^{239}$ [18]**
**(barns)**

| | | | | | |
|---|---|---|---|---|---|
| $E_n = 550 \pm 10$ keV | | *Q = 300—200 keV* | *Q = 200—90 keV* | *Q = 90—0 keV* | |
| | $U^{235}$ | $0.20 \pm 0.05$ | $0.25 \pm 0.05$ | $5.40 \pm 0.2$ | |
| | $Pu^{239}$ | $0.10 \pm 0.05$ | $0.13 \pm 0.05$ | $6.45 \pm 0.2$ | |
| $E_n = 980 \pm 44$ keV | | *Q = 750—500 keV* | *Q = 500—150 keV* | *Q = 150—0 keV* | |
| | $U^{235}$ | $0.31 \pm 0.06$ | $0.35 \pm 0.06$ | $4.70 \pm 0.2$ | |
| | $Pu^{239}$ | $<0.06$ | $0.16 \pm 0.06$ | $5.06 \pm 0.2$ | |
| $E_n = 2000 \pm 30$ keV | | *Q = 1750—1500 keV* | *Q = 1500—1000 keV* | *Q = 1000—500 keV* | *Q = 500—0 keV* |
| | $U^{235}$ | $0.42 \pm 0.1$ | $0.67 \pm 0.15$ | $0.27 \pm 0.05$ | $4.14 \pm 0.2$ |
| | $Pu^{239}$ | $0.24 \pm 0.08$ | $0.24 \pm 0.08$ | $0.19 \pm 0.05$ | $4.19 \pm 0.2$ |

the processes leading to the energy degradation of the neutron are believed to be complex.

Work now in progress should result in a much better understanding of scattering from $U^{235}$. However, it is not justifiable to assume that a complete knowledge of scattering from all fissile isotopes will soon be available. The reactor theorist will have to rely on integral experiments, nuclear theory, and the extrapolation of good measurements of the scattering from one fissile isotope, $U^{235}$, for an understanding of scattering in the fissile region.

## Scattering from structural materials

### *Heavy materials*

The metallurgical properties of heavy elements, particularly at elevated temperatures, make them very useful in many reactor applications. A typical example of such a metal is tungsten. This nucleus is the only one of this type whose elastic and inelastic scattering properties have been measured in detail [18]. As a result, it is informative to examine its scattering properties not only with the objective of utilizing it in reactor applications but also with the intention of understanding, experimentally and theoretically, the behaviour of a typical heavy structural material.

Using the fast-timing techniques described above, the angular distribution of elastically scattered neutrons has been measured [18]. The results are presented in Fig. 6. The excitation functions for inelastic scattering resulting in the excitation of residual nuclear levels at 120, 350, 630, 730, 930, 1030, and 1130 keV are given in Fig. 7. The combined elastic and inelastic scattering cross-sections are in good agreement with the known total scattering cross-section [30]. Utilizing the results of this experiment, evidence from Coulomb excitation studies and the known systematics of even-even nuclei, the spin and parity assignments shown in the figure are postulated. The illustrated errors on the actual data points include the uncertainties relative to this particular measurement and the absolute error in the elastic scattering cross-section of carbon which was used as the standard. The first group of inelastically scattered neutrons was found to be isotropically distributed (see Fig. 6). This is what one would expect from the predominantly s- & d-wave contribution to the scattering to this level. The solid curves in Fig. 7 are based upon calculations of the Hauser-Feshback type [11], including the effect of neutron width fluctuations [19]. The optical model phase shifts of Campbell, Feshback, Porter, and Wiesskopf were employed to calculate the neutron strength functions [20]. The spin-orbit force was taken into account by adjusting the radius of the Saxon-Woods potential [21]. In addition, the strength functions were varied to account for the known strong deformation of this nucleus. It is evident from Fig. 7 that this adjustment of the strength functions is necessary in order to obtain reasonable theoretical agreement with the experimental results, particularly in the lower, better defined, levels. The higher-level agreement between theory and experiment is reasonable in view of the uncertainties in the spins and parities.

For this heavy nucleus, modern experimental techniques have given a good measurement of inelastic scattering, its magnitude, its angular distribution, and its associated neutron energy loss. In addition, the experimental results serve as a good qualitative measure of the theoretical knowledge of inelastic

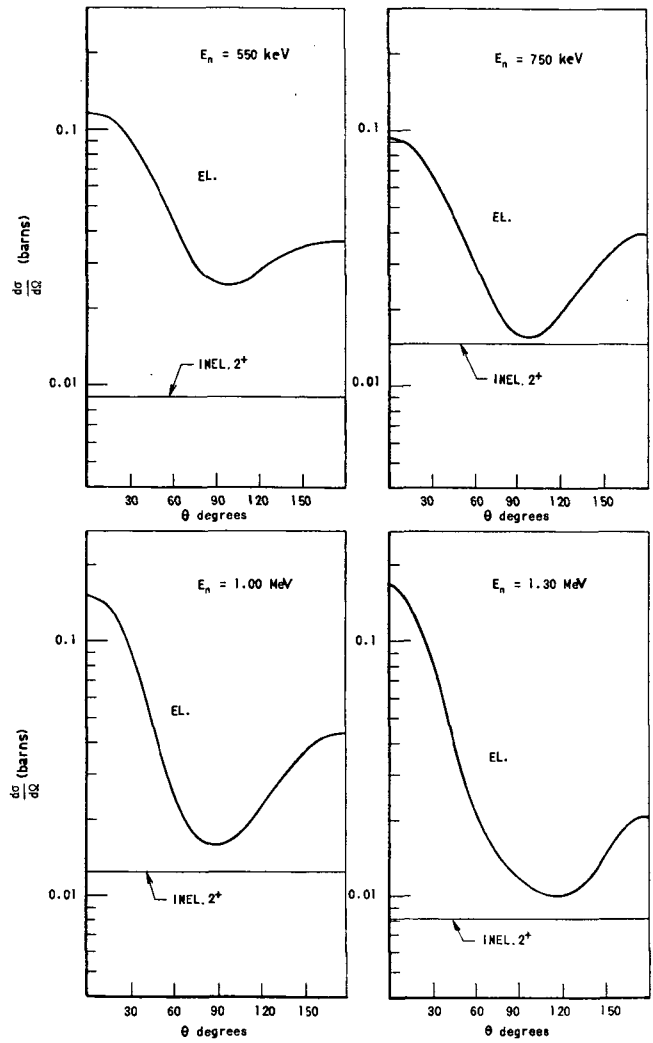


Fig. 6
The angular distribution of elastically scattered neutrons from tungsten and the distribution of inelastically scattered neutrons resulting in the excitation of the first residual nuclear level.

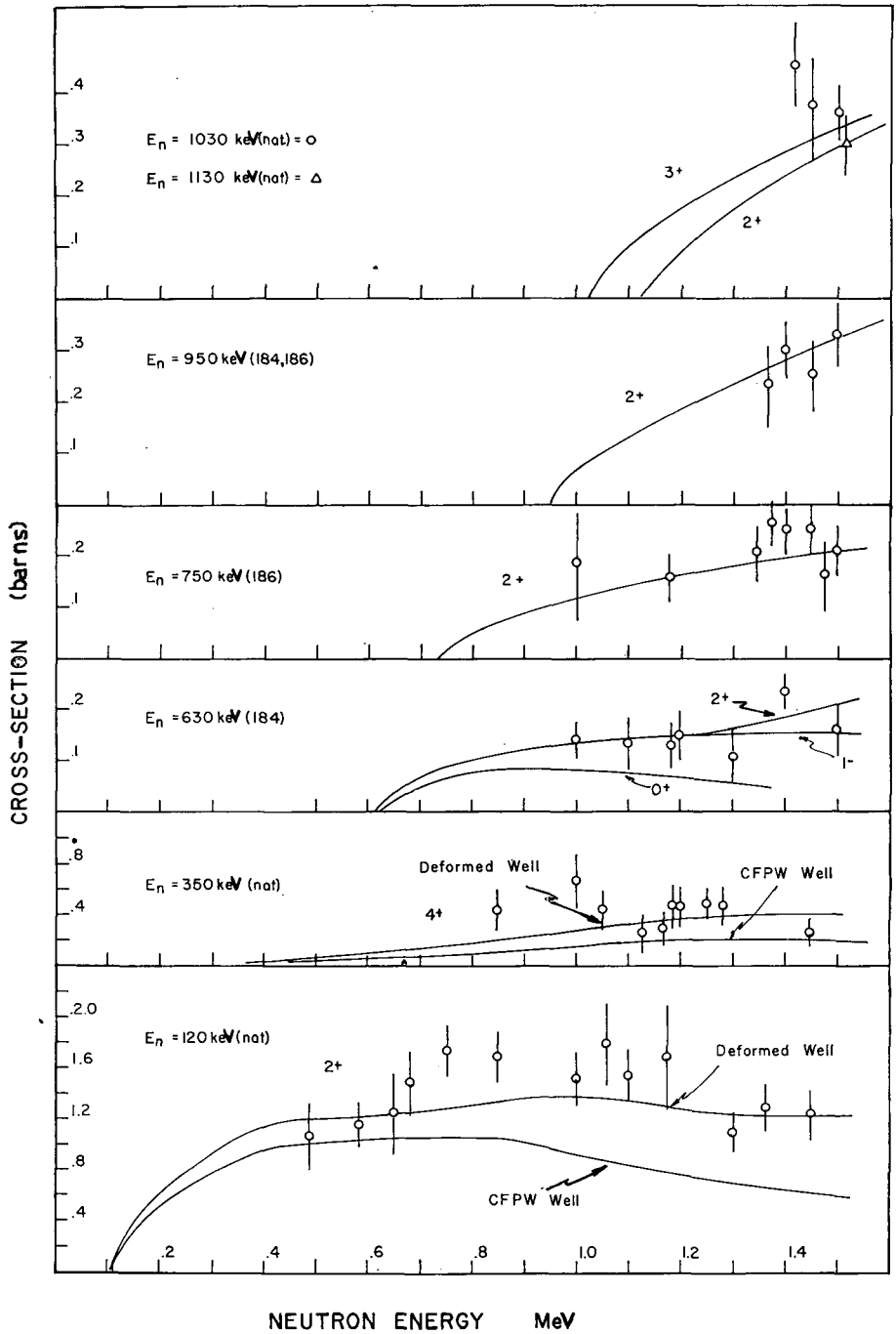


Fig. 7
The excitation functions for inelastic neutron scattering from tungsten as a function of incident neutron energy.

scattering from heavy materials. It is evident that the theoretical understanding is inadequate to predict inelastic scattering from heavy structural materials with an appreciable degree of quantitative precision.

*Light and intermediate materials*

The scattering of fast neutrons from medium- and light-weight structural materials and coolants displays a widely varying behaviour due to the differing types of nuclear structure involved. As a result, the experimental problems are often quite different and have been successfully treated in a number of ways. In the absence of low-lying nuclear levels, flat detection systems have proven very successful [1]. Where nuclear levels and associated inelastically scattered neutron groups are widely spaced, the biased counter and threshold detector have been employed to determine the cross-sections for elastic and inelastic scattering [22, 23]. In cases involving nuclei with low-lying levels separated by a few hundred kilo-electron-volts or less, most successful scattering measurements have utilized fast-time-of-flight techniques.

Fig. 8 shows the angular distribution of neutrons elastically scattered from $O^{16}$ [24, 25, 26]. These distributions are characteristic of those obtained throughout the region of light nuclei. The total cross-section displays a broad and widely spaced resonance structure that can be carefully measured with existing techniques [30]. Thus the reactor theorist has available to him the basic data necessary for the determination of the effect on reactive systems of resonance structure in light nuclei. A contrasting situation exists in the region of $A \sim 100$, where the structure of the nucleus is far too complex to be resolved with present techniques and where the theoretical understanding must be based upon average nuclear properties [19]. Typical examples of elastic scattering in this region are the angular distributions of niobium and zirconium given in Fig. 9. Both of these nuclei have essentially the same total scattering cross-section, but inelastic scattering resulting in the excitation of the greater density of residual nuclear levels in niobium leads to a larger inelastic cross-section for this element [27]. Scattering to a pair of levels at $\sim 800$ keV in niobium accounts for a 0.45-b inelastic cross-section, an inelastic component equal to the entire non-elastic cross-section of Zr at the same incident energy.

For comparison, Fig. 9 also shows the elastic distribution from iron. This lighter nucleus, $A = 56$, demonstrates a qualitatively different distribution from that of niobium and zirconium in accord with the predictions of optical model [28]. In Fig. 10, the angular distributions of elastically scattered neutrons from iron are given for a rather wide range of incident neutron energies [27]. All of these measurements employ energy resolutions of $\sim 15$ keV. In nuclei with $A \sim 100$, such as zirconium and niobium, this energy spread is more than sufficient to average over the details of the nuclear structure. In the case of iron this is not true. The total cross-section and the inelastic cross-section display structure within energy intervals somewhat exceeding available instrumental resolutions [30, 27]. The complexity of this structure makes theoretical interpretation difficult. The energy intervals involved are such as to make detailed experimental measurements very formidable. Thus the theoretical reactor physicist employing multi-group cross-sections in the region $A \sim 50$ would do well to consider the merit of decreasing the group energy interval beyond the point where the available microscopic parameters can be meaningfully represented by averages over many resonances.

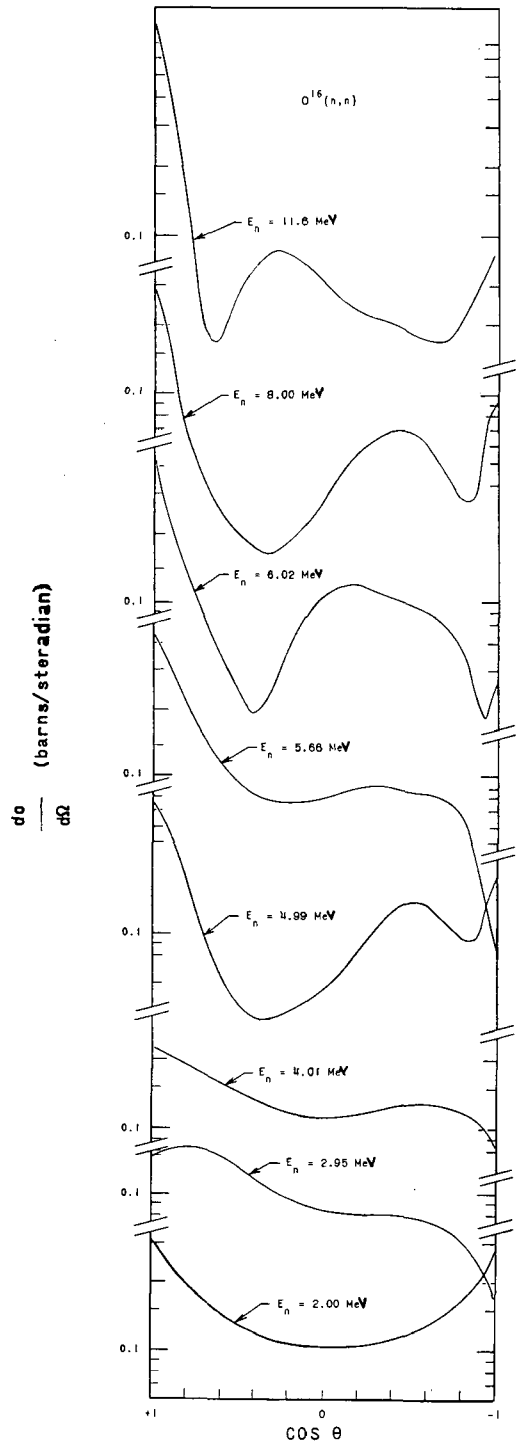


Fig. 8
The angular distribution of neutrons elastically scattered from $O^{16}$. The scattering angle is in the centre of mass system [24, 25].

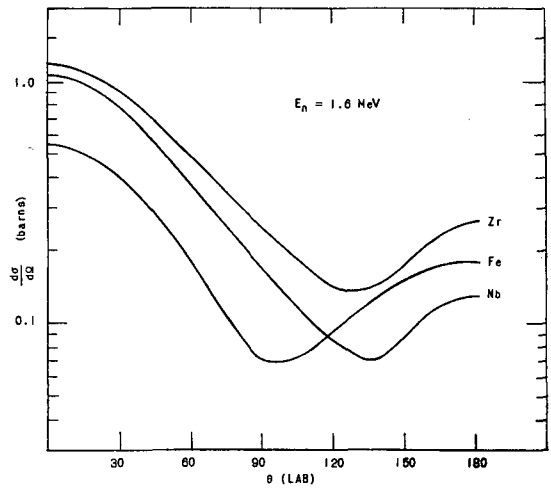


Fig. 9
The angular distribution of neutrons elastically scattered from Fe, Zr, and Nb at a 1.6-MeV incident neutron energy. Time-of-flight techniques were employed to remove the inelastically scattered components [13].

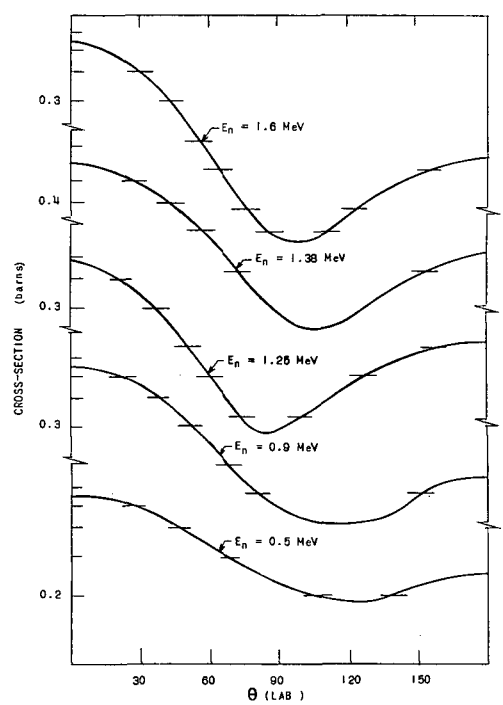


Fig. 10
The angular distribution of neutrons elastically scattered from Fe as a function of incident neutron energy [27].

## Fast neutron capture

### Experimental methods

The experimental determination of fast-neutron capture cross-sections requires a relative measurement of energy dependence and an absolute normalization. These two problems are not always dealt with simultaneously.

Many measurements are actually determinations of the cross-section for the production of a given active isotope through neutron capture. Indeed, the classic work of Fermi and co-workers was of this type [29]. Where it is applicable, the method is amenable to a high degree of precision, particularly in those cases where the characteristics of the decaying product are such as to permit an absolute determination of the activity through beta-gamma coincident counting. In less favorable cases, the normalization must rely upon the absolute standardization of a detector system or must be referenced to a standard source.

A method that does not require an active product and which uniquely avoids the problems of standardization is the spherical-transmission technique. This method has been employed for the standardization of key capture cross-sections used as the basis of much wider work [31]. Unfortunately, the method requires rather lengthy and complex multiple-interaction corrections.

Recent work at the Los Alamos Scientific Laboratory has resulted in the development of large liquid scintillators having gamma-ray detection efficiencies of as high as $\sim 95\%$. An example of this detector as utilized in capture measurements is shown in Fig. 11 [8]. A small capturing sample is placed near the centre

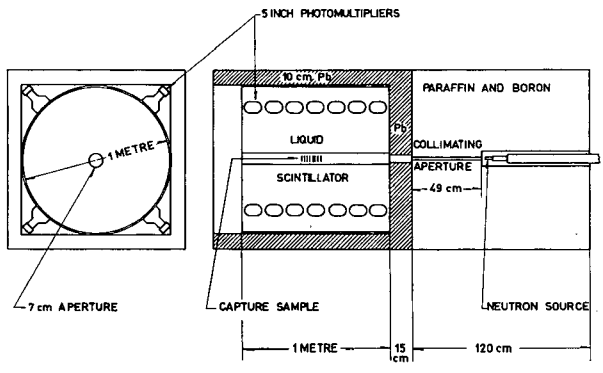


Fig. 11
A schematic diagram of a large liquid scintillator used in capture and alpha measurements [8].

of the large liquid scintillator. Some of the monoenergetic neutrons produced in a burst at a nearby target proceed down a collimated tube and strike the sample. Any resulting neutron capture is immediately followed by the release of about 6 MeV of prompt gamma radiation, nearly all of which is converted into a massive light pulse within the large liquid scintillator. The time correspondence between the production of the neutron burst and the observation of the light pulse resulting from capture permits an accurate determination of the time independent background. In studying fissile samples, the scintillator is loaded with material having a large thermal capture cross-section. Fission

events occurring within the sample are experimentally evident from the prompt fission gamma-ray pulse coincident with the incident neutron burst, followed later by one or more pulses due to the fission neutrons which have been moderated and captured within the scintillator liquid. The neutron-detection efficiency is very high, thus the device is a powerful tool for studies of $\bar{\nu}$ as well as for capture measurements (see below). Using a fissile sample, the detector can simultaneously measure the capture and fission rates and thus directly determine the ratio of the capture to the fission cross-section $\equiv \alpha$ of fissile materials. Although descriptively the device may appear complex, it is a very powerful tool and is being utilized at a number of laboratories throughout the world [10, 34, 52].

## Capture in fissile materials

Employing the unique capabilities of the liquid scintillator described above, Diven *et al.* have made precise measurements of alpha for $U^{233}$, $U^{235}$, and

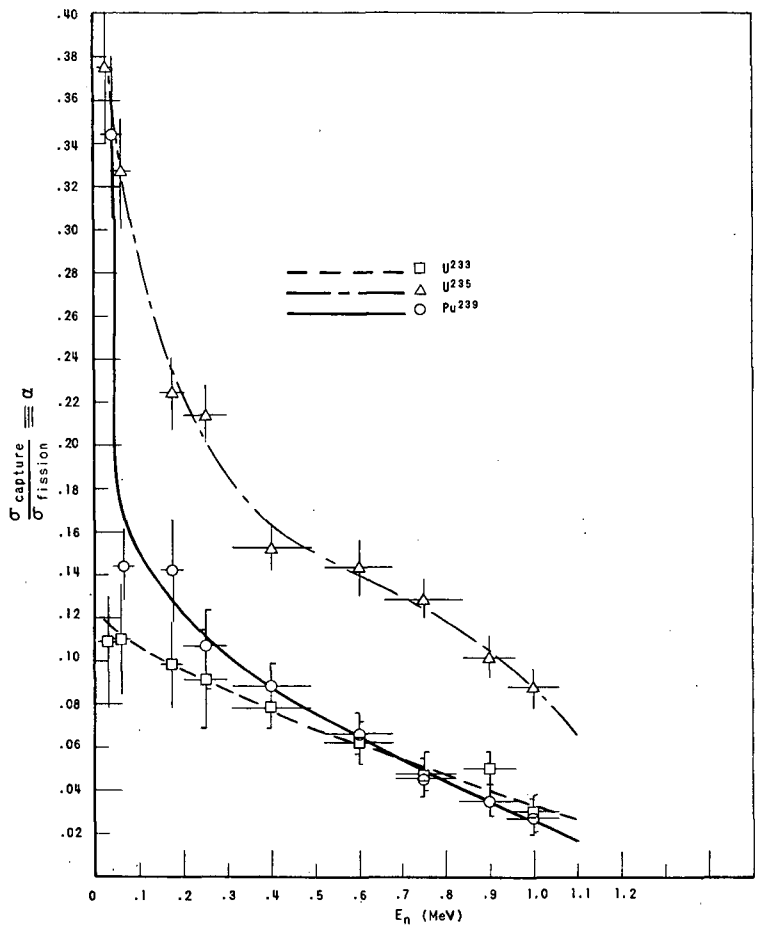


Fig. 12
$\alpha$ as a function of incident neutron energy for $U^{233}$, $U^{235}$ and $Pu^{239}$ [35].

$Pu^{239}$ [35]. These are shown in Fig. 12, where $\alpha$ is given as a function of incident neutron energy. The results can be combined with the measured fission cross-sections (see below) to obtain the respective capture cross-sections. The values are in good agreement with estimates based upon macroscopic measurements [12]. An example of activation techniques employed in the fission region is the measurement of the capture cross-section of $U^{236}$ shown in Fig. 13 [36]. Studies of this

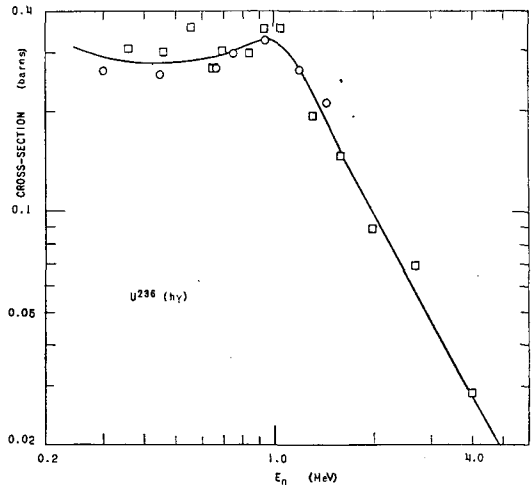


*Fig. 13*
The capture cross-section of $U^{236}$ as a function of incident neutron energy.

type are difficult, due to the inherently high natural activity of the samples and their daughters. Often a major problem associated with the measurements is the proper preparation of the sample so as to suppress this source of high background.

## Capture in non-fissile materials

Utilizing a large liquid scintillator, the capture properties of a wide range of materials have been studied up to an incident neutron energy of 1.0 MeV [8]. A somewhat different application of a liquid scintillator has been used by Gibbons *et al.* [10] to measure capture cross-sections in the incident neutron region $\sim$10–300 keV. These measurements are standardized against selected materials, whose capture cross-sections have been carefully determined with sphere-transmission measurements [31]. Many workers have carried out relative and absolute fast-capture measurements utilizing the activation approach [37, 5–7]. With this profusion of overlapping experimental work, fast-neutron capture cross-sections should be well known. Unfortunately, this is not the case, as is illustrated in Fig. 14, which summarizes a portion of the studies of capture in gold. The absolute normalizations are often inconsistent to better than $>25\%$, particularly in the region $\sim$100 keV. Even the relative shapes of the measured cross-sections are not consistent in the lower-energy region. While not all materials are as poorly known as gold, this example is fairly typical of the current status of experimental knowledge of fast-neutron capture.

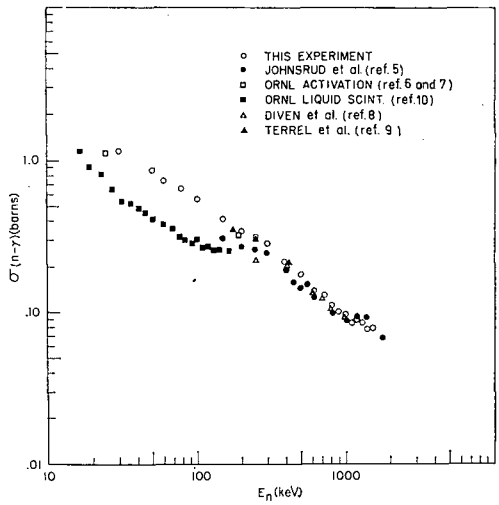


Fig. 14
A comparison of the fast-neutron capture cross-section of gold as determined by various techniques.

Theoretical understanding of fast-neutron capture is based upon a knowledge of average nuclear resonance structure. Qualitative theoretical interpretation leads to reasonable agreement with experiment in the 100-keV region, where incident neutron p-wave effects are pronounced. More detailed theoretical understanding of capture processes requires a knowledge of the average fluctuations and characteristics of neutron-level spacings, and must be a part of a unified theory of compound nuclear reactions [41]. Unfortunately, experimental evidence, as outlined in this paper, is too fragmentary to form a foundation upon which to construct a complete understanding of fast-neutron reactions.

## Fast-neutron-induced fission

### Fast-fission cross-sections

Requisite to the absolute measurement of the fast-fission cross-section is the determination of the incident neutron flux. The well-known n-p cross-section is usually used for this purpose. Employing this approach, accuracies of 3–5% have been obtained over the incident neutron energy range 500–1000 keV. It is noteworthy that such precisions exceed those obtainable in measurements of the thermal-fission cross-section of $U^{235}$. Utilizing the absolutely measured $U^{235}$ fast-fission cross-section as a secondary flux standard, the fast-fission cross-sections of other nuclei have been determined to a relative accuracy of $\sim 1\%$. Many of the transuranium isotopes are very highly alpha-active. The recent development of gaseous scintillation and solid-state detection devices with extremely short response times has made it possible to study the fission cross-sections of these materials with a precision not obtainable with previous techniques [43].

It is qualitatively evident from fission theory that the even-odd isotopes are most unstable to fission, possessing negative energy fission thresholds of

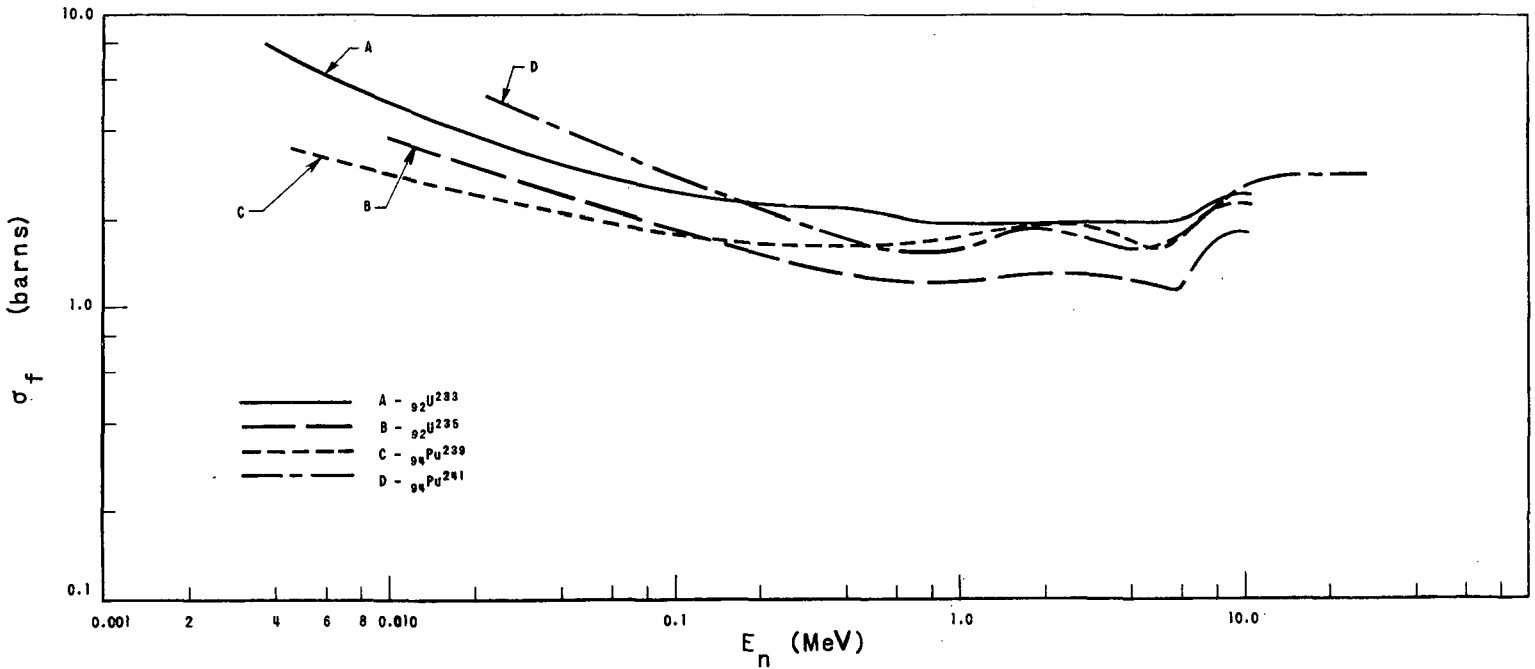


Fig. 15a
The fast-fission cross-sections of the even-odd nuclei $U^{233}$, $U^{235}$, $Pu^{239}$, and $Pu^{241}$ [30, 45, 46, 47, 48].

some number of MeV [44, 45]. Fig. 15a graphically summarizes the fast-fission cross-sections of even-odd nuclei most useful in reactor design. The line representation results from a subjective fit to the experimental data taking into account the method of standardization, experimental techniques employed, and the errors assigned to the individual measurements [30, 46, 47, 48, 45].

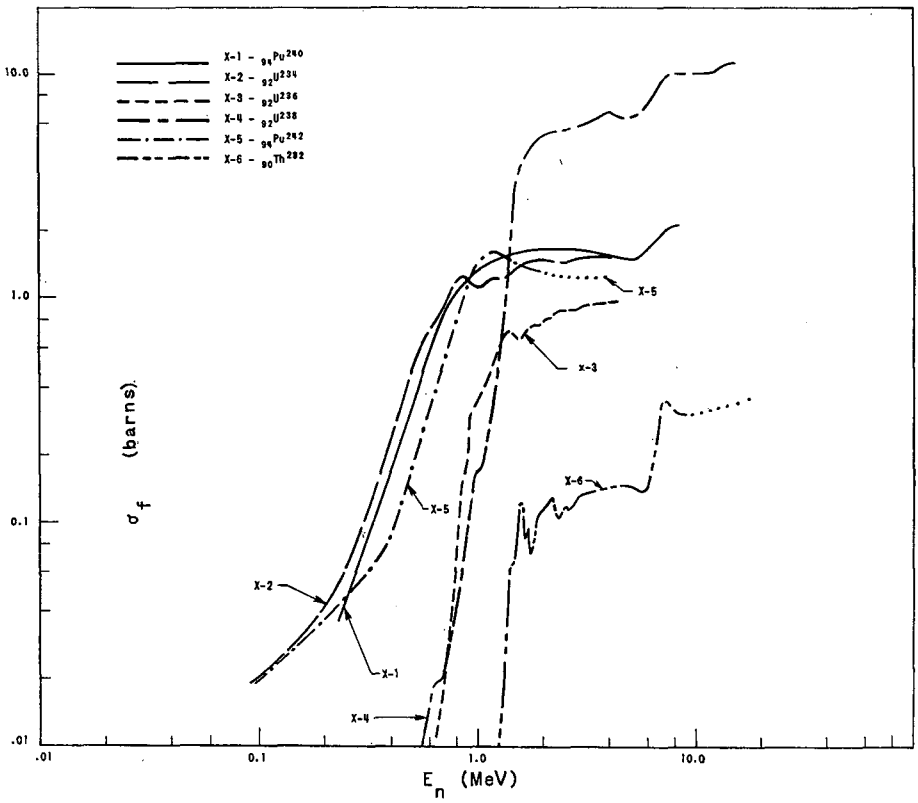


Fig. 15b
The fast-fission cross-sections of the even-even nuclei $Th^{232}$, $U^{234}$, $U^{238}$, $Pu^{240}$, and $Pu^{242}$ [30, 45, 48, 49].

The fast-fission cross-sections of even-even nuclei are summarized in Fig. 15b [45, 48, 49]. These processes are, characteristically, threshold reactions. Their fission cross-sections exhibit varying degrees of detailed structure. The plateau-like behaviour is qualitatively explained by theory, but the detailed structure stems from not well-understood characteristics of the particular nuclei [44]. A similar threshold behaviour is evident in the odd-even fissile nuclei shown in Fig. 15c [45, 47]. Notably absent from the figures are odd-odd nuclei. The beta decay half-lives of these isotopes are generally too short to permit an experimental measurement of their fission cross-sections. Fortunately, the short half-lives also result in only small concentrations in reactive systems.

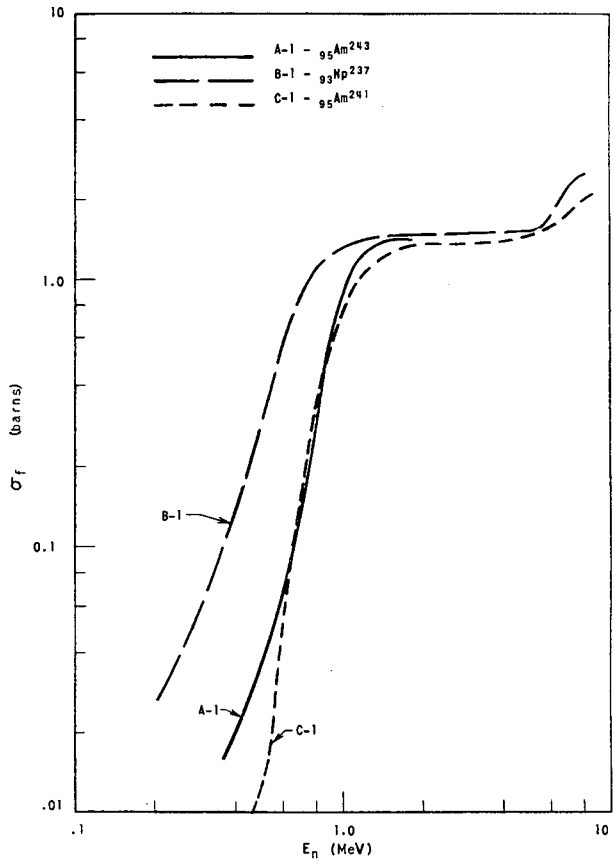


Fig. 15c
The fast-fission cross-sections of the odd-even nuclei $Np^{237}$, $Am^{241}$, and $Am^{243}$ [30, 43, 45].

Future work in the measurement of fast-fission cross-sections will be devoted largely to the transuranium region. Most of the measurements will utilize the $U^{235}$ fission cross-section as a standard. The need for increased accuracy in measurements of the $U^{235}$ fission cross-section from 1 to 100 keV is not evident from Fig. 15a, due to the omission of the actual data points. The uncertainty throughout this region may be as large as $\sim 20\%$. As fast-breeding systems grow larger and are characterized by softer spectra, this energy region assumes increasing importance. As a result, it is expected that the precision of the $U^{235}$ fission cross-section below 100 keV will soon be improved by a factor of 3–5.

## Fission-neutron emission

Fission neutrons are defined as all neutrons emitted at or following the fission. Of these $\sim 99\%$ are emitted within an immeasurably short time of the actual scission. The absolute average number of neutrons emitted per fission, $\bar{\nu}$, and the dependence of $\bar{\nu}$ on incident neutron energy are of fundamental importance

in reactor design. Experimental measurements of these quantities utilize large neutron-detection systems of high and known sensitivity or relatively small devices, the response of which is usually calibrated relative to a "standard" $\bar{\nu}$ value. Outstanding examples of the large detection systems are the carbon pile and large liquid scintillator [50, 34]. Such large detectors can provide fission-neutron-detection efficiencies as high as 95% or more, and have determined $\bar{\nu}$ with an accuracy of $\sim 1\%$. The smaller devices utilize a limited neutron-detection volume and are not amenable to absolute determinations, due to the inherent uncertainty in their sensitivity [51]. However, they are simple, easy to use experimentally, and capable of relative $\bar{\nu}$ measurements to a precision of $\sim 1\%$.

Existing experimental knowledge of neutron emission from fissile isotopes of applied interest is summarized in Figs. 16 and 17. In Fig. 16, $\bar{\nu}$ is expressed in the linear form $\bar{\nu} = \bar{\nu}(t) + (d\bar{\nu}/dE)\,E_n$ (incident neutron energy in MeV) for the neutron-induced fission of ${}_{90}Th^{232}$, ${}_{92}U^{233}$, ${}_{92}U^{238}$, ${}_{94}Pu^{239}$, ${}_{94}Pu^{240}$ and ${}_{94}Pu^{241}$. The experimental points shown largely refer to measurements made with essentially monoenergetic neutrons. The parameters pertaining to each isotope are the result of an objective least square fit of the linear $\bar{\nu}$ relation to the experimental data. Where applicable, spontaneous fission $\bar{\nu}$ values associated with the actual fissioning nucleus are utilized to provide $\bar{\nu}$ values at effective negative incident neutron energies. The measured $\bar{\nu}$ values for $U^{233}$ and $Pu^{239}$ are in reasonable agreement with the linear $\bar{\nu}$ relation shown, but are not precise enough to provide a detailed knowledge of the variation of $\bar{\nu}$ with incident neutron energy. As is evident from Fig. 16, $\bar{\nu}$ for $Th^{232}$ is not well known, but the experiments indicate that it is anomalously low. Recent measurements at incident neutron energies of 1.58, 3.5, and 15.0 MeV have resulted in a much better understanding of $\bar{\nu}$ for $U^{238}$ [51, 52]. The remaining distributions given in Fig. 16 are based upon fragmentary experimental evidence. They emphasize the need for much further work, particularly in the transuranium region.

Fig. 17 summarizes, in detail, the published knowledge of $\bar{\nu}$ for $U^{235}$. The incident neutron energies are separated into two ranges. The first energy interval extends from thermal to 1.5 MeV. Recent precision measurements in this region lead to $\bar{\nu}(U^{235}) = 2.43 + 0.115\,E_n$. In the second energy interval, extending from 1.5 to 15 MeV, $\bar{\nu}(U^{235}) = 2.406 + 0.138\,E_n$. The $\bar{\nu}$ in the upper energy interval is adjusted so as to correspond to the value of $\bar{\nu}$ at 1.5 MeV obtained from the fit over the lower-energy range. From the above it is evident that $\bar{\nu}$ for $U^{235}$ is not simply linearly dependent on incident neutron energy. Rather the initial rise of $\bar{\nu}$ for $U^{235}$ with incident neutron energy is somewhat less than the average slope over the entire interval thermal to 15.0 MeV. This conclusion is, to a certain extent, verified by the analysis of fast critical experiments.

In addition to the outstanding need for greatly increased accuracy in $\bar{\nu}$ measurements pertaining to fissile isotopes of applied usefulness, it should be emphasized that a standard $\bar{\nu}$ value that can be referred to throughout the world is of fundamental importance. For such a standard application, $\bar{\nu}$ resulting from the spontaneous fission of $Cf^{252}$ is unexcelled. Efforts to determine this quantity with the very highest precision are now under way at several laboratories.

---

Fig. 16 — The average number of neutrons emitted per neutron-induced fission of $Th^{232}$, $U^{233}$, $Pu^{239}$, $Pu^{241}$ as a function of incident neutron energy [30, 34, 50, 52, 53, 54, 55, 56, 57, 58, 59, 60, 61, 62, 63, 64, 65, 66, 67, 68].

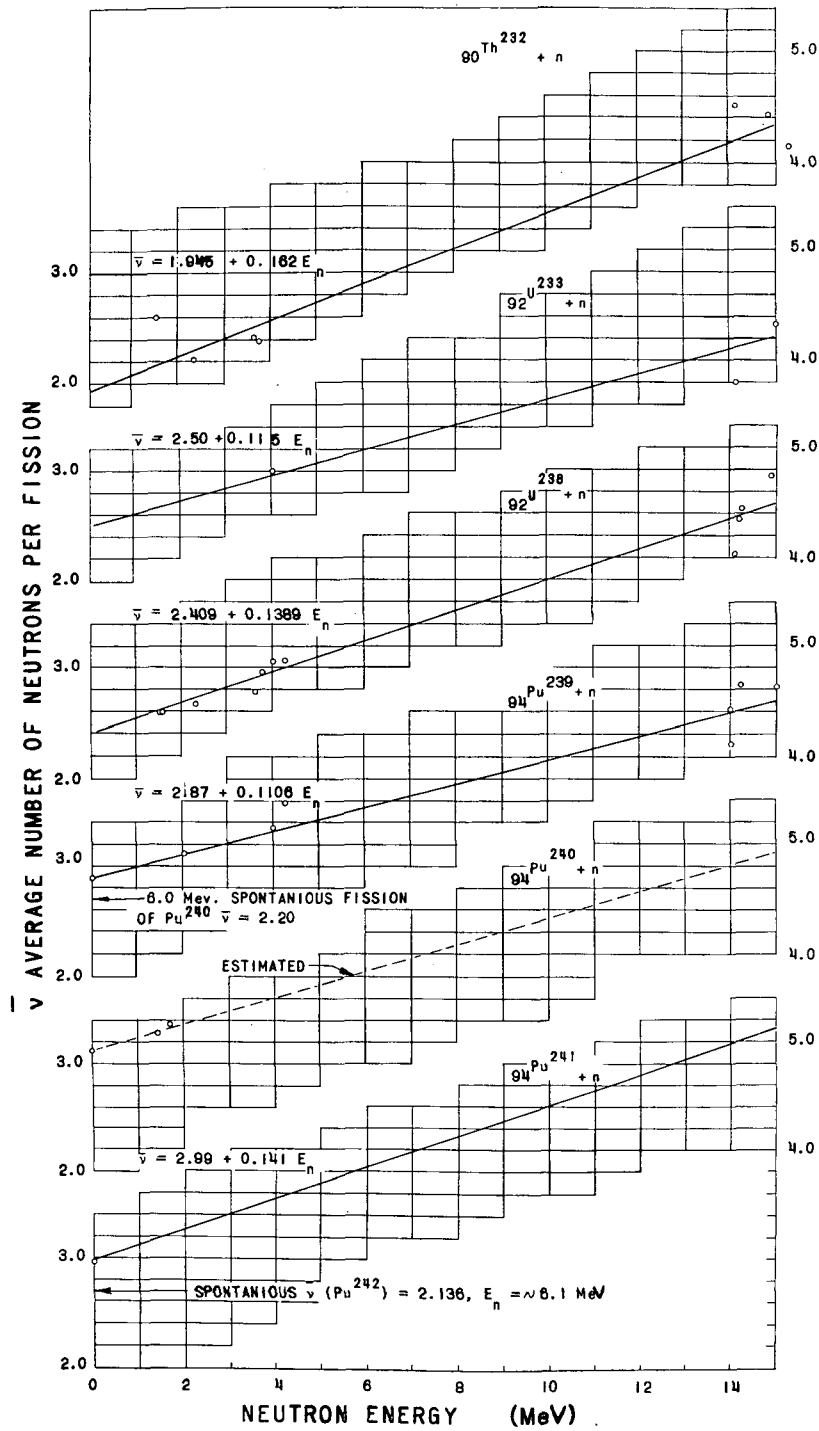
90Th232 + n
92U233 + n
92U238 + n
94Pu239 + n
94Pu240 + n
94Pu241 + n
v̄ = 1.945 + 0.162 En
v̄ = 2.50 + 0.115 En
v̄ = 2.409 + 0.1389 En
v̄ = 2.87 + 0.1108 En
6.0 Mev. SPONTANIOUS FISSION OF Pu240 v̄ = 2.20
ESTIMATED
v̄ = 2.99 + 0.141 En
SPONTANIOUS ν (Pu242) = 2.136, En = ~6.1 MeV
v̄ AVERAGE NUMBER OF NEUTRONS PER FISSION
NEUTRON ENERGY (MeV)
2.0
3.0
4.0
5.0
0
2
4
6
8
10
12
14

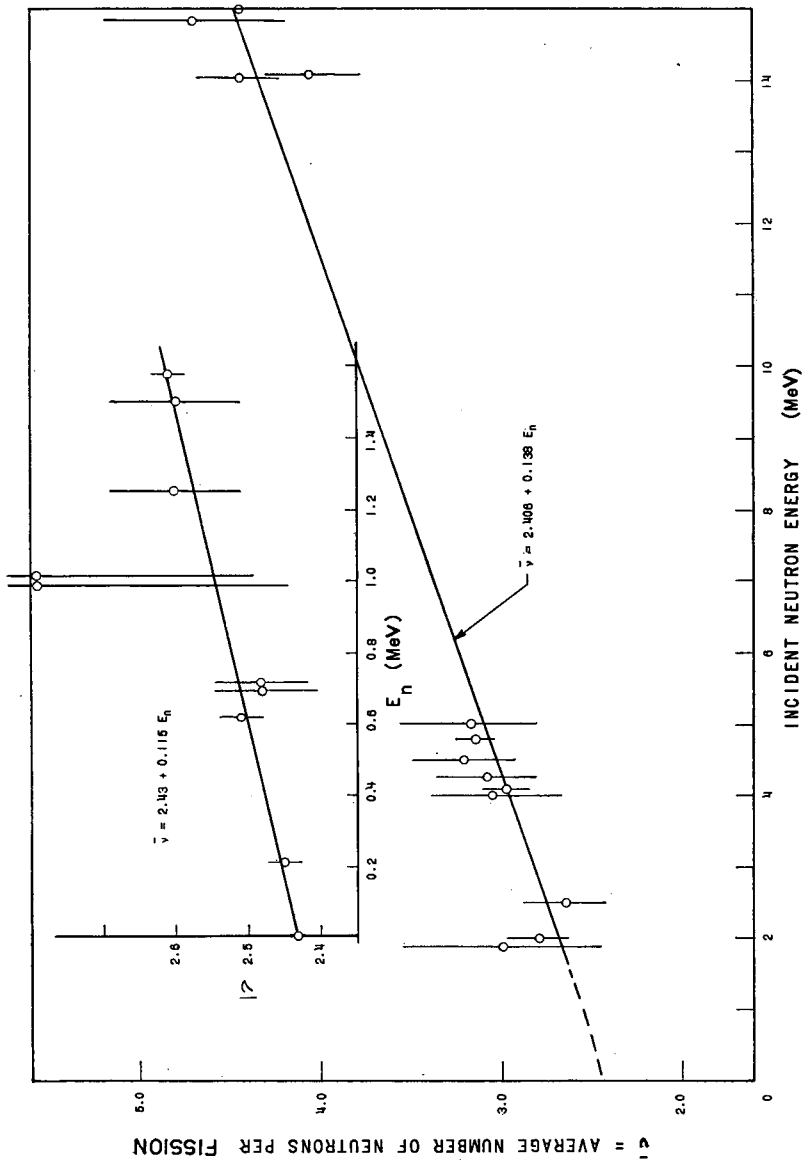


Fig. 17
The average number of neutrons emitted per $U^{235}$ fission as a function of incident neutron energy [30, 34, 50, 52, 53, 54, 58, 59, 60, 61, 62, 65, 69, 70, 71].

As a result of continuing refinement of existing techniques, it is probable that $\bar{\nu}$ thermal of $U^{235}$, $U^{233}$, and $Pu^{239}$ will soon be known to an absolute accuracy of $\sim$0.75%. Precision measurements of $d\bar{\nu}/dE$ similar to those shown in Fig. 17 will be extended to a wider energy range and to more fissile isotopes. As increasing quantities of the transuranium nuclei become available, knowledge of $\bar{\nu}$ for such important reactor-formed materials as $Pu^{241}$ will greatly improve. Unfortunately, the physical basis of fission-neutron emission is not well known.

As a consequence, fission theory can be expected to provide only qualitative guidance in establishing $\bar{\nu}$ values. Precise knowledge must come from individual experimental measurements and empirical relations derived thereof.

## Conclusion

Recent improvements in experimental techniques and methods employed in fast-neutron measurements have been described. Implicit in these advances has been the very considerable improvement in supporting equipment, particularly charged particle accelerators and electronic and electronuclear devices. Examples illustrating advances in fast-neutron scattering have been given. There is every indication that these studies of neutron scattering are only the initial portion of major progress in this field. From the discussion of capture processes it is evident that, while the basic information is steadily improving, an unfortunate number of experimental discrepancies persist. Knowledge of fission cross-sections and fission properties is consistently improving. Future work in these two associated fields will increasingly be devoted to the study of those transuranium isotopes found in appreciable quantities within high-burn-up breeding systems. Certainly the experimental physicist is providing the reactor theorist with basic nuclear data. If the theorist is to continue to obtain this requisite information and to properly plan for its future utilization, it is necessary that he fully comprehend the magnitude of the effort required on the part of the experimental worker. He must realize that even an appreciable improvement in the technological methods will only shift the region in which understanding changes from discrete to statistical and move back slightly the limit of knowledge. The experimental problems will still exist in associated areas and will usually be considerably more complex.

## REFERENCES

[1] ALLEN, W. D., Neutron Detection, New York Philosophical Library (1960).
[2] CRANBERG, L., UN Int. Conf. PUAE **4** (1955) 40.
[3] MARION, J. and FOWLER, J., Fast Neutron Physics, Part I, Interscience Publishers Inc., New York (1960).
[4] STEPHENS *et al.*, *Phys. Rev. Letters* **3** (1959) 435.
[5] JOHNSRUD *et al.*, *Phys. Rev.* **116** (1959) 927.
[6] MACKLIN, R. L. *et al.*, *Phys. Rev.* **107** (1957) 504.
[7] LYON, W. and MACKLIN, R. L. *Phys. Rev.* **114** (1959) 1619.
[8] DIVEN, B. C. *et al.*, *Phys. Rev.*, **20** (1960) 556—Also see these proceedings, vol. I, p. 149.
[9] TERRELL *et al.*, Proc. Conf. on Physics of Breeding, ANL-6122.
[10] GIBBONS, J. H. *et al.*, ORNL-2910.
[11] HAUSER, W. and FESHBACH, H., *Phys. Rev.* **87** (1952) 366.
[12] YIFTAH, OKRENT and MOLDAUER, Fast Reactor Cross Sections, Pergamon Press, New York, (1960).
[13] SMITH, A. B., Unpublished.
[14] MOLDAUER, P., Private communication.
[15] BLATT, J. and WIESSKOPF, V., Theoretical Nuclear Physics, John Wiley and Sons, New York (1952).
[16] CRANBERG, L. and LEVIN, J., *Phys. Rev.* **103** (1956) 343.
[17] CRANBERG, L., LA-2177 (1959).
[18] SMITH, A. and MOLDAUER, P., *Bull. Amer. phys. Soc.*, Ser. II, **5** (1960).
[19] MOLDAUER, P., "Theory of average neutron reaction cross-sections", to be published in *Phys. Rev.*
[20] CAMPBELL *et al.*, Some Optical Model Calculations, MIT report TID-5820.

[21] WOOD, R. and SAXON, D., *Phys. Rev.* **95** (1954) 577.
[22] ALLEN, R. C. *et al.*, *Phys. Rev.* **104** (1956) 731.
[23] WALT and BEYSTER, *Phys. Rev.* **98** (1955) 677.
[24] CHASE, L. *et al.*, Unpublished [1961].
[25] HUNZINGER and HUBER, *Helv. phys. Acta* **18** (1960) 570.
[26] LANGSDORF *et al.*, Neutron Scattering Angular Distributions, ANL-5567 (1956).
[27] SMITH, A. B., Unpublished [1961].
[28] BEYSTER *et al.*, *Phys. Rev.* **104** (1956) 1319.
[29] FERMI, E., The Collected Papers of Enrico Fermi, Vol. I, University of Chicago Press (1961).
[30] Neutron Cross-Sections, BNL-325.
[31] SCHMITT, H. and COOK, C., *Nucl. Phys.* **20** (1960) 202.
[32] BATCHELOR, R., *Proc. phys. Soc.* (*Lond.*) **A 69** (1956) 214.
[33] SMITH, A. B., *Bull. Amer. phys. Soc.*, Ser. II, **5**, (1960) 19.
[34] MOAT *et al.*, Private communication. Also see these proceedings, vol. **I**, p. 139.
[35] HOPKINS, J. and DIVEN, B., In press. Also see these proceedings, vol. **I**, p. 111.
[36] STUPEGIA *et al.*, To be published.
[37] COX, S. A., *Phys. Rev.* **122** (1961) 1281.
[38] KERMAN, A., Nuclear Reactions, North Holland Publishing Co., New York (1959).
[39] ALLEN, R. C., *Nucl. Sci. Engng* **2** (1957) 787.
[40] WALT, M. and BARSCHALL, H., TID-5157 (1953).
[41] MOLDAUER, P., *These proceedings*, vol. **I**, p. 171.
[42] CRANBERG, L., *Phys. Rev.* **109** (1958) 2063.
[43] BUTLER, D. K., "The fast-fission cross-section of $Am^{243}$", To be published.
[44] BOHR, N. and WHEELER, J., *Phys. Rev.* **561** (1939) 426.
[45] NORTHRUP *et al.*, *Phys. Rev.*, **115** (1959) 1277.
[46] SMITH, L. *et al.*, LASL WASH-1028 (1960) 34.
[47] BUTLER, D. K., "The fast-fission cross-section of $Pu^{241}$", To be published.
[48] BUTLER, D. K., *Phys. Rev.* **117** (1960) 1305.
[49] HENKEL, R. L. *et al.*, Progress in Nuclear Energy Series I, Physics & Mathematics, Vol. 2, Pergamon Press, New York (1958).
[50] DIVEN, B. C. *et al.*, *Phys. Rev.* **101** (1959) 1016.
[51] BUTLER, D. *et al.*, *These proceedings*, vol. **I**, p. 125.
[52] CONDI, H. and STARFELT, N., FDA-4, Rapport A 4190-411 (1961).
[53] KALASHNIKOVA *et al.*, Unpublished [1955]. This is Ref. 63 in Leachman, R. B., Proc. 2nd UN Int. Conf. PUAE **15** (1958) 229.
[54] TERRELL, S., *Phys. Rev.* **108** (1957) 783.
[55] SMITH, A. B. *et al.*, *Phys. Rev.*, **115** (1959) 1242.
[56] Average $Pu^{241}$, U.K., NSA, NSSR, AERE unpublished Report [1955]. Ref. 84 in Leachman, R. B., (see Ref. [53] above).
[57] JAFFEY, A., ANL-5396 (1955).
[58] KUZMINOV, B. D., Unpublished [1956]. Ref. 68 in Leachman, R. B. (see Ref. [53] above).
[59] JOHNSTONE, I., Unpublished AERE report. Ref. 75 in Leachman, R. B. (see Ref. [53] above).
[60] BETHE, H. *et al.*, Unpublished LASL report [1955]. Ref. 73 in Leachman, R. B. (see Ref. [53] above).
[61] GRAVES, E. R., Unpublished LASL report [1954]. Ref. 78 in Leachman, R. B. (see Ref. [53] above).
[62] FLOROV, N. and TAMANOV, E., *Atomn. Energ.* (In press).
[63] LEROY, J., C.E.N. Saclay, Compte Rendu.
[64] SMITH, A. B. *et al.*, "$Pu^{241}$ $\bar{\gamma}$ values", To be published in *Phys. Rev.*
[65] ANDREEV, V. N., Ref. 11 in Leachman, R. B. (see Ref. [53] above).
[66] DE SAUSSURE, G. and SILVER, E., ORNL-2081 (1956) 105.
[67] HICKS *et al.*, *Phys. Rev.* **101** (1956) 1016.
[68] FOWLER, S. L., ORNL Report (1956). Ref. 67 in Leachman, R. B., (see [53] above).
[69] SMIRENKIN *et al.*, *Atomn. Energ.* **4** (1958) 188.
[70] BONDARENKO, I. I. *et al.*, Proc. 2nd UN Int. Conf. PUAE **15** (1958) 353.
[71] PROTOPOPOV, A. and BLINOV, M., *Atomn. Energ.* **4** (1958) 374.

# MESURES DE SECTIONS EFFICACES INTÉRESSANT LES RÉACTEURS RAPIDES

F. CHEYNIER, R. JOLY, J. R. LEROY, A. MICHAUDON ET P. RIBON
COMMISSARIAT A L'ÉNERGIE ATOMIQUE,
FRANCE

**Abstract — Résumé — Аннотация — Resumen**

**Measuring cross-sections in fast reactors.** Measurements of cross-sections of significance for fast reactors have recently been carried out at Saclay.

The measurements on intermediate neutrons were made with a 28-MeV electron linear accelerator using the time-of-flight method, with a resolution $\Delta t/L$ of 0.01 μs/m. The results of the uranium-235 fission cross-section measurements are given and analysed.

For fast neutrons, an arrangement giving fast beam pulsation has been evolved and applied to measurement of total cross-sections by the time-of-flight method, and can be adapted to either of the accelerators available (300 and 600 kV).

**Mesures de sections efficaces intéressant les réacteurs à neutrons rapides.** Des mesures de sections efficaces intéressant les réacteurs à neutrons rapides ont été récemment effectuées à Saclay.

Dans le domaine des neutrons intermédiaires, ces mesures ont utilisé un accélérateur linéaire d'électrons de 28 MeV et ont été effectuées par la méthode du temps de vol, avec une résolution $\Delta t/L$ de 0,01 μs/m. Les résultats des mesures des sections efficaces de fission de l'uranium-235 sont présentés et analysés.

Dans le domaine des neutrons rapides, on a construit et utilisé, pour des mesures de sections efficaces totales par la méthode du temps de vol, un système de pulsation rapide du faisceau pouvant être adapté à l'un ou l'autre des deux accélérateurs (300 et 600 kV) dont le Centre dispose.

**Измерение эффективных сечений для расчета реакторов на быстрых нейтронах.** Недавно в центре ядерных исследований в Сакле были проведены измерения эффективных сечений, касающихся реакторов на быстрых нейтронах.

Для измерения эффективных сечений промежуточных нейтронов использовался линейный ускоритель электронов на 28 Мэв, причем измерения проводились методом времени пролета с разрешающей способностью $\Delta t/L$ 0,01 μs/m. В докладе даются и анализируются результаты измерения эффективных сечений деления урана-235.

Для измерения полных эффективных сечений быстрых нейтронов методом времени пролета была построена и использовалась система быстропульсирующего пучка, которая может использоваться с обоими ускорителями (300 и 600 кв), которыми располагали авторы.

**Medición de secciones eficaces de interés para el diseño de reactores rápidos.** Recientemente se han realizado en el Centre d'études nucléaires de Saclay mediciones de secciones eficaces de interés para el diseño de reactores de neutrones rápidos.

En la gama de las energías neutrónicas intermedias, se utilizó para estas mediciones por el método del tiempo de vuelo un acelerador lineal de electrones, de 28 MeV, con un poder de resolución $\Delta t/L$ de 0,01 μs/m. Los autores exponen y analizan los resultados de la medición de las secciones eficaces de fisión del uranio-235.

En lo que respecta a los neutrones rápidos, se ideó y empleó para la medición de secciones eficaces totales por el método del tiempo de vuelo un sistema de pulsación rápida del haz que puede adaptarse a cualquiera de los dos aceleradores (de 300 y 600 kV) de que se dispone en el mencionado centro.

## Introduction

Des recherches ont été poursuivies au Centre d'études nucléaires de Saclay dans le but d'améliorer notre connaissance des constantes nucléaires nécessaires à l'établissement des projets inscrits au programme français de réacteurs à neutrons rapides. Ces recherches ont été poursuivies selon deux axes principaux. D'une part, nous avons essayé de déterminer l'influence des différentes constantes nucléaires sur la taille critique et la propagation des flux neutroniques à longue distance dans un réacteur à neutrons rapides. D'autre part, nous avons construit et équipé un certain nombre d'appareils de physique permettant la mesure de constantes neutroniques; le programme de travail de ces appareils a été établi en tenant compte, dans la mesure du possible, des besoins mis en lumière par les études évoquées précédemment.

Des calculs destinés à déterminer l'influence des constantes neutroniques ont été faits en se basant sur divers modèles du projet RAPSODIE, qui sera un réacteur de 10 MW utilisant un combustible contenant environ 20% de plutonium, le restant étant de l'uranium enrichi à 20%. Le volume du cœur sera de l'ordre de 40 l. Les méthodes employées pour faire ces calculs étant exposées dans d'autres communications, nous nous contenterons d'énumérer nos principales conclusions, pour indiquer ensuite leurs relations avec le programme de mesures que nous avons établi.

TABLEAU I

**$\delta k/k$ EXPRIMÉ EN pcm POUR UNE AUGMENTATION DE 10% DES CONSTANTES CONSIDÉRÉES DU PLUTONIUM-239**

| $E_n$ (MeV) | $i$ | $\nu$ | $\sigma_f$ | $\sigma_c$ | $\sigma_{in}$ | $\sigma_{er}$ | $\sigma_{tr}$ |
|---|---|---|---|---|---|---|---|
| ∞ à 1,35 | 1 | 1058,39 | 701,21 | —7,14 | —18,36 | —0,25 | 77,25 |
| 1,35 à 0,825 | 2 | 766,25 | 532,92 | —11,67 | 3,39 | —0,05 | 39,9 |
| 0,825 à 0,50 | 3 | 983,21 | 681,32 | —24,15 | 3,25 | 0,17 | 32,14 |
| 0,5 à 0,30 | 4 | 948,32 | 647,30 | —36,12 | 2,13 | 0,4 | 28,4 |
| 0,3 à 0,18 | 5 | 718,65 | 484,21 | —46,89 | 0,49 | 0,22 | 17,62 |
| 0,18 à 0,0674 | 6 | 893,23 | 597,45 | —102,53 | — | 0,54 | 15,24 |
| 0,0674 à 0,0091 | 7 | 378,07 | 243,98 | —57,31 | — | 0,08 | 2,15 |
| 0,0091 à 0 | 8 | 24,78 | 15,61 | —4,58 | — | — | 0,087 |

A titre d'exemple, le tableau I, extrait d'un travail de SOLANES et KAUFMANN [1, 2], montre l'influence d'une variation de 10% de l'une des constantes nucléaires du plutonium-239 sur la réactivité de RAPSODIE. Il ressort clairement de ces résultats que les grandeurs les plus importantes dans ce cas sont $\nu$ et $\sigma_f$. Pour des énergies supérieures à 1 MeV, les résultats relatifs à $^{235}U$ et $^{238}U$ montrent également l'importance de $\nu$, $\sigma_f$ et $\sigma_{in}$ (diffusion inélastique). Les premiers résultats des études de propagation de flux [3] montrent la nécessité d'une bonne connaissance des sections efficaces de capture, de diffusion élastique et inélastique, notamment dans le sodium et le fer, afin de déterminer correctement la distribution spatiale du spectre d'énergie des neutrons, l'échauffement des parties internes de la protection du réacteur et l'activité des circuits de refroidissement.

D'autres auteurs se sont également efforcés d'établir des listes de grandeurs nucléaires dont la mesure serait souhaitable, dans le cadre du développement

des réacteurs à neutrons rapides. C'est ainsi que KANIA, MOINEREAU, VENDRYÈS et ZALESKI [4] envisagent le cas d'un réacteur d'un volume beaucoup plus grand que RAPSODIE. De leur travail, il découle notamment qu'il est nécessaire d'améliorer notre connaissance des sections efficaces de fission, de capture et de diffusion dans le domaine d'énergie des résonances, tant au point de vue de la détermination de la taille critique que de la propagation des flux et du facteur de régénération.

Par ailleurs, SCHMIDT [5] a montré la nécessité de faire un grand nombre de mesures dans le domaine d'énergie des résonances, et de déterminer, si possible, les paramètres de ces résonances. La connaissance de ces paramètres est nécessaire si l'on veut calculer la variation de réactivité due à l'effet Doppler lors d'un brusque changement de température du cœur du réacteur, c'est-à-dire lors d'une brusque variation de puissance. De plus, la connaissance de ces paramètres ainsi que des états de spin et des parités des niveaux excités correspondant aux résonances est nécessaire à l'établissement d'une théorie satisfaisante des réactions nucléaires, laquelle permettrait d'interpoler avec certitude entre des valeurs expérimentales voisines.

Pour faire face à ces besoins, le Centre d'études nucléaires de Saclay dispose, dans le domaine des résonances, d'un accélérateur linéaire à électrons [6] et d'un choppeur rapide [7] installé auprès de la pile EL3.

Les caractéristiques de l'accélérateur linéaire sont les suivantes:

Tube à onde progressive de 3000 MHz
Energie: 10 à 36 MeV
Courant crête: 120 mA à 28 MeV pour des impulsions de 0,1 μs
120 mA à 26 MeV pour des impulsions de 2 μs
Durée de l'impulsion électronique: 0,1 μs*, 0,25 μs, 0,5 μs, 1 μs, 1,5 μs, 2 μs
Fréquence de répétition: 125 Hz, 250 Hz ou 500 Hz ou coup par coup ou fréquence continûment variable de 0 à 30 Hz.

Les neutrons sont produits par des réactions (γ, n) et (γ, f) induites par le rayonnement de freinage des électrons de 28 MeV; l'intensité crête de la source de neutrons ainsi constituée est environ $10^{16}$ n/s dans une géométrie $4\pi$. Ces neutrons sont ralentis jusque dans le domaine d'énergie des résonances par deux écrans de paraffine de 3 cm d'épaisseur entourant la cible.

La cible est environnée d'un massif de béton qui laisse passer les neutrons dans cinq directions. Chacune de ces directions constitue une base de vol sur laquelle sont disposées des stations permettant d'installer les détecteurs de neutrons à des distances pouvant aller jusqu'à 200 m. Les temps de vol sont mesurés au moyen d'un sélecteur à mémoire à tores magnétique. Nous disposons actuellement de sélecteurs à 1000 et 1024 canaux, la largeur du canal pouvant prendre l'une des valeurs suivantes: 0,25 μs, 0,5 μs, 1 μs, ...jusqu'à 40 μs. Un sélecteur à 1000 canaux dont la largeur de canal peut être réduite à 0,1 μs a, par ailleurs, été récemment mis en service. Avec cet appareil, en réglant la durée de la bouffée neutronique à 0,1 μs, et en plaçant le détecteur de neutrons à 100 m, la résolution nominale de l'ensemble se trouve donc portée à 1 ns/m. Malheureusement, la dispersion en temps introduite par le ralentissement des neutrons dans le manchon de paraffine entourant la cible est de 0,15 μs à 10 eV et de 0,05 μs à 100 eV pour une épaisseur de paraffine de 2,75 cm. Il semble

* Cette valeur n'est utilisable que depuis un mois.

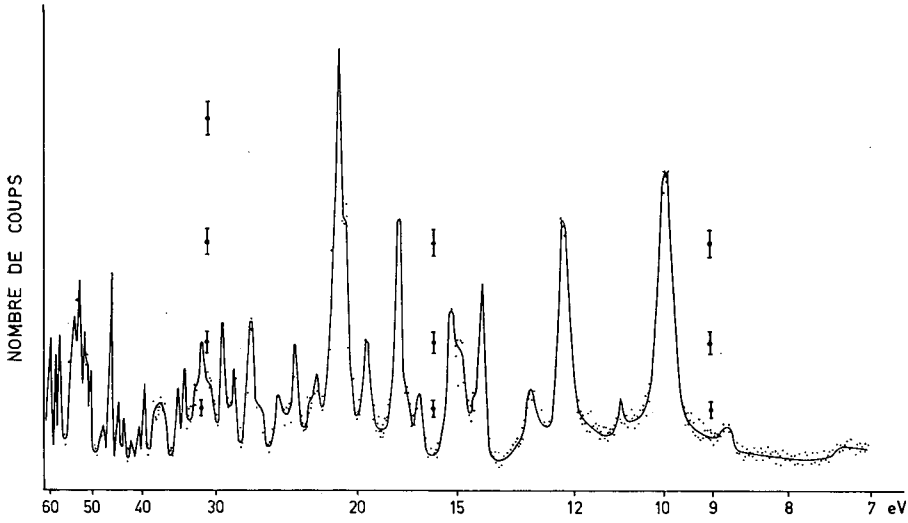


Figure 1
Scintillateur gazeux.

donc que la résolution de 0,1 μs ne puisse être atteinte réellement que pour des neutrons d'énergie supérieure à 50 eV environ.

Pour illustrer les possibilités de l'accélérateur linéaire comme source pulsée de neutrons, il est intéressant de le comparer avec le «chopper» installé au voisinage de la pile EL 3: le flux de neutrons obtenu avec l'accélérateur linéaire est, à résolution égale, deux cents fois celui donné par le «chopper», celui-ci étant par ailleurs comparable aux meilleurs appareils de ce type. En revanche, le «chopper» permet d'utiliser en transmission des échantillons beaucoup plus petits, ce qui donne la possibilité d'utiliser des isotopes séparés, alors que cela serait prohibitif avec les dimensions d'échantillons nécessaires pour travailler avec l'accélérateur linéaire.

Nous allons maintenant passer en revue les différents types de mesures possibles à l'accélérateur linéaire.

## Mesures de section efficace de fission

Les premières mesures de la section efficace de fission de l'uranium-235 ont été faites en 1958 [8], entre 4 eV et 20 keV. Elles ont été reprises par la suite [9] entre 7 et 95 eV, afin de mieux séparer les résonances dans le domaine d'énergie où on pouvait espérer calculer les paramètres de ces résonances; le sélecteur à 1024 canaux était alors calé à 0,5 μs de largeur de canal, la base de vol était de 50 m. La résolution nominale était donc de 10 ns/m. Les fissions étaient détectées par une chambre d'ionisation pouvant contenir dix dépôts d'uranium enrichi à 45% d'uranium-235, de 240 mm de diamètre et d'épaisseur 2 mg/cm$^2$.

L'analyse des résultats a mis en évidence l'existence d'un effet Doppler plus grand que l'effet attendu. Pour expliquer cette différence, il faut admettre une température de Debye très élevée (600° K) pour l'oxyde d'uranium constituant les dépôts de la chambre. Afin d'élucider cette question, un cryostat à hélium liquide a été mis en service par A. Michaudon.

Des mesures de la section efficace de fission de $^{239}Pu$ et de $^{233}U$ de 1 eV à 50 keV environ seront faites prochainement. A cause de la forte réactivité de ces éléments, il a été nécessaire de mettre au point un détecteur de fission par scintillation gazeuse (fig. 1); nous disposons actuellement d'un scintillateur de xénon contenant 1 g d'uranium-233 [10]. Des résultats préliminaires concernant la section efficace de fission de l'uranium-233 entre 7 et 60 eV sont présentés sur la figure 2.

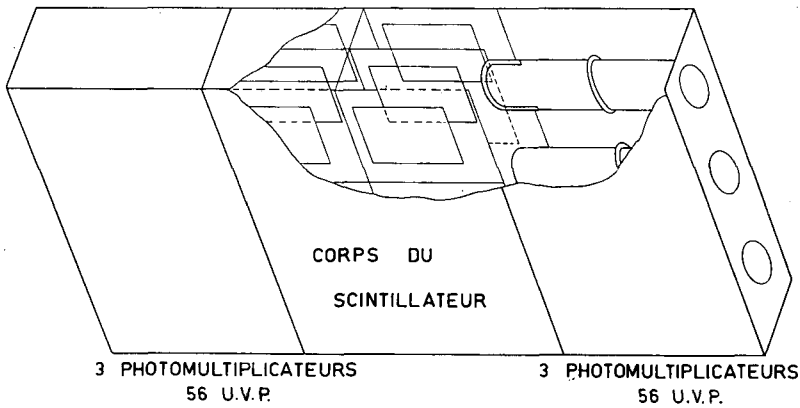


Figure 2
Section efficace de fission de $^{233}U$ de 7 à 60 eV.

## Mesures de sections efficaces totales

Le détecteur de neutrons est alors constitué par un écran de 500 cm² de bore-10 enrichi à 92%; le gamma de 478 keV de désexcitation du lithium-7 produit par la réaction $^{10}B$ (n, $\gamma$) $^{7}Li$, est décelé par un des six ensembles cristal NaI-photomultiplicateur qui entourent l'écran de bore. Cet ensemble est maintenant bien au point, et il nous permettra de produire des courbes de transmission d'une manière quasi industrielle. La mesure de la section efficace totale de l'uranium-238 entre 1 et 20 keV est notamment prévue pour un avenir prochain par Julien, Corge et Netter.

A titre d'exemple, citons l'expérience de transmission réalisée récemment [11] sur l'uranium-235 entre 8 et 22 eV afin d'obtenir une meilleure détermination des paramètres des résonances étudiées dans les mesures de section efficace de fission réalisées précédemment. L'échantillon était sous forme $^{4}UF$ enrichi à 92,9%; deux épaisseurs ont été utilisées:

$$\frac{1}{N} = 1109 \text{ b/atome}$$

$$\frac{1}{N} = 583 \text{ b/atome.}$$

La résolution utilisée était de 10 ns/m. Cinq résonances (12,4 eV — 14,5 eV — 16,10 eV — 16,69 eV — 19,29 eV) ont été analysées par la méthode des aires partielles, particulièrement convenable ici, et, quand ce fut possible, à l'aide du minimum de transmission. Les résultats de ces analyses sont donnés par le tableau II.

TABLEAU II

**PARAMÈTRES DES RÉSONANCES DE L'URANIUM-235**

| $E_0$ (eV) | $\Gamma$ (meV) | $\sigma_0 f$ (b) | $\sigma_0$ (b) | $2\,g\,\Gamma n$ (meV) | $\Gamma F$ (meV) | $\Gamma\gamma$ (meV) | $\eta/\bar{\nu}$ | |
|---|---|---|---|---|---|---|---|---|
| | | | | | | | (1) | (2) |
| 12,40 | $61 \pm 6$ | 772 | $2210 \pm 300$ | $1,29 \pm 0,09$ | $21 \pm 3$ | $38 \pm 6$ | 0,35 | $0,39 \pm 0,03$ |
| 15,41 | $106 \pm 10$ | 112 | $260 \pm 50$ | $0,33 \pm 0,06$ | $45 \pm 10$ | $61 \pm 10$ | 0,42 | $0,52 \pm 0,10$ |
| 16,10 | $55 \pm 7$ | 182 | $640 \pm 120$ | $0,43 \pm 0,04$ | $16 \pm 5$ | $39 \pm 7$ | 0,29 | $0,28 \pm 0,05$ |
| 16,69 | $117 \pm 12$ | 120 | $205 \pm 40$ | $0,30 \pm 0,05$ | $68 \pm 12$ | $49 \pm 12$ | 0,58 | $0,50 {}^{+0,05}_{-0,07}$ |
| 18,05 | 116 | 103 | | | | | | |
| 19,29 | $108 \pm 7$ | 947 | $2150 \pm 200$ | $3,45 \pm 0,25$ | $48 \pm 6$ | $57 \pm 9$ | 0,45 | $0,43 \pm 0,02$ |
| 20,10 | 290 | 17 | — | — | — | — | — | — |
| 20,60 | 72 | 62 | — | — | — | — | — | — |
| 21,06 | 56 | 500 | — | — | — | — | — | — |
| 22,93 | 81 | 140 | — | — | — | — | — | — |
| 27,80 | 101 | 160 | — | — | — | — | — | — |
| 28,35 | 181 | 26 | — | — | — | — | — | — |
| 29,63 | 122 | 27 | — | — | — | — | — | — |
| 30,57 | 126 | 38 | — | — | — | — | — | — |
| 30,85 | 36 | 165 | — | — | — | — | — | — |
| 32,06 | 107 | 340 | — | — | — | — | — | — |
| 33,52 | 80 | 317 | — | — | — | — | — | — |
| 35,18 | 207 | 490 | — | — | — | — | — | — |

(1) Valeur de $\eta/\bar{\nu} = \Gamma F\,(\Gamma F + \Gamma\gamma)$ calculée à partir des paramètres.
(2) Valeur de $\eta/\bar{\nu}$ mesurée directement (Harwell).

## Etudes sur les gammas de capture

Ce travail est cité pour mémoire seulement, car le dispositif actuel ne permet pas de détecter tous les gammas, donc de faire une mesure de section efficace de capture. Il a été utilisé pour déterminer les fluctuations des largeurs partielles de la transition donnant le gamma le plus énergique quand on passe d'une résonance à une autre [12].

## Mesures de $\eta$

Une série de mesures de $\eta$ est prévue sur l'uranium-235, et ultérieurement, sur le plutonium-239, entre 1 eV et 50 keV.

Pour faire des mesures dans le domaine des énergies supérieures à 100 keV, le Centre d'études nucléaires de Saclay dispose:

1° D'un Van de Graaff de 5 MeV [13], mais cet appareil a un programme de travail en particules chargées très important, et, par ailleurs, la disposition de la salle des cibles ne se prête pas à toutes les expériences de physique des neutrons. Néanmoins des expériences de diffusion inélastique sur différents noyaux, notamment $^{56}Fe$, $^{127}I$, $^{209}Bi$ [14], ont été réalisées, pour des énergies de neutrons incidents allant jusqu'à 6,5 MeV. Cet appareil pourra peut-être, dans un proche avenir, être utilisé d'une manière plus intense pour faire des mesures intéressant les pilologues.

2° D'un générateur de neutrons type Cockroft-Walton de 300 keV, construit par Hæfely, d'un générateur électrostatique de 150 kV et d'un accélérateur

électrostatique Felici-Sames de 600 kV, qui, bien qu'installé à Fontenay-aux-Roses, est utilisé partiellement par une équipe de Saclay. Avec ces appareils, les seules réactions pouvant donner des neutrons monocinétiques sont (d, d) et (d, t). Les énergies ainsi obtenues, 2 à 3 MeV d'une part, et 14 MeV d'autre part, sont d'un intérêt médiocre pour les réacteurs rapides.

Aussi, après une série de mesures sur $\nu$ à 14 MeV [15], le générateur Hæfely est utilisé pour des études de caractère plus fondamental.

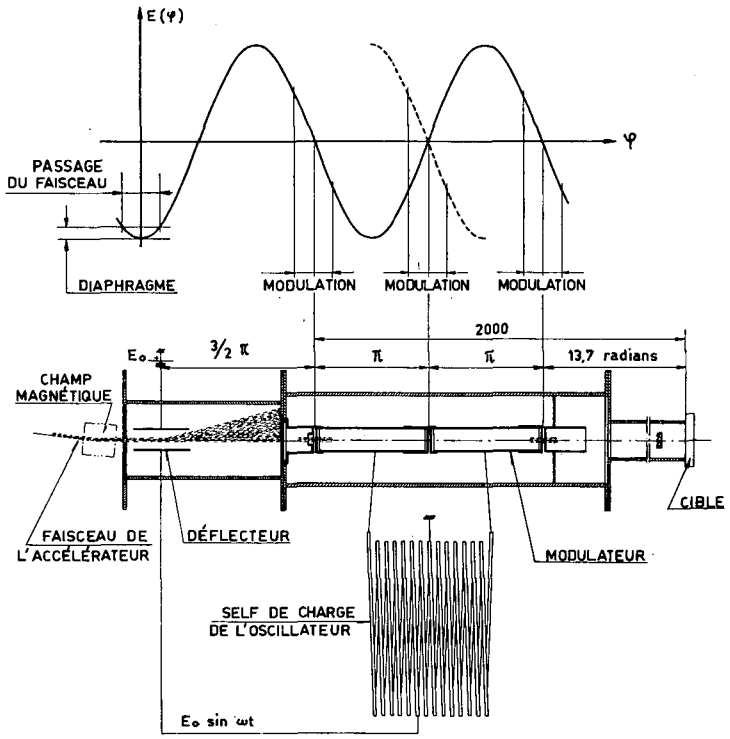


Figure 3
Schéma du dispositif de pulsation pour un accélérateur électrostatique de basse énergie.

3° D'un accélérateur Sames de 600 kV avec dispositif de pulsation rapide [16]. Les possibilités de mesures neutroniques réalisables avec un accélérateur électrostatique de 600 kV sont grandement augmentées par l'adjonction d'un dispositif de pulsation permettant d'utiliser les techniques du temps de vol rapide.

Dans le système que nous avons construit, le faisceau sortant de l'accélérateur pénètre, après analyse magnétique, dans un déflecteur qui se compose essentiellement de deux plaques planes parallèles, placées de chaque côté du faisceau, et d'un diaphragme placé après les plaques, à 1 m environ du centre de celles-ci. A l'une des plaques on applique une tension continue, et à l'autre plaque une tension alternative haute fréquence de 6 MHz. Avec un réglage correct de l'amplitude de la tension haute fréquence et de la tension continue, le faisceau ne peut

passer à travers le diaphragme qu'une fois par période, et pendant 1/6 de la période environ.

Le paquet d'ions ainsi formé traverse successivement deux électrodes de modulation cylindrique auxquelles on applique des tensions sinusoïdales égales entre elles mais de signe contraire. La relation de phase entre le champ électrique transversal de déflection et le champ électrique axial de modulation est telle que le début du paquet d'ions ayant traversé le diaphragme est freiné tandis que la fin du paquet est accélérée.

La longueur des électrodes de modulation est choisie de manière que la variation de phase de la tension alternative soit de $\pi$ pendant le temps de transit des particules à travers une des électrodes. De cette manière, l'effet des dernières fentes s'ajoute bien à celui de la première.

On peut obtenir sur la cible de l'accélérateur, grâce à ce dispositif, des impulsions de courant d'une amplitude crête de 2 mA et d'une durée de 1 à 2 ns.

Les expériences de physique des neutrons réalisables au moyen de cet appareil peuvent être divisées en deux catégories:

*a*) Celles dans lesquelles le faisceau de deutons produit des neutrons monocinétiques qui seront envoyés sur une cible dans laquelle ils produisent des neutrons secondaires dont l'énergie est mesurée par temps de vol. Cette méthode a donné de très beaux résultats dans plusieurs laboratoires, mais dans ce cas notre appareillage souffre d'une infériorité grave: l'énergie des neutrons ne peut pas être réglée d'une manière continue.

*b*) Dans d'autres expériences, on produit des bouffées brèves de neutrons de plusieurs énergies au moyen de la réaction (d, Li) ou de la réaction (d, Be) ou même en dégradant l'énergie des neutrons produits par la réaction (d, t) par diffusion inélastique sur un petit bloc d'uranium placé au voisinage immédiat de la cible. Les neutrons sont ensuite sélectionnés en temps de vol, comme on le fait avec l'accélérateur linéaire, mais dans une gamme d'énergies beaucoup plus grandes. Parmi les expériences de ce type et qui intéressent le programme de réacteurs rapides, nous pouvons citer les mesures de transmission, entre 1 et 14 MeV, les variations d'une section efficace de fission entre 1 et 14 MeV, les variations de $\nu$ entre 1 et 14 MeV.

La mesure de transmission du sodium-23 pour des neutrons d'énergie supérieure à 4 MeV est actuellement en cours selon cette méthode. La même mesure sera ensuite effectuée sur d'autres éléments.

## RÉFÉRENCES

[1] SOLANES, M. et KAUFMANN, S., Rapport interne CENS.
[2] SOLANES, M. et MOINEREAU, P., vol. II des présents Comptes rendus, p. 27.
[3] KANIA, A., PASQUET, P., SOLANES, M., PÉPIN, P. et RASTOIN, J., vol. I des présents Comptes rendus, p. 387.
[4] KANIA, A., MOINEREAU, P., VENDRYÈS, G., et ZALESKI, C. P., vol. II des présents Comptes rendus, p. 301.
[5] SCHMIDT, J. J., EANDC(E)-9 L.
[6] LEBOUTET, PICARD, VASTEL, CEA-686.
[7] JULIEN, J. *et al.*, Actes 2e Conf. Genève 7 (1958) 15 et *Onde élect.* 388 (1957).
[8] BILLAUD, P. *et al.*, Actes 2e Conf. Genève 7 (1958) 526.
[9] MICHAUDON, A., BERGÈRE, R., COIN, A. et JOLY, R., *J. Phys. Radium* 21 (1960) 429.

[10] NIFENECKER, H. *et al.*, Nuclear Electronics I, IAEA, Vienna (1962) 115.
[11] MICHAUDON, A. et RIBON, P., à paraître dans *J. Phys. Radium.*
[12] NIFENECKER, H., HAZONI, Y., MICHAUDON, A. et PAYA, D., à paraître dans *J. Phys. Radium.*
[13] WINTER, S. D., *Onde élect.* **344** (1955) 995.
[14] NAGGIAR, V., *J. Phys. Radium* **21** (1960) 384.
[15] LEROY, J. L., *J. Phys. Radium* **21** (1960) 617.
[16] CHEYNIER, B., LEROY, J. L. et PRÉLEC, K., *J. Phys. Radium* **21** (1960) 393.

SM-18/85

# ИЗМЕРЕНИЕ ПАРАМЕТРОВ РЕЗОНАНСНОЙ СТРУКТУРЫ СЕЧЕНИЙ, ВЛИЯЮЩИХ НА РАСПРОСТРАНЕНИЕ БЫСТРЫХ НЕЙТРОНОВ В СРЕДАХ

М. Н. НИКОЛАЕВ, В. В. ФИЛИППОВ И И. И. БОНДАРЕНКО
АКАДЕМИЯ НАУК СССР, МОСКВА,
СССР

**Abstract — Résumé — Аннотация — Resumen**

**Measurement of resonance parameters of cross-sections affecting fast-neutron propagation in various media.** In compiling a system of multi-group constants for fast- and intermediate-reactor calculations, it is frequently necessary to account for the self-shielding effect associated with the resonance structure of the cross-sections. The energy region in which the resonance structure has a considerable influence on neutron propagation in the material extends up to several decades of kilo-electron-volts for heavy nuclei and to several mega-electron-volts for intermediate nuclei. To compute resonance effects in calculating group parameters, it is essential to know not only the average interaction cross-sections between neutrons and materials, but also values such as $\langle 1/\Sigma_t \rangle$, $\langle 1/\Sigma_t^2 \rangle$, etc. (the brackets signify averaging over the energy group).

Present information about resonance parameters for fast neutrons is not sufficient to calculate these values with the necessary precision. In this connection it is interesting to take direct measurements of the values $\langle 1/\Sigma_t \rangle$, $\langle 1/\Sigma_t^2 \rangle$ and other analogous characteristics.

The paper describes the results obtained from measurements of a number of parameters (such as $\langle \Sigma_t \rangle$, $\langle \Sigma_t^2 \rangle$, $\langle 1/\Sigma_t \rangle$, $\langle 1/\Sigma_t^2 \rangle$, $\langle 1/\Sigma_t^3 \rangle$ etc.), which characterize the cross-section structure of a number of intermediate nuclei within the range from 300 keV to 3 MeV. These values were arrived at by an analysis of transmission curves obtained by good geometry for transmissions up to $\sim 10^{-2}$. The data show that resonance effects exercise a strong influence on the diffusion characteristics of the material.

**Mesure des paramètres de résonance de sections efficaces liés à la propagation des neutrons dans différents milieux.** Lorsqu'on établit un système de constantes multi-groupes pour les calculs de réacteurs à neutrons rapides et intermédiaires, il est souvent nécessaire de tenir compte de l'effet d'auto-protection lié à la structure de résonance des sections efficaces. Le domaine d'énergie dans lequel la structure de résonance a une grande influence sur la propagation des neutrons dans la matière va de plusieurs dizaines de keV, pour les noyaux lourds, à plusieurs dizaines de MeV pour les noyaux intermédiaires. Pour évaluer les effets de résonance lors du calcul des paramètres de groupes, il faut connaître non seulement les sections efficaces d'interaction moyenne entre les neutrons et la matière, mais aussi certaines valeurs telles que $\langle 1/\Sigma_t \rangle$, $\langle 1/\Sigma_t^2 \rangle$, etc. — les signes $\langle\rangle$ signifiant que l'on prend la moyenne du groupe d'énergie.

Actuellement, les données dont on dispose sur les paramètres de résonance dans le domaine des neutrons rapides ne sont pas suffisantes pour calculer ces moyennes avec la précision nécessaire. A cet égard il est intéressant de mesurer directement les moyennes $\langle 1/\Sigma_t \rangle$, $\langle 1/\Sigma_t^2 \rangle$ et d'autres caractéristiques analogues.

Les auteurs décrivent les résultats obtenus par la mesure d'un certain nombre de paramètres (tels que $\langle \Sigma_t \rangle$, $\langle \Sigma_t^2 \rangle$, $\langle 1/\Sigma_t \rangle$, $\langle 1/\Sigma_t^2 \rangle$, $\langle 1/\Sigma_t^3 \rangle$ etc.) qui caractérisent la structure de la section efficace de divers noyaux intermédiaires dans une gamme d'énergie allant de 300 keV à 3 MeV. On est parvenu à mesurer ces moyennes par une analyse des courbes de transmission obtenues grâce à une bonne configuration géométrique pour des taux de transmission allant jusqu'à $\sim 10^{-2}$. Les données recueillies montrent que les effets de résonance influent fortement sur les caractéristiques de diffusion de la matière.

**Измерение параметров резонансной структуры сечений, влияющих на распространение быстрых нейтронов в средах.** При составлении систем многогрупповых констант для расчета реакторов на быстрых и промежуточных нейтронах во многих случаях необходимо учитывать эффекты самоэкранировки, связанные с резонансной структурой сечений. Энергетическая область, в которой резонансная структура оказывает существенное влияние на распространение нейтронов в веществе, простирается вплоть до нескольких десятков кэв для тяжелых ядер и до нескольких Мэв для ядер среднего веса. Для учета резонансных эффектов при вычислении групповых параметров необходимо знать не только средние сечения взаимодействия нейтронов с веществами, но и такие величины, как $\langle 1/\Sigma_t \rangle$, $\langle 1/\Sigma_t^2 \rangle$ и другие (скобки означают усреднение по энергетической группе).

Имеющиеся в настоящее время сведения о резонансных параметрах в области быстрых нейтронов недостаточны для того, чтобы указанные величины могли быть вычислены с необходимой точностью. В связи с этим представляет интерес непосредственное измерение величин $\langle 1/\Sigma_t \rangle$, $\langle 1/\Sigma_t^2 \rangle$ и других аналогичных характеристик.

В докладе приводятся результаты измерений ряда параметров (таких как $\langle \Sigma_t \rangle$, $\langle \Sigma_t^2 \rangle$, $\langle 1/\Sigma_t \rangle$, $\langle 1/\Sigma_t^2 \rangle$, $\langle 1/\Sigma_t^3 \rangle$ и другие), характеризующих структуру сечений ряда ядер среднего веса в области от 300 кэв до 3 Мэв. Указанные величины были получены путем анализа кривых пропускания, снятых в хорошей геометрии вплоть до пропусканий $\sim 10^{-2}$. Полученные данные указывают на сильное влияние резонансных эффектов на диффузионные характеристики вещества.

**Medición de los parámetros de resonancia de las secciones eficaces que afectan a la propagación de los neutrones rápidos en distintos medios.** En el planteo de los sistemas de constantes que intervienen en la teoría de los multigrupos para el cálculo de reactores de neutrones rápidos y de neutrones intermedios, es preciso considerar en muchos casos los efectos de autoblindaje relacionados con la estructura resonante de las secciones eficaces. El intervalo energético dentro del cual la resonancia ejerce una influencia decisiva sobre la propagación de los neutrones en la materia abarca desde algunas decenas de kiloelectrón-voltios, para los núcleos pesados, hasta unos cuantos megaelectrón-voltios, para los núcleos intermedios. Para poder tener en cuenta los efectos de resonancia en el cálculo de los parámetros de los grupos, es indispensable conocer no sólo las secciones eficaces medias correspondientes a las reacciones de los neutrones con la materia, sino también algunas magnitudes tales como $\langle 1/\Sigma_t \rangle$, $\langle 1/\Sigma_t^2 \rangle$ etc. (los corchetes indican que se toman valores promedios de los grupos energéticos).

La información de que se dispone actualement acerca de los parámetros de resonancia en el terreno de los neutrones rápidos no permite calcular las magnitudes mencionadas con la exactitud necesaria. Por tal razón interesa medir directamente $\langle 1/\Sigma_t \rangle$, $\langle 1/\Sigma_t^2 \rangle$ y otros valores análogos.

Los autores presentan los resultados de las mediciones de una serie de parámetros (tales como $\langle \Sigma_t \rangle$, $\langle \Sigma_t^2 \rangle$, $\langle 1/\Sigma_t \rangle$, $\langle 1/\Sigma_t^2 \rangle$ $\langle 1/\Sigma_t^3 \rangle$ etc.), que caracterizan la estructura de las secciones eficaces de una serie de núcleos intermedios para neutrones de energía comprendida entre 300 keV y 3 MeV. Dichos valores se dedujeron analizando las curvas de paso a través de la materia, obtenidas con una geometría favorable, hasta un valor límite de $10^{-2}$, aproximadamente. Los datos obtenidos demuestran que los efectos de resonancia ejercen una notable influencia sobre las características de la difusión en la materia.

## 1. Необходимость учета резонансной структуры сечений составлении многогрупповых констант

До последнего времени при расчетах реакторов на быстрых нейтронах использовались многогрупповые системы констант, составленные на основании имеющихся данный о средних сечениях (см. [1], [2]). Подобный подход к вычислению групповых параметров является обоснованным только в том случае, когда сечения в пределах энергетической группы являются достаточно плавными функциями энергии. В случаях, когда в сечениях проявляется резонансная структура, при составлении многогрупповых констант необходимо учитывать резонансную блокировку сечений. До сих пор учет резонансной блокировки производился, как правило, только в области изолированных резонансов при вычислении групповых сечений радиационного захвата и деления для тяжелых ядер [3], [4]. При вычислении же таких групповых параметров, как коэффициент диффузии (или соответствующее ему „транспортное" сечение) и сечение замедления, влиянием резонансных эффектов пренебрегалось. Однако, эффекты, связанные с блокировкой резонансов, могут оказать существенное влияние и на эти величины. Это обстоятельство отмечалось в работе [5], в которой, в частности, был произведен учет резонансной блокировки при составлении многогрупповой системы констант для $U^{238}$ (см. также работу [6]).

Как видно из результатов этих работ, даже в случае такого тяжелого ядра как $U^{238}$ и сравнительно высоких энергий (порядка нескольких десятков Кэв) резонансная блокировка оказывает заметное влияние не только на сечение захвата, но также и на транспортное сечение.

В случае ядер среднего веса резонансная структура сечений проявляется вплоть до энергий порядка нескольких Мэв [7]. Поэтому можно думать, что для этих ядер эффект блокировки будет существенен во всей энергети-

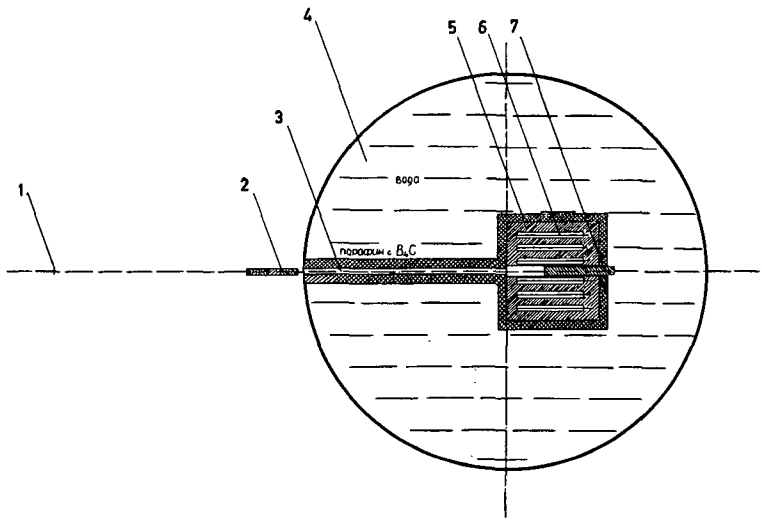


Рис. 1

1 — мишень; 2 — рассеиватель; 3 — коллимационное отверстие; 4 — бак с водой; 5 — детектор; 6 — борные счетчик и 7 — полиэтиленовая пробка.

ческой области, представляющей интерес с реакторной точки зрения. Этот вывод подтверждается и экспериментальными данными [5].

Как известно, уравнение переноса нейтронов некоторой группы получается путем усреднения точного уравнения, учитывающего энергетическую зависимость нейтронного потока и сечений, по спектру нейтронов рассматриваемой группы. В получающиеся при этом групповые уравнения входят соответствующим образом усредненные значения сечений. Например, отвлекаясь от анизотропии рассеяния и плавных изменений спектра можно придти к следующим выражениям для групповых значений коэффициента диффузии и сечения замедления:

$$\langle D\rangle = \frac{1}{3}\frac{\left\langle\frac{1}{\Sigma}\right\rangle}{\left\langle\frac{1}{\Sigma^2}\right\rangle}\ ;\quad \langle\Sigma_{\text{зам}}\rangle = \frac{\xi}{\Delta u}\frac{1}{\left\langle\frac{1}{\Sigma}\right\rangle} \tag{1}$$

Здесь $\xi$ — средне-логарифмическая потеря энергии,
$\Delta u$ — ширина группы в масштабе летаргии,
$\Sigma$ — макроскопическое сечение рассеяния.

Скобки означают усреднение по рассматриваемой группе.

Имеющиеся в настоящее время сведения о резонансных параметрах в области быстрых нейтронов недостаточно точны и полны для того, чтобы величины $\langle 1/\Sigma\rangle$ и $\langle 1/\Sigma^2\rangle$ могли быть вычислены с необходимой степенью точности.

Отметим также, что на эти величины оказывают сильное влияние интерференционные эффекты, которые почти не изучены в рассматриваемой энергетической области. В связи с этим представляет интерес непосредственное измерение величин $\langle 1/\Sigma\rangle$, $\langle 1/\Sigma^2\rangle$ и других аналогичных параметров, характеризующих флуктуации сечения.

## 2. Выражение для кривой пропускания, позволяющее по ее форме определить среднее сечение $\langle\Sigma\rangle$

Интересующие нас величины могут быть определены следующим образом. Рассмотрим кривую пропускания $T(t)$ нейтронов, равномерно распределенных в интервале усреднения $\Delta E$ через толщину $t$:

$$T(t) = \frac{1}{\Delta E}\int\limits_{\Delta E} e^{-\Sigma(E)t}\,dE\,. \tag{2}$$

Площадь под кривой пропускания равна средней длине свободного пробега $\langle 1/\Sigma\rangle$:

$$\int\limits_0^\infty T(t)\,dt = \frac{1}{\Delta E}\int\limits_{\Delta E}\frac{dE}{\Sigma(E)} = \left\langle\frac{1}{\Sigma}\right\rangle. \tag{3}$$

Производя двойное интегрирование кривой пропускания, получаем средний квадрат длины пробега, $\langle 1/\Sigma^2\rangle$:

$$\int\limits_0^\infty dt\int\limits_t^\infty T(t')\,dt' = \frac{1}{\Delta E}\int\limits_{\Delta E}\frac{dE}{\Sigma^2(E)} = \left\langle\frac{1}{\Sigma^2}\right\rangle. \tag{4}$$

Аналогичным образом могут быть определены средние от более высоких степеней $1/\Sigma$.

Если в выражении (2) вынести $\exp[-\langle\Sigma\rangle t]$ из под знака интеграла, а оставшееся выражение разложить в ряд Тэйлора и почленно проинтегрировать, то получаем:

$$T(t) = e^{-\langle\Sigma\rangle t}\left[1 + \frac{\langle\Sigma^2\rangle - \langle\Sigma\rangle^2}{2!}t^2 + \ldots\right] \tag{5}$$

Пользуясь этим выражением можно по форме кривой пропускания при малых толщинах определить среднее сечение и оценить дисперсию сечения $\langle\Sigma^2\rangle - \langle\Sigma\rangle^2$.

## 3. Экспериментальная установка для измерения кривых пропускания

Установка с помощью которой измерялись кривые пропускания, изображена на рис. 1. В качестве источника нейтронов использовалась реакция $T(p, n)$ $He^3$. Протоны, ускоренные на электростатическом генераторе, попадали на тритий-циркониевую мишень (I), толщина которой составляла 300 кэв. Измерения производились, под углом 0° к пучку протонов. Нейтроны, вылетевшие из мишени и прошедшие через рассеиватель (2) без столкновения, через коллимационное отверстие (3) в защитном баке с водой (4) попадали в детектор (5). Рассеиватели имели форму цилиндра диаметром 50 мм. Они составлялись из отдельных секций различной толщины, подвешенных на стальных нитях. Используя различные наборы секций, можно было изменять толщину рассеивателя.

Регистрация нейтронов производилась с помощью 48-ми пропорциональных счетчиков (6) с обогащенным бором (типа СНМО-5) Счетчики располагались внутри цилиндрического блока из парафина. Вдоль оси блока проходил канал диаметром 50 мм, наполовину заполненный полиэтиленовой пробкой (7). Нейтроны, прошедшие через коллиматор, рассеивались в этой пробке и, замедлившись в парафиновом блоке, регистрировались счетчиками. Детектор помещался внутри защитного бака (4) с диаметром и высотой равными 2-м метрам. В коллимационное отверстие бака ⌀ 45 мм попадали только нейтроны, которые прошли через рассеиватель. Для измерения фона, входное отверстие коллиматора закрывалось от мишени медным конусом длиной 800 мм. Фон составлял 0,1% от счета при открытой мишени. Угловое разрешение установки равнялось примерно 1°. Максимальная толщина рассеивателей соответствовала более чем стократному ослаблению пучка нейтронов.

## 4. Результаты проведенных экспериментов

Кривые пропускания были сняты для алюминия, серы, железа, никеля, меди, циркония, ниобия, молибдена, свинца, висмута и тория в интервале энергий от 0,3 до 2,7 Мэв. Результаты анализа кривых пропускания приведены в таблицах I—XI. Точность определения величин $\langle\sigma\rangle$ и $\langle\sigma^2\rangle^{1/2}$ составляет 4%; погрешности в величинах $\langle 1/\sigma\rangle^{-1}$, $\langle 1/\sigma^2\rangle^{-1/2}$ и $\langle 1/\sigma^3\rangle^{-1/3}$ равны соответственно 1%, 3% и 5%.

Полученные нами средние сечения в большинстве случаев лежат на несколько процентов выше данных, приведенных в атласе 7. Эти расхождения

можно понять, если учесть, что в работах по измерению полных сечений, данные которых приводятся в атласе, толщины рассеивателей обычно берутся достаточно большими (порядка одной длины пробега), вследствие чего на результатах экспериментов может сказываться резонансная блокировка.

Формы большинства кривых пропускания оказались отличными от экспоненциальных, что свидетельствует о флуктуациях сечений в пределах интервалов усреднения. Поэтому средние характеристики, определяемые различными законами усреднения, в этих случаях не совпадают между собой. Отклонених кривый пропусканий от экспоненциального закона (вплоть до $T \leq 10^{-2}$) не обнаружено только в случаях молибдена и тория, у которых в изучавшейся области энергий уровни практически полностью перекрыты.

В то же время для таких ядер, как железо, никель, медь и др. эффекты резонансной структуры сечений оказываются весьма существенными во всем исследованном диапазоне энергий. Например, среднее значение коэффициента диффузии может для этих ядер отличаться от значения, полученного при использовании среднего сечения в 1,5 2 раза.

Таблица I

**СРЕДНИЕ ХАРАКТЕРИСТИКИ СЕЧЕНИЯ АЛЮМИНИЯ**

| Энергия, Мэв | 0,3—0,6 | 0,6—0,9 | 0,9—1,2 | 1,2—1,5 | 1,5—1,8 | 1,8—2,1 | 2,1—2,4 |
|---|---|---|---|---|---|---|---|
| $\langle\sigma\rangle$ барн | 4,26 | 3,95 | 3,16 | 3,44 | 2,99 | 3,22 | 2,69 |
| $\langle\sigma^2\rangle^{\frac{1}{2}}$ барн | 4,57 | 4,26 | 3,50 | 3,82 | 3,20 | 3,29 | 2,76 |
| $\left\langle\frac{1}{\sigma}\right\rangle^{-1}$ барн | 3,23 | 3,43 | 2,94 | 2,86 | 2,76 | 3,12 | 2,48 |
| $\left\langle\frac{1}{\sigma^2}\right\rangle^{-\frac{1}{2}}$ барн | 2,82 | 3,15 | 2,80 | 2,80 | 2,70 | 3,11 | 2,44 |
| $\left\langle\frac{1}{\sigma^3}\right\rangle^{-\frac{1}{3}}$ барн | 2,47 | 2,92 | 2,66 | 2,70 | 2,62 | 3,08 | 2,39 |

Таблица II

**СРЕДНИЕ ХАРАКТЕРИСТИКИ СЕЧЕНИЯ СЕРЫ**

| Энергия, Мэв | 0,9—1,2 | 1,2—1,5 | 1,5—1,8 | 1,8—2,1 | 2,1—2,4 |
|---|---|---|---|---|---|
| $\langle\sigma\rangle$ барн | 2,90 | 2,91 | 3,07 | 3,05 | 3,28 |
| $\langle\sigma^2\rangle^{\frac{1}{2}}$ барн | 3,18 | 3,13 | 3,59 | 3,35 | 3,70 |
| $\left\langle\frac{1}{\sigma}\right\rangle^{-1}$ барн | 2,34 | 2,46 | 2,22 | 2,46 | 2,86 |
| $\left\langle\frac{1}{\sigma^2}\right\rangle^{-\frac{1}{2}}$ барн | 2,24 | 2,37 | 2,06 | 2,31 | 2,72 |
| $\left\langle\frac{1}{\sigma^3}\right\rangle^{-\frac{1}{3}}$ барн | 2,18 | 2,31 | 1,97 | 2,25 | 2,64 |

Таблица III

**СРЕДНИЕ ХАРАКТЕРИСТИКИ СЕЧЕНИЯ ЖЕЛЕЗА**

| Энергия, Мэв | 0,3—0,6 | 0,6—0,9 | 0,9—1,2 | 1,2—1,5 | 1,5—1,8 | 1,8—2,1 | 2,1—2,4 | 2,4—2,7 |
|---|---|---|---|---|---|---|---|---|
| $\langle\sigma\rangle$ барн | 4,20 | 3,30 | 2,67 | 2,99 | 3,30 | 3,41 | 3,87 | 3,57 |
| $\langle\sigma^2\rangle^{\frac{1}{2}}$ барн | 5,15 | 3,53 | 2,83 | 3,24 | 3,61 | 3,51 | 4,11 | 3,63 |
| $\left\langle\frac{1}{\sigma}\right\rangle^{-1}$ барн | 2,70 | 2,69 | 2,15 | 2,50 | 2,73 | 3,15 | 3,26 | 3,40 |
| $\left\langle\frac{1}{\sigma^2}\right\rangle^{-\frac{1}{2}}$ барн | 2,23 | 2,33 | 1,91 | 2,30 | 2,55 | 3,01 | 3,06 | 3,37 |
| $\left\langle\frac{1}{\sigma^3}\right\rangle^{-\frac{1}{3}}$ барн | 1,90 | 2,08 | 1,72 | 2,14 | 2,40 | 2,70 | 2,85 | 3,33 |

Таблица IV

**СРЕДНИЕ ХАРАКТЕРИСТИКИ СЕЧЕНИЯ НИКЕЛЯ**

| Энергия, Мэв | 0,3—0,6 | 0,6—0,7 | 0,9—1,0 | 1,2—1,5 | 1,5—1,8 | 1,8—2,1 | 2,1—2,4 | 2,4—2,7 |
|---|---|---|---|---|---|---|---|---|
| $\langle\sigma\rangle$ барн | 4,35 | 3,20 | 3,20 | 3,23 | 2,97 | 2,80 | 3,21 | 3,06 |
| $\langle\sigma^2\rangle^{\frac{1}{2}}$ барн | 5,05 | 3,32 | 3,63 | 3,30 | 2,97 | 2,85 | 3,37 | 3,09 |
| $\left\langle\frac{1}{\sigma}\right\rangle^{-1}$ барн | 3,08 | 2,35 | 2,78 | 3,03 | 2,87 | 2,70 | 2,87 | 2,87 |
| $\left\langle\frac{1}{\sigma^2}\right\rangle^{-\frac{1}{2}}$ барн | 2,68 | 2,03 | 2,35 | 2,88 | 2,79 | 2,60 | 2,74 | 2,79 |
| $\left\langle\frac{1}{\sigma^3}\right\rangle^{-\frac{1}{3}}$ барн | 2,38 | 1,78 | 1,75 | 2,75 | 2,72 | 2,50 | 2,59 | 2,71 |

Таблица V

**СРЕДНИЕ ХАРАКТЕРИСТИКИ СЕЧЕНИЯ МЕДИ**

| Энергия, Мэв | 0,3—0,6 | 0,6—0,9 | 0,9—1,2 | 1,5—1,8 | 1,8—2,1 | 2,1—2,4 |
|---|---|---|---|---|---|---|
| $\langle\sigma\rangle$ барн | 5,32 | 4,18 | 3,52 | 3,20 | 3,02 | 3,18 |
| $\langle\sigma^2\rangle^{\frac{1}{2}}$ барн | 6,50 | 4,43 | 3,62 | 3,21 | 3,02 | 3,26 |
| $\left\langle\frac{1}{\sigma}\right\rangle^{-1}$ барн | 4,03 | 3,68 | 3,31 | 3,04 | 2,98 | 2,91 |
| $\left\langle\frac{1}{\sigma^2}\right\rangle^{-\frac{1}{2}}$ барн | 3,52 | 3,56 | 3,25 | 3,04 | 2,98 | 2,81 |
| $\left\langle\frac{1}{\sigma^3}\right\rangle^{-\frac{1}{3}}$ барн | 3,09 | 3,46 | 3,18 | 2,97 | 2,96 | 2,72 |

Таблица VI

**СРЕДНИЕ ХАРАКТЕРИСТИКИ СЕЧЕНИЯ ЦИРКОНИЯ**

| Энергия, Мэв | 0,3—0,6 | 0,6—0,9 | 0,9—1,2 | 1,2—1,5 | 1,5—1,8 | 1,8—2,1 | 2,1—2,4 | 2,4—2,7 |
|---|---|---|---|---|---|---|---|---|
| $\langle\sigma\rangle$ барн | 9,51 | 7,79 | 7,00 | 7,13 | 5,78 | 5,33 | 5,00 | 5,03 |
| $\langle\sigma^2\rangle^{\frac{1}{2}}$ барн | 9,73 | 7,88 | 7,00 | 7,20 | 5,85 | 5,45 | 5,06 | 5,21 |
| $\left\langle\frac{1}{\sigma}\right\rangle^{-1}$ барн | 8,81 | 7,31 | 7,00 | 6,71 | 5,50 | 4,96 | 4,75 | 4,66 |
| $\left\langle\frac{1}{\sigma^2}\right\rangle^{-\frac{1}{2}}$ барн | 8,43 | 7,01 | 7,00 | 6,66 | 5,42 | 4,83 | 4,68 | 4,53 |
| $\left\langle\frac{1}{\sigma^3}\right\rangle^{-\frac{1}{3}}$ барн | 8,08 | 6,77 | 7,00 | 6,61 | 5,34 | 4,74 | 4,66 | 5,41 |

Таблица VII

**СРЕДНИЕ ХАРАКТЕРИСТИКИ СЕЧЕНИЯ НИОБИЯ**

| Энергия, Мэв | 0,3—0,6 | 0,6—0,9 | 0,9—1,2 | 1,2—1,5 | 1,5—1,8 | 1,8—2,1 | 2,1—2,4 | 2,4—2,7 |
|---|---|---|---|---|---|---|---|---|
| $\langle\sigma\rangle$ барн | 9,14 | 7,48 | 7,08 | 5,86 | 5,94 | 5,57 | 5,09 | 5,05 |
| $\langle\sigma^2\rangle^{\frac{1}{2}}$ барн | 9,28 | 7,48 | 7,23 | 5,86 | 5,94 | 5,70 | 5,09 | 5,24 |
| $\left\langle\frac{1}{\sigma}\right\rangle^{-1}$ барн | 8,23 | 7,48 | 6,29 | 5,86 | 5,75 | 5,11 | 4,67 | 4,63 |
| $\left\langle\frac{1}{\sigma^2}\right\rangle^{-\frac{1}{2}}$ барн | 7,92 | 7,48 | 6,38 | 5,86 | 5,35 | 4,98 | 4,61 | 4,52 |
| $\left\langle\frac{1}{\sigma^3}\right\rangle^{-\frac{1}{3}}$ барн | 7,53 | 7,48 | 6,36 | 5,86 | 5,23 | 4,87 | 4,55 | 4,43 |

Таблица VIII

**СРЕДНИЕ ХАРАКТЕРИСТИКИ СЕЧЕНИЯ СВИНЦА**

| Энергия, Мэв | 0,3—0,6 | 0,6—0,9 | 0,9—1,2 | 1,2—1,5 | 1,5—1,8 | 1,8—2,1 | 2,1—2,4 | 2,4—2,7 |
|---|---|---|---|---|---|---|---|---|
| $\langle\sigma\rangle$ барн | 5,92 | 6,01 | 5,32 | 5,45 | 6,26 | 6,81 | 7,83 | 8,12 |
| $\langle\sigma^2\rangle^{\frac{1}{2}}$ барн | 6,14 | 6,34 | 5,55 | 5,65 | 6,55 | 7,13 | 7,95 | 8,40 |
| $\left\langle\frac{1}{\sigma}\right\rangle^{-1}$ барн | 5,38 | 5,26 | 4,83 | 5,11 | 5,85 | 6,23 | 6,64 | 7,06 |
| $\left\langle\frac{1}{\sigma^2}\right\rangle^{-\frac{1}{2}}$ барн | 5,22 | 4,97 | 4,70 | 5,03 | 5,74 | 6,11 | 6,37 | 6,81 |
| $\left\langle\frac{1}{\sigma^3}\right\rangle^{-\frac{1}{3}}$ барн | 5,07 | 4,42 | 4,56 | 4,99 | 5,62 | 5,99 | 6,31 | 6,56 |

Таблица IX

**СРЕДНИЕ ХАРАКТЕРИСТИКИ СЕЧЕНИЯ ВИСМУТА**

| Энергия, Мэв | 0,3—0,6 | 0,6—0,9 | 0,9—1,2 | 1,2—1,5 | 1,5—1,8 | 1,8—2,1 | 2,1—2,4 | 2,4—2,7 |
|---|---|---|---|---|---|---|---|---|
| $\langle\sigma\rangle$ барн | 6,80 | 6,27 | 5,38 | 5,22 | 6,92 | 7,54 | 8,33 | 8,47 |
| $\langle\sigma^2\rangle^{\frac{1}{2}}$ барн | 7,18 | 6,60 | 5,45 | 5,38 | 7,55 | 7,95 | 8,68 | 8,90 |
| $\left\langle\frac{1}{\sigma}\right\rangle^{-1}$ барн | 6,56 | 5,27 | 5,07 | 5,14 | 5,62 | 6,17 | 7,58 | 7,70 |
| $\left\langle\frac{1}{\sigma^2}\right\rangle^{-\frac{1}{2}}$ барн | 6,38 | 5,17 | 5,00 | 5,07 | 5,50 | 5,20 | 7,24 | 7,47 |
| $\left\langle\frac{1}{\sigma^3}\right\rangle^{-\frac{1}{3}}$ барн | 5,98 | 5,08 | 4,94 | 4,99 | 5,40 | 4,57 | 7,00 | 7,29 |

Таблица X

**СРЕДНИЕ ХАРАКТЕРИСТИКИ СЕЧЕНИЯ ТОРИЯ**

| Энергия, Мэв | 0,3—0,6 | 0,6—0,9 | 0,9—1,2 | 1,2—1,5 | 1,5—1,8 | 1,8—2,1 | 2,1—2,4 |
|---|---|---|---|---|---|---|---|
| $\langle\sigma\rangle$ барн | 8,25 | 7,72 | 6,91 | 6,72 | 7,27 | 7,47 | 7,52 |
| $\langle\sigma^2\rangle^{\frac{1}{2}}$ барн | 8,25 | 7,72 | 6,91 | 6,72 | 7,27 | 7,47 | 7,52 |
| $\left\langle\frac{1}{\sigma}\right\rangle^{-1}$ барн | 8,25 | 7,72 | 6,91 | 6,72 | 7,27 | 7,47 | 7,52 |
| $\left\langle\frac{1}{\sigma^2}\right\rangle^{-\frac{1}{2}}$ барн | 8,25 | 7,72 | 6,91 | 6,72 | 7,27 | 7,47 | 7,52 |
| $\left\langle\frac{1}{\sigma^3}\right\rangle^{-\frac{1}{3}}$ барн | 8,25 | 7,72 | 6,91 | 6,72 | 7,27 | 7,47 | 7,52 |

Таблица XI

**СРЕДНИЕ ХАРАКТЕРИСТИКИ СЕЧЕНИЯ МОЛИБДЕНА**

| Энергия, Мэв | 0,3—0,6 | 0,6—0,9 | 0,9—1,2 | 1,2—1,5 | 1,6—1,9 | 1,9—2,2 | 2,2—2,5 | 2,6—2,9 |
|---|---|---|---|---|---|---|---|---|
| $\langle\sigma\rangle$ барн | 8,52 | 7,80 | 6,22 | 5,61 | 5,02 | 4,77 | 4,57 | 4,25 |
| $\langle\sigma^2\rangle^{\frac{1}{2}}$ барн | 8,50 | 7,80 | 6,22 | 5,61 | 5,02 | 4,77 | 4,57 | 4,25 |
| $\left\langle\frac{1}{\sigma}\right\rangle^{-1}$ барн | 8,50 | 7,80 | 6,22 | 5,61 | 5,02 | 4,77 | 4,57 | 4,25 |
| $\left\langle\frac{1}{\sigma^2}\right\rangle^{-\frac{1}{2}}$ барн | 8,50 | 7,80 | 6,22 | 5,61 | 5,02 | 4,77 | 4,57 | 4,25 |
| $\left\langle\frac{1}{\sigma^3}\right\rangle^{-\frac{1}{3}}$ барн | 8,50 | 7,80 | 6,22 | 5,61 | 5,02 | 4,77 | 4,57 | 4,25 |

## ЛИТЕРАТУРА

[1] ГОРДЕЕВ, И. В., КАРДАШЕВ, Д. А., МАЛЫШЕВ, А. В. Справочник по ядерно-физическим константам для расчета реакторов. Москва, Атомиздат, 1960.
[2] ЛЕВЕНШТЕЙН, В. и ОКРЕНТ, Д. Основные положения физики энергетических реакторов на быстрых нейтронах. Материалы 2-ой Международной конференции по мирному использованию атомной энергии, том 3 стр. 261, Москва, изд-во Главатома, 1959.
[3] ГОРДЕЕВ, И. В., ОРЛОВ, В. В., СЕДЕЛЬНИКОВ, Г. Х. *Атомная энергия* **9** (1957) 252.
[4] ROACH, W., *Nucl. Sci. and Engng* 8 (1960) 621.
[5] ЛЕЙПУНСКИЙ, А. И. и др. *Атомная энергия* **9** (1958) 277.
[6] ЛУКЬЯНОВ, А. А. и ОРЛОВ, В. В. *Атомная энергия* (в печати).
[7] Д., ЮЗ, ШВАРЦ, Р. Атлас нейтронных сечений. Атомиздат, 1959.

# ANGULAR DISTRIBUTIONS OF FAST NEUTRONS SCATTERED BY Al, Si, P, S, AND Zn

K. Tsukada, S. Tanaka, M. Maruyama and Y. Tomita
Japan Atomic Energy Research Institute, Tokai-mura, Japan

**Abstract — Résumé — Аннотация — Resumen**

**Angular distributions of fast neutrons scattered by Al, Si, P, S and Zn.** Differential scattering cross-sections of Al, Si, P, S and Zn for fast neutrons have been measured in an energy range of 3.4 to 4.6 MeV by using the time-of-flight method. Angular distributions of the inelastically scattered neutrons are nearly isotropic in all cases. These results are discussed on the basis of the Hauser-Feshbach theory.

**Distributions angulaires des neutrons rapides diffusés par Al, Si, P, S et Zn.** Les sections efficaces différentielles de diffusion de Al, Si, P, S et Zn pour des neutrons rapides ont été mesurées dans la gamme d'énergies de 3,4 à 4,6 MeV, en employant la méthode du temps de vol. Les distributions angulaires des neutrons diffusés inélastiquement sont presque isotropes dans tous les cas. Les auteurs analysent ces résultats en se fondant sur la théorie de Hauser-Feshbach.

**Условия распределения быстрых нейтронов, рассеянных алюминием, кремнием, фосфором и цинком.** Дифференциальное сечение рассеяния алюминия, кремния, фосфора, серы и цинка для быстрых нейтронов измерено в диапазоне энергии от 3,4 до 4,6 Мегаэлектронвольт использованием метода времени пролета. Угловые распределения неупруго рассеянных нейтронов являются почти во всех случаях изотропными. Эти результаты обсуждаются на основе теории Хаузера-Фешбаха.

**Distribuciones angulares de neutrones rápidos dispersados por Al, Si, P, S y Zn.** Los autores han medido por el método del tiempo de vuelo las secciones eficaces diferenciales de dispersión del Al, Si, P, S y Zn para neutrones rápidos de energía comprendida entre 3,4 y 4,6 MeV. Las distribuciones angulares de los neutrones dispersados inelásticamente son casi isotrópicas en todos los casos. Los autores analizan los resultados obtenidos basándose en la teoría de Hauser-Feshbach.

## Introduction

The angular distribution of inelastically scattered neutrons is one of the most important clues to the clarification of the mechanism of nuclear reactions in the low-energy region. The compound-nucleus process, direct process and a combination of these two have been introduced for this purpose with fair success. But there are still many problems to be solved. One of these is the fluctuation [1] in the cross-sections which accompanies the variation of the energy of the incident particles.

In a programme of the study [2] of the fast-neutron elastic and inelastic scattering by the time-of-flight method, cross-sections of Al, Si, P, S, Ti, Fe, Zn and Se have been measured for the neutrons of 3.5 to 4.8 MeV. Results for Ti, Fe, Zn, and Se have already been discussed in paper I in [2]. In this paper the differential inelastic scattering cross-sections of Al, Si, P, S and Zn are compared

with results calculated by using the HAUSER-FESHBACH formula [3]. Fluctuations were observed in these angular distributions with variation of the energy of incident neutrons, and correlations between these fluctuations and those in the neutron total cross-sections [4] are pointed out.

The reasons for the choice of those elements which are discussed in this paper are as follows:

(*a*) Low-lying levels of these elements can be resolved by the time-of-flight method;
(*b*) The statistical assumption [3] in the compound-nucleus process is satisfied to a rough approximation;
(*c*) Calculations [5] with the optical potential of the surface-absorption type suggest that there is no resonance of any partial wave in this mass region for the neutrons of 3.5 to 4.8 MeV. Therefore, the angular distribution of the inelastically scattered neutrons is expected to be asymmetric about 90°, if the direct process predominates over the compound-nucleus process;
(*d*) Al, Si, P and S belong to the rotational region, in which the direct process is expected [6] to contribute to the inelastic scattering even at low energies.

## 1. Experimental

Neutrons were generated from the D (d, n) $He^3$ reaction by using a 2-MV Van de Graaff accelerator, and the spectra of the scattered neutrons were measured by the pulsed-beam time-of-flight method [2, 7]. The experimental arrangement and the block diagram of the time-of-flight spectrometer are shown in Figs. 1 and 2. The yield of neutrons at the target was monitored by a current integrator which was arranged so as to measure the deuteron beam entering the gas target. The spreads in the neutron energy were 250 and 150 keV at 3.5 and 4.8 MeV, respectively. The angular resolution of the apparatus was $\pm 7°$. The time-resolution, which was determined from the half-width of the peak for the gamma-rays in the time spectrum, was 7.2 ns. An example of the time spectrum is shown in Fig. 3. The efficiency of the detector was determined by using the data [8]

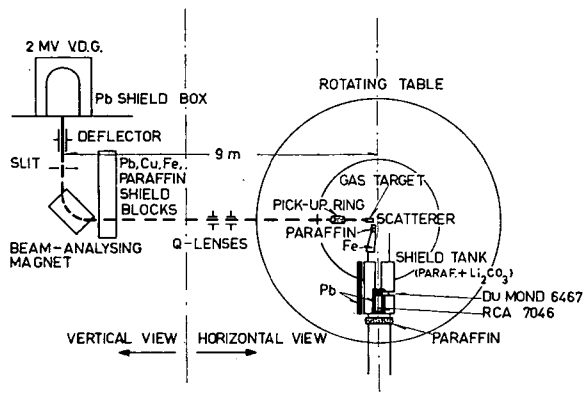


Fig. 1
Schematic diagram of the experimental arrangement

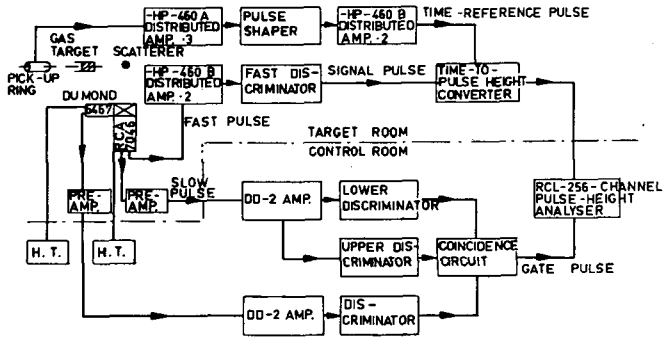


Fig. 2
Block diagram of the time-of-flight spectrometer for fast neutrons.

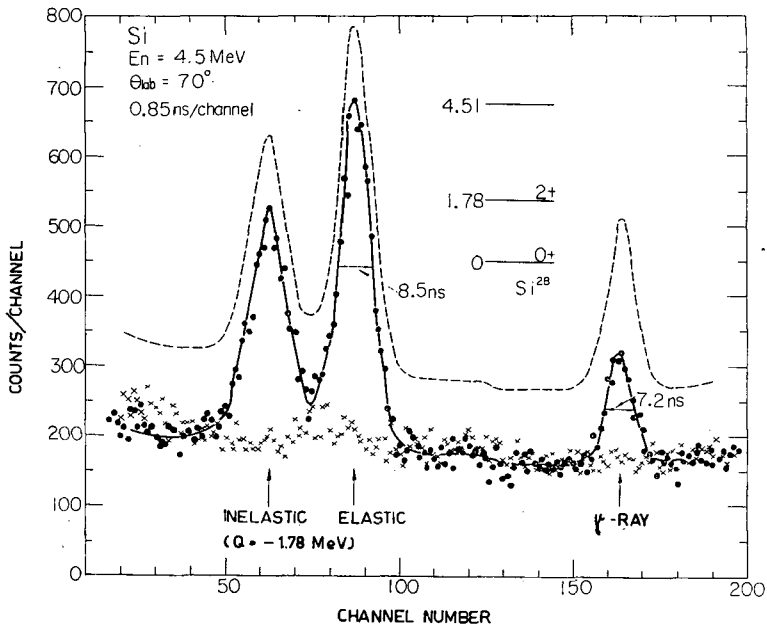


Fig. 3
Time spectrum showing the scattering of 4.5-MeV neutrons by Si.

of the yield of neutrons from the D (d, n) $He^3$ and T (p, n) $He^3$ reactions as a function of the energy.

## 2. Results

Some of the elastic scattering cross-sections observed are shown in Figs. 4, 5 and 6 together with data published by other authors [9, 10, 11]. Corrections for the multiple scattering are estimated to be small and not applied in the present results.

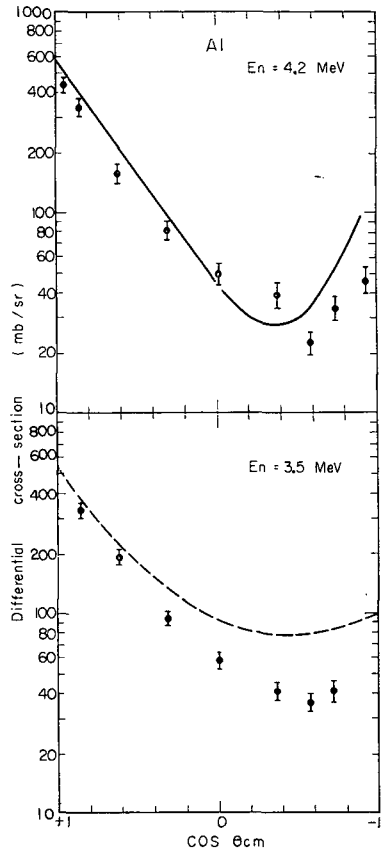


Fig. 4
Angular distributions for the elastic scattering of neutrons by Al at incident energies of 4.2 and 3.5 MeV. The solid curve shows data given by Walt and Beyster (in [9]) at an incident energy of 4.1 MeV, and the dashed curve shows data of Snowdon *et al.* (see [10]) at an incident energy of 3.7 MeV.

The angular distributions of those inelastically scattered neutrons which lead to the low-lying levels of Al, Si, P, S and Zn are shown in Figs. 7 to 11. Errors shown in these figures are the sum of the following: the statistical error, error due to subtraction of the background, error due to peeling-off of the individual peaks in the time spectrum, error in the estimation of the detector efficiency ($\pm 7\%$), and error in the cross-section [8] for the D (d, n) $He^3$ reaction ($\pm 3\%$).

Results calculated by using the Hauser-Feshbach formula are also shown in Figs. 7 to 11. In these calculations, a statistical assumption [3] for the levels of the compound nuclei is adopted, and the contributions from the higher levels of the residual nuclei, the spins and parities of which are not known, and those from the (n, p) and (n, $\alpha$) reactions are neglected, and penetration factors calculated by BEYSTER *et al.* [12] are used. For Zn, the cross-sections were calculated

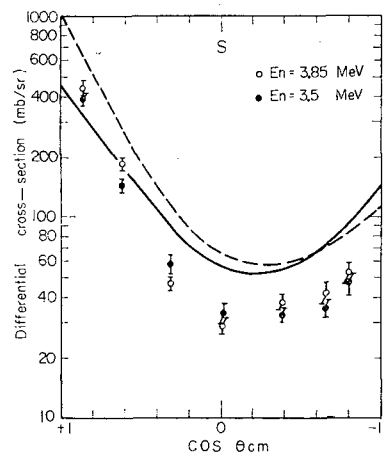


Fig. 5
Angular distributions for the elastic scattering of neutrons by S at incident energies of 3.5 MeV and 3.85 MeV. The solid and dashed curves show data of Snowdon *et al.* and those of Morgan (see [11]) respectively, at an incident energy of 3.7 MeV.

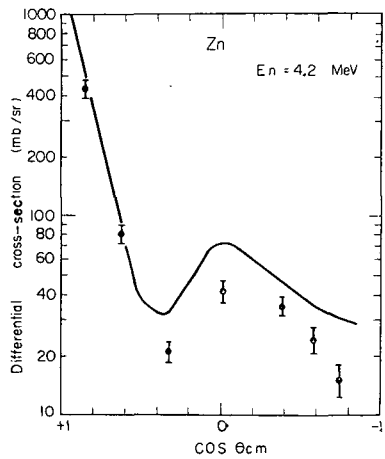


Fig. 6
Angular distribution for the elastic scattering of neutrons by Zn at incident energy of 4.2 MeV. The solid curve shows data given by Walt and Beyster (see [9]) at an incident energy of 4.1 MeV.

with a formula [2] which was modified from the Hauser-Feshbach formula so as to be used without detailed knowledge about the levels of high excitation.

The cross-sections of elastic scattering ($\sigma_e$), those of inelastic scattering ($\sigma_i$) and the sum of $\sigma_e$ and $\sigma_i$, which are obtained by integrating the observed differential cross-sections, are shown in Figs. 12 to 16. The neutron total cross-

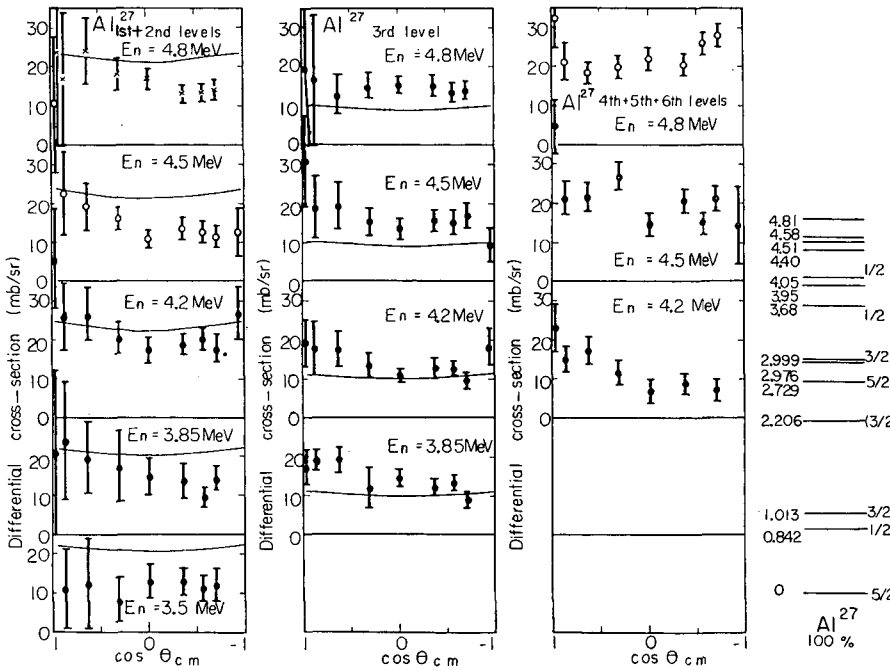


Fig. 7
Angular distributions for the inelastic scattering of neutrons leading to the low-lying levels in $Al^{27}$ at incident energies of 3.5, 3.85, 4.2, 4.5 and 4.8 MeV. The solid curves show the angular distributions calculated by using the Hauser-Feshbach formula.

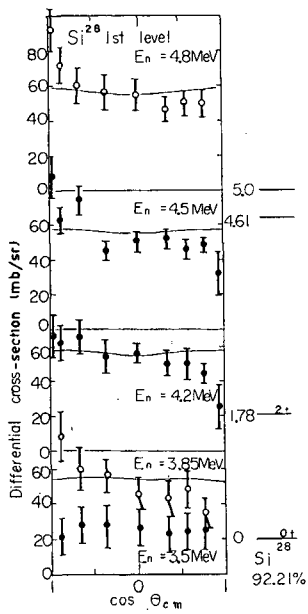


Fig. 8
Angular distributions for the inelastic scattering of neutrons leading to the 1st level in $Si^{28}$ at incident energies of 3.5, 3.85, 4.2, 5.5 and 4.8 MeV. The solid curves show the angular distributions calculated by using the Hauser-Feshbach formula.

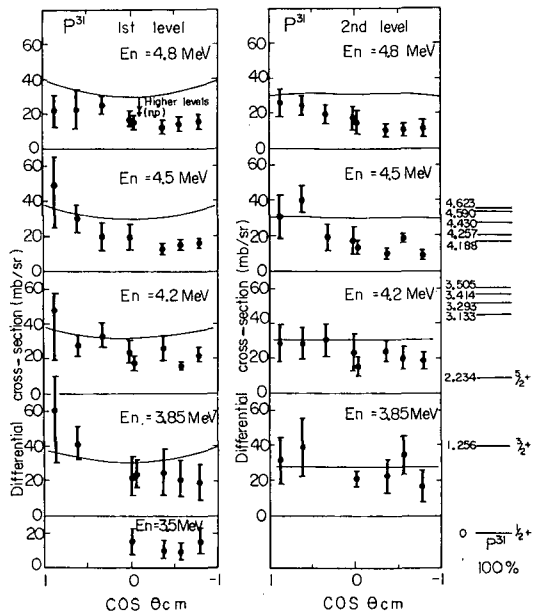


Fig. 9

Angular distributions for the inelastic scattering of neutrons leading to the 1st and 2nd levels in $P^{31}$ at incident energies of 3.5, 3.85, 4.2, 4.5 and 4.8 MeV. The solid curves show the angular distributions calculated by using the Hauser-Feshbach formula and the arrows show the reduction in the cross-section due to the contributions of the higher levels and (n, p) reaction.

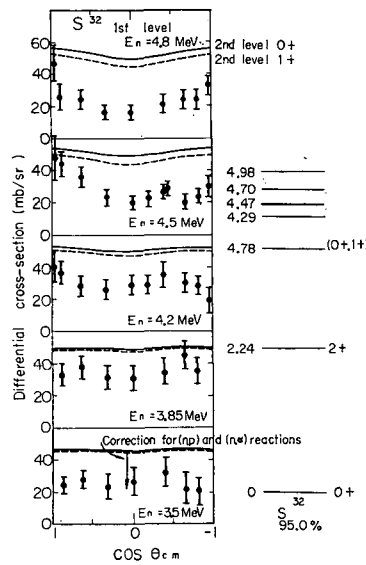


Fig. 10

Angular distributions for the inelastic scattering of neutrons leading to the 1st level in $S^{32}$ at incident energies of 3.5, 3.85, 4.2, 4.5 and 4.8 MeV. The solid or dashed curves show the angular distributions calculated by using the Hauser-Feshbach formula on the assumption that the spin and parity of the 2nd level are 0+ or 1+. The arrow shows the reduction in the cross-section due to the contribution of (n, p) and (n, α) reactions.

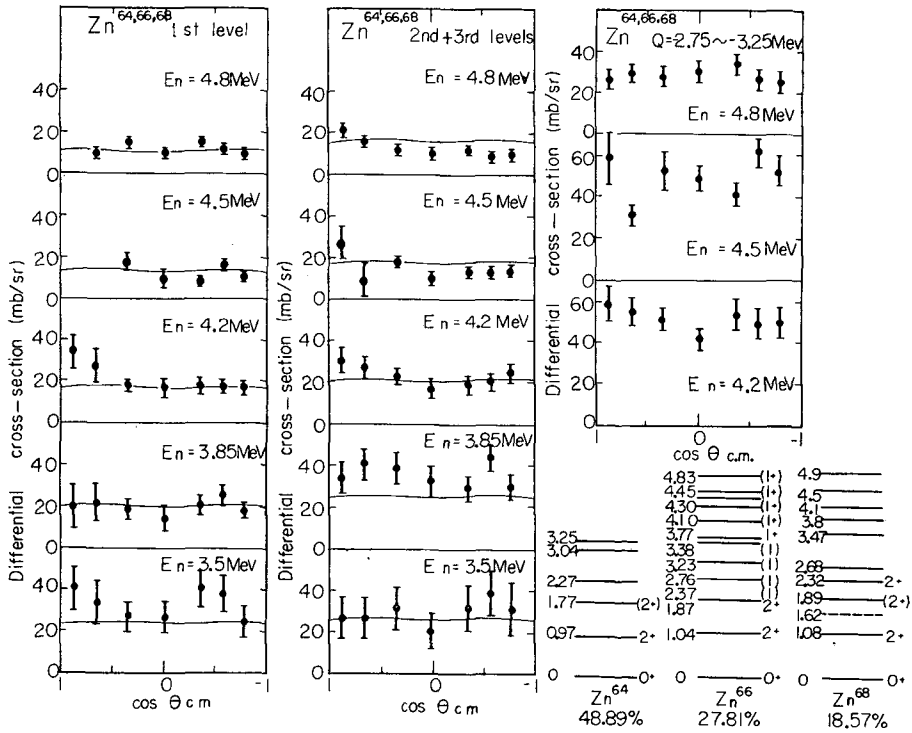


Fig. 11
Angular distributions for the inelastic scattering of neutrons leading to the low-lying levels in $Zn^{64}$, $Zn^{66}$ and $Zn^{68}$ at incident energies of 3.5, 3.85, 4.2, 4.5 and 4.8 MeV. The solid curves show the angular distributions calculated by using the formula (see [4]) modified from the Hauser-Feshbach formula and normalized to the angular distribution for the 1st level observed at an incident energy of 4.8 MeV.

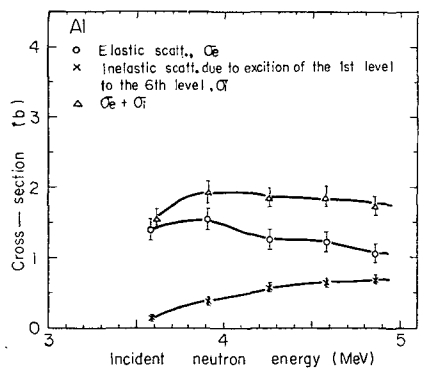


Fig. 12
Cross-sections obtained by integrating the observed differential cross-sections for the elastic and inelastic scattering of neutrons by Al and the sum of these cross-sections.

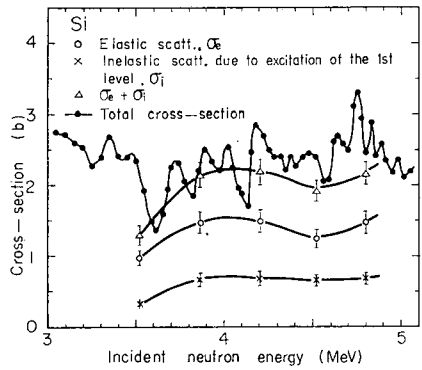


Fig. 13
Cross-sections obtained by integrating the observed differential cross-sections for the elastic and inelastic scattering of neutrons by Si. The sum of these cross-sections is compared with the neutron total cross-section (see [3]).

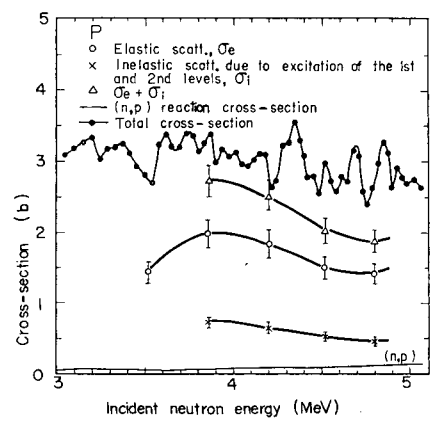


Fig. 14
Cross-sections obtained by integrating the observed differential cross-sections for the elastic and inelastic scattering of neutrons by P. The sum of these cross-sections, together with (n, p) reaction cross-sections (from BNL-325), is also shown for the purpose of comparison with the neutron total cross-section (see [3]).

sections [4], which were measured with an energy resolution and accuracy of $\pm 15$ keV and $\pm 3\%$ respectively, are also shown in Figs. 13 to 15. Agreement between the neutron total cross-sections and the sum of the elastic and inelastic scattering cross-sections would be fairly good, if the cross-sections of the (n, p), (n, $\alpha$) reaction [13] and the inelastic scattering leading to the higher levels of the residual nuclei were taken into account.

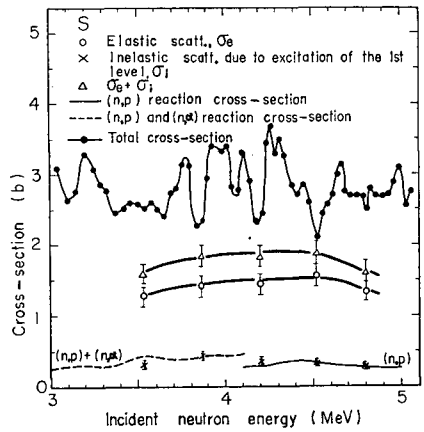


Fig. 15
Cross-sections obtained by integrating the observed differential cross-sections for the elastic and inelastic scattering of neutrons by S. The sum of these cross-sections, together with (n, p) and (n, α) reaction cross-sections (from BNL 325), is also shown for the purpose of comparison with the neutron total cross-section (see [3]).

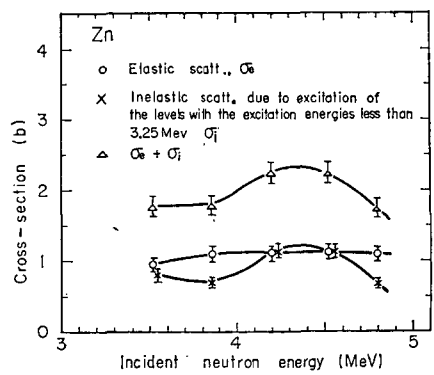


Fig. 16
Cross-sections obtained by integrating the observed differential cross-sections for the elastic and inelastic scattering of neutrons by Zn and the sum of these cross-sections.

## 3. Discussion

The angular distributions observed are nearly isotropic or symmetric about 90 degrees as shown in Figs. 7 to 11, though there is a slight indication of a forward peak in the case of Si. The results of the calculations of the Hauser-Feshbach formula are also nearly isotropic. Absolute values of the observed results for Si agree well with the calculated ones, but for the other elements the observed results are smaller than the calculated ones. This discrepancy between the observed and calculated results will be due to the neglection of some channels done in the course of the calculation of the Hauser-Feshbach formula, i.e. the

(n, p) and (n, $\alpha$) reactions and the inelastic scattering leading to the higher levels. In the case of Zn, the calculated value of the inelastic scattering cross-section leading to the first level of the residual nucleus is normalized to the observed value at 4.8 MeV in Fig. 11. The agreement between the observed and calculated results is fairly good, not only for the scattering to the first level, but also for scatterings leading to other levels in the whole energy range.

It may be concluded from these results together with those of paper I [2] that the compound-nucleus process is a predominant mechanism in the energy range of 3 to 5 MeV and in the mass region of Al to S and Ti to Zn.

The detailed patterns of the angular distributions of the inelastically scattered neutrons are rather complicated: the patterns show fluctuations with variation of the incident-neutron energy. On the other hand, as seen in Figs. 13 to 15, the neutron total cross-sections of Si, P and S fluctuate with a period of 100 keV [4]*. These fluctuations will be related with those in the angular distributions of the inelastic scattering, because only two or three peaks of the fluctuation of the total cross-sections are covered by the energy-resolution of the spectrometer.

## ACKNOWLEDGEMENTS

The authors would like to express their appreciation to Dr. T. Momota for his invaluable help and advice. The authors are greatly indebted to Mr. Kobayashi and Mr. Y. Sato for operation and maintenance of the Van de Graaff accelerator and to Dr. A. Sugie and Dr. K. Harada for discussions of the results.

## REFERENCES

[1] ODA, Y., *et al.*, *J. phys. Soc. Japan* **15** (1960) 51.
[2] TSUKADA, K., TANAKA, S. and MARUYAMA, M., *J. phys. Soc. Japan* **16** (1961) 166.
[3] HAUSER, W. and FESHBACH, H., *Phys. Rev.* **87** (1957) 366.
[4] TSUKADA, K. and TANAKA, O., to be published.
[5] HARADA, K., SUGIE, A., IMAI, H. and MORIGUCHI, K., JAERI-1008, in Japanese.
[6] UI, H., *Progr. theor. Phys. (Osaka)* **18** (1957) 163.
[7] WEBER, W., JOHNSTONE, C. and CRANBERG, L., *Rev. sci. Instrum.* **27** (1956) 166.
[8] MARION, J. B. and FOWLER, J. L., Fast neutron physics, **1**, Interscience, New York (1960).
[9] WALT, M. and BEYSTER, J. R., *Phys. Rev.* **98** (1955) 677.
[10] WHITEHEAD, W. D. and SNOWDON, S. C., *Phys. Rev.* **92** (1953) 114.
[11] MACHWE, M. K., KENT, D. W. Jr., and SNOWDON, S. C., *Phys. Rev.* **114** (1959) 1563; HUGHES, D. J. and CARTER, R. S., BNL-400.
[12] BEYSTER, J. R., SCHRANDT, R. G., WALT, M. and SALMI, E. W., LA-2009.
[13] HUGHES, D. J. and SCHWARTZ, R. B., BNL-325.
[14] ERICSON, T., *Nucl. Phys.* **11** (1959) 481.
[15] HIBDON, C. T., *Phys. Rev.* **114** (1959) 179.

* These peaks of the fluctuation of the total cross-sections do not correspond to individual levels of the compound nuclei, because the level spacings of the compound nuclei of these elements are estimated to be a few keV or less [14, 15]. There is no difference between the patterns of the fluctuation of an odd-odd nucleus ($P^{32}$) and those of even-odd nuclei ($Si^{29}$ and $S^{33}$), though the effective excitation energy of the former is higher than those of the latter by 1 MeV. In this estimation, a pairing energy [14] for the even-odd nucleus is taken into account in addition to the binding energy.

# NEUTRON INELASTIC SCATTERING BY SODIUM-23

J. H. TOWLE AND W. B. GILBOY
ATOMIC WEAPONS RESEARCH ESTABLISHMENT, ALDERMASTON, UNITED KINGDOM

**Abstract — Résumé — Аннотация — Resumen**

**Neutron inelastic scattering by sodium-23.** A programme of measurements of the neutron scattering cross-sections of materials of importance in fast reactors for neutrons of energies up to 4 MeV is in progress at AWRE. The time-of-flight technique is used. In this paper detailed results are presented for Na up to 2 MeV, together with some provisional results at 3.97 MeV.

Differential cross-sections have been measured for the elastic and inelastic scattering of 1.5-MeV neutrons by $Na^{23}$. The results were corrected for multiple scattering and other effects due to the finite size of the $Na^{23}$ metal sample, using a new Monte Carlo computer programme. The sum of the integrated cross-sections is in agreement with the total cross-section measured by transmission with the same apparatus.

The variation of the cross-section for inelastic scattering was obtained over the incident neutron energy range 0.5 to 2.0 MeV by measuring the yield of 0.44-MeV $\gamma$-rays at an angle of 125° to the incident neutron flux. At this angle the $\gamma$-ray yield is proportional to the tottal inelastic cross-section for an angular distribution of the form $1 + A\,P_2(\cos\theta)$ which is expected for this transition. The angular distribution of $\gamma$-rays was found experimentally to be $1 + 0.14\,P_2$ with 1.5-MeV incident neutrons. The inelastic cross-section curve was normalized at 1.5 MeV to the value obtained by observing the neutrons. The overall errors on the points are $\pm 6\%$.

**Diffusion inélastique des neutrons par le sodium-23.** Le Centre d'Aldermaston poursuit l'exécution d'un programme de mesures des sections efficaces de diffusion des neutrons (dont l'énergie peut atteindre 4 MeV) pour des matières ayant une grande importance dans les réacteurs à neutrons rapides. Les mesures sont faites d'après la méthode du temps de vol. Les auteurs du mémoire donnent le détail des résultats obtenus pour le sodium avec des énergies allant jusqu'à 2 MeV, ainsi que les résultats provisoires obtenus à 3,97 MeV.

On a mesuré les sections efficaces différentielles de diffusion élastique et inélastique par $^{23}Na$ de neutrons de 1,5 MeV. On a corrigé les résultats, d'après une nouvelle méthode de Monte-Carlo, pour tenir compte de la diffusion multiple et des autres effets dus aux dimensions finies de l'échantillon de $^{23}Na$ métal. La somme des sections efficaces intégrées correspond bien à la section efficace totale mesurée par transmission avec le même appareil.

La variation de la section efficace de diffusion inélastique a été obtenue, dans la gamme d'énergie des neutrons incidents comprises entre 0,5 et 2 MeV, en mesurant l'intensité des rayons gamma de 0,44 MeV émis sous un angle de 125° par rapport au faisceau des neutrons incidents. L'intensité des rayons gamma émis sous cet angle est proportionnelle à la section efficace totale de diffusion inélastique pour une distribution angulaire de la forme: $1 + A\,P_2\,(\cos\theta)$, qui est prévue dans ce cas. Les expériences ont montré que la distribution angulaire des rayons gamma était de $1 + 0{,}14\,P_2$, avec des neutrons incidents de 1,5 MeV. La courbe de section efficace de diffusion inélastique a été normalisée, pour 1,5 MeV, d'après la valeur obtenue en observant les neutrons; les écarts des points à la courbe sont de l'ordre de $\pm 6\%$.

**Неупругое рассеяние нейтронов натрием-23.** В Научно-исследовательском центре по разработке атомного оружия выполняется программа измерений сечения рассеяния нейтро-

нов с энергией до 4 Мэв для материалов, имеющих значение для реакторов на быстрых нейтронах. При этом используется метод времени пролета. В настоящем докладе подробно излагаются результаты, полученные для рассеяния нейтронов с энергией до 2 Мэв ядрами натрия совместно с некоторыми предварительными результатами при 3,97 Мэв.

Были измерены дифференциальные сечения для упругого и неупругого рассеяния натрием-23 нейтронов с энергией в 1,5 Мэв. Результаты были исправлены для многократного рассеяния и других эффектов, объясняющихся ограниченным размером образца металлического натрия-23, с использованием вычислительного метода Монте Карло. Сумма интегральных сечений согласуется с общим сечением, измеренным пропусканием при помощи той же аппаратуры.

Вариация сечения для неупругого рассеяния была получена для диапазона энергий бомбардирующих нейтронов от 0,5 до 2,0 Мэв путем измерения выхода гамма-лучей с энергией в 0,44 Мэв при угле в 125° к потоку бомбардирующих нейтронов. При этом угле выход гамма-лучей пропорционален общему сечению неупругого процесса для углового распределения вида $1 \div AP_2$ (Cos Q), которое предполагается для этого перехода. Экспериментальным путем было найдено, что угловое распределение гамма-лучей равняется $1 \div 0{,}14\ P_2$ при бомбардирующих нейтронах с энергией в 1,5 Мэв. Кривая сечения неупругого процесса была приведена при 1,5 Мэв к значению, полученному из опытов с нейтронами. Общие погрешности в сравниваемых точках равняются $\div 6 \div\div$.

**Dispersión inelástica de neutrones en el sodio-23.** En el Atomic Weapons Research Establishment se está llevando a cado un programa de mediciones de las secciones eficaces de dispersión neutrónica de sustancias de interés para la construcción de reactores rápidos. La energía máxima de los neutrones utilizados con arreglo al método del tiempo de vuelo es del orden de los 4 MeV. En la memoria se recogen detalladamente los resultados obtenidos para el Na con energías de hasta 2 MeV y algunos resultados provisionales obtenidos con energías de 3,97 MeV.

Se han medido las secciones eficaces diferenciales correspondientes a la dispersión elástica e inelástica de neutrones de 1,5 MeV en el $^{23}$Na. Los resultados obtenidos se han corregido para tener en cuenta la dispersión múltiple y otros efectos derivados del tamaño finito de la muestra metálica de $^{23}$Na, utilizando un nuevo programa de cómputo de Monte Carlo. La suma de las secciones eficaces integradas coincide con la sección eficaz total medida por transmisión con el mismo aparato.

Se evaluó también la variación de la sección eficaz de dispersión inelástica para los neutrones incidentes de energía comprendida entre 0,5 y 2,0 MeV, midiendo la intensidad de los rayos $\gamma$ de 0,44 MeV emitidos en un ángulo de 125° respecto del haz de neutrones incidentes. En dicho ángulo, la intensidad de los rayos $\gamma$ es proporcional a la sección eficaz total de dispersión inelástica para una distribución angular de la forma: $1 + A\ P_2\ (\cos\theta)$, que es de esperar para esta transición. Se comprobó experimentalmente que la distribución angular de los rayos $\gamma$ viene dada por la expresión $1 + 0{,}14\ P_2$ cuando la energía de los neutrones incidentes es de 1,5 MeV. La curva de la sección eficaz correspondiente a la dispersión inelástica se normalizó al nivel de 1,5 MeV en función del valor obtenido por observación del comportamiento de los neutrones. El margen de error de sus diversos puntos es del orden de $\pm$ 6 por ciento.

## Introduction

Accurate data on the scattering of fast neutrons by $Na^{23}$, and on the inelastic process in particular, is required for the design of fast reactors using liquid Na as coolant. This element has received first priority in the programme of measurements of the scattering cross-sections of important fast-reactor materials now in progress at Aldermaston. In this paper we present the inelastic cross-section from threshold to 2 MeV, the differential cross-sections for elastic and inelastic scatter-

ing of 1.5-MeV neutrons, and the angular distribution of 0.44-MeV gamma-rays, at 1.5 MeV neutron energy, together with preliminary results on the inelastic cross-section at 3.97 MeV.

Very little relevant data has been obtained previously for $Na^{23}$. The differential cross-section for the total scattering of neutrons has been measured from 0.05 to 1.40 MeV by LANGSDORF *et al.* [1], but no differentiation was made between elastic and inelastic events. From observations of the 0.44-MeV gamma-ray with a NaI-detector in ring scattering geometry, FREEMAN *et al.* [2] have measured the inelastic cross-section from threshold to 1.4 MeV with an overall accuracy of $\pm 20\%$. For the measurements to be of the fullest use, an accuracy of $\pm 5\%$ on the inelastic cross-section is desirable.

## 1. Time-of-flight spectrometer

The basic details of the T.O.F. spectrometer have been described previously by BATCHELOR and TOWLE [3]. Since then the apparatus has been improved by the introduction of a large and versatile detector shield, and by the application of pulse-shape discrimination against gamma-rays. These facilities have led to large reductions in background at neutron energies of several MeV. The detector rests in a collimating channel in the centre of the main body of the shield, which is a cylindrical tank of water of 1.2 m diameter and 1.2 m height. The shield is extended in the direction towards the scattering sample by means of three sections of truncated cone each filled with water. The length of the cone may thus be suited to the shielding and flight-path requirements. A flight-path of 1.7 m was used in the present measurements. Further attenuation of neutrons leaving the source in the direction of the counter is achieved with a 30-cm-long Cu bar which is adjusted to suit the scattering angle. The detector is a liquid scintillator, type NE-213, viewed by two RCA-6810A photomultipliers operated in coincidence. Full details of the detector and electronics and an account of the gamma-ray discriminator have been given by BATCHELOR *et al.* [4].

Neutrons are produced by proton-bombardment of a cell 2.5-cm-long filled to 760 mm Hg pressure with tritium, and the scatter is placed 11 cm away at 0° to the proton direction. The total energy spread of 1.5-MeV neutrons incident on the sample, due to target thickness and the energy-angle variation, is about 0.08 MeV.

The Na-scatterer was made by filling a light aluminium can with pure sodium under an argon atmosphere. An analysis of a sample of the sodium used indicated an impurity content (chiefly oxygen) of not greater than 0.5%. The can was cylindrical, 4.5 cm in diameter, 5 cm in length, and with a wall thickness of 0.040 cm. Four polythene scatterers were made for comparison measurements. These were 5.0 cm long with an inner dimension of 0.48 cm; the outer dimensions were 0.591, 0.682, 0.884 and 1.082 cm. A quantitative chemical analysis of a sample of the polythene used gave a hydrogen content of $(14.35 \pm 0.01)\%$ which differs only slightly from the theoretical value of 14.37% for $(CH_2)_n$.

## 2. Experimental procedure

### DIFFERENTIAL CROSS-SECTIONS

The differential cross-sections were measured at 12 angles from 30° to 137°. At each angle, runs were made with the Na scatterer and, for an equal number of counts in a long counter-monitor, with a duplicate empty can. The time-of-flight

spectrum due to scattering from Na was then obtained from a channel-by-channel subtraction of the two spectra recorded.

In order to establish the cross-sections relative to the n-p cross-section, runs with the polythene samples were made at an angle of 40°. The several sample sizes were used in order to check on the consistency of a neutron-attenuation correction which has been applied in the manner described by CRANBERG [5]. Allowance has also been made for the non-parallel paths of the incident neutrons, the angular distribution of the source neutrons being obtained experimentally. The corrected yield of neutrons scattered from hydrogen was obtained to $\pm 1\%$ accuracy.

Corrections have been applied to the data to account for the finite size of the Na sample, using two efficient new Monte Carlo programmes written at Aldermaston by PARKER *et al.* [6]. One of these calculates the flux-attenuation factor, and a correction for multiple scattering to the ratio $\sigma_{in}/\sigma_{el}$. The other programme corrects the shape of the differential elastic cross-section for the effect of multiple scattering and for the finite angular resolution ($\pm 11°$) of the source-sample system. The input cross-sections for the Monte Carlo were estimated true microscopic data, obtained by applying rough corrections to the experimental results. The output from the first Monte Carlo run was then used to prepare more accurate input data for a second run. In this second Monte Carlo run the experimental scattering process was very closely simulated, and further iterations of the programmes were not necessary.

The variation with neutron energy of the detector-efficiency was measured in a subsidiary experiment, by comparison with a calibrated long counter.

EXCITATION CURVE

To obtain the excitation curve for inelastic scattering, the yield of 0.44-MeV gamma-rays was measured at an angle of 125° to the incident flux. At this angle (or its supplement) the differential cross-section is equal to $(4\pi)^{-1}$ times the integrated cross-section for an angular distribution of the form $W(\theta) = 1 + A P_2 (\cos\theta)$, which holds for a pure dipole transition. The 0.44-MeV transitions are predominantly M1 with a very small admixture of E2 transitions, the ratio of probabilities E2/M1 being $0.003 \pm 0.001$ (RASMUSSEN *et al.* [7] and BERENBAUM *et al.* [8]), and $W(\theta)$ may be taken to have the above form.

The relative gamma-ray intensity was obtained from time-spectra recorded at each energy with the pulse-shape discrimination circuit rendered inoperative.

After subtracting the spectra obtained with Na-filled and empty cans, the gamma-ray peak represented the 0.44-MeV gamma-rays detected. To relate the gamma-ray yield to the incident neutron flux it was necessary to measure the flux leaving the source at 0° by means of a long counter placed 1.3 m away. This measurement was made with the sample removed at each bombarding energy. Some measurements of the angular distribution of the gamma-ray were also obtained by this time-of-flight method.

## 3. Results

The differential cross-sections for 1.5-MeV neutrons are shown in Fig. 1. The upper solid curve represents the elastic scattering after all corrections have been made. The corresponding experimental points have been corrected for flux attenuation before plotting so that the residual effect due to multiple scattering and finite source-sample angular resolution is easily noted. Both these effects tend to decrease the anisotropy of the observed scattering.

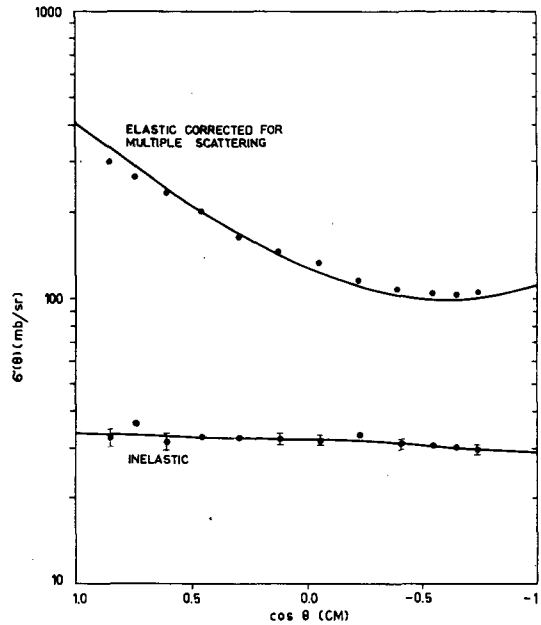


Fig. 1
Differential elastic and inelastic cross-sections for the scattering of 1.5-MeV neutrons by $Na^{23}$, in the centre-of-mass system.

The lower curve is the best fit to the points for inelastic scattering. Before plotting, these data were first multiplied by a factor allowing for the flux attenuation and overall multiple scattering corrections. Since this curve is almost isotropic, any correction to the shape would not be significant compared to the experimental errors, and this correction was therefore not calculated. The relative errors on the inelastic points are shown, and on the elastic data are represented, by the size of the plotted points. The integrated cross-sections at 1.5 MeV are as follows: $\sigma_{el} = 2.10 \pm 0.06$; $\sigma_{in} = 0.400 \pm 0.016$; and $\sigma_T = 2.50 \pm 0.08$ b. This total cross-section is in agreement with a value of $2.45 \pm 0.08$ b obtained from a transmission measurement on the same sample.

The departure from symmetry about 90° of the inelastic scattering is thought to be due to interference between neighbouring levels in the compound nucleus, since the inelastic and total cross-sections show resonances in the region of 1.5 MeV.

The angular distribution of 0.44-MeV gamma-rays at 1.5 MeV was of the form $W(\theta) = 1 + (0.14 \pm 0.03)\, P_2(\cos\theta)$. A measurement of the anisotropy of the gamma-rays at 1.3, 1.5 and 1.7 MeV gave values for $W(137°)/W(90°)$ of 1.01, 1.13 and 0.98 respectively, showing a marked change of $W(\theta)$ with energy. This effect is again attributed to contributions from a small number of compound-nuclear levels.

The inelastic cross-section from 0.5 to 2.0 MeV is shown in Fig. 2. This data has been normalized at 1.5 MeV to the value $0.400 \pm 0.016$ b given above. The overall standard errors on the points are $\pm 6\%$. The width at half-height of the triangles represents the neutron-energy spread due to the target thickness and the finite angle subtended by the scatterer.

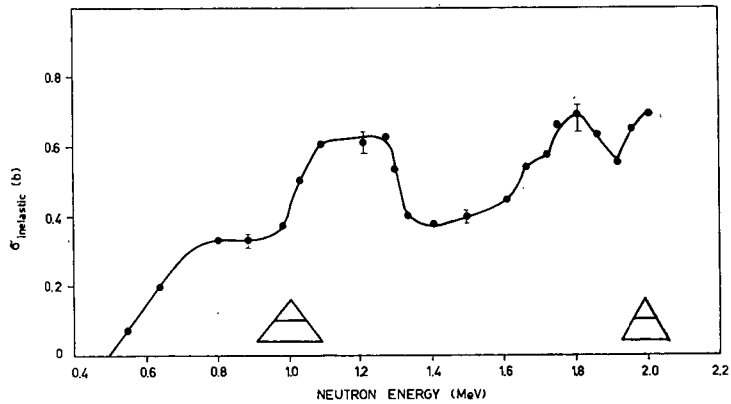


Fig. 2
Inelastic scattering cross-section for neutrons of energy up to 2 MeV on $Na^{23}$.

Preliminary results on the inelastic cross-section at 3.97 MeV are shown in Table I. Cross-sections for excitation of different levels are given. These were obtained by integration of the appropriate differential cross-sections, which were found to be isotropic within experimental error. The levels at 2.64 and 2.70 MeV were not resolved.

TABLE I

**$Na^{23}$ (n–n′) $Na^{23}$* AT 3.97 MeV AND HAUSER-FESHBACH RESULTS**

Optical potential: $V+i\ (W+W'E)$, with $V=41.5$, $W=0.1$, $W'=2$, and Saxon-Woods form factor ($r_0=1.4$, $a=0.35$) gives reasonable fit to $\sigma_T$ and $\sigma_{el}\ (\theta)$.

| $Na^{23}$ level (MeV) | $\sigma$ (mb) Experiment | $\sigma$ (H-F) Run 1 | $\sigma$ (H-F) Run 2 |
|---|---|---|---|
| 0.438 | 280* | 331 ($^5/_2+$) | 324 ($^5/_2+$) |
| 2.08 | 180 ± 15 | 153 ($^7/_2+$) | 149 ($^7/_2+$) |
| 2.39 | 70 ± 8 | 69 ($^1/_2+$) | 127 ($^5/_2+$) |
| 2.64 | 140 ± 14 | 96 ($^5/_2+$) | 52 ($^1/_2+$) |
| 2.70 | | 55 ($^9/_2+$) | 54 ($^9/_2+$) |
| 2.98 | 100 ± 10 | 48 ($^3/_2+$) | 47 ($^3/_2+$) |
| 3.68 | — | 0.8($^9/_2+$) | 0.8($^9/_2+$) |

* SHIPLEY *et al.* [9].

The table also shows the results of Hauser-Feshbach calculations made by Dr. K. Parker. Two sets of level spins were considered. There is considerable evidence that the 0.438-MeV level is $5/2^+$, and previous work suggests that the spins of the 2.08, 2.70, and 2.98-MeV levels are $7/2^+$, $9/2^+$, and $3/2^+$ respectively. The rotational model for $Na^{23}$ [10] predicts these levels and also suggests two more levels below 4 MeV with spins $1/2^+$ and $5/2^+$. These levels might possibly correspond to those at 2.39 and 2.64 MeV, and the Hauser-Feshbach calculation is consistent with spins 1/2 and 5/2 respectively for these levels. The calculation with spins reversed disagrees with the experimental results.

## ACKNOWLEDGEMENT

The authors express their thanks to Dr. L. A. Warren, who kindly undertook a chemical analysis of the polythene used in these investigations.

## REFERENCES

[1] LANGSDORF, A., LANE, R. O., MONAHAN, J. E., *Phys. Rev.* **107** (1957) 1077—1087. See also LANE, R. O., and MONAHAN, J. E., *Phys. Rev.* **118** (1960) 533—535.
[2] FREEMAN, J. M., and MONTAGUE, J. H., *Nucl. Phys.* **9** (1958), 181—197.
[3] BATCHELOR, R. and TOWLE, J. H., *Proc. phys. Soc.* **73** (1959) 193—200.
[4] BATCHELOR, R., *et al.*, *Nucl. Instrum. and Meth.* 8 (1960) 146—150.
[5] CRANBERG, L., LA-2177 (1959).
[6] PARKER, J. B., *et al.* (to be published).
[7] RASMUSSEN, V. K., METZGER, F. R. and SWANN, C. P., *Nucl. Phys.* **13** (1959) 95—103.
[8] BERENBAUM, R., TOWLE, J. H. and MATTHEWS, J. H., *Proc. phys. Soc.* **69** (1956) 858—861.
[9] SHIPLEY *et al.*, *Phys. Rev.* **115** (1959) 122.
[10] PAUL. E. B. and MONTAGUE, J. H., *Nucl. Phys.* 8 (1958) 61.

SM—18/73

# NEUTRON CAPTURE CROSS-SECTIONS FOR ENERGIES ABOVE A FEW HUNDRED ELECTRON-VOLTS

J. H. NEILER
OAK RIDGE NATIONAL LABORATORY, OAK RIDGE, TENN.,
UNITED STATES OF AMERICA

**Abstract — Résumé — Аннотация — Resumen**

**Neutron capture cross-sections for energies above a few hundred electron-volts.** A series of measurements at Oak Ridge National Laboratory provides extensive information on neutron radiative capture cross-sections at intermediate energies. The cross-sections of about 50 elements have been determined, relative to the known absorption cross-section of indium, for neutron energies near 30 and 65 keV obtained with a pulsed positive-ion accelerator. Normalizing to these cross-sections, the radiative capture cross-sections of about 30 elements have been measured as a function of neutron energy from 0.2 to 170 keV. To cover this range both chopper and pulsed-accelerator techniques have been utilized. Statistical model curve-fits of the latter data for heavy nuclei, where the keV cross-sections are an average over many resonances, are generally in good agreement with the average nuclear parameters obtained from recent low-energy total cross-section results.

**Mesures de sections efficaces de capture de neutrons au-dessus de quelques centaines d'électronvolts.** Une série de mesures faites au Laboratoire national d'Oak Ridge donnent des renseignements très complets sur les sections efficaces de capture radiative de neutrons intermédiaires. On a déterminé les sections efficaces d'une cinquantaine d'éléments par rapport à la section efficace d'absorption déjà connue de l'indium, au moyen de flux pulsés de neutrons d'énergies voisines de 30 et de 65 keV, produits par un accélérateur d'ions positifs. En normalisant par rapport à ces sections efficaces, on a mesuré les sections efficaces de capture radiative d'une trentaine d'éléments en fonction de l'énergie des neutrons entre 0,2 et 170 keV. Pour couvrir ce domaine d'énergie, on a utilisé des méthodes faisant appel à la fois aux sélecteurs rapides et aux accélérateurs pulsés. Les courbes types ajustées statistiquement à ces dernières données pour les noyaux lourds — où les sections efficaces, pour des énergies de l'ordre du kiloélectronvolt, sont une moyenne prise sur de nombreuses résonances — sont généralement en bon accord avec les paramètres nucléaires moyens obtenus à partir des mesures récentes de sections efficaces totales pour des basses énergies.

**Сечение захвата нейтронов для энергий выше нескольких сотен электрон-вольт.** Серия измерений в Окриджской национальной лаборатории (1, 2, 3) предусматривает широкую информацию по вопросам сечения радиационного захвата нейтронов промежуточных энергий. Определены поперечные сечения почти 50 элементов относительно известного сечения поглощения индия для энергий нейтронов близких к 30 и 65 килоэлектроновольт при помощи импульсного ускорителя положительно заряженных ионов. Нормированные к этим поперечным сечениям, сечения радиационного захвата приблизительно 30 элементов были измерены как функция энергии нейтронов от 0,2 до 170 килоэлектроновольт. Чтобы покрыть этот диапазон использовались селектор нейтронов и импульсный ускоритель. Статистическая модель подгонок экспериментальных кривых для тяжелых ядер согласно последним данным, где поперечные сечения в килоэлектронвольтах являются средним числом для многих резонансов, находятся в хорошем соответствии со средними ядерными параметрами, полученными из недавних результатов о полных сечениях при малых энергиях.

**Secciones eficaces de captura neutrónica para energías superiores a algunos cientos de electrón-voltios.** En el Oak Ridge National Laboratory se ha efectuado una serie de mediciones que proporcionan una amplia información sobre las secciones eficaces de captura radiativa de neutrones a energías intermedias. Se han determinado las secciones eficaces de captura de unos 50 elementos, refiriéndolas a la sección eficaz de absorción del indio, ya conocida, para energías neutrónicas del orden de 30 y 65 keV, obtenidas con un acelerador pulsado de iones positivos. Tomando como norma esas secciones eficaces, se han medido las secciones eficaces de captura radiativa de unos 30 elementos en función de energías neutrónicas comprendida entre 0,2 y 170 keV. Para abarcar ese intervalo, se han empleado interruptores de haz y aceleradores pulsados. La representación gráfica de estos últimos datos correspondientes a núcleos pesados conforme al modelo estadístico, en que las secciones eficaces keV constituyen un promedio que abarca muchas resonancias, concuerda por lo general en forma satisfactoria con los parámetros nucleares medios obtenidos a partir de los resultados recientes de las secciones eficaces totales a bajas energías.

## Introduction

The availability of intense beams of thermal and low-energy neutrons from moderated reactors has made possible extensive studies of neutron-capture processes by direct observation of the radiations from the capturing nuclide. Until recently, studies of the capture process at neutron energies of 1 keV or higher have been primarily dependent upon activation [1—18] or spherical shell transmission [19, 20] methods. Direct measurements of keV neutron radiative capture have been essentially impossible because of the low intensities of keV neutron sources, low detector-efficiencies and the large scattering-to-capture ratio which results in high beam-associated backgrounds. The means to overcome these difficulties have been provided only recently by the development of the pulsed positive-ion accelerator as a high-intensity neutron source, fast timing-techniques which provide both background elimination and neutron-energy selection over relatively short flight paths [21], and large tank scintillators as capture radiation detectors [22].

The ORNL measurements of neutron capture cross-sections above a few hundred eV, which are being summarized here, fall into categories based on the type and manner of use of the neutron source [23, 24]. One set of measurements utilized a fast-pulsed positive ion accelerator and thin lithium or tritium target to provide neutrons of energy near 30 and 65 keV. Pre-acceleration pulsing was used to increase the available peak current, and to reduce and permit measurement of the beam-associated background in a large liquid-scintillator. The same detector was used in a second set of experiments measuring capture cross-section as a function of neutron energy from 10 to 200 keV. Here the pulsing allowed both background suppression and neutron time-of-flight measurement. A third set of measurements at ORNL essentially closes the gap between the eV work and that of Diven and others in the hundreds of keV. Again a large tank-scintillator was used, this time with a fast chopper as neutron source.

## Apparatus and techniques

### Detector and electronics

The scintillator tank used with the ORNL pulsed accelerator is shown in Fig. 1. The one used in the chopper work was similar, although smaller. The shape approximates a sphere 1.2 m in diameter; it contains about 1000 l of xylene-terphenyl

solution. The size was dictated by the desire for high (>90%) probability of detection of an average radiative capture event which involves 6—8 MeV and has a multiplicity of decay gammas $\geq 3$. This can be achieved even for 2 gammas of

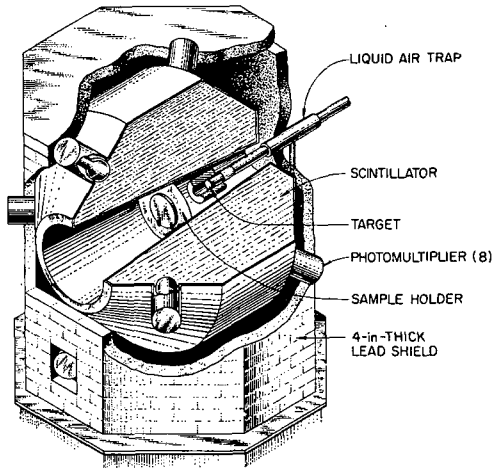


Fig. 1
Liquid-scintillator tank (1.2 m) as used for measuring capture cross-sections with kinematically collimated neutron sources.

nearly equal energies. However, the high background rates at 1—2 MeV require that a bias be set above 2 MeV in actual operation. Thus a change in the spectrum to a predominance of 5—7-MeV gammas followed by gammas totalling less than 2 MeV could reduce the efficiency to 50—60%.

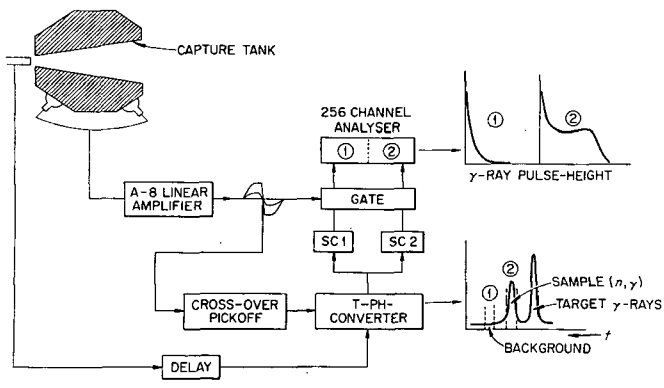


Fig. 2
Block diagram of scintillator tank and associated electronic apparatus connected for capture gamma-ray pulse-amplitude measurements. When cross-sections are to be measured, the inputs to the single channel analyser (SC 1) and 256 channel are interchanged; a time spectrum of pulses is then gated into the multi-channel by a selected range of gamma pulse-amplitudes.

The operation of the electronics associated with the tank and pulsed Van de Graaff beam is block diagrammed in Fig. 2; here the apparatus is arranged to allow study of the spectrum of gamma-ray pulse-amplitudes from the tank. A time-to-pulse amplitude converter provides an analogue presentation of the spectrum of time intervals between "start" pulses obtained from the tank and "stop" pulses provided by the amplified accelerator-beam-current pulse at the neutron-producing target. Single channel windows placed over amplitude ranges corresponding to the time of arrival of neutrons and to a time when only background is present allow simultaneous recording of the signal plus background and the background gamma pulse-amplitude spectra from the tank. A typical pulse-amplitude spectrum with background subtracted is shown in Fig. 3. A similar

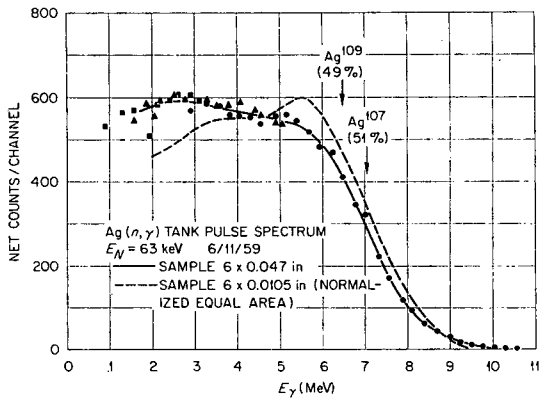


Fig. 3
Net pulse-amplitude spectrum of capture gamma-rays from two silver samples of different thickness.

spectrum is necessary for each sample since the detection efficiency for a capture event is determined by the ratio of spectrum area above the bias level to total area under the curve. The accuracy with which the tank can be used to measure cross-sections relative to a standard is excellent ($\pm 5\%$) but absolute measurements are much less certain ($\pm 10$—$15\%$). This is due to such uncertainties as (1) neutron flux measurements, (2) total escape probability of capture gamma-rays, and (3) absolute gamma-ray counting efficiency (within the pulse-height window).

## Neutron source

In order to measure low cross-sections and to provide sufficient intensity for the determination of gamma-ray pulse-amplitude spectra, use was made of "kinematic collimation" of the neutrons from $Li^7$ (p, n) and T (p, n) reactions. At incident proton energies very near the threshold these reactions provide intense forward-directed beams of 30- and 65-keV neutrons. The proton energy was adjusted in each case to cause the entire reaction-yield to appear within a forward cone of about 10° half-angle. In the case of $Li^7$ (p, n) for example, at a proton energy 2.0 keV above threshold the number of neutrons ($E = 30$ keV) incident per second on the sample *during* the pulse was approximately $3 \times 10^8$. This inten-

sity was sufficient to permit measurement of cross-sections as small as a few millibarns in samples of material 5—7 in in diameter with thicknesses no greater than that resulting in $1/e$ attenuation of 150-keV gamma-rays. The general arrangement of detector, sample and target is shown in Fig. 1.

## Results of measurements

### "THRESHOLD" NEUTRON SOURCE

In the first series of measurements, once the gamma pulse-amplitude spectrum was obtained, the roles of the single channel and multi-channel in Fig. 2 were interchanged. A time spectrum was recorded in the multi-channel for a known energy range of gamma pulse-amplitudes in the single channel window. The area under the time peak was then proportional to the capture cross-section for the known amount of sample material. Primarily because of the difficulty of measuring precisely and absolutely a neutron flux in the keV energy range, a single standard cross-section (indium) was chosen and all other cross-sections were measured relative to this value. The absolute neutron-absorption cross-sections at 24 keV of SCHMITT and COOK [19], which are probably the most direct and accurate values

TABLE I

**RESULTS OF THRESHOLD MEASUREMENTS WITH 30, 65, AND 167 keV AVERAGE ENERGY NEUTRONS**

Capture cross-sections are given in millibarns. The estimated absolute error (S.D.) is $\pm 10\%$ except where noted. The neutron energy resolution was approximately triangular with width at half-maximum of $\pm 7$ keV, and $\pm 20$ keV at 30 and 65 keV, respectively, and about $\pm 3$ keV at 167 keV.

| Element | 30 | 65 | 167 | Element | 30 | 65 | 167 |
|---|---|---|---|---|---|---|---|
| C | $0.2 \pm 0.4$ | $0.0 \pm 0.3$ | $1.3 \pm 2$ | Sn | 88 | 51 | — |
| F | $4.5 \pm 1.0$ | — | — | Sb | 436 | 245 | — |
| Mg | $0.4 \pm 0.2$ | $2.1 \pm 0.7$ | — | I | 733 | 440 | — |
| Al | $2.8 \pm 0.7$ | — | — | La | 55 | 18 | — |
| Si | $13 \pm 2$ | — | — | Ce | 35 | 8.0 | — |
| S | $25 \pm 5$ | — | — | Pr | 115 | 59 | — |
| V | $30 \pm 5$ | — | — | Sm | 875 | 450 | 330 |
| Cr | $10 \pm 2$ | $3.5 \pm 1$ | — | Gd | 1175 | 670 | 310 |
| Fe | $12 \pm 2$ | $6.3 \pm 1.5$ | — | Tb | 1850 | 1070 | 600 |
| Co | 88 | — | — | Dy | 775 | — | 240 |
| Ni | $16 \pm 3$ | $6.5 \pm 1.5$ | — | Ho | 1720 | 1070 | 515 |
| Cu | $39 \pm 5$ | $25 \pm 4$ | — | Er | 960 | — | 230 |
| Zn | $31 \pm 5$ | $20 \pm 4$ | — | Tm | 1310 | 700 | 400 |
| Ge | — | 39 | — | Yb | 575 | 390 | 170 |
| Br | 650 | 345 | — | Lu | 2520 | 1200 | — |
| Sr | 155 | 24 | — | Ta | 735 | 440 | 270 |
| Y | 13.5 | 6.9 | — | W | 270 | 190 | — |
| Zr | 14 | 10.3 | — | Pt | 330 | 234 | — |
| Nb | 264 | 135 | — | Au | 515 | 332 | 230 |
| Mo | 140 | 69 | — | Hg | 295 | 103 | — |
| Rh | — | 540 | — | Tl | 71 | 35 | — |
| Pd | 454 | 265 | 175 | Pb | $3 \pm 3$ | $1 \pm 2$ | — |
| Ag | 951 | 586 | 375 | Bi | $1 \pm 4$ | $4 \pm 3$ | — |
| Cd | 330 | 183 | — | $U^{238}$ | 473 | 302 | — |
| In | (763) | (448) | (258) | | | | |

available in this energy range, were then used to calculate a weighted indium cross-section of $760 \pm 50$ mb at 30 keV. The standard value at 65 keV was obtained by two measurements. One derived the ratio of the 30- to 65-keV cross-sections by determining the ratio of the neutron fluxes with a $B^{10}$—NaI (Tl) detector [21]; the other utilized activation of indium at the two energies with fluxes measured by the $4\pi$ graphite-sphere method [25]. The cross-section ratios, 65 keV to 30 keV for the two methods were 0.597 and 0.583, respectively, and the average was used to determine a standard value of $450 \pm 40$ mb for indium at 65 keV. The final results, corrected for resonance self-protection and increased average path-lengths due to scattering are shown in Table I.

### Cross-section as a function of energy

The second series of measurements was also based on the gamma-ray pulse-amplitude spectra obtained for the threshold work. The neutron source, however, was changed to a relatively thick $Li^7$ or T target, extensive collimation, as shown in Fig. 4, being used to confine the neutrons into a beam. A flight path of 1.2 m

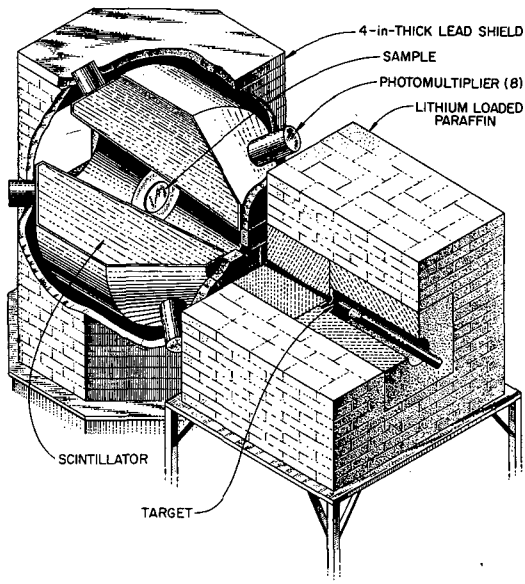


Fig. 4
Liquid scintillator tank and collimator as used for measuring capture cross-section as a function of energy.

was used; with the timing resolution of the overall system being about 20 ns this provided an energy resolution varying from 5% at 10 keV to 20% near 150 keV. All measurements of capture cross-sections as a function of energy were made relative to the shape of the capture cross-section of indium. Considerable effort was therefore expended in determining the shape of the indium cross-section relative to the shape of the total absorption cross-section of $U^{235}$ above 100 keV, and relative to the shape of the $B^{10}$ (n, $\alpha\gamma$) $Li^7$ cross-section below 140 keV. The

shape of the $U^{235}$ absorption cross-section was constructed from the fission cross-section given in the Brookhaven compilation and the value of $\alpha$ given by DIVEN *et al.* [26]. The shape of the $B^{10}$ (n, $\alpha_1 \gamma$) $Li^7$ cross-section as a function of energy was obtained in the following manner. The $B^{10}$ (n, $\alpha_0$) $Li^7$ cross-section was calculated from reciprocity using the $Li^7$ ($\alpha$, n) $B^{10}$ cross-section measurements [27]. This was subtracted from the cross-section for producing alpha-particles which was measured most recently by BICHSEL and BONNER [28]. The result is the shape of the $B^{10}$ (n, $\alpha_1$) $Li^7$ cross-section. The two shapes were internormalized by careful fitting in the overlap region and the final shape normalized to the standard indium values at 30 and 65 keV. This, rather than use of the absolute absorption cross-section of $U^{235}$, was decided upon because of the uncertainty in the spectrum shape, and thus the detection efficiency, for $U^{235}$ absorption gamma-rays, introduced mainly by the high counting rates from the natural radioactivity of the sample. Based upon these standards the neutron flux was determined at

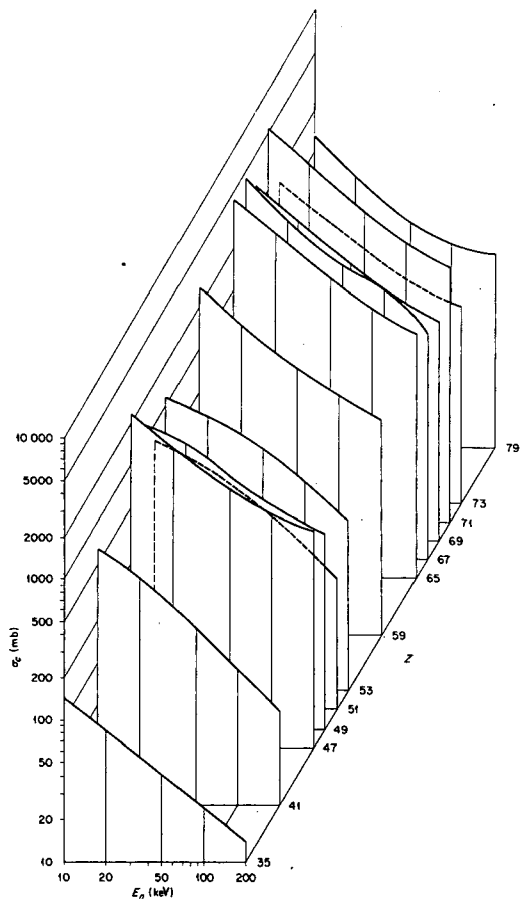


Fig. 5
Capture cross-section of odd-$Z$ elements as a function of neutron energy. The results are presented in this fashion for conciseness only.

frequent intervals during the measurement. The cross-sections of 22 elements were measured in this manner. The results, after the usual corrections for resonance self-protection and average path-lengths, are shown in Figs. 5 and 6. The errors

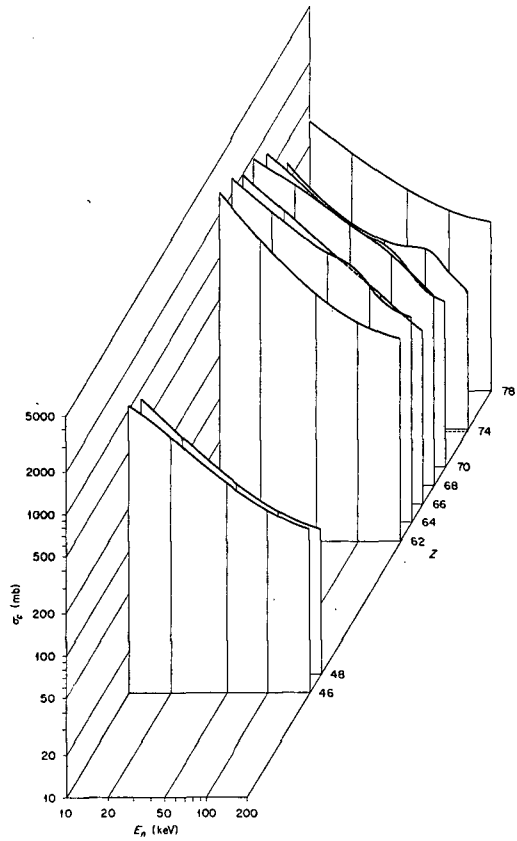


Fig. 6
Capture cross-sections of even-$Z$ elements as a function of neutron energy.

in these cross-sections are, of course, dependent on the element and on the neutron energy. They are a minimum (standard deviations of about 10%) at the normalization points of 10 and 65 keV. At energies below 15 keV the poor signal-to-background ratio results in errors rising to perhaps 15% at 10 keV. The error rises again to 15% between 100 to 140 keV where the standard shapes are least well known.

The initial results of the third set of ORNL measurements have recently been reported [24]. For this work a fast chopper was used as neutron source, the shape of the neutron flux *versus* energy being determined with $BF_3$ counters. At present the results are normalized to the pulsed accelerator work in the region of 6 keV. It is planned to obtain absolute cross-sections at a later date. The 24 elements so far measured in the energy range 0.2 keV to 10 keV are shown in Figs. 7, 8 and 9.

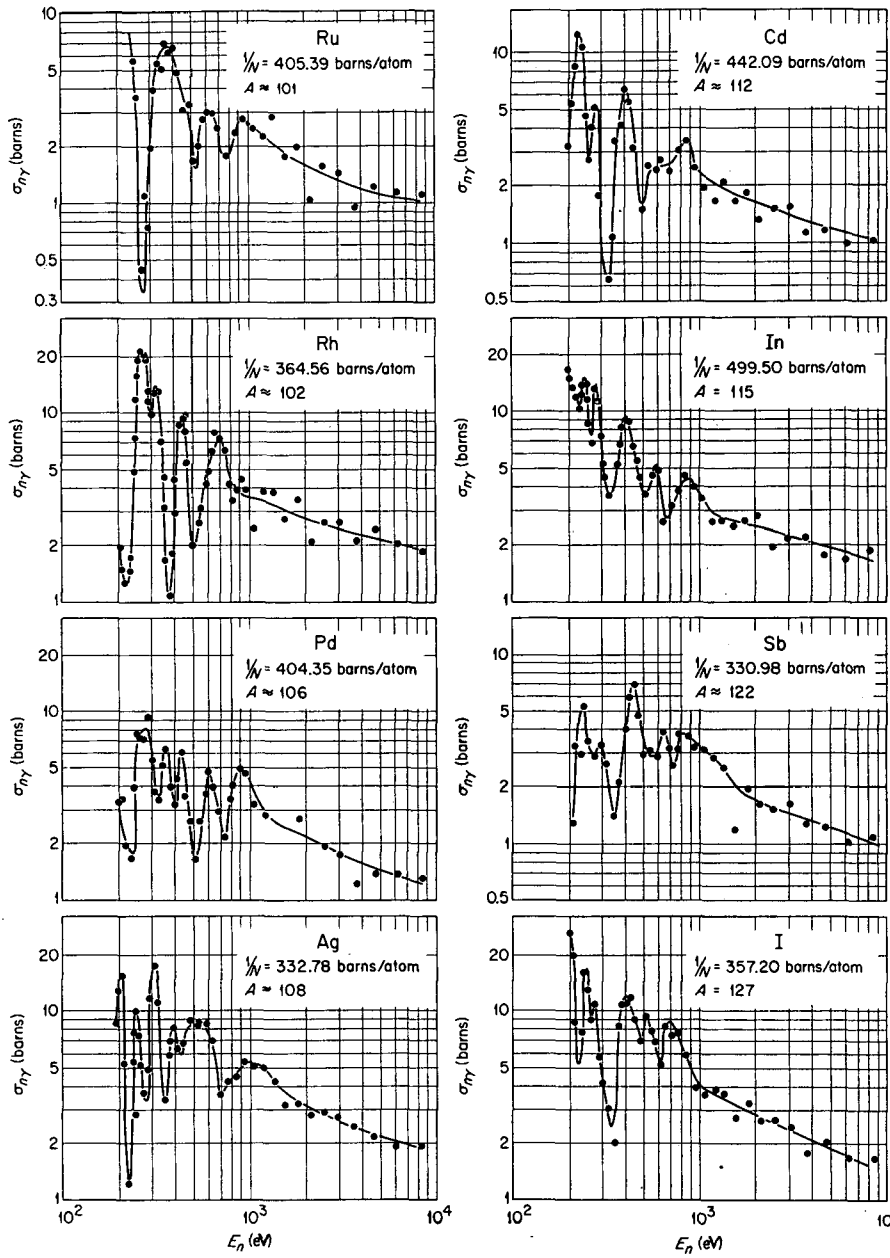


Fig. 7
Capture cross-sections as a function of energy for elements near atomic weight 115.

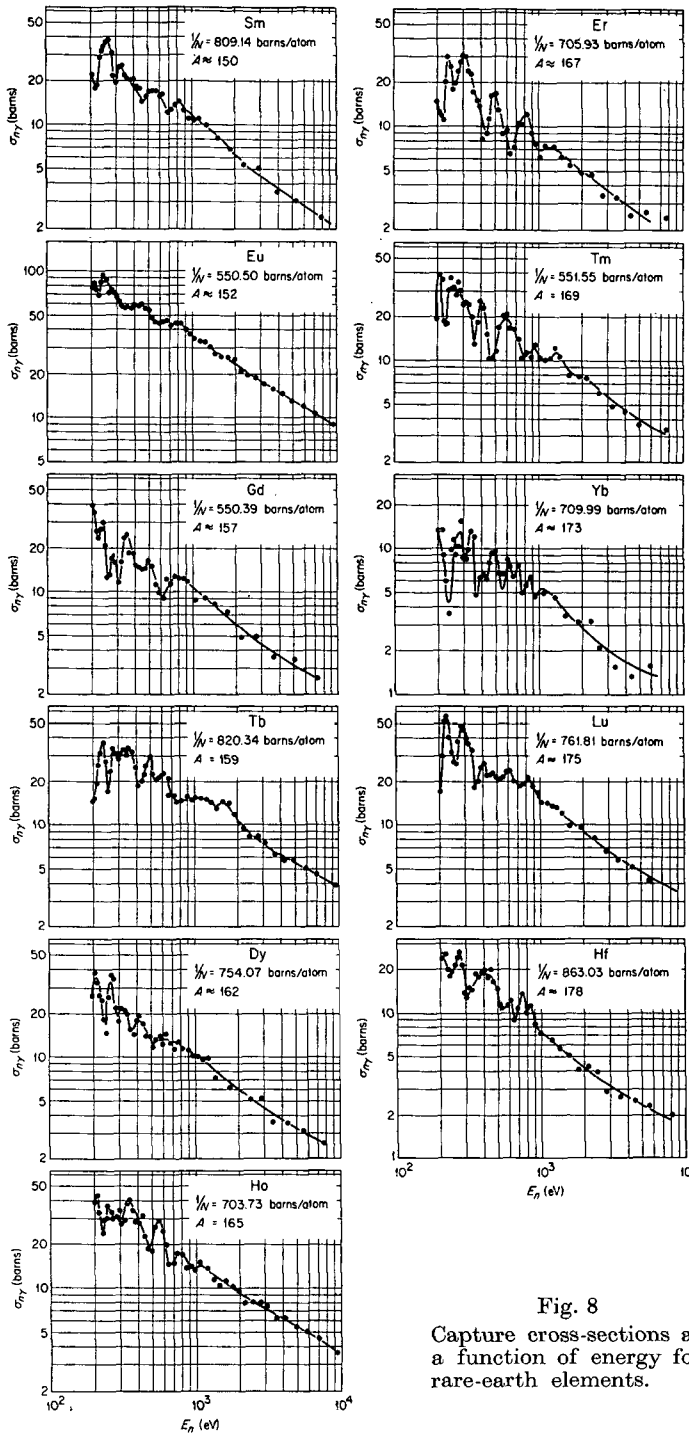


Fig. 8
Capture cross-sections as a function of energy for rare-earth elements.

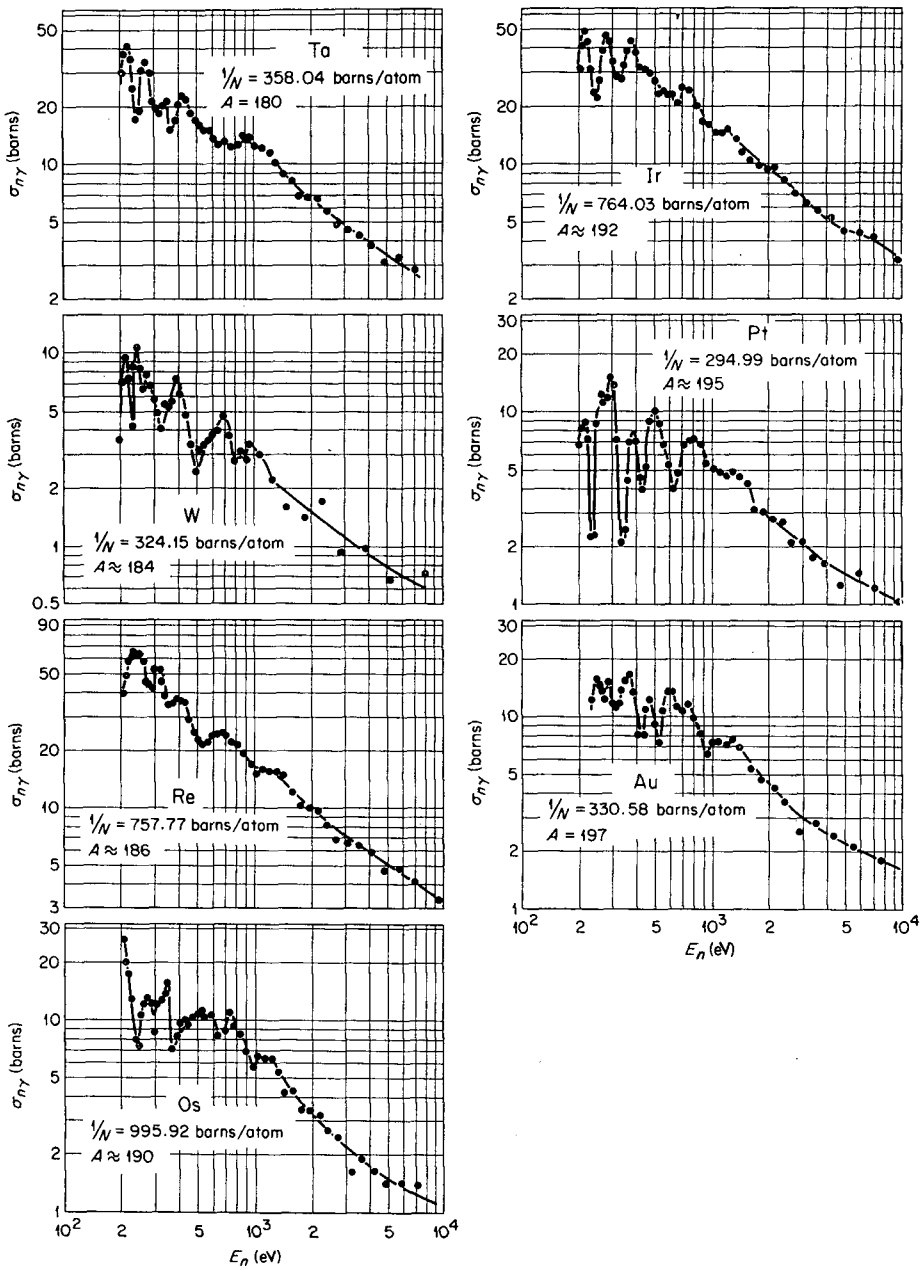


Fig. 9
Capture cross-sections as a function of energy for some heavy elements.

## Analysis and discussion

Some of the results of the various experiments described here plus most of the published results from other measurements for each element are plotted in Figs. 10 through 14. These are chosen as representative from the recently published work of GIBBONS *et al.* [23] where the references and detailed discussion may be found. The dotted line is drawn through the data points only to indicate the general behaviour. Characteristic of these data is the large fluctuation in cross-section for the lower incident energies, showing the effects of individual resonances or groups of resonances. As the energy increases, the cross-section becomes a smoothly varying function, indicating here that averages over many resonances are being observed. It is in this region that one can apply a quantitative fit to the data utilizing parameters obtained from total cross-section measurements in the eV range. These parameters are the average s-wave level-spacing, radiative-width and strength-function. Restricting the energy to less than 100 keV, the only remaining parameter is the p-wave strength-function. The radiative capture cross-section as a function of energy can then be computed as an average over many resonances. In a rather surprising number of cases, good fits are obtained with reasonable assumptions for the p-wave strength-function. See, for example, the results for tantalum, iodine and indium, Figs. 10, 11 and 12. Note in these cases the increasing contribution from p-wave capture as $A$ decreases toward the p-wave strength-function maximum in the vicinity of $A \approx 100$. In the case of terbium, Fig. 13, where from the optical model one would expect a rather small p-wave strength-function, serious disagreement occurs. Fairly good agreement in

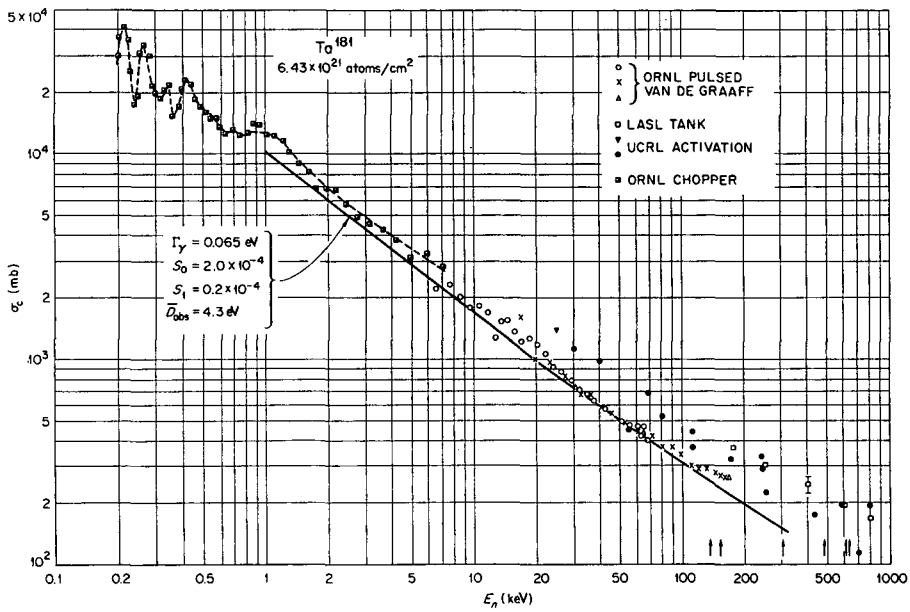


Fig. 10
Compilation of neutron capture cross-section results for tantalum. The solid line and level parameters represent the best fit obtained by Gibbons *et al.* [23].

fit can be obtained, however, by assuming a somewhat larger $\Gamma_\gamma/D$, which would be consistent with missed levels in the total cross-section measurement. In other cases similar to this, the agreement has improved as more recent s-wave experi-

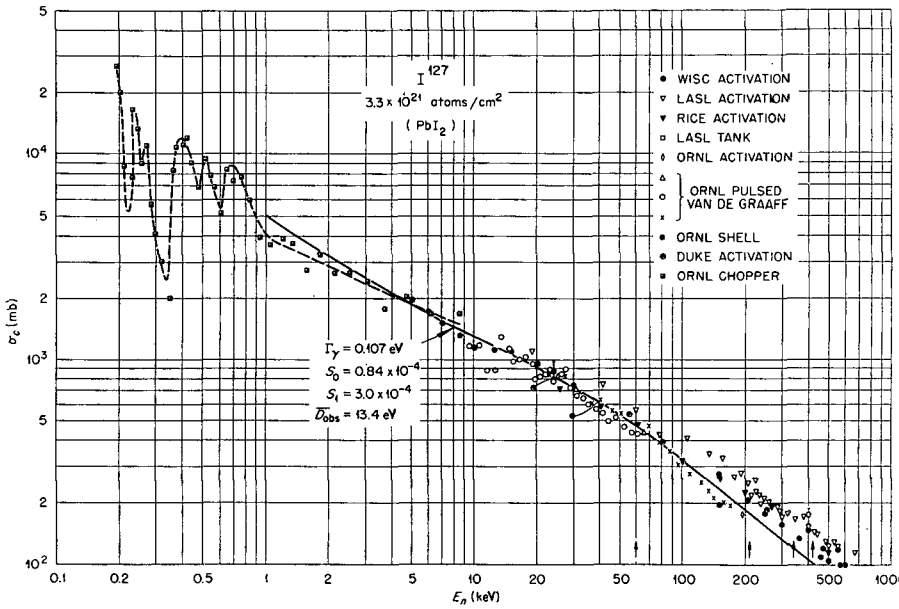


Fig. 11
Compilation of neutron capture cross-section results for iodine.

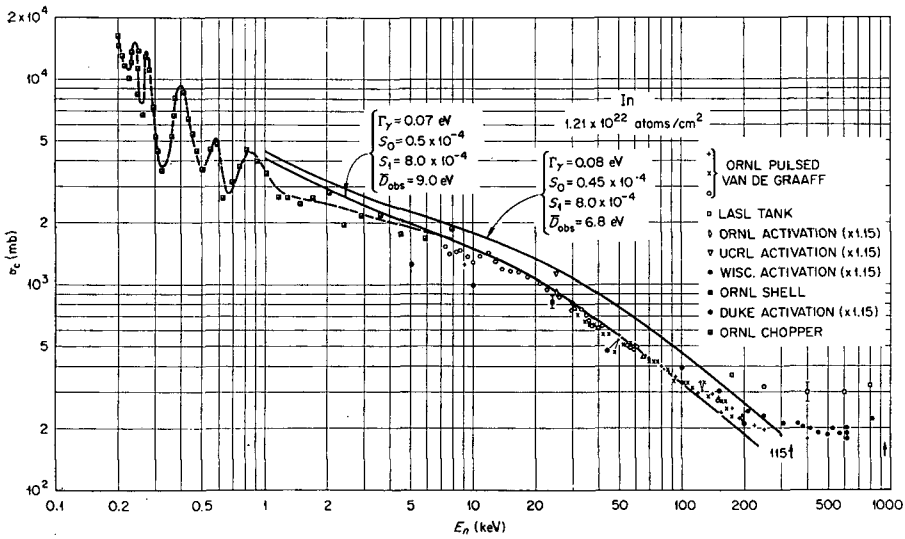


Fig. 12
Compilation of neutron capture cross-section results for indium.

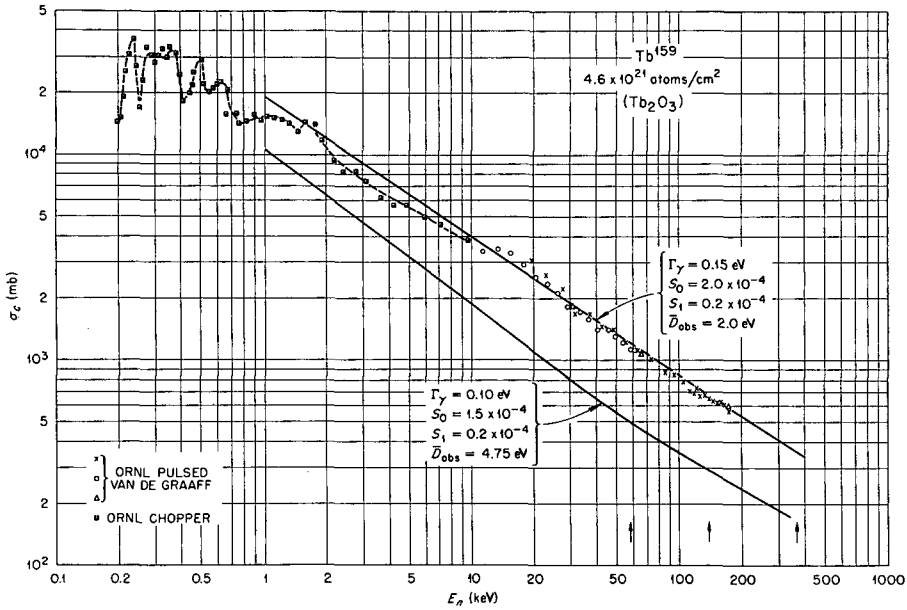


Fig. 13
Compilation of neutron capture cross-section results for terbium. The lower curve was calculated using results of low-energy cross-section measurements for s-wave parameters and a reasonable p-wave strength-function. The upper curve is a fit obtained by changing s-wave parameters. The change required was far outside error limits quoted for the low-energy total cross-section results.

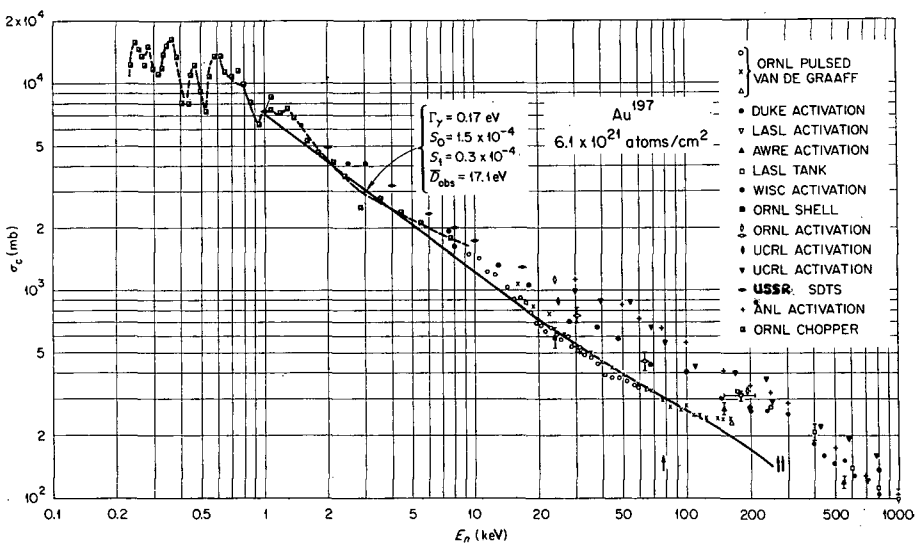


Fig. 14
Compilation of neutron capture cross-section results for gold.

mental parameters became available. Finally, the case of gold, Fig. 14, is an example of good agreement in fit to the ORNL data when the most recent s-wave parameters are used with a reasonable assumption for the p-wave strength-function. Unfortunately, the agreement between various experimental results is particularly bad for this element. This situation is in serious need of clarification; several recent measurements have been made, those of COX [29] and WESTON [30] with results that seem mostly to accentuate the difficulties of neutron measurements in the 10—200-keV energy range. In general the ORNL results are only about 30% lower than those of DIVEN *et al.* [22] and are not often more than 25% lower than the activation measurements, which have been made in the 10—200-keV range. This disagreement is outside the assigned experimental errors and is not yet understood.

## REFERENCES


[1] HUMMEL, V. and HAMERMESH, B., *Phys. Rev.* **82** (1951) 67.
[2] KIMBALL, C. and HAMERMESH, B., *Phys. Rev.* **89** (1953) 1306.
[3] MACKLIN, R. L., LAZAR, N. H. and LYON, W. S., *Phys. Rev.* **107** (1957) 504.
[4] BOOTH, R., BALL, W. P. and MACGREGOR, M. H., *Phys. Rev.* **112** (1958) 226.
[5] LEIPUNSKY, A. I. *et al.*, Proc. 2nd UN Int. Conf. PUAE **15** (1958) 50 (2219).
[6] PASECHNIK, M. V., *et al.*, Proc. 2nd UN Int. Conf. PUAE **15** (1958) 18 (2030).
[7] BAME, S. J. and CUBITT, R. L., *Phys. Rev.* **113** (1959) 256.
[8] GABBARD, F., DAVIS, R. H. and BONNER, T. W., *Phys. Rev.* **114** (1959) 201.
[9] LYON, W. S. and MACKLIN, R. L., *Phys. Rev.* **114** (1959) 1619.
[10] JOHNSRUD, A. E., SILBERT, M. G. and BARSCHALL, H. H., *Phys. Rev.* **116** (1959) 927.
[11] MISKEL, J. A., *et al.*, *Bull. Amer. phys. Soc.* **4** (1959) 475.
[12] FERGUSON, A. T. G. and PAUL, E. B., *J. nucl. Energy* **A 10** (1959) 19.
[13] VERVIER, J. F., *Nucl. Phys.* **9** (1959) 569.
[14] BILPUCH, E. G., WESTON, L. W. and NEWSON, H. W., *Ann. Phys.* **10** (1960) 455.
[15] WESTON, L. W., *et al.*, *Ann. Phys.* **10** (1960) 477.
[16] PERKIN, J. L., O'CONNOR, L. P., and COLEMAN, R. F., *Proc. phys. Soc. (Lond.)* **A 72** (1958) 505.
[17] KONONOV, V. N., STAVISKII, I. I. and TOLSTIKOV, V. A., *J. nucl. Energy* **A 11** (1959) 46.
[18] HANNA, R. C. and ROSE, B., *J. nucl. Energy* **8** (1959) 197.
[19] SCHMITT, H. W. and COOK, C. W., *Nucl. Phys.* **20** (1960) 202.
[20] BELANOVA, T. S., *J. exp. theor. Phys.* **34** (1958) 574. (Translation: *Soviet Phys.* — JETP 34 (7) (1958) 397).
[21] NEILER, J. H. and GOOD, W. M., Fast Neutron Physics, Part I, (edited by J. L. Fowler and J. B. Marion), Interscience Publishers, Inc., New York (1960) Chap. IVa.
[22] DIVEN, B. C., TERRELL, J. and HEMMENDINGER, A., *Phys. Rev.* **120** (1960) 556.
[23] GIBBONS, J. H., *et al.*, *Phys. Rev.* **122** (1961) 182.
[24] BLOCK, R. C., VONDERLAGE, F. C. and WESTON, L. W., *Bull. Amer. phys. Soc.* **6** (1961) 274.
[25] MACKLIN, R. L., *Nucl. Instrum.* **1** (1957) 335.
[26] DIVEN, B. C., TERRELL, J. and HEMMENDINGER, A., *Phys. Rev.* **109** (1958) 144.
[27] GIBBONS, J. H. and MACKLIN, R. L., *Phys. Rev.* **114** (1959) 571.
[28] BICHSEL, H. and BONNER, T. W., *Phys. Rev.* **108** (1957) 1025.
[29] COX, S. A., *Phys. Rev.* **122** (1961) 1280.
[30] WESTON, L. W. and LYON, W. S., *Phys. Rev.* (1961, to be published.)
[31] BERQVIST, I. and SLARFELT, N., *Nucl. Phys.* **22** (1961) 513.
[32] FIRK, F.W.K. and GIBBONS, J. H., *Bull. Amer. phys. Soc.* **6** (1961) 252.

SM—18/55

# MEASUREMENTS OF $\alpha$ FOR $U^{233}$, $U^{235}$ AND $Pu^{239}$ FOR MONOENERGETIC NEUTRONS

J. C. HOPKINS AND B. C. DIVEN
LOS ALAMOS SCIENTIFIC LABORATORY,
UNIVERSITY OF CALIFORNIA, LOS ALAMOS, N. MEX.,
UNITED STATES OF AMERICA

**Abstract — Résumé — Аннотация — Resumen**

**Measurements of $\alpha$ for $U^{233}$, $U^{235}$ and $Pu^{239}$ for monoenergetic neutrons.** The ratio of neutron capture to fission cross-sections, $\alpha$, has been measured for $U^{233}$, $U^{235}$ and $Pu^{239}$ at nine incident neutron energies from 30 keV to 1000 keV. A pulsed and collimated neutron beam is passed through the target at the centre of a large cadmium-loaded liquid scintillator. Captures and fissions are detected by means of their prompt gamma-rays; elastic and inelastic scattering events are ignored because of their smaller pulse heights. Fission events are identified by the neutrons which accompany the fission process. These neutrons are thermalized in the scintillating solution and provide delayed pulses which characterize a fission event. Capture events are not followed by delayed pulses from the scintillator. Corrections are applied for the fission events not followed by delayed-neutron pulses and for the effect of background counts. The capture, capture plus fission, and background events are recorded simultaneously. This procedure yields values of $1+\alpha$ to an accuracy of 1 or 2%.

**Mesures de $\alpha$ pour $^{233}U$, $^{235}U$ et $^{239}Pu$ pour des neutrons monoénergétiques.** Les auteurs ont mesuré le rapport, $\alpha$, section efficace de fission/section efficace de capture pour $^{233}U$, $^{235}U$ et $^{239}Pu$, pour neuf énergies de neutrons incidents (de 30 keV à 1000 keV). Un faisceau de neutrons, pulsé et collimaté, bombarde une cible placée au centre d'un grand scintillateur liquide chargé au cadmium. Les captures et les fissions sont détectées au moyen des rayons gamma instantanés qui les accompagnent; les diffusions élastiques et inélastiques ne sont pas détectées, car les hauteurs des impulsions associées sont plus faibles. Les fissions sont identifiées au moyen des neutrons qui accompagnent les processus de fission. Ces neutrons sont ralentis dans le scintillateur et donnent des impulsions retardées qui caractérisent les fissions. Les captures ne sont pas suivies d'impulsions retardées venant du scintillateur. Il faut appliquer des corrections pour tenir compte des fissions qui ne sont pas suivies d'impulsions de neutrons retardés et du bruit de fond. La capture, la capture suivie de fission, le bruit de fond sont enregistrés simultanément. Ce procédé donne une valeur de $1+\alpha$ avec une précision de 1 à 2% près.

**Измерения $\alpha$ для $U^{233}$, $U^{235}$ и $Pu^{239}$ для моноэнергетических нейтронов.** Отношение сечения захвата нейтронов к сечению деления, $\alpha$, измерялось для урана-233, урана-235 и плутония-239 при 9 энергиях бомбардирующих нейтронов от 30 кэв до 1.000 кэв. Пульсирующий и коллимированный пучок нейтронов пропускается через мишень в центре крупного жидкостного сцинтиллятора с кадмием. Захваты и деления обнаруживаются посредством гамма-лучей мгновенных нейтронов; акты упругого и неупругого рассеяния игнорируются ввиду малых размеров их импульсов. Акты деления опознаются по нейтронам, которые сопровождают процесс деления. Эти нейтроны доводятся до тепловой энергии в сцинтиллирующем растворе и дают запаздывающие импульсы, которые характеризуют акт деления. Акты захвата не дают запаздывающих импульсов от сцинтиллятора. Поправки применяются к актам деления, за которыми не следуют импульсы запаздывающих нейтронов и к эффекту обусловленного счетом фона. Акты захвата, захвата плюс деления и фона записываются одновременно. Этот метод дает значения $1+\alpha$ с точностью 1 или 2%.

**Mediciones de $\alpha$ para neutrones monoenergéticos correspondientes a los isótopos $^{233}$U, $^{235}$U y $^{239}$Pu.** Se han medido los cocientes $\alpha$ entre las secciones eficaces de captura y de fisión de los isótopos $^{233}$U, $^{235}$U y $^{239}$Pu para neutrones incidentes de nueve niveles energéticos comprendidos entre 30 y 1000 keV. A tal efecto se hace pasar un haz pulsado y colimado de neutrones a través de un blanco que se coloca en el centro de un gran centelleador líquido cargado con cadmio. Las capturas y las fisiones se detectan por los rayos gamma inmediatos emitidos; los fenómenos de dispersión elástica o inelástica son ignorados porque la amplitud de sus impulsos es menor. Las fisiones se identifican gracias a los neutrones a que dan origen. Estos neutrones se termalizan en la solución de centelleo y producen impulsos retardados que caracterizan al suceso de fisión. Las capturas no van seguidas de impulsos retardados en el centelleador. Se aplican factores de corrección para tener en cuenta las fisiones que no van seguidas de impulsos neutrónicos retardados, así como la actividad de fondo. Las capturas, capturas más fisiones y la actividad de fondo se registran simultáneamente. Por este procedimiento se obtienen valores de $1+\alpha$ con una precisión de 1 a 2 por ciento.

A measurement of $\alpha$, the ratio of neutron capture to neutron-induced fission cross-sections for $U^{233}$, $U^{235}$ and $Pu^{239}$ has been completed recently at Los Alamos. This ratio was measured as a function of neutron energy from 30 keV to 1000 keV.

Ultimately we desire a knowledge of $\eta$, the number of neutrons per fission available for fission and breeding. The parameters $\eta$ and $\alpha$ are related by the expression, $\eta=\bar{\nu}/(1+\alpha)$, where $\bar{\nu}$ is the average number of neutrons emitted per fission. There are two approaches to the determination of $\eta$, namely the direct measurement of $\eta$ as in the manganese-bath experiments [1] and the indirect method of separate measurements of $\bar{\nu}$ and of $\alpha$. We chose the second technique, and this report will describe the measurement of $\alpha$.

This experiment involves the detection of gamma-radiation accompanying neutron capture or fission. A pulsed beam of neutrons from the T (n, p) $He^3$ reaction is allowed to strike a target placed at the centre of a large liquid scintillator. Three processes can be initiated by the neutrons interacting with the target nuclei: neutron scattering, radiative capture and fission. Proton recoil pulses from the scintillator due to thermalization of scattered neutrons are discriminated against because of their low amplitude. On the other hand, both capture and fission are accompanied by gamma-radiation in coincidence with the beam pulse. This radiation will be detected with almost 100% efficiency by the large liquid scintillator and produces a prompt pulse which allows the selection of capture and fission events while discriminating against scattering. Since the total energy of the fission gamma-rays is approximately the same as the total energy of the capture gamma-rays, it is not possible to distinguish between the two events by observation only of the prompt pulses.

Fission, however, is also accompanied by neutron emission. This fact provides the basis for the technique of distinguishing fission from capture events. The scintillator is large enough to cause most of the fission neutrons to be thermalized and finally captured in the liquid. The solution is cadmium loaded to ensure that most neutrons will be captured within 32 μs. The 9-MeV pulse produced by neutron capture in the cadmium provides a delayed pulse to identify fission events.

If we neglect all background corrections and the fact that not all fission events are followed by delayed pulses, the experiment is very simple. The prompt pulse is used as a trigger to open a 32-μs gate between the scintillator and some sort of

pulse-detector. If any pulses occur during the gate, the prompt pulse was due to a fission event. However, if no pulses occur during the gate, the prompt pulse was due to radiative capture. The ratio of the number of capture to the number of fission pulses is $\alpha$. The corrections for background radiation and the fact that not all fissions are accompanied by delayed pulses in the scintillator are discussed below.

Fig. 1 shows the arrangement of neutron source, collimator, scintillator and shielding. The scintillator tank is 1 m in diameter and 1 m long. It is filled with a

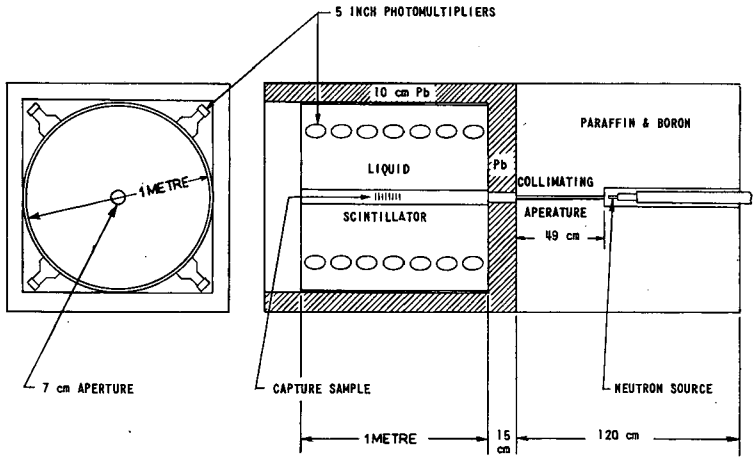


Fig. 1
End view and cross-section of the scintillator, neutron source, and shielding. A collimated and pulsed beam of neutron is passed through the target at the centre of the scintillator.

mixture of toluene, terphenyl, POPOP (a wave-length shifter) and cadmium propionate. The scintillating solution is viewed by 28 5-in photomultiplier tubes connected in parallel.

The isotope whose $\alpha$ is to be measured is placed in the centre of the scintillator. Through this target is passed a pulsed beam of fast neutrons, collimated so as not to enter the scintillating volume. The duration of the pulse is 0.1 μs and the pulses are separated by 32 μs. The scintillator has a very high efficiency and must therefore be well shielded.

The fraction of fission not followed by delayed pulses in the scintillator was measured by substituting a fission counter for the target in the centre of the scintillator. A coincidence between the fission counter and the scintillator establishes the fact that a fission took place and the gate is then opened. The probability of detecting a pulse during the gate is then measured.

The coincidence work is performed with a time-to-pulse-height converter. It measures the time between scintillator pulses and the beam pulse and puts out a pulse with height proportional to the time interval. Fig. 2 shows the output of the time-converter displayed on a 100-channel pulse-height analyser. The target is $U^{235}$. This is a plot of counting rate against time over a 1-μs interval. There is a constant background counting rate on which is superimposed a peak due to

fission and capture gamma-rays. Most of the counts in the peak are due to fission. The output of the time-to-pulse-height converter is fed to a single-channel pulse-height analyser, centred on the prompt interval. The single-channel pulse-height analyser selects those scintillator pulses in coincidence with the beam pulse. The

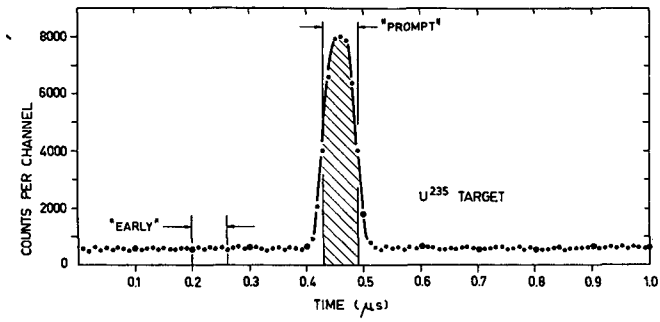


Fig. 2
Time distributions of scintillator pulses with the $U^{235}$ sample in the scintillator. The prompt channel includes the pulses due to radiative capture and fission. The "early" channel contains background pulses.

coincidence pulse is then used to trigger the gating circuit, between the scintillator and a pulse-detector. Meanwhile a 50-channel pulse-height analyser has analysed, but not stored, the prompt pulse from the scintillator. If any pulses occur during the 32-μs gate the analysed pulse is not stored. However, if no pulses occur during the 32-μs gate the analysed pulse is stored.

Thus the 50-channel pulse-height analyser displays those pulses occurring at prompt time that are not followed by delayed pulses. These pulses are mostly due to capture events. The trigger pulses, or coincidences, are mostly due to captures plus fissions.

The preceding was a description of one-half of a dual system. Another identical system with a single-channel pulse-height analyser centred on an interval of the time spectrum preceding a beam pulse is used to correct for the background radiation.

A correction for the effect of prompt capture of scattered neutrons in the scintillator construction materials is determined by substituting a mock-up sample for the fissionable sample. The characteristic of the mock-up is that it produces the same scattering as the fissionable sample, but does not fission or capture neutrons. A polyethylene mock-up was used for this purpose. With these corrections for background pulses we obtain the scintillator pulse-height spectra for capture plus fissions not followed by delayed pulses.

Fig. 3 shows the results of the present experiment for $U^{233}$. Almost no data are available for comparison. $\alpha$ is plotted as a function of the incident neutron energy from 30 keV to 1000 keV. The absolute standard deviations are based on a combination of statistical uncertainties, related to the number of events observed, and estimates of uncertainties in the extrapolation of the spectra to zero energy. The neutron energy spread is due to the tritium target thickness and the time resolution of the timing circuits.

Fig. 4 shows our results for $\alpha$ of $U^{235}$; $\alpha$ is plotted *versus* incident neutron energy between 30 keV and 1000 keV. The curve drawn is meant only to guide the eye.

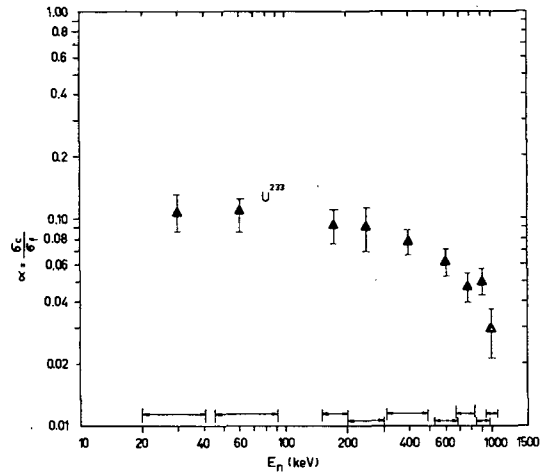


Fig. 3
The ratio of neutron capture to fission cross-sections, α, is plotted as a function of incident neutron energy from 30 to 1000 keV for $U^{233}$. The horizontal arrows indicate the incident neutron energy spread.

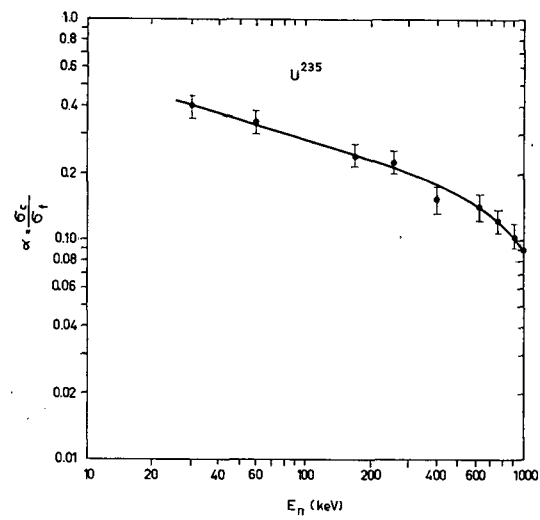


Fig. 4
The ratio of neutron capture to fission cross-sections, α, is plotted *versus* incident neutron energy between 30 and 1000 keV for $U^{235}$.

A theoretical prediction of α in this energy region is a matter of some difficulty, involving the effects of various angular momenta, competition with inelastic scattering, and varying fission and radiation widths.

Fig. 5 shows our results and results of other groups for α of $U^{235}$. The solid black line is the curve shown in Fig. 4; it represents our measurements. The data of DIVEN *et al.* [2] are not shown here, since our present experiment supersedes these

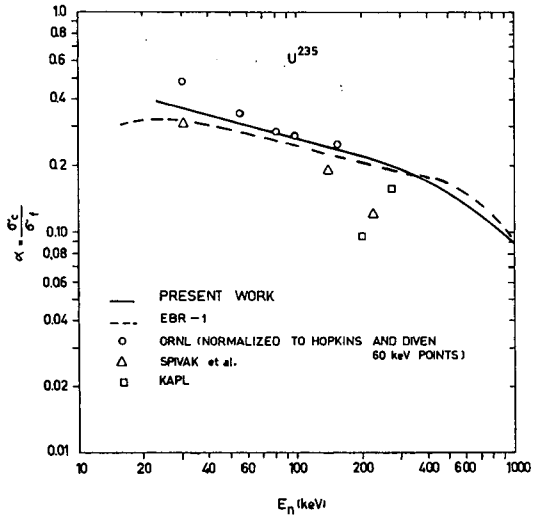


Fig. 5
The ratio of neutron capture to fission cross-sections, $\alpha$, is plotted as a function of incident neutron energy from 30 to 1000 keV for $U^{235}$.

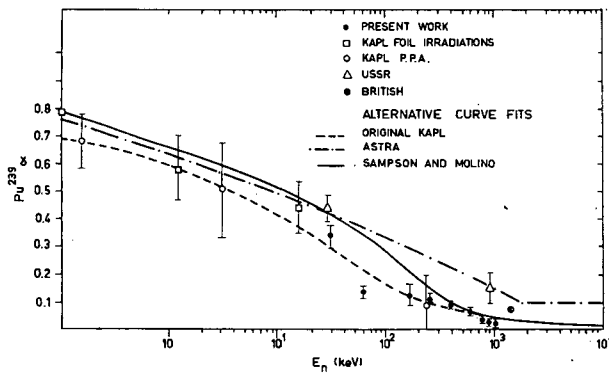


Fig. 6
The experimental values for $\alpha$, the ratio of neutron capture to fission cross-sections are plotted as a function of the incident neutron energy for $Pu^{239}$. An explanation of the curves is given in the text.

measurements. The dashed curve was taken from a neutron capture cross-section curve obtained from EBR-1 data of KAFALAS *et al.* [3] and reported by YIFTAH *et al.* [4].

The ORNL data [5] are from a comparison of the total absorption cross-section of $U^{235}$ to the capture cross-section of indium normalized to our 60-keV point. The KAPL data [6] were obtained with appropriately shielded foils in reactor spectra. Mass-spectrometer and radiochemical analysis were used for a determination of the neutron capture and fission yields. SPIVAK and his co-workers [7] measured $\eta$ using photoneutron sources and computed $\alpha$.

An analysis of the previous data on $\alpha$ for $P^{239}$ was made by SAMPSON and MOLINO at KAPL [8]. Fig. 6 shows the results of that analysis with the data from the present experiment. The KAPL foil-irradiation measurements are those of KANNE, STEWART and WHITE [6]. Appropriately shielded $Pu^{239}$ foils were exposed to reactor spectra and the $\alpha$ determined from the observed induced fission-product activity and the change in isotopic composition. The KAPL, PPA and United Kingdom measurements were obtained from the reactivity effect of $Pu^{239}$ upon various critical assemblies. The USSR data were based upon a measurement of $\eta$ using a ($\gamma$, n) neutron source. The Astra curve, suggested by Baraff and Mallon, is based upon data published about the time of the first Geneva conference. It includes the United Kingdom and USSR data but not the PPA data. The "original KAPL" curve was based upon the KAPL measurements. The Sampson and Molino curve is based on all previous measurements plus the EBR-1 data of Kafalas *et al.* [3]. This curve is consistent with all previous measurements except for the high-energy USSR measurement. Sampson and Molino conclude that $\alpha$ undergoes a sharp decrease with increasing energy near 100 keV. Our results indicate a sharp decrease in $\alpha$ near 60 keV neutron energy.

## REFERENCES

[1] MACKLIN, R. L., *et al.*, Reports to the AEC Nuclear Cross Sections Advisory Group, WASH-1026 (1959) 42.
[2] DIVEN, B. C., TERRELL, J. and HEMMENDINGER, A., *Phys. Rev.* **109** (1958) 144—150.
[3] KAFALAS, P., LEVENSON, M. and STEVENS, C. M., *Nucl. Sci. and Engng* **2** (1957) 657—663.
[4] YIFTAH, S., OKRENT, D. and MOLDAUER, P. A., Fast Reactor Cross Sections, Pergamon Press, New York (1960) 80—88.
[5] GIBBONS, J. H. *et al.*, Reports to the AEC Nuclear Cross Sections Advisory Group, WASH-1026 (1959) 48.
[6] KANNE, W. R., STEWART, H. B. and WHITE, F. A., Proc. UN Int. Conf. PUAE **4** (1955) 315—320.
[7] Reactor Physics Constants, ANL-5800 (1958) 55.
[8] SAMPSON, J. B. and MOLINO, D. F., KAPL-1793 (May 1957).

SM—18/79

# EFFECTIVE RESONANCE ABSORPTION INTEGRALS FOR ZIRCONIUM AND NIOBIUM

E. HELLSTRAND, G. LINDAHL AND G. LUNDGREN
AKTIEBOLAGET ATOMENERGIS,
SWEDEN

**Abstract — Résumé — Аннотация — Resumen**

**Effective resonance absorption integrals for zirconium and niobium.** The resonance absorption integrals of zirconium and niobium have been measured at the Swedish reactor R 1 with the pile-oscillator technique. In the case of niobium, measurements were also made by activation. The results of the two methods agree within the limits of error.

**Intégrales d'absorption par résonance effective du zirconium et du niobium.** Les intégrales d'absorption par résonance du zirconium et du niobium ont été déterminées par la technique de l'oscillateur de pile, dans le réacteur suédois R 1. Dans le cas du niobium, les mesures ont été faites anssi par la méthode d'activation. Les résultats donnés par les deux méthodes coïncident dans la limite des erreurs expérimentales.

**Эффективное интегральное поглощение циркония и ниобия.** На шведском реакторе R 1 при помощи реакторного осциллятора измерялось эффективное интегральное поглощение циркония и ниобия. Измерение поглощения ниобия осуществлялось также с помощью активации. Полученные результаты этих двух методов измерения согласуются в пределах погрешности.

**Integrales de absorción de resonancia efectiva para el zirconio y el niobio.** Empleando la técnica del oscilador, se han medido en el reactor sueco R-1 las integrales de absorción de resonancia del zirconio y del niobio. En el caso del niobio, se realizaron también mediciones por activación. Los resultados de ambos métodos concuerdan dentro de les límites de error experimental.

## Introduction

A series of measurements of resonance integrals has been undertaken at the Swedish reactor R1. Results for thorium metal and for copper, manganese, cobalt, molybdenum and sodium have recently been published [1, 2]. The present paper will deal with measurements on zirconium and niobium.

The measurements were made at the reactor centre, where the energy distribution of the epithermal neutron flux had earlier been studied with a fast chopper [3]. The deviation from the $1/E$ distribution is about 6% over the energy range 5 eV to 10 keV, the flux per unit lethargy, $\Phi(u)$, being larger at high energy than at low. Above 10 keV, no experimental information is available but it is likely that $\Phi(u)$ decreases slightly with increasing energy.

## Zirconium

For zirconium, the main resonance absorption occurs in the $Zr^{91}$ isotope. As neutron capture in that isotope leads to the stable $Zr^{92}$ isotope, the activation technique cannot be used for the determination of the resonance integral for zirconium. The measurements were therefore made with pile-oscillator technique.

Pure zirconium samples of desired geometrical form could not be obtained. Plates of zircaloy-2 of known composition were therefore chosen as samples. The plates had a length of 200 mm and a width of 40 mm; the thickness varied between 0.2 mm and 6.4 mm. The measurements were made in the total reactor spectrum, and thus the reactor response was proportional to the sum of the thermal and epithermal absorption of the samples. The proportionality constant was determined by oscillating boron samples prepared by pipetting known amounts of boric acid on to filter paper.

The evaluation of the effective resonance integrals, R$I$, for the different plate thicknesses requires a knowledge of the thermal absorption cross-section, $\sigma_0$, and of the quantity $r\sqrt{T/T_0}$ ($T$ is the neutron temperature in the Maxwellian part of the reactor spectrum, $T_0$ is 293 °K and $r$ is defined by WESTCOTT [4]). $\sigma_0$ was determined from BNL-325, 2nd ed. and Suppl. No. 1, and the known composition of the alloy including impurities. $r\sqrt{T/T_0}$ was obtained from the cadmium ratio for gold, assuming $\sigma_0$ and R$I$ for gold to be known.

The result of the measurement is shown in Fig. 1. The effective resonance integral for zirconium is there given as a function of the effective plate thickness, $d_{\mathrm{eff}}$ ($d_{\mathrm{eff}}$ is the thickness of an infinite plate giving the same surface to mass ratio as the actual plates). A crude extrapolation to zero plate thickness gives a value for the dilute integral. One obtains: R$I = 0.85 \pm 0.15$ b*.

## Niobium

The measurements on niobium were performed both with pile-oscillator technique and with activation technique. For the oscillations, samples with suitable length and width were prepared by rolling. The final thickness was 0.05 mm, and either a single foil or two or three foils on top of each other were oscillated. The resonance integral was then evaluated in the same way as for zirconium.

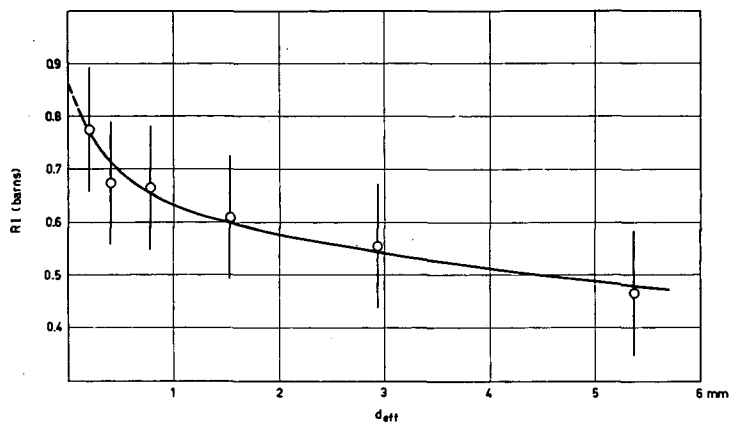


Fig. 1
The effective resonance integral of zirconium as a function of plate thickness.

* A more detailed account of the measurements has been submitted to *Arkiv för Fysik* for publication.

The activation measurements were made by comparing the cadmium ratio for gold and niobium in the same neutron spectrum. Assuming values for $\sigma_0^{Au}$, $R\,I^{Au}$ and $\sigma_0^{Nb}$ to be known, the resonance integral for niobium may be obtained. As the energy distribution of the neutron flux differs from $1/E$, a small correction factor has to be applied to account for the fact that the main resonance absorption in gold and niobium does not occur at the same energy. The correction amounts to about 4%.

The *preliminary* values from the activation and pile-oscillator measurements are given in Table I.

TABLE I

**EFFECTIVE RESONANCE INTEGRALS FOR NIOBIUM**
**Preliminary values**

| Method | Foil thickness (mm) | R $I$ (b) |
|---|---|---|
| Activation | 0.05 | 7.80 ± 0.30 |
| Pile oscillator | 0.05 | 7.35 ± 0.70 |
| Pile oscillator | 0.10 | 7.70 ± 0.70 |
| Pile oscillator | 0.15 | 7.20 ± 0.70 |

The results obtained with the two methods agree within the limits of error. Extrapolation of results from activation experiments with different numbers of foils placed on top of each other yields a self-screening effect of about 5% for a single foil. Tentatively, a value of 8.2 b may therefore be given for the dilute integral. Earlier values are 7.8 b [4] and 13 ± 5 b [5].

## REFERENCES

[1] HELLSTRAND, E. and WEITMAN, J., *Nucl. Sci. Engng* **9** (1961) 507.
[2] DAHLBERG, R., JIRLOW, K. and JOHANSSON, E., *J. nucl. Energy*, Part A/B **12** (1961) 53.
[3] JOHANSSON, E., LAMPA, E. and SJÖSTRAND, N. G., *Ark. Fys.* **18** (1960) 513.
[4] MACKLIN, R. L. and POMERANCE, H. S., Proc. UN Int. Conf. PUAE **5** (1956) 96.
[5] TATTERSALL, R. B., ROSE, H., PATTENDEN, S. K. and JOWITT, D., *J. nucl. Energy*, Part A **12** (1960) 32.

# I. 3. FISSION PROPERTIES

# EXPERIMENTAL STUDIES OF FISSION PROPERTIES UTILIZED IN REACTOR DESIGN*

D. BUTLER, S. COX, J. MEADOWS, J. ROBERTS, A. SMITH AND J. WHALEN
ARGONNE NATIONAL LABORATORY, ARGONNE, ILL.,
UNITED STATES OF AMERICA

**Abstract — Résumé — Аннотация — Resumen**

**Experimental studies of fission properties utilized in reactor design.** A programme of experimental studies of fission parameters useful in reactor design is described including the following:

(*a*) The periods and yields of delayed-neutron groups emitted following the neutron-induced fission of $Pu^{241}$ are measured. Evidence for systematic isotopic dependence of delayed-neutron yields is presented. An experimental investigation of the relation between the time behaviour of delayed-neutron emission and the energy of the incident neutron inducing fission is described.

(*b*) The cross-section for the inducing of fission in $Am^{243}$, $Pu^{242}$ and $Pu^{241}$ with neutrons in the energy range 0.030 to 1.8 MeV is measured. Emphasis is placed upon the detailed dependence of the fission cross-section on the incident-neutron energy. The absolute values of the cross-sections are given to a precision of ~25%.

(*c*) Detailed results of a measurement of the $Pu^{241}$ fission-neutron spectrum are given, including the spectral shape and average fission-neutron energy. Techniques and methods of measuring prompt-fission-neutron spectra are described.

(*d*) The dependence of $\bar{\nu}$ (the average number of neutrons emitted per fission) of $U^{235}$ on the incident neutron energy is measured from 100 keV to 1.6 MeV. $\bar{\nu}$ of $U^{238}$ and other fissile isotopes is compared to $\bar{\nu}$ of $U^{235}$ (thermal). The relative precision of the measurements is $\gtrsim 1.2\%$.

**Etude expérimentale des propriétés de la fission utilisées dans les études de réacteurs.** Les auteurs décrivent un programme d'études expérimentales sur les paramètres de la fission dont il faut tenir compte dans les études de réacteurs.

*a*) On a mesuré les périodes et les rendements de groupes de neutrons retardés libérés par la fission induite de $^{241}Pu$. Les auteurs établissent la relation existant entre les rendements en neutrons retardés et la composition isotopique. Ils décrivent des recherches expérimentales sur le rapport entre le comportement dans le temps de l'émission des neutrons retardés et l'énergie du neutron incident provoquant la fission.

*b*) On a mesuré les sections efficaces de fission de $^{243}Am$, $^{242}Pu$ et $^{241}Pu$ provoquée par des neutrons dont l'énergie varie entre 0,030 et 1,8 MeV. Les auteurs soulignent la relation étroite qui existe entre la section efficace de fission et l'énergie des neutrons incidents. Ils indiquent les valeurs absolues des sections efficaces avec une précision d'environ 25%.

*c*) Les auteurs exposent en détail les résultats de la mesure du spectre des neutrons de fission de $^{241}Pu$, notamment la forme du spectre et l'énergie moyenne des neutrons de fission. Ils décrivent les techniques et les méthodes utilisées pour mesurer le spectre des neutrons instantanés de fission.

*d*) La dépendance de $\bar{\nu}$ (nombre de neutrons libérés par fission) de $^{235}U$ vis-à-vis de l'énergie des neutrons incidents a été mesurée dans le domaine de 100 keV à 1,6 MeV. Les auteurs comparent le $\bar{\nu}$ de $^{238}U$ et celui d'autres isotopes fissiles au $\bar{\nu}$ de $^{235}U$ (thermique) d'autre part. Les mesures ont été faites avec une précision de l'ordre de 1,2%.

* Work performed under the auspices of the United States Atomic Energy Commission.

**Экспериментальное изучение характеристик деления, используемых при расчете реакторов.** В докладе описывается программа экспериментальных исследований параметров деления, полезных при расчете реакторов, включая нижеследующее.

*a*) Измеряются периоды и выходы групп запаздывающих нейтронов, испускаемых в результате деления плутония-241, вызванного нейтронами. Доказывается очевидность систематической изотопной зависимости выхода запаздывающих нейтронов. Описывается экспериментальное изучение связи между временным режимом эмиссии запаздывающих нейтронов и энергией бомбардирующих нейтронов, вызывающих деление.

*b*) Измеряется сечение деления $Am^{243}$, $Pu^{242}$ и $Pu^{241}$ нейтронами в области энергии от 0,030 до 1,8 Мэв. Особое внимание уделяется зависимости сечения деления от энергии бомбардирующих нейтронов. Абсолютные значения сечений даются с точностью $\sim 25\%$.

*c*) Даются подробные результаты измерения спектра нейтронов деления $Pu^{241}$, включая форму спектра и среднюю энергию нейтронов деления. Описываются приемы и методы измерения спектров мгновенных нейтронов деления.

*d*) Измеряется зависимость $\bar{\nu}$ (среднее число нейтронов, испускаемых на одно деление) урана-235 от энергии бомбардирующих нейтронов в области энергии от 100 кэв до 1,6 Мэв. $\bar{\nu}$ урана-238 и других расщепляющихся изотопов сравнивается с $\bar{\nu}$ урана-235 (тепловые). Точность измерений равняется $\gtrsim 1{,}2\%$.

**Estudio experimental de las propiedades de fisión utilizadas en el diseño de reactores.** Los autores describen un programa de estudios experimentales de los parámetros de fisión que se han de tener en cuenta en el diseño de reactores.

*a*) Medición del período y rendimiento de los grupos de neutrones retardados emitidos a raíz de la fisión del $^{241}Pu$, inducida por neutrones. Los autores demuestran que hay una relación de dependencia sistemática entre el rendimiento de neutrones retardados y la composición isotópica empleada. Describen estudios experimentales de la relación existente entre el comportamiento en el tiempo de la emisión de neutrones retardados y la energía del neutrón incidente que provoca la fisión.

*b*) Medición de las secciones eficaces de fisión del $^{243}Am$, $^{242}Pu$ y $^{241}Pu$ inducida por neutrones de energía comprendida entre 0,030 y 1,8 MeV. Los autores examinan con particular detenimiento la variación de la sección eficaz en función de la energía del neutrón incidente. Indican los valores absolutos de las secciones eficaces con una precisión del orden del 25%.

*c*) Exposición detallada de los resultados de la medición del espectro de los neutrones de fisión del $^{241}Pu$, inclusive la forma del espectro y la energía media de los neutrones de fisión. Los autores describen técnicas y métodos para medir los espectros de los neutrones inmediatos de fisión.

*d*) Medición, en el caso del $^{235}U$, de la variación de $\bar{\nu}$ (número medio de neutrones emitidos por fisión), en función de la energía del neutrón incidente, para el intervalo 100 keV — 1,6 MeV. Los autores comparan el valor $\bar{\nu}$ del $^{238}U$, y de otros isótopos fisionables con el valor de $\bar{\nu}$ correspondiente al $^{235}U$ (neutrones térmicos). Las mediciones se efectuaron con una precisión del orden del 1,2 por ciento.

## Introduction

The precise calculation of the properties of fast reactors cannot be made without knowledge of the nuclear characteristics of the materials used in the reactors. At present our limited understanding of the physics of the fission process makes it necessary to obtain most of these characteristics from direct measurements. However, by proper choice and design of experiments, the results can be made to be not only of applied usefulness, but also of value in increasing basic understanding of fission. This paper will describe four experiments performed with both of these objectives in mind.

The first experiment is a measurement of the periods and yields of the delayed neutrons from $Pu^{241}$. This information is directly useful in determining the properties of fast reactors utilizing recycled fuel. It will also be shown, together with other delayed-neutron data, to suggest a systematic dependence of delayed-neutron yields on charge and mass number. The second experiment is the measurement of the fission cross-sections of $Pu^{241}$, $Pu^{242}$ and $Am^{243}$. These cross-sections are useful both for reactor calculations and for extending knowledge of the systematics of fission. The third and fourth measurements are most meaningful for applied use, because they represent phenomena where basic understanding is still extremely rudimentary. They are the determination of the energy spectrum of prompt neutrons from the fission of $Pu^{241}$, and measurements of $\bar{\nu}$ for $U^{238}$ and $U^{235}$, the latter as a function of incident neutron energy.

## Periods and yields of delayed neutrons from $Pu^{241}$

The experimental set-up used for the measurement of the periods and yields of delayed neutrons from $Pu^{241}$ is shown schematically in Fig. 1. A collimated

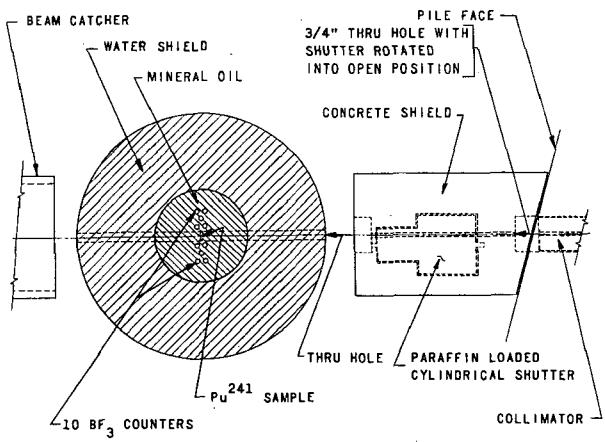


Fig. 1
Schematic diagram of the apparatus used for the measurement of delayed neutrons from $Pu^{241}$.

thermal-neutron beam from the Argonne research reactor was passed through a shutter and then through the shield tank. The fissionable sample was placed in the beam at the centre of the tank and surrounded by an array of $BF_3$ proportional counters to detect the delayed neutrons. After an irradiation of several minutes, the shutter was closed and the decay of the delayed neutrons was followed using a digital time analyser.

The delayed-neutron decay was measured for both $Pu^{241}$ and $U^{235}$. The $U^{235}$ served as a check of the counter response and also as a standard for the determination of the total yield of delayed neutrons from the $Pu^{241}$. The results of the delayed-neutron yield measurements are listed in Table I together with data obtained by Keepin *et al.* [1], which is included for comparison. Because of physical limitations imposed by the shutter support, the data of this experiment

TABLE I

**PLUTONIUM DELAYED-NEUTRON EMISSION**

| Group index | $Pu^{239}$* | $Pu^{240}$* | $Pu^{241}$ |
|---|---|---|---|
| | *Delayed-neutron yields*** | | |
| 1 | 2.1 ±0.6 | 2.2 ±0.3 | 1.54 ±0.4 |
| 2 | 18.2 ±2.3 | 23.8 ±1.6 | 36.5 ±1 |
| 3 | 12.9 ±3.0 | 16.2 ±4.4 | 27.5 ±4.0 |
| 4 | 19.9 ±2.2 | 31.5 ±2.7 | 62.0 ±8.0 |
| 5 | 5.2 ±1.8 | 11.9 ±1.8 | 29.0 ±3.0 |
| 6 | 2.7 ±1.0 | 2.4 ±0.5 | — |
| Total | 61 ±3 | 88 ±6 | 154 ±15 |
| | *Delayed-neutron periods (seconds)* | | |
| 1 | 54.28 ±2.34 | 53.56 ±1.21 | 54.0 ±1 |
| 2 | 23.04 ±1.67 | 22.14 ±0.38 | 23.2 ±0.5 |
| 3 | 5.60 ±0.4 | 5.14 ±0.42 | 5.6 ±0.6 |
| 4 | 2.13 ±0.24 | 2.08 ±0.19 | 1.97 ±0.1 |
| 5 | 0.618 ±0.213 | 0.511 ±0.077 | 0.43 ±0.04 |
| 6 | 0.257 ±0.045 | 0.172 ±0.033 | — |

* The $Pu^{239}$ and $Pu^{240}$ data are from KEEPIN *et al.* [1].
** *All values are absolute number of delayed-neutrons/fission* $\times 10^4$.

could not be analysed until after 0.5-s decay time had elapsed, by which time no measurable yield from the 0.2-s group remained.

The results indicate a delayed fraction, $\beta$, for $Pu^{241}$ a little over twice that for $Pu^{239}$. Therefore the build-up of $Pu^{241}$ in a reactor will increase the difference in reactivity between delayed and prompt critical, thus helping in the problem of reactor control. The periods measured for the five observed groups are also given in Table I. These are, within the limits of experimental error, the same as those observed by Keepin. It should be emphasized that the assignment of these groups is not unique. Recently, precursors with periods of 16.3 and 24.4 s have been separated using radiochemical techniques [3, 4]. That a least squares fit to Keepin's extensive data cannot separate these two, suggests that there may be other groups as yet unresolved as well. Fortunately for the reactor scientists, the fact that the data can be fitted so well with six periods means that no more need be included in reactor kinetics calculations.

A graphical presentation of the absolute delayed-neutron group yields is given as a function of mass number from isotopes of Th, U, Pu, and Cf in Fig. 2 [1, 2]. The total delayed-neutron yields for each isotope are shown in Fig. 3. The curves drawn through the experimental points are for purposes of emphasizing the systematics of Fig. 2 and Fig. 3. For a given atomic number, the delayed-neutron yield increases strongly with mass number, except for the 54-s period. For a given mass number there is a sharp decrease in delayed-neutron yield with increasing atomic number. The dependence on atomic number appears to be much stronger than the dependence on mass number. For example, the extrapolated $Pu^{238}$ yields are roughly an order of magnitude smaller than the $U^{238}$ yields. For an addition of two mass units, however, the delayed-neutron yield increases only about a factor of three. An examination of the fission mass distribution [5] for the three uranium isotopes represented here shows immediately

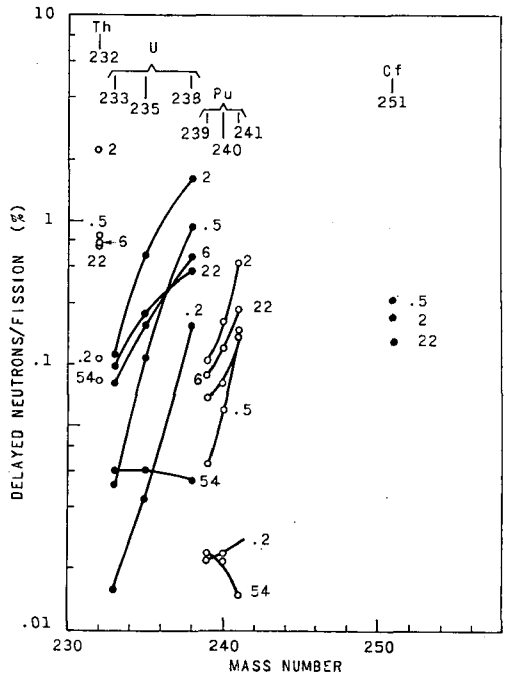


Fig. 2
Absolute individual delayed-neutron group yield from isotopes of Th, U, Pu and Cf. The numbers beside the experimental points and curves represent the approximate half-life for the associated delayed-neutron group. The curves drawn through the experimental points for U and Pu are for the purpose of emphasizing the systematic behaviour.

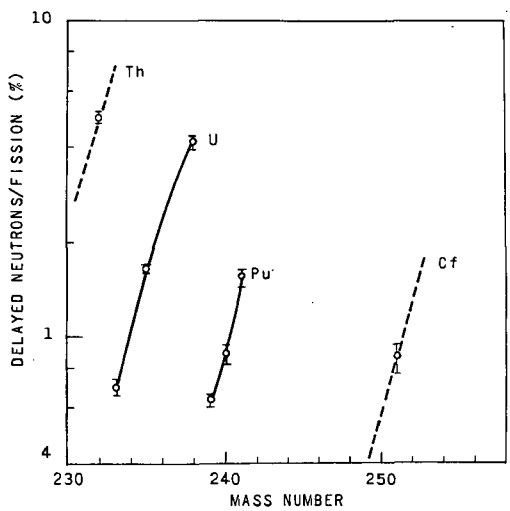


Fig. 3
Absolute total delayed-neutron yields for isotopes of Th, U, Pu and Cf. The dashed curves through Th and Cf represent the possible behaviour of the delayed-neutron yield of Th and Cf as suggested by the behaviour of the delayed-neutron yield for U and Pu.

that the change in the mass distribution between $U^{233}$ and $U^{238}$ is inadequate to account for the large increase in the delayed-neutron yield. The alternative to a dependence of delayed-neutron yield on mass distribution is a dependence on the charge distribution of the fission fragments [6, 7, 8, 9]. This means that the sharp decrease in yield between $U^{238}$ and $Pu^{239}$, and $Th^{232}$ and $U^{233}$, is due to an abrupt shift in the charge distribution resulting from the addition of two charges to the fissionable nucleus.

The systematic trends of the delayed-neutron yields from the uranium and plutonium isotopes appear to be clear enough to justify approximate determination of the yields of unmeasured isotopes by interpolation and extrapolation. Such determination of delayed-neutron yields is very useful in the study of reactors utilizing high nuclear burn-ups, or re-cycled fuel.

## Neutron-induced fission cross-sections of $Pu^{241}$, $Pu^{242}$, and $Am^{243}$

The cross-sections for neutron-induced fission of $Pu^{241}$, $Pu^{242}$ and $Am^{243}$ were determined by measuring the ratio of the cross-sections to that of $U^{235}$ [10, 11]. The measurements were made with a back-to-back gas scintillation counter as shown in Fig. 4. A gas scintillator was chosen because the short duration

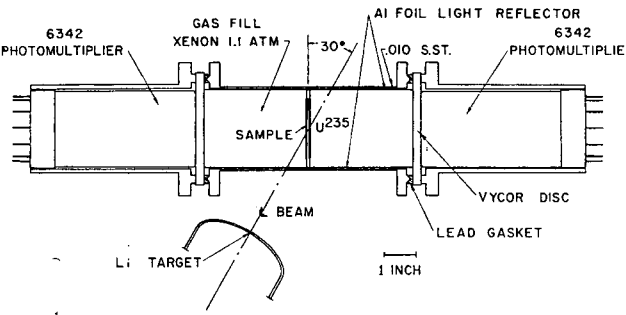


Fig. 4
Back-to-back gas scintillation counter used in the fission cross-section measurements.

of its pulses made it possible to eliminate most of the pile-ups of alpha pulses. The counter was filled with an argon-nitrogen mixture or with pure xenon, both of which gave good performance.

The neutrons for the measurements were produced by the $Li^7$ (p, n) $Be^7$ reaction using protons from an electrostatic generator. For most of the measurements the counter was placed at 0° with respect to the neutron beam. However, for the $Pu^{241}$ measurements below 150 keV, the counter was placed at 115.5° in order to avoid the second geometric group of neutrons. At this angle, because of physical limitations, the counter had to be located twice as far from the neutron source as at 0°. The increased distance together with the reduced yields from the target at 115.5° reduced the count rate almost a factor of 10. The result was an increase in the relative background count caused by low-energy neutrons scattered back by the surrounding air and structural materials. A check of the background was made by measuring the dependence of the count rate of a $BF_3$ proportional counter on distance from the neutron source. The departure of this

dependence from $1/R^2$ indicated that 20% of the $B^{10}$ count rate at the fission counter position was due to scattered neutrons, and that 80% of this background was below the cadmium cut-off. Estimating that the 0.26-V resonance [10] may subtend as much as a quarter of the background neutron spectrum, the effect of the $Pu^{241}$ measurement would be 5%. This must be considered as a possible systematic error causing as much as a 5% error in the $Pu^{241}$ fission cross-section below 150 keV. For all the data above 150 keV, the error would be 1% or less, and for the $Pu^{242}$ and $Am^{243}$ measurements less than 0.5%.

The fissionable samples were all thin deposits on platinum foils. Their masses were determined by alpha counting. The alpha counter was calibrated using the $U^{235}$ sample activity as a standard. The absolute activity of the $U^{235}$ sample was known from its mass spectrum and total mass, the latter being determined in its preparation by quantitative electrodeposition.

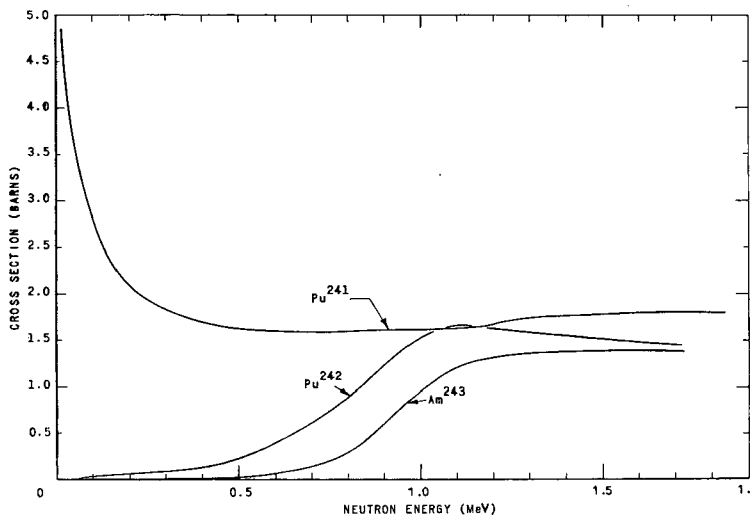


Fig. 5
Fission cross-sections of $Pu^{241}$, $Pu^{242}$ and $Am^{243}$.

The results of the fission cross-section measurements are shown in Fig. 5. They have been corrected for the second group of neutrons from the $Li^7$ (p, n) $Be^{7*}$ reaction above 600 keV [12, 13]. The total energy spread of the neutrons due to geometry and target thickness was maintained less than 70 keV for all data above 200 keV. For the $Pu^{241}$ measurements below 200 keV, it tapered down to a 17-keV spread at 21 keV incident energy.

The statistical errors in the $Pu^{242}$ and $Am^{243}$ measurements were 4% on the high energy plateaux, and in the $Pu^{241}$ measurements were 1.2% above 200 keV and about 5% between 20 and 200 keV. In addition to the statistical errors, it is necessary to consider systematic errors in the normalization of the curves. These arise primarily in the determination of the sample masses and in the correction for fissions not causing large enough pulses to be seen above the alpha pulses. No truly quantitative measure of these normalization errors is possible, but they can be estimated to be 6% for the $Am^{243}$ measurements, 5% for the

$Pu^{242}$ measurements, and 7% for the $Pu^{241}$ measurements above 150 keV. For the $Pu^{241}$ measurements below 150 keV, the low-energy air and room scattered neutrons may have caused as much as an additional 5% error.

As with the delayed-neutron yields, it appears now to be possible to make systematic generalizations with the fission cross-sections allowing the prediction of unmeasured cross-sections in the MeV region. For this purpose, the 2.5-MeV cross-sections [10, 14, 15, 16, 17] of the heavy elements, extrapolated from 1.7-MeV data where necessary, are plotted in Fig. 6 against $Z^2/A$ [14]. It can be

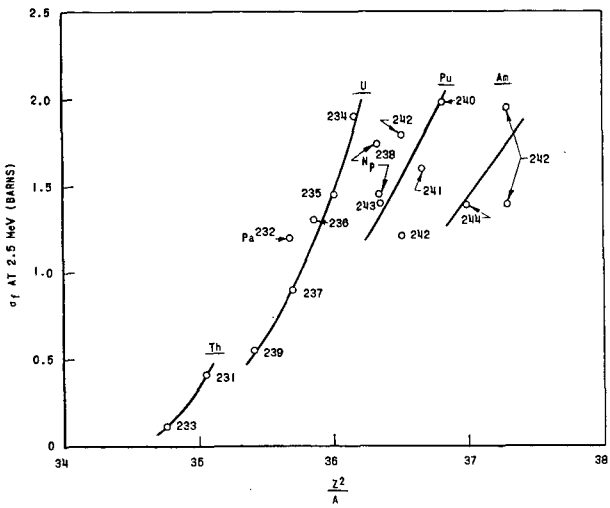


Fig. 6
Fission cross-sections at 2.5 MeV. Labels are the masses of the compound nuclei.

seen that great regularity exists for each element, suggesting the possibility of interpolation and extrapolation. Some of the plutonium and americium cross-sections, indicated by arrows in the figure, do not fit the curves well. However, in each instance of a poor fit, there are at least two independent measurements in disagreement with each other, so that additional data are needed before a final judgement of the validity of the systematic scheme can be made.

## Prompt fission-neutron spectrum of $Pu^{241}$

The energy spectrum of prompt neutrons from the fission of $Pu^{241}$ was determined using two techniques, measurement of neutron time of flight and measurement of the range of proton recoils in nuclear emulsions. The time-of-flight apparatus is shown in Fig. 7. A thermal-neutron beam was incident on a thin sample of fissionable material contained in a gas scintillation counter. Some of the neutrons resulting from fissions induced within the sample proceeded down the well-collimated flight path to the neutron scintillation detector $\sim$1 m distant. The time between the response of the fission detector and the arrival of the neutron at the scintillation detector was determined with a time to pulse height converter. By interchanging $Pu^{241}$ and $U^{235}$ fissionable samples within the gas

scintillator, a direct comparison of the velocity spectra of prompt fission-neutrons from the two isotopes was obtained. This comparison method was free from errors associated with the absolute sensitivity of the neutron detector.

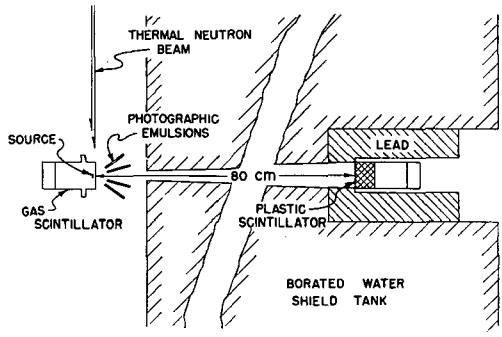


Fig. 7
Schematic diagram of the experimental apparatus utilized in the measurement of the $Pu^{241}$ prompt-fission-neutron spectrum. The photographic emulsions were removed during the time-of-flight measurements.

In order to obtain good energy resolution and improved statistical accuracy in the high-energy portion of the spectrum, a nuclear-emulsion technique was employed. For this measurement, a larger sample of $Pu^{241}$ of sufficient purity so that 90% of the thermally induced fissions were due to $Pu^{241}$ was placed in

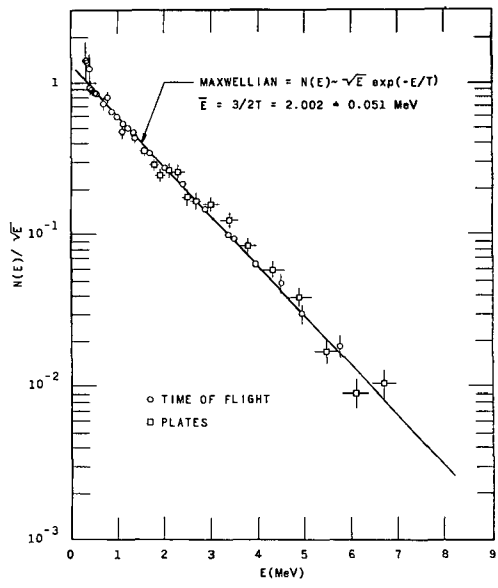


Fig. 8
Typical experimental measurement of the $Pu^{241}$ fission-neutron energy spectrum. Circular points are from the time-of-flight measurements, square points are the results of the measurements of proton recoil tracks in nuclear emulsions. The solid curve represents a least squares fit of a Maxwellian distribution to the experimental points.

the thermal-neutron beam. The sample was surrounded by a set of nuclear track plates in such a way that fission neutrons were incident on the emulsion surfaces at a small tangential angle. Proton recoils were measured if they fell within a square prism whose axis was parallel to the neutron direction and whose half-angle was 20°. In order to check the recoil measurement technique, the $Pu^{241}$ recoils were compared with those obtained from a $U^{235}$ sample using the same experimental conditions.

The results of the measurements are shown in Fig. 8. This spectrum was obtained by assuming a Maxwellian spectrum for $U^{235}$ of the form

$$N\,(\mathrm{E}) \sim \sqrt{E}\,\mathrm{e}^{-E/T}$$

where $N$ (E) is the number of neutrons per unit energy interval, $E$ is the energy in mega-electron-volts, and $T$ a "temperature" constant assumed to be 1.290 MeV [20]. The $Pu^{241}$ distribution itself then fits the same formula with a "temperature" of 1.335 MeV. The resulting average $Pu^{241}$ fission-neutron energy is 2.002 MeV.

Statistical arguments have been used to relate the average number of neutrons emitted per fission, $\bar{\nu}$, to the average fission-neutron energy, $\bar{E}$. TERRELL [20] obtained the following correlation:

$$\bar{E} = 0.78 + 0.62\sqrt{\bar{\nu} + 1}\,.$$

This expression leads to a value $\bar{\nu}$(t) ($Pu^{241}$) = 2.88, which is, within statistical errors, in good agreement with the more directly measured value [21] of $\bar{\nu}$(t) ($Pu^{241}$) = 2.95.

## Energy dependence of $\bar{\nu}$

The number of prompt neutrons per fission, $\bar{\nu}$, was measured for $U^{235}$ and $U^{238}$. In addition, the dependence of $\bar{\nu}$ for $U^{235}$ was measured as a function of the energy between 0.2 and 1.58 MeV.

The principal experimental difficulty in the measurement of $\bar{\nu}$ for high incident-neutron energies is the detection of the fission neutrons in the presence of the background produced by the neutrons causing the fissions. The fission-neutron detector was designed to be sensitive to neutrons of all energies from epi-cadmium to beyond 10 MeV. The separation of fission neutrons from background was accomplished by observing the time correlation between the fissions and neutrons.

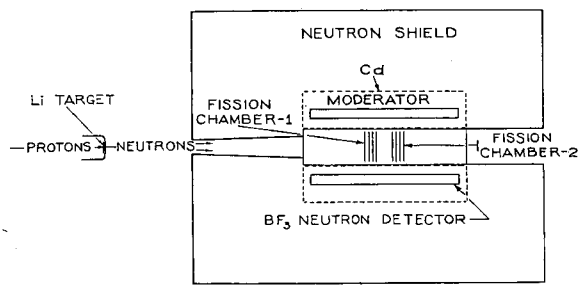


Fig. 9
Schematic diagram of the experimental apparatus used to measure $\bar{\nu}$.

The measurement was performed using the experimental arrangement shown schematically in Fig. 9. Two fission-pulse ionization counters in a common container were placed in the centre of a large shield tank. A beam of neutrons from a $Li^7$ (p, n) $Be^7$ source on an electrostatic generator, collimated by the input hole in the shield tank, was passed through the chamber. One chamber contained the fissionable material to be studied, and the other contained $Cf^{252}$ as an intermediate standard. The chamber was surrounded by a ring of $BF_3$ proportional counters embedded in moderator to detect the fission neutrons. The fission and neutron pulses were all fed into a time-analysing circuit* which separately recorded the total number of fissions and the time distribution of neutron counts after a fission in either chamber. Each of these distributions consisted of a rapid rise followed by an exponential fall during the time corresponding to the moderation and leakage-absorption time distributions of the neutrons in the moderator. The distributions were on top of a constant background corresponding to neutrons scattered from the incident beam and neutrons from fissions not seen by the time analyser. By recording the time distributions from both fission counters simultaneously, the ratio of the $\bar{\nu}$ for the two fissioning materials was measured. The elaborate time analyser was used to insure that the fission neutrons could be successfully separated from the background. The separation was only achieved by taking great care to minimize scattering of the incident-neutron beam into the fission-neutron counters. This was done by using gold leaf for the fissionable sample backings and thin aluminium end-windows on the counter body. The result was that the scattering by the supporting materials was reduced to the point where 50% of the scattering was due to the counter gas.

In addition to allowing for separation of the fission neutrons from scattered neutrons, the time analyser also permitted an experimental check of the number of fissions being produced by thermal-neutron background due to moderation in the water of the shield tank and materials, including air, surrounding the experiment. This check was made by pulsing the incident-neutron beam and observing the time distribution of fissions following the beam pulse. It was found that about 9% of the fissions in $U^{235}$ were produced by thermal-neutron background. The results were corrected accordingly. Corrections were also made for the second group of neutrons produced by $Li^7$ (p, n) $Be^{7*}$ reaction in the Li target.

The results of the measurements of $\bar{\nu}$ of $U^{235}$ as a function of neutron energy are shown in Fig. 10, together with results obtained by other workers [10, 23–26]. These are based on the value of the prompt thermal $\bar{\nu}$ of $U^{235}$ of 2.42 [10], chosen because at present it is more accurately known than the value for the $Cf^{252}$ monitor. Using the $U^{235}$ standard, the data gives a value of the $\bar{\nu}$ for spontaneous fission of $Cf^{252}$ of $3.73 \pm 0.03$, and for $U^{238}$ at 1.58 MeV of $2.56 \pm 0.03$. The errors quoted do not include any error in the $U^{235}$ standard. The $Cf^{252}$ and $U^{238}$ values are in agreement with those obtained by DIVEN *et al.* [25, 27] of $3.81 \pm 0.08$ and $2.61 \pm 0.09$ respectively, normalized to the above $\bar{\nu}$ of $U^{235}$.

The $U^{235}$ measurements are sufficiently accurate to determine that the trend indicated by previous results in this energy interval is correct. The initial increase of $\bar{\nu}$ with incident-neutron energy is indeed slower than the straight line drawn between the thermal and high-energy data. An immediate implication of these results is that the values of $\bar{\nu}$ of $U^{235}$ currently used in fast-reactor calculations

* The analyser, except for very minor modification, was that described in Ref. [22].

are too large, and should be reduced in accordance with these data. It is reasonable to assume that some reduction continues to be warranted up to an energy close to that corresponding to second chance fission.

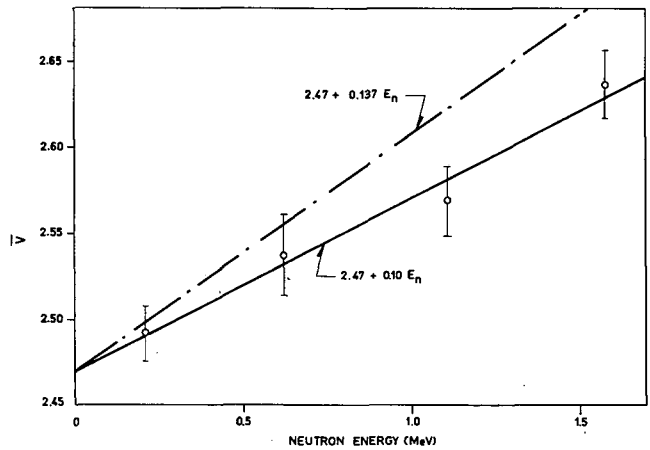


Fig. 10
$\bar{\nu}$ of $U^{235}$ as a function of incident-neutron energy. The broken line represents a straight line fit to all existing data below 15 MeV. The figure is normalized to an older value of $\bar{\nu}$ of 2.47 (see text).

## REFERENCES

[1] KEEPIN, G. R., WIMETT, T. F. and ZEIGLER, R. K., *Phys. Rev.* **107** (1957) 1044.
[2] COX, S. A., FIELDS, P. R., FRIEDMAN, A. M., SJOBLOM, R. J. and SMITH, A. B., *Phys. Rev.* **112** (1958) 960.
[3] PERLOW, G. J. and STEHNEY, A. F., *Phys. Rev.* **113** (1959) 1269.
[4] STEHNEY, A. F. and PERLOW, G. J., *Bull. Amer. phys. Soc.* Ser. II **6** (1961) 62.
[5] KATCOFF, S., *Nucleonics* **16** (1958) 78.
[6] WAHL, A. C., *J. inorg. nucl. Chem.* **6** (1958) 263.
[7] KENNETH, T. J. and THODE, N. G., *Phys. Rev.* **103** (1956) 323.
[8] STEINBERG, E. P. and GLENDENIN, L. E., Proc. UN Int. Conf. PUAE **7** (1956) 3.
[9] GLENDENIN, L. E., CORYELL, C. D. and EDWARDS, R. R., Radiochemical Studies: The Fission Products, National Nuclear Energy Series, McGraw-Hill Book Co., Inc., New York (1951) 489.
[10] HUGHES, D. J. and SCHWARTZ, R., Neutron Cross Sections, 2nd ed. BNL-325 and Suppl. No. 1, U.S. Govt. Print. Office, Washington, D.C. (1958).
[11] ALLEN, D. W. and HENKEL, R. L., Progress in Nuclear Energy Series I—Physics and Mathematics, II, Pergamon Press, London (1958) 28.
[12] SMITH, A. B., Private communication.
[13] BEVINGTON, P. R., ROLLAND, W. W. and LEWIS, H. W., *Phys. Rev.* **121** (1961) 871.
[14] KAZARINOVA, M. E., ZAMYATNIN, Yu S. and GORBACHEF, V. M., *Atomn. Energia* 8 (1960) 139.
[15] BUTLER, D. K., *Phys. Rev.* **117** (1960) 1305.
[16] NESTEROV, V. G. and SMIRENKIN, G. N., *Soviet Phys.* JETP 8 (1959) 367. Also private communication.
[17] SCHMITT, H. W. and MURRAY, R. B., *Phys. Rev.* **116** (1959) 1575.

[18] JACKSON, J. D., Proc. of the Symposium on the Physics of Fission (Chalk River, May 1956), CRP-642-A (1956) 125.
[19] SMITH, A. B., FIELDS, P. R. and ROBERTS, J. H., *Phys. Rev.* **108** (1957) 411.
[20] TERRELL, J., *Phys. Rev.* **113** (1959) 527.
[21] DeSAUSSURE, G. and SILVER, E. G., *Nucl. Sci. and Engng* **5** (1959) 49.
[22] WHALEN, J. F., MEADOWS, J. W. and NELSON, C. H., *Rev. sci. Instrum.* **30** (1959) 991.
[23] KALASHNIKOVA, V. I., *et al.* Meetings of the Division of Physical-Mathematical Sciences, Session of the Academy of Science of the U.S.S.R. on the Peaceful Use of Atomic Energy, July 1—5, 1955. Publishing House of the Academy of Science of the U.S.S.R., Moscow (1955) 156. Translated in AEC-tr-2435 Pt. 1, p. 123.
[24] USACHEV, L. N. and TRUBITSYN, V. P., Report of FIGU Institut Atomnoi Energii (1953). Quoted in BONDARENKO, I. E., *et al.*, Proc. 2nd UN Int. Conf. PUAE **15** (1958) 353.
[25] DIVEN, B. C., *et al.*, Unpublished. See TERRELL, J., *Phys. Rev.* **108** (1957) 783.
[26] GRAVES, E. R., Unpublished. Quoted in HYDE, E. K., UCRL-9036 (1960) 246.
[27] DIVEN, B. C., *et al.*, *Phys. Rev.* **101** (1956) 1012.

SM—18/18

# THE NUMBER OF PROMPT NEUTRONS FROM $U^{235}$-FISSION OVER THE RANGE 0.04 TO 3 MeV

A. Moat, D. S. Mather and P. Fieldhouse
Atomic Weapons Research Establishment, Aldermaston,
United Kingdom

**Abstract — Résumé — Аннотация — Resumen**

**The number of prompt neutrons from $U^{235}$-fission over the range 0.04 to 3 MeV.** The number, $\bar{\nu}$, of prompt neutrons from the neutron-induced fission of $U^{235}$ has been measured as a function of neutron energy in the range 0.04 to 3.0 MeV. The reactions Li (p, n) and T (p, n) were used, the protons being accelerated by a 6-MV Van de Graaff. A collimated beam of neutrons from the target was incident on a fission ionization chamber, which was placed at the centre of a spherical 240-l loaded liquid scintillation counter. This counter had an efficiency of about 88%; it was surrounded by a massive neutron shield. Spot measurements of $\bar{\nu}$ were made to a statistical accuracy of about 1%, and will be quoted relative to the 0.04 MeV value. It was necessary to prove that fissions were induced only by neutrons of the wanted energy: this was achieved by pulsing the proton beam from the Van de Graaff and applying time-of-flight selection to the neutrons from the target.

**Nombre de neutrons instantanés provenant de la fission de $^{235}U$ dans la gamme d'énergie de 0,04 à 3 MeV.** Le nombre $\bar{\nu}$ de neutrons instantanés provenant de la fission de $^{235}U$ provoquée par des neutrons a été mesuré en fonction de l'énergie des neutrons dans la gamme d'énergie de 0,04 à 3 MeV. On a utilisé les réactions Li (p, n) et T (p, n), les protons étant accélérés par un accélérateur de Van de Graaff de 6 MV. Un faisceau collimaté de neutrons émanant de la cible frappait la chambre à fission qui se trouvait placée au centre d'un compteur sphérique contenant 240 l de scintillateur liquide. Ce compteur, d'un rendement de 88% environ, était entouré d'un écran compact contre les neutrons. La mesure de $\bar{\nu}$, faite en différents points avec une précision statistique d'environ 1%, est exprimée par rapport à la valeur pour 0,04 MeV. Il fallait s'assurer que la fission n'était provoquée que par des neutrons de l'énergie voulue: on y est parvenu en pulsant le faisceau de protons provenant de l'accélérateur de Van de Graaff et en opérant une sélection par temps de vol des neutrons provenant de la cible.

**Число мгновенных нейтронов получаемых в результате деления урана-235, в диапазоне 0,04—3 Мэв.** Число $\bar{\nu}$ мгновенных нейтронов, получаемых в результате вызванного нейтронами деления урана-235, измерялось как функция энергии нейтронов в диапазоне от 0,04 до 3,0 Мэв. Использовались реакции Li (p, n) и T (p, n), причем протоны ускорялись генератором Ван де Граафа мощностью в 6 Мв. Коллимированный пучок нейтронов из мишени падал на ионизационную камеру деления, которая находилась в центре сферического жидкостного сцинтилляционного счетчика объемом 240 литров. Этот счетчик имел коэффициент полезного действия приблизительно 88%; он был окружен массивным экраном для защиты от нейтронов. Измерения $\bar{\nu}$ были сделаны со статистической точностью приблизительно в 1%; они будут сообщены для значения в 0,04 Мэв. Необходимо было доказать, что деления вызывались лишь нейтронами желаемой энергии; это было достигнуто за счет пульсирования пучка нейтронов из генератора Ван де Граафа и применения отбора по методу времени пролета для нейтронов из мишени.

**Número de neutrones inmediatos emitidos en la fisión del $^{235}U$ para la gama de energía de 0,04 a 3 MeV.** Se ha medido el número $\bar{\nu}$ (neutrones inmediatos emitidos en la fisión del $^{235}U$) como función de la energía neutrónica en el intervalo comprendido

entre 0,04 y 3,0 MeV. Para ello se utilizaron las reacciones Li (p, n) y T (p, n), acelerándose los protones mediante un generador Van de Graaff de 6 MV. Un haz colimado de neutrones procedente del blanco incide sobre una cámara de fisión, colocada en el centro de un contador esférico de 240 l conteniendo un centelleador líquido. Este contador, cuyo rendimiento es de 88% aproximadamente, se halla rodeado de un pesado blindaje neutrónico. Las mediciones de $\bar{\nu}$ efectuadas en distintos puntos con una precisión estadística del orden del 1% se expresan respecto del valor para 0,04 MeV. Era necesario asegurarse de que las fisiones sólo eran inducidas por neutrones de la energía elegida, lo que se consiguió pulsando el haz de protones del generador Van de Graaff y efectuando una selección, por el método del tiempo de vuelo, de los neutrones procedentes del blanco.

## Introduction

The work reported here was carried out as part of a programme at AWRE for the accurate determination of the average number ($\bar{\nu}$) of prompt neutrons from fission induced by neutrons in the energy range 0–20 MeV. Measurements up to a few mega-electron-volts are of particular application to the design of fast reactors which may have neutron energy spectra peaking between 50 keV and 1 MeV.

A table which lists the majority of $\bar{\nu}$ measurements up to a few mega-electron-volts appears in a paper by LEACHMAN [1]. Fig. 1 shows available data for $U^{235}$ below 3 MeV; this data has been prepared by PARKER [9] and has been normalized to a thermal value of 2.43.

It has been generally assumed that $\bar{\nu}$ is a linear function of energy, and slopes of 0.12 to 0.18 per MeV have been deduced from available measurements up to 14 MeV. Parker [9] finds a slope of $0.130 \pm 0.003$ as the least squares fit to all available measurements for $U^{235}$ up to 15 MeV.

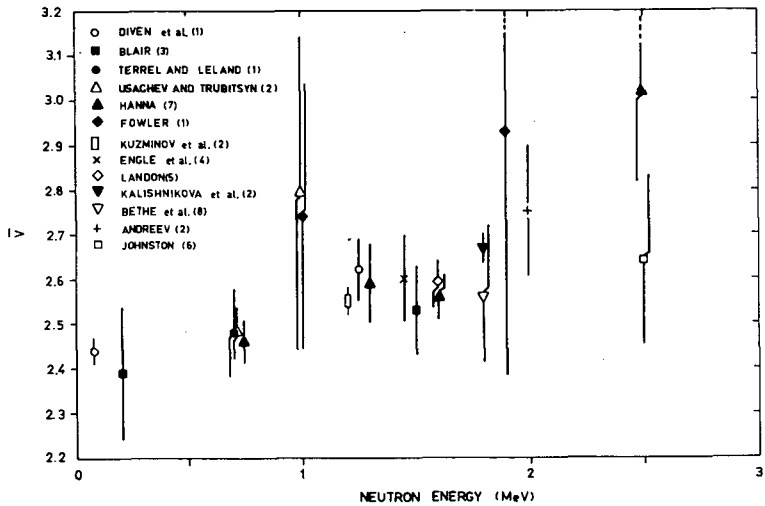


Fig. 1
Previous measurements of $\bar{\nu}$, the average number of neutrons per fission, as a function of the neutron energy inducing fission in the range 0—3 MeV.

The present experiment was carried out using a large loaded-liquid scintillation counter as the neutron detector. This technique was used by DIVEN *et al.* [10] and HICKS *et al.* [11] for the measurement of $\bar{\nu}$ in spontaneous fission, and for fission induced by low-energy neutrons. At AWRE the method has been extended to high neutron energies [12] by housing the scintillator in a massive neutron shield. The technique has been further refined by applying the time-of-flight method to ensure that no significant errors in $\bar{\nu}$ were introduced due to fissions induced by thermal neutrons or other neutrons below the primary energy.

## The scintillation counter

The scintillation counter, which was made by Nuclear Enterprises (G.B.) Ltd., is spherical, having a diameter of 76 cm. It contains approximately 240 l of liquid, type NE-213, loaded with $^1/_2$% gadolinium, and is fitted with 12 photomultiplier tubes, type EMI-9618-A.

Neutrons are moderated in the liquid and are finally captured, after a mean life of 10 μs, in the loading element Gd. The gamma-rays emitted at capture produce a pulse in the scintillator. The efficiency of the present counter, averaged over a fission spectrum, is about 88% for neutrons originating at the centre. It has been measured by placing a $Cf^{252}$ fission chamber at the centre of the $2^1/_2$ in diameter tube which runs diametrically through the scintillation counter. The number of capture pulses observed per fission, divided by 3.77, gave the counter efficiency. The number 3.77 is $\bar{\nu}$ for $Cf^{252}$, as reported in Ref. [12], after correction for the difference between $Cf^{252}$ and $Pu^{240}$ spontaneous fission-neutron spectra, as noted in that reference. Frequent checks on the efficiency, using the $Cf^{252}$ fission chamber, were made during the course of the $\bar{\nu}$ measurements. Similar fission chambers containing $U^{235}$, or other nuclides, may be placed in the same position for the $\bar{\nu}$ determinations. The $U^{235}$ chamber contains 16 nickel foils 3-cm diameter, coated on both sides with about 1 mg/cm$^2$ $U^{235}$. It is used with a continuous flow of 90% argon and 10% methane.

The scintillation counter is operated with three banks of photomultiplier tubes set in coincidence (resolving time 40 ns). It is considered necessary to use a coincidence arrangement to eliminate any chance of after-pulses giving rise to a false efficiency. We find that, using three banks of four tubes, a longer and flatter plateau of efficiency versus gain is achieved than when using two banks, each of six tubes.

## The shielding system

The scintillation counter is used in the vicinity of an intense neutron source and has therefore been provided with an efficient shield. Fig. 2 shows the counter in position in the shield. The "nose" of the shield, adjacent to the neutron source, is of copper 10-cm thick; behind this is an iron block 46-cm thick, and finally there is a water-tank 63-cm thick. A water jacket 46-cm thick shields the counter on the remaining sides from the less energetic room-scattered neutrons. The water in the shield contains 4% by weight of boric acid, so that neutrons thermalized in the water will be preferentially absorbed by boron rather than hydrogen, thus producing background gammas of 0.48 MeV instead of 2.2 MeV.

Through the cone of the shield runs a narrow tapered collimating hole, designed to form a neutron beam 3-cm diameter at the position occupied by the fission chamber. The collimator consists of plugs, 10 cm in length, the five nearest the source being iron and the remainder polythene.

Neutrons were produced at a 2-mm-diameter spot on a lithium fluoride or titanium tritide target, bombarded by protons from a 6-MV Van de Graaff. The target was situated at the apex of the shielding tank and on the axis of the collimator.

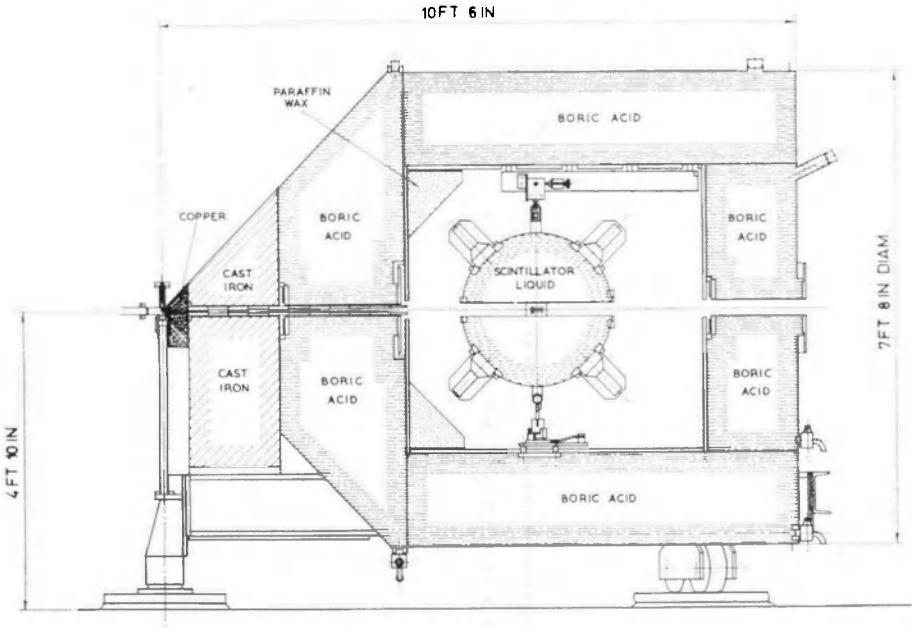


Fig. 2
Horizontal shielding system.

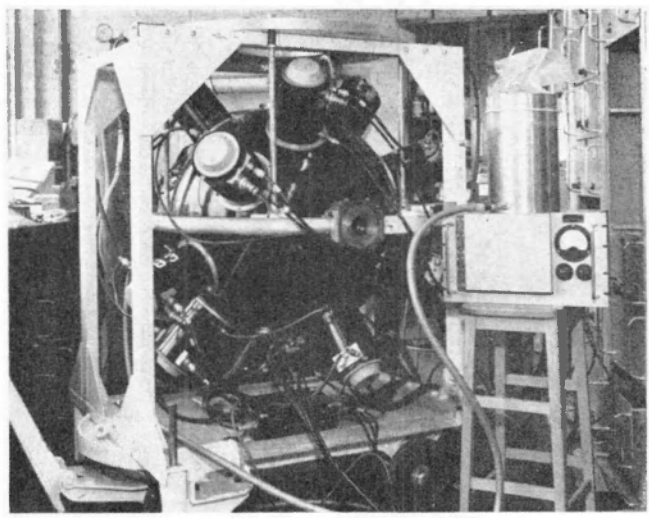

Fig. 3
The 240-l spherical scintillation counter.

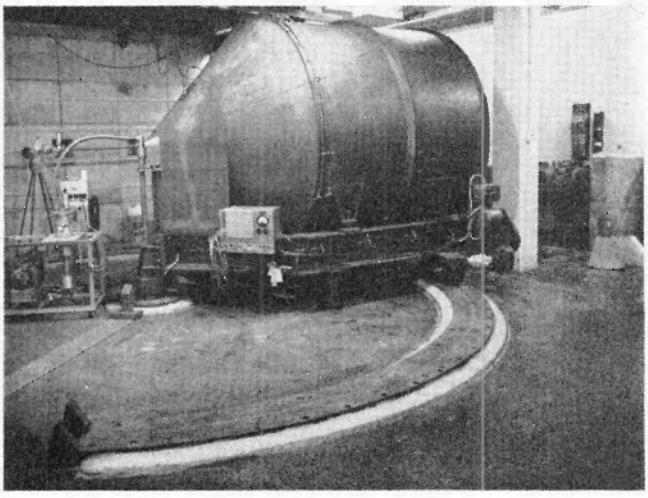

Fig. 4
The pivoted shielding system that houses the scintillation counter.

The shielding system is mounted on a trolley, pivoted beneath the target, so that targets may be observed at the angles necessary to give the maximum energy coverage over the range 0—23 MeV. Figs. 3 and 4 show photographs of the spherical scintillation counter and the pivoted shielding system.

**Method for $\bar{\nu}$ measurements**

A small fraction of the neutrons produced at the target will travel through the collimator, and these must pass through the fission chamber, which is about 2 m from the target. Gamma rays from a fission event will produce a prompt pulse in the scintillator, and fissions are identified by a coincidence (recorded by "slow coincidence" unit, on the electronics block diagram, Fig. 5) between a scintillator pulse, and a large pulse from the fission chamber. The output from the slow-coincidence unit opens a 40-μs gate, during which interval the multiple event analyser (MEA) may accumulate scintillator pulses [13]. The MEA gives an output, which is displayed on a pulse height analyser, with amplitude proportional to the number of scintillator pulses accumulated during the gating time.

After correction for background contribution, dead-time losses and counter efficiency (as described in [12]), the data from a run give the probabilities $P_0$, $P_1$, $P_2$ etc. of emission of 0, 1, 2 etc. neutrons from fission. The mean number of neutrons $\bar{\nu}$ is given by $(0 \times P_0) + (1 \times P_1) + (2 \times P_2) + \ldots$ etc.

**Neutron spectrum incident on the fission chamber**

All the measurements, except that at 40-keV energy, were made using the T (p, n) reaction, the tritium targets being chosen in thickness to give an energy spread of about 50 keV. For the 40-keV point, a lithium target was bombarded with protons 8 keV above the threshold for the $Li^7$ (p, n) reaction.

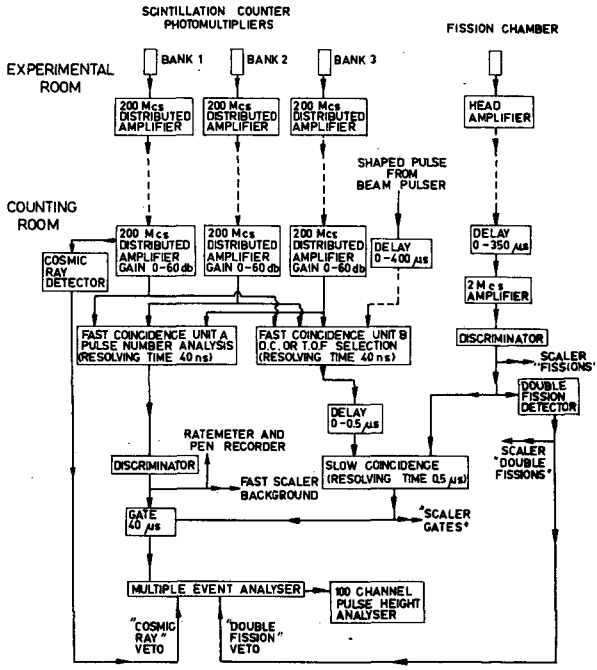


Fig. 5
Block diagram of electronics.

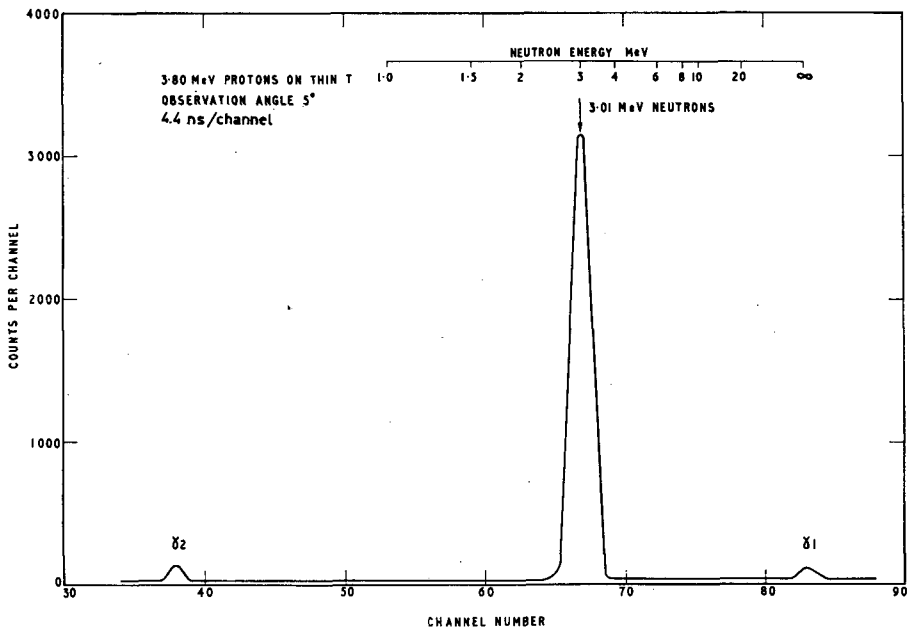


Fig. 6
Time spectrum of 3-MeV neutrons arriving at the counter from the T (p, n) reaction.

It was essential to show that the neutron spectra incident on the fission chamber were free from neutrons of energies other than the primary group. Such degraded neutrons could conceivably have arisen from the target or from the walls of the collimator tube. Thermal neutrons could be particularly important because of the high thermal-fission cross-section of $U^{235}$. We have used three techniques to show that the spectra were sufficiently clean; these are discussed below.

(*a*) Using a pulsed proton beam and a small organic scintillator in place of the fission counter, the time-of-flight technique was employed for neutrons of various primary energies. The time spectra obtained (Fig. 6 is the result for 3-MeV neutrons) showed that, for primary energies up to nearly 5 MeV produced by the T (p, n) reaction (using tritium-titanium on gold backings), no degraded neutrons were present above 0.5 MeV. This lower energy limit was imposed by the energy response of the organic scintillator.

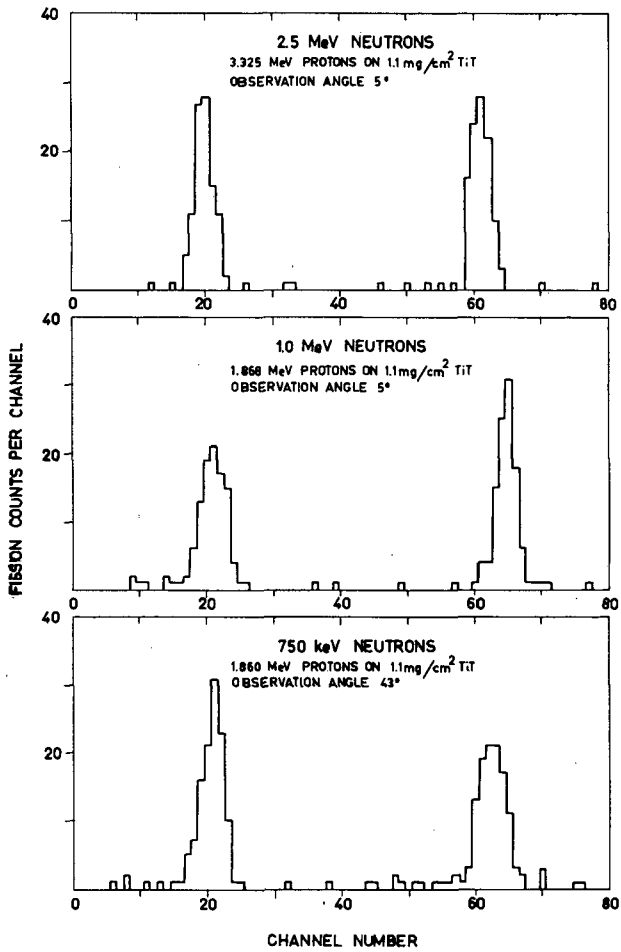


Fig. 7
Fission-time sorting for fissions induced by neutrons of energies 750 keV, 1.0 MeV and 2.5 MeV.

(*b*) At 3-MeV primary energy, a measurement of $\bar{\nu}$ for $U^{235}$ was made using a pulsed beam, and selecting only those fissions occurring at the time 3-MeV neutrons passed through the fission chamber. (With $2.5 \times 10^6$ pulses per second and a fast coincidence resolving time of 40 ns, this system would reject 90% of the randomly occurring, e.g. thermal, fissions.) The same statistical accuracy of 0.8% was obtained in a DC measurement (i.e. beam not pulsed) at 3-MeV energy. The two values were 0.5% from the mean, indicating that there was no serious contamination of the neutron spectrum at 3 MeV.

(*c*) An alternative approach has been used to show that fissions are being induced by neutrons of the correct energy. In this method, which we call "fission-time sorting", the organic scintillator of the conventional time-of-flight apparatus, described in (*a*), was replaced by the $U^{235}$ fission chamber. A pulsed beam was used, and the time-sorter was started by the fast pulse (due to the prompt fission gammas) from the large scintillator which surrounded the fission chamber: the appropriate scintillator pulse was gated by the slow pulse from the fission chamber. A stop-pulse for the time-sorter was derived from the beam deflection oscillator. The displays obtained (Fig. 7) show sharp peaks corresponding to fissions induced by primary energy neutrons, and a few fissions occurring at random times. From the fraction of fissions which are random in time one can predict the maximum error which would be made in a DC measurement, i.e. assuming all randomly occurring fissions are thermal induced. At 1 MeV, for example, an error of 1% in the $\bar{\nu}$ value would require that at least 25% of the fission rate is due to thermals. At 3 MeV, 9% thermal fissions would give a 1% error. The fission-time plots of Fig. 7 show that, even assuming all fissions occurring between the peaks to be thermal induced, the neutron spectra were sufficiently free from low energy contamination for DC measurements of $\bar{\nu}$ to be made.

Procedure (*c*) is a quick method for assessing the reliability of any proposed DC measurement of $\bar{\nu}$.

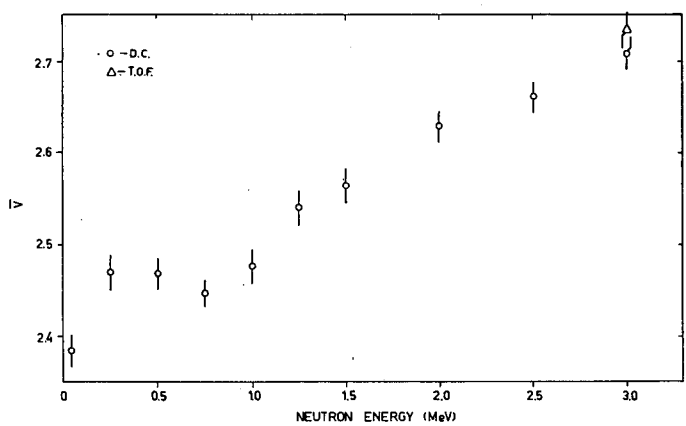


Fig. 8
Present measurements of $\bar{\nu}$ $U^{235}$ in the range 0.04—3 MeV.

## Results for prompt $\bar{\nu}$ of $U^{235}$

In Fig. 8 are shown the results of our $U^{235}$ $\bar{\nu}$ measurements up to 3 MeV; Table I tabulates the results together with the ratios to the "40-keV" value.

TABLE I

THE AVERAGE NUMBER $\bar{\nu}$ OF PROMPT NEUTRONS FROM FISSION OF $U^{235}$

| Incident neutron energy—$E$ (MeV) | $\bar{\nu}$(E)* | $\bar{\nu}$(E)/$\bar{\nu}$ (40keV)** |
|---|---|---|
| 0.04 | 2.384 ±0.018 | 1.000 — |
| 0.25 | 2.469 ±0.021 | 1.036 ±0.012 |
| 0.5 | 2.468 ±0.018 | 1.035 ±0.011 |
| 0.75 | 2.447 ±0.014 | 1.026 ±0.010 |
| 1.0 | 2.475 ±0.018 | 1.038 ±0.011 |
| 1.25 | 2.540 ±0.019 | 1.065 ±0.011 |
| 1.5 | 2.565 ±0.019 | 1.076 ±0.011 |
| 2.0 | 2.629 ±0.017 | 1.103 ±0.011 |
| 2.5 | 2.661 ±0.017 | 1.116 ±0.011 |
| 3.0 DC | 2.708 ±0.018 | 1.136 ±0.012 |
| 3.0 TOF | 2.735 ±0.021 | 1.147 ±0.012 |

* Errors are statistical only and are based on an assumed $\bar{\nu}$ $Cf^{252}$ = 3.77.
** The errors include that of the 40-keV value.

At 3 MeV, the time-of-flight (TOF) result and the DC result are shown separately. A weighted least squares fit to the present data gives:

$$\bar{\nu} = (2.398 \pm 0.014) + (0.107 \pm 0.007)\, E\,.$$

The variation of $\bar{\nu}$ with energy is clearly not linear from thermal to 14 MeV, since this would require a slope of about 0.14 per MeV. Even over the restricted energy range 0—3 MeV, the measured points suggest a non-linear function, and this is particularly noticeable below about 1 MeV.

## Future work

The present measurements are to be extended to about 9 MeV for $U^{235}$. In the important region below 1 MeV where the data appear to depart from the linear fit, measurements will be made to greater relative accuracy, and with better energy resolution to determine whether this effect is real.

Similar procedures will be followed for a number of other nuclides, including $Th^{232}$, $U^{233}$, $U^{238}$, $Pu^{239}$ and $Pu^{240}$.

Our future work will be considerably helped by the installation of top terminal pulsing on the 6-MV Van de Graaff. The greater ion source current available, and also the absence of neutron background from the beam deflection system, should enable time-of-flight measurements to be made as quickly as the present DC determinations.

## REFERENCES

[1] LEACHMAN, R. B., Proc. 2nd UN Int. Conf. PUAE **15** (1958) 229.
[2] BONDERENKO, I. I., *et al.*, Proc. 2nd UN Int. Conf. PUAE **15** (1958) 353.
[3] BLAIR, J. M., AERE unpublished report [1957].
[4] ENGLE, L. B., HANSEN, G. E. and PAXTON, H. C., *Nucl. Sci. and Engng* 8 (1960) 543.
[5] LANDON, H. H., AERE unpublished report [1957].
[6] JOHNSTONE, I., AERE, NP/R-1912 (1956).
[7] HANNA, R. C., NRDC-94 (1956).
[8] LEACHMAN, R. B., LA-1863 (1954).
[9] PARKER, K., Private communication.
[10] DIVEN, B. C. *et al.*, *Phys. Rev.* **101** (1956) 1012.
[11] HICKS, D. A., ISE, J. and PYLE, R. V., *Phys. Rev.* **101** (1956) 1016.
[12] MOAT, A., MATHER, D. S. and McTAGGART, M. H., *Reactor Sci. and Technol.* **15** (1961) 102.
[13] GORE, W. G., *Nucl. Instrum. and Meth.* **7** (1960) 320.

SM—18/56

# NUMBERS OF PROMPT NEUTRONS PER FISSION FOR $U^{233}$, $U^{235}$, $Pu^{239}$ AND $Cf^{252}$ *

B. C. Diven and J. C. Hopkins
Los Alamos Scientific Laboratory,
University of California, Los Alamos, N. Mex.,
United States of America

**Abstract — Résumé — Аннотация — Resumen**

**Numbers of prompt neutrons per fission for $U^{233}$, $U^{235}$, $Pu^{239}$, and $Cf^{252}$.** An absolute measurement of $\bar{\nu}$, the average number of prompt neutrons emitted per fission, is being made for the spontaneous fission of $Cf^{252}$. The relative values of $\bar{\nu}$ are being measured for neutron-induced fission of $U^{233}$, $U^{235}$, and $Pu^{239}$, and are being compared with the spontaneous fission $\bar{\nu}$ of $Cf^{252}$. Neutrons with energies between thermal and 15 MeV are used. Particular emphasis is put on studying the dependence of $\bar{\nu}$ on the incident neutron energy. A fission counter containing the appropriate isotope is placed in the centre of a large cadmium-loaded liquid scintillator. Through the fissionable isotope is passed a collimated beam of neutrons. Fission events, identified by pulses from the fission counter, open an electronic gate between the large liquid scintillator and a scaler. Scintillator pulses due to capture in the scintillating solution of thermalized fission neutrons are counted during the gate. The fission neutrons are detected almost independently of energy and with very high efficiency. With this technique values of $\bar{\nu}$ to an accuracy of 1% are expected.

**Nombre de neutrons instantanés émis par la fission de $^{233}U$, $^{235}U$, $^{239}Pu$ et $^{252}Cf$.** Les auteurs ont mesuré la valeur absolue de $\bar{\nu}$, nombre moyen de neutrons instantanés émis par la fission, dans le cas de la fission spontanée de $^{252}Cf$. Ils ont mesuré les valeurs relatives de $\bar{\nu}$ pour la fission induite par neutrons de $^{233}U$, $^{235}U$ et $^{239}Pu$ et les ont comparées à la valeur de $\bar{\nu}$ pour la fission spontanée de $^{252}Cf$. Ils ont utilisé des neutrons dont l'énergie était comprise entre l'énergie thermique et 15 MeV. L'accent a été mis sur l'étude de la dépendance de $\bar{\nu}$ vis-à-vis de l'énergie des neutrons incidents. Un compteur à fission contenant l'isotope approprié est placé au centre d'un grand scintillateur liquide chargé de cadmium. Un faisceau collimaté de neutrons traverse l'isotope fissile. Les fissions, identifiées à l'aide des impulsions provenant du compteur à fission, déclenchent une porte électronique située entre le grand scintillateur liquide et une échelle de comptage. Les scintillations produites par capture dans le scintillateur des neutrons de fission thermalisés sont comptés pendant la durée de l'ouverture de la porte. La détection des neutrons de fission se fait presque indépendamment de l'énergie et atteint un rendement très élevé. A l'aide de cette technique, les auteurs espèrent pouvoir mesurer la valeur de $\bar{\nu}$ avec une précision de 1%.

**Число мгновенных нейтронов на одно деление для $U^{233}$, $U^{235}$, $Pu^{239}$ и $C^{252}$.** Абсолютное измерение $\bar{\nu}$ среднего числа мгновенных нейтронов, испускаемых на одно деление, проводится для самопроизвольного деления $Cf^{252}$. Относительные значения $\bar{\nu}$ измеряются для деления урана-233, урана-235 и плутония-239, вызываемого нейтронами, и сравниваются с $\bar{\nu}$ самопроизвольного деление $Cf^{252}$. Используются нейтроны в области от тепловой энергии до 15 Мэв. Особое внимание уделяется изучению зависимости $\bar{\nu}$ от энергии бомбардирующих нейтронов. Счетчик делений, содержащий соответствующий изотоп, помещается

* Work performed under the auspices of the United States Atomic Energy Commission.

в центре крупного жидкостного сцинтиллятора с кадмием. Через расщепляющийся изотоп пропускается коллимированный пучок нейтронов. Акты деления, обнаруживаемые импульсами от счетчика делений, открывают электронную схему пропускания между крупным жидкостным сцинтиллятором и пересчетным устройством. Импульсы сцинтиллятора, вызываемые захватом в сцинтиллирующем растворе замедленных до тепловой энергии нейтронов деления, отсчитываются во время пропускания. Нейтроны деления обнаруживаются почти независимо от энергии и с очень большой эффективностью. Используя этот метод, можно ожидать измерения значений $\bar{\nu}$ с точностью до 1%.

**Número de neutrones inmediatos emitidos por fisión de los isótopos $^{233}$U, $^{235}$U, $^{239}$Pu y $^{252}$Cf.** Se está realizando la medición absoluta de $\bar{\nu}$, el número medio de neutrones inmediatos emitidos por fisión, en el caso de la fisión espontánea del $^{252}$Cf. El dato obtenido se comparará con los valores relativos de $\bar{\nu}$ que se está determinando para las fisiones de los isótopos $^{233}$U, $^{235}$U y $^{239}$Pu inducidas por neutrones. Se emplean neutrones cuyas energías abarcan desde los valores térmicos hasta 15 MeV, y se estudia con particular atención la manera en que $\bar{\nu}$ varía con la energía de los neutrones incidentes. En el centro de un gran centelleador líquido cargado con cadmio se coloca un contador de fisión que contiene el isótopo de que se trata, a través del cual se hace pasar un haz colimado de neutrones. Las fisiones, identificadas por los impulsos que emite el contador de fisión, abren una puerta electrónica entre el centelleador líquido y un escalímetro. Los impulsos del centelleador debidos a la captura de neutrones de fisión termalizados en el líquido de centelleo se cuentan mientras la puerta está abierta. Los neutrones de fisión se detectan con un rendimiento muy elevado y casi independientemente de su energía. Se espera que esta técnica permita determinar los valores de $\bar{\nu}$ con una precisión del 1 por ciento.

Several years ago, REINES *et al.* [1] at Los Alamos developed a neutron detector whose efficiency was nearly 100%. With this detector a detailed study can be made of the number of neutrons emitted in the fission process. If all of the neutrons emitted in each individual fission event were detected, then not only would the average number of neutrons emitted per fission be found but also the probability that no neutrons be emitted, the probability that two neutrons be emitted and so forth. This is precisely what we measure in our experiment. The techniques to be described are similar to those developed by DIVEN *et al.* [2] in 1955 for a previous measurement of neutron multiplicities. The differences are in the scintillator and associated electronics, which have improved with the state of the art.

Since the neutron detector is the key to the experiment, it will be described first. This device is a large liquid scintillator. It consists of an 870-l tank of a solution of terphenyl in toluene with various additives, including a cadmium salt. Twenty-eight 5-in DuMont 6364 photomultiplier tubes on the surface of this tank are used to pick up light from scintillations which are produced in the liquid. Since the liquid is hydrogenous, the neutron will very rapidly lose energy by collisions with the hydrogen nuclei. In fact it will only take a small fraction of a microsecond for a million-electron-volt neutron to lose most of its energy—say to be reduced in energy by a factor of $10^3$. In this slowing-down process, the neutron energy is transferred to energy of recoiling hydrogen nuclei. These recoil protons cause a pulse to be produced in the detector which is, for our purposes, in coincidence with the introduction of the neutron. However, considerable time is required for the neutron to reach thermal energy. When the neutron is finally slowed down to near thermal energy, there is a good chance for it to be captured by the cadmium which is present in the solution. The average length of time

elapsed between the introduction of a neutron into the solution and its capture by cadmium is about 28 μs. When the capture occurs, several gamma rays are emitted from the cadmium and produce a pulse in the scintillator. This is a second pulse and it occurs at a variable time after the first one. An explanation of how these pulses are used is given below.

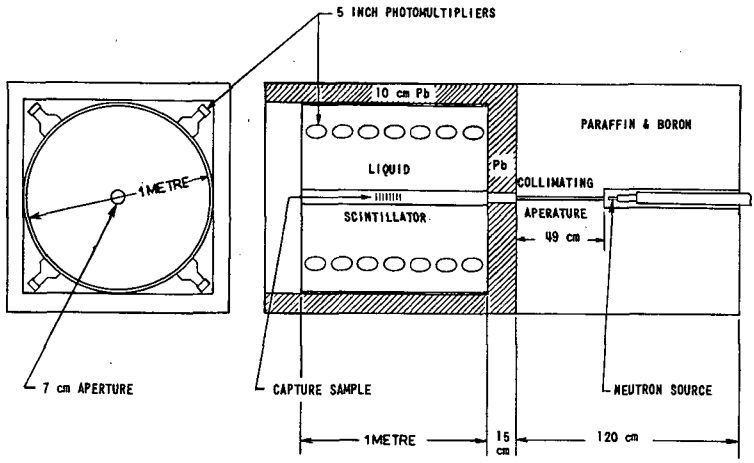


Fig. 1
End view and cross-section of the scintillator, neutron source and shielding. A collimated beam of neutrons is passed through the fission counter at the centre of the scintillator.

Fig. 1 is a diagram of our experimental set-up. The scintillation counter is a circular cylinder about 1 m in diameter and 1 m long. There is a hole down the axis of this cylinder. In this hole, at the centre of the counter, is placed an ionization chamber containing fissionable material. If we are investigating spontaneous fission, then this is all of the equipment needed. However, our main interest is in neutron-induced fission. For this work, we use a collimated beam of neutrons which pass down the axial opening of the scintillator and through the fission counter without striking the scintillator. The source of fast neutrons is a 2.5-MeV Van de Graaff generator. For neutron energies between thermal energies and one million electron-volts the T (p, n) $He^3$ reaction is used, for energies between 3.5 and 5 MeV the D (D, n) $He^3$ reaction is used, and for neutrons of 15 MeV the T (d, n) $He^4$ reaction is used.

In order to keep the background radiation low, the neutron source is enclosed in shielding which absorbs all neutrons except those which pass through the collimator. Lead is used to stop gamma rays which are produced by the capture of neutrons in the shield. Neutrons from the source pass through the collimator, the axial opening of the scintillator, and into the fission counter where fissions are produced.

When a fission occurs, the pulse produced in the ionization chamber by the fission fragments is used to open a 64-μs gate. The output of the scintillator is fed through the gate to a scaler which determines the number of pulses which arrive during the gate. When the fission occurs, both gamma rays and neutrons

are emitted. These enter the scintillator and both contribute to a pulse which occurs at the same time as the fission event. The neutrons lose energy by multiple scattering in the solution, and one by one are captured by cadmium which produces pulses that are detected by the scaler at the time each neutron is captured.

If the efficiency of the scintillator were 100% and there were no background, then there would appear on the scaler as many pulses as there were neutrons emitted in the fission event. Actually, some corrections are needed because the efficiency is only about 80% and there is a background of about one pulse in every two to ten gates.

In order to deduce the mean number of neutrons per fission from the observed number of pulses per gate, it is necessary to know the efficiency of the detector for fission neutrons. Several effects contribute to a reduction of the efficiency from 100%. A few of the neutrons leak out of the detector. A Monte-Carlo calculation indicates that the leakage of neutrons varies from less than 1% for 1-MeV neutrons to 5% for 5-MeV neutrons. For the fission spectrum, about 98.5% of the neutrons are captured in the detector.

A larger cause of reduction of efficiency is leakage of the cadmium gamma rays from the scintillator. For about 12% of the neutron capture events, enough of the gamma ray energy escapes from the scintillator so that the resulting pulse is unacceptably small. These and other smaller effects result in a reduction of the detector efficiency to about 80%.

The efficiency is determined in two ways. The first is to assume the accurately known value of $\bar{\nu}$ for $U^{235}$ at thermal energy. The detector efficiency is the mean number of neutrons detected per gate divided by the known value of $\bar{\nu}$. Another method is to replace the fission detector with a proton recoil neutron detector such as a hydrogen-filled proportional counter that is inserted into the centre of the liquid scintillator in place of the fission counter. Then monoenergetic neutrons are passed through the proportional counter, and the gate opened with pulses produced by recoil protons. Every proportional counter pulse is associated with the scattering of a neutron out of the beam and into the liquid scintillator by a hydrogen nucleus in the counter. Furthermore, if gates are opened only if the pulse height from the recoil proton falls within a narrow range of energies, then both the energy and the direction of the scattered neutron are known. The neutron-detection efficiency for a neutron of this energy is the mean number of pulses per gate less background. With a knowledge of the efficiency as a function of energy, the efficiency can be computed for the detection of fission neutrons.

This apparatus has been used for the measurement of $\alpha$ and of $\bar{\nu}$. Only the measurement of $\bar{\nu}$ is described here. This experiment has two parts: (*a*) the measurement of $\bar{\nu}$ for neutron-induced fission of $U^{233}$, $U^{235}$ and $Pu^{239}$ relative to the $\bar{\nu}$ for spontaneous fission of $Cf^{252}$; and (*b*) the determination of an absolute $\bar{\nu}$ for the spontaneous fission of $Cf^{252}$. Preliminary data on the absolute value of $\bar{\nu}$ for $Cf^{252}$ yields a value of 3.73 with a standard deviation of 3%.

The results of the analysis of the data for the relative measurements of $\bar{\nu}$ are shown in Fig. 2 and Table I. Relative measurements of $\bar{\nu}$ have been made for spontaneous fission of $Pu^{240}$ and for the neutron-induced fission of $U^{233}$, $U^{235}$ and $Pu^{239}$. Since we have not yet made a sufficiently accurate measurement of the efficiency of the neutron detector, all of the data are normalized to the thermal value for $\bar{\nu}$ of $U^{235}$: $2.43 \pm 0.03$. The standard deviations shown in Fig. 2 reflect the statistical uncertainty due to the number of fission events observed and to the 1.2% uncertainty in the $\bar{\nu}$ of $U^{235}$ for thermal-neutron-induced fission.

TABLE I

$\bar{\nu}$ AND $d\bar{\nu}/dE$ AS A FUNCTION OF ENERGY FOR $U^{233}$, $U^{235}$, AND $Pu^{239}$

| Isotope | $E_n$ | Prompt neutrons per fission | Delayed neutrons per fission | Total $\bar{\nu}$ | $d\bar{\nu}/dE_n$ |
|---|---|---|---|---|---|
| $U^{233}$ | Thermal | 2.440 ±0.041 | 0.007 | 2.447 ±0.041 | 0.126 ±0.014 |
| | 4.0 MeV | 2.943 ±0.040 | — | 2.950 ±0.063 | |
| $U^{235}$ | Thermal | 2.414 ±0.030 | 0.016 | 2.430* ±0.030 | 0.122 ±0.008 |
| | 4.0 MeV | 2.903 ±0.048 | — | 2.919 ±0.048 | |
| $Pu^{240}$ | —6.28 MeV | 2.167 ±0.036 | 0.009 | 2.176 ±0.036 | 0.098 ±0.005 |
| $Pu^{239}$ | Thermal | 2.814 ±0.046 | 0.006 | 2.820 ±0.046 | 0.150 ±0.012 |
| | 4.0 MeV | 3.415 ±0.063 | — | 3.421 ±0.063 | |
| $Cf^{252}$ | Spont.[1] | 3.739 ±0.051 | 0.009 | 3.748 ±0.051 | — |
| | Spont.[2] | 3.722 | — | 3.731 | — |

* "U.S. value", all other points normalized to this. D. J. Hughes *et al.*, BNL-325 Supplement No. 1 (1960) 4.

[1] $Cf^{252}$ spontaneous fission $\bar{\nu}$ normalized to "U.S. value" for $\bar{\nu}$ of $U^{235}$.

[2] $Cf^{252}$ spontaneous fission $\bar{\nu}$ obtained from our preliminary absolute measurement.

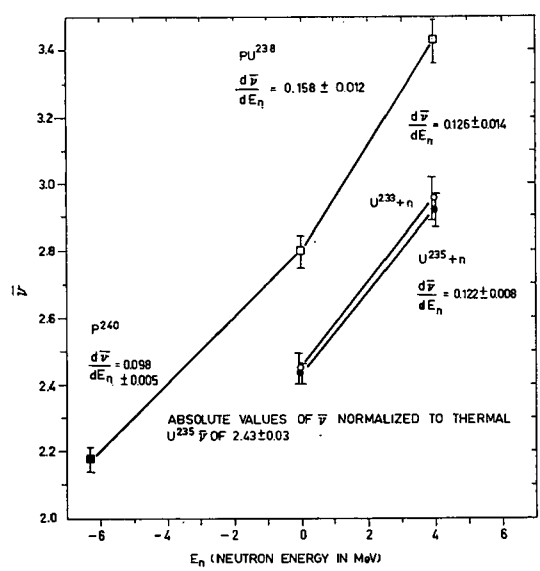


Fig. 2

$\bar{\nu}$ as a function of incident-neutron energy for $U^{233}+n$, $U^{235}+n$ and $Pu^{239}+n$.

TABLE II
**PRELIMINARY VALUES FOR $\bar{\nu}$**

| Isotope | $E_n$ (keV) | Prompt neutrons per fission | Delayed neutrons per fission | Total $\bar{\nu}$ |
|---|---|---|---|---|
| $U^{233}$ | Thermal | $2.465 \pm 0.041$ | 0.007 | $2.472 \pm 0.041$ |
| | $325 \pm 93$ | $2.479 \pm 0.043$ | | $2.486 \pm 0.043$ |
| | $475 \pm 75$ | $2.492 \pm 0.043$ | | $2.499 \pm 0.043$ |
| | $842 \pm 59$ | | | |
| | $992 \pm 54$ | $2.546 \pm 0.046$ | | $2.553 \pm 0.046$ |
| | $4000 \pm 300$ | $2.973 \pm 0.040$ | | $2.980 \pm 0.063$ |
| $U^{235}$ | Thermal | $2.414 \pm 0.030$ | 0.016 | $2.430 \pm 0.030$* |
| | $325 \pm 93$ | $2.424 \pm 0.039$ | | $2.440 \pm 0.039$ |
| | $475 \pm 75$ | $2.431 \pm 0.038$ | | $2.447 \pm 0.038$ |
| | $842 \pm 59$ | $2.458 \pm 0.038$ | | $2.474 \pm 0.038$ |
| | $1106 \pm 52$ | $2.519 \pm 0.040$ | | $2.535 \pm 0.040$ |
| | $4000 \pm 300$ | $2.903 \pm 0.048$ | | $2.919 \pm 0.048$ |
| $Pu^{240}$ | —6280 | $2.187 \pm 0.036$ | 0.009 | $2.196 \pm 0.036$ |
| $Pu^{239}$ | Thermal | $2.824 \pm 0.046$ | 0.006 | $2.830 \pm 0.046$ |
| | 4000 | $3.462 \pm 0.063$ | | $3.468 \pm 0.063$ |
| $Cf^{252}$ | Spontaneous** | $3.761 \pm 0.051$ | 0.009 | $3.770 \pm 0.051$ |

* "U.S. value", all other points normalized to this. D. J. Hughes *et al.*, BNL 325 Supplement No. 1 (1960) 4.
** $Cf^{252}$ spontaneous fission $\bar{\nu}$ normalized to "U.S. value" for $\bar{\nu}$ of $U^{235}$.

The standard deviation in the slope, $d\bar{\nu}/dE_n$, is mainly due to the uncertainty associated with the relative measurement. These relative errors are from 0.9 to 1.5%. Thus the slope is more accurately known than would be implied by the error bars on the individual points.

The salient feature of these data is that the average slope, $d\bar{\nu}/dE_n$, for $Pu^{239} + n$ between —6.28 MeV and thermal energies differs from the average slope between thermal energies and 4.0 MeV. Often, for simplicity, the slope has been assumed to be constant and approximately equal to $1/E_0$, where $E_0$ is the average of the binding energy plus the kinetic energy of the emitted neutron [3]. However, it is well known that the fragment mass distribution changes with bombarding energy [4] and that the neutron emission per fragment is dependent upon fragment mass [5]. For these reasons it is easy to see that a slope change with energy is reasonable.

It should be emphasized that the absolute values quoted are the result of preliminary data and should be considered as tentative. Measurements of $\bar{\nu}$ are in progress now. We hope to extend the relative measurements to 14 MeV and to make a more accurate absolute determination of $\bar{\nu}$.

## REFERENCES

[1] REINES, F. *et al.* *Rev. sci. Instrum.* **25** (1954) 1061.
[2] DIVEN, B. C. *et al.*, *Phys. Rev.* **101** (1956) 1012.
[3] TERRELL, J. *Phys. Rev.* **108** (1957) 783.
[4] KATCOFF, S. *Nucleonics* **16** (1958) 78.
[5] WHETSTONE, S. L., quoted in LEACHMAN, R. B., Proc. 2nd UN Int. Conf. PUAE **15** (1958) 229.

SM — 18/75

# AN ABSOLUTE MEASUREMENT OF $\bar{\nu}$ OF CALIFORNIUM-252

I. Asplund, H. Condé and N. Starfelt
Research Institute of National Defence, Stockholm, Sweden

**Abstract — Résumé — Аннотация — Resumen**

**An absolute measurement of $\bar{\nu}$ of $Cf^{252}$.** An absolute determination of the average number of neutrons, $\bar{\nu}$, emitted in the spontaneous fission of $Cf^{252}$ has been made by counting the fission neutrons in a large liquid scintillator. The detection efficiency of this counter was measured as a function of neutron energy. Well-collimated neutrons were scattered into the scintillator by an anthracene crystal, which detected the corresponding recoil protons. Pulse-shape discrimination was employed to eliminate $\gamma$-ray background. The detection efficiency for $Cf^{252}$ fission neutrons was found to be $0.703 \pm 0.007$, giving a value of $3.78 \pm 0.04$ for the average number of prompt neutrons emitted per $Cf^{252}$ fission.

**Mesure absolue de $\bar{\nu}$ de $^{252}$Cf.** Les auteurs ont procédé à une détermination absolue du nombre moyen de neutrons, $\bar{\nu}$, émis au cours de la fission spontanée de $^{252}$Cf en comptant les neutrons de fission dans un grand scintillateur liquide. L'efficacité de la détection de ce compteur a été mesurée en fonction de l'énergie des neutrons. Un faisceau collimaté de neutrons a été diffusé dans le scintillateur par un cristal d'anthracène qui détectait les protons de recul correspondants. On a utilisé un discriminateur de formes d'impulsions pour éliminer le bruit de fond dû aux rayons gamma. On a constaté que, pour les neutrons libérés par la fission de $^{252}$Cf, l'efficacité de la détection était de $0{,}703 \pm 0{,}007$, soit une valeur de $3{,}78 \pm 0{,}04$ pour le nombre moyen de neutrons rapides émis par la fission de $^{252}$Cf.

**Абсолютное измерение $\bar{\nu}$ калифорния-252.** Было проведено абсолютное определение среднего числа нейтронов $\bar{\nu}$, испускаемых при самопроизвольном делении калифорния-252, путем подсчета нейтронов деления в большом жидкостном сцинтилляторе. Эффективность обнаружения с помощью этого счетчика измерялась как функция нейтронной энергии. Хорошо коллимированные нейтроны рассеивались в сцинтиллятор с помощью кристалла антрацена, который обнаруживает соответствующие протоны отдачи. Использовался дискриминатор формы импульса для устранения фона гамма-излучения. Эффективность обнаружения для нейтронов деления калифорния-252 составила $0{,}70 \pm 30{,}007$, что дает $3{,}78 \pm 0{,}04$ для среднето числа быстрых нейтронов, испускаемых на одно деление калифорния-252.

**Medición del valor absoluto de $\bar{\nu}$ para el $^{252}$Cf.** Los autores han efectuado una determinación absoluta del número medio de neutrones, $\bar{\nu}$ emitidos en la fisión espontánea del $^{252}$Cf, contando los neutrones de fisión mediante un contador de centelleo líquido de grandes dimensiones. El rendimiento de detección de este contador se midió en función de la energía neutrónica. El haz neutrónico bien colimado se dispersó en el medio de centelleo con ayuda de un cristal de antracenio que detecta los correspondientes protones de retroceso. Para eliminar el fondo de rayos $\gamma$, los autores procedieron a discriminar la forma de los impulsos. Encontraron que el rendimiento de detección de los neutrones de fisión procedentes del $^{252}$Cf era de $0{,}703 \pm 0{,}007$, lo que da un valor de $3{,}78 \pm 0{,}04$ para el número medio de neutrones inmediatos emitidos en la fisión de cada núcleo de $^{252}$Cf.

## Introduction

Absolute values of the average number of neutrons, $\bar{\nu}$, emitted per fission have been determined in several different ways [1]. Most of the measurements have been made for fission of $U^{235}$ induced by thermal neutrons, but results also exist for spontaneous fission of $Cf^{252}$. It is comparatively easy to measure the ratio of $\bar{\nu}$ for two elements, so the $Cf^{252}$ value is a suitable standard for relative measurements as well as $\bar{\nu}$ for $U^{235}$.

One class of measurements relies on the calibration of the fission-neutron counter by using standard neutron sources and the accuracies of the $\bar{\nu}$ values obtained in this way depend on the calibration of the standard sources. Using this method, KENWARD, RICHMOND and SANDERS [1, 2] obtained the value of $2.420 \pm 0.037$ for thermal fission of $U^{235}$, and in a similar way MOAT, MCTAGGART and MATHER [3] measured the value of $3.65 \pm 0.07$ for $Cf^{252}$. CRANE, HIGGINS and THOMPSON [4] obtained a value of $3.53 \pm 0.15$ for $Cf^{252}$ using the $Mn\,SO_4$ bath techniques.

By comparing the measured and calculated critical masses of a $U^{235}$ sphere, ENGLE, HANSEN and PAXTON [5] obtained a $\bar{\nu}$ for $U^{235}$ which, when corrected to thermal neutrons, yields a value of $2.37 \pm 0.07$. A third type of experiment was performed by DIVEN *et al.* [6, 7]. They calibrated their fission-neutron detector by means of a reaction, the $\bar{\nu}$ value of which is equal to 1, i.e. the scattering of neutrons against protons in an anthracene crystal. Their results were $2.426 \pm 0.06$ for thermal fission of $U^{235}$, and $3.81 \pm 0.09$ for $Cf^{252}$. A similar method was used by COLVIN and SOWERBY [1, 8], yielding a value of $2.418 \pm 0.039$ for thermal fission of $U^{235}$. In this case, the detector was a boron pile and the nuclear reaction used for the efficiency calibration was the photo-disintegration of the deuteron.

In the present experiment, the method first described by DIVEN *et al.* [6] has been employed, thus avoiding the use of a standard neutron source. The difficulty caused by gamma-ray background in the anthracene crystal has been overcome by separating recoil proton pulses from those of gamma rays by pulse-shape discrimination. Furthermore, the determination of the detection efficiency of the fission-neutron counter has been made simpler by making the counter spherical instead of cylindrical and by mounting the photomultipliers in spherical symmetry.

The limit to the accuracy attainable in this experiment is set by the lack of knowledge of the exact shape of the fission-neutron spectrum. In the present case, with a tank of a diameter of 60 cm, this leads to an uncertainty of about $\pm 0.5\%$ in $\bar{\nu}$.

The experimental arrangement has been described earlier by CONDÉ and STARFELT [9], who also give a more complete list of references to earlier experiments.

## Experimental arrangement

The neutron-detection efficiency of the cylindrical detector, earlier used [9] for relative measurements of $\bar{\nu}$ values and equipped with photomultipliers only at one end appeared to be non-isotropic. Thus this detector is not suitable for an absolute measurement of $\bar{\nu}$ and has been replaced by a spherical tank with twelve 5-in photomultipliers uniformly distributed over the surface of the sphere (Fig. 1). The tank is a glass bulb with a diameter of 60 cm and painted white

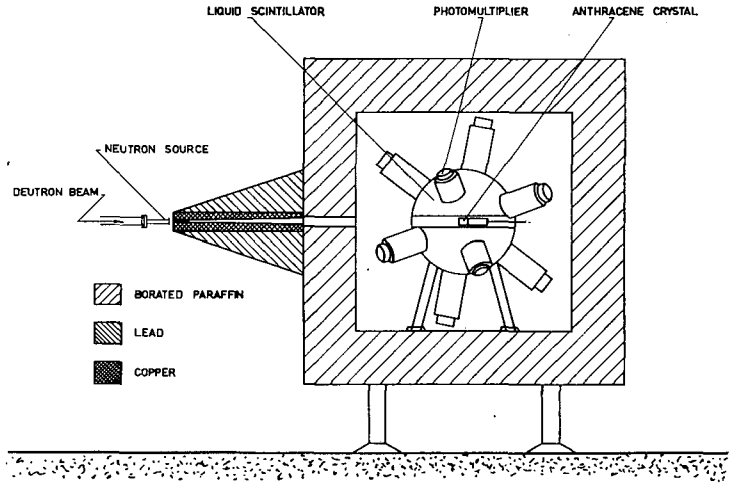


Fig. 1
Experimental arrangement for the absolute measurement of $\bar{\nu}$.

on the outside. The scintillator solution is triethylbenzene with $p$-terphenyl, POPOP and Cd-octoate to capture the thermalized neutrons. The cadmium-to-hydrogen atomic ratio is about 0.002.

In the centre of the axial tube through the tank a fission chamber containing the $Cf^{252}$ sample was mounted. The tube has a diameter of 6 cm. The $Cf^{252}$ sample gave about 80 spontaneous fisssions per minute.

In the measurement of the neutron-detection efficiency of the scintillator, the fission chamber was replaced by an anthracene crystal, 2 in in diameter and 0.5 in in length, mounted on a 2-in photomultiplier. A narrow beam of neutrons from the collimator passed through the axial tube, and the neutrons were scattered into the liquid scintillator by the crystal. The neutrons were

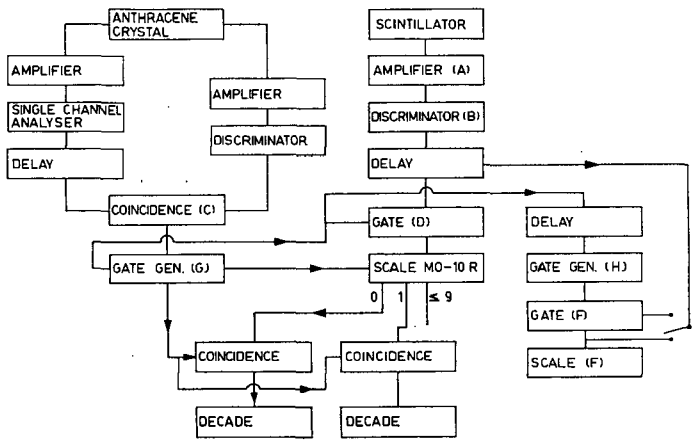


Fig. 2
Block diagram of the electronic circuits.

produced at a 300 kV electrostatic accelerator by $H^2$ (d, n) $He^3$ and $H^3$ (d, n) $He^4$ reactions in thin, adsorbed targets. The average neutron energies were 3.0 and 14.9 MeV at the D-D and D-T reactions, respectively.

Fig. 2 shows a block diagram of the electronic circuits. When a pulse caused by a recoil proton of preselected energy occurs in the anthracene crystal, a gate is opened and the pulses from the liquid scintillator are counted during a time of 30 μs. To distinguish between recoil protons and γ-ray background, pulse-shape discrimination according to the method of OWEN [10] is used. The pulses from the last dynode of the multiplier tube are different in pulse heights for protons and electrons, thus making it possible to discriminate against Compton electrons down to about 0.8 MeV of proton-recoil energy. A pulse which is linear in proton-recoil energy is obtained from another dynode in the tube. The linear pulse passes an amplifier and a single-channel analyser, while the pulse from the last dynode passes an amplifier and a pulse-height discriminator. A coincidence between the two pulses opens the gate of the liquid scintillator. The scintillator pulses are counted by a beam switching tube, MO-10R. This tube can accumulate from zero to nine pulses which are counted in ten registers after the end of the gate time. The over-all resolving time is 0.16 μs.

With a delay of 175 μs, the pulse from the gate generator (G) also starts the gate generator (H), which produces a 30-μs gate pulse to the fast background counting system (F).

## Experimental procedure

The measurements of the detection efficiency for different neutron energies were made alternately with measurements of $\bar{\nu}$ for $Cf^{252}$ complemented with measurements of the stability of the electronic equipment.

First, the amplification and bias setting for the scintillation pulses were adjusted by counting pulses over a certain discriminator level from a standard $Co^{60}$ source. The length of the gate of the background counting system relative to that counting fission-neutrons was obtained by observing the counting rates in the two branches when the gates were opened by a signal from a pulse generator. Then a 30-min run with the $Cf^{252}$ fission chamber was made resulting in about 1500 fissions.

For energy calibration of the anthracene crystal, the Compton-electron spectrum from a standard $Na^{22}$ γ-ray source was measured on a 100-channel pulse analyser. Then, with the anthracene crystal in position in the tank, a 3-h run was made at a certain energy of the scattered neutrons, i.e. at a certain setting of the single channel analyser. This resulted in about 6000 registered events. The pulse-height spectrum of the recoil protons, the setting of the single-channel analyser and the discriminator bias of the pulse-shape discriminating circuit were registered on a 100-channel analyser during the 3-h run.

After these measurements, the same cycle of measurements was repeated at another setting of the single-channel analyser, i.e. at another neutron energy.

The background was not a serious problem. The number of pulses per gate in the background was kept at about 0.5 in the runs with the anthracene crystal. To make sure that there was no variation of the sensitivity of the neutron detector with counting rate, $Cf^{252}$ runs were made with different backgrounds ranging from 0.5 down to the natural background of 0.02 pulses per gate. No variation was observed.

A correction for pile-up of neutron pulses in the scintillator has to be performed as described in reference [9].

For capture pulses following a fission, the probability, $K$, of two pulses being detected as one was equal to 0.02; for background pulses, it was equal to 0.01. With these low values of $K$, no corrections had to be made for pile-up of more than two pulses, and the approximate formula given by Diven *et al.* [6] was sufficient.

This correction was 2.6% to the observed $Cf^{252}$ $\bar{\nu}$-values and around 0.2% to the anthracene $\bar{\nu}$-values.

**Neutron detection efficiency**

A typical pulse distribution obtained from the anthracene crystal when irradiated with monoenergetic neutrons is shown in Fig. 3. The distribution of the pulses selected by the single-channel analyser in determination of the

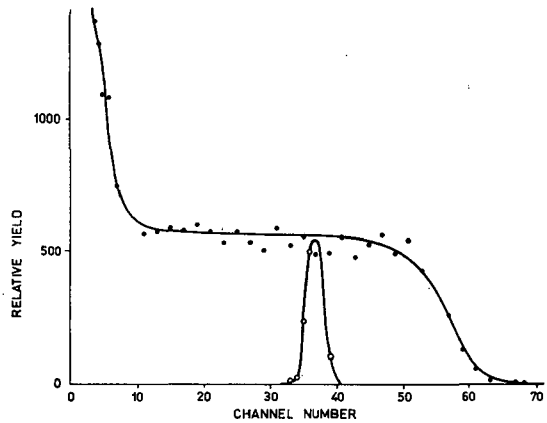


Fig. 3
Pulse distribution from the anthracene crystal for 14.9-MeV neutrons (filled circles), and distribution of pulses selected by the single-channel analyser (open circles).

detection efficiency for a certain neutron energy, $E''_n$, is also given. In the case of strictly monoenergetic neutrons of energy $E'_n$ entering the crystal, and when these neutrons are scattered just once in the anthracene crystal against a proton, the energy $E_p$ of the recoil proton gives a unique measure of the energy, $E''_n = E'_n - E_p$, and the direction, $\theta$, of the scattered neutron ($\cos^2\theta = E''_n/E'_n$). However, the deuterium targets used in this experiment had a small contamination of tritium giving a component of 14.9-MeV neutrons to the 3.0-MeV runs. This effect can easily be corrected for by extrapolating to lower energies the recoil-proton spectrum observed above 3 MeV.

The (n, $\alpha$) reaction in $C^{12}$ in the anthracene crystal induced by 14.9-MeV neutrons gives rise to pulses equivalent in height to protons up to 1.6 MeV, thus setting a lower limit to the proton energy which can be used in the measurements both with tritium and with deuterium target.

As a result of scattering of neutrons in the collimator, a small fraction of the neutrons entering the anthracene crystal has an energy lower than the energy $E'_n$ given by the source. Thus a recoil-proton energy $E_p$ may correspond to

TABLE I

**NEUTRON DETECTION EFFICIENCY ($\eta$) OF THE LIQUID SCINTILLATOR FOR DIFFERENT NEUTRON ENERGIES, $E''_n$**

**(The angle $\theta$, indicates the neutron direction with respect to the axis of the scintillator)**

| Neutron source | $E''_n$ (MeV) | $\theta°$ | $\eta_{obs.}$ (%) | Pile-up correction | Other corrections | $\eta_{corr.}$ (%) |
|---|---|---|---|---|---|---|
| D—D | 0.24 | 73.6 | 72.3 ± 1.5 | 0.0 | +0.4 | 72.7 |
| D—D | 0.65 | 62.3 | 73.9 ± 1.2 | 0.0 | +0.4 | 74.3 |
| D—D | 1.07 | 53.3 | 73.9 ± 1.1 | 0.0 | +0.4 | 74.3 |
| D—D | 1.55 | 44.0 | 73.3 ± 1.2 | 0.0 | +0.5 | 73.8 |
| D—T | 0.48 | 79.7 | 71.5 ± 1.7 | +0.2 | +0.3 | 72.0 |
| D—T | 1.65 | 70.6 | 72.2 ± 1.7 | +0.2 | +0.5 | 72.9 |
| D—T | 3.01 | 63.3 | 70.4 ± 1.7 | +0.2 | —0.5 | 70.1 |
| D—T | 3.46 | 61.2 | 67.3 ± 2.1 | +0.5 | —0.5 | 67.3 |
| D—T | 4.27 | 57.6 | 63.9 ± 1.8 | +0.2 | —0.6 | 63.5 |
| D—T | 5.45 | 52.8 | 58.9 ± 1.7 | +0.8 | —0.7 | 59.0 |
| D—T | 6.69 | 47.9 | 53.2 ± 1.8 | +0.2 | —0.7 | 52.7 |
| D—T | 7.94 | 43.1 | 53.3 ± 1.7 | +0.2 | —0.8 | 52.7 |
| D—T | 10.75 | 31.9 | 42.4 ± 1.6 | +0.2 | —0.7 | 41.9 |

a scattered neutron of energy lower than $E'_n - E_p$. As the neutron detection efficiency of the scintillator tank decreases with increasing neutron energy, this fact results in a measured efficiency for neutron energies above about 3 MeV, which is slightly larger than the true efficiency. The corresponding correction can be calculated.

As the pulse height per unit kinetic energy in anthracene is negligibly small for carbon nuclei as compared with protons, scattering of neutrons against carbon in the crystal is equivalent to degradation in the collimator and the correction can be performed in the same way.

A certain pulse height, $E_p$, in the anthracene crystal does not uniquely define the recoil-proton energy. In the first place, the pulse-height versus proton-energy relation is non-linear in such a way that a single scattering event where one recoil proton gets the energy $E_p$ gives a pulse which is larger than that obtained from two or more recoil protons of total energy $E_p$ resulting when a neutron is multiply scattered in the crystal. Secondly, a recoil proton may escape from the crystal having deposited only part of its energy in the crystal. For these reasons a pulse height, $\varepsilon$, corresponding to the single energy $E_p$, may be connected with scattered neutrons not only of energy $E'_n - E_p$ but also with neutrons of lower energy. These effects can be calculated and corrected for. They are important only above $E''_n \simeq 3$ MeV.

Table I gives the measured detection efficiency of the fission-neutron detector at different neutron energies, $E''_n$, for neutrons emitted at the angle $\theta$ (single scattering) to the detector axis. Because of the spherical symmetry of the detector, these values also represent the efficiency in all directions except those where the open channel through the tank is of importance. The corrections to the raw data are also given. The efficiency as a function of neutron energy is shown in Fig. 4. The fact that the low-energy portion of the curve lies around 70% and not at 100% is due mainly to the escape of capture $\gamma$-rays from the tank and to the bias setting for the $\gamma$-ray pulses, which has to be at a fairly high level to reduce the background counting rate.

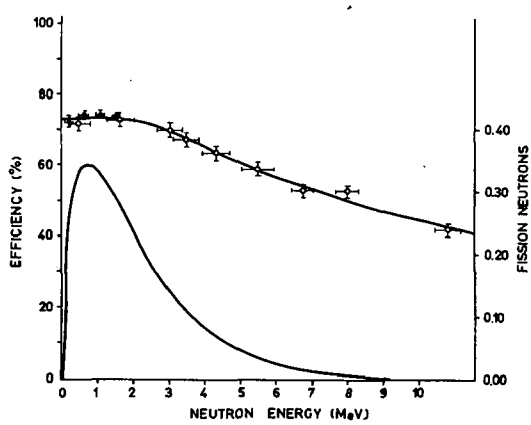


Fig. 4
Neutron-detection efficiency for the liquid scintillator as a function of neutron energy, $E''_n$. Filled and open circles represent D–D and D–T neutrons, respectively. Counting statistics and energy spread are also shown. The lower curve shows the fission-neutron spectrum of $Cf^{252}$.

From the efficiency curve of Fig. 4 the detection efficiency for the neutrons from spontaneous fission of $Cf^{252}$ has to be calculated. Several measurements of this fission-neutron spectrum have been performed, but still there are uncertainties. Two different representations have been used: the Watt spectrum $N(E) \sim \sinh\sqrt{bE'}\ e^{-aE}$ and the Maxwell spectrum $N(E) \sim \sqrt{E}e^{-E/T}$. In his review article on fission spectra, TERRELL [11] compared three theories, the two mentioned above and a third given by Feather, with the experimentally given spectra. His conclusion is that the Watt spectrum and the Maxwellian spectrum can equally well be fitted to the experiments.

In either case, it is evident that the spectrum of $Cf^{252}$ is harder than the spectrum of $U^{235}$, for example. Terrell [12] has given a relation between $\bar{E}$ $(=3T/2)$ and $\bar{\nu}$: $\bar{E}=0.78+0.62\ (\bar{\nu}+1)^{1/2}$. Assuming $\bar{\nu}$ $(Cf^{252})=3.8$, one obtains $T=1.43$. This value is in fairly good agreement with the results of SMITH *et al.* [13] and of HJALMAR *et al.* [14]. Smith *et al.* preferred to fit a Watt spectrum to the experimental data.

Recently, BONNER [15] published a new measurement on the $Cf^{252}$ spectrum. He used a new type of neutron spectrometer [16] and obtained $T=1.367+0.039$ in the Maxwellian representation.

In our calculation of the detection efficiency for $Cf^{252}$ fission neutrons, we used a Maxwell spectrum with the parameter $T=1.4$.

Finally, a correction for the neutrons escaping through the channel in the detector has to be applied. A simple calculation shows that this correction is quite small: $0.9\pm0.2\%$. The finally adopted value of the detection efficiency, $\bar{\eta}$, of the liquid scintillator to $Cf^{252}$ fission neutrons was $0.703\pm0.007$. The uncertainty of $\pm0.007$ in this value includes counting statistics and estimated errors of 10% in the pile-up corrections and 25% in the other corrections. Furthermore, the inaccuracy in the fission-neutron spectrum is estimated to give a contribution of 0.5%.

**Result and discussion**

With the neutron-detection efficiency determined as described above, a final value of $3.78 \pm 0.04$ was obtained for the average number of prompt neutrons emitted per spontaneous fission of $Cf^{252}$. The stated uncertainty includes counting statistics and the estimated error in the pile-up correction for the measurements of the $Cf^{252}$ fission neutrons, together with the uncertainty in $\overline{\eta}$. Adding to the prompt $\bar{\nu}$ the number of delayed neutrons per fission of $0.86 \times 10^{-2}$ [17], a $\bar{\nu}$-value of $3.79 \pm 0.04$ for prompt and delayed neutrons is obtained. This is in good agreement with the value of $3.81 \pm 0.09$ obtained by Diven *et al.* [6] and with the value of 3.77 reported by MOAT *et al.* [18], but not with the value of $3.53 \pm 0.15$ given by CRANE *et al.* [4].

Both Diven *et al.* and Moat *et al.* made exact measurements of the ratio between $\bar{\nu}$ for $Cf^{252}$ and $\bar{\nu}$ for fission of $U^{235}$ with 80-keV neutrons with the results: $1.566 \pm 0.025$ and $1.565 \pm 0.019$, respectively. Using our value for $Cf^{252}$ of $3.78 \pm 0.04$ for $\bar{\nu}$ of $Cf^{252}$, these relative measurements result in a $\bar{\nu}$ of $2.42 \pm 0.04$ for thermal fission of $U^{235}$ when $1.6 \times 10^{-2}$ delayed neutrons per fission are added.

The accuracy of the present experiment is limited mainly by counting statistics. However, to improve the accuracy by a factor of 2 or more it is not sufficient only to increase counting time. In such a case, the errors in the corrections would dominate, and it would be necessary to make these corrections smaller by using a larger neutron detector and faster electronics and by making more accurate calculations of multiple scattering and other small effects in the anthracene crystal.

## ACKNOWLEDGEMENTS

The authors wish to thank Mr. J. Hansén and Mr. I. Lindgren for skilful technical assistance.

## REFERENCES

[1] SAFFORD, G. J. and HAVENS, W. W., Jr., *Nucleonics* **17** 11 (1959) 134.
[2] KENWARD, C. J., SANDERS, J. E. and RICHMOND, R., AERE R/R-2212 (1957).
[3] MOAT, A., McTAGGART, M. H. and MATHER, D. S., AWRE NR/P—1/59 (1959).
[4] CRANE, W. W. T., HIGGINS, G. H. and THOMPSON, S. G., *Phys. Rev.* **97** (1955) 242 and **101** (1956) 1804.
[5] ENGLE, L. B., HANSEN, G. E. and PAXTON, H. C., *Nucl. Sci. and Engng* **8** (1960) 543.
[6] DIVEN, B. C. *et al.*, *Phys. Rev.* **101** (1956) 1012.
[7] TERRELL, J., ANL-6122 (1959) 33.
[8] COLVIN, D. W. and SOWERBY, M. G., EANDC (UK) 3 (1960).
[9] CONDÉ, H. and STARFELT, N., *Nucl. Sci. and Engng* **11** (1961) 397.
[10] OWEN, R. B., *IRE Trans. nucl. Sci.* NS-5 **3** (1958) 198.
[11] TERRELL, J., *Phys. Rev.* **113** (1959) 527.
[12] TERRELL, J., *Phys. Rev.* **108** (1957) 783.
[13] SMITH, A. B., FIELDS, P. R. and ROBERTS, J. H. *Phys. Rev.* **108** (1957) 411.
[14] HJALMAR, E., SLÄTIS, H. and THOMPSON, S. G. *Ark. f. Fys.* **10** (1956) 357.
[15] BONNER, T. W., *Nucl. Phys.* **23** (1961) 116.
[16] BRAMBLETT, R. L., EWING, R. I. and BONNER, T. W., *Nucl. Instrum.* **9** (1960) 1.
[17] COX, S. *et al.*, *Phys. Rev.* **112** (1958) 960.
[18] MOAT, A. *et al.*, *These proceedings*, vol. **1**, p. 139.

# I. 4. NUCLEAR THEORY

SM—18/88

# STATISTICAL EMISSION IN NUCLEAR REACTIONS

E. Erba, U. Facchini and E. Menichella Saetta
Istituto di Fisica dell'Università, Milan,
and
Laboratori C.I.S.E., Milan,
Italy

**Abstract — Résumé — Аннотация — Resumen**

**Statistical emission in nuclear reactions.** Statistical model in nuclear reactions has been extensively developed in the past decades, mainly by V. Weisskopf. However, a clear understanding of the experimental situation regarding low- and medium-energy nuclear reaction is not yet settled.

The interpretation is complicated by the fact that often the reactions proceed *via* other mechanisms, for instance direct effects.

The purpose of the present paper is to show how a great number of experiments can be put in agreement with the statistical formulas, and particularly the resonance measurements for slow neutrons, the evaporation spectra from medium-energy (n, n′), (p, n) and (n, p) reactions and the (n, p) cross-sections at 14 MeV.

From the set of experiments discussed it is possible to obtain a consistent table of $a$, the parameter of the level density formula.

**Emission statistique dans les réactions nucléaires.** Au cours de ces dernières décennies, de nombreuses études ont été faites, notamment par V. Weisskopf, en vue d'élaborer un modèle statistique relatif aux réactions nucléaires. Cependant, on n'est pas encore parvenu à expliquer totalement les résultats des expériences dans le domaine des réactions à faible ou moyenne énergie.

Leur interprétation est d'autant plus complexe que ces réactions s'opèrent souvent selon d'autres mécanismes, par exemple sous la forme d'effets directs.

Le mémoire a pour objet de montrer comment il est possible de faire concorder les résultats de multiples expériences avec ceux que donnent les formules statistiques, notamment les mesures des résonances dans le cas des neutrons lents, le spectre d'évaporation obtenu à partir de réactions (n, n′), (p, n) et (n, p) à énergie moyenne et les sections efficaces (n, p) correspondant à une énergie incidente de 14 MeV.

La série d'expériences examinée permet de tabuler le paramètre $a$ de la formule qui exprime la densité des niveaux d'énergie.

**Статистическая эмиссия в ядерных реакциях.** Статистическая модель в ядерных реакциях была широко развита в последние десятилетия, главным образом, В. Вейсскопфом. Однако все еще не пришли к ясному пониманию экспериментальной ситуации относительно ядерной реакции малых и средних энергий.

Объяснение усложняется тем фактом, что часто реакции имеют другие механизмы, например, прямые эффекты.

Настоящий доклад имеет целью показать, как значительное число экспериментов может быть приведено в соответствие со статистическими формулами и, в частности, с резонансными измерениями для медленных нейтронов, спектра испарения из реакций средних энергий (n, n′), (p, n) и (n, p) и поперечных сечений (n, p) при 14 Мэв.

Из ряда обсуждаемых экспериментов можно получить согласующуюся таблицу параметра $\alpha$ формулы уровня плотности.

**Emisión estadística en las reacciones nucleares.** El modelo estadístico en las reacciones nucleares ha sido estudiado extensamente en las últimas décadas, principalmente por V. Weisskopf. Sin embargo, aún no se ha logrado interpretar cabal-

mente los datos experimentales en lo que respecta a las reacciones nucleares a energías bajas e intermedias.

Complica la interpretación el hecho de que a menudo las reacciones se desarrollan en virtud de otros mecanismos (efectos directos, por ejemplo).

Los autores de la presente memoria se proponen demostrar que es posible ajustar los resultados de un gran número de experimentos a las fórmulas estadísticas, particularmente en el caso de las mediciones de las resonancias de neutrones lentos, de los espectros de evaporación correspondientes a reacciones (n, n′), (p, n) y (n, p) de energía media y de las secciones eficaces para la reacción (n, p) a 14 MeV.

Partiendo de los resultados de la serie de experimentos estudiada, es posible establecer una tabla de valores satisfactorios para el parámetro $a$ que aparece en la fórmula que da el nivel de densidad.

## Introduction

The statistical model for nuclear reactions has been developed for a number of years, especially by V. Weisskopf, and has formed a basis of discussion in the field of nuclear reactions at low and medium energies.

However, the information we have on the various parameters that intervene in the model and on the field of validity of the model itself is still not cleared.

In the present work [1], an attempt is made to show the possibility of explaining a certain group of nuclear reactions with a statistical model, assuming a nuclear model of independent and equidistant particles to deduce statistically the density $\varrho$ of the nuclear levels.

The experiments discussed refer to:

(*a*) The measurements of the total cross-sections for slow neutrons in the resonance areas of about 110 nuclei;

(*b*) Energy spectra of particles emitted in the reactions (n, p) and (n, n′) and (p, n) for incident energies ranging between 4 and 16 MeV (56 spectra);

(*c*) Cross-sections of (n, p) and (n, n′) reactions for medium nuclei (32 nuclei).

From the results of experiments (*a*) and (*b*), we have deduced for the various nuclei the parameter $a$ entering $\varrho$; we have then used this formula of $\varrho$ to compare the results of experiments (*c*) with the statistical model of the nuclear reactions.

We may point out that as far as the following data analysis is concerned, the essential condition that should be satisfied in order to apply a statistical model to the nuclear reaction is the formation and decay of the compound nucleus as two independent processes.

We have used WEISSKOPF tables [2] for proton and neutron transparencies, taking as "effective nuclear radius" the value $R=r_0A^{1/3}$, with $r_0=1.5$ fermi for protons and 1.4 fermi for neutrons.

For the density of the levels $\varrho\ (E, j)$ of the nucleus, containing $A$ nucleons at excitation energy $E$ and with spin $j$, we have used the formula of the equidistant spacing model.

The pairing interaction is introduced through the "effective excitation energy" $U$ given by

$$U=E+\Delta$$

where $\Delta$ is a negative term representing the pairing energy of the last two protons when $Z$ is even, of the last two neutrons when $N$ is even, the sum of both pairing

energies for even-even nuclei; $\Delta$ is zero for odd-odd nuclei; $\varrho\,(E, j)$ is given by the formula:

$$\varrho(E,j) = \frac{6^{-\frac{1}{2}}}{2^{\frac{3}{2}}}\pi\hbar^3(2j+1)\frac{e^{-\left(j+\frac{1}{2}\right)^2/2ct}}{12}g_0^{\frac{1}{2}}J^{-\frac{3}{2}}\frac{e^{2\sqrt{aU}}}{(U+t)^2}. \tag{1}$$

The equidistant spacing model is the simplest of those discussed hitherto by various authors. With this formula, $\varrho\,(E, j)$ is expressed as a function of the average density $g_0$ of the single particle at the top of the potential well.

Assuming $g_n$ and $g_p$ as the densities for neutrons and protons respectively we have:

$$\left.\begin{aligned} g_0 &= g_n + g_p \\ a &= \frac{\pi^2}{6}g_0\,. \end{aligned}\right\} \tag{2}$$

The thermodynamic temperature is obtained from

$$U = at^2 - t\,. \tag{3}$$

$J$ is the moment of inertia of the nucleus and $c$ is given by

$$C = \frac{J}{\hbar^2}\,.$$

**Resonance of slow neutrons**

In reactions with slow neutrons, the presence of well-defined and separated width levels shows that in the reaction a compound nucleus is formed whose mean life is much greater than the relaxation time.

The experimental information analysed here is the average distance $D_{obs}$ among the various levels corresponding to values of the energy of incident neutrons below 200 keV.

Though no special hypotheses are formulated, it may be supposed that all the possible levels, in accordance with the rules of the conservation of spin and parity, are excited (with a greater or lesser probability), and therefore $D_{obs}^{-1}$ represents the density of the nuclear levels of the compound nucleus at the excitation energy $E$ and with given value of the spin $j$. The binding energy of the neutrons gives with good approximation the excitation energy $E$ of the compound nucleus.

Taking account of the spin $I$ of the target nucleus we have:

$$D_{obs} = \frac{1}{2}\varrho\left(E; j = \frac{1}{2}\right);\ I = 0 \tag{4}$$

$$D_{obs} = \frac{1}{2}\left[\varrho\left(E; I + \frac{1}{2}\right) + \varrho\left(E; I - \frac{1}{2}\right)\right];\ I \mp 0\,. \tag{5}$$

Since the initial state has a well-defined parity (the $l$ value of the incident neutrons is 0) the observed levels have only one of the two possible parities. Then we introduced in formulae (4) and (5) the factor $^1/_2$, which is due to the hypothesis of the equiprobability of the two parities for nuclear levels.

The measurements conducted by various groups and reported in BNL [3] reports and in other papers [4, 5] give the value $D_{obs}$ for 110 nuclei. From formulae (1—5) we can obtain the value of $g_0$.

We have introduced for $J$ the value $^2/_5\, M\, A\, R^2$, $M$ mass of nucleons, $r_0 = 1.4$ fermi, corresponding to a rigid nucleus following the advice of ERICSON [6]. Varying $J$ by some 10—30% the set of $a$ (MeV$^{-1}$) values obtained does not change appreciatively.

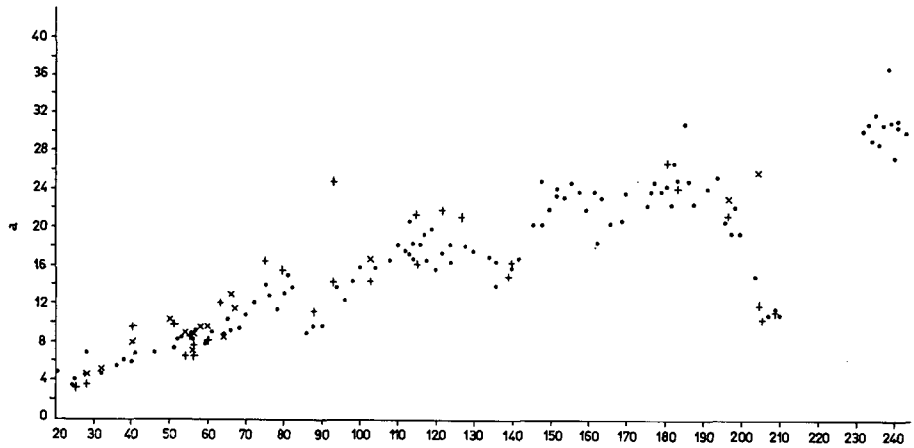


Fig. 1
Values of $a$ (MeV$^{-1}$) as a function of the number of mass $A$.
$\cdot\, a$ from $D_{\text{obs}}$
$\times\, a$ from spectra ($U > 5.5$ MeV)
$+\, a$ from spectra ($U < 5.5$ MeV)

We have obtained the values of $a$, with an electronic calculation. Fig. 1 represents the values of $a$ corresponding to each nucleus.

These values show a regular behaviour of $a$ with mass number $A$ and present the known minima for values of $A$ corresponding to nuclei having a magic neutron number ($A \simeq 90$, 140, 210).

## Spectra of neutrons and protons

In a previous work [8], we discussed the emission of nucleons and particles by various nuclei in various reactions. There we showed how a certain number of energy spectra, usually taken at backward angles, where the direct effects are reduced, give a result consistent with the statistical model.

In fact, according to such model, the ratio between the $n(\varepsilon)$ and the inverse cross-section $\sigma_c$ times the energy $\varepsilon$ of the emitted particle represents the density of states of the residual nucleus; $\sigma_c$ is derived from Weisskopf tables [2].

A work on (n, n′) reactions has been recently conducted by THOMSON and CRANBERG [7] for a certain number of medium and heavy nuclei. These authors have shown that for (n, n′) reactions with incident neutrons of 4—7-MeV energy the direct effects are not very important, and that they are isolable from evaporative emission, by comparing spectra obtained at various incident energies.

We have therefore, in this work, collected spectra that could be relied on, such as evaporative emissions [8], and the values of $a$ obtained by comparing all these spectra with formulae (1) and (3). The results collected represent all spectra regarding nucleon emission discussed in [8], the more recent results on (n, p) (n, n′) and (p, n) results at incident energies below 16 MeV.

It is pointed out that the $(U+t)^{-2}$ factor in formula (1) changes by 50% the values of $a$ obtained from the (n, n′) reactions by Thomson [7].

It must be remembered that formula (1) in a small range of values of $U$ is not quite different from an exponential shape

$$\varrho \sim C e^{U/\theta} \tag{6}$$

with $\theta$ constant.

It is interesting to note that, $a$ values obtained from the spectra are in good agreement with those obtained with the resonances of slow neutrons (Fig. 1), and that particularly the deep minima at magic $N$ nuclei and the average shape of the $a$ curves *versus* $A$ are substantiated.

## (n, p) cross-sections at 14 MeV

All the cross-sections $\sigma$ (n, p) for medium nuclei bombarded with 14-MeV neutrons have already been shown to be in agreement with the statistical model in Ref. [1], in which, as a first approximation, formula (6) for the density of nuclear levels was used, with $\theta$ constant, in rough agreement with the spectra.

ALLAN [9] has also shown an agreement with statistical model using formula (1) with $a = A/8$. These values of $a$, however, are not quite in good agreement with the $a$ values deduced by the experimental spectra of protons.

It is important to check the agreement of the experimental ratio [$\sigma$ (n, p)]/[$\sigma$ (n, n′)] with the corresponding ratio calculated with the statistical model, taking formula (1) as level density and using the $a$ values obtained and represented in Fig. 1.

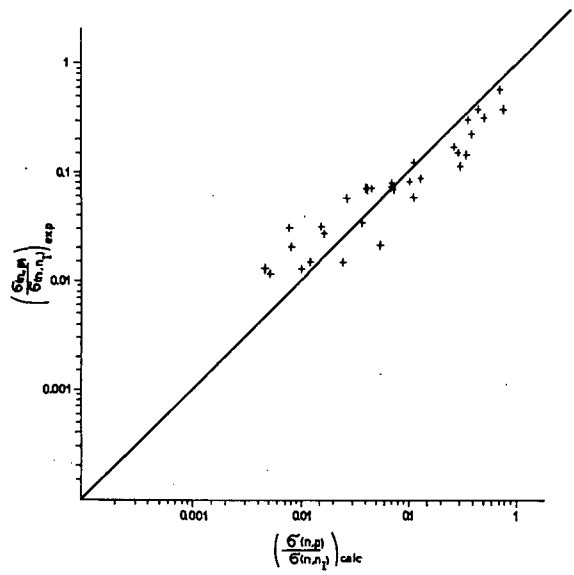


Fig. 2

$$\frac{\sigma\,(\mathrm{n,\,p})}{\sigma\,(\mathrm{n,\,n'})_{\mathrm{exp}}} \text{ as function of } \frac{\sigma\,(\mathrm{n,\,p})}{\sigma\,(\mathrm{n,\,n'})_{\mathrm{calc}}}\,.$$

The calculation performed electronically has given, for medium nuclei, the results shown in Fig. 2, demonstrating that the agreement is of the same kind as the one found in Ref. [1] and as the one found by Allan [9].

## Conclusions

The consistence of the whole group of experimental results discussed under the evaporation rules gives a wide experimental basis to the evaporation model and proves the validity of the $a$ values and of the formula of level density given with sufficient accuracy by (1) in the field of the energies and reactions studied.

A more extensive paper will be published in *Il Nuovo Cimento*.

## REFERENCES

[1] FACCHINI, U., IORI, I. and MENICHELLA, E., *Nuovo Cim.* **16** (1960) 1109–1131.
[2] BLATT, J. and WEISSKOPF, V., Theoretical Nuclear Physics, New York, Wiley and Sons (1952).
[3] BNL-325, Neutron cross section, 2nd ed. (1958).
[4] CAMERON, A. G. W., *Canad. J. Phys.* **36** (1958) 1040.
[5] STOLOVY, A. and HARVEY, J. A., *Phys. Rev.* **108** (1957) 353.
[6] ERICSON, T., *Advanc. Phys.* **9** (1960) 425.
[7] THOMSON, D. B. (Advisor L. Cranberg), Nuclear level densities and reaction mechanisms from inelastic neutron scattering, Thesis, Los Alamos Scientific Laboratories (1960).
[8] COLLI, L., *et al.*, *Nuovo Cim.* **13** (1959) 730.
[9] ALLAN, D. L., *Nucl. Phys.* **24** (1961) 274.

SM—18/35

# CALCULATION OF FAST-NEUTRON REACTION CROSS-SECTIONS*

P. A. MOLDAUER
ARGONNE NATIONAL LABORATORY, ARGONNE, ILL.,
UNITED STATES OF AMERICA

**Abstract — Résumé — Аннотация — Resumen**

**Calculation of fast-neutron reaction cross-sections.** The radiative-capture and inelastic-scattering cross-sections in reactor materials of neutrons having energies between 1 keV and several mega-electron-volts are of great importance in the analysis and design of fast reactors. Recent improvements in the theoretical description of such processes and the evaluation of the necessary nuclear parameters have made it possible to obtain reliable estimates of their cross-sections. Examples of such calculations are presented.

**Calcul des sections efficaces pour les neutrons rapides.** Les sections efficaces de capture radiative et de diffusion inélastique des neutrons dont l'énergie varie entre 1 keV et plusieurs méga-électronvolts jouent un rôle très important dans l'analyse et l'étude des réacteurs à neutrons rapides. Des améliorations récentes dans la description théorique de ces processus et l'évaluation des paramètres nucléaires nécessaires ont permis d'obtenir des valeurs satisfaisantes de leurs sections efficaces. La précision de ces évaluations ressort des comparaisons entre les sections efficaces calculées et toutes les mesures récentes dont les résultats sont connus. L'auteur présente des exemples de tels calculs.

**Вычисление сечений реакции на быстрых нейтронах.** Сечения радиационного захвата и сечения неупругого рассеяния нейтронов с энергией от одного кэв до нескольких Мэв в реакторных материалах имеют большое значение при анализе и расчете реакторов на быстрых нейтронах. Недавние успехи в теоретическом обосновании таких процессов и оценка необходимых ядерных параметров сделали возможным точно оценивать их сечения. Это показывается на примере сравнения вычисленных сечений со всеми имеющимися последними измерениями. Представлены примеры таких вычислений.

**Cálculo de secciones eficaces para neutrones rápidos.** Las secciones eficaces de captura radiativa y de dispersión inelástica de los materiales para reactores, a energías neutrónicas comprendidas entre 1 KeV y varios megaelectrón-voltios revisten considerable importancia para el análisis y diseño de reactores rápidos. Gracias a los recientes progresos en la descripción teórica de estos procesos y en la determinación de los parámetros nucleares necesarios, es posible evaluar con cierta seguridad tales secciones eficaces. Ello puede comprobarse comparando las secciones eficaces calculadas con los resultados de mediciones recientes. El autor presenta algunos ejemplos de los mencionados cálculos.

---

* Work performed under the auspices of the United States Atomic Energy Commission.

In intermediate and fast reactors having neutron fluxes predominantly at energies below a few mega-electron-volts, the crucial processes of fission, neutron capture and inelastic neutron scattering proceed almost exclusively through compound-nucleus formation. At these neutron energies, furthermore, the compound nuclei concerned occur in states which, for a given isotope and given total angular momentum and parity, form a sequence of distinct resonances. This resonance structure is in most cases not relevant to reactor calculations, either because it is smoothed out by the superposition of several sequences belonging to different angular momenta, parities and isotopes, or because it is much finer than the group structure employed in the calculations. Also the energy resolutions of neutrons employed in measuring cross-sections in this region are generally much broader than the resonance structures. Exceptions occurring primarily for the lighter nuclei will be mentioned later.

In general, therefore, one is interested in measuring or estimating the average over resonances of the neutron-reaction cross-sections. In Ref. [1] it has been shown that under the above-mentioned conditions these averages are well represented by the following expressions:

$$\sigma_{\mathrm{nf}} = \frac{2.045}{E\,(2I+1)} \sum_{J,\,\pi,\,l,\,j} (2J+1) \left\langle \frac{\Gamma_{\mathrm{f}}\,\Gamma_{\mathrm{n}}^{lj}}{D_{J,\pi}\,D_{J,\pi}} \middle/ \frac{\Gamma}{D_{J,\pi}} \right\rangle_{J,\,\pi} \tag{1}$$

$$\sigma_{\mathrm{nc}} = \frac{2.045}{E\,(2I+1)} \sum_{J,\,\pi,\,l,\,j} (2J+1) \left\langle \frac{\Gamma_{\mathrm{c}}}{D_{J,\pi}} \frac{\Gamma_{\mathrm{n}}^{lj}}{D_{J,\pi}} \middle/ \frac{\Gamma}{D_{J,\pi}} \right\rangle_{J,\,\pi} \tag{2}$$

$$\sigma_{\mathrm{n,n_i}} = \frac{2.045}{E\,(2I+1)} \sum_{J,\,\pi,\,l,\,j,\,l',\,j'} (2J+1) \left\langle \frac{\Gamma_{\mathrm{n}}^{lj}}{D_{J,\pi}} \frac{\Gamma_{\mathrm{n}_i}^{l'j'}}{D_{J,\pi}} \middle/ \frac{\Gamma}{D_{J,\pi}} \right\rangle_{J,\,\pi}. \tag{3}$$

Here $\sigma_{\mathrm{nf}}$, $\sigma_{\mathrm{nc}}$, $\sigma_{\mathrm{n,n}_i}$ are the average cross-sections in barns for fission, capture, and inelastic scattering to the $i^{\mathrm{th}}$ excited state of the target nucleus, respectively; $E$ is the incident neutron energy in MeV; $I$ is the spin of the target nucleus; $D_{J,\,\pi}$ is the average spacing of resonances of angular momentum $J$ and parity $\pi$; $\Gamma_{\mathrm{f}}$, $\Gamma_{\mathrm{c}}$, $\Gamma$ are the fission capture and total widths of individual resonances; $\Gamma_{\mathrm{n}}^{lj}$ and $\Gamma_{\mathrm{n}_i}^{lj}$ are the widths for emitting a neutron with orbital angular momentum $l$ and total angular momentum $j = l \pm {}^1/_2$, leaving the residual nucleus respectively in the ground state or in the $i^{\mathrm{th}}$ excited state. The brackets $\langle\quad\rangle_{J,\,\pi}$ indicate an average over all resonances with angular momentum $J$ and parity $\pi$ lying in an energy interval around $E$. The sums are carried over all values of the indicated angular momenta which are consistent with conservation of angular momentum and parity. The average of the type $\left\langle \frac{\Gamma_{\mathrm{A}}}{D_{J\pi}} \frac{\Gamma_{\mathrm{B}}}{D_{J\pi}} \middle/ \frac{\Gamma}{D_{J\pi}} \right\rangle_{J\pi}$ are certain functions of the quantities $\left\langle \frac{\Gamma_{\mathrm{A}}}{D_{J\pi}} \right\rangle_{J\pi}$, $\left\langle \frac{\Gamma_{\mathrm{B}}}{D_{J\pi}} \right\rangle_{J\pi}$, $\left\langle \frac{\Gamma}{D_{J\pi}} \right\rangle_{J\pi}$; see Refs. [1], [2] and [3]. Typically, these functions differ by at most a factor of 2 from $\left\{ \left\langle \frac{\Gamma_{\mathrm{A}}}{D_{J\pi}} \right\rangle_{J\pi} \left\langle \frac{\Gamma_{\mathrm{B}}}{D_{J\pi}} \right\rangle_{J\pi} \middle/ \left\langle \frac{\Gamma}{D_{J\pi}} \right\rangle_{J\pi} \right\}$, for the cases of interest here.

In order to estimate cross-sections by means of Eqs. (1), (2) and (3), it is necessary to obtain estimates of the various average width-to-spacing ratios involved. At neutron energies small compared to the excitation energy of the compound nucleus (e.g. $E < 100$ keV), one may reasonably expect $\left\langle \frac{\Gamma_{\mathrm{f}}}{D_{J\pi}} \right\rangle_{J\pi}$ for fissile isotopes, and $\left\langle \frac{\Gamma_{\mathrm{c}}}{D_{J\pi}} \right\rangle_{J\pi}$ to differ little from their values at electron-volt energies

as determined by the analysis of individual resonances occurring there [4]. Strictly speaking, this can be justified only for those $(J, \pi)$ sequences produced by s-wave neutrons. Above $E \sim 1$ keV, higher angular momentum neutrons are absorbed. While almost all capture cross-section data are consistent with the assumption that $\Gamma_c$ varies little with $(J, \pi)$, this should not be expected of $\Gamma_f$, in view of the BOHR theory of fission [5]. At neutron energies above several hundred kilovolts, the energy dependence of $\left\langle \frac{\Gamma_c}{D} \right\rangle_{J\pi}$ can be estimated by the method of MARGOLIS [6] employing information on the energy dependence of level spacing, obtained from capture-gamma-ray spectra [7] and from emitted particle spectra [8]. In the absence of resonance data on $\left\langle \frac{\Gamma_c}{D_{J\pi}} \right\rangle_{J\pi}$, reliable estimates of average capture cross-sections are impossible because of the large fluctuations in the level spacings from nuclide to nuclide. This difficulty can be overcome to some extent when treating mixtures of large numbers of different nuclides such as fission products [9]. In that case, systematic trends in level spacings [10] can be expected to provide adequate averaging over the fluctuations. The estimation of fission cross-sections and capture-to-fission ratios at these higher energies is not possible without further information on the dependence of $\left\langle \frac{\Gamma_f}{D_{J\pi}} \right\rangle_{J\pi}$ on $J$, $\pi$ and $E$.

Neutron-width-to-spacing ratios can be expressed directly in terms of the parameters of the fairly successful optical model of neutron scattering [11] using expressions given in Ref. [1]. Several sets of such parameters fitted to experimental data exist [12], as well as an adaptation of one of these sets to permit rapid determination of $\left\langle \frac{\Gamma_n^{lj}}{D_{J\pi}} \right\rangle_{J\pi}$ [13]. What is principally lacking are optical model calculations for deformed nuclei which are needed for reliable determinations of $\left\langle \frac{\Gamma_n{}^{lj}}{D_{J\pi}} \right\rangle_{J\pi}$ in all of the heavy fissionable materials as well as several potentially interesting structural materials such as tantalum and tungsten.

The methods described have been used to estimate average cross-sections [9] and to interpolate or extrapolate existing measurements [14]. Further calculations using improved computing methods and parameters are in progress.

Several examples of estimates of neutron inelastic-scattering and capture cross-sections, together with comparisons with experimental data, are discussed here.

Inelastic-scattering cross-sections in uranium and plutonium were calculated with neutron-width-to-spacing ratios obtained from a simple optical model without spin-orbit force or deformation. The principal effect of this is to enhance $(l=1)$ and $(l=3)$ neutron absorption and emission over what would be expected from a perfectly absorbing nucleus. Fig. 1 shows the resulting excitation curves for the first three excited states of $U^{238}$ ($2^+$, $4^+$, $6^+$ levels at 44, 146, and 300 keV, respectively). Excitation of the higher levels of this ground-state rotational band is not appreciable at these energies, because of the large orbital angular momenta required. Curves for the excitation of levels belonging to rotational bands based on a $1^-$ level at about 700 keV and a $0^+$ level at about 900 keV have been estimated and are shown in Ref. [14].

Fig. 2 shows similar results for $U^{235}$, which has been studied also by RAE, MARGOLIS and TROUBETZKOY [15].

The levels assumed are those belonging to rotational bands based on the $7/2^-$ ground state, the $1/2^+$ isomeric level at $\sim 100$ eV and a $5/2^+$ level at 234 keV. Only levels having spins differing by less than 4 units from the ground state

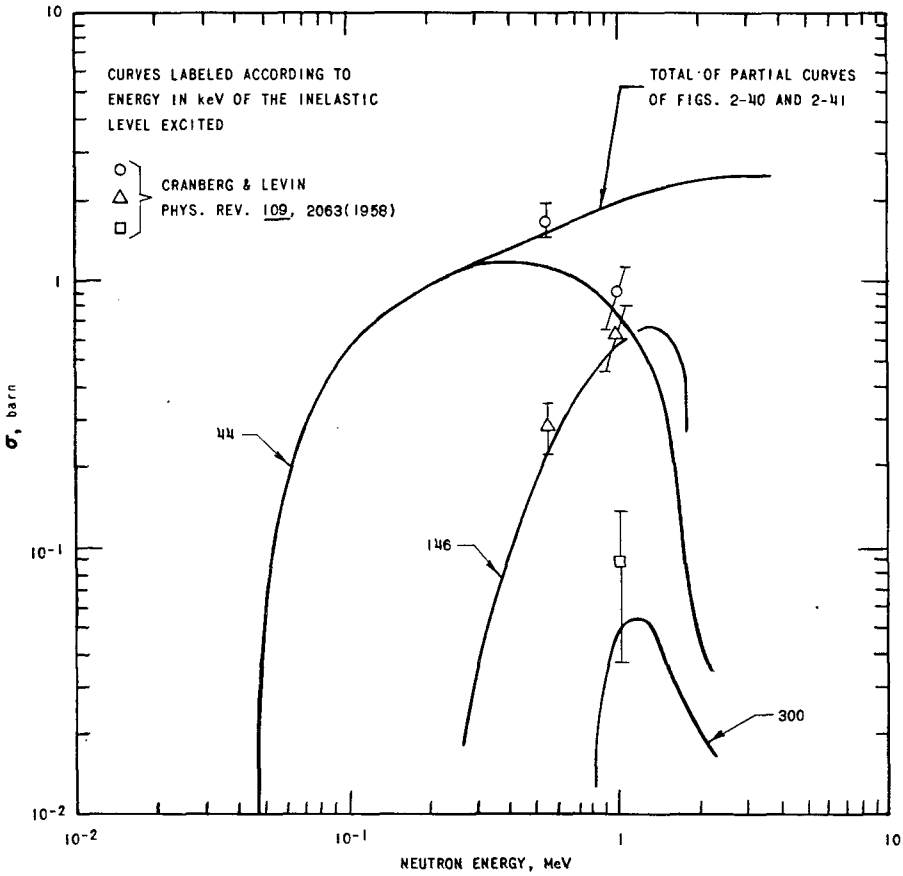


Fig. 1
Excitation of the first three excited states of $U^{238}$ by neutrons of energies up to 2 MeV. Data points from Ref. [16].

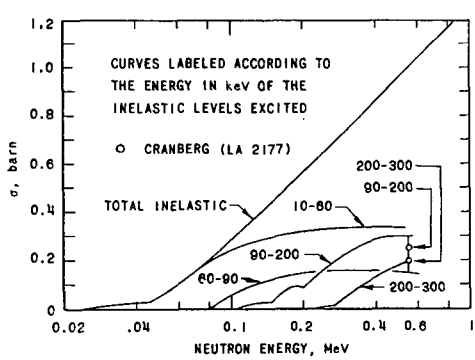


Fig. 2
Inelastic scattering of neutrons with energies up to 600 keV from $U^{235}$. Data points from Ref. [17].

have been calculated. This still leaves ten levels below 300 keV, and these have been collected into four groups for graphical presentation.

Similar results for $Pu^{239}$ are shown in Fig. 3, calculated on the basis of the rotational bands of levels based on the $1/2^+$ ground state, a $5/2^+$ level at 286 keV

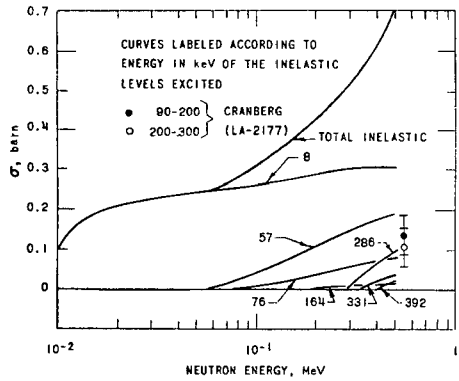


Fig. 3
Inelastic scattering of neutrons with energies up to 500 keV from $Pu^{239}$. Data points from Ref. [17].

and a $7/2^-$ level at 392 keV. The calculations in Figs. 1, 2 and 3 are compared with the experimental data of Refs. [16] and [17].

Figs. 4, 5 and 6 show interpolated neutron-capture cross-sections for chromium, iron and nickel. Again optical model neutron-resonance parameters were used. For the capture-width-to-spacing ratios, the measured average level-spacings for s-wave resonance neutrons from Ref. [4] were used, together with the assumptions that the average spacing for sequences with different $J$ values behaves like $(2J+1)^{-1}$ and is independent of parity. For the energy dependence of the level spacings, the formula of Ref. [18] was employed. The capture widths for all resonances of all isotopes of the same element were arbitrarily assumed to be the same, and their values adjusted to bring the calculations into agreement with the measurements of Refs. [19] and [20]. The values of $\Gamma_c$ thus obtained are of the order of 1 eV.

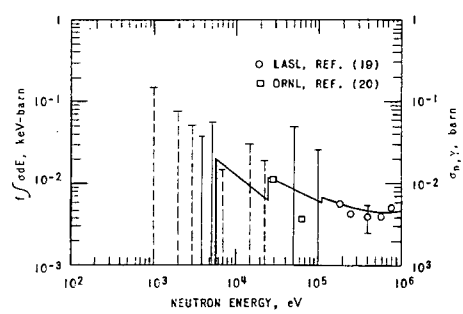


Fig. 4
Neutron capture in chromium. Data points from Refs. [19] and [20].

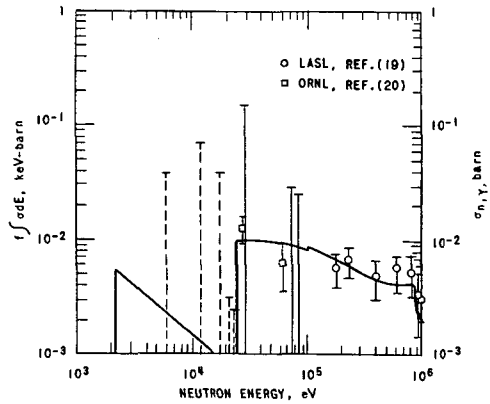


Fig. 5
Neutron capture in iron. Data points from Refs. [19] and [20].

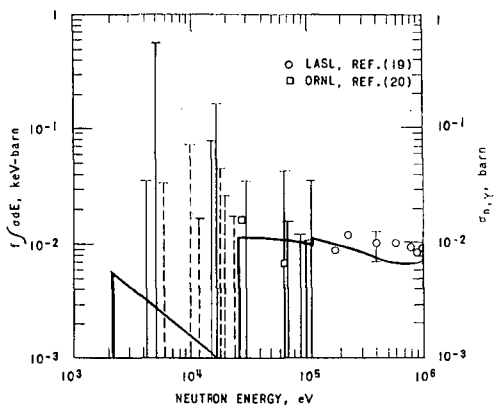


Fig. 6
Neutron capture in nickel. Data points from Refs. [19] and [20].

The level spacings in these lighter elements are of the order of kilovolts and may thus be as large as or larger than the size of energy groups employed in the analysis of intermediate or fast reactors. In such cases, particularly where the flux varies appreciably with neutron energy, it may be important to know the details of the capture resonance structure, rather than just the average cross-section over a region which may contain only one or two or even no resonances. In Figs. 4, 5 and 6, average cross-sections have been drawn in those energy groups of Ref. [14] containing several resonances due to a particular isotope and neutron orbital angular momentum. The effect of other, more isolated resonances has been indicated by placing a bar at the resonance energy in question with a height proportional to the value of $f\int\sigma dE$, where $f$ is the abundance of the isotope to which the resonance belongs, $\sigma$ is the atomic resonance capture cross-section of the isotope, and the range of integration is several full resonance widths in the vicinity of the resonance energy $E_0$. The contribution of such a

resonance to the average cross-section over any energy region $\Delta$ with respect to a flux $\Phi$ is then given by

$$\int_{\Delta} \Phi \sigma_{n,\gamma}^{res} \, dE = \Phi(E_0) \left[ f \int \sigma \, dE \right]. \tag{4}$$

A consistent application of this procedure requires the specific representation of resonances produced by $l=1$ and even $l=2$ neutrons whose resonance positions are unknown. Such resonances have been indicated in Figs. 4, 5 and 6 correctly as regards their spacings and the magnitude of their contributions but at fictitious positions. The first piece of average cross-section curve up to 25 keV in each of these figures represents the contribution from the odd A isotopes only. The second piece, between 25 and 110 keV, contains the contributions of the odd A isotopes and the p- and d-wave neutrons captured in the even A isotopes. Above 110 keV, all capture is represented by the average cross-section curve. Capture processes not included in the average cross-section curve are represented by the resonance lines. At energies below which no resonance bars or average cross-section curve is shown, the capture cross-section can be represented by the extension of the thermal $1/v$ cross-section. An exception would be the presence of direct capture [21] in that region, regarding which there is as yet very little quantitative information.

## REFERENCES


[1] MOLDAUER, P. A., "Theory of average neutron-reaction cross-sections in the resonance region". *Phys. Rev.* **123** (1961) 968.
[2] LANE, A. M. and LYNN, J. E., *Proc. phys. Soc. (Lond.)* **A 70** (1957) 557.
[3] DRESNER, L., Proc. Int. Conf. on Neutron Interactions with the Nucleus, CU-175 (1957) 71.
[4] BOLLINGER, L. M., Nuclear Spectroscopy, Part A, Academic Press, Inc., New York (1960) 416.
HUGHES, D. J. *et al.*, Neutron Cross Sections, 2nd ed. and Suppl. No. 1 BNL-325 (1958 and 1960).
[5] BOHR, A., Proc. UN Int. Conf. PUAE **2** (1956) 151.
[6] MARGOLIS, B., *Phys. Rev.* **88** (1952) 327.
[7] STRUTINSKII, V. M., GROSHEV, L. V. and AKIMOVA, M. K., *Nucl. Phys.* **16** (1960) 645.
[8] LECOUTEUR, K. J. and LANG, D. W., *Nucl. Phys.* **13** (1959) 32.
[9] MOLDAUER, P. A., Proc. Conf. on Physics of Breeding, ANL-6122 (1959) 67.
[10] NEWTON, T. D., *Canad. J. Phys.* **34** (1956) 804. — CAMERON, A. G. W., AECL PD-292 (1957). — ERICSON, T., *Nucl. Phys.* **6** (1958) 62.
[11] FESHBACH, H., PORTER, C. E. and WEISSKOPF, V. F., *Phys. Rev.* **96** (1954) 448.
[12] BEYSTER, J. R. *et al.*, LA-2099 (1957). — EMMERICH, W. S., WRLR 60-94511-6-R17. — CAMPBELL, E. J., *et al.* TID-5820.
[13] MOLDAUER, P. A., ANL-6323.
[14] YIFTAH, S., OKRENT, D. and MOLDAUER, P. A., Fast Reactor Cross-Sections, Pergamon Press, Inc., New York (1960).
[15] RAE, E. R., MARGOLIS, B. and TROUBETZKOY, E. S., *Phys. Rev.* **112** (1958) 492.
[16] CRANBERG, L. and LEVIN, J. S., *Phys. Rev.* **109** (1958) 2063.
[17] CRANBERG, L., LA-2177 (1959).
[18] LANG, J. M. B. and LECOUTEUR, K. J., *Proc. phys. Soc. (Lond.)* **A 67** (1954) 585.
[19] DIVEN, B. C., TERRELL, J. and HEMMENDINGER, A., *Phys. Rev.* **120** (1960) 556.
[20] GIBBONS, J. H. *et al.*, *Phys. Rev.* **122** (1961) 182.
[21] LANE, A. M., *Nucl. Phys.* **11** (1959) 625.

# NEUTRON FISSION-PRODUCT CROSS-SECTIONS

V. BENZI AND A. M. SARUIS
COMITATO NAZIONALE ENERGIA NUCLEARE, BOLOGNA,
ITALY

**Abstract — Résumé — Аннотация — Resumen**

**Neutron fission-product cross-sections.** Absorption cross-sections for some fission products have been calculated in the $10^3$—$10^5$-eV energy range using the statistical model. Neutron angular momenta $l=0$ and $l=1$ have been considered. The results are compared with those obtained by Greebler *et al.* for the energy dependence of the cross-sections, and with those given by Walker for the unresolved resonance integrals.

**Sections efficaces des produits de fission.** Les auteurs ont calculé, au moyen du modèle statistique, les sections efficaces d'absorption d'un certain nombre de produits de fission pour la gamme d'énergies de $10^3$ à $10^5$ eV. Dans les cas étudiés, les moments cinétiques étaient de $l=0$ et $l=1$. Les auteurs comparent les résultats de leurs calculs avec ceux obtenus par Greebler et ses collaborateurs, afin de voir dans quelle mesure les sections efficaces dépendent de l'énergie, et à ceux qui ont été fournis par Walker pour les intégrales de résonance non résolues.

**Поперечные сечения нейтронов продуктов деления.** Сечения поглощения некоторых продуктов деления вычислены в диапазоне энергии в $10^3-10^5$ эв с помощью статистической модели. Рассмотрены угловые моменты количества движения нейтронов $l=0$ и $l=1$. Результаты сравниваются с результатами, полученными Гриблером и др. для зависимости сечений от энергии, и с результатами, полученными Уолкером для неразрешенных резонансных интегралов.

**Secciones eficaces neutrónicas de los productos de fisión.** Empleando el modelo estadístico, los autores calculan las secciones eficaces de absorción de algunos productos de fisión en el intervalo de energía de $10^3$—$10^5$ eV. Estudian los momentos angulares neutrónicos $l=0$ y $l=1$. Comparan los resultados con los obtenidos por Greebler y colaboradores para la variación de las secciones eficaces en función de la energía, y con los que da Walker para las integrales de resonancia no resuelta.

## Introduction

As it is well known, fission-product poisoning calculations at high and intermediate energies are not so easily made as in the case of thermal energies, because of the greater difficulty in obtaining the required experimental information.

However, in lack of experimental data, an estimate of these cross-sections can be obtained by means of theoretical models, bound to reproduce known experimental results.

Such a phenomenological approach has been recently adopted, for example, by GIBBONS *et al.* [1], in analysing by means of the statistical model the experimental results obtained in the keV region for various elements.

In the field of fission-product cross-sections, the statistical model was early used by BUSINARO *et al.* [2], and more recently has been adopted by GREEBLER, HURWITZ and STORM [3], and by GORDEEV and PUPKO [4].

In these papers, the contribution of neutrons of orbital angular momentum $l > 0$ to the capture cross-section was approximately obtained by multiplying the $(l = 0)$ cross-sections by a corrective factor, or using some experimentally known strength-functions for p-neutrons to make appropriate extrapolations.

As we will see in the following, the p-wave contribution may be very important in the keV region, so that if only rough estimates are quite satisfactory for thermal reactors, where the greater contribution to the resonance integral is generally due to the epithermal absorption, a more precise evaluation of p-wave effects is required for intermediate and fast reactors.

In this paper, an attempt is made to evaluate the average radiation capture cross-section for some fission-product nuclides, taking into account the neutron orbital angular momenta of order 0 and 1.

## The statistical model formula

Following the statistical model, the mean cross-section for radiative capture of neutron is [5]:

$$\overline{\sigma}_{n\gamma}(E) = 2\pi^2 \lambda\!\!\!^{-2} \sum_{l=0}^{\infty} \sum_{j} \sum_{J=|l-j|}^{l+j} \frac{g_J}{\overline{D}_{J\pi}} \left\langle \frac{\Gamma_n^{lJ\pi} \Gamma_\gamma^{J\pi}}{\Gamma^{J\pi}} \right\rangle$$

where:

$2\pi \lambda\!\!\!^{-}$ = neutron wavelength
$l$ = neutron orbital angular momentum
$j$ = entrance channel spin ($= I \pm 1/2$ for $I \neq 0$; $1/2$ for $I = 0$)
$I$ = spin of target nucleus (ground state)
$J$ = spin of compound nucleus
$g_J$ = $(2J+1)/2(2I+1)$
$\overline{D}_J$ = average spacing between resonances of given spin $J$ and parity.

$\Gamma_n^{lJ\pi}$, $\Gamma_\gamma^{J\pi}$ and $\Gamma^{J\pi}$ are respectively the entrance channel neutron width for channel spin $j$, the radiation width and the total width for a resonance of spin $J$ and parity $\pi$.

The brackets indicate an average over all resonances of spin $J$ and parity $\pi$. Usually, it is assumed that $\Gamma_\gamma^{lJ\pi}$ is independent of $J$, $\pi$ and energy, $\Gamma^{lJ\pi}$ is independent of $J$, $\pi$ and $j$, and $\overline{D}_{J\pi}$ is independent of $\pi$; so we will use the symbols $\Gamma_n^l$, $\Gamma_\gamma$ and $\overline{D}_J$.

Taking into account s- and p-components only, we define the strength-functions

$$\overline{S}^0 = (\Gamma_n^0/\overline{D}_J)_{l=0}$$

$$\overline{S}^1 = (\Gamma_n^0/\overline{D}_J)_{l=1}$$

and the penetrability factors

$$v_0 = 1$$

$$v_1 = k^2 R^2 / (1 + k^2 R^2)$$

where $k = 1/\lambda\!\!\!^{-}$ is the wave number of the incident neutron and $R$ the channel radius of the compound nucleus.

The reduced neutron widths at 1eV of the resonances with angular momentum $l$

$$(\Gamma_n^0)_l = (\Gamma_n^l / v_l E^{1/2})$$

are assumed distributed according to the Porter-Thomas law. Then, averaging on this distribution, the expression for $l$-neutrons capture cross-section is

$$\bar{\sigma}_{n\gamma}(E) = \frac{\pi^2 \lambda^2}{(2I+1)} \left(\frac{\bar{\Gamma}_\gamma}{\bar{D}_0}\right) \sum_J \varepsilon_I^{jl} (2J+1)^2 \Big\{1 - \\ - \pi^{1/2} (Z_l{}^J/2)^{1/2} (1 - E\, rf\, [(Z_l{}^J/2)^{1/2}]) \exp (Z_l{}^J/2)\Big\}$$

with

$$\bar{D}_0 = (2J+1)\, \bar{D}_J$$

and

$$Z_l{}^J = \frac{(\bar{\Gamma}_\gamma)}{\bar{D}_0} \frac{(2J+1)}{\varepsilon^{lj}{}_J\, \bar{S}^l\, v_l\, E^{1/2}} .$$

The $\varepsilon^{lj}{}_J$ are the accessible reaction channel numbers:
$\varepsilon^{lj}{}_J = 2$ if both values of $j$ are contained in the limits $|J-1| \leq j \leq |J+1|$
$= 1$ if only one value of $j$ is contained in the above limits
$= 0$ otherwise.

**Results of calculations**

In order to obtain the "total" radiative cross-section

$$\bar{\sigma}_{n\gamma}(E) = \bar{\sigma}^0{}_{n\gamma}(E) + \bar{\sigma}^1{}_{n\gamma}(E)$$

it is necessary to know the quantities $\bar{\Gamma}_\gamma$, $\bar{D}_0$, $\bar{S}^0$ and $\bar{S}^1$.

The average radiation width $\Gamma_\gamma$ is usually the parameter experimentally better known. However, an uncertainty of $\sim 40\%$ frequently appears.

From the knowledge of the average spacing between observed resonances, $\bar{D}_0$ can be obtained in principle by means of the relations

$$\bar{D}_0 = 2\,(2I+1)\,\bar{D}_{obs} \quad \text{if } I \neq 0$$
$$\bar{D}_0 = \bar{D}_{obs} \quad \text{if } I = 0.$$

$\bar{D}_{obs}$ is equal to the difference between the resonance energies of the first and the $N^{th}$ resolved levels divided by $(N-1)$. $\bar{D}_{obs}$ may be also obtained by plotting the number of levels up to energy $E$ *versus* $E$ and then considering the slope of this curve as $\bar{D}_{obs}$.

In this way missed resonances can be sometimes discovered.

For every resolved resonance $\Gamma_n^0$ is generally known, although with very large uncertainty in some cases. Thus, averaging $\Gamma_n^0$, $\bar{S}^0$ can be "experimentally" obtained for several elements.

The optical model can be used in order to get an idea of the "goodness" of the strength-functions so obtained.

For some elements, the values of $\bar{S}^0$ are very far from the theoretical ones, showing too poor statistical accuracy in determining $\bar{\Gamma}_n^0$ or $\bar{D}_{obs}$. Obviously, in such an analysis, one has to consider carefully the effects on the level spacing deriving from the even, odd or magic values of $Z$ and $N$.

Among the various fission-product elements, we have so considered only those for which sufficient consistency was obtained between empirical and calculated values of $\bar{S}^0$ (and also between graphical and numerical estimates of $\bar{D}_{obs}$).

$\bar{S}^1$ strength-functions are much more difficult to obtain. Observed values are affected by very large errors, and only few elements have been tested from

this point of view. However, optical model calculation [6] seems in quite good agreement with these values in the high mass-number region.

In this work, an empirical fit of the optical-model-obtained $\bar{S}^1$ strength-functions has been used.

The fit gives

$$\bar{S}^1 = 10^{-4}\left[0.25 + \frac{42.50}{6.25 + 1.20\,(A - 92.50)^2} + \frac{5.75}{2.30 + 0.12\,(A - 109)^2}\right]$$

where $A$ is the mass number of the nuclide considered.

In Table I, experimentally known and calculated values of $\bar{S}^1$ are listed.

TABLE I

**EXPERIMENTAL AND CALCULATED VALUES FOR $\bar{S}^1$ STRENGTH-FUNCTIONS**

| Element | $\bar{S}^1 \cdot 10^4$ | | Reference |
|---|---|---|---|
| | Exp. | Calc. | |
| $Zr^{92}$ | $7.5 \pm 2.5$ | 6.7 | a |
| $Nb^{93}$ | $6.0 {+1.5 \atop -1}$ | — | b |
| ,, | $6.0 \pm 2.0$ | 6.5 | c |
| ,, | $4.6 \pm 1.0$ | | d |
| $Zr^{94}$ | $5.8 \pm 2.4$ | 5.2 | a |
| $Mo^{100}$ | $1.0 \pm 1.0$ | 1.3 | a |
| $Rh^{103}$ | $2.5 \pm 1.5$ | 1.4 | a |
| $Ag^{107}$ | $2.6 {+1.9 \atop -0.8}$ | 2.5 | a |
| $Pd^{108}$ | $2.5 {+4.5 \atop -1.0}$ | 2.7 | a |
| $Ag^{109}$ | $3.3 \pm 1.0$ | 2.8 | a |
| $In^{115}$ | $2.0 {+2.0 \atop -0.8}$ | 1.2 | a |
| $I^{127}$ | $3.0 {+1 \atop -1.5}$ | 0.45 | b |
| $Pr^{141}$ | 0.1 | 0.25 | b |
| $Tb^{159}$ | $0.2 {+0.1 \atop -0.2}$ | 0.25 | b |
| $Ta^{181}$ | $0.2 {+0.1 \atop -0.2}$ | 0.25 | b |
| $Au^{197}$ | $0.33 \pm 0.3$ | 0.25 | a |
| ,, | 0.3 | | b |

a) WESTON, L. W., *et al.*, *Ann. Phys.* **10** (1960) 477.
b) GIBBONS, J. H., *et al.*, *phys. Rev.* **122** (1961) 182.
c) ROSEN, J. L. *et al.*, *Bull. Amer. phys. Soc.* **4** (1959) 473.
d) DESJARDINS, J. S., Ph. D. Thesis, Columbia Univ. (1959).

In determining $\bar{\Gamma}_\gamma$, $\bar{D}_0$ and $\bar{S}^0$ values, the parameters given by HUGHES, MAGURNO and BRUSSEL [7] were used; the results of our calculations for the chosen fission-products (direct or indirect) are given in Table II. The value $R = 1.35 \times 10^{-13} \times A^{1/3}$ cm was used for the nuclear radius.

Table III gives the average radiative capture cross-sections for energies of $10^3$, $10^4$ and $10^5$ eV. For each energy, the first column gives the $l=0$ contribution, the second $l=1$ contribution (which is frequently very small for

TABLE II

**AVERAGE PARAMETERS USED IN $\bar{\sigma}_{n\gamma}$ CALCULATION**

| Isotope | $\overline{D}_0$ (eV) | $\overline{\Gamma}_0$ (eV) | $\overline{S}^0 \cdot 10^4$ | $\overline{S}^1 \cdot 10^4$ |
|---|---|---|---|---|
| $Se^{77}$ | 1332 | 0.250 | 1.46 | 0.45 |
| $Br^{81}$ | 544 | 0.280 | 1.20 | 0.60 |
| $Rb^{85}$ | 10800 | 0.250 | 1.36 | 0.90 |
| $Rb^{87}$ | 17096 | 0.250 | 1.46 | 1.30 |
| $Y^{89}$ | 15000 | 0.250 | 0.59 | 2.25 |
| $Mo^{95}$ | 2100 | 0.210 | 0.43 | 3.40 |
| $Mo^{97}$ | 1740 | 0.260 | 0.33 | 1.90 |
| $Tc^{99}$ | 344 | 0.280 | 0.55 | 1.40 |
| $Rh^{103}$ | 120 | 0.155 | 0.28 | 1.40 |
| $Pd^{105}$ | 144 | 0.140 | 0.36 | 1.85 |
| $Cd^{111}$ | 109 | 0.115 | 0.33 | 2.30 |
| $In^{113}$ | 160 | 0.080 | 0.62 | 1.65 |
| $In^{115}$ | 70 | 0.078 | 0.41 | 1.20 |
| $Sb^{121}$ | 119 | 0.090 | 0.66 | 0.55 |
| $Sb^{123}$ | 420 | 0.064 | 0.69 | 0.50 |
| $Te^{123}$ | 127 | 0.100 | 0.93 | 0.50 |
| $Te^{125}$ | 232 | 0.100 | 0.47 | 0.45 |
| $I^{127}$ | 156 | 0.100 | 0.96 | 0.45 |
| $I^{129}$ | 282 | 0.100 | 0.57 | 0.35 |
| $Cs^{133}$ | 320 | 0.110 | 1.30 | 0.35 |
| $Pr^{141}$ | 1284 | 0.150 | 4.16 | 0.30 |
| $Pm^{147}$ | 37 | 0.080 | 5.32 | 0.25 |
| $Sm^{147}$ | 116 | 0.059 | 6.20 | 0.25 |
| $Eu^{153}$ | 10 | 0.097 | 3.75 | 0.25 |
| $Tb^{159}$ | 34 | 0.100 | 1.17 | 0.25 |
| $Dy^{161}$ | 28 | 0.120 | 1.84 | 0.25 |
| $Dy^{162}$ | 574 | 0.140 | 1.56 | 0.25 |
| $Dy^{163}$ | 132 | 0.103 | 0.86 | 0.25 |

$E = 10^3$ eV). Column III contains the sum of the two components, while in column IV the values calculated by GREEBLER *et al.* are given. At lower energy, $10^2$ eV say, the behaviour of $\sigma_{n\gamma}$ generally can be better obtained from the resolved resonances, whereas at higher energies, $E > 5 \cdot 10^5$ eV say, the inelastic scattering may become important.

As one can see, at energies of $10^5$ eV, our values are in many cases two or three times greater than those given by GREEBLER *et al.* [3] due to $l = 1$ contribution; this order of magnitude was predicted in the Greebler paper.

In thermal reactors, however, $l = 1$ contribution is not so important. Using effective Westcott cross-sections, for a given nuclide one has

$$\hat{\sigma} = \sigma_0 \, (g + rs)$$

where $\sigma_0$ is the absorption cross-section at 2200 m/s, $r$ an index which represents the relative strength of the epithermal component, $g\,\sigma_0$ is the effective Maxwellian cross-section, and

$$s = \sqrt{\frac{4T}{\pi\, T_0}}\, \frac{I'}{\sigma_0}$$

$T$ is the Maxwellian temperature, $T_0 = 293.6$ °K and $I'$ is the resonance absorption integral.

TABLE III

**FISSION PRODUCT CROSS-SECTIONS AS A FUNCTION OF ENERGY (in barns)**

| Isotope | $E = 10^3$ eV | | | | $E = 10^4$ eV | | | | $E = 10^5$ eV | | | |
|---|---|---|---|---|---|---|---|---|---|---|---|---|
| | $\bar{\sigma}_0$ | $\bar{\sigma}_1$ | $\bar{\sigma}_T$ | $\bar{\sigma}_T^*$ | $\bar{\sigma}_0$ | $\bar{\sigma}_1$ | $\bar{\sigma}_T$ | $\bar{\sigma}_T^*$ | $\bar{\sigma}_0$ | $\bar{\sigma}_1$ | $\bar{\sigma}_T$ | $\bar{\sigma}_T^*$ |
| $Se^{77}$ | 1.362 | — | 1.362 | — | 0.158 | 0.079 | 0.237 | — | 0.017 | 0.045 | 0.062 | — |
| $Br^{81}$ | 3.939 | — | 3.939 | — | 0.550 | 0.101 | 0.651 | — | 0.067 | 0.123 | 0.190 | — |
| $Rb^{85}$ | 0.468 | 0.044 | 0.512 | 0.33 | 0.051 | 0.074 | 0.125 | 0.04 | 0.006 | 0.015 | 0.021 | 0.08 |
| $Rb^{87}$ | 0.221 | 0.088 | 0.309 | 0.11 | 0.023 | 0.049 | 0.072 | 0.014 | 0.002 | 0.008 | 0.010 | 0.002 |
| $Y^{89}$ | 0.145 | 0.118 | 0.263 | 0.15 | 0.015 | 0.048 | 0.063 | 0.017 | 0.002 | 0.007 | 0.009 | 0.003 |
| $Mo^{95}$ | 1.192 | 0.158 | 1.350 | 1.1 | 0.162 | 0.310 | 0.472 | 0.20 | 0.020 | 0.065 | 0.085 | 0.044 |
| $Mo^{97}$ | 1.387 | — | 1.387 | 0.98 | 0.207 | 0.292 | 0.499 | 0.20 | 0.027 | 0.086 | 0.113 | 0.032 |
| $Tc^{99}$ | 4.729 | — | 4.729 | 3.50 | 0.958 | 0.243 | 1.201 | 0.82 | 0.156 | 0.387 | 0.543 | 0.208 |
| $Rh^{103}$ | 2.567 | — | 2.567 | 3.2 | 0.473 | 0.274 | 0.747 | 0.71 | 0.071 | 0.248 | 0.319 | 0.164 |
| $Pd^{105}$ | 3.206 | — | 3.206 | 2.8 | 0.663 | 0.462 | 1.125 | 0.61 | 0.110 | 0.361 | 0.471 | 0.174 |
| $Cd^{111}$ | 2.593 | — | 2.593 | 2.2 | 0.447 | 0.503 | 0.950 | 0.56 | 0.064 | 0.259 | 0.322 | 0.11 |
| $In^{113}$ | 4.351 | — | 4.351 | — | 0.782 | 0.450 | 1.232 | — | 0.115 | 0.309 | 0.425 | — |
| $In^{115}$ | 4.006 | — | 4.006 | 4.5 | 0.934 | 0.033 | 0.967 | 0.91 | 0.170 | 0.446 | 0.616 | 0.18 |
| $Sb^{121}$ | 4.378 | — | 4.378 | — | 0.766 | 0.032 | 0.798 | — | 0.110 | 0.198 | 0.308 | — |
| $Sb^{123}$ | 2.202 | — | 2.202 | — | 0.072 | 0.118 | 0.190 | — | 0.008 | 0.024 | 0.032 | — |
| $Te^{123}$ | 3.562 | — | 3.562 | — | 0.496 | 0.081 | 0.578 | — | 0.061 | 0.130 | 0.191 | — |
| $Te^{125}$ | 1.900 | — | 1.900 | — | 0.267 | 0.107 | 0.374 | — | 0.033 | 0.086 | 0.119 | — |
| $I^{127}$ | 4.975 | — | 4.975 | 4.7 | 0.790 | 0.026 | 0.816 | 0.95 | 0.106 | 0.167 | 0.273 | 0.20 |
| $I^{129}$ | 3.238 | — | 3.238 | 3.5 | 0.534 | 0.045 | 0.579 | 0.62 | 0.074 | 0.125 | 0.199 | 0.18 |
| $Cs^{133}$ | 4.650 | — | 4.650 | 4.7 | 0.668 | 0.054 | 0.723 | 0.85 | 0.083 | 0.124 | 0.207 | 0.20 |
| $Pr^{141}$ | 2.226 | — | 2.226 | 2.6 | 0.251 | 0.090 | 0.341 | 0.393 | 0.027 | 0.050 | 0.077 | 0.065 |
| $Pm^{147}$ | 20.905 | — | 20.905 | 6.40 | 3.066 | — | 3.066 | 1.1 | 0.389 | 0.197 | 0.586 | 0.185 |
| $Sm^{147}$ | 9.940 | — | 9.940 | 11.0 | 1.240 | — | 1.240 | 1.7 | 0.141 | 0.132 | 0.273 | 0.378 |
| $Eu^{153}$ | 33.494 | — | 33.494 | 19.0 | 6.921 | — | 6.921 | 6.2 | 1.147 | 0.060 | 1.207 | 1.30 |
| $Tb^{159}$ | 9.368 | — | 9.368 | — | 1.757 | — | 1.757 | — | 0.268 | 0.199 | 0.467 | — |
| $Dy^{161}$ | 15.696 | — | 15.696 | — | 3.145 | — | 3.145 | — | 0.508 | 0.217 | 0.725 | — |
| $Dy^{162}$ | 1.370 | — | 1.370 | — | 0.161 | 0.051 | 0.212 | — | 0.018 | 0.044 | 0.062 | — |
| $Dy^{163}$ | 5.180 | — | 5.180 | — | 0.867 | — | 0.867 | — | 0.121 | 0.146 | 0.267 | — |

* Starred values are obtained from Ref. [3].

This last parameter can be obtained as a sum of resolved and unresolved resonance integrals, using Breit-Wigner formula for the resolved integrals, while for the unresolved resonance integrals, without statistical variation of reduced neutron widths, the following expression was given by DRESNER [8]:

$$I^*_{\mathrm{nr}} = \frac{4\pi^2}{k^{*2}} \sum_J g_J \frac{\overline{\Gamma}_\gamma}{\overline{D}_J} \left[ \frac{B - \ln(1+B)}{B^2} \right]$$

where $k^*$ is the neutron wave-number at a given energy $E^*$ for which the resonance integral is evaluated, and $B = \overline{\Gamma}_\gamma / \overline{\Gamma}^0_{\mathrm{n}} E^{*1/2}$.

Following WALKER [9], no serious error arises in using the above expression for $I^*_{\mathrm{nr}}$, but neglecting $l=1$ contribution.

TABLE IV

**RESONANCE INTEGRALS OF SOME FISSION-PRODUCT ELEMENTS (in barns)**

| Isotope | $I_{\mathrm{res}}$ | $I_0$ | $I_1$ | $I^*_{\mathrm{nr}}$ | $I$ total | $I^*$total |
|---|---|---|---|---|---|---|
| $Se^{77}$ | 10 | 1.5 | 0.35 | 2 | 12 | 12 |
| $Br^{81}$ | 42 | 17 | 0.70 | 23 | 60 | 65 |
| $Rb^{85}$ | 0.077 | 0.076 | 0.15 | 0.082 | 0.3 | 0.16 |
| $Rb^{87}$ | 0.05 | 0.03 | 0.08 | 0.03 | 0.16 | 0.08 |
| $Y^{89}$ | 0.09 | 0.014 | 0.054 | 0.012 | 0.16 | 0.10 |
| $Mo^{95}$ | 98 | 1.9 | 1.6 | 3 | 102 | 101 |
| $Mo^{97}$ | 9.8 | 2.7 | 1.3 | 4 | 14 | 14 |
| $Tc^{99}$ | 177 | 20 | 2 | 25 | 199 | 202 |
| $Rh^{103}$ | 1013 | 9 | 1.5 | 10 | 1024 | 1026 |
| $Pd^{105}$ | 45 | 21 | 2.7 | 25 | 69 | 70 |
| $Cd^{111}$ | 31 | 13 | 2 | 14 | 46 | 45 |
| $In^{113}$ | 199 | 47 | 2 | 59 | 248 | 258 |
| $Sb^{121}$ | 175 | 32 | 0.9 | 40 | 208 | 215 |
| $Sb^{123}$ | 109 | 16 | 0.6 | 23 | 126 | 132 |
| $Te^{123}$ | 3683 | 19 | 0.7 | 22 | 3703 | 3705 |
| $Te^{125}$ | 8.7 | 6 | 0.6 | 7 | 15 | 16 |
| $I^{127}$ | 128 | 22 | 0.8 | 30 | 151 | 158 |
| $I^{129}$ | 13 | 17 | 0.6 | 22 | 30 | 35 |
| $Cs^{133}$ | 355 | 18 | 0.6 | 25 | 374 | 380 |
| $Pr^{141}$ | 17 | 1.4 | 0.4 | 1.6 | 19 | 19 |
| $Pm^{147}$ | 1967 | 288 | 0.8 | 384 | 2256 | 2351 |
| $Sm^{147}$ | 491 | 83 | 0.6 | 118 | 576 | 609 |
| $Eu^{153}$ | 1209 | 380 | 1.0 | 557 | 1590 | 1766 |
| $Tb^{159}$ | 302 | 72 | 1.5 | 84 | 375 | 384 |
| $Dy^{161}$ | 798 | 126 | 0.9 | 156 | 925 | 954 |
| $Dy^{162}$ | 2564 | 2.2 | 0.3 | 2.8 | 2567 | 2567 |
| $Dy^{163}$ | 1190 | 38 | 0.6 | 48 | 1239 | 1238 |

* Starred values are obtained using the formula given by Dresner.

This can be seen from Table IV, where calculated results for unresolved $l=0$ and $l=1$ integrals are listed; approximate $I^*_{\mathrm{nr}}$ values are also given for comparison.

Although the sum $I_0 + I_1$ is sometimes quite different from the $I^*_{\mathrm{nr}}$ value, the total resonance integrals do not differ so much because of the predominant importance of resolved resonances.

## ACKNOWLEDGEMENTS

The authors are grateful to Prof. E. Clementel for many discussions on the subject and helpful assistance. They also wish to thank Miss F. Fabbri and Mr. G. Panini for their assistance in the computation of numerical results.

## REFERENCES

[1] GIBBONS, J. H. *et al.*, *Phys. Rev.* **122** (1961) 182.
[2] BUSINARO, U. L., GALLONE, S. and MORGAN, D., *J. nucl. Energy* **4** (1957) 319.
[3] GREEBLER, P., HURWITZ, H. Jr. and STORM, M. L., *Nucl. Sci. and Engng* **2** (1957) 334.
[4] GORDEEV, I. V. and PUPKO, V. Y., Proc. 2nd UN Int. Conf. PUAE **16** (1958) 141.
[5] LANE, A. M. and LYNN, J. E., *Proc. phys. Soc.* (*Lond.*) **A 70** (1957) 557.
[6] WESTON, L. W. *et al.*, *Ann. Phys.* **10** (1960) 477.
[7] HUGHES, D. I., MAGURNO, B. A. and BRUSSEL, M. K., Neutron Cross-Sections, Suppl. No. 1 to BNL-325 (1960).
[8] DRESNER, L., Resonance Absorption in Nuclear Reactors, Pergamon Press, London (1960) 97—98.
[9] WALKER, W. H., AECL-1054, CRRP-913 (1960).

# I. 5. MULTI-GROUP CROSS-SECTIONS

SM—18/65

# GROUP CROSS-SECTIONS FOR FAST REACTORS

P. F. ZWEIFEL* AND G. L. BALL
ATOMIC POWER DEVELOPMENT ASSOCIATES, INC., DETROIT, MICH., UNITED STATES OF AMERICA

**Abstract — Résumé — Аннотация — Resumen**

**Group cross-sections for fast reactors.** A general discussion of the multi-group-diffusion equations is given, and the correct form of the group cross-sections discussed. In particular, it is shown that the average transport cross-section may be written to a certain approximation in terms of an average mean free path. The calculation of this quantity is lengthy because it is not amenable to expression in terms of elemental averages; however, several inequalities are proved which simplify the averaging procedure required.

Three further aspects of group cross-sections which are frequently ignored, but may be important in detailed design study, are discussed:

(*a*) The use of the same set of group-averaged cross-sections for all fast reactors is invalid if the spectra in different reactors are dissimilar and if the cross-sections vary rapidly over the group, conditions which frequently hold. An iteration procedure is described by which the correct averages are found; it is then used to determine the sensitivity of reactor calculations to spectral effects.

(*b*) In transport calculations such as $S_n$, averages must be made over both angle and energy. Since the flux is non-separable in angle and energy, extreme care is necessary to avoid erroneous results. The $S_n$ equation is studied in terms of a simple model, and a criterion is derived which may prove useful in determining the importance of angular non-separability in reactor calculations.

(*c*) A consistency relation among group-diffusion coefficients, slowing-down power and absorption cross-sections is derived from neutron-conservation arguments. It is shown that a frequently used definition of group absorption cross-section in terms of effective resonance integrals is not correct, but must be modified according to the type of multi-group scheme being used.

**Sections efficaces de groupes pour les réacteurs à neutrons rapides.** Les auteurs procèdent à une étude générale des équations de diffusion à plusieurs groupes et de la forme exacte des sections efficaces de groupes. Ils montrent notamment que la section efficace moyenne de transport peut, avec une certaine approximation, s'exprimer en termes de libre parcours moyen. Le calcul de cette quantité prend beaucoup de temps, car elle ne peut se réduire en moyennes élémentaires; néanmoins, on a démontré certaines inégalités, qui simplifient la méthode de calcul des moyennes qui doit être utilisée.

Les auteurs analysent trois autres aspects des sections efficaces de groupes, que l'on néglige souvent, mais qu'il peut être important de connaître pour les études de réacteurs.

*a*) Il est injustifié d'utiliser pour tous les réacteurs à neutrons rapides le même ensemble de sections efficaces dont la moyenne par groupe a été calculée si les spectres des différents réacteurs sont dissemblables et si les sections efficaces varient rapidement à l'intérieur du groupe, comme c'est le cas le plus souvent. Les auteurs décrivent une méthode d'itération qui permet d'obtenir les valeurs moyennes correctes; ils déterminent ensuite, à l'aide de cette méthode, dans quelle mesure les calculs de réacteurs sont influencés par les effets de spectre.

---

* University of Michigan, Ann Arbor, Mich.

*b*) Dans les calculs de transport (la méthode $S_n$, par exemple), les moyennes doivent être calculées en tenant compte à la fois de tous les angles et de toutes les énergies. Etant donné qu'on ne peut dissocier dans le flux une partie angulaire et une partie énergétique, la plus grande attention est nécessaire pour éviter les erreurs. Les auteurs étudient l'équation obtenue par la méthode $S_n$ sous la forme d'un modèle simple, et en tirent un critère qui pourrait aider à déterminer l'importance de la non-séparabilité angulaire dans les calculs de réacteurs.

*c*) A partir de raisonnements fondés sur la conservation du nombre de neutrons, il est possible d'obtenir une relation consistant entre les coefficients de diffusion de groupe, le pouvoir de ralentissement et les sections efficaces d'absorption. Les auteurs montrent qu'il n'est pas exact de définir, comme c'est souvent le cas, la section efficace de groupe en terme d'intégrales de résonance efficace, mais qu'il faut modifier cette définition suivant le type de schéma multigroupe utilisé.

**Групповые сечения реакторов на быстрых нейтронах.** Дается общий обзор многогрупповых диффузионных уравнений и рассматривается правильная форма групповых поперечных сечений. В частности, показано, что среднее поперечное сечение переноса может до некоторой степени приблизительно быть выражено в виде средней величины свободного пробега. Подсчет такого количества занимает много времени, так как он не поддается выражению в виде элементарного усреднения; однако подтвердились некоторые неравномерности что упрощает необходимый метод усреднения.

Рассматриваются три следующих вопроса групповых поперечных сечений, которые часто игнорируются, но которые могут иметь значение при детальном изучении проекта:

*a*) Использование одной и той же серии усредненных по группам сечений для всех реакторов на быстрых нейтронах ничего не дает, если спектры различных реакторов не одинаковы и если сечения быстро изменяются в группе; такое положение часто имеет место. Дается описание метода повторения, посредством которого устанавливается правильное усреднение, и этот метод используется для определения влияния спектральных эффектов на реакторные расчеты.

*b*) При расчетах переноса, таких, как $S_n$ усреднения должны быть выполнены как по углу, так и по энергии. Так как поток нельзя разделить на „угловой" и „энергетический", необходимо очень тщательно избегать ошибочных результатов. Уравнение $S_n$ изучается в виде простой модели, и получается критерий, который может оказаться полезным при определении значения угловой неразделимости в реакторных расчетах.

*c*) На основе аргументов о сохранении нейтронов выводится постоянное отношение между групповыми коэффициентами диффузии, уменьшением энергии и абсорбцией поперечных сечений. Показано, что часто используемое определение группового поперечного сечения абсорбции в виде интегралов эффективного резонанса является неправильным, однако оно должно быть изменено в соответствии с используемым типом многогрупповой схемы.

**Secciones eficaces de grupos para reactores rápidos.** La memoria discute en términos generales las ecuaciones de difusión de grupos múltiples y la forma correcta de las secciones eficaces correspondientes. En particular, demuestra que la sección eficaz media de transporte puede expresarse con bastante precisión en términos de un promedio de recorridos libres medios. Esta magnitud es difícil de calcular porque no se puede expresar en función de promedios elementales; sin embargo, se demuestran varias desigualdades que simplifican el procedimiento de determinación de promedios.

La memoria discute otros tres aspectos de las secciones eficaces de grupos que con frecuencia se ignoran, pero que pueden ser importantes al estudiar detalladamente un diseño.

*a*) El empleo de los mismos valores medios correspondientes a las secciones eficaces de grupos para todos los reactores rápidos no se justifica si los espectros de los diferentes reactores no son similares y si las secciones eficaces varían rápidamente dentro del grupo, como ocurre a menudo. Los autores describen un método de iteración, que

permite obtener valores medios correctos y determinar en qué medida los efectos espectrales ejercen influencia sobre los cálculos de reactores.

*b*) En los cálculos de transporte (método $S_n$ por ejemplo), los promedios deben evaluarse en función del ángulo y de la energía. Como el flujo no es separable en una parte ángulo y en una parte energética, es necesario proceder con sumo cuidado para evitar errores. La ecuación $S_n$ se estudia sobre la base de un modelo sencillo, y de este estudio se deduce un criterio que puede ser de utilidad al determinar la importancia de la no-separabilidad angular en los cálculos de reactores.

*c*) Basándose en los argumentos de conservación neutrónica, se deriva una relación de compatibilidad entre coeficientes de difusión de grupos, capacidad de moderación y secciones eficaces de absorción. Se demuestra que la definición de las secciones eficaces de absorción de grupos basada en integrales de resonancia eficaz que se emplea frecuentemente no es correcta, siendo preciso modificarla de acuerdo con el método de grupos múltiples que se utilice.

## Introduction

In multi-group diffusion calculations [1, 2], one attempts to solve the energy-dependent $P_1$ equations by breaking the entire reactor energy range into a set of energy intervals or "groups" in each of which the neutrons are treated by one-velocity theory. The basic energy-dependent* equations are [1, 2]:

$$\Sigma_{\mathrm{T}}(\mathbf{r},u)\,\varphi(\mathbf{r},u)+\nabla\cdot\mathbf{J}(\mathbf{r},u)=\sum_{i=1}^{N}\left\{\int_{u-\ln 1/\alpha_i}^{u}\varphi(\mathbf{r},u)\,\Sigma_{\mathrm{s}\,i\,0}(\mathbf{r},u'\to u)\,\mathrm{d}u'\right.$$

$$\left.+\int_{0}^{u}\varphi(\mathbf{r},u')\,\Sigma_{\mathrm{in}i0}(\mathbf{r},u'\to u)\,\mathrm{d}u'\right\}+X(u)\int_{0}^{\infty}\nu\,\Sigma_{\mathrm{f}}(\mathbf{r},u')\,\varphi(\mathbf{r},u')\,\mathrm{d}u' \qquad (1\mathrm{a})$$

$$\Sigma_{\mathrm{T}}(\mathbf{r},u)\,\mathbf{J}(\mathbf{r},u)+\frac{1}{3}\nabla\varphi(\mathbf{r},u)=\sum_{i=1}^{N}\left\{\int_{u-\ln 1/\alpha_i}^{u}\mathbf{J}(\mathbf{r},u')\,\Sigma_{\mathrm{s}i1}(\mathbf{r},u'\to u)\,\mathrm{d}u'\right.$$

$$\left.+\int\mathbf{J}(\mathbf{r},u')\,\Sigma_{\mathrm{in}i1}(\mathbf{r},u'\to u)\,\mathrm{d}u'\right\}. \qquad (1\mathrm{b})$$

Here $\varphi$ is the neutron flux, $\mathbf{J}$ is the current, $\Sigma_{\mathrm{T}}$ is the total cross-section, and $\Sigma_{\mathrm{s}i}(u'\to u)$ and $\Sigma_{\mathrm{in}i}(u'\to u)$ the elastic and inelastic differential scattering cross-sections of the $i$th material from lethargy $u$ into lethargy $\mathrm{d}u'$ at $u'$. The subscripts 0 and 1 represent the zeroth and first Legendre moments. $\Sigma_{\mathrm{f}}$ is the fission cross-section and $X(u)$ the fission spectrum; the summation $i$ runs over all elements in the mixture, each of which has a maximum logarithmic energy decrement in an elastic collision $\ln 1/\alpha_i=2\ln\left(\frac{A_i+1}{A_i-1}\right)$, where $A_i$ is the mass of the $i$th nucleus in units of the neutron mass.

In order to reduce Eqs. (1) to a set of group equations for $\varphi$, it is necessary to replace the integrals by summations and also to eliminate $\mathbf{J}$ between (1a) and (1b), obtaining in this way a single equation for $\varphi$. To do this, we first make the

* The lethargy variable $u=\ln(10\ \mathrm{MeV}/E)$ is used here.

approximation that $\Sigma_{\mathrm{in}\,i\,1}=0$, a relation which holds rigorously (except for the small difference between centre-of-mass and laboratory angles for heavy scatterers) for cross-sections calculated according to the Hauser-Feshbach model [3] which predicts a cross-section symmetric about 90°. Furthermore, the usual Fermi-age approximation, valid for heavy moderators, permits us to write the degradation integral in Eq. (1b) as

$$\sum_{i=1}^{N} \int_{u-\ln 1/\alpha_i}^{u} \mathbf{J}(\mathbf{r}, u')\, \Sigma_{\mathrm{s}\,i\,1}(\mathbf{r}, u' \to u)\, \mathrm{d}u' \approx \mathbf{J}(\mathbf{r}, u) \sum_{i=1}^{N} \bar{\mu}_{0i}(\mathbf{r}, u)\, \Sigma_{\mathrm{s}\,i}(\mathbf{r}, u) \tag{2}$$

where $\bar{\mu}_{0i}(u)$ is the average cosine of the scattering angle when a neutron of lethargy $u$ collides with the $i$th nucleus [4]. For isotropic scattering in the centre-of-mass system, $\mu_{0i}$ is a constant $=2/3A_i$. $\Sigma_{\mathrm{s}\,i}$, the total scattering cross-section, is given by

$$\int_{u'}^{u' + \ln 1/\alpha_i} \Sigma_{\mathrm{s}\,i\,0}(u' \to u)\, \mathrm{d}u\,.$$

Combining Eqs. (1b) and (2) gives the well-known Fick's rule for neutron diffusion,

$$\mathbf{J}(\mathbf{r}, u)\, \Sigma_{\mathrm{tr}}(\mathbf{r}, u) + 1/3\, \nabla \varphi(\mathbf{r}, u) = 0 \tag{3}$$

where

$$\Sigma_{\mathrm{tr}}(\mathbf{r}, u) \equiv \Sigma_{\mathrm{T}}(\mathbf{r}, u) - \sum_{i=1}^{N} \bar{\mu}_{0\,i}(\mathbf{r}, u)\, \Sigma_{\mathrm{s}\,i}(\mathbf{r}, u)\,. \tag{3a}$$

It is clear now that if Eq. (3) is integrated over the $m$th group* we obtain

$$\mathbf{J}^m(\mathbf{r})\, \Sigma_{\mathrm{tr}}^m(\mathbf{r}) + 1/3\, \nabla \varphi^m(\mathbf{r}) = 0 \tag{4}$$

where

$$\mathbf{J}^m = \int_{\Delta u^m} \mathbf{J}^m(\mathbf{r}, u)\, \mathrm{d}u \tag{4a}$$

with a similar equation for $\varphi^m$ and

$$\Sigma_{\mathrm{tr}}^m(\mathbf{r}) = \int_{\Delta u^m} \mathbf{J}^m(\mathbf{r}, u)\, \Sigma_{\mathrm{tr}}(\mathbf{r}, u)\, \mathrm{d}u \Big/ \mathbf{J}^m(\mathbf{r})\,. \tag{4b}$$

Note that even if $\Sigma_{\mathrm{tr}}(\mathbf{r}, u)$ does not depend on $\mathbf{r}$, $\Sigma_{\mathrm{tr}}^m$ will depend on $\mathbf{r}$ unless $\mathbf{J}(\mathbf{r}, u)$ is separable in space and energy, a situation which does not hold in general, but is a reasonable approximation for narrow groups. If $\mathbf{J}(\mathbf{r}, u)$, and $\varphi(\mathbf{r}, u)$ are indeed separable in space and energy, from Eqs. (3b) and (4) we have

$$\Sigma_{\mathrm{tr}}^m = \int_{\Delta u^m} \Phi(u)\, \mathrm{d}u \Big/ \int_{\Delta u^m} \Sigma_{\mathrm{tr}}^{-1}\, \Phi(u)\, \mathrm{d}u \equiv (\lambda_{\mathrm{tr}}^m)^{-1} \tag{4b'}$$

where $\Phi(u)$ is the energy-dependence of $\varphi(\mathbf{r}, u)$ and $\lambda_{\mathrm{tr}}^m$ is a flux-averaged quantity; i.e., for the separable case, assuming Eq. (3) holds, the current average of $\Sigma_{\mathrm{tr}}$ is equal to the reciprocal of the flux average of $\lambda_{\mathrm{tr}}$.

* The element index $i$ will always appear as a subscript; the group index $m$ will appear as a superscript.

Inserting these results in Eq. (1a) and integrating over the $m$th energy group, we obtain (for the general case)

$$\Sigma_{\mathrm{T}}^{m}(\mathbf{r})\,\varphi^{m}(\mathbf{r}) - \nabla\cdot D^{m}(\mathbf{r})\,\nabla\varphi =$$

$$= \sum_{i=1}^{N}\left\{\int\limits_{\Delta u^{m}} \mathrm{d}u \int\limits_{u-\ln 1/\alpha_i}^{u} \varphi(\mathbf{r},u')\,\Sigma_{\mathrm{s}\,i\,0}(\mathbf{r},u'\to u)\,\mathrm{d}u'\right.$$

$$\left. + \int\limits_{\Delta u^{m}} \mathrm{d}u \int\limits_{0}^{u} \varphi(\mathbf{r},u')\,\Sigma_{\mathrm{in}\,i\,0}(\mathbf{r},u'\to u)\,\mathrm{d}u'\right\}$$

$$+ X^{m}\int\limits_{0}^{\infty}\varphi(\mathbf{r},u')\,\Sigma_{\mathrm{f}}(\mathbf{r},u')\,\mathrm{d}u'\,. \tag{5}$$

Here $X^{m} = \int\limits_{\Delta u^{m}} X(u)\,\mathrm{d}u$ and $D^{m} = (3\,\Sigma_{\mathrm{tr}}^{m})^{-1}$ where $\Sigma_{\mathrm{tr}}^{m}$ is defined by Eq. (4b). The integrations on the right-hand side of Eq. (5) merit special attention, however. In general, $\Sigma_{\mathrm{s}i0}(\mathbf{r}, u'\to u)$ may be written in the form of a sum of products [4, 5].

$$\Sigma_{\mathrm{s}\,i\,0}(\mathbf{r},u'\to u) = \sum_{\mathrm{L}'=0}^{\infty} B_{\mathrm{L}'\,i}^{C}(\mathbf{r},u')\,T_{0\mathrm{L}'\,i}(u-u')\,. \tag{6}$$

Here the $B_{\mathrm{L}'}^{C}$ are the Legendre components of the differential angular scattering cross-section in the centre-of-mass system ($C$) and the $T_{0\mathrm{L}'}$ are the elements of a matrix defined in [4]. For isotropic scattering in $C$

$$B_{\mathrm{L}'i}^{C} = \Sigma_{\mathrm{s}\,i}\,\delta_{0\mathrm{L}'};\; T_{00i} = \frac{\mathrm{e}^{-(u-u')}}{1-\alpha_i}\,. \tag{6a}$$

The first integral on the right side of Eq. (5) becomes ($u_{+}^{m} - u_{-}^{m} = \Delta u^{m}$)

$$\sum_{i=1}^{N}\sum_{\mathrm{L}=0}^{\infty}\int\limits_{u^{m}_{-}}^{u^{m}_{+}}\mathrm{d}u \int\limits_{u-\ln 1/\alpha i}^{u}\mathrm{d}u'\,B_{\mathrm{L}'\,i}^{C}(\mathbf{r},u')\,T_{0\mathrm{L}'}(u-u')\,\varphi(\mathbf{r},u)\,. \tag{7}$$

Letting $u - u' = U$ we have, changing variables to $U$ and $u$,

$$\sum_{i=1}^{N}\sum_{\mathrm{L}'=0}^{\infty}\int\limits_{u^{m}_{-}}^{u^{m}_{+}}\mathrm{d}u \int\limits_{0}^{\ln 1/\alpha i}\mathrm{d}U\,B_{\mathrm{L}'\,i}^{C}(\mathbf{r},u-U)\,T_{0\mathrm{L}'\,i}(U)\,\varphi(\mathbf{r},u-U) \tag{7a}$$

which may or may not be a more convenient form for numerical use than Eq. (7). For isotropic scattering in $C$, Eq. (7a) reduces to

$$\sum_{i=1}^{N}\int\limits_{u^{m}_{-}}^{u^{m}_{+}}\mathrm{d}u \int\limits_{0}^{\ln 1/\alpha i}\mathrm{d}U\,\Sigma_{\mathrm{s}\,i}(\mathbf{r},u-U)\,\frac{\mathrm{e}^{-U}}{1-\alpha_i}\,\varphi(\mathbf{r},u-U) \tag{7b}$$

which is still rather complicated.

An inspection of Eqs. (7) makes it clear that if the usual procedure of replacing this degradation integral by a sum of the form

$$\sum_i \sum_{j=0}^{k} \varphi^j(\mathbf{r})\, \Sigma_{\mathrm{el}\,i}^{j\to k}(\mathbf{r}) \tag{8}$$

is to be accurate, extreme care must be exercised in the definitions of the transfer coefficients $\Sigma_{\mathrm{el}}^{j\to k}$ as well as the $\varphi^j$. In fact, because of the peculiar limits on the $\mathrm{d}u'$ integral in (7) it is clearly *not* correct to define $\Sigma_{\mathrm{el}\,i}^{j\to k}$ simply as proportional to the probability that a neutron which collides with a nucleus of the $i$th species in group $j$ will be degraded to group $k$. Usually, for fast reactors, the group-width is wider than any of the $\ln 1/\alpha_i$.* Then elastic degradation takes place only between adjacent groups and it is possible to write, for a single element, and for $u$ in the $m$th group,

$$\int_{u-\ln 1/\alpha_i}^{u} \varphi(\mathbf{r}, u')\, \Sigma_{\mathrm{s}\,i\,0}(u'\to u)\, \mathrm{d}u' =$$
$$= \varphi^{m-1}(\mathbf{r})\, \Sigma_{\mathrm{el}\,i}^{m-1,\,m}(\mathbf{r}, u) + \varphi^m(\mathbf{r})\, \Sigma_{\mathrm{el}\,i}^{m,\,m}(\mathbf{r}, u) \tag{9}$$

where $\varphi^m(\mathbf{r})$ has the same definition as before and

$$\Sigma_{\mathrm{el}\,i}^{m-1,\,m}(\mathbf{r}, u) = \int_{u-\ln 1/\alpha}^{u^m_-} \varphi(\mathbf{r}, u')\, \Sigma_{\mathrm{s}\,i\,0}(u'\to u)\, \mathrm{d}u' \big/ \varphi^{m-1}(\mathbf{r}) \tag{10a}$$

and

$$\Sigma_{\mathrm{el}\,i}^{m,\,m}(\mathbf{r}, u) = \int_{u^m_-}^{u} \varphi(\mathbf{r}, u')\, \Sigma_{\mathrm{s}\,i\,0}(u'\to u)\, \mathrm{d}u' \big/ \varphi^{m}(\mathbf{r}) \tag{10b}$$

and

$$\Sigma_{\mathrm{el}\,i}^{j\to k} = \int_{\Delta u^k} \mathrm{d}u\, \Sigma_{\mathrm{el}\,i}^{j,\,k}(\mathbf{r}, u). \tag{10c}$$

Since this method of averaging the elastic transfer coefficients is too complicated to be practical, approximations are generally used. One useful approximation is to assume that the integral of $\varphi(\mathbf{r}, u')\, B_{\mathrm{L}'i}^{C}(\mathbf{r}, u')\; T_{0\mathrm{L}'}(u-u')$ can be written as the product of integrals. One then finds Eq. (8) applies if we write

$$\Sigma_{\mathrm{el}\,i}^{j\to k}(\mathbf{r}) = \sum_{\mathrm{L}=0}^{\infty} B_{\mathrm{L}\,i}^{C\,j} \int_{u^k_-}^{u^k_- + \ln 1/\alpha_i} \mathrm{d}u \int_{u_+^j - \ln 1/\alpha_i}^{u_+^j} \mathrm{d}u'\; T_{0\mathrm{L}'\,i}(u-u'). \tag{11}$$

This equation simplifies for the case of isotropic scattering in $C$ and can be evaluated in closed form even in the general case. However, so far as we know, this particular approach to the determination of the elastic transfer coefficients has never been used.

A simpler procedure is to use the Fermi-age approximation on the degradation integral (7), a procedure followed by Ehrlich and Hurwitz [6], and which

* For carbon, the lightest element in most fast reactors, $\ln 1/\alpha = 0.3365 = \Delta u_{\max}$, while the minimum width of groups usually exceeds $\Delta u = 0.5$.

will not be described in detail here. (See, however, Section 4 of this paper.) This particular procedure leads to one equation for two unknowns, which makes it rather awkward to solve, but at least it does have the merit of simplifying the calculation of the elastic transfer coefficients.

The inelastic degradation term in Eq. (5) is fairly straightforward in the "product of integrals" approximation. One writes it as

$$\sum_{j=1}^{k} \varphi^j(\mathbf{r})\, \Sigma_{\mathrm{in}\,i\,0}^{j\to k} \tag{12}$$

where

$$\Sigma_{\mathrm{in}\,i\,0}^{j\to k} = \int_{\Delta u^j} \mathrm{d}u'\, \varphi(\mathbf{r}, u')\, \Sigma_{\mathrm{in}\,i\,0}(\mathbf{r}, u') \int_{\Delta u^k} \pi_{\mathrm{in}\,i\,0}(u'\to u)\, \mathrm{d}u / \varphi^j(\mathbf{r}). \tag{12a}$$

Here $\pi_{\mathrm{in}\,i\,0}(u'\to u)$ is the scattering frequency (probability) portion of $\Sigma_{\mathrm{in}}(u'\to u)$, and $\Sigma_{\mathrm{in}\,0}(u') = \int_0^\infty \mathrm{d}u\, \Sigma_{\mathrm{in}}(u'\to u)$. Eq. (12) differs from the comparable Eq. (11) for the group coefficients only in that one need not exercise care with the limits of integration. Basically the same approximation has been made for both cases, namely that in performing the average over the initial group the dependence of the scattering frequency on initial lethargy may be neglected.

The purpose of the present paper is to discuss some of the fundamental problems inherent in the multi-group procedure, in so far as cross-section averages are concerned. In Section 1 we consider the problem of finding $\Sigma_{\mathrm{tr}}^m$; in Section 2 we consider the sensitivity of reactor parameters to the spectrum over which the average is taken, while in Section 3 we consider the problem of non-separability of flux, not only in space and energy, but in energy and angle. Finally, in Section 4, some remarks are made concerning the most appropriate definition of the group constants for various multi-group schemes.

## 1. Averaging of the transport mean free path

In the Introduction we showed that the correct diffusion coefficient for the $m$th group, $D^m$, is given by

$$D^m = \frac{1}{3\Sigma_{\mathrm{tr}}^m}, \quad \Sigma_{\mathrm{tr}}^m = (\lambda^m)^{-1}, \tag{13}$$

where $\lambda^m$ is the flux-weighted transport mean free path. This definition was, of course, based on the assumption of Fick's rule, Eq. (3), and space-energy separability of flux and current, both of which assumptions we adopt for the purposes of the present section.

Since it would be an Herculean task to average $\lambda$ each time a reactor composition is changed, it would be desirable to find a scheme whereby elemental averages could be combined in some fashion. Then, if reactor composition is changed but it is assumed that the spectrum is not violently affected, these elemental averages could be combined for the new calculation without lengthy reaveraging.

Two possible definitions come to mind.

$$\overset{a}{\Sigma}{}^{m}_{\mathrm{tr}} = \sum_{i=1}^{N} \left(\lambda^{m}_{i}\right)^{-1} \tag{14a}$$

and

$$\overset{b}{\Sigma}{}^{m}_{\mathrm{tr}} = \sum_{i=1}^{N} \Sigma^{m}_{\mathrm{tr}\,i}\,. \tag{14b}$$

We will prove the following inequalities:

$$\overset{a}{\Sigma}{}^{m}_{\mathrm{tr}} \leqslant \Sigma^{m}_{\mathrm{tr}} \leqslant \overset{b}{\Sigma}{}^{m}_{\mathrm{tr}}\,; \tag{15}$$

this, at least, permits error limits to be set on $\Sigma^{m}_{\mathrm{tr}}$ if it is calculated from elemental averages according to both (14a) and (14b).

We prove the theorem first for a binary mixture containing materials of transport cross-sections $\Sigma_1$ and $\Sigma_2$.

$$\frac{\overset{b}{\Sigma}{}^{m}_{\mathrm{tr}}}{\Sigma^{m}_{\mathrm{tr}}} = (<\Sigma_1> + <\Sigma_2>)\left\langle \frac{1}{\Sigma_1 + \Sigma_2} \right\rangle = <\Sigma_1 + \Sigma_2> \left\langle \frac{1}{\Sigma_1 + \Sigma_2} \right\rangle. \tag{16}$$

Consider

$$<\sigma> <1/\sigma> = \int \sigma\, \varphi\, \mathrm{d}u \int \frac{1}{\sigma}\, \varphi\, \mathrm{d}u\,. \tag{17}$$

Here $\varphi$ is a normalized weighting function and $\sigma$ is an arbitrary cross-section. Further, we are dealing with cases in which $\sigma$ and $\varphi$ are both positive-definite. We can then define two functions $\alpha$ and $\beta$ by

$$\alpha = \sqrt{\sigma\varphi}\,, \tag{18a}$$

$$\beta = \sqrt{\frac{\varphi}{\sigma}} \tag{18b}$$

which are elements of Hilbert space [7]*. Defining the scalar product $(\alpha, \beta)$ by

$$(\alpha, \beta) = \int \alpha\, \beta\, \mathrm{d}u, \tag{19}$$

we have, from the Schwarz inequality [7]

$$\int \alpha^2\, \mathrm{d}u \int \beta^2\, \mathrm{d}u \geqslant \left(\int \alpha\, \beta\, \mathrm{d}u\right)^2 \tag{20}$$

or

$$\int \sigma\, \varphi\, \mathrm{d}u \int \frac{1}{\sigma}\, \varphi\, \mathrm{d}u \geqslant \left(\int \varphi\, \mathrm{d}u\right)^2 = 1. \tag{21}$$

Letting $\sigma = \Sigma_1 + \Sigma_2$, we see that

$$\overset{b}{\Sigma}{}^{m}_{\mathrm{tr}} \geqslant \Sigma^{m}_{\mathrm{tr}} \tag{22}$$

* Clearly, since $\varphi$ is a distribution function, it does not follow that $\alpha$ and $\beta$ will in general be elements of Hilbert space. However, for practical cases both the fluxes and the cross-sections are sufficiently well behaved that $\alpha$, $\beta$ $\varepsilon$ $L_2$. If this condition is not fulfilled, our proof is not necessarily valid.

and one of the inequalities (15) is proven.

Next, consider $\overset{a}{\Sigma}{}^m_{\mathrm{tr}} - \Sigma^m_{\mathrm{tr}} = \delta$. We shall prove $\delta \leqslant 0$.

$$\delta = \left\langle \frac{1}{\Sigma_1} \right\rangle^{-1} + \left\langle \frac{1}{\Sigma_2} \right\rangle^{-1} - \left\langle \frac{1}{\Sigma_1 + \Sigma_2} \right\rangle^{-1} \tag{23}$$

$$\delta = \frac{\left(\left\langle \frac{1}{\Sigma_1} \right\rangle + \left\langle \frac{1}{\Sigma_2} \right\rangle\right)\left\langle \frac{1}{\Sigma_1 + \Sigma_2} \right\rangle - \left\langle \frac{1}{\Sigma_1} \right\rangle \left\langle \frac{1}{\Sigma_2} \right\rangle}{\left\langle \frac{1}{\Sigma_1} \right\rangle \left\langle \frac{1}{\Sigma_2} \right\rangle \left\langle \frac{1}{\Sigma_1 + \Sigma_2} \right\rangle}. \tag{24}$$

Since the denominator is always positive, we need consider only the numerator; call it $\delta'$:

$$\delta' = \left\langle \frac{\Sigma_1 + \Sigma_2}{\Sigma_1 \Sigma_2} \right\rangle \left\langle \frac{1}{\Sigma_1 + \Sigma_2} \right\rangle - \left\langle \frac{1}{\Sigma_1} \right\rangle \left\langle \frac{1}{\Sigma_2} \right\rangle \tag{25}$$

$$= \int \frac{\Sigma_1 + \Sigma_2}{\Sigma_1 \Sigma_2} \varphi \, \mathrm{d}u \int \frac{1}{\Sigma_1 + \Sigma_2} \varphi \, \mathrm{d}u - \int \frac{1}{\Sigma_1} \varphi \, \mathrm{d}u \int \frac{1}{\Sigma_2} \varphi \, \mathrm{d}u . \tag{26}$$

This may be written in the form:

$$\delta' = (1/2) \iint \mathrm{d}u \, \mathrm{d}u' \varphi(u) \varphi(u') \left\{ \frac{\Sigma_1 + \Sigma_2}{\Sigma_1 \Sigma_2} \frac{1}{\Sigma'_1 + \Sigma'_2} + \frac{\Sigma'_1 + \Sigma'_2}{\Sigma'_1 \Sigma'_2} \frac{1}{\Sigma_1 + \Sigma_2} - \right.$$
$$\left. - \frac{1}{\Sigma_1 \Sigma'_2} - \frac{1}{\Sigma'_1 \Sigma_2} \right\} \tag{27}$$

where we have abbreviated $\Sigma^m \equiv \Sigma^m(u)$ and $\Sigma^{m\prime} \equiv \Sigma^m(u')$.

After a little algebraic manipulation, we find

$$\delta' = -(1/2) \iint \mathrm{d}u \, \mathrm{d}u' \varphi(u) \varphi(u') \frac{(\Sigma_2 \Sigma'_1 - \Sigma_1 \Sigma'_2)^2}{\Sigma_1 \Sigma_2 \Sigma'_1 \Sigma'_2 (\Sigma_1 + \Sigma_2)(\Sigma'_1 + \Sigma'_2)} . \tag{28}$$

Clearly, $\delta' \leqslant 0$, which proves

$$\Sigma^m_{\mathrm{tr}} \geqslant \overset{a}{\Sigma}{}^m_{\mathrm{tr}} \tag{29}$$

or comparing with (22)

$$\overset{a}{\Sigma}{}^m_{\mathrm{tr}} \leqslant \Sigma^m_{\mathrm{tr}} \leqslant \overset{b}{\Sigma}{}^m_{\mathrm{tr}}$$

and inequality (15) is proved.

The extension of this theorem to the general mixture rather than the binary mixture for which it is proved above is straightforward. Inequality (22) follows from the general case simply by writing $\Sigma_1 = \sum_{i=1}^{n} \Sigma_i + \sum_{i=n+1}^{N} \Sigma_i$, where $i$ is the elemental index, $N$ is the total number of components in the mixture, and $n$ is completely arbitrary. The extension of inequality (29) to the general mixture may be made in the following manner. We wish to show that

$$\sum_{i=1}^{N} \left\langle \frac{1}{\Sigma_i} \right\rangle^{-1} \leqslant \left\langle \frac{1}{\sum_{i=1}^{N} \Sigma_i} \right\rangle^{-1} . \tag{30}$$

Since we have shown [inequality (24)] that

$$\left\langle \frac{1}{\Sigma_1} \right\rangle^{-1} + \left\langle \frac{1}{\Sigma_2} \right\rangle^{-1} \leqslant \left\langle \frac{1}{\Sigma_1 + \Sigma_2} \right\rangle^{-1} \tag{31}$$

we set $\Sigma_2 = \Sigma_3 + \Sigma_4$ so that (31) becomes

$$\left\langle \frac{1}{\Sigma_1} \right\rangle^{-1} + \left\langle \frac{1}{\Sigma_3 + \Sigma_4} \right\rangle^{-1} \leqslant \left\langle \frac{1}{\Sigma_1 + \Sigma_3 + \Sigma_4} \right\rangle^{-1}. \tag{32}$$

But from (31)

$$\left\langle \frac{1}{\Sigma_3} \right\rangle^{-1} + \left\langle \frac{1}{\Sigma_4} \right\rangle^{-1} \leqslant \left\langle \frac{1}{\Sigma_3 + \Sigma_4} \right\rangle^{-1}$$

so that (32) may be written

$$\left\langle \frac{1}{\Sigma_1} \right\rangle^{-1} + \left\langle \frac{1}{\Sigma_3} \right\rangle^{-1} + \left\langle \frac{1}{\Sigma_4} \right\rangle^{-1} \leqslant \left\langle \frac{1}{\Sigma_1 + \Sigma_3 + \Sigma_4} \right\rangle^{-1} \tag{33}$$

which proves the theorem for a tertiary mixture. We could now define $\Sigma_4 = \Sigma_5 + \Sigma_6$ and continue the process $N$ times for an $N$-fold mixture. Note that this inequality is weakened each time a new element is added to the mixture so that more care is required in using the approximation $\overset{a}{\Sigma}{}^m{}_{\mathrm{tr}}$ to $\Sigma^m{}_{\mathrm{tr}}$ the greater the number of components in the mixture. Thus, if for a given mixture (the correct) $\Sigma^m{}_{\mathrm{tr}}$ is known and one (or more) components are added to the mixture, it is better to take the group transport cross-section for the new mixture (call it $\Sigma^{m\prime}{}_{\mathrm{tr}}$) as

$$\Sigma^{m\prime}_{\mathrm{tr}} = \left\langle \frac{1}{\Sigma^m_{\mathrm{tr}}} \right\rangle^{-1} + \sum_j \left\langle \frac{1}{\Sigma_j} \right\rangle^{-1} \tag{34}$$

than as

$$\Sigma^{m\prime}_{\mathrm{tr}} = \sum_i \left\langle \frac{1}{\Sigma_i} \right\rangle^{-1}. \tag{35}$$

In Eq. (34) the sum is taken over the additional elements while in (35) it goes over all the elements, old and new, in the mixture. This of course only applies to cases in which, for some reason or other, the group transport cross-section for part of the mixture has been computed from the correct definition (13). This suggests that in many calculations, particularly of the survey type, it might be wise to calculate $\Sigma^m{}_{\mathrm{tr}}$ by the correct definition for the invariant components of the reactor (if any). "Invariant" means any components whose *relative* density will remain unchanged throughout the survey. Then a stronger lower limit can be placed on inequality (15) than otherwise. It is also interesting to note, since the usual approximation [8] is to take $\Sigma^m{}_{\mathrm{tr}} = \overset{a}{\Sigma}{}^m{}_{\mathrm{tr}}$, the diffusion coefficient and hence the leakage are always over-estimated, a consistent error which could probably not be tolerable if more serious approximations (such as energy-space separability of the flux) were not made. This error could be particularly important in the case of danger-coefficient calculations of such materials as sodium (for which an appreciable fraction of the coefficient may be due to leakage) because $\Delta\Sigma^m{}_{\mathrm{tr}}$ is not related in any simple manner, except through the inequalities previously derived, to the transport cross-section of the material whose danger coefficient is being studied.

There are ways to estimate the magnitude of the effect discussed here. We consider the fractional difference between the extreme members of inequality (15);

$$\varepsilon \equiv \frac{\overset{b}{\Sigma}{}^{m}_{\mathrm{tr}} - \overset{a}{\Sigma}{}^{m}_{\mathrm{tr}}}{\overset{a}{\Sigma}{}^{m}_{\mathrm{tr}}} = \frac{\sum_i \left\{\langle \Sigma_i \rangle - \left\langle \frac{1}{\Sigma_i} \right\rangle - 1\right\}}{\sum_i \left\langle \frac{1}{\Sigma_i} \right\rangle^{-1}}. \tag{36}$$

(Note $\varepsilon > 0$). Equation (36) can be written

$$\varepsilon = \frac{\sum_i \left\langle \frac{1}{\Sigma_i} \right\rangle^{-1} \left\{\langle \Sigma_i \rangle \left\langle \frac{1}{\Sigma_i} \right\rangle - 1\right\}}{\sum_i \left\langle \frac{1}{\Sigma_i} \right\rangle^{-1}}, \tag{37}$$

from which it is clear that*

$$[\langle \sigma_i \rangle \langle 1/\sigma_i \rangle - 1]_{\min} \leqslant \varepsilon \leqslant [\langle \sigma_i \rangle \langle 1/\sigma_i \rangle - 1]_{\max} \tag{38}$$

where $[\ldots\ldots\ldots]_{\min}$ means the value of the bracketed quantity for that element in the mixture which makes the quantity a minimum and $[\ldots\ldots]_{\max}$ has an analogous definition. Clearly, the relationship can be written in terms of the microscopic cross-section because the product $\langle \Sigma_i \rangle \langle 1/\Sigma_i \rangle$ does not depend on the number density. Thus, the quantity $\langle \sigma_i \rangle \langle 1/\sigma_i \rangle$ could be made a part of cross-section libraries in order to permit rapid error-analyses when multi-group calculations are being performed.

For isotropic scattering in $C$, $\sigma_{\mathrm{tr}} = (1 - 2/3A)\sigma_{\mathrm{s}} \cong \sigma_{\mathrm{s}}$ for heavy elements. Then a fair approximation to (38) might be to take $(\sigma^m{}_{\mathrm{s}i}/\sigma^m{}_{\mathrm{tr}i})^{-1}$, where $\sigma^m{}_{\mathrm{s}i}$ is the group-averaged microscopic scattering cross-section of the $i$th element and $\sigma^m{}_{\mathrm{tr}i} = N_i^{-1}\langle \lambda_i \rangle^{-1}$. Unfortunately, group averages of scattering cross-sections are not easily found in tabulations of group constants. Instead, "elastic transfer coefficients" are generally given (see Introduction). Whether or not $\sigma^m{}_{\mathrm{s}}$ can be obtained from these transfer coefficients depends upon how they were defined to form the tabulation; more often than not it cannot be so obtained.

In closing this section, it might be remarked that many thermal or near-thermal reactors are treated by means of spectral codes, such as MUFT [9], which rapidly generate group constants for a given problem, and themselves use only unaveraged microscopic cross-section data as input. As yet, no severe numerical tests have been made of the points raised in this section—if such tests show that more care in cross-section averaging should be taken than has been done in the past, it may well be that fast and intermediate reactors should be treated in a fashion similar to the MUFT procedure.

## 2. Some remarks on flux separability in transport calculations

In order to investigate the dependence of group constants on angle (resulting from flux non-separability), a very simple calculation was performed assuming a fission spectrum flux in a graphite medium. The energy range was from 10 MeV

* Eq. (38) follows from the fact that the $\langle 1/\Sigma_i \rangle$ terms act merely as a weighting function in Eq. (37), and $\varepsilon$, the weighted average of the $\{\langle \Sigma_i \rangle \langle 1/\Sigma_i \rangle - 1\}$ cannot assume a value outside the range of those terms.

to 2.25 MeV ($u=0$ to $u=1.5$). For the case considered, the group-averaged cross-section did not vary by more than about 3% over the entire range of position* and angle. This is probably a small uncertainty compared with many other approximations made, although one should be cautious in assuming that the variation will be small in another case. Fortunately, the check employed here is so simple (because of its highly approximate nature) that it can readily be used to check any case of practical interest. If the results indicate large variations of group-averaged quantities with space and angle, appropriate steps must be taken. Such steps might involve procedures similar to the iteration method used in the next section to investigate a different problem, i.e., the flux as a function of position and angle could be calculated from group constants which do not depend on position or angle**; the resultant position- and angle-dependent spectrum can then be used to compute the new group constants which are then inserted as functions of position and angle, from which a new spectrum is computed and new averages are found. The process is continued until it converges, but it is highly likely that one iteration would be sufficient.

In referring to a cross-section as a function of "angle", we have two points in mind. One is the definition of $\Sigma^m{}_{\mathrm{tr}}$ in the Introduction as an average over the current rather than the flux. Of course, if the spectrum does not depend on angle, the two averages will be identical. However, in group-diffusion calculations, no further note need be taken of the angular dependence of the spectrum than to average $\Sigma_{\mathrm{tr}}$ over current.

The situation is different in transport calculations such as $S_n$ [10]. In such calculations the process of forming one-velocity equations from the energy-dependent Boltzmann equation introduces an implicit dependence of the group cross-sections on angle as well as space, in the same manner that, in the Introduction, the cross-section was seen to become a function of position in the diffusion scheme. As a matter of fact, since transport calculations are used in cases for which great accuracy is desired, the motivation for considering effects on non-separability should be highest there. Thus, before using $S_n$ or similar calculations, these effects should be considered. As was mentioned earlier, the angular dependence introduces a companion spatial dependence because of the inherent non-separability of the one-velocity Boltzmann equation in space and angle. This spatial dependence may, in general, be much smaller than that introduced even in diffusion calculations by the presence of boundaries. This latter effect is not considered at all in the present paper—the only feasible method for studying it seems to be an iterative procedure such as is mentioned earlier in this section.

A brief description of the calculation will now be given. Taking as a first approximation the energy-angle-space dependent flux, $\psi\,(u, \mu, x)$,*** to be separable and to be given by the diffusion theory result, we have****

$$\psi\,(u, \mu, x) = 1/2\,\{\varphi\,(u, x) + 3\,\mu\,J\,(u, x)\}. \tag{39}$$

Separating $\varphi\,(u, x)$ in the form $f\,(u)\cos Bx$ and writing $J = -D\,\dfrac{\mathrm{d}\varphi}{\mathrm{d}x}$, we have

* The angular dependence introduces a position-dependence as is discussed later in this section.

** Strictly speaking, a group *constant* must be independent of position and angle, otherwise it would be a group *variable*.

*** For simplicity, only one dimension is considered.

**** $\mu$ is the cosine of the angle between the velocity vector of the neutron and the $x$-axis.

$$\psi(u, \mu, x) = 1/2\, f(u)\, [\cos Bx + 3\, \mu DB \sin Bx]. \tag{40}$$

Here $B$ is the "buckling" of the reactor [1, 2]. Then we can write

$$\Sigma^m(\mu, x) = \frac{\cos B \int_{\Delta u^m} f(u)\, \Sigma(u)\, \mathrm{d}u + 3\, \mu B \sin Bx \int_{\Delta u^m} f(u)\, D(u)\, \Sigma(u)\, \mathrm{d}u}{\cos B \int_{\Delta u^m} f(u)\, \mathrm{d}u + 3\, \mu B \sin Bx \int_{\Delta u^m} f(u)\, D(u)\, \mathrm{d}u} \tag{41a}$$

or

$$\Sigma^m(\mu, x) = \frac{\cos Bx\, \langle \Sigma \rangle + 3\, \mu B \sin Bx\, \langle \Sigma D \rangle}{\cos Bx + 3\, \mu B \sin Bx\, \langle D \rangle}. \tag{41b}$$

Here the symbol $\langle x \rangle$ refers to the ordinary flux-average defined in the Introduction. Equations (41) may now be used to investigate the effect of angular dependence of group constants. Note how the spatial dependence is introduced at the same time because of the inherent non-separability of flux in angle and space.

Eq. (41b) reduces simply to $\langle \Sigma \rangle$ if the numerator and denominator are integrated over all angles (which is how $\langle \Sigma \rangle$ enters in diffusion calculations); if $\Sigma^m{}_{\mathrm{tr}} = 3\, D^m$ is calculated in the same way from Eq. (41) and if the numerator and denominator are multiplied by $\mu$ and integrated over all angles, we obtain simply the familiar result of the Introduction, $\Sigma^m{}_{\mathrm{tr}} = \langle \lambda_{\mathrm{tr}} \rangle^{-1}$.

Using Eq. (1) for the graphite medium case discussed earlier in this section ($B = 0.08\ \mathrm{cm}^{-1}$), we obtain the results given in Table I.

TABLE I

$\bar{\Sigma}(\mu, x)$ **FOR GRAPHITE**

| $\mu \downarrow$ \ $x \rightarrow$ | 0 | $\frac{\pi}{4B}$ | $\frac{\pi}{2B}$ |
|---|---|---|---|
| 1 | 0.1425 | 0.1418 | 0.1406 |
| 0.5 | 0.1425 | 0.1421 | 0.1406 |
| 0 | 0.1425 | 0.1425 | 0.1406 |
| —0.5 | 0.1425 | 0.1432 | 0.1406 |
| —1 | 0.1425 | 0.1450 | 0.1406 |

This gives only a rough idea of the magnitude of the result, so that each individual case should be treated separately. Note that the effect increases with increasing buckling, so that it may be more important in intermediate- (or thermal-) spectrum propulsion reactors than in fast power reactors.

## 3. Effect of spectrum on reactor parameters

In order to determine the sensitivity of various reactor parameters to the spectrum over which the cross-section is averaged, a spherical uranium-graphite system, similar to a critical experiment described by LONG *et al.* [11], was studied. The composition is given in Table II.

TABLE II

**REACTOR COMPOSITION**

| Material | Core* | | Blanket** | |
|---|---|---|---|---|
| | Vol. % | Number density | Vol. % | Number density |
| $U^{235}$ | 9.4 | $4.516 \times 10^{21}$ | 0.19 | $9.128 \times 10^{19}$ |
| $U^{238}$ | 0.7 | $3.365 \times 10^{20}$ | 83.3 | $4.004 \times 10^{22}$ |
| Fe | 9.15 | $7.747 \times 10^{21}$ | 7.31 | $6.189 \times 10^{21}$ |
| C | 73.6 | $5.352 \times 10^{22}$ | | |

* Spherical core radius, $r = 26.566$ cm.
** For blanket $\Delta r = 30.0$ cm.

The basic microscopic cross-section data were taken from the Bettis library [12], and an iteration procedure was used. In the first iteration, in which the reactor radius was varied until criticality was achieved, the cross-sections were averaged without regard to a spectral weighting function. In the second iteration, the microscopic cross-section data were averaged over the spectrum obtained in the first iteration, obtained by drawing a smooth curve through the mid-points of the group-lethargy histogram obtained from the 10-group calculation. The criticality of the reactor was then calculated using the spectrum-weighted cross-sections. In each case, graphite danger-coefficients were computed by removing uniformly 10% of the graphite in the core.

TABLE III

**GROUP STRUCTURE**

| Group No. | Energy (MeV) | Lethargy |
|---|---|---|
| 1 | 10 —2.23 | 0 — 1.5 |
| 2 | 2.23 —1.35 | 1.5— 2.0 |
| 3 | 1.35 —0.50 | 2.0— 3.0 |
| 4 | 0.50 —0.30 | 3.0— 3.5 |
| 5 | 0.30 —0.18 | 3.5— 4.0 |
| 6 | 0.18 —0.067 | 4.0— 5.0 |
| 7 | 0.067 —0.025 | 5.0— 6.0 |
| 8 | 0.025 —0.0091 | 6.0— 7.0 |
| 9 | 0.0091—0.0034 | 7.0— 8.0 |
| 10 | 0.0034—thermal | 8.0—19.8 |

In Table III we give the group boundaries used in the problem, run with the AIM-6 code, an unpublished modification of the AIM-5 code [13]. Table IV lists $k_{\text{eff}}$ and the graphite danger-coefficient from each iteration described above, as well as from a calculation performed using a 10-group cross-section library, based generally upon the 11-group set listed in ANL-5800 [8].

Fig. 1 shows the histogram spectra obtained from the first two iterations. Their fairly close agreement indicated that the calculation had probably converged sufficiently to be stopped at that point.

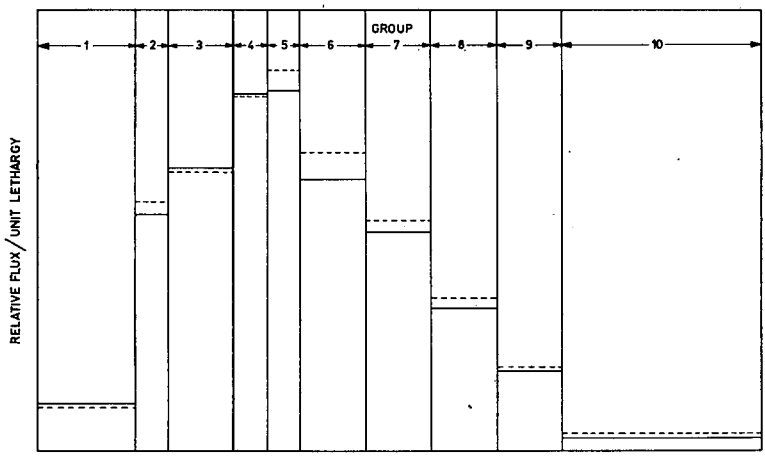


Fig. 1
Comparison of group fluxes for zeroth and first iterations. The comparison refers to the assembly described in Table II. The solid lines represent the zeroth iteration fluxes, the dotted lines the first iteration fluxes. The lethargies corresponding to group boundaries are given in Table III.

TABLE IV
**SPECTRAL WEIGHTING EFFECTS**

| Run No. | Iteration | Remarks | $k_{eff}$ | $\Delta k_{eff}$ | $(\Delta k_{eff}/k_{eff})$/mole* |
|---|---|---|---|---|---|
| 1 | Zeroth | Nominal carbon | 1.000 02 | — | — |
| 2 | Zeroth | 10% reduced carbon | 0.971 49 | 0.028 53 | $4.089 \times 10^{-6}$ |
| 3 | First | Nominal carbon | 0.970 42 | — | — |
| 4 | First | 10% reduced carbon | 0.944 48 | 0.025 94 | $3.718 \times 10^{-6}$ |
| 5 | 10-group library used | Nominal carbon | 1.012 60 | — | — |
| 6 | | 10% reduced carbon | 0.991 17 | 0.021 43 | $3.071 \times 10^{-6}$ |

* Carbon danger-coefficient.

From Table IV, it is seen that the spectrum over which cross-sections are averaged may be important—the reactor criticality in Run No. 3 can be assumed to be correct. The use of unaveraged cross-sections (Runs 1 and 2) produces an error in $k_{eff}$ of approximately 3% although the graphite danger-coefficient is close. The use of the 10-group library is seen to lead to a 4% error in $k$ and a 20% error in the graphite danger-coefficient. It is true that the particular 10-group library used here is not the most up-to-date data by any means; however, the results are indicative of the pitfalls which may occur in reactor design if proper care is not exercised.

## 4. Some remarks on definitions of group constants*

In the Introduction it was pointed out that the correct definition of $D^m$ was in terms of a transport cross-section averaged over current which is, for fluxes separable in space and energy, the reciprocal of the average of the transport mean free path over flux.

The group absorption cross-section is usually straightforward for fast reactors (if the microscopic data are known!). On the other hand, for intermediate reactors one frequently attempts to deduce group absorption cross-sections from resonance integral data [14]. Here care must be taken since the result, in general, will depend on the definition of the elastic transfer coefficient.

To see this, let us suppose that one writes for the $m$th group:

$$q^m = \xi^m \Sigma^m{}_s \varphi^m = \omega^m{}_1 q^I{}_m + \omega^m{}_2 q^0{}_m \tag{42}$$

where $q^I{}_m$ and $q^0{}_m$ are, respectively, the slowing-down densities (products of flux and $\xi\,\Sigma_s$) into and out of the $m$th group, i.e., $q^I{}_m$ is the slowing-down source into the $m$th group and $q^0{}_m$ the slowing-down source into the $(m+1)$ group. Ehrlich and Hurwitz [6] used this notation in dealing with the multi-group age equation and gave various "schemes" for choosing $\omega_1$ and $\omega_2$. Note that the elastic transfer coefficients $\Sigma^{j\to k}$ discussed in the Introduction can be related to the $\omega$'s rather than calculated directly (so long as elastic transfer is restricted to the adjacent group), since clearly

$$q^I{}_m = \Sigma^{m-1\to m}\,\varphi^{m-1} \tag{43a}$$

and

$$q^0{}_m = \Sigma^{m\to m+1}\,\varphi^m\,. \tag{43b}$$

Ehrlich and Hurwitz describe three schemes in Ref. [6].

(*a*) $\omega_1 = \omega_2 = 1/2$:

(*b*) $\omega_1 = f,\ \omega_2 = 0$;

(*c*) $\omega_1 = \dfrac{1}{2}\dfrac{(\xi\,\Sigma_s)^I{}_m}{(\xi\,\Sigma_s)^m}\,,\quad \omega_2 = \dfrac{1}{2}\dfrac{(\xi\,\Sigma_s)^0{}_m}{(\xi\,\Sigma_s)^m}\,.$

The last scheme, the so-called "Oak Ridge Scheme", is equivalent to assuming a linear relation among the fluxes rather than the slowing-down densities. If $\xi\Sigma_s$ is essentially constant, there is little difference. Clearly, another possible scheme is to modify (*b*) above to a flux relation

(*d*) $\omega_1 = \dfrac{f\,(\xi\,\Sigma_s)^I{}_m}{(\xi\,\Sigma_s)^m}\,,\qquad \omega_2 = 0\,.$

The schemes (*b*) and (*d*) have been found by experience to be generally superior although care is required in choosing the $f$. Usually after solving the multi-group problem one should check to make sure that the final solution is consistent with the choice of $f$.

---

* The work outlined here was performed originally by D. B. Wehmeyer and one of the authors (P.F.Z.), unpublished.

If one of the above schemes is chosen, it is simple to express $\Sigma_{\text{in}}^{m\to m+1}$ in terms of the $\omega$'s. The algebra will not be reproduced here. However, the computation of the $\Sigma^{m\to m+1}$ from basic cross-section data, as is described in the Introduction, is seen to be equivalent to still another scheme for the $m$th group:

$$(e)\quad \omega_1 = 0\,, \quad \omega_2 = \frac{(\xi\,\Sigma_{\text{s}})^m}{\Sigma^{m\to m+1}}\,.$$

In general, the group constants should be chosen so as to conserve neutrons. Thus

$$(\Sigma^m{}_a + D^m B^2)\,\varphi^m \Delta u^m = \frac{N I^m{}_{\text{eff}} e^{-B^2 \tau^m}}{(\xi\,\Sigma_{\text{s}})^m}\, q^I{}_m \tag{44}$$

where $I^m{}_{\text{eff}}$ is the effective resonance integral for the $m$th group, $N$ is the number density of absorber atoms and $\tau^m$ is the Fermi age in the $m$th group.

Then from Eqs. (42, 44), and the fact that $q^0{}_m = q^I{}_m \dfrac{N I^m_{\text{eff}}}{(\xi\,\Sigma_{\text{s}})^m} e^{-B^2 \tau^m}$ we find

$$\Sigma^m{}_a = \frac{\dfrac{N I^m_{\text{eff}}}{\Delta u^m} e^{-B^2 \tau^m}}{\omega_1 + \omega_2 \dfrac{N I^m_{\text{eff}}}{(\xi\,\Sigma_{\text{s}})^m} e^{-B^2 \tau^m}} - D^m B^2\,. \tag{45}$$

This may be taken as a consistency relation between $D^m$, $(\xi\Sigma_{\text{s}})^m$, and $\Sigma^m{}_a$ or it may be taken as a definition of $\Sigma^m{}_a$ if the other two group cross-sections are assumed known. Note that in Scheme ($b$) above, if we ignore the effect of leakage, $\Sigma^m{}_a$ is defined as

$$\Sigma^m{}_a = \frac{N I^m_{\text{eff}}}{f \Delta u^m} \tag{46}$$

which may differ appreciably from a frequently used approximation in which $\Sigma^m{}_a$ is taken to be $N I_{\text{eff}}/\Delta u^m$.

As yet, no numerical tests have been made of the relative accuracy of the various schemes, or of the various definitions of the cross-sections. Such tests will comprise the contents of a future paper.

## REFERENCES


[1] WEINBERG, A. M. and WIGNER, E. P., The Physical Theory of Neutron Chain Reactors. The University of Chicago Press, Chicago (1958).
[2] GLASSTONE, S. and EDLUND, M. C. The Elements of Nuclear Reactor Theory, D. Van Nostrand Co., Inc., New York (1952).
[3] HAUSER, W. and FESHBACH, H., *Phys. Rev.* **87** (1952) 366.
[4] ZWEIFEL, P. F. and HURWITZ, H., Jr., *J. appl. Phys.* **25** (1954) 1241.
[5] AMSTER, H., *J. appl. Phys.* **4** (1957) 623.
[6] EHRLICH, R. and HURWITZ, H. Jr., *Nucleonics* **12** a (1954) 23.
[7] ZAANEN, A. C., Linear Analysis, Interscience Publishers, Inc., New York (1953).
[8] YIFTAH, S., OKRENT, D. and MOLDAUER, P. A., Fast Reactor Cross Sections, Pergamon Press, New York (1960); and Reactor Physics Constants, ANL-5800 (1958).
[9] BOHL, H. Jr., GELBARD, E. M., and RYAN, G. H., WAPD-TM-72 (July 1957).
[10] CARLSON, B. G. and BELL, G. I. Proc. 2nd UN Int. Conf. PUAE **16** (1958) 535.
[11] LONG, J. K. *et al.*, Proc. 2nd UN Int. Conf. PUAE **12** (1958) 119.
[12] HENRY, A. F., WAPD-TM-224 (1960).
[13] FLATT, H. P. and BALLER, D. C., NAA-SR-4694 (1960).
[14] ADLER, F. T., HINMAN, G. W. and NORDHEIM, L. W. Proc. 2nd UN Int. Conf. PUAE **16** (1958) 155.

# A PUNCHED-CARD LIBRARY OF NEUTRON CROSS-SECTIONS

## and its use in the mechanized preparation of group cross-sections for use in Monte Carlo, Carlson $S_n$ and other multi-group neutronics calculations on high-speed computers*

K. PARKER
ATOMIC WEAPONS RESEARCH ESTABLISHMENT, ALDERMASTON,
UNITED KINGDOM

**Abstract — Résumé — Аннотация — Resumen**

**A punched-card library of neutron cross-sections and its use in the mechanized preparation of group cross-sections for use in Monte Carlo, Carlson $S_n$ and other multi-group neutronics calculations on high-speed computers.** The AWRE punched-card library of neutron cross-sections is described together with associated IBM-7090 programmes which process this data to give group-averaged cross-sections for use in Monte Carlo, Carlson $S_n$ and other multi-group neutronics calculations.

The methods developed to deal with both isotropic and anisotropic elastic scattering are described. These include the multi-group transport approximation and the full treatment of anisotropic scattering using the Legendre polynomial moments of the scattering transfer matrix.

The principles of group-constant formation are considered and illustrated by describing systems of group constants suitable for fast-reactor calculations. Practical problems such as the empirical adjustment of group constants to reproduce integral results and the collapsing of a many-group set of constants to give a few-group set are discussed.

**Fichier, à cartes perforées, de sections efficaces neutroniques: emploi dans la préparation de sections efficaces de groupes pour les calculs par les méthodes de Monte-Carlo, $S_n$ de Carlson et autres calculs neutroniques multigroupes sur calculatrices rapides.** L'auteur décrit le fichier de cartes perforées sur lesquelles on enregistre à l'Atomic Weapons Research Establishment (AWRE) les sections efficaces neutroniques ainsi que les programmes IBM-7090 associés qui sont employés pour le traitement de ces informations, en vue d'obtenir des sections efficaces moyennes par groupe pouvant servir aux calculs de neutroniques à plusieurs groupes, effectués à l'aide des méthodes de Monte-Carlo, $S_n$ de Carlson et autres méthodes.

L'auteur expose ensuite les méthodes mises au point pour étudier la diffusion élastique, tant isotrope qu'anisotrope. Elles comprennent l'approximation de transport à plusieurs groupes, ainsi que le traitement complet de la diffusion anisotrope par les moments polynomiaux de Legendre de la matrice de transfert de la diffusion.

L'auteur examine les principes de la formation des constantes de groupes; à titre d'illustration, il décrit les systèmes de constantes de groupes qui se prêtent aux calculs de réacteurs à neutrons rapides. Il expose quelques problèmes pratiques, tels que l'ajustement empirique des constantes de groupes pour reproduire des mesures intégrales et la simplification d'une série de constantes pour un grand nombre de groupes en vue d'obtenir une série de constantes pour un petit nombre de groupes.

* This paper reports work carried out by J. H. Bird, F. J. Birkin, P. M. Blackall, B. E. Blythe, B. R. S. Buckingham, M. J. Clements, E. C. Evans, S. Francescon, R. Hinves, F. J. Hooper, W. M. M. Kerr, J. C. Parish, J. B. Parker, K. Parker, E. D. Pendlebury, L. M. Russell, J. B. Taylor and L. H. Underhill.

**Библиотека перфорированных карточек сечений нейтронов и ее применение для механизированной подготовки усредненных по группам сечений для использования в вычислениях по методам Монте Карло, Карлсона $Sn$ и в других многогрупповых нейтронных вычислениях на быстродействующих счетно-решающих устройствах.** В докладе дается описание находящейся в Научно-исследовательском центре по разработке атомного оружия библиотеки перфорированных карточек сечений нейтронов совместно с программами IBM 7090, которые обрабатывают эти данные для получения усредненных по группам сечений, которые используются в нейтронных вычислениях по методам Монте Карло, Карлсона $Sn$ и в других многогрупповых вычислениях.

Описываются методы, касающиеся как изотропного, так и анизотропного упругого рассеяния. Они включают многогрупповое транспортное приближение и полную обработку анизотропного рассеяния, используя моменты многочлена Лежандра матрицы передачи рассеяния.

Принципы образования групповой постоянной обсуждаются и иллюстрируются при помощи описания систем групповых постоянных, подходящих для расчетов реакторов на быстрых нейтронах. Обсуждаются такие практические проблемы, как эмпирическое согласование групповых постоянных для воспроизводства интегральных результатов и приведение многогрупповой системы постоянных к малогрупповой системе.

**Fichero de tarjetas perforadas de secciones eficaces neutrónicas: su empleo en la preparación mecanizada de secciones eficaces de grupos para trabajar con calculadoras rápidas según los métodos de Montecarlo, $S_n$ de Carlson y otros procedimientos de grupos múltiples.** La memoria describe el fichero de tarjetas perforadas sobre las que se registran en el Atomic Weapons Research Establishment (AWRE) las secciones eficaces neutrónicas, así como los programas correspondientes de la calculadora IBM-7090 que se emplean para la elaboración de estos datos con miras a obtener promedios por grupo de secciones eficaces apropiadas para cálculos neutrónicos de grupos múltiples por los métodos de Montecarlo, de $S_n$ de Carlson y otros procedimientos.

El autor expone seguidamente los métodos desarrollados para estudiar la dispersión elástica isotrópica y anisotrópica. Comprenden la aproximación de transporte de grupos múltiples y el tratamiento completo de la dispersión anisotrópica empleando los momentos polinómicos de Legendre de la matriz de transferencia por dispersión.

El trabajo expone los principios de la formación de constantes de grupo y, a título ilustrativo, describe sistemas de constantes de grupo que sirven para cálculos de reactores rápidos. Analiza algunos problemas prácticos como la adaptación empírica de las constantes de grupo para reproducir resultados de mediciones integrales, y la reducción de un sistema de constantes de muchos grupos a otro de pocos grupos.

## Introduction

Neutronics calculations are basic to the physics of fast and intermediate reactors. While simple approximate methods have been developed, the more exact calculations are of considerable complexity and are only really feasible when high-speed computers are available. Investigators who have used Monte Carlo, Carlson $S_n$ or other numerical methods of solving the neutron transport equation will probably agree that it is not only the actual calculations which are complex; the assembly, classification and processing of the required neutron cross-section data presents a formidable problem. The obvious way of solving this problem is to use the same high-speed computers in processing the data. Several groups of workers have been active in this field. In this paper we discuss the general philosophy of mechanized handling of neutron cross-section data for use in neutronics calculations with particular reference to fast- and inter-

mediate-reactor problems; this general philosophy is illustrated by describing various features of the particular system devised at AWRE for use with IBM-704, 709 and 7090 computers.

In most large-scale neutronics calculations the region of allowed neutron energy is sub-divided into a number of ranges in each of which appropriate averages ("group cross-sections") of the various microscopic cross-sections are calculated. The mechanized preparation of nuclear data for neutronics calculations then falls naturally into two stages.

In the first stage the experimental and theoretical data on neutron cross-sections for a given element or isotope must be surveyed and criticized and a set of best values tabulated. Where there is no experimental information available, cross-sections must be estimated by the best theoretical method available (graphical interpolation, detailed calculations using nuclear theory or, if all else fails, the best guess based on nuclear systematics). The assembled best data on microscopic cross-sections is then represented on punched cards or magnetic tape in a form suitable for further processing. In this stage the machine programmes are relatively simple and most of the work is involved in surveying and evaluating the data. This stage of the operation is discussed in more detail in Section 1.

In the second stage the stored data from stage one is converted into group cross-sections using machine programmes. Once the criteria for determining the grouping have been settled, according to the requirements of the particular types of neutronics calculation to be made, and an appropriate machine programme written, the procedure is simple and straightforward. In this second stage the main effort is expended in the often formidable task of determining and programming appropriate grouping techniques. In Sections 2 and 3 we describe how this can be done for the Monte Carlo, Carlson $S_n$ and certain other methods.

## 1. Neutron cross-section libraries

### 1.1 General philosophy

In the setting-up of a record of neutron cross-sections on either punched cards or magnetic tape, certain principles must be kept in mind:

(*a*) For the purposes of neutronics calculations it is necessary to specify cross-sections, angular distributions at secondary neutrons and energy distributions of secondary neutrons for *all* processes which are energetically possible in the energy region of interest (ignoring one is equivalent to assuming that its cross-section is zero).

(*b*) The arrangement of the data on cards or tape must be as simple as possible, but must be capable of accommodating not only the currently available data but also that likely to become available in years to come if further modification of the system is to be avoided. In this respect it must be possible to incorporate revised values of the data easily.

(*c*) A good referencing system for measured and calculated data is essential and it is desirable to be able to see, at any given time, just which data is well determined and which is poorly determined. Frequent revision of the data is to be avoided if comparative calculations are of importance and it is necessary to strike a balance between frequency of revision and extent of comparative calculations.

(*d*) In the compiling, tabulating and recording of the data, all possible cross-checks against error must be employed.
(*e*) The final "best" data should give reasonable answers when used in making calculations on simple integral systems.

### 1.2 Collection of data

In a consideration of the data for any particular nuclide, certain well-known reference works such as the "barn book" [1, 2] and the compilations of Howerton [3] can be used as a starting point. These give a good deal of information on many cross-sections of interest. BNL-400 [4] details many angular distributions for elastic scattering but information on energy and angular distributions for inelastic processes is generally scanty and must be gleaned from the original literature.

When all the available information has been gathered together, recommended values can be derived. These will be based on experimental data, theoretical considerations, and interpolations and extrapolations, and as far as the latter are concerned, will undoubtedly reflect the personal prejudices of the particular compiler. One hopes that the regions of uncertainty will be those where the neutronics calculations are not very sensitive to the data but this is not always the case. In all this it is desirable to pay attention to the uncertainties in the experimental data; these are often larger than one thinks and it is unfortunate that the "barn book" [1] does not show experimental errors. The ultimate test of the recommended data is its use in calculations on experimentally well-determined simple integral systems (e.g. bare cores of $U^{235}$ and $Pu^{239}$). Disagreement here marks a failure of the data. Unfortunately the converse is not true, although confidence in the data will increase as it successfully reproduces the features of more and more integral systems.

AWRE Report 0-27/60 [5] details recommended neutron cross-sections of beryllium in the energy range 0.025 eV—15 MeV compiled in accordance with the principles discussed. AWRE Report 0-28/60 [6] summarizes recommended data for H, $H^2$, $H^3$, $He^3$, $He^4$, Be, B, $B^{10}$, C, N, O, F, Na, Al, Si, Cl, Ca, Cr, Fe, Ni, Cd, Pb, $Th^{232}$, $U^{233}$, $U^{235}$, $U^{238}$, $Pu^{239}$, $Pu^{240}$ and $Pu^{241}$. Similar compilations of recommended data have been published by a number of United States laboratories.

### 1.3 Representation of data

Initial representation on punched cards is conveniently made in decimal mode. Machine programmes can then transfer the data to punched cards written in binary mode or to magnetic tape. It is necessary to have a scheme of identification for nuclide and reaction type. Use of atomic mass $A$ and atomic number $Z$ identifies the nuclide, $A$ being omitted for a natural element having several stable isotopes. The reaction type can be identified by a simple numbering system.

Cross-sections may be arranged as (energy, cross-section) point-pairs in order of increasing energy. At AWRE the points are the end-points of linear segments of the cross-section graph plotted on a log-log scale (as in BNL-325 [1]). Sufficient points are chosen so that the error on linear interpolations is small, and thus the cross-sections can be determined quite accurately at all energies. In resonance regions large numbers of points are needed.

The average number of neutrons per fission, $\bar{\nu}$, can be represented in the same way as a cross-section except that a linear-linear plot is more useful.

A number of ways of representing angular distributions of secondary neutrons has been suggested. In the case of elastic scattering, the energy loss is a known function of this angular distribution and the mass of the scattering nucleus. This function is best evaluated when the angular distribution is given in the centre-of-mass co-ordinate system. One method of representation is to expand the distribution in a series of Legendre polynominals in the cosine of the scattering angle and to tabulate the energy-dependent coefficients. This system has been developed by Nuclear Development Associates workers. At AWRE the incident neutron range is subdivided into a number of ranges in each of which a particular probability distribution for scattering as a function of cos $\theta$ ($\theta$ = centre-of-mass scattering angle) is assumed to hold. The punched cards record the starting energy of the range together with pairs of (cos $\theta$, probability) values. These are determined from a linear plot of the probability curve so that again interpolation in cos $\theta$ is possible. In addition the value of the atomic (or isotopic) weight is given so that energy loss in an elastic collision can be calculated. This method of representation is open to some objection in that average values of cos $\theta$ are discontinuous in energy. An improvement would be obtained if the probability distributions were specified at definite incident energies, $E$, with the possibility of double interpolation in $E$ and cos $\theta$.

Angular distributions of non-elastic processes—inelastic scattering [the (n, n′) reaction], fission, (n, 2n) reaction, etc.—are generally taken as isotropic in the laboratory co-ordinate system. This is not necessarily correct, although anisotropies are expected to be small compared with those found in elastic scattering. This problem will need attention as more measurements on non-elastic processes become available.

In the case of secondary energies of non-elastic processes the correlation between angle and energy is generally unknown. It is convenient to consider several secondary energy laws, e.g.:

(*a*) Neutrons emitted with a known discrete energy (a simple assumption which is not based on nuclear theory).

(*b*) Neutrons emitted with energy $k\,(E_0 - E_d)$, where $k$ is a constant, $E_0$ is the initial neutron energy and $E_d$ is a discrete energy. This approximates to the excitation of a single level in an (n, n′) reaction.

(*c*) Continuous spectra independent of the initial energy, e.g. fission spectrum (approximately).

(*d*) Neutrons emitted with secondary energy, $E$, represented by the probability function, $p$, with

$$p\,(E/E^q{}_0) = f\,(E_0, E/E^q{}_0)$$

where $f$ is some function, $E_0$ is the initial energy and $q$ can take the values $0, {}^1/_2$ or 1. In the $q = {}^1/_2$ class is the "boil-off" spectrum found in the (n, n′) reaction for a continuum of final states.

Linear combinations of these and any further laws may be allowed.

In recording the data on magnetic tape or punched cards it is essential to apply all possible checks such as printing from the library and comparing with the original data, checking monotonic energy increase, checking that partial cross-sections sum to the total cross-section at each energy and so on.

Full details of the AWRE punched-card library of neutron cross-sections have been given by the author elsewhere [7].

### 1.4 Uses of neutron cross-section libraries

The principal use of a neutron cross-section library is in the preparation of data for neutronics problems as described in Sections 2 and 3. In addition it is possible to supply printed lists of cross-sections at given energy points. At AWRE a Benson-Lehner Electro-Plotter Model H has been used to prepare the graphs of cross-sections and elastic scattering angular distributions given in [6]. Average cross-sections for various spectra are readily computed.

## 2. Group constants for Monte Carlo calculations

### 2.1 General philosophy

In Monte Carlo work there are two broad conceptions of the way to present nuclear data advantageously, depending on what type of machine is available to perform the calculations. With a high-speed machine of large storage-capacity such as the IBM-7090, the neutron cross-sections can be well represented in step-function form, the neutron incident energy in a collision being used as an entry in a vast table, which consists of the several cross-sections, stored in the machine. The secondary energy and angular distribution laws likewise can be stored in blocks, each block corresponding to a specified energy range.

If the calculations are to be performed on a machine of small storage-capacity the data can be stored in the form of a series of polynomials; the penalty of representing the data in this form is that at each collision it may be necessary to appeal to a large number of polynomials (or other analytic functions) and to interpolate in energy.

In Monte Carlo work, the choice of a random number determines which of a particular set of reactions a neutron will have when it collides with a nucleus. The angular and energy distribution of any secondary neutrons is again determined by sampling and the use of random numbers.

### 2.2 Methods of processing the basic cross-sections

The processing of the basic cross-sections can be illustrated by describing methods used at AWRE.

The cross-sections are read into the machine from the library cards, and cross-sections are calculated by interpolation at each of a large number $N$ of pre-assigned energies for all nuclides and elements of interest to form a "library tape".

The main processing programme accepts data from the library tape and first calculates the partial cross-sections $(\theta_{ij})_E$ according to the formula

$$(\theta_{ij})_E = p_i \cdot (\sigma_{ij})_E \tag{1}$$

where $(\sigma_{ij})_E$ is the cross-section of element (or isotope) $i$ of type $j$ ($j$ refers to elastic scatter, fission, absorption, etc.) and $p_i$ is the proportion, by atoms, of element $i$ in the material. $\sum_i (\theta_{i,\,\mathrm{tot}})_E$ is defined as the total cross-section for the material, which will be written $\Theta_E$.

Next, cross-sections relevant to the $N$—1 energy *ranges* $g_m$ ($m=1, 2, \ldots N$—1) defined by the $N$ pre-assigned points are computed according to the formula

$$\varphi_m = (\theta_m \Theta_{m+1} + \theta_{m+1}\Theta_m)/(\Theta_m + \Theta_{m+1}) \tag{2}$$

where $\theta_m = (\theta_{ij})_m$ relates to the $j$th cross-section of element $i$. This procedure implies reciprocal averaging of the total cross-sections, and direct averaging of the proportional partial cross-sections $\theta_m/\Theta_m$.

The next procedure is to reduce the number of ranges, $N$—1, to that number required in the Monte Carlo, which is generally 128. We therefore define, for each pair of successive energy bands, a quantity

$$Q_{m,\,m+1} = W_{ij} \left| \frac{\varphi_m - \varphi_{m+1}}{\varphi_m + \varphi_{m+1}} \right| \tag{3}$$

where $m = 1, 2 \ldots N-2$. $Q_{m,\,m+1} = (Q_{ij})_{m,\,m+1}$ is a measure of the proportional change in the $j$th cross-section of element $i$ and is computed for all $m$, $i$ and $j$. $W_{ij}$ is any pre-assigned number that may be used to weight the proportional change in the $j$th cross-section of element $i$, and is generally set equal to unity.

The machine now selects

$$R_{m,\,m+1} = \max_{ij} Q_{m,\,m+1} \tag{4}$$

and examines all the $R_{m,\,m+1}$. The pair of energy ranges with the least $R_{m,\,m+1}$ are now combined to form one new energy range, the cross-sections for which are computed by means of formulae analogous to (2), and the procedure is repeated until only the desired number of ranges remains.

Generally, we have

$$\varphi_r = (n_p\theta_p\Theta_q + n_q\theta_q\Theta_p)/(n_p\Theta_q + n_q\Theta_p) \tag{5}$$

where $p$, $q$ relate to the two abutting ranges about to be amalgamated and $r$ to the new energy range; $n_p$, $n_q$ are weights equal to the number of ranges that have, as it were, gone into the making of ranges $p$ and $q$.

The master tape of AWRE contains the data for 29 elements or isotopes interpolated at a fixed set of 395 energy points between 1/40 eV and 14 MeV. The two programmes described above have the following additional features:

(*a*) The programme for writing the library tape ensures that the sum of the partial cross-sections is identical to the total cross-section for the element or isotope by multiplying each partial cross-section by the ratio $(\sigma_{i,\,\mathrm{tot}})_E / \Sigma\,(\sigma_{i,j})_E$. This assumes that the total cross-section after interpolation is correct, and it is necessary to offset the small errors obtained in interpolating the partial cross-sections.

(*b*) The main programme, during the process of reduction from a large to a smaller number of energy bands, will ensure, if desired, that certain stipulated energy bands will be preserved in the final result.

The form of the criterion (3) calls for comment. The use of *proportional* rather than *absolute* variation of a cross-section in this connection is, we believe, right; the use of the latter idea would tend to lead to the amalgamation of groups where the variation of the large, and often relatively unimportant, cross-sections was low, though the small cross-sections, which might be of far greater interest, may alter by a large proportion. The factor $W_{ij}$ can be introduced whenever it is judged desirable to choose the grouping in such a way that the proportional variation of a particular cross-section, or series of cross-sections, is to be given more weight than that of others.

When the criterion has been used to suppress an energy range, the new cross-sections are calculated according to formula (2). As was pointed out, this method

is equivalent to averaging the mean free paths for successive energy ranges and also the proportions of occasions when a given action occurs. It can be shown that this procedure is justified if the energy spectrum of neutrons, in the Monte Carlo, is uniform over the range; since this spectrum is determined by the cross-sections themselves, this assumption is not strictly legitimate. Since the neutron spectrum varies from problem to problem, the best method of grouping should depend also upon the problem under consideration; to avoid defining the energy bands in different ways for different problems, the methods described above must be used throughout.

Neutron secondary energy laws occur in either a continuous or a discrete form. Where the laws are of a discrete nature no processing is required, the appropriate expressions being programmed as part of the main Monte Carlo tracking programme.

The continuous laws comprise:

(*a*) Secondary energy laws of the continuous-energy-spectrum type, the spectrum depending on the neutron's incident energy;

(*b*) Fission spectra, and other special spectra; and

(*c*) Elastic scatter spectra; here the basic quantity obtained is emergent angle, and the emergent energy is calculated as a function of this.

The main way of handling these continuous laws is the same in all three cases. If the appropriate spectrum in the laboratory system is $f(E)$ (implying that there is a probability $f(E)\,\mathrm{d}E$ that the emergent energy lies between $E$ and $E+\mathrm{d}E$) a set of quantities $\{E_l\}$ is defined by the equations

$$\int_{-\infty}^{E_l} f(E)\,\mathrm{d}E = a_l \int_{-\infty}^{\infty} f(E)\,\mathrm{d}E = a_l\,. \tag{6}$$

$E$ relates to energy except in case (*c*), where $E$ is the cosine of the scatter angle. In both cases $f(E)$ will vanish over part of the range of integration. The $a_l$ are a specified set of numbers.

The fidelity of the representation of the spectrum $f(E)$ by $\delta$-functions at the $E_l$ depends on the size and the spacing of the set $a_l$. In practice the choice of the $E_l$ is resolved by drawing at random one from a set of $2^m$ random numbers. Thus the $a_l$ are equally spaced and defined by

$$a_l = -2^{-m-1} + l\cdot 2^{-m}\ (l=1, 2 \ldots 2^m)\,. \tag{7}$$

Thus what is required in the storage of the machine when doing Monte Carlo calculations are the quantities $\{E_l\}$, and these are obtained by solving (6). The programme is, in addition, equipped to deal with special requirements such as the conversion from centre-of-mass to laboratory co-ordinates in the case of elastic scatter.

The programme accepts the co-ordinates of points on the curve $y=f(E)$ selected (and available from the punched-card library) in such a way that interpolation provides a sufficiently accurate representation of the function. The maximum number of points is 200 and the output is generally 32 values of $\{E_l\}$. Some examples of the use of the programme are given below.

*Angular distribution of elastically scattered neutrons*

Values of differential cross-sections as a function of $\cos\theta$, $\theta$ being angle in the centre-of-mass system, are available from the punched-card library. These

quantities are fed into the programme as point-pairs, and 32 equiprobable values of $\cos\theta$ are selected by solving (6). These are converted into the laboratory system by the formula

$$\cos\varphi = (1 + A\cos\theta)/(1 + 2A\cos\theta + A^2)^{1/2} \tag{8}$$

where $A$ is the atomic weight of the isotope or element. Associated with each scatter angle is an energy-loss factor, $p(\theta)$, the neutron's new energy being given by the formula

$$E/E_0 = p(\theta) = (A^2 + 2A\cos\theta + 1)/(A+1)^2 \tag{9}$$

where $E_0$ is the incident energy.

The machine-time taken for such a calculation is quite short. For a given element, several runs (perhaps ten or more) will be required, since the functional form of the differential cross-section varies with incident energy.

*Energy at inelastic scatter*

Direction after an inelastic collision (n, n′) is normally assumed to be isotropic in the laboratory system, but where other evidence is available, the angular distribution can be prepared in a manner similar to that explained above. For energy loss, three types of law are in general use, these being of the form $E = tE^q{}_0$, where $q$ is either 0, $^1/_2$ or 1. The probability distribution of $t$ is available and 32 equiprobable values of $t$ are selected by the programme.

Fuller details of the AWRE system of producing data for Monte Carlo calculations are given in [7].

There are at least two disadvantages in the procedure outlined above in that (*a*) the preparation programme must generally be run for each new task, and (*b*) all neutron cross-sections occurring within a material are represented by $n$ quantities, where $n$ is the number of energy groups: if the cross-section occurs non-zero over only a small energy range, most of the $n$ quantities will be zero.

A revised collision routine programme now being written will overcome these difficulties in the following manner.

(*a*) The input consists of appropriate (to the nuclides in question) cards from the "punched-card library of neutron cross-sections" giving direct input from this library to the tracking programme.

(*b*) Cross-sections are grouped individually so that, for a particular nuclide, one cross-section may be specified by only three step-functions while another may be specified by as many as 100 independent step-functions.

## 3. Group constants for Carlson $S_n$ and other calculations

### 3.1 Derivation of group equations and definitions of group constants

The time-dependent neutron transport equation can be written

$$\frac{1}{v}\frac{\partial f}{\partial t}(\mathbf{r}, E, \mathbf{\Omega}, t) + \mathbf{\Omega}.\,\mathrm{grad}\, f(\mathbf{r}, E, \mathbf{\Omega}, t) + \alpha(\mathbf{r}, E, t)\, f(\mathbf{r}, E, \mathbf{\Omega}, t) =$$
$$= \int\int \beta(\mathbf{r}, E' \to E, \mathbf{\Omega}' \to \mathbf{\Omega}, t)\, f(\mathbf{r}, E', \mathbf{\Omega}', t)\, \mathrm{d}E'\, \mathrm{d}\mathbf{\Omega}' + S(\mathbf{r}, E, \mathbf{\Omega}, t). \tag{10}$$

In this equation $f(\mathbf{r}, E, \mathbf{\Omega}, t)$ is the angular flux, and $f(\mathbf{r}, E, \mathbf{\Omega}, t)\,\mathrm{d}r\,\mathrm{d}E\,\mathrm{d}\mathbf{\Omega}$ is equal to the number of neutrons in volume element $\mathrm{d}\mathbf{r}$ about $\mathbf{r}$ and in energy element $\mathrm{d}E$ about $E$ crossing the element $\mathrm{d}\mathbf{\Omega}$ on the unit sphere per unit time

at time $t$ ($\mathrm{d}\mathbf{\Omega}$ is normal to the direction $\mathbf{\Omega}$). The neutron speed is $v$, and $\mathbf{\Omega}$ is a unit vector in the direction of motion of the neutron. $\alpha(\mathbf{r}, E, t)$ is the macroscopic total neutron cross-section for neutrons of energy $E$ at position $\mathbf{r}$ at time $t$, while $\beta(\mathbf{r}, E' \to E, \mathbf{\Omega}' \to \mathbf{\Omega}, t)\,\mathrm{d}E\,\mathrm{d}\mathbf{\Omega}$ is the number of secondary neutrons with $E$ in $(E, E+\mathrm{d}E)$ and $\mathbf{\Omega}$ in $(\mathbf{\Omega}, \mathbf{\Omega}+\mathrm{d}\mathbf{\Omega})$ produced by one primary neutron with energy $E'$ travelling in direction $\mathbf{\Omega}'$ per unit path-length at position $\mathbf{r}$ and time $t$.

$S(\mathbf{r}, E, \mathbf{\Omega}, t)\,\mathrm{d}\mathbf{r}\,\mathrm{d}E\,\mathrm{d}\mathbf{\Omega}$ is the number of neutrons released per unit time with $E$ in $(E, E+\mathrm{d}E)$ and $\mathbf{\Omega}$ in $(\mathbf{\Omega}, \mathbf{\Omega}+\mathrm{d}\mathbf{\Omega})$ in volume element $\mathrm{d}\mathbf{r}$ about $\mathbf{r}$ at time $t$.

If the time-dependence is separated out in the form $\mathrm{e}^{\lambda t}$ the first term on the left-hand side of (10) is replaced by $(\lambda/v)\,f(\mathbf{r}, E, \mathbf{\Omega})$ where $f$ is now independent of $t$.

The directional derivative $\mathbf{\Omega}.\,\mathrm{grad}\,f$ takes on different forms according to the geometry of the system under consideration.

From (10), group equations for non-overlapping groups are conventionally derived by integration over each energy group, assuming that the mean free path and scattering cross-sections can be regarded as constant both within each group and between each group and any other.

The form of the group equations is then

$$\frac{1}{v_g}\frac{\partial \Phi_g}{\partial t}(\mathbf{r}, \mathbf{\Omega}, t) + \mathbf{\Omega}.\,\mathrm{grad}\,\Phi_g(\mathbf{r}, \mathbf{\Omega}, t) + \alpha_g(\mathbf{r}, t)\,\Phi_g(\mathbf{r}, \mathbf{\Omega}, t) = \\ = \sum_{g'} \int \beta_{g'g}(\mathbf{r}, \mathbf{\Omega}' \to \mathbf{\Omega}, t)\,\Phi_{g'}(\mathbf{r}, \mathbf{\Omega}', t)\,\mathrm{d}\mathbf{\Omega}' + S_g(\mathbf{r}, \mathbf{\Omega}, t) \tag{11}$$

with

$$\frac{1}{v_g} = \frac{1}{(\Delta E)_g}\int_g \frac{1}{v}\,\mathrm{d}E \tag{12}$$

$$\alpha_g(\mathbf{r}, \mathrm{t}) = \frac{1}{(\Delta E)_g}\int_g \alpha(\mathbf{r}, E, t)\,\mathrm{d}E \tag{13}$$

$$\beta_{g'g}(\mathbf{r}, \mathbf{\Omega}' \to \mathbf{\Omega}, t) = \frac{1}{(\Delta E)_g}\int_{g'} \mathrm{d}E' \int_g \mathrm{d}E\,\beta(\mathbf{r}, E' \to E, \mathbf{\Omega}' \to \mathbf{\Omega}, t) \tag{14}$$

and

$$S_g(\mathbf{r}, E, \mathbf{\Omega}, t) = \int_g S(\mathbf{r}, E, \mathbf{\Omega}, t)\,\mathrm{d}E \tag{15}$$

as "reasonable" definitions of the group parameters. The angular flux per group is $\Phi_g$, while $(\Delta E)_g = \int_g \mathrm{d}E$, the group width.

The above derivation of the group equations is not very convincing, being more plausible than rigorous, and this has led to investigations of other methods of deriving group equations with a view to seeing just which approximations are involved. One method of approach is to expand the angular flux $f$ in a finite or infinite series as follows:

$$f(\mathbf{r}, E, \mathbf{\Omega}, t) = \sum \Phi_g(\mathbf{r}, \mathbf{\Omega}, t)\,F_g(E). \tag{16}$$

Usually the $F_g(E)$ are taken to be orthornormal and in this case substitution of (16) in (10) followed by multiplication by $F_{g'}(E)$ and integration over energy

leads to group equations of type (11) but with different definitions of the group constants.

Later work has shown that an expansion of type (16) is too restricted and that the properties of equation (10) are such that it must be considered in conjunction with the adjoint equation. When source terms are neglected and an $e^{\lambda t}$ time dependence is introduced, the transport equation and its adjoint become

$$\mathcal{L} f = -\frac{\lambda}{v} f \tag{17}$$

$$\mathcal{L}^* f^* = -\frac{\lambda^*}{v} f^* \tag{18}$$

where the operator $\mathcal{L}$ and its adjoint $\mathcal{L}^*$ are defined by

$$\mathcal{L} \equiv \mathbf{\Omega}.\,\mathrm{grad} + \alpha(\mathbf{r}, E) - \iint \beta(\mathbf{r}, E' \to E, \mathbf{\Omega}' \to \mathbf{\Omega})\,\mathrm{d}E'\,\mathrm{d}\,\mathbf{\Omega}' \tag{19}$$

$$\mathcal{L}^* \equiv -\mathbf{\Omega}.\,\mathrm{grad} + \alpha(\mathbf{r}, E) - \iint \beta(\mathbf{r}, E \to E', \mathbf{\Omega} \to \mathbf{\Omega}')\,\mathrm{d}E'\,\mathrm{d}\,\mathbf{\Omega}'. \tag{20}$$

The boundary condition on $f$ is that $f(\mathbf{r}, E, \mathbf{\Omega}, t)$ shall be zero on the boundaries for all values of $\mathbf{\Omega}$ corresponding to inward motion while that on $f^*$ is that $f^*(\mathbf{r}, E, \mathbf{\Omega}, t)$ shall be zero on the boundaries for all values of $\mathbf{\Omega}$ corresponding to outward motion.

The starting point for the derivation of group equations is then the variational principle which states that the integral

$$J = \frac{\int f^*(\mathbf{r}, E, \mathbf{\Omega})\,\mathcal{L} f(\mathbf{r}, E, \mathbf{\Omega})\,\mathrm{d}\mathbf{r}\,\mathrm{d}E\,\mathrm{d}\mathbf{\Omega}}{\int f^*(\mathbf{r}, E, \mathbf{\Omega})\,\frac{1}{v} f(\mathbf{r}, E, \mathbf{\Omega})\,\mathrm{d}\mathbf{r}\,\mathrm{d}E\,\mathrm{d}\mathbf{\Omega}} \tag{21}$$

is stationary with respect to variation of $f$ and $f^*$ if, and only if, $f$ and $f^*$ are solutions of the normal and adjoint transport equations respectively and the value that $J$ then attains is an eigenvalue of the operators $\mathcal{L}$ and $\mathcal{L}^*$.

It can be shown that the solutions of (17) and (18) which are everywhere non-negative have the same eigenvalue so that $\lambda = \lambda^*$ and probably all the eigenvalues of $\mathcal{L}$ are also eigenvalues of $\mathcal{L}^*$.

To obtain group equations one substitutes trial functions for $f$ and $f^*$ of the form

$$f(\mathbf{r}, E, \mathbf{\Omega}) = \sum_{g=1}^{G} \Phi_g(\mathbf{r}, \mathbf{\Omega})\,F_g(E) \tag{22}$$

$$f^*(\mathbf{r}, E, \mathbf{\Omega}) = \sum_{g=1}^{G} \Phi^*_g(\mathbf{r}, \mathbf{\Omega})\,H_g(E) \tag{23}$$

and requires that (21) be stationary for small variations of $\Phi_g$ and $\Phi_g{}^*$. Alternative separations of the variables may introduce an artificial polarity into the medium. Initially the only restrictions on the functions $F_g(E)$ and $H_g(E)$ are that they are mutually orthogonal so that

$$\int H_{g'}(E)\,F_g(E)\,\mathrm{d}E = K_g\,\delta_{g'g} \tag{24}$$

where $K_g$ are constants and the integral extends over the whole range of $E$.

The expansions (22) and (23) can be exact in general only if the $F_g(E)$ and $H_g(E)$ form complete sets and in this case the number of functions will generally be infinite. In the case of finite $G$, (22) and (23) generally represent an approximation which may be improved by suitable choice of $F_g$ and $H_g$ or by increase of $G$.

Substitution of (22) and (23) into (21) and satisfaction of the variational principle lead to the equations

$$\mathbf{\Omega}.\ \text{grad}\ \Phi_g + \sum_{g'=1}^{G} \alpha_{g'g}(\mathbf{r})\,\Phi_{g'}(\mathbf{r},\mathbf{\Omega}) - \sum_{g'=1}^{G} \int \beta_{g'g}(\mathbf{r},\mathbf{\Omega}'\to\mathbf{\Omega})\,\Phi_{g'}(\mathbf{r},\mathbf{\Omega}')\,\mathrm{d}\mathbf{\Omega}' = \\ = -\lambda \sum_{g'=1}^{G} \frac{1}{v_{g'g}}\,\Phi_{g'}(\mathbf{r},\mathbf{\Omega}) \tag{25}$$

and

$$-\mathbf{\Omega}.\ \text{grad}\ \Phi^*_g + \sum_{g'=1}^{G} \alpha^*_{g'g}(\mathbf{r})\,\Phi^*_{g'}(\mathbf{r},\mathbf{\Omega}) - \sum_{g'=1}^{G} \int \beta^*_{g'g}(\mathbf{r},\mathbf{\Omega}\to\mathbf{\Omega}')\,\Phi^*_{g'}(\mathbf{r},\mathbf{\Omega}')\,\mathrm{d}\,\mathbf{\Omega}' = \\ = -\lambda \sum_{g'=1}^{G} \frac{1}{v^*_{g'g}}\,\Phi^*_{g'}(\mathbf{r},\mathbf{\Omega}) \tag{26}$$

subject to the same boundary conditions for $\Phi_g$ and $\Phi_g{}^*$ as for $f$ and $f^*$ below equation (20). The various group constants are defined by

$$\alpha_{g'g}(\mathbf{r}) = \frac{1}{K_g}\int H_g(E)\,\alpha(\mathbf{r},E)\,F_{g'}(E)\,\mathrm{d}E \tag{27}$$

$$\alpha^*_{g'g}(r) = \frac{1}{K_g}\int F_g(E)\,\alpha(\mathbf{r},E)\,H_{g'}(E)\,\mathrm{d}E \tag{28}$$

$$\beta_{g'g}(r,\mathbf{\Omega}'\to\mathbf{\Omega}) = \frac{1}{K_g}\int \mathrm{d}E\,H_g(E)\int \mathrm{d}E'\,F_{g'}(E')\,\beta(\mathbf{r},E'\to E,\mathbf{\Omega}'\to\mathbf{\Omega}) \tag{29}$$

$$\beta^*_{g'g}(\mathbf{r},\mathbf{\Omega}\to\mathbf{\Omega}') = \frac{1}{K_g}\int \mathrm{d}E\,F_g(E)\int \mathrm{d}E'\,H_{g'}(E')\,\beta(\mathbf{r},E\to E',\mathbf{\Omega}\to\mathbf{\Omega}') \tag{30}$$

$$\frac{1}{v_{g'g}} = \frac{1}{K_g}\int H_g(E)\,\frac{1}{v}\,F_{g'}(E)\,\mathrm{d}E \tag{31}$$

$$\frac{1}{v_{g'g}{}^*} = \frac{1}{K_g}\int F_g(E)\,\frac{1}{v}\,H_{g'}(E)\,\mathrm{d}E. \tag{32}$$

If the energy range is now divided into $G$ intervals and $F_g(E)$ and $H_g(E)$ are required to be non-zero in the energy interval $g$ and zero elsewhere, then the off-diagonal terms in (27), (28), (31) and (32) disappear, but off-diagonal terms remain in (29) and (30).

Thus far the functions $F_g$ and $H_g$ remain very general. It is useful (but not essential) to ensure that $\beta^*_{gg'}(\mathbf{r},\mathbf{\Omega}'\to\mathbf{\Omega}) = \beta_{g'g}(\mathbf{r},\mathbf{\Omega}'\to\mathbf{\Omega})$ and examination

of (29) and (30) shows that this is true provided $K_g = K_{g'} =$ constant. In this case (24) is replaced by

$$\int H_{g'}(E) F_g(E) \, \mathrm{d}E = K \delta_{g'g} \, . \tag{33}$$

Another desirable feature for group constants is that they should exhibit the same conservation rules as the neutron cross-sections from which they are derived. For example, in the elastic scattering of neutrons by a light nucleus there is slowing-down, but the number of neutrons is unchanged so that

$$\alpha^{\mathrm{e}}(\mathbf{r}, E) = \int\int \beta^{\mathrm{e}}(\mathbf{r}, E \to E', \mathbf{\Omega} \to \mathbf{\Omega}') \, \mathrm{d}E' \, \mathrm{d}\mathbf{\Omega}' \tag{34}$$

the index e denoting elastic scattering with $\alpha^{\mathrm{e}}$ corresponding to the integrated elastic cross-section. If the group constants produced from $\alpha^{\mathrm{e}}(\mathbf{r}, E)$ and $\beta^{\mathrm{e}}(\mathbf{r}, E \to E', \mathbf{\Omega} \to \mathbf{\Omega}')$ are $\alpha^{\mathrm{e}}_g(r)$ and $\beta^{\mathrm{e}}_{gg'}(\mathbf{r}, \mathbf{\Omega} \to \mathbf{\Omega}')$ then one must satisfy

$$\alpha^{\mathrm{e}}_g(\mathbf{r}) = \sum_{g'=1}^{G} \int \beta^{\mathrm{e}}_{gg'}(\mathbf{r}, \mathbf{\Omega} \to \mathbf{\Omega}') \, \mathrm{d}\mathbf{\Omega}' \, . \tag{35}$$

This and similar relations can only be true in general if $H_g(E)$ is a constant at all energies for which it is non-zero.

A final restriction has to be placed on the $F_g(E)$ in order that the dependent variable $\Phi_g(\mathbf{r}, \mathbf{\Omega})$ has the conventional dimensions of angular flux per group and from (22) this means

$$\int F_g(E) \, \mathrm{d}E = 1 \, . \tag{36}$$

Bearing the above considerations in mind, one can simplify equations (25) — (32) to give the following group equations and definitions of group constants:

*Normal group equation*

$$\mathbf{\Omega} . \operatorname{grad} \Phi_g(\mathbf{r}, \mathbf{\Omega}) + \alpha_g(\mathbf{r}) \Phi_g(\mathbf{r}, \mathbf{\Omega}) - \sum_{g'=1}^{G} \int \beta_{g'g}(\mathbf{r}, \mathbf{\Omega}' \to \mathbf{\Omega}) \Phi_{g'}(\mathbf{r}, \mathbf{\Omega}') \, \mathrm{d}\mathbf{\Omega}' = -\frac{\lambda}{v_g} \Phi_g(\mathbf{r}, \mathbf{\Omega}) \tag{37}$$

*Adjoint group equation*

$$-\mathbf{\Omega} . \operatorname{grad} \Phi^*_g(\mathbf{r}, \mathbf{\Omega}) + \alpha_g(\mathbf{r}) \Phi^*_g(\mathbf{r}, \mathbf{\Omega}) - \sum_{g'=1} \int \beta^*_{g'g}(\mathbf{r}, \mathbf{\Omega} \to \mathbf{\Omega}') \Phi^*_g(\mathbf{r}, \mathbf{\Omega}') \, \mathrm{d}\mathbf{\Omega}' = -\frac{\lambda}{v_g} \Phi^*_g(\mathbf{r}, \mathbf{\Omega}) \tag{38}$$

with

$$\alpha_g(\mathbf{r}) = \int_g \alpha(\mathbf{r}, E) \, F_g(E) \, \mathrm{d}E \tag{39}$$

$$\frac{1}{v_g} = \int_g \frac{1}{v} F_g(E) \, \mathrm{d}E \tag{40}$$

$$\beta_{g'g}(\mathbf{r}, \mathbf{\Omega}' \to \mathbf{\Omega}) = \beta^*_{gg'}(\mathbf{r}, \mathbf{\Omega}' \to \mathbf{\Omega}) = \int_g \mathrm{d}E \int_{g'} \mathrm{d}E' \, F_{g'}(E') \, \beta(\mathbf{r}, E' \to E, \mathbf{\Omega}' \to \mathbf{\Omega}) \tag{41}$$

$$\int_g F_g(E)\,\mathrm{d}E = 1\,. \tag{42}$$

In (39)—(42) $\int_g \mathrm{d}E$ denotes the integral over the energy range where $F_g(E)$ is non-zero.

Since it has been arranged that $\Phi_g(\mathbf{r}, \mathbf{\Omega})$ represents angular flux per group, it follows that $\Phi^*_g(\mathbf{r}, \mathbf{\Omega})$ represents the importance of a neutron of any energy in group $g$ at position $\mathbf{r}$ moving in direction $\mathbf{\Omega}$.

It should be noted that the variable $E$ in $f(\mathbf{r}, E, \mathbf{\Omega}, t)$ may be replaced by either $v$, the neutron velocity, or $u$ the lethargy, the derivation being virtually unchanged except in regard to dimensions of quantities.

The set of equations (37—40) provides a basis for the multi-group solution of the transport equation, and inspection of (37) and (38) shows that $\Phi^*_g(\mathbf{r}, \mathbf{\Omega})$ satisfies the same type of equation at $\Phi_g(\mathbf{r}, -\mathbf{\Omega})$. Although their derivation is much more satisfactory than that of equations (11—15) a number of difficulties remains unsolved, particularly as regards the physical significance of the adjoint quantities under the various restrictions and their relation to the concept of neutron importance.

The choice of $G$ and the group boundaries to give maximum accuracy in the solution is discussed in Section 3.3.

### 3.2 Specializations and simplifications

A number of simplifications can often be made in equations (37) and (42).

The form of the derivative operator $\mathbf{\Omega}.\,\mathrm{grad}$ depends on the geometry considered. For instance, in spherical geometry there are two space variables $r$ and $\mu$ and $\Phi_g(\mathbf{r}, \mathbf{\Omega}) \to \Phi_g(r, \mu)$, while

$$\mathbf{\Omega}.\,\mathrm{grad} = \mu \frac{\partial}{\partial r} + \frac{1-\mu^2}{r}\frac{\partial}{\partial \mu} \tag{43}$$

where $\cos^{-1}\mu$ is the angle between the outward radius vector and the direction of motion of the neutron.

For all processes leading to secondary neutrons normally considered, $\beta$ depends only on $E$, $E'$ and $\overline{\mu}$, where $\cos^{-1}\overline{\mu}$ is the angle between the directions of the incident and secondary neutrons. In isotropic scattering $\beta$ is in fact independent of $\overline{\mu}$ and this leads to considerable simplifications in the terms involving $\beta$. In spherical geometry we have

$$\int \beta_{g'g}(\mathbf{r}, \mathbf{\Omega}' \to \mathbf{\Omega})\,\Phi_{g'}(\mathbf{r}, \mathbf{\Omega}')\,\mathrm{d}\,\mathbf{\Omega}' \to \frac{1}{2}\beta_{g'g}(r)\,\varphi_{g'}(r) \tag{44}$$

with

$$\varphi_{g'}(r) = \int_{-1}^{1} \Phi_{g'}(r, \mu')\,\mathrm{d}\,\mu' \tag{45}$$

$$\beta_{g'g}(r) = \int_g \mathrm{d}E \int_{g'} \mathrm{d}E'\,F_{g'}(E)\,\beta(r, E' \to E) \tag{46}$$

where

$$\beta(r, E' \to E) = 2\,\beta(r, E' \to E, \overline{\mu}) = 4\pi\,\beta(r, E' \to E, \mathbf{\Omega}' \to \mathbf{\Omega}). \tag{47}$$

Formally similar equations hold in plane geometry.

Unfortunately, isotropic elastic scattering of neutrons is scarcely ever encountered in practice. In many instances it is possible to make some kind of transport approximation in which an isotropic-scattering problem is solved with modified group constants. Alternatively the anisotropy of scattering may be allowed for to any desired accuracy. These topics form the subject of another paper submitted to this Seminar [8]. For our purposes it is sufficient to note that in the so-called "diagonal transport approximation", a transport equation of the normal form is solved with $\bar{\alpha}_g$, $\bar{\beta}_{g'g}$ replacing $\alpha_g$ and $\beta_{g'g}$ where

$$\bar{\alpha}_g = \alpha_g - \beta^1_{gg} \tag{48}$$

$$\bar{\beta}_{g'g} = \beta^0_{g'g} - \delta_{g'g}\beta^1_{gg} \tag{49}$$

where the moments of the scattering matrix are given by

$$\beta^l_{g'g}(\mathbf{r}) = \int_{-1}^{+1} \beta_{g'g}(\mathbf{r}, \bar{\mu}) P_l(\bar{\mu})\, \mathrm{d}\bar{\mu}\,. \tag{50}$$

These moments are used in the "exact" solution of the transport equation when anisotropic scattering is taken into account. In the compiling of group constants it is therefore desirable to compute the values of the $\beta^l_{g'g}(r)$.

Thus far our development of the theory has been made with a view to applying it to the Carlson $S_n$ method of solving the group equations derived from the exact transport equation. A similar development can be made using the diffusion theory equation and for the present purposes it is only necessary to note that the group-averaged quantities which arise have a somewhat different form from those already derived. Quantities to be calculated include

$$\left(\frac{1}{\bar{\sigma}_{\mathrm{tr}}}\right)_g = \int_g \frac{1}{\sigma_{\mathrm{tr}}} F_g(E)\, \mathrm{d}E \tag{51}$$

$$(\overline{\nu\sigma_{\mathrm{f}}})_g = \int \nu\sigma_{\mathrm{f}} F_g(E)\, \mathrm{d}E \tag{52}$$

$$(\bar{\sigma}_{\mathrm{f}})_g = \int \sigma_{\mathrm{f}} F_g(E)\, \mathrm{d}E \tag{53}$$

and

$$(\sigma_{\mathrm{abs}})_g = \int \sigma_{\mathrm{abs}} F_g(E)\, \mathrm{d}E \tag{54}$$

where $\sigma_{\mathrm{abs}}$ is the cross-section for parasitic absorption. Any machine programme for calculating group-averaged quantities can readily be adapted to calculate these quantities.

### 3.3 Principles of group-constant formation

The derivation of group equations and the discussion of the possible simplifications already given show just what quantities must normally be calculated.

In the forming of group constants with non-overlapping groups (overlapping groups are possible but are not considered here), a choice must be made of the number of groups $G$, group boundaries and weighting spectra $F_g(E)$. This choice depends on the nature of the problem to be solved, and the rules governing the choice are of a semi-empirical nature. Among the factors which should be taken into account are the following:

(*a*) Increase in the number of groups generally increases the amount of computation involved.
(*b*) Intelligent increase in the number of groups increases accuracy.
(*c*) The weighting spectra $F_g(E)$ should be chosen to approximate as closely as possible to the spectrum of the system under investigation. For instance, in a bare lump of highly enriched uranium, $F_g(E)$ might be taken as segments of the fission spectrum or a spectrum slightly degraded from the fission spectrum.
(*d*) Empirical adjustments can be made to group constants so that calculations reproduce the results of integral experiments.
(*e*) A highly accurate set of group constants (for a known type of problem) may be condensed to get a few-group set for use in rapid comparative calculations.

Although we have used the term group constants rather loosely throughout this paper, it is in fact most convenient to calculate group cross-sections (having dimensions of area) rather than true group constants which are obtained by multiplying the group cross-sections by the number of nuclei per unit volume, in other words, to deal with the microscopic rather than the macroscopic group constants. Group cross-sections are easier to handle than group constants in forming data for a mixture of materials, and with group constants one more item of information, the standard density, must be specified.

We can now distinguish "transfer cross-sections", consisting of data analogous to the usual "group constants", the data consisting of an array of order $G^2$ where $G$ is the number of groups, and "reaction rate cross-sections", which are vectors of order $G$ such that multiplication by quantities related to neutron densities and summation over groups give the number of reactions occuring per unit time.

In making detailed calculations of transfer cross-sections one can work in terms of energy, velocity or lethargy, the latter being defined by

$$u = A \ln (B/E). \tag{55}$$

$A$ and $B$ are suitable constants.

If $\sigma(E)$ is the cross-section for a neutron scattering (elastic or inelastic) reaction as a function of $E$, and if $\Gamma(E', E, \bar{\mu})\, \mathrm{d}E\, \mathrm{d}\bar{\mu}$ is the probability that an incident neutron of energy $E'$ is scattered through an angle whose cosine lies between $\bar{\mu}$ and $\bar{\mu} + \mathrm{d}\bar{\mu}$ and leaves with an energy between $E$ and $E + \mathrm{d}E$, then for this particular process we can define [using (39) and (41)]

$$\beta_{g'g}(\bar{\mu}) = \int_g \mathrm{d}E \int_{g'} \mathrm{d}E'\, F_{g'}(E')\, \sigma(E')\, \Gamma(E', E, \bar{\mu}) \tag{56}$$

$$\alpha_g = \int_g \sigma(E)\, F_g(E)\, \mathrm{d}E \tag{57}$$

with

$$\int_g F_g(E)\, \mathrm{d}E = 1\,. \tag{42}$$

$F_g(E)$ is the weighting spectrum for group $g$.

All the above formulae apply if energy is replaced throughout by lethargy.

In the case of absorption processes (i.e. processes in which *no* secondary neutrons are produced) $\beta_{g'g} = 0$ for all $g'$ and $g$, and only $\alpha_g$ is non-zero.

In the case of fission and other multiplicative processes (e.g., (n, 2n) and (n, 3n) reactions), there is an additional factor in (56) depending on the number of secondaries per primary.

The moments of the $\beta_{g'g}$ $(\overline{\mu})$ are defined by (50).

The values of $\alpha_g$ and $\beta^l_{g'g}$, to be inserted in the transport equation are, of course, the sums of the $\alpha_g$ and $\beta^l_{g'g}$ over all possible reactions.

The actual form of (56) is dependent on the form in which the differential cross-section is specified. The choice made in this paper is determined by the form of specification of angular distributions in the AWRE punched-card library of neutron cross-sections [7], where the angular distribution is specified as a normalized probability distribution in $\overline{\mu}$ for inelastic processes and in cos $\theta$ ($\theta$ = centre-of-mass scattering angle) for elastic scattering.

Reaction rate cross-sections are defined by

$$\sigma^p{}_g = \int_g \sigma^p(E)\, F_g(E)\, \mathrm{d}E \tag{58}$$

$\sigma^p$ $(E)$ is the cross-section for a particular reaction as a function of energy. This definition is, of course, formally the same as (57).

With this definition the number of reactions occurring per unit time per gram of material is given by

$$\dot{R}^p = N \sum_g \varphi_g\, \sigma_g{}^p \tag{59}$$

where $N$ is the number of nuclei present per gram and $\varphi_g$ is the scalar flux per group (i.e. the integral over angle of the angular flux per group $\Phi_g(\mu)$).

The group velocities $v_g$ are simply given by (40).

It is often convenient to provide information on the average energy-release per reaction in the various groups. This enables one to calculate the rate of energy gain by material due to the neutrons present. It is convenient to calculate quantities given by

$$\left(\overline{\sigma}\overline{E}\right)_g = \sum_p \int F_g(E)\, U^p(E)\, \sigma^p(E)\, \mathrm{d}\, E \tag{60}$$

where $\dot{U}^p$ $(E)$ is the average energy given to the material by a neutron of energy $E$ in a collision of type $p$ (again (42) is assumed to hold). $U^p$ $(E) = E - E_f + Q$, where $E$ is the incident neutron energy, $E_f$ is the average energy of the secondary neutrons and $Q$ is the energy released in the reaction.

If $\dot{U}$ is the rate of energy gain per gram by the material, we have (for a single nuclide)

$$\dot{U} = N \sum_g (\sigma E)_g\, \varphi_g \tag{61}$$

where $N$ is the number of nuclei present per gram.

Similar formulae hold for adjoint quantities and it is worth noting that the preceding definitions still apply in the limit of zero group-width, corresponding to monoenergetic or $\delta$-function groups.

There are at least two possible methods of treating neutrons which are slowed down below the lowest energy covered by the groups used in any particular problem. If such neutrons are treated as being absorbed the transfer cross-sections

are referred to as *non-saving*. If one pretends that all neutrons slowed below the lowest energy covered are retained in the lowest energy group, the transfer cross-sections are referred to as *saving*. In this case the neutrons remain in the group until they are either absorbed (true absorption) or cause a fission, in which case fission neutrons appear in other groups covering the fission spectrum. It is perhaps best to distribute the elastically scattered neutrons isotropically.

Transfer cross-sections are generally specified for individual nuclides and it is often necessary to produce data for a mixture.

Suppose that, in a small region, the mixture is composed of nuclides $t=1$ (1) $T$ of atomic mass $A_t$ in proportions by nuclei $X_t$.

The concentration $x_t$ is given by

$$x_t = AX_t \Big/ \sum_{t=1}^{T} A_t X_t \tag{62}$$

(number of nuclei of type $t$ per gram of material)

where $A \times 10^{-24}$ is Avogadro's number, i.e. $A=0.6023$. Group constants for the mixture at 1 g/cm$^3$ can be found by evaluating scalar products of the form

$$\sum_{t=1}^{T} x_t \beta^t_{g'g} \quad \text{and} \quad \sum_{t=1}^{T} x_t \alpha^t_g \tag{63}$$

$\alpha^t_g$ and $\beta^t_{g'g}$ being measured in barns.

Similarly, the rate of energy gain per gram by the mixture becomes, when (61) is generalized,

$$\dot{U} = \sum_{t=1}^{T} x_t \sum_{g=1}^{G} \left(\overline{\sigma E}\right)^t_g \varphi_g \tag{64}$$

and, when (59) is generalized, the number of reactions of type $p, t$ occurring per second per gram of mixture is given by

$$\dot{R}^{p,t} = x_t \sum_{g=1}^{G} \varphi_g \sigma^{p,t}_g. \tag{65}$$

In some cases a mixture may be specified, for example, as "2 molecules water to 1 atom natural uranium", while in the library of group-averaged cross-sections there might be data for a molecule of water and for an atom of natural uranium. In this case the cross-sections would be combined as if two nuclides were involved, one of mass 18 and the other of mass 238.07. In general, cross-sections for a molecule will be found by summing those of the constituent atoms, while for a natural element averages of cross-sections and masses will be used.

It is desirable that sets of group constants should lead to agreement between measurement and calculation for integral systems. Leaving aside experimental errors, any disagreement may be due either to approximations in the calculation or errors in the neutron cross-sections used in constructing the group cross-sections. The following remarks essentially assume that the neutron cross-sections are correct, adjustment being made to take up errors caused by the finite group approximation.

If group constants are constructed by means of known formulae, they can then be adjusted to give agreement between theory and experiment for a number of integral experiments. Such adjustment is particularly desirable for systems involving fissile nuclides. Of course, one expects that with good methods of calculation and good neutron cross-sections the adjustment will be small. It should be noted that adjustment takes account of errors of calculation (e.g. use of the transport approximation) as well as of errors in the basic neutron cross-sections.

Two methods of adjustment have been used at AWRE. In the first, there is a uniform scaling in $\nu$, the number of neutrons per fission $\nu' = y\nu$, and in the second, new values of $\alpha_g$ and $\beta_{g'g}$ are calculated as follows:

$$\alpha'_g = \alpha_g - x\alpha_g^{\text{elastic}} \tag{66}$$

$$\beta'_{g'g} = \beta_{g'g} - x\,\delta_{g'g}\alpha_g^{\text{elastic}} \tag{67}$$

the value of $x$ being variable. *First and higher moments of $\beta$ are unaltered.*

The reason for this choice is that the first kind of adjustment can be used for the infinite medium time constant ($\lambda$) while the second can then be used for adjusting to give correct critical sizes without alteration of the infinite medium time constant.

Other and better methods of adjustment can be devised. The important thing is to specify what is being done and to be satisfied that the amount of adjustment is reasonable. This does not seem to have been done by all investigators.

It is often desirable to take a many-group set of group constants and condense it to give a few-group set of group constants, the two sets having certain common group boundaries. In this process it may be required to give different weights to the groups of the many-group set, this weighting being determined by the proportions of some calculated or measured spectrum falling within the various groups of the many-group set.

For convenience the many-group set may be referred to as class A constants and the few-group set as class B constants.

Suppose class A constants are denoted by the subscript $n$ and that group $g$ of the class B constants extends from the lower boundary of class A group $n_g$ to the upper boundary of class A group $m_g$, and suppose that $f_n$ is the proportion of the weighting spectrum in group $n$ of the class A set.

The class B constants are now given in terms of the class A constants by the formulae

$$\alpha^{\text{B}}_g = \sum_{n_g}^{m_g} \alpha^{\text{A}}_n f'_n \tag{68}$$

$$\left(\frac{1}{v_g}\right)^{\text{B}} = \sum_{n_g}^{m_g} \left(\frac{1}{v_n}\right)^{\text{A}} f'_n \tag{69}$$

$$\beta^{\text{B}}_{g'g} = \beta^{*\text{B}}_{gg'} = \sum_{n=n_g}^{m_g} \sum_{n'=n_{g'}}^{m_{g'}} \beta^{\text{A}}_{n'n} f'_{n'} \tag{70}$$

where
$$f'_n = f_n \Big/ \sum_{n=n_g}^{m_g} f_n \,. \tag{71}$$

### 3.4 Machine production of group cross-sections

The machine production of group constants obviously depends on the machine and on the form in which the microscopic (or macroscopic) cross-sections are supplied. In this section the systems and programmes developed at AWRE are described. These will be of practical interest to those having access to IBM 704, 709 or 7090 machines and of general interest to others.

The form in which the group cross-sections (or constants) are specified is governed principally by the input requirements of the Carlson $S_n$ or other programme with which they are to be used. It is desirable to have the constants available in print, on punched-cards and on tape.

Group constants (cross-sections) used at AWRE are classified by the following terms:

| | |
|---|---|
| *Number of groups* | —self-explanatory. |
| *Set number* | —distinguishes between different boundaries and weighting spectra for the same number of groups. |
| *Class* (useful rather than necessary for classification purposes) | —gives a guide to which sets are for use in high-accuracy calculations and which are for use in high-speed calculations. |
| *Transport number* | —distinguishes between sets having the same number of groups, same weighting spectra and same boundaries but different transport or empirical corrections. |
| *Data type* | —distinguishes between different forms of printed and punched-card output. |
| *Mark number* | —distinguishes between different sets of basic (input) neutron cross-sections. |
| *Composition* | —distinguishes between different nuclides, elements, etc. |
| *Saving or non-saving constants* | —distinguishes different ways of handling low-energy neutrons. |

The detailed meaning of these terms is as follows:

*Set number*. This is a number which distinguishes between sets of group constants having the same number of groups but having different group boundaries or different weighting spectra $F_g(E)$ or both. The set number is not used to distinguish between differences arising from different empirical adjustments of constants (see transport number) or the use of different sets of data from the AWRE punched-card library of (microscopic) cross-sections (see *Mark number*).

Note that there need be no connection whatever between, for example, 5-group, set 6 constants and 7-group, set 6 constants.

It is worth noting that groups are always ordered by decreasing energy (or increasing lethargy), i.e. the highest energy neutrons, are in group 1.

*Class*. Many-group constants for use in very high accuracy calculations or as a basis for collapse to fewer groups are said to be of class A.

Fewer- (but still "large") group constants for use in high-accuracy calculations, whether calculated directly from the microscopic cross-sections or by collapse of class A constants, are known as class B constants.

Few-group constants for use in high-speed fair-reliability routine calculations, whether calculated directly from the microscopic cross-sections or by collapse of class A or of class B constants, are known as class C constants. (These are useful where high reliability is not required or where the reliability can be inferred by other means.)

The differentiation between the three classes A, B and C is somewhat arbitrary but class will serve as some indication to an investigator of which particular set of constants should be used in his work.

*Transport number.* The transport number distinguishes between the different transport and empirical corrections applied to the same basic cross-sections (see Section 3.3) and is varied mainly during the construction of data-types 1 and 4 (see below for data-types 1 and 4).

*Data type.* Classification by data type distinguishes between transfer cross-sections (1—9) and reaction rate cross-sections (10—15). Typical data types used to date are as follows:

*Data-type 1.* These are isotropic (zeroth order moment) transfer cross-sections summed over all individual reactions with a diagonal transport correction applied. In most cases, further empirical adjustments will have been made (see *Transport number* above). Individual nuclides and mixtures of nuclides can be dealt with. This data is suitable for use in isotropic Carlson $S_n$ calculations except in programmes using a fission-source technique such as TDC.

*Data-type 3.* These are transfer cross-sections *for individual reactions.* No transport correction is applied and the zeroth, first, second... moments of the $\beta$'s are supplied separately. The main use of data-type 3 is in checking the cross-sections and studying the effects of varying microscopic cross-sections. Data-type 3 is not generally suitable as input in a machine solution of the transport equation.

*Data-type 4.* These are transfer cross-sections, summed over all individual reactions except fission. No transport correction is applied and the zeroth, first, second... moments of the $\beta$'s are supplied separately. The angular distribution of neutrons from fission is taken to be isotropic in the laboratory system so that fission neutrons only contribute to the zeroth moment of the $\beta$'s. In data-type 4, values of $(\nu\,\sigma_f)_g$ and the proportion of the fission spectrum in each group are given. Empirical adjustments to the data can be made as described in Section 3.3 (different adjustments implying different transport numbers).

These cross-sections can be used for anisotropic scattering calculations or for calculations involving a full transport correction.

*Data-type 5.* This data is the same as data-type 1 but is arranged in a form suitable for use with the Los Alamos TDC programme in which a fission-source term technique is used. It is similar to data-type 4 except that the first and higher moments of $\beta$ are omitted while a diagonal transport correction is applied to $\alpha$ and $\beta^0$.

*Data-type 10.* These are neutron-induced reaction cross-sections. A simplified, possibly incomplete, reaction specification is employed in that in many cases only the neutron fate is specified and not necessarily the nuclear particles. Thus the $C^{12}$ (n, n′) cross-section specified might consist of the sum of cross-sections for two possible reactions $C^{12}$ (n, n′) $3\alpha$ and $C^{12}$ (n, n′) $C^{12*}$.

Data-type 10 cards are suitable for reaction-rate analysis of calculations made using data-type 1 and 5 cards as basic data but are not generally suitable for

calculations requiring an exact specification of the reaction (e.g., isotopic concentration in irradiated plutonium).

*Data-type 11.* These are neutron-induced reaction cross-sections with a detailed specification of each reaction included. Only nuclides can be included in this type of data.

*Mark number.* The mark number distinguishes, for a fixed number of groups and fixed set number, between different initial microscopic cross-sections. For instance, when revised data is introduced for a particular nuclide in the AWRE

TABLE I

**BOUNDARIES OF GROUP CROSS-SECTION SETS**

| Class A | | Class B | | | | Class C | | |
|---|---|---|---|---|---|---|---|---|
| 32-group set 5 | 23-group Set 5 | 16-group Set 5 | 13-group Set 5 | 10-group Set 6 | 7-group Set 4 | 4-group Set 5 | 8-group Set 5 | 7-group Set 7 |
| (MeV) | (MeV) | (MeV) | (MeV) | (MeV) | (MeV) | (MeV) | (MeV) | (MeV) |
| 14.0 | 14.0 | 14.0 | — | 14.0 | — | — | — | — |
| 13.5 | 13.5 | 13.5 | — | 13.5 | — | — | — | — |
| 12.5 | 12.5 | — | — | — | — | — | — | — |
| 11.0 | 11.0 | 11.0 | 11.0 | 11.0 | 11.0 | 11.0 | 11.0 | 11.0 |
| 9.5 | 9.5 | — | — | — | — | — | — | — |
| 8.0 | 8.0 | — | — | — | — | — | — | — |
| 6.5 | 6.5 | 6.5 | — | 6.5 | — | — | — | — |
| 5.0 | 5.0 | — | — | — | — | — | — | — |
| 3.4 | 3.4 | — | — | — | — | — | — | — |
| 2.4 | 2.4 | 2.4 | 2.4 | 2.4 | 2.4 | — | — | — |
| 1.6 | 1.6 | — | — | — | — | 1.6 | 1.6 | 1.6 |
| 1.1 | 1.1 | 1.1 | 1.1 | 1.1 | 1.1 | — | — | — |
| 0.78 | 0.78 | — | — | — | — | 0.78 | 0.78 | 0.78 |
| 0.55 | 0.55 | 0.55 | 0.55 | 0.55 | 0.55 | — | — | — |
| 0.37 | 0.37 | — | — | — | — | — | — | — |
| 0.26 | 0.26 | 0.26 | 0.26 | 0.26 | 0.26 | — | — | — |
| 0.18 | 0.18 | — | — | — | — | 0.18 | 0.18 | 0.18 |
| 0.13 | 0.13 | 0.13 | 0.13 | 0.13 | 0.13 | — | — | — |
| (keV) | (keV) | (keV) | (keV) | (keV) | (keV) | (keV) | (keV) | (keV) |
| 80 | 80 | — | — | — | — | — | — | — |
| 43 | 43 | 43 | 43 | 43 | 43 | — | — | — |
| 22 | 22 | — | — | — | — | — | — | — |
| 10 | 10 | 10 | 10 | 10 | 10 | 10 | 10 | 10 |
| 4 | 4 | — | — | | | | — | — |
| 1.6 | 1.6 | 1.6 | 1.6 | | | | — | — |
| 0.65 | | — | — | | | | — | — |
| 0.26 | | 0.26 | 0.26 | | | | 0.26 | 0.26 |
| 0.11 | | — | — | | | | — | — |
| (eV) | | (eV) | (eV) | | | | (eV) | (eV) |
| 42 | | 42 | 42 | | | | — | — |
| 15 | | — | — | | | | 15 | 15 |
| 5.5 | | 5.5 | 5.5 | | | | — | — |
| 2.0 | | — | — | | | | — | — |
| 0.4 | | 0.4 | 0.4 | | | | 0.4 | 0.4 |
| Thermal | | Thermal | Thermal | | | | Ther-mal | |

punched-card library of (microscopic) cross-sections, there will be a new mark number for data for that nuclide in the library of group-averaged data.

*Composition.* Data can be specified for a single nuclide, a mixture of nuclides (including elements with several stable isotopes) or molecules.

*Saving or non-saving constants.* The distinction between saving and non-saving constants has already been discussed in Section 3.3.

Full details of the machine print-outs associated with the various data types are given in reference [9].

The vital link in the chain for producing group cross-sections is CANDY, an IBM-709 programme (an IBM-704 version is also available), which takes the data contained in the AWRE punched-card library of neutron cross-sections [7] and produces group cross-sections of the desired type.

There are two versions of CANDY. In CANDY-1, class A constants are formed using lethargy weighting. These can then be condensed using any given weighting spectrum. In CANDY-2, the restriction to lethargy weighting in the forming of class A constants has been removed and class A constants can be formed with any prescribed weighting (in accordance with formulae given in Section 3.3). The condensation part of the programme remains unaltered.

A full description of CANDY is given in reference [9]. Typical (IBM 709) machine-times are 3 min to produce output in two or three data-types for one nuclide (with off-line printing) using card input. Tape input is most economical when output of several data types is required for many nuclides. Data-type 4 with several moments takes a longer time (roughly 6 min for 4 moments, 9 min for 6 moments).

Many sets of group cross-sections have been prepared at AWRE. Indeed, with the availability of CANDY, one problem is to prevent the proliferation of sets of group cross-sections. With some thought it is possible to prepare standard sets applicable to a wide range of problems. At AWRE these sets are generally obtained from a basic class A 32-group (set 5) set formed by averaging the microscopic cross-sections with respect to lethargy. These are then condensed with appropriate weighting spectra to give derived class B and class C sets. Table I shows group boundaries for some standard sets currently in use. All these sets have been used in calculations on integral systems of interest in the physics of fast and intermediate reactors. Fuller details of the weighting spectra used in their construction are given in reference [9].

## 4. The future of mechanized processing of neutron cross-section data

There can be no doubt that, with the growing use of high-speed computers, libraries of neutron cross-sections will be more widely used in the next few years. Already many laboratories are showing great interest in the developments that have taken place so far. Neutronics calculations on high-speed computers are uneconomical without their use.

In the fast-reactor field the problems remaining appear to be relatively few. The systems of representation need extending to take account of the increasing data on non-elastic processes and to make fullest use of elastic scattering angular-distribution measurements. The main factor governing progress is the rate at which accurate measurements of microscopic data accumulate.

In the intermediate energy region the problems associated with resonances and with temperature effects—Doppler broadening, etc.—are still a formidable

barrier to the approach to perfection. It seems likely that below 1 keV the cross-sections of heavy nuclides should be generated from tabulated resonance parameters with a facility for including Doppler broadening. The definition of group cross-sections in this energy region is also a matter of some difficulty.

It is in the intermediate energy region (1 eV—1 keV for heavy nuclides) that we can expect in the next few years more important developments in the subject of mechanized processing of neutron cross-section data.

## ACKNOWLEDGEMENTS

The work reported here has only been made possible by the excellent team spirit of many past and present members of the Mathematical Physics Divisions at AWRE.

## REFERENCES

[1] HUGHES, D. J. and SCHWARTZ, R. B., BNL-325 2nd ed., Superintendent of Documents, U.S. Government Printing Office, Washington 25, D.C. (1958).
[2] HUGHES, D. J., MAGURNO, B. A. and BRUSSEL, M. K., BNL-325 2nd ed. suppl. No. 1, Superintendent of Documents, U.S. Government Printing Office, Washington 25, D.C. (1960).
[3] HOWERTON, R. J., UCRL-5226 (1958) and UCRL-5226 Revised (1959).
[4] HUGHES, D. J. and CARTER, R. S., BNL-400 (1956).
[5] PARKER, K., AWRE Report 0—27/60 (1960).
[6] BUCKINGHAM, B.R.S., PARKER, K. and PENDLEBURY, E. D., AWRE Report 0—28/60 (1960).
[7] PARKER, J. B. and PARKER, K., AWRE Report 0—20/60 (1960).
[8] PENDLEBURY, E. D. and UNDERHILL, L. H., *These proceedings*, vol. **II** p. 73.
[9] PARKER, K., AWRE Report 0—1/61 (1961).

SM—18/45

# AN ACCURATE TREATMENT OF RESONANCE SCATTERING IN LIGHT ELEMENTS IN FAST REACTORS*

H. HUMMEL AND A. RAGO
ARGONNE NATIONAL LABORATORY, ARGONNE, ILL.,
UNITED STATES OF AMERICA

**Abstract — Résumé — Аннотация — Resumen**

**An accurate treatment of resonance scattering in light elements in fast reactors.** The question of how to deal with the rapid fluctuation with energy of scattering cross-sections of the light- and medium-weight elements present in fast reactors has always been troublesome. Previous group cross-section evaluation work by one of the present authors and by others has treated this problem crudely. An IBM-704 code, ELMOE, has been prepared, which combines any desired standard cross-section set containing 10 to 20 groups available in a library of such sets with detailed data on the energy variation of the Legendre coefficients of the scattering cross-section of resonance scatterers. A fine group fundamental mode calculation is carried out using several hundred groups, and diffusion coefficients and elastic removal cross-sections are evaluated for the resonance scatterers for the standard groups. Application of the code has been made to various mixtures of uranium, aluminium, stainless steel and oxygen, corresponding to recent ZPR-III critical experiments. It is found that effective light- and medium-element group cross-sections show a significant variation with composition, particularly below about 500 keV, where resonance structure is more pronounced. This variation in a few extreme cases amounts to a factor of 2 or more.

**Traitement approprié de la diffusion par résonance dans les éléments légers dans les réacteurs à neutrons rapides.** On a toujours éprouvé des difficultés à tenir compte de la rapidité avec laquelle, dans les réacteurs à neutrons rapides, les sections efficaces de diffusion des éléments légers et intermédiaires varient en fonction de l'énergie. Des estimations de sections efficaces de groupes déjà publiées par l'un des auteurs et par d'autres ont donné une solution rudimentaire de ce problème. On a établi ici un code, ELMOE, pour une calculatrice IBM-704, qui réalise la combinaison entre n'importe quel ensemble de valeurs standard des sections efficaces pour 10 à 20 groupes pris dans un fichier *ad hoc* et les données détaillées relatives aux variations en fonction de l'énergie des coefficients de Legendre dans les expressions des sections efficaces de diffusion des diffuseurs résonnants. Par subdivision des groupes, on a effectué les calculs des modes fondamentaux avec plusieurs centaines de groupes et obtenu les coefficients de diffusion et les sections efficaces de déplacement élastique des milieux diffuseurs à résonance pour les groupes types.

Les auteurs ont appliqué le code à plusieurs mélanges d'uranium, d'aluminium, d'acier inoxydable et d'oxygène qui correspondent aux expériences critiques effectuées avec un réacteur du type ZPR-III. Ils ont constaté qu'en fait les sections efficaces de groupes composés d'éléments légers et intermédiaires varient sensiblement selon leur composition, notamment au-dessous de 500 keV environ, où la structure de résonance est plus prononcée. Dans quelques cas extrêmes, cette variation atteint un facteur 2 ou plus.

**Точное определение резонансного рассеяния в легких элементах в реакторах на быстрых нейтронах.** Обычно большие затруднения представляют быстрые изменения эффективных

* Work done under the auspices of the United States Atomic Energy Commission.

сечений рассеяния легких и средних элементов в зависимости от энергии нейтронов в реакторах на быстрых нейтронах. В предыдущей работе по оценке сечения по группам, проделанной одним из авторов данного доклада и другими, эта проблема не решена до конца. Был подготовлен код счетно-решающего устройства IBM-704, ELMOE, который совмещает любую желаемую стандартную систему сечений, состоящую из 10—20 групп, имеющихся в библиотеке таких систем, с подробными данными об энергетических вариациях коэффициентов Лежандра сечения рассеяния резонансных рассеивателей. Путем использования нескольких сотен групп выведен прекрасный фундаментальный групповой метод расчета; определены коэффициенты диффузии и сечения удаления (из пучка) в результате упругого рассеяния для резонансных рассеивателей стандартных групп.

Данный код применялся к различным смесям урана, алюминия, нержавеющей стали и кислорода, соответствующим недавно проведенным критическим опытам на реакторе нулевой мощности ZPR-III. Установлено, что значительные вариации эффективных сечений групп легких и средних элементов зависят от состава, особенно ниже примерно 500 кэв, когда более резко выражена резонансная структура. Эта вариация в нескольких предельных случаях составляет коэффициент порядка два или больше.

**Cálculos de precisión de la dispersión por resonancia en los elementos ligeros presentes en los reactores rápidos.** Siempre ha resultado difícil resolver los problemas que plantea la rápida fluctuación, en función de la energía, de las secciones eficaces de dispersión de los elementos ligeros e intermedios presentes en los reactores rápidos. Las evaluaciones de secciones eficaces de grupo ya publicadas por uno de los autores del presente trabajo y otros expertos brindan una solución parcial del problema. Se ha preparado una clave, llamada ELMOE, para la calculadora IBM-704, que permite combinar cualquier conjunto de secciones eficaces que se desee, para 10 a 20 grupos que figuren en un fichero *ad hoc*, con datos detallados sobre la variación, en función de la energía, de los coeficientes de Legendre en las expresiones de secciones eficaces de dispersión para los dispersadores por resonancia. Por subdivisión en grupos, se han calculado los modos fundamentales con varios centenares de grupos, obteniéndose los coeficientes de difusión y las secciones eficaces de eliminación elástica para los dispersadores por resonancia.

Los autores han aplicado esta clave a diversas mezclas de uranio, aluminio, acero inoxidable y oxígeno, que corresponden a experimentos críticos efectuados con el reactor ZPR-III. Se ha comprobado que las secciones eficaces de grupo de los elementos ligeros e intermedios varían sensiblemente según su composición, especialmente para energías inferiores a los 500 keV, en las que la estructura de resonancia es más pronunciada. El algunos casos extremos, esta variación alcanza un factor de 2 o superior.

## Introduction

Elastic scattering resonances in the light elements present in fast power reactors have always been troublesome since they cause rapid fluctuations in the scattering cross-sections of these materials, while variations of cross-sections of fissile and fertile materials in the fast region are comparatively slow. The change in the neutron leakage and flux caused by adding or removing the light materials is difficult to calculate exactly, because the elastic moderation introduced by these materials causes perturbation in the neutron energy spectrum in the vicinity of the resonances.

In order to deal more effectively with problems of this type, an IBM-704 code, ELMOE, has been prepared. This code calculates the Fourier transform of the neutron flux for a mixture of moderators heavier than H, with the moderator-scattering law rigorously taken into account. Approximations available in the

flux calculations are the usual P-1 and "consistent" P-1 and B-1 [1—3]. This code thus performs approximately the same calculation for moderators heavier than H as that which the MUFT codes [4] carry out for H. Although designed specifically for fast-reactor calculations, it can also be applied to thermal and intermediate reactors. No special provisions have yet been incorporated for dealing with capture resonances, however.

A feature of the code is that certain parameters which are slowly varying need be specified only for "coarse" groups which are much wider in energy than the "fine" groups used to take detailed account of elastic moderation. This greatly reduces the amount of input data required.

The coarse groups are those ordinarily used in fast-reactor calculations with a total of 10 to 20 groups spanning the fast region. A fine-group structure is superimposed over all or a part of the usual groups. Associated with each of the fine groups is a set of Legendre polynomial expansion coefficients of the scattering cross-section of each element. The original intention was that the fine group network be fine enough to trace out the detailed variation of each scattering cross-section. This has proved practicable except for the high resolution data of HIBDON [5] for scattering from Na, which are being specially handled as described later. From the Legendre polynomial expansion coefficients, elastic-transfer, transport, and elastic-removal cross-sections for the light elements are calculated for each fine group. Fission, capture, and inelastic-removal cross-sections are normally kept constant for the fine groups corresponding to a given coarse group. Variable capture cross-sections for the fine groups may be supplied if desired. Inelastic transfers and normally the fission source entering the fine groups are distributed in proportion to the fine-group energy widths. A variable fission source for the fine groups may be supplied if desired. No provision is made for inelastic transfers within coarse groups.

The fine groups all have the same lethargy width. Meshing of the coarse and fine groups is accomplished by a slight redefinition of the coarse-group energy limits. Although the fine-group lethargy width is arbitrary, in practice the labour involved in changing it except by integral multiples is such that only one width (and in some cases twice this width) has so far been used. This lethargy width is such that twenty times it corresponds to the maximum energy loss per collision in Na. With this width, 691 groups are required to cover the energy region from 3.67 MeV to 9 keV, which is the present range of the library of Legendre polynomial expansion coefficients. This is about as many groups as it seems practicable to handle on an IBM-704 with 32 000-word memory from the standpoint both of storage space and of machine time.

At least one coarse group at the top and bottom of the energy range must be handled in the usual way, i.e., not subdivided. Otherwise the fine-group region may cover any desired part of the energy spectrum. The groups not subdivided are calculated according to the usual equations for the Fourier transform. The equations for the fine-group region are given below.

## 1. P-1 approximation

For the P-1 approximation, the equation for the flux in the $k^{\text{th}}$ group is

$$\varphi^i{}_k = \frac{\beta_k + \psi_k}{\dfrac{B^2{}_i}{3\,\Sigma^k_{\text{tr}}} + \Sigma^k{}_{\text{a}} + \Sigma^k_{\text{elr}}} \tag{1}$$

where

$\varphi^i_k$ = $i^{\text{th}}$ iterate of the flux group $k$

$\beta_k$ = fraction of fission source in group $k$ (assumed same for all isotopes)

$\psi_k = \sum_{j=1}^{k-1} (\Sigma^{j\to k}_{\text{eltr}} + \Sigma^{j\to k}_{\text{intr}})\ \varphi^i_j$ = scattering source from higher energies

$\Sigma^{j\to k}_{\text{eltr}}$ = elastic-scattering transfer cross-section, group $j$ to group $k$

$\Sigma^{j\to k}_{\text{intr}}$ = inelastic-scattering transfer cross-section, group $j$ to group $k$

$\Sigma^k_{\text{a}}$ = absorption (total non-elastic removal) cross-section for group $k$

$\Sigma^k_{\text{elr}}$ = elastic-removal cross-section for group $k$

$\Sigma^k_{\text{tr}}$ = transport cross-section for group $k$

$B^2_i$ = the $i^{\text{th}}$ iterate of the buckling.

This equation is calculated by iteration until convergence on $B^2$ which is decided by

$$\sum_{k=1}^{N} \nu_k \Sigma^{\text{f}}_k \varphi^i_k = 1 - \varepsilon \tag{2}$$

where

$\nu_k \Sigma^{\text{f}}_k$ = neutrons per fission times fission cross-section for group $k$

$\varepsilon$ = convergence criterion for iterative scheme.

In the further discussion, the superscript "$i$" is dropped as a convergence is assumed.

Details of the calculation of elastic-scattering matrices, elastic-removal cross-sections and transport cross-sections are given in the Appendix.

## 2. "Consistent" P-1 approximation

In the ordinary P-1 approximation, the angular distribution of the slowing-down source is not properly taken into account. The equations correctly taking it into account in the P-1 approximation are given in [1] as Eqs. (11.31a) and (11.31b). For simplicity, these are given here with spatial variation in the $Z$ direction only assumed.

$$\frac{1}{4\pi}\frac{\partial J(E,Z)}{\partial Z} = \int_0^\infty \varphi(E',Z)\, S_0(E'\to E)\, \mathrm{d}E' - \frac{\Sigma_{\text{tot}}(E)\,\varphi(E,Z)}{4\pi} + S_{00}(E,Z) \tag{3}$$

$$\frac{1}{4\pi}\frac{\partial \varphi(E,Z)}{\partial Z} = \int_0^\infty J(E',Z)\, S_1(E'\to E)\, \mathrm{d}E' - \frac{3\,\Sigma_{\text{tot}}(E)\, J(E,Z)}{4\pi} \tag{4}$$

$J(E,Z)$ = current

$\varphi(E,Z)$ = flux

$4\pi S_{00}(E,Z)$ = inelastic-scattering plus fission sources (assumed isotropic).

For the Fourier transform one can set

$$J(E,Z) = -\mathrm{i}\, J(E)\, \mathrm{e}^{\mathrm{i}BZ} \tag{5a}$$

$$\varphi(E, Z) = \Phi(E)\, e^{iBZ} \tag{5b}$$

$$S_{00}(E, Z) = S_{00}(E)\, e^{iBZ}. \tag{5c}$$

In multi-group notation, with E′ and E corresponding to groups $j$ and $k$ respectively,

$$S_0(E' \to E) \to S_0{}^{j\to k} = \frac{1}{4\pi} \Sigma_{\text{eltr}}^{j\to k}$$

$$S_1(E' \to E) \to S_1{}^{j\to k} = \frac{1}{4\pi} \frac{3}{2} \left(\frac{E_k}{E_j}\right)^{1/2} \left[(A+1) - \frac{(A-1)}{\frac{E_k}{E_j}}\right] \Sigma_{\text{eltr}}^{j\to k}.$$

$E_j$ and $E_k$ may be taken as the lower group limits:

$$J(E) \to J_k$$

$$\varphi(E) \to \varphi_k.$$

Writing Eq. (3) in multi-group form with the use of Eq. (5)

$$BJ_k = \sum_{j=k-n}^{k-1} \varphi_j [\Sigma_{\text{eltr}}^{j\to k} + \Sigma_{\text{intr}}^{j\to k}] - (\Sigma^k{}_{\text{a}} + \Sigma_{\text{elr}}^k)\, \varphi_k + \beta_k. \tag{6}$$

Eq. (4) can be similarly rewritten as

$$\frac{J_k}{B} = \frac{\varphi_k}{3\Sigma_{\text{tot}}^k} + \frac{1}{3\Sigma_{\text{tot}}^k} \sum_{j=k-n}^{k-1} \frac{J_j}{B} \frac{3}{2} \left(\frac{E_k}{E_j}\right)^{1/2} \left[(A+1) - \frac{(A-1)}{\frac{E_k}{E_j}}\right] \Sigma_{\text{eltr}}^{j\to k}. \tag{7}$$

Solving Eqs. (6) and (7) for the flux one obtains

$$\varphi_k = \frac{\beta_k + \sum_{j=k-n}^{k-1} \varphi_j [\Sigma_{\text{eltr}}^{j\to k} + \Sigma_{\text{intr}}^{j\to k}] - \frac{1}{3\Sigma_{\text{tot}}^k} \sum_{j=k-n}^{k-1} \frac{3}{2} \left(\frac{E_k}{E_j}\right)^{1/2} BJ_j \left[(A+1) - \frac{(A-1)}{\frac{E_k}{E_j}}\right] \Sigma_{\text{eltr}}^{j\to k}}{\frac{B^2}{3\Sigma_{\text{tot}}^k} + \Sigma^k{}_{\text{a}} + \Sigma_{\text{elr}}^k}. \tag{8}$$

Eqs. (7) and (8) are a coupled set which are solved iteratively to obtain the group fluxes and currents and the eigenvalue $B^2$.

## 3. "Consistent" B-1 approximation [2, 3]

If one substitutes $\gamma_k \Sigma^k{}_{\text{tot}}$ for $\Sigma^k{}_{\text{tot}}$, where $\gamma_k$ is defined as

$$\gamma_k = \frac{\alpha_k \tan^{-1}\alpha_k}{3\left(1 - \frac{\tan^{-1}\alpha_k}{\alpha_k}\right)} \qquad \alpha_k = \frac{B}{\Sigma_{\text{tot}}^k} \tag{9}$$

one obtains the "consistent" B-1 approximation, in which a rigorous solution for the Fourier transform is obtained except that only a P-1 expansion of the scattering cross-sections in the laboratory system is used. For this case Eqs. (7) and (8) are transformed to

$$\frac{J_k}{B} = \frac{\varphi_k}{3\gamma_k \Sigma^k_{\text{tot}}} + \frac{1}{3\gamma_k \Sigma^k_{\text{tot}}} \sum_{j=k-n}^{k-1} \frac{J_j}{B} \frac{3}{2} \left(\frac{E_k}{E_j}\right)^{1/2} \left[(A+1) - \frac{(A-1)}{\frac{E_k}{E_j}}\right] \Sigma^{j\to k}_{\text{eltr}} \tag{10}$$

and

$$\varphi_k = \frac{\beta_k + \sum_{j=k-n}^{k-1} \varphi_j [\Sigma^{j\to k}_{\text{eltr}} + \Sigma^{j\to k}_{\text{intr}}] - \frac{1}{3\gamma_k \Sigma^k_{\text{tot}}} \sum_{j=k-n}^{k-1} \frac{3}{2} \left(\frac{E_k}{E_j}\right)^{1/2} B J_j \left[(A+1) - \frac{(A-1)}{\frac{E_k}{E_j}}\right] \Sigma^{j\to k}_{\text{eltr}}}{\frac{B^2}{3\gamma_k \Sigma^k_{\text{tot}}} + \Sigma^k_{\text{a}} + \Sigma^k_{\text{elr}}} . \tag{11}$$

Again the solution involves coupling Eqs. (10) and (11), with iteration on $B^2$.

## 4. Treatment of narrow resonances

The ratio of final to initial fine-group energies thus far being used is 0.991 33, so that at 100 keV the group width is 0.87 keV and at 200 keV 1.74. Since many of the resonances in Na reported by HIBDON [5] in this energy region have widths less than 1 keV, this group spacing cannot be used to describe such resonance shapes. The method of dealing with these very narrow resonances is as follows. First a problem is run with the low resolution data for Na given in [8], which can be adequately traced out with the group spacing being used. The usual assumption of the narrow-resonance approximation is made, that over one of the fine groups the total source is constant and equal to that calculated with the low-resolution data. For the P-1 approximation the actual magnitude of the source for each group need not be known. In this case the assumption is made that the source $S$ equals $\varphi(E)\,\Sigma_{\text{tot}}(E)$ within the fine group. An average transport cross-section for fine groups is obtained from

$$\frac{1}{\Sigma^j_{\text{tr}}} = \frac{\int_{E_{j-1}}^{E_j} \frac{\mathrm{d}E}{\Sigma_{\text{tot}}(E)\,\Sigma_{\text{tr}}(E)}}{\int_{E_{j-1}}^{E_j} \frac{\mathrm{d}E}{\Sigma_{\text{tot}}(E)}} .$$

$\Sigma_{\text{tot}}(E)$ and $\Sigma_{\text{tr}}(E)$ are obtained from the detailed Na data, with the contributions of material other than Na being held at the values for the original ELMOE calculation. Finally, the values of $1/\Sigma^j_{\text{tr}}$ are weighted with the fluxes from the ELMOE calculation to obtain a revised coarse-group value.

To obtain a corrected scattering cross-section for elastic-removal calculation, the following integral is computed:

$$\sigma_{\text{s Na}}(j) = \frac{\int_{E_{j-1}}^{E_j} \frac{\sigma_{\text{s Na}}(E)\,\mathrm{d}E}{\Sigma_{\text{tot}}(E)}}{\int_{E_{j-1}}^{E_j} \frac{\mathrm{d}E}{\Sigma_{\text{tot}}(E)}} .$$

These values of $\sigma_{sNa}(j)$ are used in conjunction with the original ELMOE fluxes to obtain a corrected elastic-removal cross-section for Na.

In the case of the consistent P-1 calculation, a more elaborate calculation is necessary for obtaining the diffusion coefficient. The first step is to run a consistent P-1 ELMOE calculation with the low-resolution data. The elastic and inelastic sources from this calculation are used in Eqs. (7) and (8) to calculate the detailed variation within the fine groups of current and flux by allowing $\Sigma_{tot}$ and $\Sigma_{elr}$ to vary within the fine group. As before, cross-sections for materials other than Na are held constant. Integrated values of flux and current for the fine groups are obtained in this way, and used to define effective diffusion coefficients in the regular manner.

## 5. Input for ELMOE code

The coarse-group cross-sections are taken from one of a library of such sets available. These may be either in the form used in the Re-X codes [6] or in that of the SN [7] code. Elastic-removal cross-sections for the light elements used in these sets must be supplied as they are subtracted out. The Legendre polynomial expansion coefficients for the light elements may be supplied either in the centre-of-mass or laboratory system. The library of such coefficients currently available includes the following elements: Fe, Ni, Cr, Nb, V, Al, Na, C and O. These data were obtained from Refs. [8–14]. Since high-resolution angular-distribution data are available only for a few isolated resonances, the procedure usually followed was to use the highest resolution data available for the isotropic component of the scattering cross-section, with the assumption that the ratio of higher expansion coefficients to the isotropic one was the same as in the angular-distribution data.

Because of limitations of storage in the IBM-704 even with 32 000-word memory, the number of fine groups that can be used is limited. If more groups than this limit are desired, the problem is run in more than one pass, subdividing different energy regions with an overlap of at least one or two coarse groups to produce a proper elastic moderation source at the upper end of the subdivided region. The number of fine groups that can be used is a function of the maximum size of the elastic-scattering matrix. The scattering cross-section library currently in use corresponds to elastic-scattering matrices of order 20, 29 and 39 for Na, O and C respectively. When Na, O or C is the lightest element present, the maximum number of fine groups that can be used in the ordinary P-1 calculation is 755, 574 and 479 respectively. For the consistent P-1, the corresponding maximum number of groups is 450, 351 and 274 respectively.

## 6. Output information from code

For each fine group the following quantities are normally printed out: flux, current/B (except for P-1), slowing-down density, inelastic source, and elastic source. The complete elastic-transfer matrices can be obtained on option. For all coarse groups the total flux and the current are given. A diffusion coefficient is given which in the fine-group region for the P-1 calculation is simply the average of $1/3\ \Sigma_{tr}$ over the fine-group fluxes. For the consistent P-1 and B-1, it is obtained from the ratio of total current to total flux for the fine groups corresponding to the coarse groups in question.

TABLE I

**EFFECTIVE CROSS-SECTIONS FOR ADDITION OF TYPE-304 STAINLESS STEEL***
**(barns)**

| Vol. % in → mixture | $U^{235}$ / $U^{238}$ | 4.70 / 0.39 | | | 4.97 / 9.97 | | | 4.70 / 9.42 | 9.42 / 0.71 | 13.93 / 15.84 |
|---|---|---|---|---|---|---|---|---|---|---|
| | Al / O / SS (diff.) | 0 / 0 / 0—30.0 | 0 / 0 / 30.0—60.0 | 0 / 0 / 0—60.0 | 0 / 0 / 0—12.38 | 0 / 0 / 12.38—24.75 | 0 / 0 / 0—24.75 | 0 / 0 / 0—60.0 | 0 / 0 / 0—80.1 | 0 / 0 / 0—19.0 |
| Group | $E_L$ (MeV) | $\sigma_{tr}$ | | | | | | | | |
| 2 | 3.67—2.23 | 1.94 | 1.94 | 1.94 | 1.94 | 1.94 | 1.94 | 1.94 | 1.94 | 1.94 |
| 3 | 1.35 | 2.06 | 2.06 | 2.06 | 2.06 | 2.06 | 2.06 | 2.06 | 2.06 | 2.06 |
| 4 | 0.83 | 1.94 | 1.93 | 1.94 | 1.97 | 1.94 | 1.95 | 1.94 | 1.94 | 1.98 |
| 5 | 0.50 | 2.26 | 2.24 | 2.25 | 2.24 | 2.25 | 2.25 | 2.26 | 2.26 | 2.32 |
| 6 | 0.30 | 2.60 | 2.47 | 2.53 | 2.78 | 2.59 | 2.69 | 2.57 | 2.57 | 2.83 |
| 7 | 0.18 | 2.52 | 2.44 | 2.48 | 2.72 | 2.53 | 2.62 | 2.53 | 2.50 | 2.75 |
| 8 | 0.11 | 3.08 | 2.94 | 3.01 | 3.45 | 3.08 | 3.26 | 3.09 | 3.05 | 3.56 |
| 9 | 0.067 | 3.77 | 3.58 | 3.68 | 4.21 | 3.81 | 4.01 | 3.80 | 3.73 | 4.33 |
| 10 | 0.041 | 4.31 | 4.29 | 4.30 | 4.44 | 4.32 | 4.38 | 4.32 | 4.30 | 4.43 |
| 11 | 0.025 | 5.22 | 4.56 | 4.89 | 6.25 | 5.30 | 5.78 | 5.19 | 5.07 | 6.50 |
| 12 | 0.015 | — | — | — | — | — | — | — | — | — |
| 13 | 0.0091 | — | — | — | — | — | — | — | — | — |
| | | $\sigma_{elr}$ | | | | | | | | |
| 2 | 3.67—2.23 | 0.0631 | 0.0656 | 0.0643 | 0.0592 | 0.0621 | 0.0606 | 0.0629 | 0.064 | 0.0587 |
| 3 | 1.35 | 0.0965 | 0.102 | 0.0994 | 0.0884 | 0.0952 | 0.0919 | 0.0967 | 0.098 | 0.0870 |
| 4 | 0.83 | 0.121 | 0.132 | 0.127 | 0.117 | 0.120 | 0.119 | 0.125 | 0.123 | 0.117 |
| 5 | 0.50 | 0.166 | 0.207 | 0.185 | 0.142 | 0.168 | 0.155 | 0.183 | 0.174 | 0.138 |
| 6 | 0.30 | 0.144 | 0.178 | 0.161 | 0.122 | 0.156 | 0.139 | 0.162 | 0.151 | 0.111 |
| 7 | 0.18 | 0.170 | 0.172 | 0.171 | 0.173 | 0.172 | 0.172 | 0.172 | 0.169 | 0.172 |
| 8 | 0.11 | 0.218 | 0.236 | 0.227 | 0.190 | 0.222 | 0.206 | 0.226 | 0.222 | 0.183 |
| 9 | 0.067 | 0.257 | 0.283 | 0.270 | 0.225 | 0.250 | 0.237 | 0.261 | 0.262 | 0.220 |
| 10 | 0.041 | 0.217 | 0.287 | 0.252 | 0.249 | 0.252 | 0.251 | 0.267 | 0.232 | 0.235 |
| 11 | 0.025 | 0.413 | 0.485 | 0.449 | 0.379 | 0.431 | 0.405 | 0.450 | 0.428 | 0.373 |
| 12 | 0.015 | — | — | — | — | — | — | — | — | — |
| 13 | 0.0091 | — | — | — | — | — | — | — | — | — |

* Based on following values of atoms /cm³ × $10^{24}$: $U^{235}$ and $U^{238}$, 0.0480—SS, 0.0847—Al, 0.0603—O, 0.0960—Na, 0.0220.

TABLE I

**EFFECTIVE CROSS-SECTION FOR ADDITION OF TYPE-304 STAINLESS STEEL (barns)**

| 4.97<br>9.97 | | | | | | 9.27<br>0.67 | 4.97<br>9.97 | | | | | YOM |
|---|---|---|---|---|---|---|---|---|---|---|---|---|
| 12.19<br>0<br>0—<br>12.38 | 12.19<br>0<br>12.38—<br>24.75 | 12.19<br>0<br>0—<br>24.75 | 24.38<br>0<br>0—<br>12.38 | 24.38<br>0<br>12.38—<br>24.75 | 24.38<br>0<br>0—<br>24.75 | 42.82<br>0<br>0—<br>9.16 | 12.19<br>7.23<br>0—<br>12.38 | 24.38<br>7.23<br>0—<br>24.75 | 24.38<br>14.46<br>0—<br>12.38 | 24.38<br>14.46<br>12.38—<br>24.75 | 24.38<br>14.46<br>0—<br>24.75 | |
| 1.94 | 1.94 | 1.94 | 1.95 | 1.94 | 1.94 | 1.95 | 1.96 | 1.95 | 1.99 | 1.97 | 1.98 | 2.21 |
| 2.07 | 2.06 | 2.07 | 2.08 | 2.07 | 2.08 | 2.09 | 2.07 | 2.07 | 2.08 | 2.07 | 2.08 | 2.09 |
| 1.98 | 1.95 | 1.97 | 1.99 | 1.96 | 1.97 | 2.00 | 2.03 | 2.00 | 2.05 | 2.02 | 2.04 | 2.09 |
| 2.30 | 2.27 | 2.28 | 2.31 | 2.28 | 2.30 | 2.34 | 2.31 | 2.30 | 2.31 | 2.29 | 2.30 | 2.34 |
| 2.86 | 2.69 | 2.77 | 2.91 | 2.76 | 2.84 | 2.99 | 2.79 | 2.79 | 2.84 | 2.75 | 2.80 | 2.95 |
| 2.87 | 2.64 | 2.75 | 2.99 | 2.74 | 2.86 | 3.15 | 2.90 | 2.88 | 3.02 | 2.79 | 2.90 | 2.63 |
| 3.71 | 3.22 | 3.47 | 4.03 | 3.41 | 3.72 | 4.56 | 3.75 | 3.69 | 3.94 | 3.46 | 3.70 | 3.59 |
| 4.29 | 3.87 | 4.08 | 4.43 | 3.95 | 4.19 | 4.73 | 4.40 | 4.22 | 4.60 | 3.98 | 4.29 | 5.74 |
| 4.50 | 4.37 | 4.44 | 4.61 | 4.44 | 4.53 | 4.75 | 4.58 | 4.55 | 4.66 | 4.47 | 4.57 | 4.47 |
| 6.96 | 4.82 | 5.90 | 7.37 | 4.75 | 6.06 | 8.78 | 8.22 | 6.86 | 9.74 | 5.25 | 7.49 | 10.26 |
| — | — | — | — | — | — | — | 4.20 | 3.98 | 4.49 | 4.03 | 4.26 | 4.99 |
| — | — | — | — | — | — | — | 7.62 | 7.61 | 7.62 | 7.60 | 7.61 | 7.63 |
| 0.0632 | 0.0644 | 0.0638 | 0.0650 | 0.0656 | 0.0653 | 0.0631 | 0.0659 | 0.0586 | 0.0633 | 0.0639 | 0.0636 | 0.0774 |
| 0.0989 | 0.101 | 0.100 | 0.104 | 0.104 | 0.104 | 0.107 | 0.106 | 0.107 | 0.112 | 0.109 | 0.111 | 0.0849 |
| 0.125 | 0.130 | 0.127 | 0.133 | 0.136 | 0.134 | 0.136 | 0.156 | 0.151 | 0.168 | 0.165 | 0.166 | 0.118 |
| 0.183 | 0.195 | 0.189 | 0.200 | 0.205 | 0.202 | 0.199 | 0.193 | 0.206 | 0.206 | 0.209 | 0.207 | 0.154 |
| 0.165 | 0.173 | 0.169 | 0.185 | 0.185 | 0.185 | 0.184 | 0.170 | 0.180 | 0.179 | 0.182 | 0.180 | 0.191 |
| 0.190 | 0.181 | 0.185 | 0.204 | 0.195 | 0.199 | 0.209 | 0.208 | 0.212 | 0.218 | 0.212 | 0.215 | 0.162 |
| 0.312 | 0.270 | 0.291 | 0.367 | 0.302 | 0.335 | 0.413 | 0.298 | 0.314 | 0.325 | 0.292 | 0.309 | 0.221 |
| 0.319 | 0.312 | 0.316 | 0.361 | 0.342 | 0.351 | 0.390 | 0.311 | 0.334 | 0.338 | 0.323 | 0.331 | 0.322 |
| 0.195 | 0.247 | 0.221 | 0.226 | 0.266 | 0.246 | 0.228 | 0.272 | 0.283 | 0.303 | 0.298 | 0.301 | 0.241 |
| 0.706 | 0.605 | 0.655 | 0.856 | 0.701 | 0.779 | 0.953 | 0.772 | 0.801 | 0.920 | 0.698 | 0.810 | 0.569 |
| — | — | — | — | — | — | — | 0.294 | 0.287 | 0.373 | 0.319 | 0.346 | 0.253 |
| — | — | — | — | — | — | — | 0.368 | 0.416 | 0.432 | 0.470 | 0.451 | 0.393 |

## 7. Results obtained with ELMOE code

A series of calculations has been performed for compositions which are typical of experiments performed on ZPR-III including Assemblies 29, 30, 31 and 32 [15]. The cores contained varying amounts of $U^{235}$, $U^{238}$, Type-304 stainless steel (SS), aluminium, sodium and oxygen. These assemblies were of particular interest because calculations with existing cross-section sets yielded critical masses much lower than those measured. Since these assemblies contained larger amounts of light elements than any previously constructed, it was of interest to see to what extent these discrepancies were due to errors in light-element cross-sections.

The most obvious error that one would expect to find is in the method of averaging the transport cross-sections of the light elements, since in general this is accomplished by simply averaging $\sigma_{tr}$ or $1/\sigma_{tr}$ for individual elements. This takes no account of perturbations in the flux caused by the scattering resonances of the element in question or of the effect of other scatterers. Another averaging method sometimes used is to average $1/\sigma_{tr}$ weighted with $1/\sigma_{tr}$ for individual elements. This corresponds to slowing down in the pure light element and could be expected to yield a lower limit to the average transport cross-section. The coarse-group cross-section set used for the calculations was that of YIFTAH *et al.* [16]. This reference will be denoted as YOM. In this reference, averaging of $1/\sigma_{tr}$ for individual elements was used. The range covered in most cases was Groups 2 through 11, extending from 3.67 MeV to 25 keV. A few calculations were done including also Groups 12 and 13, extending down to 9.1 keV.

Because of the interaction among elements, it is not possible in general to assign a unique coarse-group transport cross-section to a given element in a mixture if some transport cross-sections vary within the group. Some effective transport and elastic-removal cross-sections for various elements (Type-304 stainless steel is handled as a single element) are given in Tables I–III. The coarse- to fine-group correspondence is given in Table III. These cross-sections are based on the difference in group-diffusion coefficient and elastic-removal cross-section caused by adding the element to a mixture as indicated. They would be appropriate for calculating the change in reactivity occasioned by the addition of the element to the assembly. The information in these tables may be used to approximate the appropriate cross-sections for a desired mixture of the indicated elements by first estimating cross-sections for adding a single light element to uranium, then estimating those for adding a second light element to this mixture, and finally a third light element if desired.

The following general comments may be made concerning the results in Tables I–III. Larger variations tend to occur in the lower-energy regions where resonance structure is more pronounced. In particular, the large variations in Group 11 are associated with strong resonances in $Fe^{56}$ and Al falling within the energy limits of this group. The presence of increasing amounts of $U^{235}$ and $U^{238}$ tends to increase effective transport cross-sections, since these elements add a constant transport cross-section to the mixture which fills in low places in the resonance scattering cross-sections. Such regions have a high weight in the averaging process because of the $1/\Sigma_{tr}$ averaging and because of a flux rise at these points. Increasing amounts of a single light element tend to decrease the transport cross-section of the element for the same reason. A mixture of light elements tends to lead to higher apparent transport cross-sections for the individual elements, because the minima in the cross-section of a given element

TABLE II

**EFFECTIVE CROSS-SECTIONS FOR ADDITION OF ALUMINIUM**

***(barns)***

| Vol. % in → mixture | $U^{235}$ / $U^{238}$ | 4.97 / 9.97 | | | 9.27 / 0.67 | | | | 4.97 / 9.97 | | | | | | 4.70 / 9.42 | 4.97 / 9.97 | | YOM |
|---|---|---|---|---|---|---|---|---|---|---|---|---|---|---|---|---|---|---|
| | SS 1 | 0 | 0 | 0 | 0 | 9.16 | 9.16 | 9.16 | 12.38 | 12.38 | 12.38 | 24.75 | 24.75 | 24.75 | 60.0 | 24.75 | 12.38 | |
| | O 2 | 0 | 0 | 0 | 0 | 0 | 0 | 0 | 0 | 0 | 0 | 0 | 0 | 0 | 0 | 14.46 | 7.23 | |
| | Al 3 | 0–12.19 | 12.19–24.38 | 0–24.38 | 0–42.82 | 0–21.42 | 21.42–42.82 | 0–42.82 | –0 12.19 | 12.19–24.38 | 0–24.38 | 0–12.19 | 12.19–24.38 | 0–24.38 | 0—17.6 | 0–24.38 | 0–12.19 | |
| | (diff.) 4 | | | | | | | | | | | | | | | | | |
| Group | $E_L$ (MeV) | $\sigma_{tr}$ | | | | | | | | | | | | | | | | |
| | 3.67— | | | | | | | | | | | | | | | | | |
| 2 | 2.23 | 1.33 | 1.32 | 1.33 | 1.32 | 1.33 | 1.32 | 1.33 | 1.33 | 1.33 | 1.33 | 1.34 | 1.33 | 1.34 | 1.34 | 1.41 | 1.39 | 1.60 |
| 3 | 1.35 | 1.94 | 1.90 | 1.91 | 1.90 | 1.92 | 1.91 | 1.92 | 1.93 | 1.92 | 1.92 | 1.94 | 1.93 | 1.93 | 1.95 | 1.97 | 1.96 | 2.00 |
| 4 | 0.83 | 2.12 | 2.11 | 2.12 | 2.10 | 2.12 | 2.10 | 2.11 | 2.14 | 2.12 | 2.13 | 2.16 | 2.14 | 2.15 | 2.19 | 2.31 | 2.28 | 2.48 |
| 5 | 0.50 | 2.77 | 2.78 | 2.78 | 2.81 | 2.84 | 2.79 | 2.81 | 2.85 | 2.81 | 2.83 | 2.87 | 2.84 | 2.86 | 2.91 | 2.88 | 2.88 | 2.97 |
| 6 | 0.30 | 3.09 | 2.97 | 3.03 | 2.99 | 3.10 | 2.97 | 3.04 | 3.20 | 3.05 | 3.13 | 3.34 | 3.15 | 3.25 | 3.56 | 3.34 | 3.29 | 3.17 |
| 7 | 0.18 | 3.20 | 2.90 | 3.06 | 2.91 | 3.21 | 2.85 | 3.03 | 3.43 | 3.07 | 3.25 | 3.59 | 3.22 | 3.41 | 3.76 | 3.52 | 3.52 | 3.82 |
| 8 | 0.11 | 3.86 | 2.87 | 3.39 | 3.06 | 3.78 | 2.95 | 3.37 | 4.25 | 3.37 | 3.81 | 4.45 | 3.65 | 4.05 | 4.57 | 4.29 | 4.46 | 5.02 |
| 9 | 0.067 | 3.68 | 2.73 | 3.20 | 2.84 | 3.34 | 2.61 | 2.98 | 3.79 | 2.92 | 3.36 | 3.87 | 3.04 | 3.45 | 3.86 | 3.92 | 4.21 | 5.98 |
| 10 | 0.041 | 2.10 | 1.91 | 2.01 | 1.87 | 1.98 | 1.94 | 1.96 | 2.20 | 2.07 | 2.14 | 2.27 | 2.17 | 2.22 | 2.36 | 2.35 | 2.31 | 2.78 |
| 11 | 0.025 | 2.87 | 0.98 | 1.94 | 1.54 | 3.23 | 1.27 | 2.25 | 3.95 | 1.55 | 2.75 | 3.27 | 1.44 | 2.35 | 1.89 | 4.11 | 5.32 | 6.34 |
| 12 | 0.015 | — | — | — | — | — | — | — | — | — | — | — | — | — | — | 0.676 | 0.602 | 0.75 |
| 13 | 0.0091 | — | — | — | — | — | — | — | — | — | — | — | — | — | — | 1.11 | 1.10 | 1.13 |
| | 3.67— | $\sigma_{elr}$ | | | | | | | | | | | | | | | | |
| 2 | 2.23 | 0.166 | 0.174 | 0.170 | 0.179 | 0.177 | 0.185 | 0.181 | 0.172 | 0.178 | 0.174 | 0.171 | 0.179 | 0.177 | 0.180 | 0.202 | 0.190 | 0.162 |
| 3 | 1.35 | 0.237 | 0.261 | 0.249 | 0.262 | 0.257 | 0.280 | 0.268 | 0.252 | 0.271 | 0.260 | 0.260 | 0.273 | 0.261 | 0.275 | 0.292 | 0.277 | 0.216 |
| 4 | 0.83 | 0.323 | 0.343 | 0.333 | 0.328 | 0.324 | 0.343 | 0.340 | 0.333 | 0.358 | 0.344 | 0.348 | 0.363 | 0.355 | 0.374 | 0.422 | 0.418 | 0.332 |
| 5 | 0.50 | 0.408 | 0.471 | 0.439 | 0.433 | 0.433 | 0.471 | 0.452 | 0.467 | 0.498 | 0.480 | 0.505 | 0.508 | 0.507 | 0.534 | 0.498 | 0.479 | 0.404 |
| 6 | 0.30 | 0.402 | 0.424 | 0.413 | 0.407 | 0.428 | 0.432 | 0.430 | 0.464 | 0.457 | 0.459 | 0.487 | 0.472 | 0.480 | 0.508 | 0.499 | 0.495 | 0.420 |
| 7 | 0.18 | 0.454 | 0.430 | 0.442 | 0.438 | 0.465 | 0.432 | 0.448 | 0.477 | 0.454 | 0.464 | 0.491 | 0.470 | 0.481 | 0.530 | 0.523 | 0.512 | 0.484 |
| 8 | 0.11 | 0.427 | 0.489 | 0.458 | 0.459 | 0.533 | 0.524 | 0.529 | 0.601 | 0.573 | 0.585 | 0.667 | 0.615 | 0.642 | 0.727 | 0.704 | 0.672 | 0.632 |
| 9 | 0.067 | 0.306 | 0.400 | 0.353 | 0.373 | 0.408 | 0.438 | 0.423 | 0.442 | 0.463 | 0.450 | 0.529 | 0.502 | 0.516 | 0.643 | 0.633 | 0.579 | 0.690 |
| 10 | 0.041 | 0.346 | 0.214 | 0.280 | 0.199 | 0.190 | 0.229 | 0.209 | 0.269 | 0.260 | 0.264 | 0.263 | 0.285 | 0.274 | 0.302 | 0.336 | 0.304 | 0.308 |
| 11 | 0.025 | 0.0691 | 0.112 | 0.0904 | 0.0883 | 0.296 | 0.221 | 0.259 | 0.535 | 0.329 | 0.431 | 0.783 | 0.462 | 0.623 | 0.976 | 0.806 | 0.755 | 0.721 |
| 12 | 0.015 | — | — | — | — | — | — | — | — | — | — | — | — | — | — | 0.672 | 0.0171 | 0.081 |
| 13 | 0.091 | — | — | — | — | — | — | — | — | — | — | — | — | — | — | 0.144 | 0.123 | 0.121 |

TABLE III

**EFFECTIVE CROSS-SECTIONS FOR ADDITION OF OXYGEN**
**(barns)**

| Vol. % in → mixture | $U^{238}$ / $U^{235}$ | 4.97 / 9.97 | | | | | | | | | | | YOM | Fine groups |
|---|---|---|---|---|---|---|---|---|---|---|---|---|---|---|
| | SS / Al / O (diff.) | 12.38 / 0 / 0—7.23 | 24.75 / 0 / 0–14.46 | 0 / 12.19 / 0—7.23 | 0 / 24.38 / 0—7.23 | 0 / 24.38 / 7.23–14.46 | 0 / 24.38 / 0–14.46 | 12.38 / 12.19 / 0—7.23 | 12.38 / 24.38 / 0–14.46 | 24.75 / 24.38 / 0—7.32 | 24.75 / 24.38 / 7.23–14.46 | 24.75 / 24.38 / 0–14.46 | | |
| Group | $E_L$ (MeV) | $\sigma_{tr}$ | | | | | | | | | | | | |
| 2 | 3.67—2.23 | 1.40 | 1.33 | 1.42 | 1.47 | 1.24 | 1.35 | 1.45 | 1.39 | 1.50 | 1.31 | 1.41 | 1.72 | 1—58 |
| 3 | 1.35 | 1.81 | 1.80 | 1.83 | 1.86 | 1.81 | 1.84 | 1.84 | 1.84 | 1.86 | 1.82 | 1.84 | 2.56 | 59—115 |
| 4 | 0.83 | 3.83 | 3.78 | 3.90 | 4.03 | 3.67 | 3.85 | 3.98 | 3.90 | 4.11 | 3.79 | 3.95 | 3.51 | 116—172 |
| 5 | 0.50 | 2.46 | 2.48 | 2.48 | 2.51 | 2.48 | 2.49 | 2.49 | 2.49 | 2.52 | 2.48 | 2.50 | 3.47 | 173—229 |
| 6 | 0.30 | 5.32 | 5.27 | 5.51 | 5.61 | 5.24 | 5.42 | 5.41 | 5.37 | 5.47 | 5.25 | 5.36 | 4.09 | 230—288 |
| 7 | 0.18 | 4.11 | 4.18 | 4.14 | 4.35 | 4.15 | 4.25 | 4.21 | 4.27 | 4.37 | 4.23 | 4.30 | 3.35 | 289—347 |
| 8 | 0.11 | 3.80 | 3.88 | 3.97 | 4.32 | 3.99 | 4.16 | 4.02 | 4.09 | 4.22 | 4.03 | 4.12 | 3.35 | 348—404 |
| 9 | 0.067 | 3.72 | 3.78 | 4.00 | 4.28 | 3.96 | 4.12 | 4.17 | 4.25 | 4.37 | 4.17 | 4.27 | 3.35 | 405—461 |
| 10 | 0.041 | 3.49 | 3.52 | 3.48 | 3.69 | 3.51 | 3.60 | 3.61 | 3.64 | 3.75 | 3.56 | 3.66 | 3.35 | 462—519 |
| 11 | 0.025 | 4.54 | 4.60 | 4.12 | 4.43 | 4.18 | 4.30 | 6.00 | 6.09 | 6.84 | 6.09 | 6.47 | 3.35 | 520—574 |
| 12 | 0.015 | — | — | — | — | 3.37 | — | — | — | — | 4.23 | — | 3.35 | 575—633 |
| 13 | 0.0091 | — | — | — | — | 3.46 | — | — | — | — | 3.46 | — | 3.35 | 634—691 |
| | | $\sigma_{elr}$ | | | | | | | | | | | | |
| 2 | 3.67—2.23 | 0.203 | 0.222 | 0.218 | 0.239 | 0.266 | 0.252 | 0.222 | 0.251 | 0.239 | 0.270 | 0.250 | 0.430 | — |
| 3 | 1.35 | 0.537 | 0.557 | 0.553 | 0.575 | 0.575 | 0.575 | 0.563 | 0.580 | 0.584 | 0.615 | 0.584 | 0.559 | — |
| 4 | 0.83 | 1.20 | 1.22 | 1.24 | 1.30 | 1.18 | 1.24 | 1.29 | 1.27 | 1.35 | 1.28 | 1.29 | 0.793 | — |
| 5 | 0.50 | 0.636 | 0.673 | 0.635 | 0.640 | 0.674 | 0.657 | 0.649 | 0.669 | 0.650 | 0.827 | 0.665 | 0.797 | — |
| 6 | 0.30 | 1.45 | 1.44 | 1.47 | 1.51 | 1.42 | 1.463 | 1.48 | 1.46 | 1.49 | 1.36 | 1.46 | 0.914 | — |
| 7 | 0.18 | 0.840 | 0.912 | 0.848 | 0.904 | 0.963 | 0.933 | 0.877 | 0.944 | 0.941 | 0.811 | 0.957 | 0.715 | — |
| 8 | 0.11 | 0.837 | 0.868 | 0.932 | 1.00 | 0.946 | 0.974 | 0.911 | 0.942 | 0.937 | 0.743 | 0.934 | 0.710 | — |
| 9 | 0.067 | 0.753 | 0.808 | 0.911 | 0.994 | 0.934 | 0.964 | 0.898 | 0.947 | 0.942 | 0.871 | 0.932 | 0.651 | — |
| 10 | 0.041 | 0.720 | 0.778 | 0.641 | 0.727 | 0.794 | 0.760 | 0.757 | 0.819 | 0.840 | 1.06 | 0.843 | 0.626 | — |
| 11 | 0.025 | 0.859 | 0.949 | 0.991 | 1.15 | 1.05 | 1.10 | 1.09 | 1.15 | 1.21 | 0.870 | 1.14 | 0.643 | — |
| 12 | 0.015 | — | — | — | — | 0.693 | — | — | — | — | 0.807 | — | 0.605 | — |
| 13 | 0.0091 | — | — | — | — | 0.702 | — | — | — | — | — | — | 0.605 | — |

are usually filled in by the other elements. It is this phenomenon which is responsible for the peculiar variations in the transport cross-section of oxygen in Group 11. In the input data, the transport cross-section of oxygen is actually assumed constant over a large energy range including Group 11 at the same value as that of YOM. However, when oxygen is added to aluminium or steel,

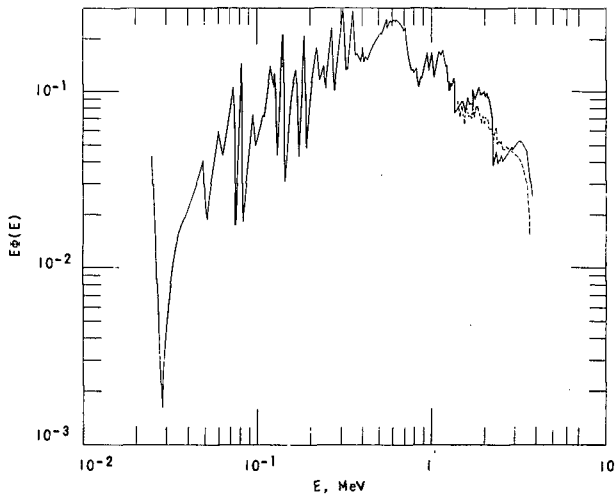


Fig. 1
Flux per unit lethargy, $E\ \varphi\ (E)$, for composition 80.1 vol. % stainless steel, 9.42 vol. % $U^{235}$, 0.71 vol. % $U^{238}$. Dashed line at high-energy end obtained from smoothed inelastic-scattering plus fission source. Normalization fixed by plotting-group fluxes from unit-fission source for lethargy width 0.0087.

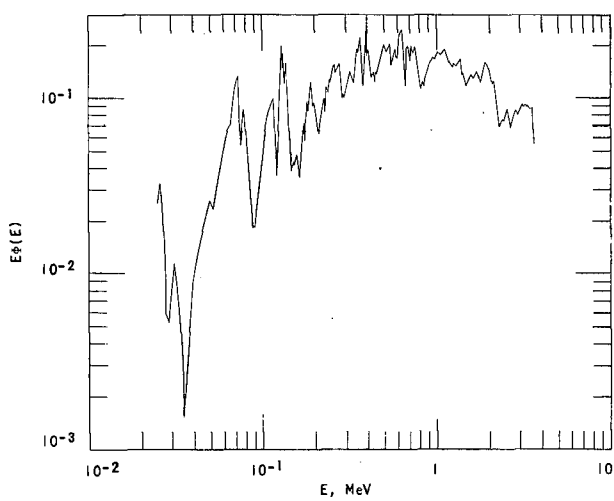


Fig. 2
Flux per unit lethargy, $E\ \varphi\ (E)$, for composition 42.82 vol. % Al, 9.16 vol. % stainless steel, 9.27 vol. % $U^{235}$, 0.67 vol. % $U^{238}$. Normalization as in Fig. 1.

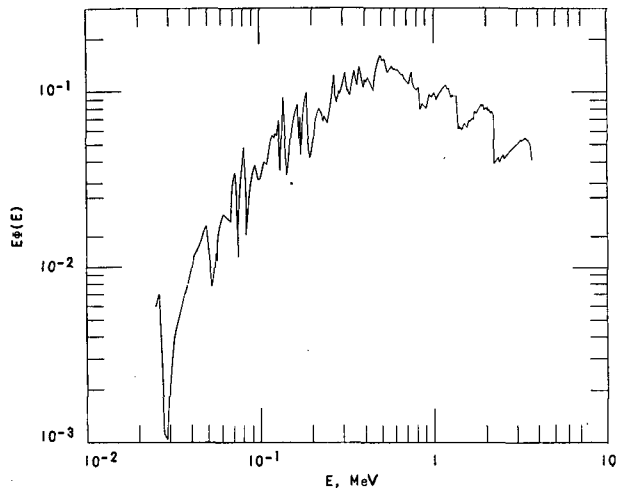


Fig. 3
Flux per unit lethargy, $E\ \varphi\ (E)$, for composition 46.50 vol. % Na, 17.62 vol. % stainless steel, 13.93 vol. % $U^{235}$, 15.84 vol. % $U^{238}$ (approximately EBR-II core). Normalization as in Fig. 1.

its effective cross-section is large because it fills in deep minima in the cross-sections of aluminium and iron. The same phenomenon is responsible for the higher effective cross-sections listed for aluminium and steel when added to mixtures already containing oxygen compared with the case of no oxygen present.

Some inaccuracy in the high-energy coarse-group cross-sections computed by the ELMOE code will be caused by the assumption of flat inelastic and fission sources, unless the coarse groups are narrower than it has been customary to use in fast-reactor calculations. This difficulty is illustrated by fine-group flux plots given in Figs. 1–3. The jumps in the flux at 1.35 and 2.23 MeV are caused by a physically unreal jump in the inelastic plus fission source at these points. This probably does not affect average transport cross-sections much, but the elastic-removal cross-sections for Groups 2 and 3 must be regarded as lower limits because the flux will actually be concentrated more heavily toward the lower group limits than in the illustrated calculations. This error can be removed by reiterating with a smoothed source inserted group by group in the high-energy region. This process has been carried out in the case of the mixture

TABLE IV

**STAINLESS-STEEL CROSS-SECTIONS AS OBTAINED DIRECTLY FROM ELMOE CODE COMPARED WITH THOSE FROM SMOOTHED SOURCE (9.42 vol.% $U^{235}$, 0.71 vol.% $U^{238}$, 0-80.1 vol.% SS)**

| Group | $E_L$ (MeV) | Original | | Corrected | |
|---|---|---|---|---|---|
| | | $\sigma_{tr}$ | $\sigma_{elr}$ | $\sigma_{tr}$ | $\sigma_{elr}$ |
| 2 | 3.67—2.73 | 1.94 | 0.064 | 1.96 | 0.093 |
| 3 | 1.35 | 2.06 | 0.098 | 2.06 | 0.116 |

TABLE V

**COMPARISON OF ORDINARY AND CONSISTENT P-1 (CP-1)**
**(Cross-sections in barns)**

| Vol. % in → mixture | $U^{235}$<br>$U^{238}$<br>SS<br>Al<br>Na | 9.42<br>0.71<br>0—80.1<br>0<br>0 | | | | 4.97<br>0.71<br>0<br>0—12.19<br>0 | | | | 13.93<br>15.84<br>17.62<br>0<br>11.60—46.50<br>(EBR-II Comp.) | | | |
|---|---|---|---|---|---|---|---|---|---|---|---|---|---|
| Group | $E_L$ (MeV) | SS | | | | Al | | | | Na | | | |
| | | $\sigma_{tr}$ | | $\sigma_{elr}$ | | $\sigma_{tr}$ | | $\sigma_{elr}$ | | $\sigma_{tr}$ | | $\sigma_{elr}$ | |
| | | P-1 | CP-1 | P-1 | CP-1 | P-1 | CP-1 | P-1 | CP-1 | P-1 | CP-1 | P-1 | CP-1 |
| 2 | 3.67—2.23 | 1.94 | 2.20 | 0.064 | 0.064 | 1.33 | 1.42 | 0.166 | 0.166 | 1.43 | 1.51 | 0.213 | 0.213 |
| 3 | 1.35 | 2.06 | 2.31 | 0.098 | 0.098 | 1.94 | 2.01 | 0.237 | 0.238 | 1.66 | 1.75 | 0.233 | 0.234 |
| 4 | 0.83 | 1.94 | 2.16 | 0.123 | 0.124 | 2.12 | 2.26 | 0.323 | 0.324 | 2.69 | 2.78 | 0.432 | 0.433 |
| 5 | 0.50 | 2.26 | 2.48 | 0.174 | 0.175 | 2.77 | 2.88 | 0.408 | 0.409 | 4.30 | 4.25 | 0.698 | 0.699 |
| 6 | 0.30 | 2.57 | 2.73 | 0.151 | 0.150 | 3.09 | 3.20 | 0.402 | 0.403 | 3.21 | 3.42 | 0.526 | 0.525 |
| 7 | 0.18 | 2.50 | 2.65 | 0.169 | 0.169 | 3.20 | 3.38 | 0.454 | 0.452 | 3.58 | 3.83 | 0.631 | 0.631 |
| 8 | 0.11 | 3.05 | 3.15 | 0.222 | 0.222 | 3.86 | 4.04 | 0.427 | 0.428 | 3.43 | 3.61 | 0.480 | 0.480 |
| 9 | 0.067 | 3.73 | 3.77 | 0.262 | 0.260 | 3.68 | 3.91 | 0.306 | 0.307 | 3.71 | 4.06 | 0.547 | 0.546 |
| 10 | 0.041 | 4.30 | 4.62 | 0.232 | 0.233 | 2.10 | 2.35 | 0.346 | 0.346 | 4.55 | 4.85 | 0.647 | 0.651 |
| 11 | 0.025 | 5.07 | 5.12 | 0.428 | 0.427 | 2.87 | 3.19 | 0.069 | 0.069 | 4.73 | 5.28 | 0.549 | 0.549 |

9.42 vol % $U^{235}$, 0.71 vol % $U^{238}$, 80.1 vol % SS. The corrected high-energy flux obtained in this way is indicated in Fig. 1. A comparison of original and corrected coarse-group cross-sections for Groups 2 and 3 for this mixture is given in Table IV.

The effect of using a lethargy width twice that employed in obtaining the results given in this paper was investigated. In most cases the cross-section changes were less than 10%. In some instances, deviations up to 20% between the single and double lethargy width results were noted. It is not believed that finer subdivision would significantly change the figures given here. The cross-section data used were the highest resolution available except in the case of Na for the results shown in Table V. In this instance the data of Ref. [8] were used. Results from the detailed processing of the data of Ref. [5] as described in Section 4 are given in Table VI.

TABLE VI

**$\sigma_{tr}$ AND $\sigma_{elr}$ FOR SODIUM USING HIBDON'S DATA (13.93 vol.% $U^{253}$—15.84 vol.% $U^{238}$—19.4 vol.% SS)**

| Vol. % {Al / Na → | | 0 / 0—11.6 | 0 / 34.8—46.5 | 18.5 / 0—11.6 | YOM |
|---|---|---|---|---|---|
| $E_L$ (MeV) | | $\sigma_{tr}$ | | | |
| 0.30—0.18 | B* | 3.71 | 3.53 | 3.67 | 3.49 |
| | H* | 4.02 | 3.78 | 4.01 | |
| 0.11 | B | 3.53 | 3.42 | 3.78 | 3.10 |
| | H | 4.33 | 4.00 | 4.67 | |
| 0.067 | B | 3.85 | 3.69 | 4.43 | 3.46 |
| | H | 4.78 | 4.40 | 5.38 | |
| | | $\sigma_{elr}$ | | | |
| 0.30—0.18 | B | 0.678 | 0.612 | 0.631 | 0.518 |
| | H | 0.605 | 0.540 | 0.549 | |
| 0.11 | B | 0.496 | 0.484 | 0.570 | 0.458 |
| | H | 0.637 | 0.603 | 0.719 | |
| 0.067 | B | 0.591 | 0.535 | 0.725 | 0.468 |
| | H | 0.749 | 0.667 | 0.935 | |

* B: BNL-325, H: Hibdon.

## 8. Use of consistent P-1 calculation

All the results previously described were obtained with the ordinary P-1 calculation. One would expect the consistent P-1 results to differ most from the ordinary P-1 when there is strong anisotropy of elastic scattering, as the term in Eq. (7) which represents coupling of the currents is proportional to the cosine of the angle of deflection of the scattered neutron in the laboratory system. If the current per unit lethargy and scattering cross-sections are constant and if scattering is isotropic in the centre-of-mass system, this term becomes proportional for each scatterer to $2/3A$, a small number. If there is a variation in the current per unit lethargy, a larger coupling of currents is produced even for isotropic scattering in the centre-of-mass system.

The accurate application of the consistent P-1 approximation is handicapped by the lack of high-resolution angular-distribution data. What error this would

be likely to introduce into the results is difficult to judge. Results of comparison of ordinary and consistent P-1 calculations for several compositions are given in Table V. Effective transport cross-sections in the latter case usually are about 5% higher than in the former. There is negligible difference in elastic-removal cross-sections, which would be expected since the slight change in leakage between the two cases would have little effect on the flux.

## 9. Significance of deviation of apparent cross-sections from YOM values

For the assemblies, the core compositions of which are given in Tables I–III, only a small fraction of the total fissions and leakage occurs below the lower limit of Group 8, 110 keV. The cross-section variations and deviations from the YOM values above 110 keV are not often extremely large, so that large variations in critical masses calculated with the different cross-sections would not be expected. A detailed study of the effect of the cross-section variations indicated in Tables I–III has not been made. MENEGHETTI [17], in a study of this series of ZPR-III assemblies, has concluded that the use of ordinary P-1 ELMOE cross-sections for light elements leads to critical-mass values 5–10% above those calculated using the YOM values. The calculated critical masses using the YOM cross-sections with the higher $\nu$ values are still 10–20% below the measured ones [17].

The detailed calculations reduce the number of parameters one feels free to adjust in interpreting critical experiments. They are also useful in understanding the results of substitution measurements, particularly with regard to non-linearity of reactivity effect with added material. Obviously, if effects occurring in the energy range below Group 8 are of interest, the detailed calculations become quite important. In such cases it may sometimes be necessary to precede a criticality calculation with an ELMOE-type calculation to generate cross-sections.

A problem which remains unsolved is how to take account of a spatial variation of neutron-energy spectrum. This variation could be local because of heterogeneity as in certain critical experiments, or on a larger scale as in the vicinity of a core-blanket or core-coolant header interface.

## APPENDIX

### Calculation of the elastic-scattering matrix

It is assumed in the calculation that data on the angular dependence of the elastic-scattering cross-sections in the centre-of-mass system are presented in the form

$$\sigma_{sc}(\omega') = \sum_l B_l P_l(\mu') \tag{A-1}$$

where $\sigma_{sc}(\omega')$ = cross-section scattering into the solid angle element $d\omega'$
$\mu'$ = cosine of the scattering angle in the centre-of-mass system
$P_l = l^{th}$ Legendre polynomial.

Data in the laboratory system are converted to the centre-of-mass system. The fractional energy in the laboratory system, $E/E_0$, per collision change of mass system in the input routine is related to $\mu'$ by [1]

$$\frac{E}{E_0} = \frac{1}{(1+A)^2}(A^2 + 1 + 2A\mu')$$

or

$$\mu' = 1 - \frac{2}{\alpha}\left(1 - \frac{E}{E_0}\right) \tag{A-2}$$

where

$$\alpha = \frac{4A}{(A+1)^2}$$

$A$ = moderator mass number
$E_0$ = initial energy of the neutron.

Integrating the scattering cross-section over azimuth angle, one obtains

$$2\pi\sigma_{SC}(\omega')\,\mathrm{d}\mu' = \sigma_{SC}(E_0 \to E)\,\mathrm{d}E. \tag{A-3}$$

Upon differentiation of Eq. (A-2) and substituting this in Eq. (A-3),

$$\sigma_{SC}(E_0 \to E)\,\mathrm{d}E = \frac{4\pi}{E_0\,\alpha}\,\mathrm{d}E \sum_l B_l P_l(\mu')\,. \tag{A-4}$$

Let $x = \frac{1}{\alpha}\left(1 - \frac{E}{E_0}\right)$.

Then, combining Eqs. (A-2) and (A-4), one may evaluate the Legendre polynomials in terms of:

$$P_1(\mu') = \mu' = 1 - 2x$$

$$P_2(\mu') = \frac{3\mu'^2 - 1}{2} = 1 - 6x + 6x^2$$

$$P_3(\mu') = \frac{1}{2}(5\mu'^3 - 3\mu') = 1 - 12x + 30x^2 - 20x^3$$

$$P_4(\mu') = \frac{1}{8}(35\mu'^4 - 30\mu'^2 + 3) = 1 - 20x + 90x^2 - 140x^3 + 70x^4\,.$$

Therefore $x$ varies from 0 to 1 as $E$ varies from $E_0$, the initial energy, to $E = (1-\alpha)E_0$, the minimum possible final energy. This range is divided into $n$ intervals chosen so that the ratio $r$ of lower to upper energy for the interval is the same for each interval, i.e.,

$$r = \frac{E_j}{E_{j-1}}\,.$$

Therefore

$$x_0 = 0$$

$$x_1 = \frac{1}{\alpha}(1 - r)$$

$$x_2 = \frac{1}{\alpha}(1 - r^2)$$

$$\vdots$$

$$x_n = \frac{1}{\alpha}(1 - r^n) = 1$$

and

$$r = (1-\alpha)^{1/n}\,.$$

If one now integrates Eq. (A-4) over the final energy interval $(E_l, E_{l-1})$ corresponding to the $x$-interval $(x_{l-1}, x_l)$,

$$\int_{E_l}^{E_{l-1}} \sigma_{SC}(E_0 \to E)\,\mathrm{d}E = 4\pi \int_{x_{l-1}}^{x_l} -\,\mathrm{d}x \left[\sum_{l=0}^{4} B_l P_l(\mu')\right]. \tag{A-5}$$

Collecting like powers of $x_1$ and denoting the coefficients as $A_1$,

$$\sigma_{\text{eltr}}^{E_0 \to l} = 4\pi \left[ A^0{}_0 (x_l - x_{l-1}) + A^0{}_1 \frac{(x^2{}_l - x^2{}_{l-1})}{2} + A^0{}_2 \frac{(x^3{}_l - x^3{}_{l-1})}{3} + \right.$$
$$\left. + A^0{}_3 \frac{(x^4{}_l - x^4{}_{l-1})}{4} + A^0{}_4 \frac{(x^5{}_l - x^5{}_{l-1})}{5} \right] \tag{A-6}$$

where

$\sigma_{\text{eltr}}^{E_0 \to l}$ = microscopic elastic-scattering cross-section from energy $E_0$ to Group $l$

$B^0{}_l$ = coefficients of the Legendre polynomial expansion at energy $E_0$

$A^0{}_0 = B^0{}_0 + B^0{}_1 + B^0{}_2 + B^0{}_3 + B^0{}_4$

$A^0{}_1 = -2\,B^0{}_1 - 6\,B^0{}_2 - 12\,B^0{}_3 - 20\,B^0{}_4$

$A^0{}_2 = 6\,B^0{}_2 + 30\,B^0{}_3 + 90\,B^0{}_4$

$A^0{}_3 = 20\,B^0{}_3 - 140\,B^0{}_4$

$A^0{}_4 = 70\,B^0{}_4$.

If one now lets $E_0$ range over $E_j$, $j = 0, \ldots, J$, the entire range under consideration, and $l$ range over the interval $k = 1, \ldots, J$

where $k = j + l$,

and $E_j$ = lower energy limit of Group $j$,

then, for the case,

$$\sigma_{\text{eltr}}^{E_j \to k} = 4\pi \left[ A^j{}_0\, x_{k-j} - x_{k-j-1} + A^j{}_1 \frac{(x^2_{k-j} - x^2_{k-j-1})}{2} + \right.$$
$$\left. + A^j{}_2 \frac{(x^3_{k-j} - x^3_{k-j-1})}{3} + A^j{}_3 \frac{(x^4_{k-j} - x^4_{k-j-1})}{4} + A^j{}_4 \frac{(x^5_{k-j} - x^5_{k-j-1})}{5} \right].$$

The elastic-scattering cross-section from Group $j$ to Group $k$ is calculated from

$$\sigma_{\text{eltr}}^{j \to k} = \frac{\sigma^{E_j \to k} + \sigma^{E_j - l \to k}}{2}.$$

**Elastic-removal cross-sections**

The elastic-removal cross-section from energy $E_j$ to below $E_{j+1}$ may be represented as

$$\sigma_{\text{elr}}^{E_j, E_{j+1}} = \sum_{k=j+2}^{j+n} \sigma_{\text{eltr}}^{E_j \to k}.$$

Substituting from Eq. (A-6), this becomes

$$\sigma_{\text{elr}}^{E_j, E_{j+1}} = 4\pi \left[ A^j{}_0 (1 - x_1) + A^j{}_1 \frac{(1 - x^2{}_1)}{2} + \right.$$
$$\left. + A^j{}_2 \frac{(1 - x^3{}_1)}{3} + A^j{}_3 \frac{(1 - x^4{}_1)}{4} + A^j{}_4 \frac{(1 - x^5{}_1)}{5} \right]. \tag{A-7}$$

The elastic-removal cross-section from Group $j$ is calculated as

$$\sigma_{\text{elr}}^{j} = \frac{\sigma_{\text{elr}}^{E_{j-1} E_j} + 4\pi\, B^j{}_0}{2}.$$

**Transport cross-sections**

The transport cross-section is given by

$$3\,\sigma_{\text{tr}}^{E_j} = 3\sigma_{\text{sc}}^{E_j} (1 - \bar{\mu}) + 3\sigma_{\text{a}} \tag{A-8}$$

where $\mu$ = average scattering angle cosine in laboratory system

$\sigma_{\text{a}}$ = total removal cross-section due to processes other than elastic scattering

$$\sigma_{\text{sc}}^{E_j} = 4\pi\, B^j{}_0.$$

From Eq. (A-8)

$$3\sigma_{\mathrm{tr}}^{E_j} = 12\pi B^j{}_0 \left(1 - \frac{2}{3A} - u_{1,1}^{-1}\frac{B^j{}_1}{3B^j{}_0} - u_{1,2}^{-1}\frac{B^j{}_2}{3B^j{}_0} - u_{1,3}^{-1}\frac{B^j{}_3}{3B^j{}_0} - u_{1,4}^{-1}\frac{B^j{}_4}{3B^j{}_0}\right) + 3\sigma_{\mathrm{a}}$$

or

$$3\sigma_{\mathrm{tr}}^{E_j} = 4\pi\left(3B^j{}_0 - \frac{2B^j{}_0}{\mathrm{A}} - u_{1,1}^{-1}\,B^j{}_1 - u_{1,2}^{-1}\,B^j{}_2 - u_{1,3}^{-1} - u_{1,4}^{-1}\,B^j{}_4\right) + 3\sigma_{\mathrm{a}}$$

where $u_{1,1}^{-1}$, $u_{1,2}^{-1}$, $u_{1,3}^{-1}$ and $u_{1,4}^{-1}$ are elements of the transformation matrix $U^{-1}$ defined in ANL-6039 transforming the $B_l$ from the centre-of-mass system to the laboratory system. As above, the cross-section at Group $j$ is calculated by

$$3\sigma_{\mathrm{tr}}^{j} = \frac{3\sigma_{\mathrm{tr}}^{E_j} + 3\sigma_{\mathrm{tr}}^{E_j-1}}{2} + 3\sigma_{\mathrm{a}}\,.$$

For use in the fundamental mode calculations, the macroscopic cross-sections are homogenized as

$$\Sigma^j{}_i = \sum_m \sigma^j{}_i\,(m)\,N\,(m)\,V\,(m)$$

where

$j$ = group index,
$m$ = material index,
$i$ = reaction, i.e., absorption, transport, etc.
$\sigma^j{}_i(m)$ = material-dependent macroscopic cross-section,
$N(m)$ = atoms per cubic centimeter of material $m$,
$V(m)$ = volume fraction of material $m$.

## ACKNOWLEDGEMENTS

Extensive assistance with the computational work was provided by K. E. Phillips, L. Kvitek and Stella Dean. Thanks are due to C. T. Hibdon for furnishing his original data on the total cross-section of aluminium.

## REFERENCES

[1] WEINBERG, A. M. and WIGNER, E. P., The Physical Theory of Neutron Chain Reactors, University of Chicago Press, Chicago (1958).
[2] SELENGUT, D. S., APEX-121 (1952).
[3] HURWITZ, H., Jr. and ZWEIFEL, P. F., *J. appl. Phys.* **26** (1955) 923.
[4] HELLENS, R. L., LONG, R. W. and MOUNT, B. H., WAPD-TM-4 (1956).
[5] HIBDON, C. T., *Phys. Rev.* **118** (1960) 514.
[6] BUTLER, M. K. and COOK, J. M., ANL-5437 (1956).
[7] CARLSON, B., LEE, C. and WORLTON, J., LAMS-2346 (1960).
[8] HUGHES, D. J. and SCHWARTZ, R. B., BNL-325, 2nd ed. (1958) and Suppl. 1 (1960).
[9] LANGSDORF, A., Jr., LANE, R. O. and MONOHAN, J. E., *Phys. Rev.* **107** (1957) 1077. See also ANL-5567 (1956).
[10] LANE, R. O. and MONOHAN, J. E., *Phys. Rev.* **118** (1956) 533.
[11] LANE, R. O., *et al.*, *Ann. Phys.* (February 1961).
[12] LUSTIG, H., GOLDSTEIN, H. and KALOS, M. H., NDA 086-2 (1958).
[13] WILLS, J. E. *et al.*, *Phys. Rev.* **109** (1958) 891.
[14] HIBDON, C. T., *Phys. Rev.* **114** (1959) 179.
[15] LONG, J K., BAKER, A. R., GEMMELL, W., KEENEY, W. P., Mc VEAN, R. L. and THALGOTT, F. W., *These proceedings*, vol. **I**, p. 271.
[16] YIFTAH, S., OKRENT, D. and MOLDAUER, P. A., Fast Neutron Cross Sections, Pergamon Press, London (1960).
[17] MENEGHETTI, D., *These proceedings*, vol. **I**, p. 457.
[18] LANE, R. O., MILLER, W. F. and HILLSTROM, R. E., ANL-6039 (1959).

# II. INTEGRAL EXPERIMENTS

## 1. CRITICAL EXPERIMENTS

# INTEGRAL EXPERIMENTS ON FAST SYSTEMS OF PLUTONIUM, URANIUM AND THORIUM*

J. J. McEnhill and J. W. Weale
Atomic Weapons Research Establishment, Aldermaston, United Kingdom

**Abstract — Résumé — Аннотация — Resumen**

**Integral experiments on fast systems of plutonium. uranium and thorium.** The paper describes two types of integral experiment which have been undertaken to provide experimental checks on nuclear data and methods of calculation.

The first consists of a cylindrical assembly of material with a point source of DD or DT neutrons at its centre. The neutron flux and various reaction rates in the cylinder material are measured as a function of position. Results obtained are compared with calculation. Experimental results for natural uranium and thorium are presented.

The second type of experiment is a low-power experimental reactor of simple regular geometry and approximately homogeneous composition. Holes can be provided as required for the insertion of counters or perturbation samples. The core composition is adjusted by the addition of a moderator to provide a neutron spectrum which tests the nuclear data in the energy region of interest. Measurements are made of the neutron-energy spectrum and various reaction rates and perturbation cross-sections as a function of position in the reactor and the results are compared with computer calculations. Results are presented for a system consisting of a core of of $U^{235}$ and graphite surrounded by a natural-uranium reflector.

**Expériences intégrales sur réacteurs à neutrons rapides de plutonium, d'uranium et de thorium.** Les auteurs décrivent deux types d'expériences intégrales visant à contrôler expérimentalement des données nucléaires et des méthodes de calcul.

Le premier dispositif expérimental est un empilement cylindrique de matériau au centre duquel est placée une source ponctuelle de neutrons DD ou DT. On mesure le flux de neutrons et l'intensité de diverses réactions dans le matériau, en fonction de la position. On compare les résultats des mesures à ceux des calculs. Le mémoire donne les résultats des expériences effectuées avec de l'uranium naturel et du thorium.

Le deuxième dispositif est un réacteur expérimental de faible puissance, ayant une géométrie régulière simple et une composition sensiblement homogène. On peut le munir, selon les besoins, de canaux pour l'introduction de compteurs ou d'échantillons de matériaux perturbateurs. On règle la composition du cœur par l'adjonction d'un ralentisseur, afin d'obtenir un spectre de neutrons tel que le contrôle des données nucléaires s'effectue dans la zone d'énergie voulue. On mesure le spectre d'énergie des neutrons, ainsi que l'intensité de diverses réactions et les sections efficaces de perturbation, en fonction de la position dans le réacteur. On compare les résultats à ceux qui sont donnés par des calculatrices. Le mémoire donne les résultats obtenus avec un réacteur ayant un cœur composé de $^{235}U$ et de graphite, entouré d'un réflecteur en uranium naturel.

**Интегральные эксперименты с системами на быстрых нейтронах с плутонием, ураном и торием.** В докладе дается описание двух экспериментальных установок, созданных для экспериментальной проверки ядерных данных и вычислительных методов.

Первая установка состоит из сборки материала цилиндрической формы с точечным источником нейтронов DD или DT расположенным в ее центре. Поток нейтронов и различные скорости реакции в цилиндре измеряются как функция положения. Полученные

* Including work by L. R. Day, J. R. Dominey, H. Goodfellow, M. H. McTaggart, H. Shieff, A. F. Thomas, K. A. Wallace.

результаты сравниваются с расчетом. Даются экспериментальные результаты для природного урана и тория.

Вторым типом установки является экспериментальный реактор низкой мощности с простой обычной геометрией и приблизительно гомогенным составом. Реактор может иметь каналы, необходимые для введения счетчиков или возмущающих образцов. Состав активной зоны регулируется добавлением замедлителя с тем, чтобы иметь спектр нейтронов, необходимый для проверки ядерных данных в интересующей области энергии. Измеряются энергетический спектр нейтронов, различные скорости реакции и изменение поперечного сечения как функции положения в реакторе, и результаты сравниваются с расчетами на вычислительных устройствах. Даются результаты для системы, состоящей из активной зоны из урана-235 и графита, окруженной отражателем из природного урана.

**Experimentos integrales realizados con reactores rápidos de plutonio, uranio y torio.** Los autores describen dos tipos de experimentos integrales que se han llevado a cabo con el propósito de comprobar experimentalmente determinados datos nucleares, así como la exactitud de los métodos de cálculo empleados.

El primer dispositivo experimental consiste en un montaje cilíndrico en cuyo centro se halla una fuente puntual de neutrones DD o DT. El flujo neutrónico y las diversas velocidades de reacción en el material del cilindro se miden en función de la posición de la fuente y los resultados así obtenidos se comparan con los calculados. La memoria presenta los resultados de experimentos efectuados con uranio natural y con torio.

Para el segundo tipo de determinaciones, se utiliza un reactor experimental de baja potencia, con una geometría regular sencilla y una composición sensiblemente homogénea. Los orificios practicados en el mismo pueden utilizarse para introducir, conforme sea necesario, contadores o muestras perturbadoras. La composición del cuerpo se regula mediante la adición de un moderador, a fin de disponer de un espectro neutrónico que permita comprobar los datos nucleares en la región energética que interesa. Se realizan mediciones del espectro de energías neutrónicas y de diversas velocidades de reacción y secciones eficaces de perturbación en función de la posición en el reactor y los resultados se comparan con los obtenidos con calculadoras. La memoria da los resultados correspondientes a un sistema que consiste en un cuerpo de $^{235}U$ y grafito, rodeado de un reflector de uranio natural.

## Introduction

A broad programme of research is in progress at Aldermaston to improve our understanding of the neutron physics of fast systems. Its primary aim is to reduce the errors and uncertainties which arise in the present calculations of nuclear characteristics for fast-reactor systems. These errors arise mainly from the inadequacy of the basic nuclear data, and the work therefore centres on an attempt to improve these data and to establish a single set of data for fast-reactor materials which is sufficiently accurate over the whole energy range of interest. The overall programme comprises three interrelated areas of work:

(*a*) Measurements of important nuclear cross-sections and parameters;

(*b*) Compilation of nuclear-data sets using results of (*a*) and other available data, and the development of methods of theoretical analysis of the nuclear characteristics of fast systems; and

(*c*) Checks of the accuracy of the nuclear data sets and system analysis against integral experiments.

Aspects of the data measurements and of the theoretical analysis are described in other Aldermaston papers presented at this Seminar. The present paper will describe some relevant integral experiments.

First of all, however, it is instructive to indicate, by reference to some of our problems at Aldermaston during the past two years, how the three programmes relate one to another and how they help to establish which microscopic

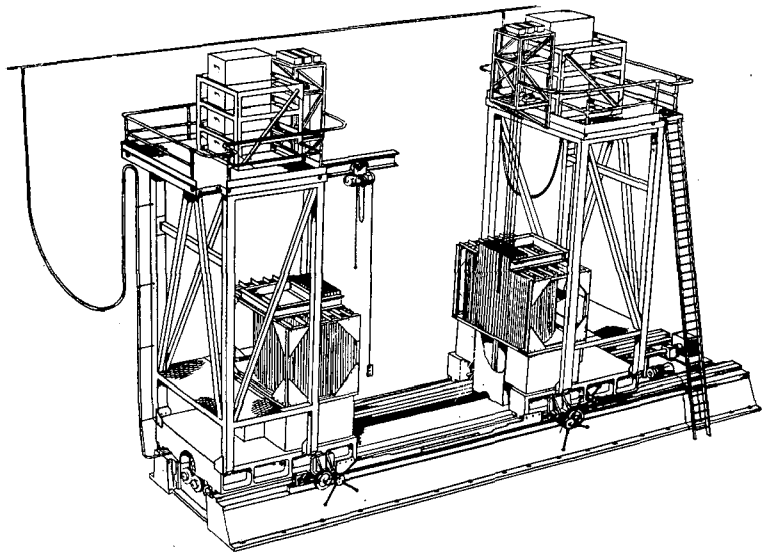

Fig. 1
Versatile experimental reactor essembly (VERA).

data need to be checked and which integral experiments are essential. During 1959 a literature review of nuclear data was made and a set of nuclear data established by selecting "best values" from the published microscopic data. These data were checked by calculating critical masses for a number of Pu- and highly-enriched U-systems, both bare and reflected by various thicknesses of natural U. The calculated critical masses were in all cases about 20% smaller than the experimental values. About this time a direct experimental measurement of $\nu$ for $U^{235}$ suggested a downward revision of this quantity. A low $\nu$ value was therefore adopted for the $U^{235}$ calculations and a corresponding reduction was applied for $Pu^{239}$. Good agreement with experimental critical masses for fast concentrated systems was then obtained and this set of nuclear data was therefore adopted for general use [1]. Nevertheless, the need for further measurements of $\nu$ and further checks against integral experiments was recognized and new work was put in hand. Later it became clear that the low $\nu$ value was incorrect and that the adopted nuclear-data set was less accurate for U-systems of lower enrichment. New experimental data had also accumulated and it was decided to make a complete revision of data for $U^{235}$, $U^{238}$ and $Pu^{239}$. As an interim measure an attempt was made to adjust the nuclear data empirically to fit integral results over a wider range of U concentration. This was done [2] by making plausible adjustments to the values of $\nu$ and $\sigma_f$ for $U^{235}$ and to $\nu$ and $\sigma$ (n, $\gamma$) for $U^{238}$. The procedure was successful, reducing the critical-mass errors to $\pm 3\%$ over the concentration range 29% to 93% $U^{235}$. It is not satisfactory,

however, to rely permanently on this expedient. New microscopic measurements and integral checks for the revised data are evidently required and these are progressing in parallel with the detailed revision of the basic nuclear-data set. Initial results for $\nu$ of $U^{235}$ are reported by MOAT [3], and initial results of a new $U^{235}$ integral experiment are reported as part of the present paper.

Our integral experiments are of three types. The first is the determination of critical mass by extrapolation of multiplication measurements made on a critical assembly machine; the second is the analysis of neutronic processes in large blocks of material in which a strong compact neutron source is located; the third is the detailed study of neutron reactions in a simple system operated as a zero-energy reactor. Some of the critical-mass measurements were done primarily to provide data for safety assessment; the other experiments were designed specifically for testing nuclear data. All the experiments have simple regular geometry and uniform composition, so that corrections relating the actual experimental system to the calculated model are minimized.

## 1. Critical mass measurements for fast systems

A number of critical-mass measurements have been made for plutonium metal in spherical geometry and for 45.5% enriched U metal in slab geometry.

The Pu measurements are for a bare sphere and for spheres reflected by natural uranium, pile-quality graphite, steel or water. The results are based on central-source multiplication measurements using Pu spheres of 4.5, 6, 7.5 and 9 kg and various thicknesses of each reflecting material. Each Pu sphere had a 2.16-cm-diameter spherical cavity at the centre to accommodate the neutron source used for multiplication measurements. The plutonium metal density was 15.64 g/cm³ and the metal in the form of two hemispheres was clad in copper foil, 0.010 in thick on the curved surfaces and 0.005 in thick on the flat surface.

Calculations for these systems have been made using the nuclear data of reference [1] in a multi-group Carlson $S_8$ code. Seven energy groups from 10 keV to 11 MeV were used for the Fe- and U-reflected systems and 13 energy groups from thermal to 11 MeV for the graphite-reflected system. The results are compared with experimental values for a number of reflector thicknesses in Table I.

TABLE I

**COMPARISON OF CALCULATED AND EXPERIMENTAL CRITICAL MASSES FOR Pu SYSTEMS**

| Reflector | Reflector thickness (in) | Experimental crit. mass (kg Pu) | Calculated crit. mass (kg Pu) |
|---|---|---|---|
| None | — | 16.8 | 17.0 |
| Natural U (18.7 g/cm³) | 2 | 8.5 ± 0.1 | 8.10 |
| | 3 | 7.4 ± 0.1 | 7.19 |
| | 6 | 6.3 ± 0.1 | 6.31 |
| Fe (7.87 g/cm³) | 2 | 10.9 | 10.3 |
| | 4 | 9.6 ± 0.1 | 8.80 |
| | 6 | 9.1 ± 0.1 | 8.11 |
| C (1.61 g/cm³) | 2 | 11.2 | 11.0 |
| | 4 | 9.2 ± 0.1 | 9.39 |
| | 6 | 8.2 ± 0.1 | 8.62 |

The experimental critical masses are derived from graphical extrapolations of graphs relating central-source multiplication to reflector thickness and the errors indicated are estimates of the probable errors of the extrapolations. In three cases the extrapolation was rather long (the largest available sphere being 9 kg) and no error is quoted for these. The result for the bare sphere was obtained by analytical extrapolation of a least-squares fit to a diffusion-theory approximation.

It should be noted that data used in the calculations are "best values" except for $\nu$, for which the low value of $\nu$ ($Pu^{239}$) $= 2.82 + 0.105\,E$ was chosen in order to obtain agreement between calculation and experiment for the bare and thick-U-reflected systems. For graphite the agreement is reasonably good but for Fe the calculated values are too small by amounts ranging from 6% to 11%. Taken with the fact that the $\nu$ value should probably be higher, the latter result suggests that the Fe scattering data need checking.

The U-slab experiments were done specifically for criticality safety assessment, to provide data against which calculations of fast-reactor melt-down configurations could be checked. Measurements of critical size were made for bare slabs and for slabs reflected by natural uranium, graphite, steel and aluminium respectively. The reflector covered both faces and edges of the slabs. The slabs were constructed of machined blocks in the form of hexagons $2\frac{3}{4}$-in across the flats and of various thicknesses. These were assembled into pseudo-cylindrical assemblies with a neutron source located at the centre, and measurements of the central-source multiplication were made as a function of thickness of the enriched-U slab. Critical thicknesses were obtained by graphical extrapolation. The results are listed in Table II.

TABLE II

**RESULTS OF U SLAB EXPERIMENTS**

| Reflector | Critical thickness of enriched U (in) | | |
|---|---|---|---|
| | 11.6 in diam. | 16.9 in diam. | 22.1 in diam. |
| None | $7.26 \pm 0.03$ | $5.47 \pm 0.04$ | — |
| Nat. U (6-in thick, 16.3 g/cm³) | $3.27 \pm 0.02$ | $2.36 \pm 0.02$ | $2.01 \pm 0.02$ |
| Graphite (6-in thick, 1.74 g/cm³) | $3.00 \pm 0.02$ | $2.14 \pm 0.02$ | $1.78 \pm 0.02$ |
| Steel (6-in thick, 7.24 g/cm³) | $4.12 \pm 0.03$ | $2.98 \pm 0.02$ | $2.57 \pm 0.02$ |
| Aluminium (6-in thick, 2.58 g/cm³) | $4.40 \pm 0.02$ | $3.21 \pm 0.02$ | $2.72 \pm 0.02$ |

The diameter indicated is that of the enriched-U slab. The natural-U reflector was solid for the first inch on the flat faces of the slab; the remainder of the reflector was a 5.7-in layer of $1\frac{1}{8}$-in rods at a packing density of 0.85. The effective density of the enriched-U slabs was 18.44 g/cm³.

These experimental results have been used to check the adjusted set of nuclear data [2] for $U^{235}$ and $U^{238}$. Calculations were carried out using a two-dimensional Carlson code ($S_4$) with 13 energy groups from thermal to 11 MeV. The results are listed in Table III.

TABLE III

**COMPARISON OF CALCULATED AND EXPERIMENTAL CRITICAL THICKNESSES FOR 45.5% U SLABS (inches)**

| Reflector / Slab diameter | None | | Graphite 6-in thick all round | |
|---|---|---|---|---|
| | Exp. | Calc. | Exp. | Calc. |
| 11.6 | 7.26 | 6.99 | 3.00 | 3.18 |
| 16.9 | 5.47 | 5.43 | 2.14 | 2.31 |
| 22.1 | — | — | 1.78 | 1.95 |

Agreement is good for the bare systems but for the graphite-reflected systems errors range from 6% to 10%, the calculated results being too large. This discrepancy is ascribed to errors in $U^{238}$ data at the lower neutron energies produced by the graphite reflector.

## 2. Accelerator-driven integral experiments with uranium and thorium

The neutron balance in a large cylindrical pile of material with a 14-MeV neutron source at its centre has been studied experimentally for natural uranium metal and for thorium metal. (A full account of the U experiment is given in a recent paper [4]). The neutron source was a Zr-$H^3$ target located at the centre of the cylinder and bombarded by a beam of deuterons brought in through a drift-tube from a 200-kV Cockcroft-Walton accelerator. Each pile was made of vertical rods packed closely together, and it was possible to remove a rod from any position to provide access for a counter to measure reaction rates and neutron spectra as a function of position in the pile. Copper cylinders were inserted and irradiated to measure the 14-MeV neutron flux by the $Cu^{63}$ (n, 2n) threshold reaction; fission rates were measured by inserting fission chambers loaded with the appropriate material; and neutron-capture rates were measured by irradiating small pellets of U or Th metal and separating and counting the $Pa^{233}$ or $Np^{239}$ activity. All the measurements were related to the strength of the central 14-MeV neutron source which was continuously monitored by counting the associated $\alpha$-particles emitted into a known solid angle at 177° to the deuteron beam. The total number of neutrons of all energies escaping from the pile for each central-source neutron was measured by means of a "long" counter mounted outside the system, its position being varied to take account of the variation of the emergent flux with angle. The fission and capture rate results were integrated to determine the total number of fissions and captures in the pile per central-source neutron.

The way in which these results can be used to draw up a detailed neutron balance is described (for the U pile) in reference [4]. Recently the results have been used to check the accuracy of nuclear data for natural U in the fast-neutron energy range. Two Monte Carlo calculations have been made by PARKER and MERCER [5] using first the nuclear data of reference [1] and secondly the same data with the original (unadjusted) values for $\nu$. The results of these calculations are compared with the experimental results in Table IV.

TABLE IV

**EXPERIMENTAL AND CALCULATED VALUES FOR THE NUMBER OF REACTIONS PER 14-MeV CENTRAL-SOURCE NEUTRON IN THE U PILE***

| Reaction | Experiment | Calculation (A) | Calculation (B) |
|---|---|---|---|
| $U^{238}$ fission | $1.18 \pm 0.06$ | 0.78 | 0.86 |
| $U^{235}$ fission | $0.28 \pm 0.02$ | 0.20 | 0.23 |
| $U^{238}$ capture | $4.08 \pm 0.24$ | 3.45 | 3.96 |
| Leakage | $0.41 \pm 0.02$ | 0.53 | 0.52 |

* The effective pile dimensions were: height 112 cm, diameter 99 cm; the effective density was 16.3 g/cm³.

Calculation (A) (Table IV) used the data of reference [1], in which $\nu$ $(U^{235}) = 2.25 + 0.132\,E$ and $\nu$ $(U^{238}) = 2.32 + 0.129\,E$.

Calculation (B) (Table IV) used the same data except that the values were taken as $\nu$ $(U^{235}) = 2.46 + 0.144\,E$ and $\nu$ $(U^{238}) = 2.53 + 0.141\,E$.

Evidently the higher values of $\nu$ give better agreement with experiment, but there is a large error in the $U^{238}$ fission calculation. This must be due to an error in the fission cross-section or in the inelastic scattering cross-section or energy distribution.

The Th pile results have not yet been compared with calculations but the experimental integral results are quoted (in Table V), as they provide useful data against which nuclear constants for this material can be checked.

TABLE V

**EXPERIMENTAL INTEGRALS FOR THE Th PILE***

| Reaction | Number of reactions per 14-MeV central-source neutron |
|---|---|
| Th (n,f) | $0.174 \pm 0.009$ |
| Th (n,γ) | $1.51 \pm 0.08$ |
| Leakage | $0.69 \pm 0.02$ |

* The pile was 110 cm high, 96.5 cm in diameter and contained 9.70 g/cm³ Th and 0.13 g/cm³ Fe.

## 3. Experiments on fast critical systems

We have recently commissioned a new Versatile Experimental Reactor Assembly (VERA) and it is being used for studies of the physics of fast critical systems. The measurements are primarily intended to provide information for a systematic check of nuclear data in the energy range 1 keV to 1 MeV. For each assembly the neutron flux, neutron spectrum, fission and capture rates and perturbation cross-sections are measured as a function of position, and the fast chain-decay constant (Rossi-$\alpha$) is measured in the region of delayed critical. Multi-group Carlson calculations are compared in detail with the experi-

mental results and discrepancies are interpreted in terms of corresponding errors in group cross-sections. The first assembly, which is now under study, has a core of $U^{235}$ and C surrounded by a reflector of natural U. The properties of this system provide a sensitive check of nuclear data for $U^{235}$ and will be used to select (within experimental cross-section errors) a set of group constants for this nuclide.

VERA is constructed of square-section fuel boxes mounted vertically in a steel lattice plate. The core and the axial portions of the reflector are composed of small square plates or bricks of material and are loaded in the fuel boxes. The radial portion of the reflector consists of closely-packed round rods which surround the square fuel boxes and are located by holes drilled in the lattice plate. The assemblies are arranged as pseudo-cylindrical cores surrounded by cylindrical reflectors and the compositions of the axial and radial portions of the reflector are adjusted to be the same. Accurate calculations are thus possible by means of the two-dimensional Carlson codes. In these calculations the core is taken as a homogeneous mixture and the experimental results, which apply to mixtures of $\frac{1}{8}$-in-thick plates, therefore require a slight correction for the fuel "bunching" effect.

To ensure safety during loading and core modifications and to provide a second shut-down mechanism, the lattice plate is divided into two portions and the reactor is correspondingly divided in half. One half is mounted on a moveable table which rests on rails and can be driven along these rails by an electrically-driven leadscrew. Loading and core modifications are only carried out when the two halves of the reactor are separated by a distance of 5 ft. A number of safety and control elements are provided. These are normal fuel boxes loaded with core and blanket material and suspended by cables from winches on the reactor superstructure. They can be dropped below their normal positions in the reactor through holes provided in the lattice plate. The safety elements are fully raised into the core before the reactor halves are driven together; the control elements are raised as the last step in the approach to criticality. The reactor is not provided with local shielding but is located in a large room with thick concrete walls, and this room is sealed during reactor operation, the reactor then being controlled remotely. No cooling system is provided as it is not intended to operate the reactor at powers above 100 W.

The dimensions and composition of the $U^{235}$/graphite assembly (referred to as VERA Assembly 2) are as follows:

| | |
|---|---|
| Core height (cm) | 27.15 |
| Core diameter (cm) | 38.10 |
| Core volume (l) | 30.8 |
| Reflector radial thickness (cm) | 37.4 |
| Reflector axial thickness (cm) | 39.4 |
| $U^{235}$ content of core (kg) | 88.96 |
| $U^{238}$ content of core (kg) | 6.80 |
| Stainless-steel content of core (kg) | 23.44 |
| Graphite content of core (kg) | 35.55 |
| Hydrogen content of core (g) | 3.0 (this is the protective lacquer) |
| Composition of reflector: U-natural (g/cm$^3$) | 14.39 |
| Stainless steel (g/cm$^3$) | 0.832 |

With all safety and control elements fully raised, the above system has an excess reactivity of 0.3%, i.e. 0.9% in core mass, assuming $\Delta K/K = \frac{1}{3}(\Delta M/M)$. Holes provided to accommodate counters at the core-reflector interface make the reactivity 0.67% less than it would be in ideal geometry. The bunching of the fuel into $\frac{1}{8}$-in plates makes the critical mass 2% smaller than it would be for a homogeneous system (reference [6]).

With these corrections the critical parameters for a homogeneous system of the above composition are:

Critical volume: 30.4 l
Critical mass: 87.8 kg $U^{235}$.

A two-dimensional Carlson calculation using the nuclear data of reference [1] in 13 energy groups predicts a critical mass of 92.1 kg $U^{235}$ for this system.

Measurements of fission rates, perturbation cross-sections and the prompt chain-decay constant for this system are now in progress. Preliminary results of measurements at the core centre are listed in Table VI.

TABLE VI

**MEASURED CROSS-SECTION RATIOS AT THE CENTRE OF THE VERA CORE**

| Fission ratios | Experimental results* | Calculated results** |
|---|---|---|
| $\frac{U^{238}}{U^{235}}$ | 0.077 | 0.074 |
| $\frac{U^{236}}{U^{235}}$ | 0.162 | 0.153 |
| $\frac{Pu^{239}}{U^{235}}$ | 1.18 | 1.12 |
| $\frac{Np^{237}}{U^{235}}$ | 0.488 | 0.365 |
| $\frac{U^{238}\ \text{(capture)}}{U^{235}}$ | 0.121 | 0.138 |
| Perturbation ratio $\frac{Pu^{239}}{U^{235}}$ | 1.72 | 1.53 |

* These results have a probable error of about 6%.
** The calculated values are from the two-dimensional Carlson calculations using data from reference [1].

## Future work

During the next two years work will be mainly concentrated on the VERA programme. The next step after completion of the $U^{235}$/C studies will be to add $U^{238}$ to the core, adjusting the C content so that the spectrum is not appreciably changed, and repeat the measurements and calculations, thus checking

the nuclear data for $U^{238}$. Subsequent systems will include $Pu^{239}$ and various diluent materials such as Fe, Al and Na, and small quantities of a moderating material will be added so that the neutron-energy spectrum is varied over the desired range. Some diluent materials of particular interest will be studied separately in accelerator-driven integral experiments of the type described for U and Th. A Na assembly is planned as the next in this series. When the revised nuclear-data sets are available, detailed analysis of the U and Th pile results will be carried out.

## ACKNOWLEDGEMENTS

Acknowledgement is due to Mr. H. Bird, Dr. L. Russell and Mr. E. Pendlebury of the theoretical physics division at Aldermaston for providing the results of their multi-group Carlson calculations and to members of the chemistry division for separating and counting $Pa^{233}$ and $Np^{239}$.

## REFERENCES

[1] BUCKINGHAM, B. R. S., PARKER, K. and PENDLEBURY, E. D., AWRE Report 0—28/60 (1960).
[2] PENDLEBURY, E. D., These proceedings, vol. **II**, p. 97.
[3] MOAT, A., *et al.* These proceedings, vol. **I**, p. 139.
[4] WEALE, J. W., *et al.*, *J. nucl. Energy* **14** (1961) 91.
[5] PARKER, J. B. and MERCER, A., unpublished information.
[6] LONG, J. K., *et al.*, Proc. 2nd UN Int. Conf. PUAE **12** (1958) 119.

SM—18/52

# CRITICAL EXPERIMENTS AND NUCLEAR CALCULATIONS—LAMPRE-I*

M. E. Battat
Los Alamos Scientific Laboratory
University of California, Los Alamos, N. Mex.,
United States of America

**Abstract — Résumé — Аннотация — Resumen**

**Critical experiments and nuclear calculations—LAMPRE-I.** As part of a programme to develop plutonium fuels for fast-breeder reactors, the Los Alamos Scientific Laboratory has constructed and is operating a 1-MW sodium-cooled test reactor whose core contains a molten alloy of plutonium and iron (90 at. % Pu, 10 at. % Fe, m.p. 410°C). Reactivity control is provided by the use of a stainless-steel reflector and four nickel control-rods located external to the core.

Experiments have been performed at core temperatures (isothermal) of 80, 160 and 480°C to determine critical mass and reflector worth at each of these temperatures. Control-rod worths, from period measurements, and temperature coefficient of reactivity were also measured.

Calculations have been made, using the $S_n$ method for solving the neutron transport problem, to determine the basic nuclear parameters of the system. The comparison between calculated and measured values of parameters such as temperature coefficient, control-element worths, and critical mass is also of interest in evaluating the reliability of the design calculations.

**Expériences critiques et calculs nucléaires concernant le LAMPRE-I.** Un réacteur d'essais de 1 MW refroidi au sodium, dont le cœur contient un alliage fondu de plutonium et de fer (90 at. % Pu, 10 at. % Fe, p. f. 410°C), a été construit et est en fonctionnement au Laboratoire scientifique de Los Alamos, dans le cadre d'un programme d'études sur les combustibles au plutonium pour réacteurs surgénérateurs à neutrons rapides. Le contrôle de la réactivité est assuré au moyen d'un réflecteur en acier inoxydable et de quatre barres de contrôle en nickel, à l'extérieur du cœur.

On a fait des expériences à des températures du cœur de 80, 160 et 480°C afin de déterminer la masse critique et la quantité de réflecteur qui correspond à chacune de ces températures. On a aussi mesuré l'efficacité des barres de contrôle, à partir de mesures de période, ainsi que le coefficient thermique de réactivité.

Afin de déterminer les paramètres nucléaires de base du réacteur, on a utilisé la méthode $S_n$ pour résoudre le problème du transport neutronique. La comparaison entre les valeurs calculées et les valeurs mesurées des paramètres, tels que le coefficient thermique, l'efficacité des barres de contrôle et la masse critique, présente aussi de l'intérêt pour évaluer le degré de confiance que l'on peut accorder aux calculs des bureaux d'études.

**Критические опыты и ядерные расчеты — ЛАМПРЕ-I.** В качестве части программы по развитию плутониевого топлива для реакторов-размножителей на быстрых нейтронах Лос-Аламосская научная лаборатория сконструировала и эксплуатирует испытательный реактор с натриевым охлаждением мощностью в 1 мегаватт, активная зона которого содержит расплавленный сплав плутония и железа (90 атомных процентов плутония, 10 атомных процентов железа при точке плавления в 410° Ц). Регулировка реактивности

* Includes work by B. M. Carmichael, R. M. Kiehn, J. L. Lundgren, R. E. Peterson, G. L. Ragan and E. O. Swickard.

обеспечена путем использования отражателя из нержавеющей стали и четырех никелиевых регулирующих стержней, расположенных вне активной зоны.

Были проведены опыты при температурах активной зоны в 80°, 160° и 480° Ц с тем, чтобы определить критическую массу и ценность отражателя при каждой из этих температур. Были измерены температурный коэффициент реактивности, а также ценность регулирующих стержней по измерениям периода.

Были сделаны расчеты с использованием метода $S_n$ для решения проблемы переноса нейтронов, чтобы определить основные ядерные параметры системы. Сравнение между расчетными и измеренными величинами параметров таких как температурный коэффициент, ценность регулирующих элементов и критическая масса представляют также интерес в оценке надежности проектных расчетов.

**Experimentos críticos y cálculos nucleares relativos al LAMPRE-I.** Como parte de un programa de ensayos de combustibles de plutonio para reactores reproductores de neutrones rápidos, se ha construido y puesto en marcha en el Los Alamos Scientific Laboratory un reactor experimental de 1 MW refrigerado por sodio, cuyo cuerpo contiene una aleación fundida de plutonio y hierro (90 atomos por ciento de Pu y 10 atomos por ciento de Fe; punto de fusión: 410°C). La reactividad se regula por medio de un reflector de acero inoxidable y de cuatro barras de control de níquel situadas fuera del núcleo.

Se han llevado a cabo experimentos a temperaturas (isotérmicas) de 80, 160 y 480°C en el cuerpo, a fin de determinar la masa crítica y la eficacia del reflector a cada una de esas temperaturas. También se midió la eficacia de las barras de control, por registro de los períodos y del coeficiente térmico de la reactividad.

Aplicando el método $S_n$ de resolución del problema del transporte neutrónico, se efectuaron cálculos para determinar los parámetros nucleares básicos del reactor. La comparación entre los valores calculados y los valores medidos de parámetros tales como el coeficiente térmico, la eficacia de las barras de control y la masa crítica, presenta también interés en lo que se refiere a la evaluación del grado de confianza que puede atribuirse a los cálculos del proyectista.

## Introduction

The Los Alamos Plutonium Reactor Experiment No. 1 (LAMPRE-I) is part of a programme to investigate the feasibility of using molten plutonium alloys as fuels for power-breeder reactors. LAMPRE-I was specifically designed to provide data for evaluating fuels and container materials; it is not considered as a prototype of a fluid-fuelled reactor. Another objective of this first experiment is to investigate the effect of gaseous-fission-product accumulation in a reactor using molten fuels. However, instead of discussing the latter aspects of the programme, this report will be mainly concerned with the nuclear data obtained during the initial phase of the experiment and comparison of these data with calculations. A brief description of the reactor will also be given.

## Description of the reactor

LAMPRE-I is a fast, sodium-cooled reactor with a design power of 1 MW(t). For the first core loading, the fuel is a plutonium-iron alloy, 90 atom % Pu and 10 atom % Fe, with a melting point of approximately 410°C [1]. The fuel is contained in Ta capsules, each having an inside diameter of 0.942 cm, 0.074 cm wall thickness, and 21.1 cm length. In order to allow for the accumulation of fission gases, each capsule is filled to three-fourths of its total height with approximately

175 g of fuel. The core can accommodate 199 capsules, those locations not used for fuel capsules being occupied by reflector pins. The core region is a cylinder approximately 15 cm in diameter and 15 cm high, with fractional volumes of about 50% fuel, 15% Ta, and 35% sodium coolant. A perspective view of the reactor is shown in Fig. 1.

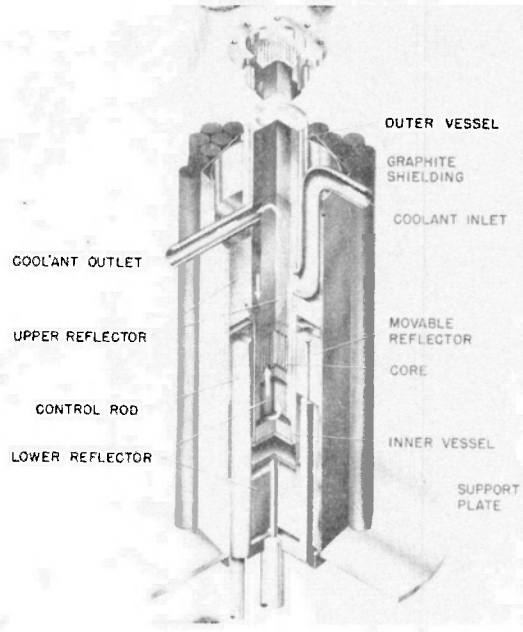


Fig. 1
Perspective view of the reactor.

As can be seen from Fig. 1, coolant sodium enters the reactor vessel and flows downward through an annulus in the radial reflector to the bottom of the vessel. From the bottom, the sodium flows up through the bottom reflector into a plenum, and then through the capsule locator plate into the core. This locator plate consists of a 4.4-cm-thick stainless-steel disc, the top of which is faced with a 0.64-cm-thick sheet of tantalum. Sockets are drilled in the tantalum plate to locate the conical capsule bottoms. The purpose of the tantalum face on the locator plate is to prevent fuel from soldering the capsule tip to the stainless-steel plate in the event of plutonium entering the socket. After flowing past and receiving heat from the core, the sodium passes into the upper-reflector region and out of the vessel. A tantalum catchpot, for containing the fuel in case of a capsule rupture, is located just below the turn-around plenum. Within the catchpot a diluent plug of iron is provided, with holes drilled so that there is about a 35% void. The plug serves to dilute the fuel which might enter the catchpot to a subcritical concentration, and also serves to alloy with and "dry up" the fuel by raising its melting point.

Heat can be supplied to the sodium loop by either or both of two methods. All piping and components are traced with electrical tubular heaters which are used for warming up the system prior to sodium charging. A second system is used to supply sufficient heat to maintain the entire coolant loop and vessel at a minimum of 450°C. The second heating system employs a transformer so constructed that part of the sodium loop is a one-turn secondary of the transformer. There is the capability of adding 40–50 kW in this fashion. It is necessary, of course, that there be some sodium flow when transformer heating is used in order to prevent overheating of the one-turn secondary.

Heat removed from the core by the sodium coolant is discharged through a stack to the atmosphere by a finned-tube, sodium-to-air heat exchanger. Coolant pumping is provided by two alternating-current electromagnetic pumps in parallel. The observed temperature rise in the coolant at 200 kW—460°C inlet Na temperature and a flow rate of 8.2 l/s—was 25°C.

An annular movable steel reflector, with a total travel of 40 cm, furnishes coarse-reactivity control. Vernier-reactivity control is provided by four separately actuated nickel control-rods which are part of the movable steel reflector. Both the reflector and control-rods are actuated hydraulically from below the reactor. The reflector can be scrammed from its maximum reactivity position in 1.5 s. The location of the reactivity-control elements is shown in Fig. 1.

## Calculational method

The method employed to calculate the nuclear parameters of LAMPRE-I was based on the $S_4$ transport scheme for spherical systems [2]. The calculation was made using ten neutron energy groups [3], and empirical methods were used to convert from spherical to cylindrical geometry. Some of the design parameters, control-rod worths for example, were determined from studies made with a critical assembly prior to the completion of the reactor. In what follows, a brief discussion of the calculations will be given; numerical results will be summarized at the end of the section.

The steps involved in the calculation of critical mass were as follows. First, $S_4$ calculations were made for a reflected spherical core using, in turn, the reflector materials and thicknesses appropriate to the system in three different directions: top, side and bottom. For these problems, the core radius was adjusted until criticality of the system was achieved. Second, the results of the latter calculations were used to compute the infinite-media buckling and reflector savings for the spherical systems. The buckling for the cylinder was obtained by averaging the spherical-system bucklings, reduced by 2% to account for inherent systematic errors in cross-sections and the $S_4$ approximation. The spherical-reflector savings were reduced by the empirical factors 0.866 for the ends of the cylinder and 0.937 for the sides. These coefficients have been analytically determined to yield, for unreflected systems, a minimum cylindrical critical mass which is 14% larger than that for a sphere, the height-to-diameter ratio for the minimum-mass cylinder being obtained from diffusion theory [4]. These coefficients essentially account for the reduced curvature of the cylindrical surface and the curvature effect on extrapolation distance. Finally, the dimensions, and hence critical mass, of the cylindrical system were obtained by substituting the computed buckling and reflector savings and the known core height in the formula for the geometric buckling of a cylinder.

The temperature coefficient of reactivity was determined from a series of critical-mass calculations in which the material densities of the fuel, container, Na coolant and reflector, appropriate to the specified temperature, were used. Results of these calculations were expressed in terms of changes in Pu critical mass per unit change in temperature, and converted to a temperature coefficient of reactivity by using the experimentally determined value of reactivity worth per gram of plutonium (see next section).

TABLE I

**CALCULATED AND EXPERIMENTAL NUCLEAR PARAMETERS—LAMPRE I**

**A. Critical mass** (kg Pu with Na in core unless otherwise indicated)

| Temperature | kg Pu—no side reflector—no rods | | kg Pu—side reflector—all rods | |
|---|---|---|---|---|
| | Calculated | Experimental | Calculated | Experimental |
| 80°C—no Na | 32.2 | 31.80 | 24.1 | 24.81 |
| 80°C—with Na | 28.3 | 27.86* | 21.0 | 22.22* |
| 160°C | 29.0 | 28.02 | 22.2 | 22.38 |
| 480°C | 28.2 | Not measured | 22.1 | 22.59 |

**B. Temperature coefficient of reactivity in cents per deg. C** (100 cents=reactivity interval between delayed and prompt critical)

| Temperature | Calculated | Experimental |
|---|---|---|
| 160°C | — | —1.3 cents per deg. C |
| 480°C | —3.2 cents per deg. C** | —2.9 cents per deg. C |

**C. Power coefficient in cents per kilowatt** (for coolant flow rate of 8.2 l/s)

| Temperature | Calculated | Experimental |
|---|---|---|
| 480°C | 0.39 cent per kilowatt | 0.60 cent per kilowatt |

* Obtained by applying correction to 160°C for fuel and Na density change.

** Calculated figure was 4.7 g Pu per deg. C. This was converted to cents per deg. C by using experimentally determined value of 0.68 cent per gram.

The power coefficient can be estimated from the temperature-reactivity coefficient calculated above. However, it is necessary to take account of the fact that the temperatures of the fuel, the coolant, and the reflector increase by different amounts as the operating power is raised. For example, it is estimated that, for full coolant flow, the average fuel temperature increases about three times as fast as the average Na temperature when power demand is increased. Hence, the main contribution to the power coefficient is due to temperature rise in the fuel and is therefore a prompt effect.

Another quantity of interest is the reactivity worth of the sodium coolant. As before, the worth of the sodium can be expressed in terms of Pu mass. This quantity is of particular importance since the experiments at a core temperature

of 80°C were made with no sodium in the reactor. However, the specification of the maximum allowable core loading, so as to provide a safe shut-down margin of reactivity, requires a knowledge of the critical mass of the system at ambient temperature with sodium and without the side reflector.

Calculational results of interest are given in Table I. Although anticipating the subsequent discussion, experimental values are also shown for comparison purposes.

**Critical experiments**

Critical-mass data were obtained by extrapolation of the curve of reciprocal multiplication, defined as plutonium mass divided by the neutron counting rate, versus plutonium mass. For these data, the reactor loading was always kept below the value which would make the system critical with only the side reflector fully inserted. Extrapolated mass data with the side reflector fully inserted were obtained only at a core temperature of 80°C. The experiments at higher temperatures were made with the side reflector restricted to three-fourths of its total travel in order to insure a maximum initial rate of reactivity decrease in case of a scram. Hence, some of the experimental critical mass values shown in Table I include a correction for this partial insertion of the side reflector. Since one of the control-rod thimbles was used to house an oscillator rod, a correction was also applied to the measured critical masses to take account of the reduced reactivity worth of this rod. The total fuel equivalent of these corrections to the experimental data was between 500 and 600 g of plutonium.

Following the extrapolated mass measurements, data were obtained for the system critical with a rod partially inserted. Period measurements were made by displacing the rod, by preselected amounts, above and below its critical position. These data were then used to compute the reactivity worth of the rod, in the vicinity of its critical position, per unit rod displacement. A calibration of the neutron-ionization-chamber levels in terms of absolute multiplication was made using the negative period data. From previous observations on the relative readings of the ionization chambers and proportional counters, the counter measurements could be converted to absolute multiplication. Units of reactivity quoted in this report are based on an assigned value of 100 cents for the reactivity interval between delayed and prompt critical. The period measurements, together with extrapolated mass data versus rod position, were combined to give a mass-reactivity worth expressible in units of cents per gram. At 160°C and 480°C, the data indicate a rod worth of 0.68 cents per gram and a total rod worth of 330 g Pu or 224 cents.

The isothermal coefficients of reactivity were measured for core temperatures in the range from 160 to 180°C, and 435 to 500°C, by appropriate adjustment of the electrical-heat input to the system. The low-temperature measurements were made by observing the change in rod displacement required to maintain the neutron level constant at a high value of multiplication. The same procedure was followed for the high-temperature measurements, except that the reactor power was held at a constant 10-W level. Data were taken at approximately 10°C-intervals, sufficient time being allowed for the system temperature to reach equilibrium at each of the measured points. From previously measured values of rod worth per unit displacement, the variation of reactivity with temperature was obtained. The experimentally determined temperature coefficients of reactivity were —1.3 and —2.9 cents per deg. C at 160 and 480°C respectively.

The difference between these two values can be partly explained by the fact that at 160°C (solid fuel) only the vertical expansion of the fuel contributes to reactivity changes. On the other hand, at 480°C (molten fuel) the total volumetric expansion contributes to the temperature coefficient.

Power coefficient measurements in the 0—50-kW range were made at coolant flow rates of 8.2 l/s with the core-inlet Na temperature held at a temperature of 480°C. Starting from a power level of a few watts, the nuclear power was raised in approximately 5-kW steps by inserting control-rods and reducing the electrical-heat input to the system so as to maintain the specified core-inlet temperature.

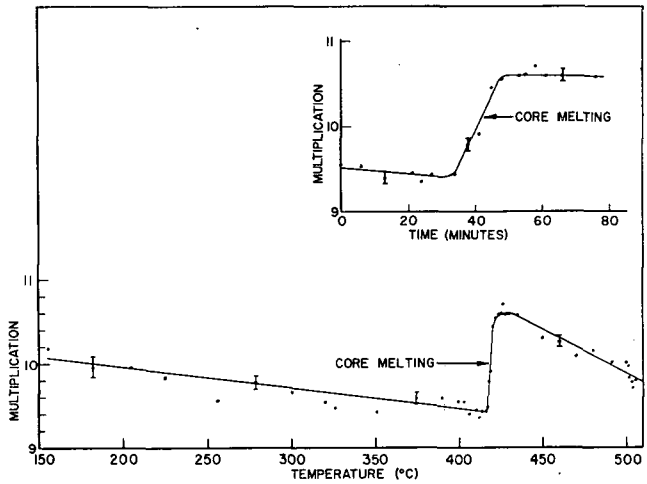


Fig. 2
*Neutron multiplication during approach to hot critical.*

At each point, the rod position and power level were recorded after the system had reached equilibrium. From a knowledge of rod worth per unit displacement, the variation of reactivity with power was inferred. At the flow investigated, the power coefficient was found to be —0.6 cent per kilowatt. This implies a totapolwer coefficient of 600 cents in bringing the reactor up to a power of 1 MW. Since the reactivity worth of a control-rod is 224 cents, a 1-MW power level can be achieved by control-rod insertion without changing the fuel loading in the core. As shown in Table I, the calculated power coefficient was —0.39 cent per kilowatt. However, in comparing the calculated and experimentally determined power coefficient, it should be noted that the calculated value was derived using parameters which involve the overall heat-transfer coefficient from the fuel to the sodium coolant. Hence, in evaluating the discrepancy between theory and experiment, the accuracy to which the heat-transfer parameters are known should be taken into account. Since a detailed analysis of these data have not as yet been made, it is not possible at this time to make any conclusive statements in regard to this discrepancy.

It might be of interest to mention the observations made while increasing the core temperature from 160°C to 500°C by electrical heating. During this time, the core loading was not changed, and multiplication data were taken as the core temperature was increased. These data are shown in Fig. 2, both as a function of time and temperature. It can be seen that a marked increase in multiplication

occurred when the melting point of the fuel was reached. This reactivity increase is attributed to the actual increase of the fuel density at the melting point, and to the effective increase in core-fuel density caused by the slumping of the fuel, upon melting, into the clearances required for the initial insertion of the fuel slugs into the capsules.

Experiments were also performed to investigate the response of the reactor to a power demand. Results of the measurement for a 30-kW power demand are shown in Fig. 3. Starting with the system in equilibrium at 1 kW, a power demand

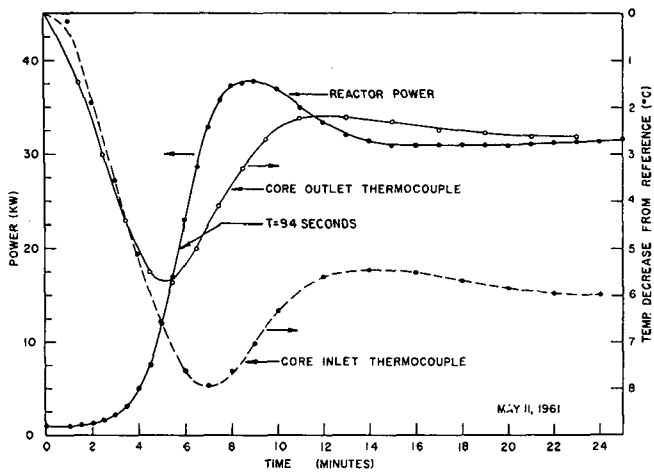


Fig. 3
Power demand experiment. $T$ is the minimum doubling time during power rise.

was made by turning off some of the electrical heat to the system. During this experiment, power and temperature readings were taken as a function of time with the control-rod position left unchanged. As can be seen from Fig. 3, an overshoot in the power *versus* time curve was observed. From the observed changes in power and inlet temperature before and after the run, together with the experimental value for temperature coefficient of reactivity, the power coefficient can be inferred. For the 30-kW case, a power coefficient of $-0.63$ cent per deg. C was computed. A similar experiment was performed starting from an initial 50-kW level and making a 100-kW demand. The results for the latter were similar to that shown in Fig. 3, except that no overshoot in the power-*versus*-time curve was observed.

## REFERENCES

[1] HALL, D. B., Proc. 2nd UN Int. Conf. PUAE **13** (1958) 300.
[2] CARLSON, B. G. and BELL, G. I., Proc. 2nd UN Int. Conf. PUAE **16** (1958) 535.
[3] KIEHN, R. M., *Nucl. Sci. Engng* 4 (1958) 166.
[4] GLASSTONE, S. and EDLUND, M. C., The Elements of Nuclear Reactor Theory, D. Van Nostrand Co., Inc., New York (1952) 213—214.

SM—18/48

# EXPERIMENTAL RESULTS ON LARGE DILUTE FAST CRITICAL SYSTEMS WITH METALLIC AND CERAMIC FUELS

J. K. Long, A. R. Baker, W. Gemmell, W. P. Keeney,
R. L. McVean and F. W. Thalgott,
Argonne National Laboratory, Argonne, Ill.,
United States of America

**Abstract — Résumé — Аннотация — Resumen**

**Experimental results on large dilute fast critical systems with metallic and ceramic fuels.** The flexibility of the ZPR-III fast critical project permits the assembly of compositions typical of large power reactors. Because oxide and carbide fuels promise attractive mechanical properties, their behaviour in critical composition has been studied. Central fission ratios, reactivity measurements, Rossi-$\alpha$ and heterogeneity effects have been determined for several uranium-blanketed cylindrical cores. Some of these are simplified compositions useful for evaluation of cross-section sets, and others are more typical of power-reactor compositions.

**Résultats d'expériences sur de grands ensembles critiques dilués à neutrons rapides avec des combustibles métalliques et céramiques.** La souplesse de l'ensemble critique à neutrons rapides ZPR-III permet de réaliser des compositions caractéristiques des grands réacteurs de puissance. Le fait que les combustibles sous forme d'oxydes et de carbures paraissent avoir des propriétés mécaniques intéressantes a incité les auteurs à étudier leur comportement en composition critique. Ils ont déterminé les taux de fission centrale, mesuré la réactivité, appliqué la technique de Rossi-$\alpha$ et les effets d'hétérogénéité pour des cœurs cylindriques à milieu fertile d'uranium. Quelques-uns de ces montages simplifiés peuvent servir à l'évaluation d'ensembles de sections efficaces, tandis que d'autres ont davantage trait aux réacteurs de puissance.

**Экспериментальные результаты по крупным разбавленным быстрым критическим системам с металлическим и керамическим топливом.** Гибкость критического реактора на быстрых нейтронах нулевой мощности ZPR-III позволяет создавать сборки композиций активных зон, типичных для крупных энергетических реакторов. Ввиду того, что окисные и карбидные топлива имеют привлекательные механические свойства, было исследовано их поведение в критической сборке. Были определены главные отношения интенсивностей деления, проведены измерения реактивности, измерение распределения во времени нейтронов, принадлежащих к одной цепи, и определены эффекты гетерогенности для нескольких цилиндрических активных зон с урановой оболочкой. Некоторые из них являются упрощенными композициями, которые можно использовать для оценок сечений, а другие более типичны для композиций энергетических реакторов.

**Resultados experimentales obtenidos en grandes conjuntos críticos diluidos de neutrones rápidos, con combustibles metálicos y cerámicos.** El reactor ZPR-III de neutrones rápidos permite, en virtud de su adaptabilidad, utilizar cuerpos cuya composición es típica de los grandes reactores de potencia. Los autores han estudiado el comportamiento de composiciones críticas de combustibles en forma de óxido y de carburo, por las interesantes propiedades mecánicas que presentan. Han determinado las razones de fisión central, la reactividad, los efectos Rossi-$\alpha$ y de la heterogeneidad para cuerpos cilíndricos con envoltura fértil de uranio. Algunos de estos montajes simplificados se prestan para la evaluación de series de secciones eficaces, en tanto que otros tienen una composición más típica de los reactores de potencia.

## Introduction

The ZPR-III is a fast-reactor critical facility characterized by the ability to handle a large inventory of fissionable and inert materials in great diversity of geometry and composition. Since the machine has been described previously [1], it will suffice here to indicate merely that it is built in two halves, each half being a framework for the insertion of 3.2-mm-thick plates of materials in any desired arrangement. The fuel which has been used up to the present time is enriched-uranium metal plates (93.3% $U^{235}$). These plates can be mingled with similar size plates of depleted uranium (0.2% $U^{235}$) or of stainless steel, sodium (in cans), aluminium or other materials of reactor interest to construct a core. The core is then surrounded with somewhat larger pieces of depleted uranium, stainless steel, etc., to simulate a reflecting and breeding blanket.

If it is desired to study the critical properties of an oxide fuel, oxygen can be introduced into the core mixture in the form of aluminium-oxide ceramic plates. Carbides can be studied by the introduction of the proper quantity of graphite plates. Aluminium is usually used to simulate the sodium of a fast reactor. Aluminium may be thought of as roughly equivalent to twice its volume in sodium in these fast reactors.

With such equipment, it is possible to determine experimentally the critical masses of various core compositions, to map the flux and the worth of materials in these configurations, to determine certain spectral indices characterizing the neutron spectrum, to measure significant quantities related to the conversion ratio, neutron lifetime, temperature coefficient, power coefficient, and to compare the results of such experiments with calculations. Similar experiments and calculations have been performed in the United Kingdom on models of the Dounreay and other reactors [2]. At Los Alamos, fast-critical studies on a variety of fast-reactor cores have been recently reported [3]. Previous fast-critical work on ZPR-III was summarized at the last Geneva Conference [4], and a coupled fast-thermal system constructed on ZPR-III was also described at that time [5]. An additional analysis of ZPR-III assemblies consists of a discussion of some of the heterogeneity effects [6], and other ZPR-III results form the basis of part of the discussion of fast reactors in the Argonne compendium of reactor physics constants [7].

The purpose of this paper is to present new critical experimental results which have been obtained on ZPR-III since 1958, most of which have not been widely distributed or tabulated for ready comparison. These results are not accompanied by any elaborate analysis beyond a simple reduction of the data to the point where a few direct comparisons between assemblies can be made. Even such simple reductions introduce enough uncertainties to make it tempting to present only the bare experimental observations with no further computations at all. Because this procedure would be unduly cumbersome, the results have been adjusted by some simple conversions, but in each case an effort will be made to give enough detail concerning these conversions so that the interested reader can relate the reported results to the actual observations.

## 1. Critical masses

The assemblies to be presented in this report can be grouped in two categories: simple compositions and reactor compositions. All the cores discussed here are cylinders with length-to-diameter ratio between 0.73 and 1.0. Each core was

TABLE I

**DESCRIPTION OF ASSEMBLIES**

| Ass'y | Core descriptive title | Critical core dimensions, length × diam. (cm) | Core critical volume (l) | Core critical mass (kg $U^{235}$) | Core composition, vol. %, density | | | | | | | Calculated reactivity*** | |
|---|---|---|---|---|---|---|---|---|---|---|---|---|---|
| | | | | | $U^{235}$ 18.75 | $U^{238}$ 19.0 | Al 2.7 | C 1.43 | SS304 7.85 | O 2.55 | Na 0.84 | YOM | Nims |
| 23 | Al diluent | 51.0 × 60.9 | 148.5 | 258.1 | 9.27 | 0.7 | 42.8 | — | 9.3 | — | — | 1.046 | — |
| 14 | C diluent | 45.9 × 46.3 | 77.4 | 136.1 | 9.38 | 0.7 | — | 74.5 | 9.3 | — | — | 1.000 | — |
| 32 | SS diluent | 61.1 × 52.2 | 130.7 | 227.5 | 9.26 | 0.7 | — | — | 81.0 | — | — | 1.056 | 1.028 |
| 33 | SS + Na diluent | 61.1 × 53.4 | 136.8 | 238 | 9.27 | 0.7 | — | — | 63.6 | — | 18.2 | 1.056 | 1.025 |
| 22 | $U^{238}$ diluent | 51.0 × 58.7 | 138.0 | 243.7 | 9.42 | 70.1 | — | — | 9.3 | — | — | 1.010 | — |
| 24 | $U^{238}$ diluent | 71.3 × 76.9 | 324.6 | 460.7 | 7.57 | 72.9 | — | — | 9.3 | — | — | 1.009 | — |
| 25 | $U^{238}$ diluent | 76.3 × 85.2 | 435.6 | 581.6 | 7.12 | 74.0 | — | — | 9.3 | — | — | 1.008 | — |
| 20* | Fermi | 76.4 × 79.3 | 378 | 431.5 | 6.09 | 19.0 | 25.1 | — | 14.3** | — | — | 1.035 | — |
| 29 | Oxide | 71.3 × 90.0 | 452 | 420.7 | 4.97 | 9.97 | 24.4 | — | 24.7 | 14.5 | — | 1.050 | 1.026 |
| 30 | Oxide | 62.2 × 82.8 | 356 | 395 | 5.92 | 9.06 | 23.4 | — | 24.6 | 7.2 | — | 1.053 | 1.024 |
| 31 | Metal | 62.2 × 90.4 | 425 | 463 | 5.81 | 9.14 | 23.5 | — | 24.5 | — | — | 1.050 | 1.020 |
| 34 | Carbide | 86.5 × 91.9 | 574.4 | 503.0 | 4.67 | 10.3 | 25.5 | 10.6 | 24.6 | — | — | 1.046 | 1.022 |

* Reduced density blanket. All other assemblies had 83.3 % $U^{238}$, 7.3 % SS blanket. Blanket at least 30 cm thick.
** Also contains 5 % Mo, 4.3 % Zr.
*** Spherical calculations. No correction has been made for shape, heterogeneity, or interface.

surrounded by at least 30 cm of blanket containing 83.3% $U^{238}$. In Table I the compositions and critical parameters of seven simple cores, containing just one or two diluent materials, are listed, together with the calculated multiplications for these geometries. In Assembly 23, aluminium is the principal diluent. This is followed by 14, an Assembly previously reported [4] but included here as a useful comparison, in which carbon in the form of graphite plates was the principal diluent. In Assembly 32, Type-304 stainless steel was the only material present in the core other than enriched uranium, and 33 differed from this by the substitution of some of the stainless steel by sodium. There follow three cores, 22, 24 and 25, in which the principal materials, $U^{238}$ and $U^{235}$, are present in the ratios 7.4, 9.6 and 10.4, respectively. Similar information is then presented for five reactor-like compositions. These include, first, Assembly 20, a simplified version of the Fermi reactor. The simplification consisted of blending the composition of the control-rods in with the rest of the core and of surrounding the core in both axial and radial directions with a blanket similar to the Fermi radial blanket. This blanket was somewhat less dense than the other assemblies listed here, 45.5% $U^{238}$, 19.4% SS, 10.1% aluminium, and 2.4% molybdenum for the first 7 cm outward from the core, and then further simplified beyond that. Assembly 29 simulates the composition of an oxide reactor, about one-fourth of the core volume being devoted to stainless-steel structural material, one-half to coolant (simulated by half that amount or one-fourth of the core volume occupied by aluminium), and the remaining one-fourth being devoted to the meat, $UO_2$, 33.3% enriched. To further clarify the role of oxygen in these assemblies, core number 30 had the oxygen content reduced by half, other materials remaining the same except for an increase in enrichment to 39.5% in order to achieve criticality within the inventory of available materials. This was followed by Assembly 31, similar to 30 except that now all oxygen was removed. The final assembly listed is a simulated uranium monocarbide fuel composition.

Because the cores are composed of thousands of individually small pieces of material, some voids are necessarily present in the core, about 10% as the usual minimum. Additional void space can be introduced uniformly by using perforated materials, and a supply of perforated aluminium is available for this purpose. In loading so many small pieces into a core, care must be taken to insure that the positions of pieces are generally reproducible and that, at least on the average, compositions and geometries can be well defined. On several occasions, identical

TABLE II

**REPRODUCIBILITY OF EXPERIMENTAL CRITICAL MASSES**

| Assembly | Date | Composition (vol. %) | | | | Observed critical mass (kg $U^{235}$) |
|---|---|---|---|---|---|---|
| | | $U^{235}$ | $U^{238}$ | SS | Al | |
| 11 | 1958 | 9.51 | 71.7 | 9.3 | | 240.5 |
| 22 | 1959 | 9.42 | 70.1 | 9.3 | | 243.7 |
| 8 | 1957 | 13.9* | 15.8 | 19.4 | 26.5 | 165.2 |
| 8A | 1960 | 13.9* | 15.8 | 19.4 | 26.5 | 166.2 |
| 2 | 1956 | 13.99 | 15.72 | 12.3 | 31.5 | 136.0 |
| 2B | 1956 | 13.99 | 15.72 | 12.3 | 31.5 | 135.8 |

* Some deviations from this composition occurred in the regions of the control and safety rods, but in this and all other respects Assemblies 8 and 8 A are as near as possible identical.

TABLE III

**16-GROUP CENTRAL FLUXES***

| Energy lower limit (MeV) | Ass'y 23 | Ass'y 14 | Ass'y 32 | Ass'y 33 | Ass'y 22 | Ass'y 24 | Ass'y 25 | Ass'y 20 | Ass'y 29 | Ass'y 30 | Ass'y 31 | Ass'y 34 |
|---|---|---|---|---|---|---|---|---|---|---|---|---|
| 3.668 | 0.035 | 0.035 | 0.019 | 0.022 | 0.020 | 0.017 | 0.016 | 0.020 | 0.019 | 0.021 | 0.021 | 0.018 |
| 2.225 | 0.074 | 0.073 | 0.043 | 0.049 | 0.034 | 0.029 | 0.028 | 0.038 | 0.038 | 0.044 | 0.044 | 0.038 |
| 1.35 | 0.116 | 0.110 | 0.084 | 0.092 | 0.054 | 0.046 | 0.044 | 0.064 | 0.067 | 0.076 | 0.078 | 0.067 |
| 0.825 | 0.145 | 0.118 | 0.123 | 0.126 | 0.109 | 0.100 | 0.097 | 0.111 | 0.098 | 0.114 | 0.123 | 0.106 |
| 0.5 | 0.166 | 0.118 | 0.199 | 0.188 | 0.199 | 0.193 | 0.191 | 0.172 | 0.141 | 0.163 | 0.180 | 0.150 |
| 0.3 | 0.147 | 0.106 | 0.162 | 0.165 | 0.209 | 0.211 | 0.211 | 0.178 | 0.137 | 0.154 | 0.167 | 0.146 |
| 0.18 | 0.115 | 0.095 | 0.150 | 0.145 | 0.157 | 0.163 | 0.165 | 0.147 | 0.138 | 0.138 | 0.136 | 0.129 |
| 0.11 | 0.076 | 0.080 | 0.099 | 0.097 | 0.108 | 0.116 | 0.118 | 0.103 | 0.108 | 0.099 | 0.093 | 0.098 |
| 0.067 | 0.055 | 0.072 | 0.052 | 0.053 | 0.048 | 0.052 | 0.053 | 0.066 | 0.081 | 0.069 | 0.061 | 0.073 |
| 0.0407 | 0.046 | 0.058 | 0.039 | 0.036 | 0.043 | 0.051 | 0.054 | 0.060 | 0.081 | 0.062 | 0.055 | 0.073 |
| 0.025 | 0.012 | 0.042 | 0.010 | 0.010 | 0.008 | 0.010 | 0.011 | 0.017 | 0.032 | 0.023 | 0.016 | 0.032 |
| 0.015 | 0.012 | 0.033 | 0.015 | 0.013 | 0.007 | 0.009 | 0.010 | 0.017 | 0.039 | 0.024 | 0.018 | 0.037 |
| 0.0091 | 0.001 | 0.023 | 0.003 | 0.003 | 0.002 | 0.003 | 0.003 | 0.004 | 0.014 | 0.008 | 0.005 | 0.017 |
| 0.0055 | 0.000 | 0.015 | 0.001 | 0.001 | 0.000 | 0.000 | 0.000 | 0.001 | 0.005 | 0.003 | 0.001 | 0.008 |
| 0.0021 | 0.000 | 0.012 | 0.001 | 0.001 | 0.000 | 0.000 | 0.000 | 0.000 | 0.000 | 0.002 | 0.000 | 0.006 |
| 0.0005 | 0.000 | 0.008 | 0.000 | 0.000 | 0.000 | 0.000 | 0.000 | 0.000 | 0.000 | 0.001 | 0.000 | 0.001 |

* Cross-section set of YIFTAH *et al.* [10].

or very similar assemblies have been constructed in the ZPR-III, and a comparison of these is some measure of the reproducibility of the procedure. A few very similar assemblies are compared in Table II. Assembly 11, described in this table, differed from 22 by minor rearrangement of the pieces and slight changes in composition as noted. Our experience indicated that the 1% difference in $U^{235}$ density between 11 and 22 is worth about 2% in critical mass, or 4.8 kg. However, Assembly 11 contains about 40 kg more $U^{238}$ than 22, which is probably worth about 1 kg of fuel, so that one should add only 3.8 kg to the mass of 11 for comparison with 22. This brings them within 0.25% in critical mass. Assemblies 8 and 8A are as identical as we can make them, yet their masses differ by 0.6%. Between Assemblies 2 and 2B all core drawers were reloaded with a slight rearrangement of pieces (although in general the identical pieces were used), and these critical masses are within 0.15%. We conclude therefore that our critical mass results are reproducible within 0.6%, which usually represents a difference in multiplication factor of 0.0015 or less.

In order to compare our measured critical masses with calculated values, the calculator must at least be aware of certain corrections. The most convenient calculations with which these masses can be compared are done in spherical geometry using the established multi-group cross-sections sets, and SNG or DSN approximations. In this case a shape factor must be used to increase the calculated mass by usually about 3% for comparison with the experimental cylinders. A number of these shape factors have been compiled by LOEWENSTEIN [8]. The calculated critical mass must then be reduced by a factor variously estimated at 4—6% [6] in order to compare the homogeneously calculated assembly with the heterogeneous experimental assembly. If the calculated critical mass is further increased by about 1%, a correction which we have estimated is reasonable to take into account the perturbation of the interfacial plane of the ZPR-III machine [4], the corrected value is often within 1% in critical mass of the direct machine calculation from which we started. For exact comparisons, individual cases must be evaluated of course, but because the corrections largely tend to cancel each other out, and because they involve some uncertainty anyway, we have listed in Table I only the uncorrected spherical-machine calculations for the multiplication of the observed critical mass. We are indebted to Nims of APDA for permission to use some of his unpublished calculations in Table I for comparison with our own. Nims uses the cross-section set of MILLS [9] with some modifications to the iron values.

Table III gives central flux for the assemblies of Table I, calculated as spheres, DS8, using the cross-section set of YIFTAH, OKRENT and MOLDAUER (YOM) [10].

## 2. Fission ratios

Fission ratios at the centre of ZPR-III have been determined using fission counters 2 in in diameter and 1 in long. The active area in these counters is flat to avoid self-absorption. Coatings contain about 100 to 200 $\mu g/cm^2$ with a total loading of about 500 $\mu g$. These counters are described in more detail by KIRN [11]. They have good reproducible plateaux and are believed to give a good measure of the spectral indices to within $\pm 2\%$ (allowing about 1% for counting statistics, 1% for uncertainty of the active mass and isotopic analysis). In addition, systematic errors may affect the $Pu^{240}$ values, for which the isotopic enrichment of the counter is less well defined.

TABLE IV

**CENTRAL FISSION RATIOS**

| Ass'y | Counter measurements | | | | | | | | | | | | Radiochemical measurements | | |
|---|---|---|---|---|---|---|---|---|---|---|---|---|---|---|---|
| | $\frac{\sigma_f U^{238}}{\sigma_f U^{235}}$ | | $\frac{\sigma_f U^{236}}{\sigma_f U^{235}}$ | | $\frac{\sigma_f U^{234}}{\sigma_f U^{235}}$ | | $\frac{\sigma_f U^{233}}{\sigma_f U^{235}}$ | | $\frac{\sigma_f Pu^{239}}{\sigma_f U^{235}}$ | | $\frac{\sigma_f Pu^{240}}{\sigma_f U^{235}}$ | | $\frac{\sigma_f U^{238}}{\sigma_f U^{235}}$ | $\frac{\sigma_\theta U^{238}}{\sigma_f U^{235}}$ | |
| | Exp. | Calc.* | Exp. | Calc. | Exp. | Calc. | Exp. | Calc. | Exp. | Calc. | Exp. | Calc. | Exp. | Exp. | Calc. |
| 23 | 0.0678 | 0.083 | — | 0.196 | 0.402 | 0.496 | 1.48 | 1.55 | 1.178 | 1.267 | — | 0.505 | 0.079 | 0.089 | 0.105 |
| 14 | 0.055 | 0.066 | — | 0.141 | 0.305 | 0.356 | 1.45 | — | 1.05 | 1.12 | — | 0.366 | — | 0.109 | 0.126 |
| 32 | 0.0451 | 0.053 | 0.116 | 0.129 | 0.367 | 0.415 | 1.51 | 1.57 | 1.203 | 1.24 | 0.382 | 0.411 | — | — | — |
| 33 | 0.048 | 0.059 | 0.118 | 0.131 | 0.370 | 0.431 | 1.51 | 1.57 | 1.208 | 1.25 | 0.40 | 0.429 | — | — | — |
| 22 | 0.036 | 0.040 | — | 0.105 | 0.293 | 0.370 | 1.53 | 1.59 | 1.16 | 1.24 | 0.333 | 0.366 | 0.041 | 0.091 | 0.113 |
| 24 | 0.028 | 0.0345 | — | 0.100 | 0.246 | 0.343 | 1.44 | 1.58 | 1.14 | 1.22 | — | 0.333 | 0.028 | 0.092 | 0.116 |
| 25 | 0.0292 | 0.0327 | — | 0.096 | 0.253 | 0.333 | — | 1.58 | 1.17 | 1.218 | — | 0.322 | — | — | — |
| 20 | 0.0381 | 0.040 | — | 0.137 | 0.292 | 0.355 | 1.52 | 1.57 | 1.15 | 1.207 | 0.332 | 0.351 | — | — | — |
| 29 | 0.0356 | 0.0404 | 0.084 | 0.095 | 0.259 | 0.295 | 1.47 | 1.537 | 1.06 | 1.139 | 0.289 | 0.294 | — | — | — |
| 30 | 0.0427 | 0.0484 | 0.098 | 0.125 | 0.300 | 0.357 | 1.49 | 1.55 | 1.12 | 1.188 | 0.328 | 0.356 | — | — | — |
| 31 | 0.0443 | 0.0504 | 0.115 | 1.134 | 0.335 | 0.391 | 1.52 | 1.56 | 1.18 | 1.218 | 0.302 | 0.389 | — | — | — |
| 34 | 0.0339 | 0.0396 | 0.080 | 0.097 | 0.247 | 0.304 | 1.45 | 1.54 | 1.067 | 1.133 | 0.271 | 0.303 | 0.04** | 0.12** | 0.127 |

* Calculations used the cross-section set of YIFTAH *et al.* [10], supplemented by values taken from BNL-325 for $U^{234}$ and $U^{236}$.
** An exceptionally large counting uncertainty of 30% must be applied to these measurements because of low activity.

The results are listed in Table IV, together with calculated values taken from Table III. The results seem to indicate a consistent discrepancy in the $U^{235}$ counter or in the corresponding cross-section set, for when the ratios are taken relative to $Pu^{239}$, agreement between experiment and calculations is consistently improved.

Also shown in Table IV are the results of radiochemical determinations of $\sigma_c^{28}/\sigma_f^{25}$ and $\sigma_t^{28}/\sigma_f^{25}$.

Because of the low-activity levels produced by activation in a critical assembly, the radiochemical methods are considered to have greater statistical uncertainty than the fission counters. Nevertheless, the agreement between the radiochemical measurements and the calculations suggests that there still may be systematic errors in the fission-counter technique. The fission counters certainly give good relative values, however, for comparing one assembly with another.

## 3. Neutron lifetimes

The Rossi-$\alpha$, or decay constant of prompt-fission chains in a particular reactor, can be related to the neutron lifetime, $l$, the effective delayed-neutron fraction, $\beta$, and the multiplication, $k$, by

$$l = \frac{\beta - (k - 1)}{\alpha}.$$

The multiplication constant, $k$, at subcritical levels, is determined by the position of a calibrated control-rod, with a source present to maintain some constant low power level. Usually, the spontaneous fission source from the $U^{238}$ blanket is sufficient for this purpose. The effective $\beta$ is estimated from studies made by MENEGHETTI [12], who showed that actually the effective $\beta$ remains relatively constant over the range of enrichments of our assemblies; $\alpha$ is measured with a ten-channel time analyser at several subcritical levels using techniques reported by BRUNSON [13]. The results are shown in Table V. The uncertainties in Rossi-$\alpha$ listed in Table V reflect mostly counting statistics. The uncertainty in $\beta$, of about 3%, is included in the uncertainty in $l$.

TABLE V

**ROSSI-$\alpha$ MEASUREMENTS**

| Ass'y | Rossi-$\alpha$ at delayed critical ($s^{-1} \times 10^{-4}$) | Estimated effective $\beta$ | Neutron lifetime ($s \times 10^{8}$) |
|---|---|---|---|
| 23 | $5.65 \pm 0.1$ | 0.0068 | $12.0 \pm 0.5$ |
| 14 | $3.85 \pm 0.1$ | 0.0075 | $19.5 \pm 0.8$ |
| 32 | $5.37 \pm 0.1$ | 0.0068 | $12.6 \pm 0.5$ |
| 33 | $5.46 \pm 0.1$ | 0.0068 | $12.4 \pm 0.5$ |
| 22 | $10.45 \pm 0.3$ | 0.0074 | $7.1 \pm 0.3$ |
| 24 | $8.51 \pm 0.1$ | 0.0073 | $8.60 \pm 0.4$ |
| 25 | $9.1 \pm 0.1$ | 0.0073 | $8.1 \pm 0.2$ |
| 20 | $4.47 \pm 0.09$ | 0.0072 | $16.15 \pm 0.8$ |
| 29 | $3.15 \pm 0.10$ | 0.0073 | $23.2 \pm 1.0$ |
| 30 | $4.10 \pm 0.10$ | 0.0073 | $17.8 \pm 0.7$ |
| 31 | $4.45 \pm 0.10$ | 0.0073 | $16.4 \pm 0.7$ |
| 34 | $2.92 \pm 0.08$ | 0.0073 | $25.0 \pm 1.0$ |

TABLE VI

**EFFECTIVE $\sigma_c$ PER MOLECULE**
**(millibarns)**

| Material | $M$* | Ass'y 20 | Ass'y 29 | Ass'y 30 | Ass'y 31 | Ass'y 34 | Ass'y 23 | Ass'y 22 | Ass'y 24 | Ass'y 25 | Ass'y 32 | Ass'y 33 |
|---|---|---|---|---|---|---|---|---|---|---|---|---|
| Ag | 13 | — | — | — | — | — | —220 | —231 | —238 | —227 | — | — |
| Bi | 6 | — | — | — | — | —6.4 | — | —27 | —24 | —2.0 | — | — |
| Y | 7 | — | — | — | — | —100 | 17.5 | —30 | —30 | — | — | — |
| Be | 27 | 18 | 61 | — | — | 57 | 66 | —4.8 | —20.5 | — | — | — |
| $U^{233}$ | 1 | — | 3575 | 3428 | 3286 | 3615 | 3233 | 3284 | 3304 | 3371 | 3290 | 3220 |
| $U^{235}$ | 1 | 1845 | 1913 | 1786 | 1795 | 1894 | 1774 | 1772 | 1842 | 1865 | 1745 | 1738 |
| $U^{238}$ | 10 | —84.5 | —100 | —66.2 | —48.3 | —104 | 40 | —84 | —89 | —95 | —18.7 | —6.7 |
| $Pu^{239}$ | 1 | 3251 | 3250 | 3280 | 3286 | 3274 | 3395 | 3238 | 3211 | 3204 | 3290 | 3310 |
| $B^{10}{}_4C$ | 0.6 | —3856 | — | — | — | —5553 | —3625 | —3130 | —3112 | —3064 | —4366 | —4270 |
| C | 16 | 4.6 | 31.2 | 31.9 | 29.6 | 33 | 39 | —10.8 | —20 | —23.8 | 70 | 64 |
| Al | 13 | —6.3 | 2.2 | 2.8 | 2.8 | 1.8 | 3.5 | —13.1 | —16.5 | —18.4 | 28.3 | 24.5 |
| Na | 4 | — | 25.9 | 17.2 | 19.4 | 12.4 | — | — | — | — | 48 | 35 |
| V | 10 | — | —16.6 | — | — | — | — | — | —19.7 | — | — | — |
| Cr | 5 | — | — | — | — | —2.3 | — | — | — | — | 14.9 | 8.6 |
| Fe | 18 | — | — | —6.9 | —6.3 | —5.3 | — | — | — | —19.4 | 0.8 | —0.5 |
| Nb | 5 | — | —112 | — | — | —112 | — | — | —88 | —80 | — | —42 |
| Mo | 13 | —60 | —71 | — | — | —67.9 | — | — | —71 | —67 | —21.2 | —22 |
| Ta | 6 | —256 | —367 | — | — | —392 | —166 | — | —267 | —253 | — | —211 |
| Pb | 7 | —2.4 | — | — | — | —1.6 | — | — | —17.3 | — | — | 11.7 |
| Th | 7 | — | —217 | — | — | —224 | — | — | —184 | — | —130 | —123 |
| SS | 18 | —13.4 | —6.7 | —6.6 | —5.6 | —6.0 | 0.9 | —23.8 | —23.8 | —21.8 | 3.6 | 2.3 |
| Zr | 9 | —19.6 | —9.2 | — | — | —8.4 | — | —34.7 | —32.4 | —35.4 | 24.6 | — |
| $Al_2O_3$ | 1.7 | — | 89 | — | 72.3 | 62.6 | 14.4 | — | —91 | —97 | 426 | 361 |
| Ph I O | 1 | —168.7 | —178 | —120 | —69 | —151 | — | — | —141 | —168 | 25 | —0.5 |
| Ph II O | 1 | — | —128 | —93 | —54 | —129 | — | — | —162 | —150 | 34 | 0 |
| O | 5 | — | 28.1 | — | 22.4 | 19.7 | 2.5 | — | —19.1 | —20 | 123 | 104 |
| Ni | 18 | — | — | — | — | —10.7 | — | — | — | — | 7.5 | 3.0 |

* $\pm 25/M$, where $M$ is number of moles in sample.

## 4. Central-reactivity measurements

Central-reactivity measurements have been made for a selection of materials for each assembly. They are shown in Table VI. For the performance of this measurement, a $2 \times 2 \times 2$-in void (smaller for fissile materials) is loaded into the centre of the assembly. Samples are inserted by hand in this void for each measurement. Thus the reactor must be shut down and the halves separated between any two consecutive measurements, but no adjustment need be made to any of the drawers or their contents. Comparisons of many measurements have shown that this procedure is reproducible to within $\pm 10^{-5}\,\Delta k$ or better. If the temperature of the assembly has varied between runs, a slight temperature correction, $-3 \times 10^{-5}$ per degree C, is made, based on experimental observations. Because of the mass and bulk of the assembly, temperature variations are usually within 0.1°C between a sample measurement and its corresponding reference measurement. Reactivity changes are measured by the critical position of calibrated control-rods, the calibrations having been made by period measurements. The periods are converted to inhours for a working unit, and again, Meneghetti has shown that this conversion is not very sensitive to core composition [12]. For the purpose of Table VI, where the various assemblies are to be compared with each other, it was considered preferable to convert the inhours to an effective capture cross-section in millibarns. This was done by computing a flux-weighted value of $(\nu - 1)\,\sigma_f - \sigma_c$ in millibarns for $Pu^{239}$ for each assembly, using the ratio of this value to the measured reactivity change for $Pu^{239}$ as a conversion factor for all the reactivity measurements of that assembly. The negative of these values is given in the table, so that the fissile materials have positive cross-section. For the reactivity measurements, the mass of the sample is known quite accurately, so that for a pure element there is no problem in converting mass to gram-moles. For stainless steel, a molecular weight of 56 was assumed. The $U^{235}$ value was determined from a measurement on 93.3% enriched uranium, with a small correction for the presence of other isotopes. The $U^{238}$ values likewise are corrected for the presence of about 0.2% $U^{235}$ in the depleted sample on which the measurement was made. The plutonium samples contain about 5% $Pu^{240}$ with the balance $Pu^{239}$. In determining the worth of the $Pu^{239}$, five parts of $Pu^{240}$ were assumed to be worth one of $Pu^{239}$, an approximation justified by the relative values of $(\nu - 1)\,\sigma_f - \sigma_c$ for the two isotopes. The boron carbide samples contain 9.9% of other chemical impurities, which are regarded as making no contribution to the measured reactivity change. The boron carbide itself is enriched to 90.7 at.% in B-10, but the results are reported on the basis of the total amount of boron carbide present, assigning it a molecular weight of 52. The physicum samples, designated Ph-I and Ph-II, are composite mixtures of the metals, oxides and salts of stable, naturally occurring elements which simulate the nuclear effects of fission products according to criteria listed in a previous report [4]. The formulae and molecular weights of these two mixtures have been recomputed to be

| *Formula* | *Molecular weight* |
|---|---|
| (Ph-I) $O_{1.519}$ | 142.2 |
| (Ph-II) $O_{1.146}$ | 136.1 |

The oxygen values listed in the table are derived from the measured worths of $Al_2O_3$ and Al. Based on an uncertainty of $10^{-5}$ in the measured reactivities,

TABLE VII

**EXPERIMENTAL AND CALCULATED CENTRAL REACTIVITY COEFFICIENTS***
**(millibarns)**

| Material | Ass'y 22 | Ass'y 23 | Ass'y 29 |
|---|---|---|---|
| $Pu^{239}$ | 3238 (3238) | 3395 (3395) | 3250 (3250) |
| $U^{235}$ | 1772 (1939) | 1774 (1964) | 1913 (2066) |
| $U^{238}$ | —84 (—94.8) | 40 (67.5) | —100 (—97.9) |
| C | | | 31.2 (18.1) |
| Al | —13.1 (—10.4) | 3.5 (12.2) | 2.2 (2.6) |
| Na | | | 25.9 (9.9) |
| Fe | (—24.4) | 0.9 (2.6) | (—8.5) |
| SS | —23.8 | | —6.7 |

* Calculated values are in parentheses. Perturbation theory (16-group) with the cross-section of Yiftah *et al.* was used. Calculated values are normalized to $(\nu-1)$. $\sigma_f - \sigma_c$ of $Pu^{239}$.

the uncertainty in the cross-section in millibarns is approximately $25/M$, where $M$ is the number of gram-moles in the measured sample. Accordingly, the values of $M$ for each material are listed in the table. For samples as large as those used in this work, self-shielding must be considered a possibility. Calculations have indicated, however, that except possibly in the cases of boron carbide and graphite, self-shielding effects are less than the uncertainties of the measurement.

Some of the more striking features of Table VI are the preponderance of negative values for the carbide assembly, 34, compared to the considerably more positive values in the steel and steel-sodium diluted assemblies, 32 and 33. Note also that the $U^{238}$ diluted assemblies, 22, 24 and 25, all have a preponderance of negative material coefficients, even for such materials as carbon and beryllium. The boron carbide coefficients in 22, 24 and 25 are not strongly negative, however, indicating the lack of neutrons in the low end of their spectra, and their relative low worth. The worths of materials are generally positive in the hard spectrum of the aluminium diluted assembly, 23, and yet the worth of oxygen here seems surprisingly low.

A few comparisons between measured and calculated central reactivities are given in Table VII. The calculations in Table VII have been made by 16-group perturbation theory and, to avoid the calculation of the volume integral in the denominators, all values are normalized to $(\nu-1)\,\sigma_f-\sigma_c$ for plutonium.

## 5. Reactivity measurements other than central

A few traverses were made with small perturbation samples to determine the worth as a function of position. Reactivity measurements can be determined within an error of $2 \times 10^{-6}$ between positions by this procedure, since the position of the halves does not require changing during a traverse. Table VIII gives the results of several such traverses for Assembly 29. Agreement between the worths of the fissionable materials measured in this traverse and the worths measured as central rectangular samples indicates that streaming along the half-inch-diameter traverse tube is a negligible effect, and that, within the limits of these experiments, the sample size of the fissionable material is unimportant. The size of the boron sample does affect its worth however, due to self-shielding in the large samples.

TABLE VIII

**AXIAL REACTIVITY COEFFICIENTS (ASSEMBLY 29)**

| Distance from interface (in) | Isotope worth ($10^{-5}$ $\Delta k$/mole) | | | |
|---|---|---|---|---|
| | $U^{235}$ ($\pm 3.0$) | $U^{238}$ ($\pm 1.0$) | $Pu^{239}$ ($\pm 2.9$) | $B^{10}$ ($\pm 1.0$) |
| —26 | 8.6* | 3.6* | — | — |
| —21 | — | — | 0.2 | — 1.03 |
| —20 | 10.4 | +3.2 | — | — |
| —14 | 26.3 | +3.1 | 31.8 | —16.6 |
| —12 | 34.2 | +0.8 | — | — |
| —10 | 44.9 | —0.3 | — | — |
| —8 | 51.9 | —1.5 | — | — |
| —7 | — | — | 83.6 | —54.7 |
| —6 | 56.6 | —2.2 | — | — |
| —4 | 64.1 | —1.9 | — | — |
| —2 | 67.3 | —3.0 | — | — |
| 0 | 67.3 | —2.7 | 111.2 | —77.0 |
| 2 | 67.3 | —1.6 | — | — |
| 4 | 65.6 | —1.4 | — | — |
| 6 | 58.2 | —1.8 | — | — |
| 7 | — | — | 87.9 | —55.1 |
| 8 | 49.1 | —0.5 | — | — |
| 10 | 44.5 | +0.3 | — | — |
| 14 | — | — | 32.4 | —19.8 |
| 20.45 | — | — | 2.8 | — 1.2 |

* Doubtful values.

The worth of materials distributed uniformly throughout the core was estimated for measurements made in a wedge-shaped sector. Although the outline of the wedge was somewhat irregular in some cases, which causes the sector to be somewhat less than an ideal representation of the uniform distribution of materials, it is believed, based on comparisons with a few full-core substitutions, that the results for heavy and intermediate elements can be trusted to within $\pm 10\%$.

TABLE IX

**REACTIVITY COEFFICIENTS FOR DISTRIBUTED MATERIALS (Inhour per kilogram)**

| Material | Ass'y 20 | Ass'y 29 | Ass'y 30 | Ass'y 32 | Ass'y 34 |
|---|---|---|---|---|---|
| SS | 0.93 | — | 2.35 | 6.82 | 1.7 |
| Na | 6.69 | — | — | 42.8 | — |
| Al | 3.80 | 4.17 | 6.90 | 26.5 | 4.6 |
| $Al_2O_3$ | 6.98 | 8.34 | 12.4 | — | — |
| $U^{238}$ | —0.33 | — | — | — | 0.85* |
| $U^{235}$ | — | — | — | — | 44.1 |
| C | — | — | — | — | 16.3 |
| Mo | —1.29 | — | — | — | — |
| Zr | 2.25 | — | — | — | — |

* This is the worth of $U^{238}$ when separated from fuel by 3.2 mm graphite.

TABLE X

**REACTIVITY WORTH OF MATERIALS AT VARIOUS RADII**
**(Inhour per kilogram)**

| Material | Ass'y 31 | | | Ass'y 32 | | | | Ass'y 33 | | | |
|---|---|---|---|---|---|---|---|---|---|---|---|
| | 6.6 cm | 28.3 cm | 43.7 cm | 2.0 cm | 7.8 cm | 16.6 cm | 19.9 cm | 2.0 cm | 5.5 cm | 16.6 cm | 27.6 cm |
| Al | .9 | 4.4 | 7.4 | — | — | — | — | — | — | — | — |
| $Al_2O_3$ | 8.9 | 8.2 | 3.1 | — | — | — | — | — | — | — | — |
| Na | 9.8 | 12.9 | 12.1 | 60 | 66 | 77 | 63 | 40 | 88 | 107 | 73 |

Experiments on Assembly 20, however, seemed to indicate that the distributed worth of light elements like aluminium and possibly sodium was sensitive to the quantity of the element and other interacting elements. The worth of $U^{238}$ is somewhat sensitive to the presence of scattering materials interposed between it and the fuel. Table IX gives some results for this type of substitution, which for the above reasons must be considered somewhat approximate. In Table X are shown the results of substitution experiments at the mid-plane of the cylinders at various radii, for Assemblies 31, 32 and 33.

## 6. Heterogeneity effects

The heterogeneity of the materials used in the ZPR-III mock-ups has an effect on reactivity which is difficult to assess experimentally. The difficulty stems from the necessity of rearranging some materials at the same time that the heterogeneity of other materials is varied, the rearrangement producing its own unknown effect on reactivity. In those assemblies which simulated actual reactor compositions, some attempt was made at clustering the materials in groups similar to their associations in the actual reactor. Thus, in Assembly 29, which simulated an oxide assembly, the plates of enriched uranium, depleted uranium and aluminium oxide were grouped together, the group being surrounded by stainless-steel plates, with aluminium separating the groups. Similarly, in Assembly 34, the carbide reactor, the enriched plates were surrounded by graphite, with depleted plates outside these, with these "fuel alloy" groups separated from each other by stainless steel and aluminium. The effects of interchanging the graphite and depleted uranium, so that the depleted was adjacent to the enriched rather than separated from it by 3.2 mm of graphite, were determined. The experiment was done in a wedge-shaped sector, and, when extrapolated to the full core, it represents a reactivity change of $+.35\%\ \Delta k/k$.

The thickness of the pieces has some effect on the reactivity of a given composition. Meneghetti has prepared a summary of previous ZPR-III experiments on varying the thickness of the pieces for the forthcoming edition of the ANL compilation of Reactor Physics Constants. It is apparent both from experimental and theoretical results that the thickness of the enriched-fuel pieces is the major contributor to heterogeneity effects. Several experiments varying the thickness of the enriched-fuel pieces were performed on Assemblies 30 and 34. The experiments were performed in wedge-shaped sectors, and Table XI gives the results extrapolated to the full cores. The experiments were planned so as to minimize any effects due to radial motion of the fuel plates. Bunching experiments in Assemblies 22, 23, 24 and 25 have been reported previously [14].

TABLE XI

**REACTIVITY OF CONFIGURATIONS CONTAINING DIFFERENT THICKNESS FUEL PLATES***

| Fuel plate | Ass'y 30 | Ass'y 32 | Ass'y 34 |
|---|---|---|---|
| 1/16 in | —0.5% | —0.5% | —0.5% |
| 1/8 in | 0 | 0 | 0 |
| 1/4 in | +1.5% | +1.5% | +1.1% |

* 1 inhour = $2.25 \times 10^{-3}$ %.

## Summary and conclusions

Although a few calculations have been made for comparison with the experimental data, the analyses are by no means complete enough to provide the basis for any major changes in the cross-section sets or methods of calculation. The results presented here do indicate certain directions where one might look for improvements in the calculations, however.

Starting with the critical-mass information, the spread in calculated reactivities of the assemblies in Table I is greater than 5%. The success in predictions of critical masses of approximately 60-l cores, reported in 1958 [4], has not continued for the larger cores. If all the large cores had about the same calculated reactivity, one might attribute the discrepancies to systematic experimental errors associated with heterogeneity or shape factors, which are not too well assessed at present. However, the contrast between calculated reactivities of Assemblies 22, 24 and 25 (all diluted with $U^{238}$) and those of the other assemblies (diluted with light elements) indicates that there are computational errors which are a function of composition. The cross-section set of Nims gives reduced reactivities for the light-element diluted assemblies, but we do not have enough experience with this set to know how it behaves for a wide variety of compositions. It is known that Nims' set (based on Mills' set) uses a different method of averaging the cross-sections within a group in the case of aluminium and iron [9]. In any case, Nims' set uses a transport cross-section for iron 25% lower than the YOM set in the region 70 to 100 keV, and 75% lower in the 25—40-keV range. Nims has also adjusted the capture cross-section for iron, and his $\sigma_c$ is about 80% higher than the YOM value in the regions 40 to 100 keV and 800 to 3600 keV. Nims' aluminium transport cross-section is considerably lower in some regions. In other respects, the cross-section sets are quite similar. These modifications have certainly improved the agreement between experimental and calculated critical masses for Assemblies 29—34.

For a number of reasons, however, we are led to suspect that there are errors in the $U^{235}$ and $U^{238}$ cross-section sets also. The central reactivity coefficients of $U^{235}$ are generally calculated higher than the measured values, indicating that the $U^{235}$ cross-section set is too reactive. If the $U^{235}$ cross-section set is substantially too reactive, the calculated criticality of Assemblies 22, 24 and 25 can be interpreted as meaning that $U^{238}$ cross-sections may be underreactive. The calculations of the central reactivity worth of $U^{238}$ are too high or too low, depending on the particular spectrum involved. Thus, it is indicated that different corrections to the $U^{238}$ cross-section set may be required in different energy regions.

As for the values of fission ratios, even if one accepts the evidence of the radiochemical measurements to the effect that the calculations are correct, it still must be remembered that the fission ratios are more sensitive to the high-energy tail of the spectrum than to the bulk of the spectrum, so that errors in the low-energy cross-sections might be contributing to calculated reactivities without affecting the fission ratios.

Our results, therefore, seem to suggest that it might be most productive to examine the cross-sections of $U^{235}$, $U^{238}$ and steel, particularly in the lower energy groups.

Even if a satisfactory set of cross-sections is devised for these materials, it is still possible that interactions between materials, which may obscure some of the resonant structure of the cross-sections, may affect reactivity measurements.

Evidence for suspecting non-linear interactions between materials was found in studies of the Fermi and EBR-II critical assemblies, where the worth of aluminium and sodium seemed to be a function of the quantities of these two materials present. To compensate for such effects, the methods of averaging the cross-sections in a region may have to be adjusted.

Future experiments and accompanying analyses are being planned with regard to these results.

## REFERENCES

[1] CERUTTI, B. C., *et al.*, *Nucl. Sci. Engng* **1** (1956) 126.
[2] BAKER, A. R., *et al.*, AERE R/R 2444 (1959).
[3] PAXTON, H. C., *Nucl. Sci. Engng* **8** (1960) 523.
[4] LONG, J. K., *et al.*, Proc. 2nd UN Int. Conf. PUAE **12** (1958) 119—141.
[5] AVERY, R., *et al.*, Proc. 2nd UN Int. Conf. PUAE **12** (1958) 151—165.
[6] MENEGHETTI, D., *et al.*, ANL-6218 (1960).
[7] Reactor Physics Constants, ANL-5800 (1958).
[8] LOEWENSTEIN, W. B., *et al.*, Proc. 2nd UN Int. Conf. PUAE **12** (1958) 16—37.
[9] MILLS, C. B., LAMS-2255 (1959).
[10] YIFTAH, S., OKRENT, D. and MOLDAUER, P. A., Fast Reactor Cross Sections, Pergamon Press (1960).
[11] KIRN, F. S., "An absolute fission counter, final program and abstracts", American Nuclear Society, 2nd Winter Meeting (1957).
[12] MENEGHETTI, D., unpublished work [1960].
[13] BRUNSON, G. S., *et al.*, *Nucleonics* **15** (1957) 132.
[14] KEENEY, W. P., *et al.*, *Trans. Amer. nucl. Soc.* **3** (1960) 327.

SM—18/60

# THE EPITHERMAL CRITICAL EXPERIMENTS

H. A. MOREWITZ AND S. G. CARPENTER
ATOMICS INTERNATIONAL, CANOGA PARK, CALIF.,
UNITED STATES OF AMERICA

**Abstract — Résumé — Аннотация — Resumen**

**The epithermal critical experiments.** The present phase of the advanced-epithermal-thorium-reactor programme consists of integral-reactor-physics experiments designed to provide neutron-cross-section information in the 10-MeV to 1-keV range. A series of nine, multi-region, slow-fast, pseudospherical critical assemblies of the honeycomb, split-table type are being studied. So far, three assemblies have been run. The outer driver-decoupler region drives an interior $U^{233}$-Th fuelled spherical test region whose neutron-flux spectrum is successively degraded by increasing the graphite moderator to fuel ratio.

A square-wave oscillator experiment defines the central reactivity worths of forty small samples of different materials to $10^{-8}$ $\Delta k$ for each assembly. Additionally, intercalibrated artificial neutron sources are oscillated to determine the various central neutron importance functions. The spectra are obtained by fission-counter measurements with calibrated foils of different thresholds and by a $Li^6$-solid-state-counter sandwich spectrometer. A digital computer routine will be used to compile all measurements into a self-consistent library of spectrum averaged cross-sections.

**Expériences critiques avec des neutrons épithermiques.** La phase actuelle du programme de réacteur au thorium à neutrons épithermiques comprend des expériences intégrales de physique des réacteurs pour obtenir des renseignements sur les sections efficaces neutroniques pour la gamme d'énergie comprise entre 1 keV et 10 MeV. Les auteurs étudient une série de neuf ensembles critiques pseudosphériques, à plusieurs régions, à couplage neutrons lents et neutrons rapides du type à alvéoles et à cœur divisé. A ce jour, trois de ces ensembles ont été mis en service. La région extérieure, mettant en service ou hors service, commande une zone d'essai intérieure de forme sphérique où le combustible est constitué de $^{233}$U-Th, dont le spectre du flux de neutrons est dégradé progressivement par augmentation du rapport entre les quantités de graphite et de combustible.

Une expérience à l'aide d'un oscillateur à ondes carrées définit les valeurs de la réactivité centrale de quarante petits échantillons de différents matériaux, jusqu'à $10^{-8}$ $\Delta k$ pour chaque ensemble. De plus, on fait osciller des sources artificielles de neutrons, étalonnées entre elles, pour déterminer les différentes fonctions neutroniques importantes au centre du montage. On obtient les spectres en procédant à des mesures à l'aide de compteurs à fission comportant des feuilles étalonnées de seuils différents et d'un spectromètre « sandwich » à compteur au $^6$Li. Une méthode de traitement numérique permettra de grouper toutes les mesures en un fichier autonome de sections efficaces moyennes par spectre.

**Надтепловые критические эксперименты.** Современная фаза программы исследований усовершенствованного надтеплового ториевого реактора состоит из полных экспериментов по реакторной физике, проводимых с целью обеспечения информацией по нейтронным сечениям в диапазоне от 10 Мэв до 1 кэв. Изучается группа девяти многозональных, медленно-быстрых, псевдосферических критических сборок „Ханикоума“ с двумя подвижными половинами активной зоны. К настоящему времени испытаны три сборки. Внешняя перемещающаяся зона двигается по отношению к внутренней сферической экспериментальной активной зоне на уране-233 — тории, спектор нейтронного потока которой успешно смягчается увеличением отношения графитового замедлителя к топливу.

Эксперимент с генератором прямоугольных импульсов определит центральную реактивную способность сорока малых образцов различных материалов до $10^{-8}$ $\Delta k$ для каждой сборки. Кроме того, взаимно калиброванные искусственные источники нейтронов осциллируются в целях определения различных функций центрального нейтронного значения. Спектры получают путем измерений счетчиком деления с помощью калиброванной фольги различных порогов, а также путем использования счетного слоистого спектрометра с $L^6$ в твердом состоянии. Для сбора всех измерений в самосогласованную библиотеку спектральных средних поперечных сечений будут пользоваться однозначным вычислительным режимом.

**Experimentos críticos con neutrones epitérmicos.** La fase actual del programa del reactor epitérmico de tipo avanzado, alimentado con torio, comprende una serie de experimentos integrales sobre física de los reactores, cuyo objeto es reunir datos sobre las secciones eficaces neutrónicas en el intervalo 1 keV a 10 MeV. Se está estudiando una serie de nueve conjuntos críticos de varias regiones, con acoplamiento térmico-rápido, de forma pseudoesférica, del tipo alveolar de cuerpo dividido. Hasta ahora se han puesto en servicio tres conjuntos de esa índole. La región externa de conexión-desconexión acciona una región de ensayo interna de forma esférica alimentada con $^{233}$U-Th, cuyo espectro neutrónico se degrada progresivamente aumentando la razón grafito-combustible.

Un experimento efectuado con un oscilador de onda cuadrada define los valores de la reactividad central de cuarenta pequeñas muestras de diferentes materiales, hasta $10^{-8}$ $\Delta k$ para cada conjunto. Además, se hacen oscilar fuentes artificiales de neutrones intercalibradas para determinar las diferentes funciones neutrónicas que revisten importancia en el centro del conjunto. Los espectros se obtienen procediendo a mediciones con contadores de fisión provistos de detectores calibrados, de umbrales diferentes, y con un espectrómetro en "emparedado" de contador de $^6$Li sólido. Se utilizará una calculadora numérica corriente para agrupar todas las mediciones en un registro sistemático de secciones eficaces promediadas respecto del espectro.

## Introduction

A series of critical experiments designed to obtain integral reactor physics information for the Advanced Epithermal Thorium Reactor (AETR) programme are being run. The 25 kg of $U^{233}$ which are available (1200 kg of $U^{233}$ are needed for a full scale critical experiment) are being used in a multi-region, slow-fast, pseudospherical critical assembly (Fig. 1) in which the central region contains the $U^{233}$-Th fuel mixtures of interest [1]. As the test series proceeds, the neutron flux spectrum in the central test region will be successively degraded by increasing the graphite moderator to fuel ratio. So far, two assemblies have been studied.

## Oscillator experiment

Because of the limited volume of the test region in each assembly, a square-wave oscillator experiment [2] has been developed to measure the central reactivity worths of small samples of fissionable, fertile, poison, coolant, and structural material. The mechanical oscillator drives a square, steel bar through a diametral hole in the assembly. The steel bar has two pockets which accept $2 \times {}^1/_2$-in capsules containing a standard material and a test material. (The diametral hole is filled by the steel bar at all times to prevent neutron streaming.) As the bar is oscillated back and forth, the standard and test pockets interchange positions so that when one of them is in the centre of the core, the other is fully removed from the assembly.

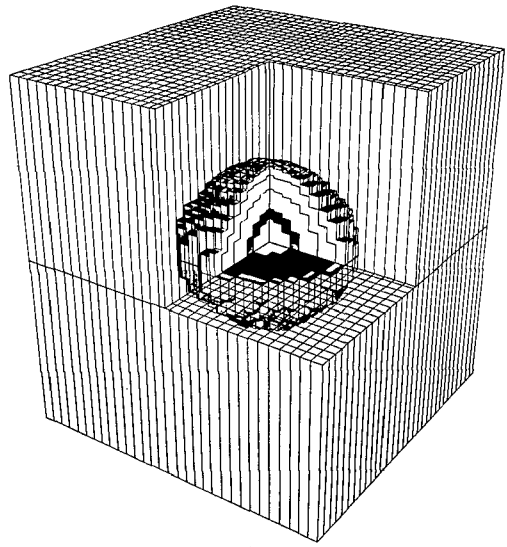

Fig. 1
ECEL pseudospherical core.

Each pocket is fed by a remote sample changer which holds up to ten capsules, so that for one closure of the critical assembly a series of measurements can be made (a measurement may require $\sim$45 min).

In order to minimize the perturbations of the test-region flux, small samples are used, thus requiring a sensitive detecting and data reduction system. The ion chamber signals, representing the modulation of the reactor power level by the reactivity of the sample, are amplified and converted to digital form by an integrating-type voltage to digital converter which generates a pulse train whose frequency is proportional to the input voltage. This pulse train is stored in a 200-channel time analyser which is gated in synchronism with the mechanical oscillator. Succeeding cycles of modulation are summed in the equiphase storage channels, while the reactor noise fills all channels uniformly. Thus, at the end of 100 cycles the signal-to-noise ratio has been increased by an order of magnitude. The stored information is then printed out on paper tape and punched on IBM cards for Fourier analysis by a digital computer routine. Only the cosine component is utilized, as this discriminates heavily against reactor drift (a 10 000-s period can be tolerated). It is possible by this method to obtain sensitivities of $\sim 10^{-8}\,\Delta k$ in reactivity.

Table I gives the results of the ratio of reactivity coefficients in Core I (stainless steel, $U^{235}$ test region).

It is to be noted that the calculated results are preliminary in that no experimentally adjusted cross-sections have been utilized. As a result, the absolute magnitude of some of the calculated reactivity coefficients differs from the experimental results by as much as 50% [3]. (The reactivity coefficients can change, but their ratios do not; thus the thorium decoupler region has little effect on the central region neutron spectrum. Only ratios of the reactivity coefficients are utilized in determining the cross-sections in this experiment.) As an example of the results to be expected, a change in the scattering cross-section of thorium

TABLE I

**REACTIVITY MEASUREMENTS**

$$\left(\frac{\Delta\rho/g \text{ material}}{\Delta\rho/g \text{ } U^{235}}\right)$$

| Material | Calculated | Measured |
|---|---|---|
| $U^{235}$ | 1 | 1 |
| $U^{238}$ | 1.83 | 2.17 |
| Th | —0.055 | —0.070 |
| Nat. U | 0.041 | 0.050 |
| $B^{10}$ | — | —14.8 |
| B | —2.3 | —3.0 |
| Polyethylene | 10.6 | 16.0 |
| Al | 0.14 | 0.046 |
| Pb | — | 0.0061 |
| Mo | — | —0.033 |
| Sb | — | —0.162 |
| Sn | 0.040 | —0.038 |
| Cd | — | —0.117 |
| C | 0.67 | 0.58 |
| Phy I (Fission product [9] mock-up) | — | —0.033 |
| Phy II | — | 0.048 |
| 304 stainless steel | 0.043 | 0.0035 |
| MgO | — | 0.748 |
| Be | 1.77 | 1.43 |
| Bi | — | 0.0078 |
| $GdO_3$ (90%) | — | —0.18 |
| Ta | — | —0.18 |
| Mixed RE (35% Sm + 45% Gd) oxides | — | —0.16 |

from the old values to the recent compilation of Roach [4] changes the Th reactivity coefficient by 100%. It is expected that the calculated absolute values will be quite improved when the experimental series are completed.

TABLE II

**IMPORTANCE MEASUREMENTS**

| Source | Intensity* | Mean energy (MeV) | Relative importance |
|---|---|---|---|
| Po-Be | $5.27 \times 10^6$ | 4.2 | 11 |
| Po-$B^{11}$ | $2.78 \times 10^6$ | 3 | 10.9 |
| Po-$Li^7$ | $8.40 \times 10^5$ | 0.484 | 13.3 |
| Po-$CaF_2$ | $9.76 \times 10^5$ | 1.4 | 13.2 |
| Sb-Be | $\sim 6 \times 10^6$ | 0.024 | — |
| Mock fiss. | $4.03 \times 10^6$ | 2 | 13 |

* The listed values were obtained by a "long counter" at Mound Laboratory. More accurate values are being measured by a Mn $SO_4$-bath technique.

## Neutron-importance experiment

In order to determine the neutron-importance spectrum, six neutron sources intercalibrated by the $MgSO_4$-bath method have been oscillated (alternately with dummy sources to cancel material reactivity effects). The individual-source spectra have been examined on a proton-recoil spectrometer [5] and shown to agree with published data [6] (see Fig. 2). The results for Core I are shown in Table II.

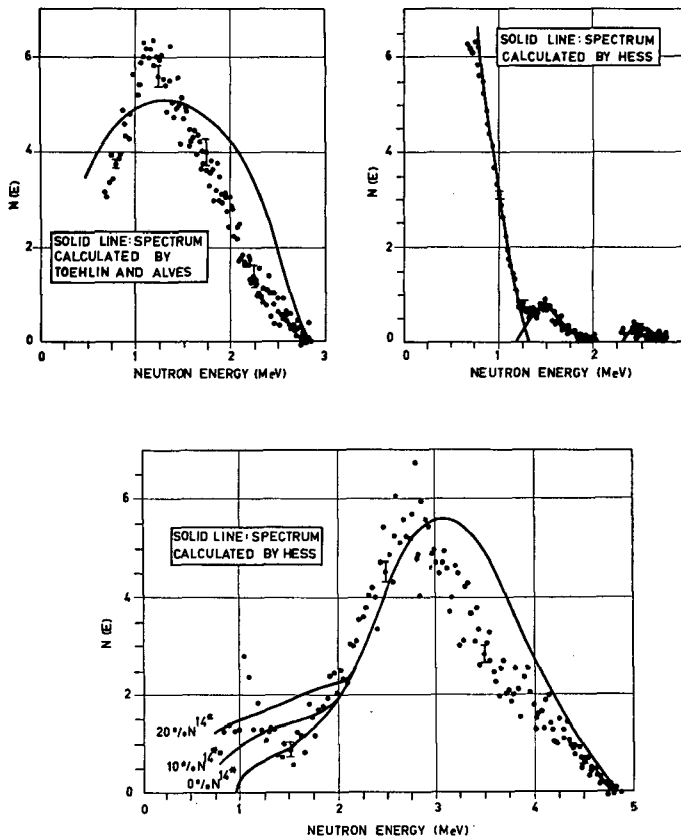


Fig. 2
Neutron spectrum for proton recoils in stilbene. *Above: left,* Po-$CaF_2$ neutron source; *right,* Po-$Li^7$ neutron source. *Below:* Po-$B^{11}$ neutron source.

## Neutron-spectra experiments

In order to determine the neutron spectrum in various regions of the core, a series of miniature fission counters, both gas-filled and solid-state diodes, have been fabricated from electroplated foils of various fissionable materials. These counters have been cross-calibrated by comparison in a thermal flux [7] (for those foils with an appreciable thermal-neutron cross-section or contaminated by

another isotope with a thermal-neutron cross-section) and 3 MeV where the cross-section *vs.* energy is relatively flat. Fig. 3 shows a series of radial traverses in the oscillator hole. Table III shows the results of these experiments on Core 1.

TABLE III

**FISSION-COUNTER MEASUREMENTS**

| Foil* | ~ Threshold | Measured ratio to $U^{235}$ | Calculated ratio to $U^{235}$ | %Diff. |
|---|---|---|---|---|
| $U^{235}$ | 0 | 1 | 1 | — |
| $U^{234}$ | 0.4 | 0.46 | 0.466 | 0 |
| $Np^{237}$ | 0.5 | 0.50 | 0.484 | 3.2 |
| $U^{236}$ | 0.9 | 0.167 | 0.168 | 0.6 |
| $U^{238}$ | 1.4 | 0.069 | 0.0764 | 11 |
| $Th^{232}$ | 1.5 | 0.0157 | 0.01695 | 8 |

* In latter cores, counters of $U^{233}$ and $Pu^{239}$ will also be used.

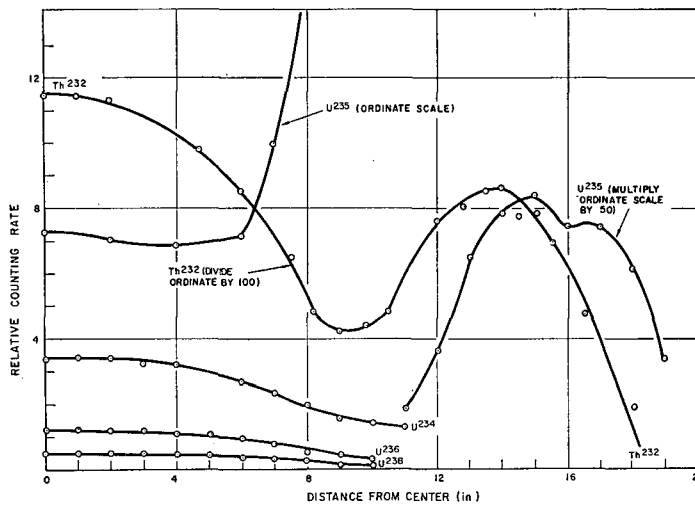


Fig. 3
Fission-counting rates of $Th^{232}$, $U^{234}$, $U^{235}$, $U^{236}$ and $U^{238}$.

## $Li^6$ spectrometer

A $Li^6$ spectrometer [8] has been constructed for use in the core interior. The pair of solid-state detectors and their pre-amplifiers have been maniaturized to fit in the $0.8 \times 0.8$-in square-oscillator hole. The spectrum in the core centre is identical with a fission spectrum above 1 MeV.

## Foil measurements

Fig. 4 shows foil measurements taken on Core 1 [10]. The aluminium (n, p) reaction shows that the high-energy flux remains constant over most of the reactor.

The calculations give the same results. Other curves have been taken with more thermal detectors and show the thermal-flux depression in the interior of the reactor.

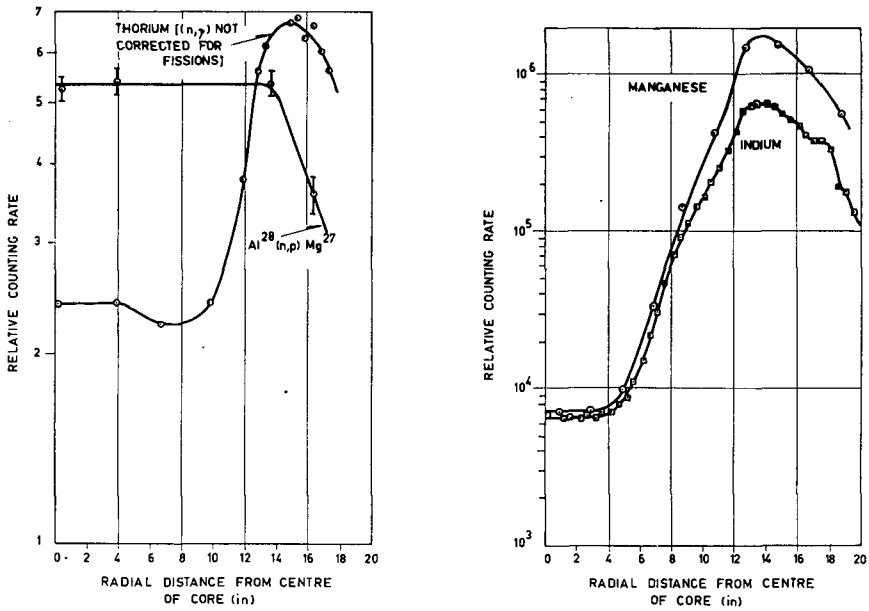


Fig. 4
Radial flux maps. *Left:* aluminium and thorium. *Right:* indium and manganese.

## REFERENCES

[1] MOREWITZ, H. A., *et al.*, Trans. ANS-4 (1), Session 12, paper 7 (1961).
[2] MOREWITZ, H. A. and CARPENTER, S. G., "The AETR oscillator system", ANL-6205 (1960) 294.
[3] KISTLER, V., Private communication.
[4] ROACH, W. H., *Nucl. Sci. Engng* 8 (1960) 621. The absorption cross-sections were obtained from resonance integral codes similar to: VERNON, R., *Nucl. Sci. Engng* 7 (1960) 252.
[5] BROCK and ANDERSON, *Rev. sci. Instrum.* **31** (1960) 10.
[6] TUTTLE, R. J., Private communication. HESS, W. N., *Ann. Phys.* **2** (1959) 115.
[7] STROMINGER, D., Private communication.
[8] LOVE, T. A. and MURRAY, R. B., ORNL Report CF-60-5-121.
[9] LONG, J. K., *et al.*, Proc. 2nd UN Int. Conf. PUAE **12** (1958) 119.
[10] ENGELHARDT, J., Private communication.

SM 18/40

# DESIGN AND CONSTRUCTION OF THE ARGONNE FAST CRITICAL FACILITY (ZPR-VI)*

W. Y. Kato and L. R. Dates
Argonne National Laboratory, Argonne, Ill.,
United States of America

**Abstract — Résumé — Аннотация — Resumen**

**Design and construction of a fast critical facility.** In a fast-power-reactor development programme, a critical facility is found to be a highly useful tool to ascertain calculational techniques, to verify neutron cross-section sets, and to obtain integral reactor-physics parameters necessary for the nuclear design of a power system. Since it is primarily a physics instrument, the design of a fast critical facility itself poses a number of different problems not found in the design of a power reactor. In addition to usual questions of site, containment, core design and instrumentation, there arise such problems as: how to obtain a large degree of flexibility consistent with safety, the determination of the size and type of facility to meet the experimental physics requirements, the determination of the number and location of control and safety rods minimizing perturbation effects and the specification of the reproducibility of control rods and other movable components to obtain the accuracy required in reactivity measurements. These are some of the problems which are discussed in this paper based on recent experience at the Argonne National Laboratory which has under construction a fast critical facility, ZPR-VI at its Lemont, Illinois site for fast-reactor-physics studies. The ZPR-VI is a movable half- or split-table-type machine similar to ZPR-III. It has a matrix about two and a half times the volume of the earlier machine and will be used to investigate the physics of large, highly dilute, metal and cermet, unmoderated and partially moderated systems having core volumes up to about 1500 l. A detailed description of the ZPR-VI with a discussion on the criteria used in the design of its various components from the point of view of reactor physics is presented. In addition, such topics as management and operating procedures, potential hazards during operation, experimental techniques to be used and construction costs are also included.

**Etude et construction d'un ensemble critique à neutrons rapides.** On considère que dans un programme de mise au point de réacteurs à neutrons rapides, un ensemble critique fournit un moyen très utile de vérifier les méthodes de calculs, les ensembles de sections efficaces neutroniques et d'obtenir l'ensemble des paramètres physiques nécessaires à la conception d'un réacteur de puissance. Puisqu'il s'agit avant tout d'un instrument de physique, la réalisation d'un ensemble critique à neutrons rapides implique la solution d'un certain nombre de problèmes qui sont très différents de ceux que pose un réacteur de puissance. Outre les problèmes habituels de site, de confinement, de construction du cœur et d'appareillage, il faut résoudre des problèmes tels que les suivants: associer une grande souplesse à la sécurité, déterminer les dimensions et le type de l'appareil qui convient le mieux aux besoins de la physique expérimentale, déterminer le nombre et l'emplacement de barres de contrôle et de sécurité en vue de réduire au minimum les effets perturbateurs, assurer la reproductibilité d'emploi des barres de contrôle et autres éléments mobiles en vue d'obtenir la précision nécessaire dans les mesures de la réactivité. Ces problèmes sont parmi ceux qui sont décrits dans le mémoire, qui découle de l'expérience acquise dernièrement

* Work performed under the auspices of the United States Atomic Energy Commission.

au Laboratoire national d'Argonne; ce dernier fait construire actuellement au Centre de Lemont (Illinois) un ensemble critique à neutrons rapides, le ZPR-VI, destiné aux études de physique d'un réacteur à neutrons rapides. Le ZPR-VI est du type à cœur divisé, comme le ZPR-III. Le volume de sa matrice est 2,5 fois supérieur à celui de la matrice du modèle précédent; il servira à étudier les propriétés physiques de grands réacteurs, hautement dilués, à combustibles métalliques et céramiques, non ralentis et partiellement ralentis, avec un cœur dont le volume peut atteindre 1500 l environ. Les auteurs donnent une description détaillée du ZPR-VI et analysent les critères qui ont servi à mettre au point ses éléments du point de vue de la physique des réacteurs. Ils présentent également des considérations sur le mode d'exploitation et de fonctionnement, sur les risques de manipulation, sur les méthodes d'expériences qu'il convient d'utiliser et sur le coût de la construction.

**Проектирование и сооружение критической сборки на быстрых нейтронах.** В программе разработки энергетических реакторов на быстрых нейтронах критическая сборка является весьма полезным средством для контролирования вычислительных методов, проверки сборников сечений нейтронов и получения всех параметров реакторной физики, необходимых для проектирования ядерной энергетической системы. Поскольку она является прежде всего физической системой, проектирование критической сборки ставит само по себе ряд трудных проблем, не встречающихся при проектировании энергетического реактора. Кроме обычных вопросов, связанных с месторасположением, оболочкой реактора, расчетом активной зоны и контрольно-измерительными приборами, возникают такие проблемы, как достижение высокой степени гибкости, совместимой с безопасностью, определение размеров и типа установки, удовлетворяющих требованиям экспериментальной физики, определение числа и размещения регулирующих и аварийных стержней, сводящих к минимуму последствия возмущений, и спецификация воспроизводимости регулирующих стержней и других подвижных компонентов с тем, чтобы обеспечить точность, необходимую при измерениях реактивности. Это лишь некоторые из проблем, которые обсуждаются в настоящем докладе, основанном на последнем эксперименте в Аргоннской национальной лаборатории, где сооружается критическая сборка на быстрых нейтронах — ZPR-VI на ее станции по изучению физики реакторов на быстрых нейтронах в Лемонте, штат Иллинойс. ZPR-VI является устройством с двумя движущимися половинами активной зоны, которое аналогично реактору ZPR-III. Он имеет объем приблизительно в два с половиной раза превышающий объем более раннего реактора, и будет использоваться для исследований физики крупных систем на сильно разбавленном топливе, металлическом и металлокерамическом топливе, без замедления или с частичным замедлением, имеющим объемы активной зоны приблизительно до 1500 литров. В докладе будет дано подробное описание ZPR-VI и будут обсуждены критерии, которые использовались при проектировании его различных компонентов с точки зрения реакторной физики. Кроме того, в доклад будут включены такие вопросы, как управление и эксплуатация, потенциальная опасность во время эксплуатации, экспериментальные методы и стоимость строительства.

**Proyecto y construcción de un conjunto crítico de neutrones rápidos.** Los conjuntos críticos constituyen auxiliares sumamente valiosos en los programas de perfeccionamiento de los reactores rápidos de potencia. Con ellos se pueden comprobar técnicas de cálculo y series de secciones eficaces neutrónicas, y se obtienen los parámetros físicos necesarios para el proyecto de reactores de potencia. Como se trata primordialmente de un instrumento de física, el diseño del propio conjunto crítico de neutrones rápidos implica la solución de problemas que difieren radicalmente de los que se plantean en el diseño de los reactores de potencia. Además de las cuestiones habituales de emplazamiento, confinamiento, proyecto del cuerpo y del instrumental, se plantean problemas como el de alcanzar un elevado grado de flexibilidad en la aplicación sin detrimento de la seguridad, hallar las dimensiones y el tipo de conjunto más adecuado para satisfacer las necesidades de la física experimental, deter-

minar el número y la posición de las barras de control y de seguridad para reducir a un mínimo los efectos perturbadores y asegurar la reproducibilidad en el empleo de las barras de control y otros elementos móviles para lograr la precisión requerida en la medición de la reactividad. La memoria discute estos y otros problemas basándose en la experiencia adquirida en el Argonne National Laboratory, que en su centro de Lemont, Illinois, está construyendo un conjunto crítico de neutrones rápidos, el ZPR-VI, destinado a la realización de estudios sobre la física de los reactores rápidos. El ZPR-VI es del tipo de cuerpo dividido, como el ZPR-III. El volumen de su matriz es 2,5 veces superior al de la matriz del modelo anterior y servirá para estudiar las propiedades físicas de los grandes reactores, altamente diluidos, de combustible metálico o cerámico, desprovistos de moderador o parcialmente moderados, con cuerpos de hasta 1500 l de volumen. Los autores describen detalladamente el ZPR-VI y analizan los criterios seguidos en el diseño de sus diversos componentes desde el punto de vista de la física de reactores. Asimismo, formulan algunas observaciones acerca de los procedimientos de explotación y manejo del reactor, los peligros que se pueden presentar durante su funcionamiento, las técnicas experimentales que conviene emplear y los costos de construcción.

## Introduction

A zero-power critical facility, ZPR-VI, the Argonne Fast Critical Facility, is under construction by the Argonne National Laboratory at its Lemont, Illinois site to further the basic understanding of the nuclear characteristics of unmoderated highly dilute reactors. This facility will be utilized to investigate at low power the physics of fast power-reactors, particularly those using carbide or oxide fuels with large core volumes ranging up to about 1500 l.

Although a great deal of microscopic cross-section data is available, uncertainties in the inelastic and absorption cross-sections especially of fissile and fertile materials, poor knowledge of the degradation of energy process and uncertainties in calculational techniques make the establishment of this fast critical facility essential. The following areas of study are representative of those to be undertaken on the ZPR-VI:

(1) The investigation of large-core, highly dilute unmoderated reactors including uranium carbide and oxide systems;
(2) The investigation of the Doppler temperature coefficient and sodium-void coefficient for dilute systems;
(3) Tests of the capability of present calculational techniques by mocking-up specific composition and geometry reactors for the comparison of parameters determined by computer methods; and
(4) The study of hypothetical melt-down configurations to determine reactivity changes of the motion of fuel. This includes such measurements as danger coefficients and power distributions on configurations where the fuel is concentrated in one section of the reactor simulating a melt-down.

## Description of the facility

### General

ZPR-VI is a split-table or two-half type of facility, which is a type used to mock up unmoderated or solid moderator reactors. This concept has been used successfully in the United States in the past eight or nine years at such labora-

tories as ANL-Idaho (ZPR-III) [1, 2], Hanford (PCTR) [3], KAPL (PPA) [4] and Atomics International (AETR) [5].

The choice of a split-table-type horizontally loaded facility was governed by the requirements of achieving a high degree of flexibility with a maximum of safety. The major considerations which led to this choice were:

(1) Ease of access to the centre of the core;
(2) Ease of loading the facility since the drawers are in small sections;
(3) Enhanced safety during loading operation due to a large decrease in reactivity by splitting the core into two halves;
(4) Availability of shut-down due to expansion of the enriched uranium in the axial direction on an excursion;
(5) Decrease in the possibility of a core-collapse-type of accident in the event of a melt-down due to the structural strength of the horizontal tubes;
(6) Availability of components of a machine which could be modified to meet the size, weight, and reproducibility tolerances;
(7) Decrease in nuclear hazards by handling small quantities of enriched materials at any given time; and
(8) Possibility of exchanging materials used on ZPR-III.

The facility consists basically of two tables, both of which are 3.7 m wide by 2.4 m long. One of the tables is stationary and the other movable with both resting on a cast-steel bed. On each table is stacked horizontally a 45-row by 45-column array of 5.52 cm square stainless-steel tubing of 1.2 m length forming half of a 2.5 m cube reactor. The tubes are constrained in position by supports on both sides. Drawers containing materials such as enriched uranium, depleted uranium, stainless steel, aluminium and zirconium are available to simulate different reactor compositions. A pictorial drawing of ZPR-VI in Fig. 1 shows the arrangement of the facility. The size of the tables was based on the desirability of being able to construct a 2.5-m cube matrix for reactor mock-ups. The width of the tables was specified to be 3.7 m so that reactors having large core-volumes with small length-to-diameter ratios could be studied.

Each half of the reactor facility has five dual-purpose control/safety rods. These rods will be of the reactor-core-removal type consisting of stainless-steel drawers, containing the core composition, fastened to drive mechanisms. In addition to the dual-purpose rods, there are available up to six $B^{10}$-loaded safety rods per half, for use when there is insufficient shut-down reactivity in the dual-purpose rods in the case of large dilute systems.

Each half of the assembly contains a polonium-beryllium start-up neutron source which may be driven in or out of the assembly by means of a motor drive.

A control console and nuclear instrumentation are available in the control room to control the movement of the table and rods, and to monitor the neutron population.

For loading and unloading operations, a platform which is hinged at the wall is swung down between the separated halves.

### Bed and table assembly

The one-piece bed is 6.5 m in length, 2.6 m in width and 43 cm in depth. It is a casting of close-grained, high-tensile (45000 lb/in$^2$ min) semi-steel, having a box-type construction and heavily ribbed for rigidity and stiffness. The bed has been designed to carry two tables with a load of 81800 kg on each. The bed

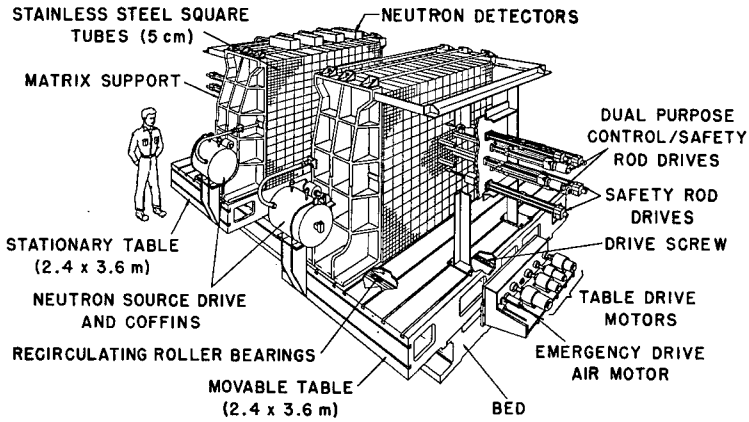


Fig. 1
Fast critical facility—ZPR VI.

has four raceways which contain alloy-steel replaceable inserts. The inserts are hardened and ground to provide a bearing surface for recirculating anti-friction roller-bearing assemblies. These anti-friction assemblies will support the movable table on the bed.

The bed supports the stationary and movable tables with the stationary table being keyed and bolted to one end. The movable table uses five anti-friction roller-bearing assemblies in the outer raceways and four assemblies in the inner raceways to affect a movement of 152 cm. The separation of 152 cm when the tables are fully apart was specified in order to insure a complete decoupling of the two halves, especially for large assemblies. The tables are 3.7 m wide, 2.4 m long and 45.7 cm deep and are of the same material as the bed. Eight parallel 2.54-cm tee-slots are machined across the loading-face parallel to the 3.7-m side of the table. These tee-slots are used to hold down the matrix supporting structure and the rod-drive mounting assembly. The movable table is guided by tapered shoes so that the two tables align accurately when they are brought together. The contact surfaces of the two tables are hand-scraped and are parallel to each other within 0.008 cm and the closed position of the tables is reproducible to at least 0.003 cm. For large assemblies this results in an uncertainty in reactivity measurements of no greater than about $\Delta k/k = 1.5 \times 10^{-5}$ due to the reproducibility of the closed position of the tables. The loading surfaces of the stationary and movable tables are parallel to the horizontal plane and to each other within 0.008 cm. This requirement is for the alignment of the cores of the two halves.

The movable table is driven by a lead screw which revolves within an anti-friction ball-bearing nut that is attached to the under-surface of the table. The maximum movement or separation of the tables is 152 cm. The lead screw is connected, through a slip clutch and a speed-reducing gear box using gears of alloy steel with flame-hardened teeth, to four three-phase motors and one air motor. Each motor is provided with a magnetic clutch and wired such that only one motor may be connected to the drive shaft at any time. Three of the motors provide the three forward speeds to bring the halves together. The fourth

motor bypasses the slip clutch and may be directly connected to the drive shaft when moving the movable table away from the stationary one. The air motor provides emergency separation of the tables on the occurrence of an electric-power failure.

The slip clutch is provided between the lead screw and speed-reducer for two purposes. If any obstruction should be left between the tables, the clutch will slip before any damage is done to the assembly. Also, when the tables are driven together, the clutch allows the movable table to be driven to an exactly reproducible position which is not dependent upon a limit switch. This is accomplished by setting the torque of the clutch somewhat higher than required to drive the table, and driving the table until the mating surfaces are in contact, causing the clutch to slip. The slip clutch is of the jaw-type, fitted with a micro-switch and collector rings in such a manner that when the clutch slips, the jaws will separate and actuate the microswitch. This microswitch is wired through collector rings to an indicator lamp on the control console. The slip clutch functions only for the forward-drive speeds.

The movable table will move forward three speeds as follows:

(1) From full separation, 152 cm to 45.7 cm at 25 cm/min with a 3/4 HP, 56 rpm, 208 V, three-phase, gear-head motor.
(2) From 45.7-cm to 7.6-cm separation at 15 cm/min using a 1/2 HP, 56 rpm, 208 V, three-phase, gear-head motor.
(3) From 7.6 cm to contact of the tables 1.27 cm/min with a 1/4 HP, 13.5 rpm, 208 V, three-phase, gear-head motor.

The three forward speeds—fast, intermediate and slow—were provided to minimize the time required to move the table 152 cm with the maximum amount of safety. The fast speed is used to minimize the start-up time. The slow speed is necessary since the reactor is normally sub-critical by an amount equal to the reactivity in the control rods. If an error in loading has been made, the slow speed insures a relatively low reactivity insertion rate, thus avoiding a serious excursion, if proper functioning of the period trip circuits is assumed. The intermediate speed was inserted to insure that there was an actual step-down in speed and that the reactor did not inadvertently assemble at the fast speed.

Upon the initiation of a scram signal [emergency shut-down], the table is driven from any position to the full-separation, 152-cm position at a rate of 1.27 cm/s by means of a 1-HP, 100-rpm, gear-head, 208-V, three-phase motor. In the event of an electric-power failure or if the table does not start to move to the 152-cm position. 0.5 s after the scram signal, a 0.9-HP, 270-rpm air motor is connected to the drive shaft through an air-operated clutch and the table is driven out at the rate of 1.27 cm/s insuring a shut-down of the reactor.

Limit switches are placed at the 45.7-cm and 7.6-cm position to shut off automatically the fast- and intermediate-speed drives respectively. In the case of the fast speed, the operator at the console need only depress a switch to start the motor; however, for the intermediate and slow speeds, the operator must hold the switch continuously in the "on" position in order to move the table.

In order to insure a positive stop at each of the speed-reduction positions, mechanical blocks which would stop the forward motion of the table in the event of a limit-switch failure or inattention by the operator are provided at the 45.7-cm and 7.6-cm positions. The table proceeds past the mechanical blocks at the next reduced speed, when the operator at the console actuates a solenoid located on the table which raises a sliding bolt out of the way of the mechanical block.

The sliding bolt and blocks are designed in such a manner that they do not stop the movable table when it is moving in the reverse direction, away from the stationary table.

In order to determine the position of the movable table accurately, a digital position indicator using selsyns, an amplifier and a read-out counter unit graduated to 0.02 mm is provided. It is possible to determine the position of the table to an accuracy of $\pm 0.025$ mm for the entire 152 cm of table travel. A linear scale graduated in centimeters showing the position of the table for the full travel is also provided to give an analogue-type indication of the table moving to the closed position.

### Matrix assembly

The honeycomb matrix is formed of 45 horizontal rows and 45 vertical columns of 5.52 cm square by 122 cm long, type-304 stainless-steel tubing whose minimum yield strength is 60000 lb/in$^2$ stacked on the two tables such that the length of the tubing is parallel to the direction of motion of the movable table. The honeycomb cross-section is a 2.5-m square, and a 2.5 m cube is formed when the tables are together. The wall thickness of the square tubing is $0.102 \pm \pm 0.003$ cm thick and the inside dimension is $5.32 \pm 0.010$ cm. The stainless-steel tubes have a stringent squareness tolerance in order to minimize sagging under load. The square stainless-steel tubes are spot-welded together in a $5 \times 5$ bundle of 25 for easy handling during alignment. In addition to the stainless-steel tubes there is available square, drawn (6061 Al) aluminium tubing of the same dimensions as the stainless-steel for use in assemblies where it is desirable to minimize steel. The aluminium tubes are also spot-welded in $5 \times 5$ bundles of 25.

The matrix of square tubes is supported by two large massively cast iron-alloy (meehanite) L-shaped knees which are bolted to the loading surface of each table. Tie-rods across the top of the L-shaped supports keep the supports in line.

Into the central portion of the matrix are placed the reactor-core-composition materials which are first loaded into 5.24-cm wide by 5.24-cm high and 38-cm or 61-cm long stainless-steel drawers. The wall thickness of the drawers is 0.081 cm so that a 5.08 cm space is available for the core materials. The drawers are provided with lugs which engage in notches in the matrix tubes so that they are accurately positioned and provide a flat surface between the assembly halves. The drawers for the aluminium tube matrix are of aluminium with the same dimesions as the stainless-steel drawers. The locating lug on the stainless-steel drawer is in a different position from that on the aluminium drawer so that it is not possible to interchange drawers between the tow matrices.

In the blanket section which surrounds the central core region, uranium blanket slugs may be loaded directly into the matrix tubes without the use of drawers.

In order to obtain a large degree of flexibility of composition and geometry for reactor mock-ups, various core materials have been fabricated into elements of thicknesses 0.16 cm and 0.32 cm. The widths of the plates are 2.54 cm and 5.08 cm; the lengths are 2.54 cm, 5.08 cm, 7.62 cm and 12.7 cm. These plates are composed of materials such as enriched uranium (partially or highly enriched), depleted uranium, natural uranium, stainless-steel, aluminium of 100, 63, 57 and 45% density, zirconium, and others. The materials are colour-coded for easy identification. Fig. 2 shows the various sizes and kinds of plate available. The

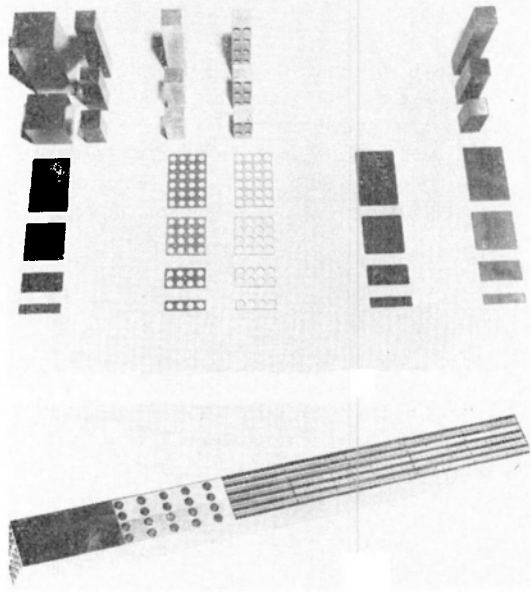

Fig. 2
Building blocks and loaded drawer.

uranium plates are coated with about a 0.001-cm-thick trifluorochloroethylene polymer coating with and without pigment, to reduce oxidation, to decrease the spread of contamination of radioactivity, and to identify the enriched, natural and depleted pieces. Approximately 60 t of depleted uranium fabricated in various sizes are available for use as blanket and core dilution plates. All the enriched uranium is fabricated into plates 0.32 cm thick in order to minimize heterogenity corrections.

There are two front drawers of different length, 38 cm and 61 cm, the size used depending on the reactor size being studied. The front drawers are those which are loaded into the honeycomb from the separation-face of the facility. In addition there are back drawers 58 cm long which are loaded from the rear side of the facility. All of the drawers are loaded by stacking the plates on the 0.32-cm or 0.16-cm edge to permit easy visual inspection of the drawer loading.

All the front drawers are provided with special leaf springs which are inserted at the back of the drawer. The drawers are 0.5 cm longer than the sum of a column of enriched uranium-pieces so that the springs may be inserted. The springs hold the plates against the front of the drawer. All the fuel pieces are fabricated so that they are slightly larger in length than the depleted-uranium or structural pieces to insure that the springs are actually holding the fuel plates against the front of the drawer. This is to insure that the fuel will expand in such a direction as to decrease reactivity upon heating of the fuel. The lugs on the drawers make it impossible to load a drawer into the matrix in such a manner that the spring is at the centre of the core, unless the spring has been incorrectly loaded into the drawer.

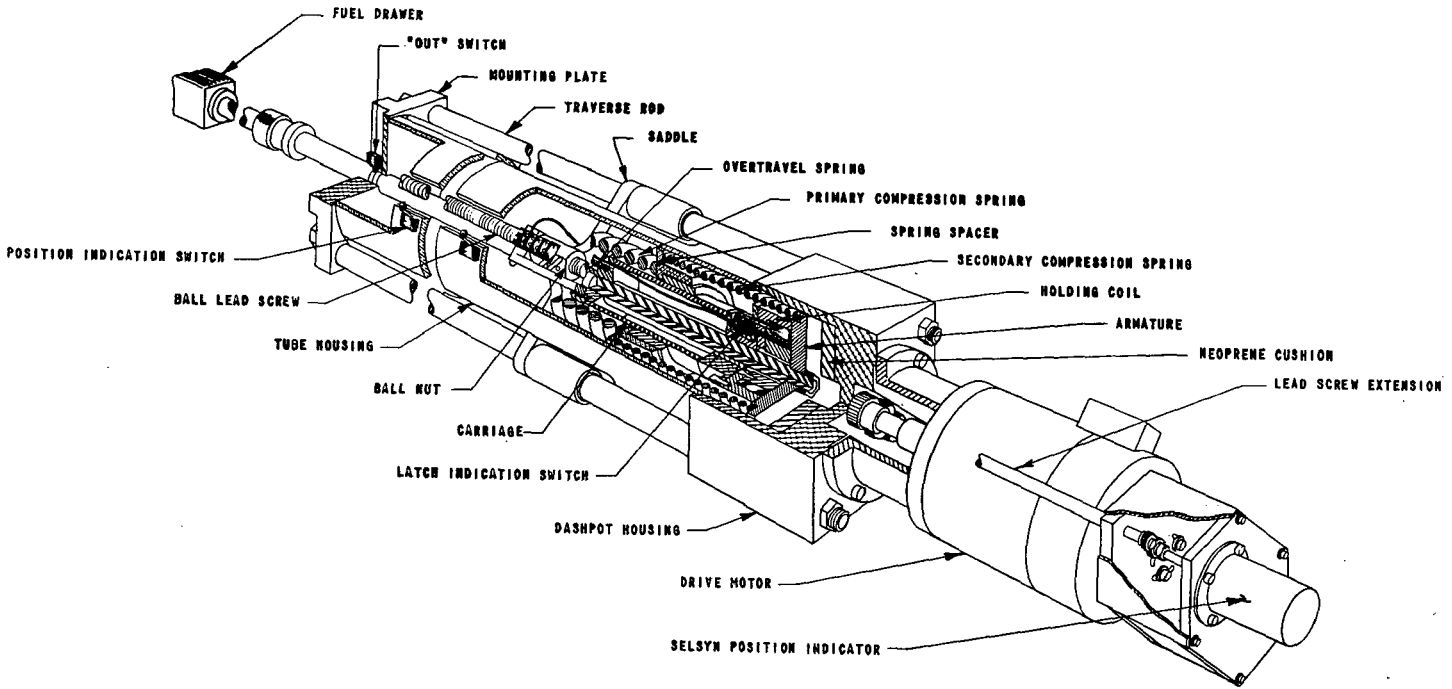


Fig. 3
Dual-purpose control/safety rod drive.

Thimbles are provided for experimental purposes at a number of points in the assembly, in both the vertical and horizontal directions. Thimble holes are located on both the vertical and horizontal centrelines. These are located approximately every 7.6 cm in each half of the assembly. For experimental counters for flux traverses and fission-rate measurements drives are provided that may be operated from the control panel in the thimbles. The travel of the drive is sufficient to move a counter to the centreline of the assembly.

### Control and safety rods

There are five dual-purpose control/safety rods of the core-composition-movement-type available on each half of the facility. The decision to use movement of sections of the core as a means of making reactivity changes for control purposes was made in order to minimize perturbation of the core. They are dual-purpose in that each may be operated as a control rod if so desired by the operator and is driven out of the reactor upon a scram signal. Of the five dual-purpose rods, at least one and up to five per half may act as control rods on a given assembly. The remaining dual-purpose rods are used as safeties. Those rods acting as safeties will be inserted at start-up and will be driven out by a spring which is held compressed by a holding magnet until a scram signal is given. All ten rods are driven out of the reactor on a scram signal. A pictorial drawing of the dual-purpose rod-drive mechanism is shown in Fig. 3.

The full travel of the dual-purpose rods is 61 cm; they are designed so that they will travel 90% of the full stroke in about 250 ms with a 32-kg-loaded drawer. The rods move the first 15 cm in about 100 ms after the initiation of the scram signal. In the event of a power failure the rods are designed to fail safe by de-energizing the holding magnet which releases the scram spring. The rods are driven by a 1/20 HP DC motor whose drive speed is variable up to a maximum of about 0.25 cm/s. There are ten selsyn-driven digital dials on the control console which indicates the dual-purpose rod positions to 0.013 cm. Microswitches and indicator lamps indicate in addition when the holding magnet is in the latched position, and when the rods are completely in the "in" and "out" positions. It is necessary to drive the holding magnet to the "out" position to latch with the rod before the rod may be driven in. It is possible to drive the holding magnet at a speed of 1.0 cm/s for latching purposes. The control drawer has a solid film lubricant (molybdenum disulfide) on all outer surfaces to minimize the danger of galling and sticking to the matrix wall. The drawers for use with the dual-purpose safety-control rods are of a much stronger wall construction than the usual drawers used for mocking-up various assembly cores. The wall thickness of these stainless-steel drawers is 0.13 cm.

In addition to the five dual-purpose rods per half, there are available up to six single-purpose $B^{10}$ insertion-type safety rods. In large dilute systems such as 800-l or 1200-l core systems the worth of a single core drawer might be less than $\Delta k = 0.2\%$. The $B^{10}$ neutron-absorber rods have been provided so that there is an additional means of decreasing reactivity when large dilute systems are being studied. The $B^{10}$ powder will be packed into a stainless-steel box about 1 cm thick, 60 cm long and 5 cm high. Special guide tubes whose outside width is 1.5 cm will allow the boron safety rod to slide into one side of a matrix tube. For these safety rods a drive unit similar to that for the dual-purposes rods will be used. The compressed spring is inverse-acting so that the boron rod is inserted into the matrix at a high speed upon a scram signal. The position of these safety

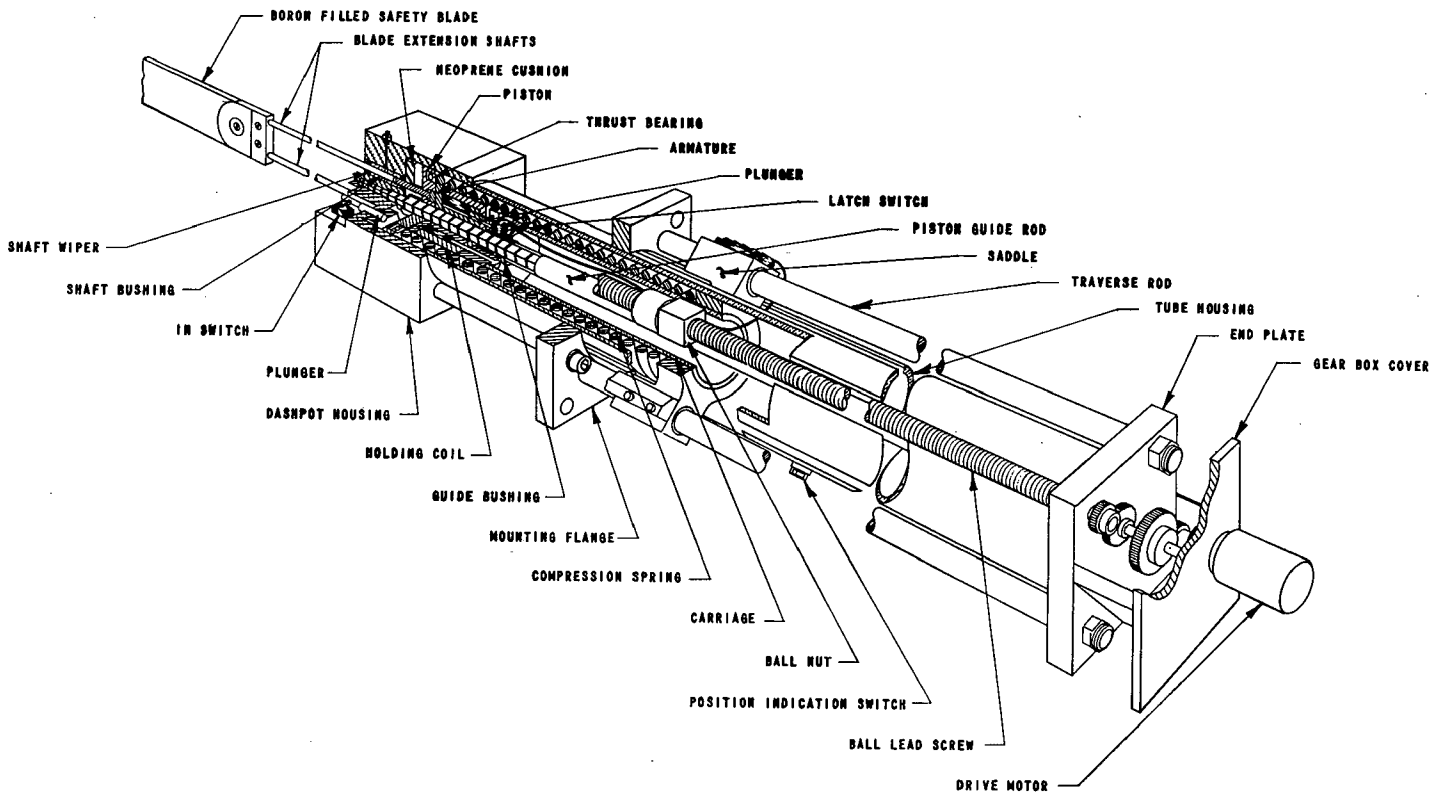


Fig. 4
Blade safety rod.

rods will be shown on the control console every 10 cm using position-indicator lamps. The withdrawal speed of the safety rods is 0.3 cm/s with the stroke being 76 cm. A drawing of the insertion-type rod-drive mechanism is shown in Fig. 4. The number of absorber-type safety rods used will depend on the type of reactor being investigated. The number of safety rods must be sufficient to introduce at least $\Delta k/k = 2\%$ shutdown. This is determined by theoretical analysis before start-up of the reactor. The locations of the dual-purpose and absorber safety rods are variable. The positions of these rods with respect to each other in the assembly will be governed by the size of the core under investigation. The dual-purpose rods will be located in the core. The absorber safety rods may be located in either the core or blanket depending on their worth.

### Source assembly

Two polonium-beryllium sources producing about $10^7$ n/s each will be used, one for each half of the assembly. In each case the source is mounted on the end of a flexible shaft and is driven from its storage shield, at the side of the assembly, approximately 10 to 20 cm from the interface and 27 cm from the centre of the core for most assemblies. Appropriate limit switches control the travel and indicate position on the control panel. Since the source is either completely in or out of the reactor, indicator lights are sufficient for indication of position. Since these sources constitute a hazard for those working around the reactor, they are placed in the storage shield when removed from the reactor. The sources are so interlocked that when the halves are apart the sources are in their respective shields and they must be replaced in the reactor before the reactor can be reassembled.

### Nuclear instrumentation and control system

The critical facility is equipped with the instrumentation shown in the block diagram of Fig. 5. The operating and usage philosophy of the instruments is as follows:

(*a*) *Channels No. 1 and 2.* Two $BF_3$ proportional counter channels both having a log count-rate meter with a minimum-level neutron trip circuit and an audible indicator.

These two channels are used during start-up to provide multiplication data during loading as well as for manual period measurements. The minimum-level neutron-trip-circuit interlock is to insure that the sources are in the reactor. The minimum-level trip (remains in tripped condition unless the count-rate exceeds the trip-rate) also provides a fail-safe indication for the entire channel.

(*b*) *Channels No. 3 and 4.* Two DC electrometer channels with recorders using uncompensated $BF_3$ ionization chambers as detectors, with channel No. 3 having a bucking current source and No. 4 having a level trip circuit. The linear electrometer is used to follow up the reactor power-level with the trip-point being set so that it is not more than one decade above the neutron level at any one time. It will have sufficient sensitivity to measure the source flux.

The linear electrometer with bucking current source will be the main operating instrument. This will be the reference used to hold the reactor neutron-level constant or to return the reactor level to a given level for rod calibration, etc. The bucking current will permit an increase in sensitivity to determine more accurately the point of criticality.

These electrometers are used to measure current from uncompensated high-sensitivity ($1 \times 10^{-12}$ A/$nv$) ionization chambers and cover a range of eight

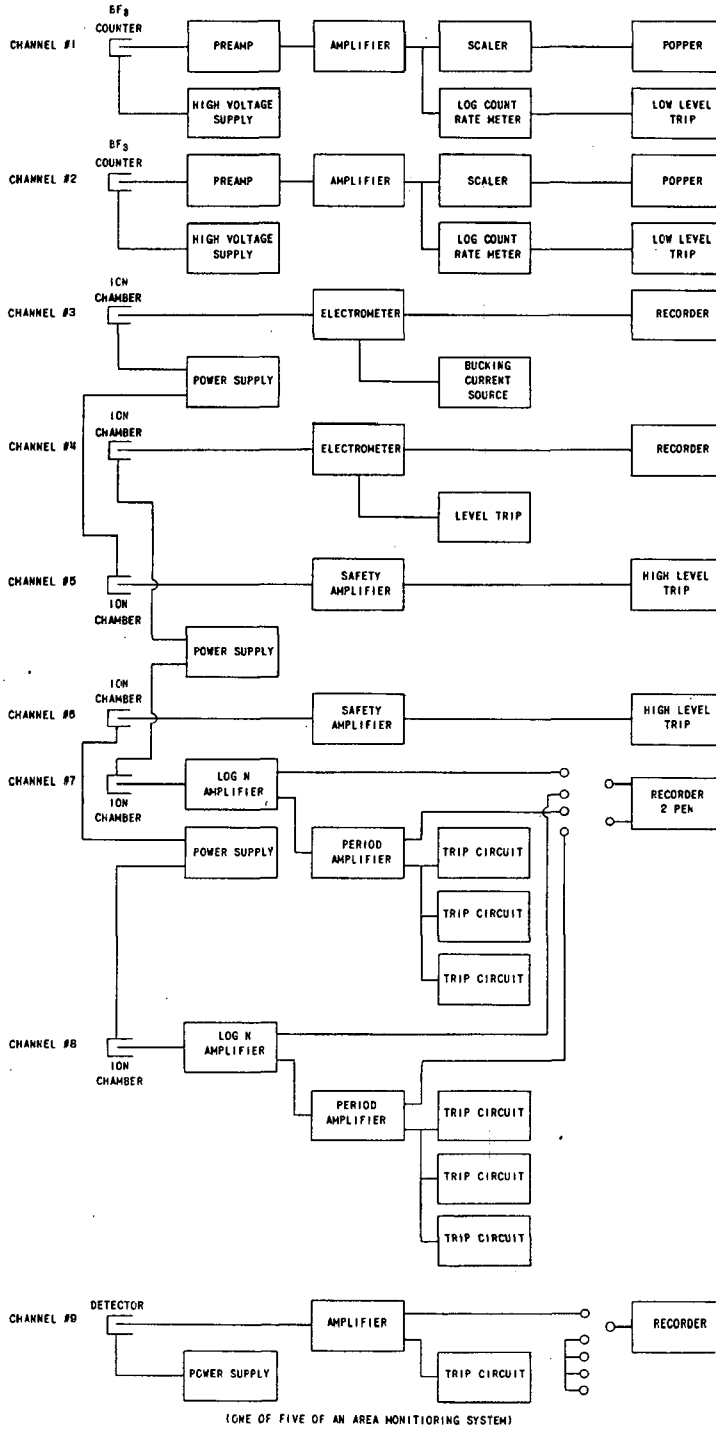


Fig. 5
Block diagram of instrumentation.

decades using appropriate resistors. There is a high-level trip circuit which is adjustable from 5 to 100% of full scale on each range on channel No. 4.

(*c*) *Channels No. 5 and 6.* Two high-level safety amplifier trip circuits using $BF_3$ uncompensated ionization chambers.

Following the initial loading and the determination of the normal operating power levels, the safety amplifier will be set to shut the reactor down if the neutron flux increases about one half to one decade above the normal operating level. They will not normally be readjusted on that core loading.

The safety amplifiers are basically DC electrometers with trip circuits and with a minimum range of three decades.

(*d*) *Channels No. 7 and 8.* Two ln amplifiers, two period meters with three period trip circuits with uncompensated $BF_3$ ionization chambers as detectors, and one recorder to be used jointly.

The period meter consists of an ionization chamber, logarithmic amplifier, and differentiating circuit of the type presently in use with other reactors. The output of the log amplifier, as well as the output of the differentiating circuit, is brought out to a two-pen recorder. This provides a single-scale record of power-level over the entire operating range without changing the scale factors, as well as a record of the variation of the reactor period.

The three period-trip circuits are used as follows:

(1) A 30-s period trip if exceeded will stop the motion of the table;
(2) A period shorter than a pre-set value will automatically shut down the reactor. This pre-set value is adjustable from 30 to 5 s;
(3) A period shorter than a fixed 5-s value will also automatically shut down the reactor.

(*e*) *Channel No. 9.* One gamma-ray monitor using a NaI scintillation detector is to be a part of an area-monitoring system.

The gamma-monitor will indicate the levels of radiation at various locations for personnel protection and is not a part of the reactor control system. Only one channel of an area-monitoring system is shown in the block diagram of Fig. 5. Instrumentation will be turned on while loading is in progress. Recorders for channels 3 and 4 and 7 and 8 will, however, be on only during operation. The audible popper will be transmitted to the reactor cell. In addition an audible 10-s alarm will sound in the reactor cell and control room when the counting rate in either channels No. 1 or 2 exceeds a pre-set value.

The control console which is located in the control room outside of the reactor cell contains the nuclear instrumentation, the switches and relays necessary for the operation of the movable table, and the dual-purpose and safety rods. It will also contain the position-indicators for the movable table and the control and safety rods. Interlocks are provided for safe and proper start-up and operation of the facility.

### Working platform

A movable 4.9 m long, 1.4 m wide, aluminium platform with a magnesium tread plate is provided for access to the matrix tubes at the interface. This platform is hinged at the nearest side wall and may be lowered between the halves when they are fully separated. During operation of the facility it is in a vertical position against the wall. The platform, after it has been lowered 90°, may be moved in the vertical direction for 1.5 m for loading personnel to gain access to the topmost tubes. It has been designed to carry a maximum load of ap-

proximately 360 kg at the outer edge. The platform position movement is controlled and indicated at the control console. It is interlocked so that it cannot be lowered unless the halves are fully separated. Conversely, the reactor may not be started up unless the platform is in the vertical position against the wall.

## 2. Description of site

### Location

The ZPR-VI facility is located in a cell of the new Zero Power Reactor Building. The building is located near the centre of the area controlled by Argonne National Laboratory and in an area where other reactor facilities such as the CP-5, EBWR and Juggernaut are located.

### Reactor cell

The interior dimensions of the reactor cell are $12 \times 9$ m with a height of 9 m. There is 1.5 m of reinforced concrete between the cell and control room. The other three sides of the cell, floor and ceiling have 1.2 m of reinforced concrete as shielding. The centreline of the ZPR-VI facility is approximately 5.5 m from the south wall, 3.4 m from the west wall and 2.1 m above the floor.

The design requirements of the reactor cell are listed below:

(*a*) The cell is designed to withstand a blast equivalent to that from 45 kg TNT at a position 1.5 m above the floor at the centre of the cell. The cell is designed to be gas-tight and to hold the explosion products until they have cooled and can be vented to the atmosphere;

(*b*) The cell is not designed to withstand high pressures or temperatures associated with a uranium fire; and

(*c*) During operation the two entrances (personnel and freight) to the cell are to be protected by gas- and pressure-tight doors. A non-pressure-tight concrete-block door provides radiation protection for the freight entrance. Missile damage resulting from an explosion is considered to be a minor consideration and no special structural design requirements for missile protection are specified.

To meet the blast-containment requirements, the concrete walls contain 1/4% of reinforcing steel-rods running in each direction of the wall faces.

While the reactor is in operation the cells are gas-tight with no air going into or out of the cell. During this period the temperature in the cell is controlled by a self-contained air-conditioning system. The cell is heated by electric heaters and cooled by a refrigerant (monochlorodifluoromethane) circulating through coils in the cell. The refrigerant is piped into the cell from compressors located in the basement of the building. While the reactor is not in operation the temperature of the room is controlled by conditioning the outside air coming into the room. Air is heated by steam heaters or cooled by an air-conditioning system in an exterior room before being forced into the cell. The cell air will be exhausted to the atmosphere through AEC absolute final filters. The temperature and humidity are maintained constant throughout the building with the air-conditioning systems.

The reactor cell has been designed to withstand an explosive energy release the equivalent of a bare charge of 45 kg TNT exploded at the centre of the reactor facility. Since the reactors are always mocked up in the stainless-steel-tube matrix, this is equivalent to surrounding the charge with a casing. In the

case of an encased charge it has been estimated by NEWMARK and HALL [5] that the cell walls would withstand approximately 86 kg TNT exploded at the centre of the matrix. This corresponds to about $1 \times 10^8$ cal or 418 MW s ($1.3 \times 10^{19}$ fissions) total energy release. Normally the pressure is atmospheric; however, it has been designed to withstand a long-duration pressure of about 2.8 bar (40 lb/in$^2$) maximum.

The personnel doors which provide the normal working access to the assembly cell from the control room are $1 \times 2$ m and are hinged along one side. The two personnel doors are electrically interlocked to prevent opening both at the same time. At least one of the two door must be completely closed and sealed at all times. These doors are designed to withstand individually a blast force of 255 lb/in$^2$ for a duration of 1.7 ms. Freight will be brought in through the $1.5 \times 3$ m door located at one end of the cell and operated manually from the cell side only. This door will be sealed at all times when the assembly is operating. An emergency-escape hatch has been provided for personnel to leave a radiation field rapidly in the event of a nuclear accident. This escape is located at the end of a ramp below the level of the floor on one wall; the exit door is operable manually from the cell side of the wall and with a key from the outside. The service and escape doors are designed to withstand a blast force of 6.9 bar (100 lb/in$^2$) for a duration of 2.9 ms. The personnel, service and emergency doors will be gas-tight before and after a blast and operable after, but not during, a temperature rise to 196 °C with a resultant long-time pressure-rise of 0.74 bar. The double personnel doors and service door are designed to provide neutron- and gamma-shielding equivalent to the walls in which they are located.

Conduits passing under the shield wall provide electrical connections to the cell from the control room. The conduits are sealed after the wires are passed through and are therefore gas-tight.

There is no water-supply line or outlet or steam line in the assembly cell. There are no floor drains except for a small drain for the condensate of the air conditioner which drains into a bucket only.

### VAULT

A vault consisting of two rooms about $7 \times 8 \times 3.4$ m high, is provided for the storage of fissionable material. One can gain access to the vault only through the vault workroom.

The enriched-uranium fuel pieces will be stored in birdcage-like structures. The fuel will be in an array four to five units high with a density of 0.06 kg/l and the separation between units of 56 cm. The concentration of fuel will not exceed 4 kg $U^{235}$ at each location, which represents an always safe configuration. Initially there will be approximately 750 kg of highly enriched uranium stored in the vault for the use of the facility.

In order to prevent accidental flooding there are no water lines, steam lines or drains in the vault. The 1.2-m thick reinforced-concrete walls of the two cells form the side walls of the vault. The other sides, floor and ceiling are constructed of 30-cm reinforced concrete.

Outside the vault on the first floor is located a vault workroom which is used for the storage in bins of the mock-up elements, such as aluminium, stainless steel and depleted uranium, and for the unloading of the drawers for the reactor. Storage space is also available for the drawers and springs. Balances for checking the weights of the uranium pieces are also available.

In the wall at one corner of the vault workroom are located three drawer-access ports for each reactor cell. These ports are approximately 10 cm in diameter and allow empty or loaded drawers to be passed into or out of the reactor cell from the workroom. When the reactor is in operation the ports will be filled with concrete shielding-plugs. When a loading or unloading operation is taking place, the shielding plug will be removed and a drawer carriage inserted which will allow a loaded or unloaded drawer to be moved through the 1.2-m thick concrete wall. There are doors on both sides of each port which are interlocked so that only one side may be open at any time.

The drawers will be loaded in the vault workroom with the proper composition of mock-up elements and enriched fuel. They will then be checked against the loading chart, passed through the port into the reactor cell and placed into the stainless-steel matrix.

## 3. Management of the facility

### Philosophy

The operation of the facility in a safe manner will be the primary concern of all personnel associated with the facility. The first line of defence against accidents is based on the selection of qualified trained personnel for the management and operation of the facility. The exercise of careful and cautious judgement on the part of these individuals is expected at all times. The second line of defence consists of the fail-safe design of the various components of the facility and the safety circuits associated with the nuclear instrumentation. The routine maintenance of the equipment and pre-operational check procedures serve to minimize the possibility of mechanical or electrical failure of the components of the system. Care in pre-planning of the experiments and agreement in regards to details before loading or making any changes in loading by at least two qualified personnel serve to prevent the introduction of unsafe experiments and conditions or faulty operating procedures.

### Reactor safety supervision

The management of the facility will be carried out along lines which have promoted the safe operation of criticals at the Argonne National Laboratory. The Reactor Supervisor is charged with the overall responsibility for the management of the facility. He reports to the Responsible Supervisor who has the responsibility for the supervision from the safety point of view of all the critical facilities on the Lemont site. The Responsible Supervisor reports to the Director of the Reactor Engineering Division who in turn reports to the Laboratory Director. The Laboratory Director with the advice of the Laboratory Reactor Safety Review Committee determines the policies for the safe management of the critical facilities.

The Reactor Safety Review Committee is composed of representative staff members from various divisions of the Laboratory and from varied professional disciplines. Its purpose is to advise and make recommendations to the Laboratory Director on the safety aspects of the operation of various nuclear machines at Argonne. It maintains a continuous review of the current operations of the Argonne reactors by giving consideration to changes made in reactor equipment and operating procedures, by considering special nuclear hazards involved in proposed reactors or nuclear multiplication experiments and by devoting special attention to reactor hazards.

## 4. Construction costs

Procurement of the various components for the facility started about January 1960. The facility will be ready for operation in 1962.
The construction costs, which does not include the engineering design time by members of the Argonne Reactor Engineering Division, are listed below. The fabrication costs for the depleted and enriched uranium are also not included.

| | |
|---|---|
| Bed and table assembly | US $ 90000 |
| Matrix assembly (stainless-steel matrix) | US $ 117000 |
| Control- and safety-rod assemblies | US $ 70000 |
| Console and instrumentation | US $ 90000 |
| Neutron source assembly | US $ 10000 |
| Mock-up plates (Al, stainless-steel, Zr, C) | US $ 140000 |
| Total | US $ 517000 |

## ACKNOWLEDGEMENT

The authors would like to express their appreciation to F. C. Beyer for the design of the Zero Power Reactor Facilities Building. The control- and safety-rod drive mechanisms were designed by J. F. Pohlman and J. N. Young. The control interlock circuitry was designed by D. C. Thompson.

## REFERENCES

[1] CERUTTI, B. C., *et al.*, ZPR-III, ANL-5513 (1956).
[2] LONG, J. K., *et al.*, Proc. 2nd UN Int. Conf. PUAE **12** (1958) 119.
[3] HEINEMAN, R. E., Proc. 2nd UN Int. Conf. PUAE **12** (1958) 650.
[4] STEHN, J. R., USAEC Report UC-81 (1958).
[5] MOROWITZ, H. A., *et al.*, *Trans. Amer. nucl. Soc.* **4** (1961) 12.
[6] KATO, W. Y., FISCHER, G. J. and DATES, L. R., "Hazards Summary Report, ZPR-VI", Appendix B, ANL-6271 (Report in preparation).

SM 18/25

# DESCRIPTION DE L'ASSEMBLAGE CRITIQUE RACHEL

P. Bourgeois, C. Clair, R. Comte et J. J. Long

Commissariat a l'énergie atomique,

France

**Abstract — Résumé — Аннотация — Resumen**

**Description of RACHEL critical assembly.** The RACHEL assembly is used for carrying out critical experiments with fast neutrons. The assembly is composed of two hemispheres of canned plutonium surrounded by a natural-uranium reflector. After the upper reflecting cap has been slowly brought close, criticality is achieved by the gradual insertion of four uranium rods which fill cylindrical ways in the lower reflector. Safety is ensured by provision for the rapid ejection downwards of a part of the lower reflector. As distance is the only form of biological protection, the hall is evacuated during experiments, the control room being situated 120 m away.

**Description de l'assemblage critique RACHEL.** L'assemblage RACHEL est destiné à la mise en œuvre d'une expérience critique en neutrons rapides. Cet assemblage se compose de deux hémisphères de plutonium gainé, entourés d'un réflecteur en uranium naturel. L'état critique est obtenu, après rapprochement lent de la calotte réflectrice supérieure, par l'enfoncement progressif de quatre barres en uranium qui obturent des logements cylindriques ménagés dans le réflecteur inférieur. L'élément de sécurité est constitué par une partie du réflecteur inférieur qui peut être rapidement éjectée vers le bas. La protection biologique n'étant assurée que par l'éloignement, le hall d'expérimentation est évacué au moment des expériences et la salle de contrôle est située à une distance de 120 m.

**Описание критической сборки РАШЕЛЬ.** Сборка РАШЕЛЬ предназначена для постановки критического эксперимента на быстрых нейтронах. Эта сборка состоит из двух полушарий заключенного в оболочку плутония, окруженных отражателем из природного урана. После медленного приближения верхнего отражателя критическое состояние достигается постепенным вводом 4 урановых стержней, которые входят в цилиндрические отверстия, находящиеся в нижнем отражателе. Безопасность обеспечивается частью нижнего отражателя, которая может быстро сбрасываться вниз. Поскольку биологическая защита обеспечивается лишь расстоянием, зал, где проходит эксперимент, освобождается от людей, а зал управления находится на расстоянии в 120 метров.

**Descripción del conjunto crítico RACHEL.** El conjunto RACHEL está destinado a la realización de experimentos críticos con neutrones rápidos. Está compuesta por dos hemisferios de plutonio recubiertos y rodeados de un reflector de uranio natural. La criticidad se alcanza, después de acercar lentamente el casquete reflector superior, por introducción gradual de cuatro barras de uranio que obturan sendos orificios cilíndricos practicados en el reflector inferior. El dispositivo de seguridad está constituido por parte del reflector inferior, que puede ser proyectado rápidamente hacia abajo. Dado que la protección radiológica sólo se logra con la distancia, la sala en que se llevan a cabo los experimentos se desaloja cuando éstos van a iniciarse; además, la sala de control se encuentra situada a 120 m del conjunto crítico.

## Introduction

Dans le cadre des études entreprises par le CEA sur les neutrons rapides, il est apparu nécessaire de déterminer expérimentalement les propriétés neutroniques d'un système possèdant un cœur en plutonium métal réfléchi à l'uranium naturel. L'assemblage critique RACHEL répond à ce but.

Domaine nouveau pour le CEA, cette expérience critique en neutrons rapides et utilisant du plutonium métal a été entourée de très nombreuses mesures de précautions.

L'assemblage RACHEL a divergé pour la première fois le 8 mars 1961.

## Assemblage (fig. 1, 2 et 3)

Une forme aussi voisine que possible de la sphère a été adoptée afin de faciliter l'interprétation des résultats. L'assemblage comprend deux hémisphères de plutonium entourés de calottes réflectrices d'uranium à contour sphérique. Entre ces deux ensembles, dont les faces planes sont horizontales, sont intercalées un certain nombre de plaquettes cylindriques de plutonium entourées des couronnes réflectrices d'épaisseurs correspondantes. Cet «empilement central», qui permet de faire varier la masse de combustible dans une certaine mesure, contribue à donner à l'ensemble une forme légèrement cylindrosphérique.

La calotte réflectrice inférieure est fixe, à l'exception de sa partie basse en forme de tronc de cône qui peut être éjectée verticalement vers le bas et constitue le «bloc de sécurité». La calotte inférieure supporte l'ensemble du cœur (hémisphères et plaquettes) ainsi que les couronnes réflectrices de l' «empilement central». La calotte réflectrice supérieure est mobile verticalement.

L'état critique est obtenu, après montée du bloc de sécurité en position haute, par la descente lente de la calotte réflectrice supérieure jusqu'au contact de la partie fixe, puis par l'enfoncement progressif de quatre barres réflectrices horizontales qui viennent obturer des logements ménagés dans la calotte réflectrice inférieure.

### 1.1 Cœur

Les éléments du cœur sont en Pu$\delta$ stabilisé de densité moyenne 15,6 g/cm$^3$. Ils sont protégés par une gaine d'épaisseur 0,1 mm.

Le jeu actuel comprend les huit éléments portés au Tableau I.

TABLEAU I

**COMPOSITION DU JEU ACTUEL D'ÉLÉMENTS**

| Elément | | Nombre d'éléments | Masse (g) |
|---|---|---|---|
| Hémisphère tronqué à 8 mm du plan équatorial<br>Rayon de la sphère: 47 mm<br>Rayon du cercle de base: 46,3 mm | | 2 | 2518 |
| Plaquettes cylindriques: | | | |
| ⌀ = 92,6 mm | e = 4, mm | 2 | 418 |
| ⌀ = 92,6 mm | e = 4,5 mm | 1 | 470 |
| ⌀ = 92,6 mm | e = 5 mm | 1 | 522 |
| ⌀ = 92,6 mm | e = 6 mm | 1 | 627 |
| ⌀ = 92,6 mm | e = 7 mm | 1 | 731 |

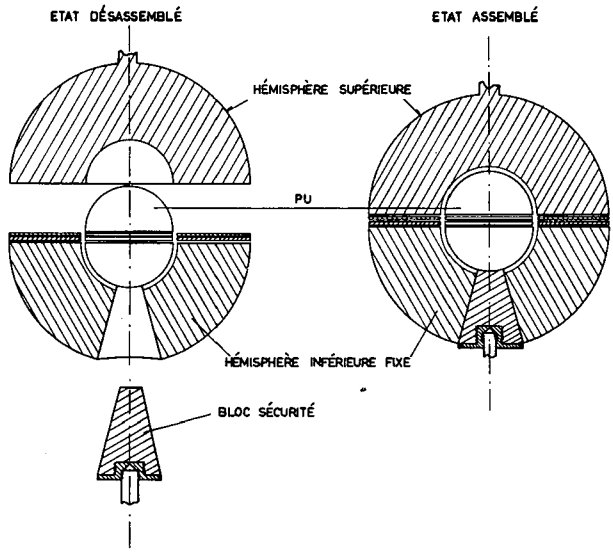


Figure 1
Schéma de principe de l'assemblage RACHEL.

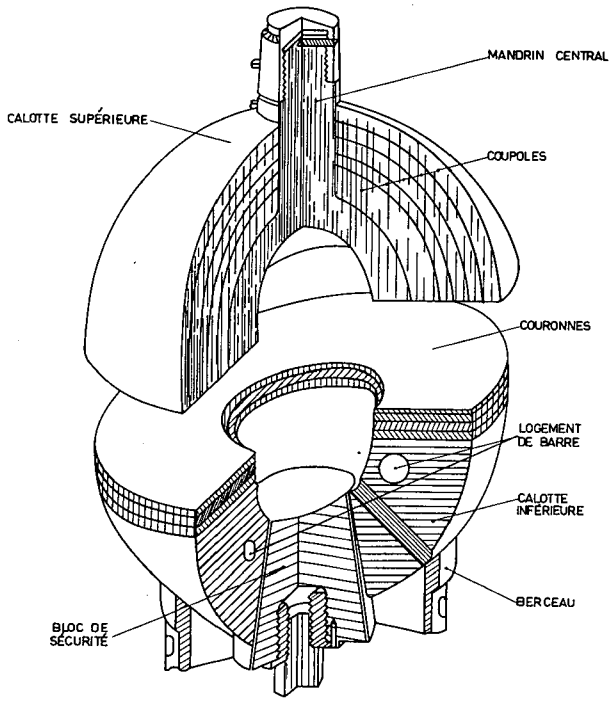


Figure 2
Ensemble réflecteur RACHEL.

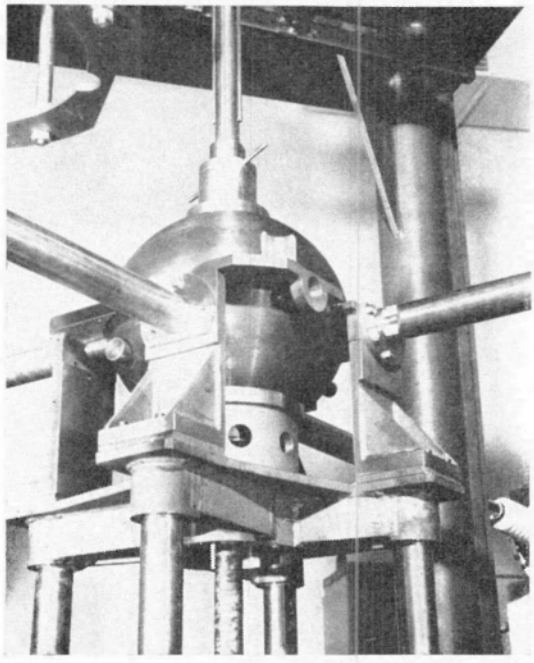

Figure 3
Assemblage RACHEL.

Ce jeu a été conçu avec le souci d'effectuer une première approche sous-critique très prudente. Il a permis, en jouant sur le nombre de plaquettes, des variations de masses de 104 g entre 5454 et 5872 g, et de 52 g au-dessus de 5872 g.

Un nouveau jeu est actuellement à l'étude, ne comportant qu'une seule plaquette intermédiaire.

## Réflecteur

Le réflecteur, en uranium naturel de densité 18.7 g/cm³, a une épaisseur de 93 mm. Il se compose essentiellement de deux hémisphères tronqués à 8 mm du plan équatorial ($\varnothing = 280$ mm) et de couronnes cylindriques d'épaisseurs correspondantes aux plaquettes de plutonium. Les parties en contact avec les hémisphères de plutonium forment deux coupoles amovibles (épaisseur: 7,5 mm) facilement transformables. Aucune gaine de dilatation n'est ménagée entre l'uranium et le plutonium (tolérance d'usinage: 0,05 mm).

La partie inférieure comporte quatre canaux horizontaux servant de logement aux barres de contrôle, deux à deux parallèles et orientées suivant deux directions perpendiculaires. Elles se présentent sous la forme de cylindres d'uranium recouvertes d'une couche d'acier inox de 0,25 mm et ont les caractéristiques données au Tableau II.

TABLEAU II

**CARACTÉRISTIQUES DES BARRES DE CONTRÔLE**

| Numéro de la barre | Rayon de la barre (cm) | Distance axe de la barre Interface cœur réflecteur | Equivalent (pcm) |
|---|---|---|---|
| 1 | 0.9 | 3.9 cm | 240 |
| 2 | 1.25 | 3.9 cm | 240 |
| 3 | 1.2 | 2.7 cm | 148 |
| 4 | 1.2 | 2.7 cm | 76 |

Deux canaux expérimentaux ($\varnothing = 12$ mm et $\varnothing = 22.8$ mm) sont ménagés suivant deux rayons dans la partie inférieure. Le bloc de sécurité, tronc de cône en uranium naturel, s'emboîte dans la partie inférieure.

La partie supérieure mobile est formée d'un empilement de coupoles concentriques. Elle permet de fair varier éventuellement la nature et l'épaisseur du réflecteur.

MÉCANISMES (fig. 4)

Un chassis unique supporte l'ensemble de l'assemblage et des mécanismes de mouvement.

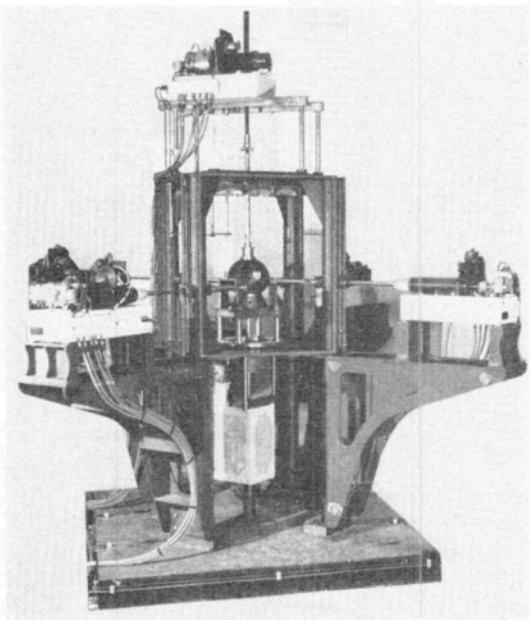

Figure 4
Assemblage RACHEL en cours de montage.

En régime normal, les mouvements des six parties mobiles (bloc de sécurité, partie supérieure, quatre barres de contrôle) sont assurés par l'énergie électrique. En régime d'urgence, le «retrait de sécurité» comporte l'éjection rapide du bloc de sécurité par un ressort maintenu bandé en marche normale à l'aide d'un électro-aimant. Dans le même temps, la remontée de la partie supérieure et le retrait des barres de contrôle sont obtenus au moyen de moteurs hydrauliques alimentés par trois accumulateurs de pression indépendants maintenus à la pression de fonctionnement en conditions de marche normale.

La partie supérieure a une course de 30 cm. La descente s'effectue pour les deux tiers (0—20 cm) à la vitesse de 10 cm/min, puis le reste de la course (20—30 cm) à la vitesse de 1 cm/min (soit une augmentation finale de réactivité d'environ 60 pcm/s). La remontée de sécurité s'effectue à une vitesse de 10 cm/min.

Le bloc de sécurité a une course de 20 cm. Son parcours est de plus de 10 cm, moins de 0,1 s après l'ordre d'éjection de sécurité.

Les barres de contrôle sont introduites à une vitesse variable de 0 à 1 mm/s (augmentation de réactivité inférieure à 1 pcm/s). La position est repérée à 0,05 mm près. Le retrait de sécurité s'effectue à une vitesse de 1 cm/s.

Des verrouillages imposent l'ordre suivant dans les opérations d'assemblages: montée du bloc de sécurité, descente de la calotte réflectrice supérieure, introduction successive des barres.

### Enceintes

L'assemblage est monté dans une boîte constituant une première enceinte étanche. Elle répond à un double but: *a*) pouvoir stabiliser ou faire varier la température de l'assemblage au moyen d'une circulation de fluide portée à la température voulue (en dehors de la puissance dégagée par les fissions, la puissance résiduelle due aux désintégrations $\alpha$ du plutonium est de l'ordre de 10 W), et *b*) limiter la contamination due à une éventuelle défaillance des gaines du plutonium et aux conséquences d'un éventuel burst de puissance.

Ces deux objectifs ont entraîné la réalisation d'une boite à gants classique sous argon en légère dépression (2 à 4 cm d'eau).

L'argon en circulation peut être envoyé soit sur un groupe de purification, soit sur une chambre de chauffe, soit sur un groupe de réfrigération.

L'ensemble de l'assemblage et de ses mécanismes est situé à l'intérieur d'un caisson métallique étanche (base : $4 \times 6$ m, hauteur : 4 m). Il constitue une deuxième enceinte en légère dépression et dont l'accès s'effectue au moyen d'un sas.

### Instrumentation

Le *pilotage neutronique* s'effectue au moyen de détecteurs extérieurs à l'assemblage.

Des compteurs comprenant des tubes $BF_3$ employés en « géométrie longue » (type Hanson McKibben) sont utilisés en régime impulsionnel. On dispose à la salle de contrôle de quatre chaînes électroniques identiques, sur lesquelles peuvent être aiguillées au choix des informations des différents compteurs sélectionnés en fonction du niveau de flux atteint. Chaque chaîne électronique (voir fig. 5) comporte un circuit commun distribuant les impulsions sur quatre voies : voie «linéaire » fournissant un enregistrement linéaire du flux, voie «logarithmique » fournissant un enregistrement du logarithme du flux ainsi que de la période, voie « Mini-Maxi » 1 envoyant un signal d'alarme lorsque la chaîne n'est pas dans des conditions normales d'utilisation (défaut d'impulsions ou saturation), et voie de comptage.

Un dispositif de sécurité envoie un signal d'alarme lorsque la période est inférieure à 3 s. L'autorisation de fonctionner n'est obtenue que si deux chaînes au moins sont en service.

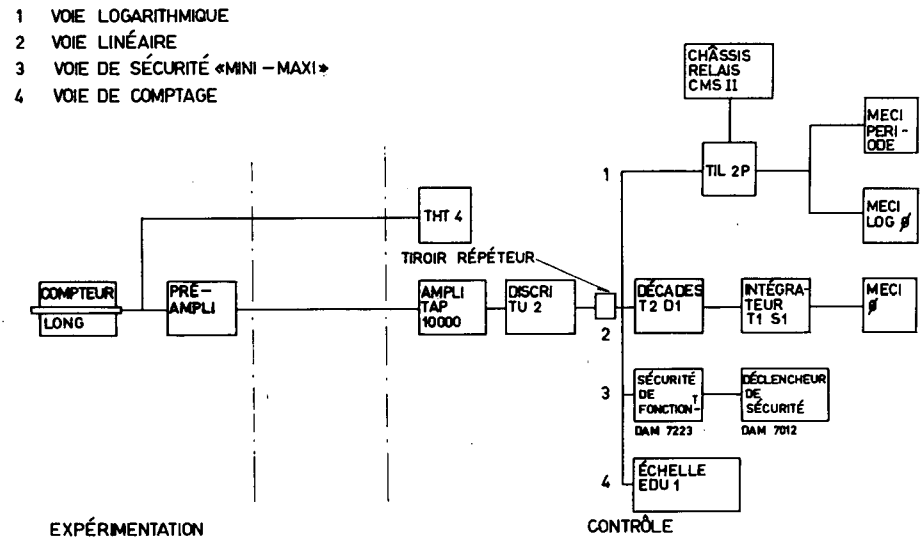


Figure 5
Diagramme chaîne électronique RACHEL.

Deux chambres à bore compensées fonctionnant en courant peuvent être utilisées pour la mesure précise des flux et périodes pour des niveaux supérieurs à $10^8$ n/cm$^2$ s.

Un photomultiplicateur muni d'un scintillateur plastique fonctionne en courant et est relié à un dispositif de sécurité rapide pouvant détecter des bursts de quelques microsecondes.

Les *températures* sont mesurées au moyen de thermocouples «cuivre-constantan ».

## Implantation

La station «Assemblages critiques » dans laquelle est installé l'assemblage RACHEL comporte un «bâtiment expérimentation » entouré d'une zone réservée de 100 m de rayon; l'accès de cette zone est interdit pendant le fonctionnement. Le «bâtiment contrôle » renfermant la salle de commande est situé à 120 m du «bâtiment expérimentation ». Aucune protection n'est ménagée au voisinage immédiat de l'assemblage, dont la durée est limitée. Des levées de terre entourent le «bâtiment expérimentation », absorbant une partie du flux direct.

Un accident atteignant $10^{18}$ fissions provoquerait à la salle de contrôle une irradiation inférieure à la dose permise intégrée pendant un an.

# PROPRIÉTÉS NEUTRONIQUES DE L'ASSEMBLAGE CRITIQUE RACHEL

C. CLAIR
COMMISSARIAT A L'ÉNERGIE ATOMIQUE,
FRANCE

**Abstract — Résumé — Аннотация — Resumen**

**Neutron properties of RACHEL critical assembly.** The critical sizes were determined experimentally and compared with the calculated results. The effect of non-fissile structural materials was studied.

**Propriétés neutroniques de l'assemblage critique RACHEL.** Les dimensions critiques ont été déterminées expérimentalement et comparées avec les résultats calculés. L'influence de matériaux de structure non fissiles a été étudiée.

**Нейтронные свойства критической сборки РАШЕЛЬ.** Критические размеры определялись экспериментально и сравнивались с результатами расчетов. Было изучено влияние нерасщепляющихся конструкционных материалов.

**Propiedades neutrónicas del conjunto crítico RACHEL.** Los autores han determinado experimentalmente las dimensiones críticas y comparado los resultados con los obtenidos mediante el cálculo. Por otra parte, han estudiado la influencia ejercida por los materiales estructurales no fisionables.

## Introduction

Depuis la mise en fonctionnement de l'assemblage RACHEL [1] un programme d'expériences a été entrepris. Ce mémoire ne prétend pas en donner les conclusions, la réalisation des expériences n'étant encore qu'à son début. Il a pour objectif de décrire les premières manipulations effectuées et d'en consigner des résultats encore partiels.

## Estimations théoriques

Pour un assemblage à cœur sphérique en plutonium $\delta$ (densité 15,6) avec un réflecteur de 9,3 cm en uranium naturel, des calculs effectués par la méthode Carlson $S_4$, au moyen du jeu classique de constantes à six groupes utilisé par G. E. Hansen, donnent une masse critique de 6350 kg.

Un calcul de perturbation à six groupes donne pour les valeurs des barres:

| *B4, B3* | *B2* | *B1* |
|---|---|---|
| 240 pcm | 148 pcm | 76 pcm |

De même l'équivalent en réactivité d'un gramme de plutonium rajouté à la surface du cœur est estimé à 3,8 pcm.

La fraction effective de neutrons retardés est calculée à partir des constantes relatives au plutonium et à l'uranium. La valeur trouvée 295 pcm équivaut à 77 g de plutonium.

Le temps de vie des neutrons immédiats, évalué par la méthode Carlson $S_4$, est estimé à $0{,}65 \cdot 10^{-8}$ s.

## L'approche sous-critique

Une approche sous-critique très prudente a été effectuée. Les éléments de combustible disponibles (deux hémisphères et six plaquettes de plutonium) permettaient de faire varier la masse de plutonium par sauts de 52 g dans la région présumée voisine de l'état critique. Cette valeur de 52 g est bien inférieure à l'équivalent masse de la fraction de neutrons retardés, soit 77 g.

Par ailleurs, le cycle d'assemblage correspondant à une certaine masse de plutonium s'effectuait toujours dans l'ordre suivant: montée du bloc de sécurité, descente de la calotte supérieure, introduction une à une des barres de contrôle. La réactivité maximum était atteinte à la fin du cycle, mais de manière aussi progressive que possible grâce à l'introduction des barres. Par contre, la variation la plus rapide de réactivité avait lieu en fin de rapprochement de la calotte supérieure (environ 60 pcm/s). Il importait donc à ce stade d'être assuré de rester sous-critique. A cet effet, la division des plaquettes et l'efficacité des barres avaient été agencées de manière que le saut discret de masse de plutonium d'un cycle à un autre, soit 52 g, reste toujours inférieur à l'équivalent masse de l'ensemble des barres de contrôle, soit 185 g (valeur estimée). De cette façon, en fin de rapprochement de la calotte supérieure, la réactivité était inférieure à celle atteinte à la fin du cycle précédent.

La source constituée par les neutrons issus des fissions spontanées du plutonium-240 a permis de s'affranchir rapidement de l'utilisation d'une source auxiliaire introduite dans un canal du réflecteur.

L'assemblage a été amené à divergence avec une masse brute de 7099 g de plutonium, la barre B4 étant enfoncée entièrement ainsi qu'une partie de la barre B3.

## Détermination de la masse critique

Des corrections ont été nécessaires afin de compenser: *a*) un ajustage défectueux des éléments de combustible entraînant la présence de vides variables suivant les plaquettes utilisées, et *b*) la présence des gaines.

On a étudié systématiquement l'effet de vides provoqués ainsi que celui d'épaisseurs supplémentaires de gaines intercalées entre les plaquettes. Ces effets ont été traduits en variations de l'inverse du taux de comptage 1/C. A l'aide de cet étalonnage, on a pu tracer la courbe d'approche sous-critique corrigée qui est représentée sur la figure 1 (inverse du taux de comptage en fonction de la masse de plutonium). La valeur de la masse critique est 6820 kg.

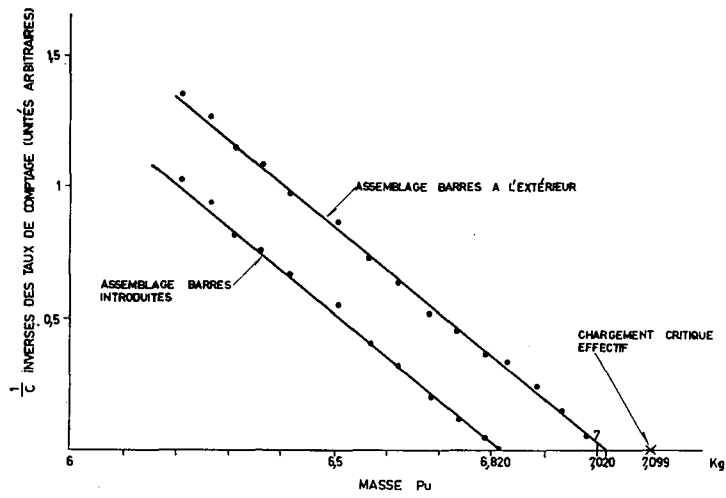


Figure 1
Approche sous-critique. Résultats corrigés.

Les paramètres de corrections, traduits en équivalent masse de plutonium, ont pour valeur:

— fuite latérale dans le réflecteur (entre deux couronnes): 0,1 mm~ 3 g
— fuite latérale dans le cœur (entre deux plaquettes): 0,1 mm~24 g
— substitution gaines-Pu: 0,1 mm~21 g.

Les valeurs de ces corrections seront vérifiées par la suite par des expériences de perturbation, car la précision est difficile à estimer.

Nous avons négligé les effets dus aux gaines sur les surfaces non planes, ainsi qu'au défaut de sphéricité (20 mm de plaquettes cylindriques).

## Etalonnage des barres de contrôle

Les barres ont été étalonnées en régime sous-critique. La valeur de l'équivalent masse de plutonium en fonction de la longueur enfoncée est portée sur la figure 2. En adoptant la valeur de correspondance calculée 3,8 pcm/g, la comparaison entre les résultats de l'expérience et du calcul:

| | *B3, B4* | *B2* | *B1* |
|---|---|---|---|
| Valeur expérimentale | 250 pcm | 163 pcm | 83 pcm |
| Valeur calculée | 240 pcm | 148 pcm | 76 pcm |

donne une assez bonne concordance. La totalité des barres représente 197 g de plutonium. Chacune d'entre elles est inférieure à l'équivalent masse de la fraction de neutrons retardés (77 g).

## Mesures en surcritique

Des mesures de période ont été effectuées lors de divergences relatives à différentes configurations de barres. Sur la figure 3, la courbe d'approche surcritique

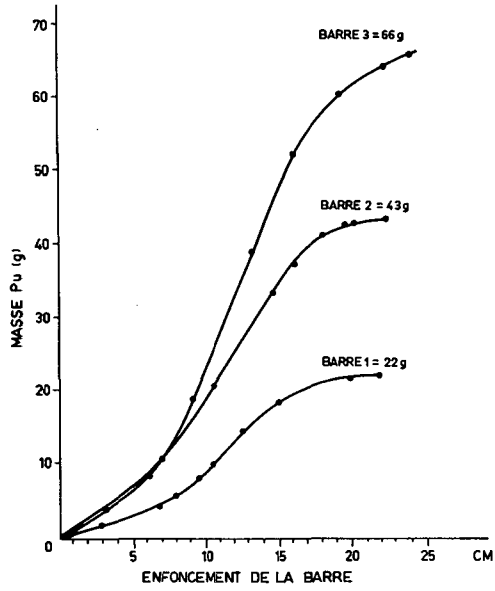


Figure 2
Etalonnage des barres de contrôle.

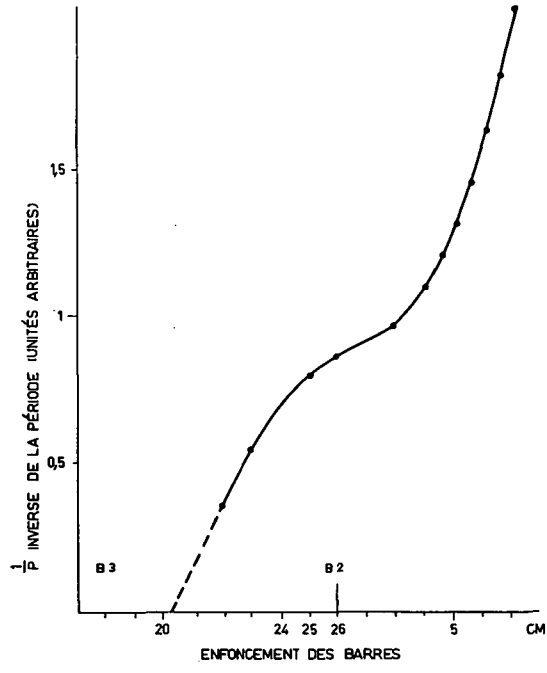


Figure 3
Approche surcritique.

montre que la configuration critique est obtenue, B4 étant complètement introduite et B3 étant à 20 cm. L'équivalent masse des barres à l'extérieur est de 70 g. Compte tenu de la correction due aux gaines (210 g), la correction globale à apporter à la masse brute de 7099 g est de 280 g. La masse critique est donc de 6820 kg.

## RÉFÉRENCE

[1] BOURGEOIS, P. *et alii*, Vol. I des présents Comptes rendus, p. 313.

SM 18/80

# ЭКСПЕРИМЕНТАЛЬНЫЕ ИССЛЕДОВАНИЯ НЕКОТОРЫХ ФИЗИЧЕСКИХ ОСОБЕННОСТЕЙ ПРОМЕЖУТОЧНЫХ РЕАКТОРОВ С БЕРИЛЛИЕВЫМ ЗАМЕДЛИТЕЛЕМ

А. И. ЛЕЙПУНСКИЙ, В. А. КУЗНЕЦОВ, Г. Я. АРТЮХОВ, А. И. МОГИЛЬНЕР, Ю. А. ПРОХОРОВ, В. М. СТЕКЛОВСКИЙ, Л. А. ЧЕРНОВ

АКАДЕМИЯ НАУК СССР, МОСКВА, СССР

**Abstract — Résumé — Аннотация — Resumen**

**Experimental studies of some of the physical features of beryllium-moderated intermediate reactors.** This paper is devoted to a review of the results obtained from a number of experiments carried out on the PF-4 critical assembly (intermediate-physical assembly), which is designed for detailed studies of the physical characteristics of intermediate reactors.

The cores and reflectors of the various critical assemblies were comprised of compact units of steel or aluminium tubes, in which discs of various materials were placed. By combining 90%-enriched uranium discs with moderating materials in various proportions, and also by introducing moderating layers of different thicknesses into the reflector, it was possible to alter the spectrum of the fission-inducing neutrons within a very broad range.

The paper describes the PF-4 critical assembly and its various subassemblies. The relative efficiency of internal and external moderation is analysed for reactors with a very low ratio of moderator nuclei to uranium nuclei in the core. The experiments show that even when thick moderating reflectors are used, this low ratio (the ratio of beryllium nuclei to uranium-235 nuclei being $\varrho_{Be}/\varrho_{U^{235}} = 1$) leads to an increase of the critical mass.

A considerable part of the paper is devoted to an analysis of heterogeneous effects in intermediate reactors. It is shown that for reactors with $\varrho_{Be}/\varrho_{U^{235}} = 30$—40 various thicknesses of highly enriched uranium, ranging from 0.023 g/cm² to 32 g/cm², have an identical effect on the reactivity of the system. The causes underlying compensation of the neutron-flux screening effect by thick layers of uranium are analysed.

The interesting fact that the efficiency of uranium increases in the neighbourhood of the absorbing rods, which was experimentally revealed in an assembly with $\varrho_{Be}/\varrho_{U^{235}}$—200, is discussed in the paper. This fact is explained by the sharp decline in the importance of neutrons absorbed by the uranium. The paper provides data, derived from the same assembly, on the efficiency of rods made of various absorbing materials. It gives the experimentally measured distribution of neutron density for neutrons of various energies in the neighbourhood of a boron-carbide rod, and the density of neutron captures by a $1/v$ detector within the rod.

The paper also discusses methods used and the results obtained from experiments designed to assess the efficiency of recompensation cylinders placed on the boundary between core and reflector.

**Etude expérimentale de quelques particularités physiques des réacteurs à neutrons intermédiaires, ralentis au béryllium.** Le mémoire analyse les résultats de plusieurs expériences effectuées sur l'ensemble critique PF-4, qui est destiné à l'étude détaillée des particularités physiques des réacteurs à neutrons intermédiaires.

Les cœurs et les réflecteurs des différents esembles critiques étaient constitués par un assemblage compact de tubes en acier ou en aluminium dans lesquels étaient

insérés des diques de diverses matières. En combinant selon différentes proportions les disques d'uranium enrichi à 90% et les matières de ralentissement et en introduisant dans le réflecteur des couches de ralentisseur de diverses épaisseurs, on a pu obtenir de grandes modifications du spectre des neutrons provoquant la fission.

Le mémoire décrit l'ensemble critique PF-4 et les différents assemblages qui le composent.

Les auteurs analysent l'efficacité relative du ralentissement intérieur et extérieur pour des réacteurs dans lesquels le rapport noyaux du ralentisseur noyaux d'uranium dans le cœur est très peu élevé. Il ressort des expériences que, même lorsqu'on emploie des réflecteurs très épais, la faible dilution de l'uranium par le ralentisseur (le rapport entre les noyaux du béryllium et de l'uranium-235 étant: $\varrho_{Be}/\varrho^{235}{}_{U} \simeq 1$) entraîne un accroissement de la masse critique.

Une partie importante du mémoire est consacrée à une analyse des effets hétérogènes produits dans les réacteurs à neutrons intermédiaires. Il est démontré que pour une réacteur dans lequel $\varrho_{Be}/\varrho^{235}{}_{U} = 30$ à 40, diverses épaisseurs d'uranium fortement enrichi, allant de 0,023 à 32 g/cm$^2$, exercent une action égale sur la réactivité du système. Les auteurs analysent les causes qui donnent lieu à une compensation de l'effet d'écran du flux de neutrons par des couches épaisses d'uranium.

Le mémoire signale comme fait intéressant l'augmentation de l'efficacité de l'uranium à proximité des barreaux absorbants, qui a été constatée expérimentalement dans un ensemble où $\varrho_{Be}/\varrho^{235}{}_{U} \simeq 200$. On explique ce fait par une diminution brusque de la quantité de neutrons absorbée par l'uranium. Pour la même installation, le mémoire cite des données relatives à l'efficacité de barreaux composés de diverses matières absorbantes. Il indique la distribution, mesurée expérimentalement, de la densité des neutrons de différentes énergies à proximité d'un barreau en carbure de bore, ainsi que la densité de capture des neutrons par un détecteur $1/v$, placé à l'intérieur du barreau.

Le mémoire expose également les méthodes appliquées et les résultats obtenus dans des expériences destinées à évaluer l'efficacité des cylindres de compensation installés à la limite du cœur et du réflecteur.

**Экспериментальные исследования некоторых физических особенностей промежуточных реакторов с бериллиевым замедлителем.** Доклад посвящен обзору некоторых экспериментальных результатов, полученных на стенде ПФ-4, предназначенном для детального исследования физических особенностей реакторов, работающих на нейтронах промежуточных энергий.

Активные зоны и отражатели различных критических сборок представляли собой плотную упаковку стальных или алюминиевых труб, в которых помещались диски из различных материалов. Комбинация дисков урана (90%-ного обогащения) и замедляющих материалов в различной пропорции, а также введение в отражатель замедляющих слоев различной толщины, позволило менять спектр нейтронов, производящих деление, в очень широких пределах.

В докладе приведено описание стенда и его отдельных узлов.

Анализируется сравнительная эффективность внутреннего и внешнего замедления для реакторов с очень малым отношением ядер замедлителя и урана в активной зоне. Эксперименты показывают, что даже в случае толстых замедляющих отражателей малое разбавление урана замедлителем (отношение ядер бериллия и урана-235 $\varrho_{Be}/\varrho_{U}{}^{5} \simeq 1$) приводит к возрастанию критической массы.

Значительное место в докладе уделено анализу гетерогенных эффектов в промежуточных реакторах. Показано, что для реактора с $\varrho_{Be}/\varrho_{US} = 30 + 40$, высокообогащенный уран в различных толщинах от 0,023 г/см$^2$ до 32 г/см$^2$ оказывает одинаковое влияние на реактивность системы. Анализируются причины, приводящие к компенсации эффекта экранировки нейтронного потока толстыми слоями урана.

В докладе приводится интересный факт возрастания эффективности урана вблизи поглощающих стержней, экспериментально обнаруженный в сбор кес $\varrho_{Be}/\varrho_{US} \simeq 200$. Этот факт

объясняется резким снижением ценности нейтронов, поглощаемых ураном. Для этой же сборки приводятся данные по эффективности стержней из различных поглощающих материалов. Приводится экспериментально измеренный ход плотности нейтронов различных энергий вблизи стержня из карбида бора и плотность захватов нейтронов $^1/\nu$-детектором внутри стержня.

В докладе приводится также методика и результаты экспериментов по оценке эффективности поворотных компенсирующих цилиндров, размещенных на границе активной зоны и отражателя.

**Estudios experimentales de algunas características físicas de los reactores intermedios moderados con berilio.** Los autores examinan algunos resultados experimentales obtenidos en el conjunto crítico PF-4, que se destina al estudio detallado de las características físicas de los reactores de neutrones intermedios.

Los cuerpos y los reflectores de los diversos conjuntos críticos están formados por un denso haz de tubos de acero o de aluminio, que contienen discos de distintos materiales. La combinación de discos de uranio (enriquecido al 90 por ciento) y de materiales moderadores en proporción variable, así como la introducción de capas moderadoras de distintos espesores en el reflector, permiten modificar dentro de límites muy amplios los espectros de los neutrones causantes de la fisión.

En la memoria se describe el conjunto crítico y sus diversas partes.

Analizan los autores la eficacia comparada de la moderación interna y externa, para reactores en que la razón de núcleos de moderador a núcleos de uranio, en el cuerpo, es muy pequeña. Los experimentos demuestran que, aun en el caso de los reflectores moderadores de gran espesor, esta baja razón ($\varrho_{Be}/\varrho^{235}U \simeq 1$) conduce a un aumento de la masa crítica.

Gran parte de la memoria se dedica al análisis de los efectos heterogéneos en los reactores intermedios. Se demuestra que para un reactor en el que la razón $\varrho_{Be}/\varrho^{235}U$ esté comprendida entre 30 y 40 distintos espesores (comprendidos entre 0,023 g/cm$^2$ y 32 g/cm$^2$) de uranio muy enriquecido ejercen un efecto de magnitud constante sobre la reactividad del sistema. Se analizan las causas de la compensación del efecto de apantallamiento del flujo neutrónico por acción de capas de uranio de gran espesor.

Los autores señalan un hecho interesante, a saber, el aumento de la eficacia del uranio en la proximidad de las barras de absorción, que se observó experimentalmente en un conjunto en el que la razón $\varrho_{Be}/\varrho^{235}U$ era del orden de 200. Este hecho se explica por el acentuado descenso del nivel energético de los neutrones absorbidos por el uranio. Para el mismo conjunto, presentan también datos sobre la eficacia de las barras de absorción fabricadas con distintos materiales absorbentes. Exponen los resultados de las mediciones experimentales de la variación de la densidad de los neutrones de distintas energías, en las cercanías de una barra de carburo de boro y la densidad de la captura neutrónica con un detector $1/\nu$ colocado en el interior de la barra.

Por último se exponen los métodos aplicados y los resultados obtenidos en la evaluación de la eficacia de los cilindros compensadores giratorios distribuidos en el límite entre el cuerpo y el reflector.

## Описание стенда

Для детального исследования физических особенностей реакторов, работающих на нейтронах промежуточных энергий, был сооружен физический стенд ПФ-4, который позволяет осуществлять и исследовать физические сборки с различным действующим спектром нейтронов, начиная от очень жесткого (быстрые реакторы) и кончая тепловым. Изменение действующего спектра нейтронов достигается вариацией соотношения между количест-

вами делящегося вещества и замедлителя. При этом имеется также возможность изменять в широких пределах размеры и состав активной зоны и отражателя реактора.

В качестве делящегося вещества на стенде ПФ-4 используется уран, обогащенный до 90% изотопом-235. Урановые элементы набираются в рабочие каналы в комбинации с замедлителем и другими материалами.

Каналы представляют собой стальные или алюминиевые трубы внешним диаметром 50 мм с толщиной стенки 1 мм. Эти трубы в количестве 825 штук с шагом 51 мм устанавливаются внутрь цилиндрической обечайки, имеющей диаметр 1602 мм и высоту 1930 мм и окруженной облегченной биологической защитой из чугунных блоков, залитых парафином. Пространство между каналами, расположенными в треугольной решетке, может заполняться алюминиевыми или стальными вытеснителями специального профиля.

В критических сборках, собираемых на стенде ПФ-4, используются ураносодержащие элементы трех типов:

*а*) металлические урановые диски диаметром 46,8 мм и толщиной 0,3 мм, покрытые защитным никелевым покрытием толщиной 15 микрон;

*б*) металлические урановые диски диаметром 46,8 мм и толщиной 5 мм, закатанные в алюминиевую фольгу толщиной 0,3 мм;

*в*) диски диаметром 46,8 мм и толщиной 0,3 мм из смеси 25% окись-закиси урана с 75% (по весу) тефлона, с тефлоновым покрытием толщиной 0,1 мм.

Часть этих элементов имеет центральное отверстие диаметром 21,5 мм. Использование, в зависимости от состава активной зоны и действующего спектра нейтронов, урановых элементов различной толщины позволяет исключить эффекты, связанные с депрессией нейтронного потока в толстых слоях урана.

В качестве замедлителя и отражателя в реакторах, собираемых на стенде, могут применяться диски из бериллия, окиси бериллия, графита и гидридов различных металлов.

Критическое состояние системы достигается путем последовательной замены пустых каналов на рабочие под контролем аппаратуры, регистрирующей умножение нейтронного источника.

Управление цепной реакции осуществляется двумя регулирующими стержнями из карбида бора диаметром 8,4 мм. Управление стержнями осуществляется дистанционно с пульта посредством сервоприводов, расположенных под реактором. Аварийное прекращение цепной реакции осуществляется двумя стержнями из карбида бора диаметром 19,4 мм, вводимыми в активную зону под действием силы тяжести противовесного груза, а также с помощью двух нормальных рабочих каналов, выпадающих из активной зоны при поступлении аварийного сигнала.

Экспериментальные каналы для помещения внутрь активной зоны и отражателя различных образцов, детекторов и ионизационных камер могут образовываться в любом месте активной зоны и отражателя путем извлечения алюминиевого (стального) вытеснителя или путем замены рабочего канала на пустой канал или на канал, заполненный дисками с отверстиями. Кроме того, имеется возможность образовать два горизонтальных канала, заходящих на различную глубину (вплоть до центра) в активную зону.

Один из горизонтальных каналов предназначается для работы с импульсным источником нейтронов, другой для вывода нейтронного пучка на се-

лектор, служащий для измерения энергетического спектра нейтронов в различных точках реактора.

Контроль за интенсивностью цепной реакции осуществляется на стенде ПФ-4 с помощью пусковой (импульсной) аппаратуры, токовой измерительной аппаратуры и аппаратуры аварийной защиты.

В пусковую аппаратуру входят 3 борных счетчика типа СНМ-5, подключаемых через усилители типа ИУ-5 либо к пересчетным установкам, либо к измерителям скорости счета. Контроль более высоких уровней мощности реактора осуществляется по 3-м токовым каналам, включающим в себя ионизационные камеры типа КНТ-53 с твердым борным покрытием. Камеры подключаются через усилители постоянного тока к гальванометрам или электронному самопишущему потенциометру. Комплект аппаратуры аварийной защиты состоит из 4-х камер КНТ-53, попарно подключенных к двум усилителям аварийной защиты. Для целей пуска реактора, поддержания его мощности на заданном уровне и перевода реактора с одного уровня мощности на другой, на стенде ПФ-4 предусмотрен автомат типа АППМ [1].

Уровень нейтронного и $\gamma$-излучения реактора в различных помещениях стендового здания контролируется обычными дозиметрическими приборами, обеспечивающими предупредительную и аварийную сигнализацию.

Стенд ПФ-4 размещен в стендовом зале, который отделен от остальной части здания бетонной защитной стеной толщиной 1,2 м.

## Реакторы с внутренним и внешним замедлением нейтронов

Замедление нейтронов, рождающихся при делении урана, и установление действующего спектра нейтронов в промежуточных реакторах определяются не только составом активной зоны и количеством замедлителя в ней, но и составом отражателя. Введение замедляющего слоя во внутренную часть отражателя приводит к существенному смягчению спектра нейтронов в активной зоне, особенно в ее периферийной области.

Внешнее замедление нейтронов (замедление в отражателе) особенно эффективно в реакторах с очень малым отношением ядер замедлителя и урана в активной зоне. Действительно, если в активную зону быстрого (без замедлителя) реактора, окруженную незамедляющим отражателем, ввести небольшое количество замедлителя (порядка нескольких ядер бериллия на ядро урана-235), то, вследствие резкого возрастания длины миграции нейтрона, значительно увеличивается утечка нейтронов из активной зоны, для компенсации которой требуется увеличение объема активной зоны, что приводит, несмотря на снижение концентрации урана в единице объема, к возрастанию критической массы. Этот результат был получен для реакторов без отражателя расчетным путем [2], [3], [4].

Если бериллий вводить не в активную зону, а во внутренние слои отражателя, то утечка нейтронов из активной зоны не увеличивается, а время жизни нейтрона за счет миграции в отражателе значительно возрастает и отражатель возвращает нейтроны в активную зону существенно замедлившимися. Действующий спектр нейтронов в активной зоне значительно мягче, чем в случае реактора с незамедляющим отражателем и в то же время критический объем и критическая масса снижаются [5]. Не совсем ясен вопрос о влиянии на критические параметры реактора введения небольших количеств

замедлителя внутрь активной зоны при наличии достаточно толстых замедляющих слоев в отражателе. В работе [2] приводятся расчетные данные по критическим параметрам уран-бериллиевых реакторов с бериллиевым отражателем, но лишь для систем, в активной зоне которых соотношение ядер бериллия и урана-235 ($\varrho_{Be}/\varrho_{U^5}$) более 15. С повышением этого соотношения критическая масса падает, несмотря на некоторое повышение критического объема. В области $\varrho_{Be}/\varrho_{U^5}<15$ нет ни расчетных, ни экспериментальных данных о поведении критических параметров систем с бериллиевым отражателем.

Таблица I

**КРИТИЧЕСКИЕ ПАРАМЕТРЫ ЦИЛИНДРИЧЕСКИХ РЕАКТОРОВ БЕЗ ЗАМЕДЛИТЕЛЯ В АКТИВНОЙ ЗОНЕ С РАЗЛИЧНОЙ ТОЛЩИНОЙ ЗАМЕДЛЯЮЩЕГО СЛОЯ ИЗ ОКИСИ БЕРИЛЛИЯ В СТАЛЬНОМ ОТРАЖАТЕЛЕ**

| Индекс сборки | Критическая масса урана в 90% обогащении [кг] | Критический объем [$10^3$ см$^3$] | Высота активной зоны [мм] | Отношение высоты к диаметру активной зоны | Средняя плотность урана в активной зоне [г/см$^3$] | Объемное содержание урана $\varepsilon_0$ [%] | Объемное содержание алюминия $\varepsilon_{Al}$ [%] | Объемное содержание окиси бериллия $\varepsilon_{BeO}$ [%] | Ядерные концентрации окиси бериллия и урана $\rho_{BeO}/\rho_{U^5}$ | Толщина окиси бериллия в отражателе $\delta_{BeO}$ [мм] |
|---|---|---|---|---|---|---|---|---|---|---|
| 01 | 57 | 4,68 | 304 | 2,17 | 12,2 | 65,2 | 23,4 | 0 | 0 | 0 |
| 02 | 31,5 | 2,59 | 168 | 1,20 | 12,2 | 65,2 | 23,4 | 0 | 0 | 50 |
| 03 | 23,8 | 1,955 | 127 | 0,91 | 12,2 | 65,2 | 23,4 | 0 | 0 | 90 |
| 04 | 22,0 | 1,81 | 117,5 | 0,84 | 12,2 | 65,2 | 23,4 | 0 | 0 | 134 |
| 05 | 21,5 | 1,76 | 114,5 | 0,82 | 12,2 | 65,2 | 23,4 | 0 | 0 | 179 |
| 06 | 25,3 | 3,17 | 206 | 1,47 | 7,98 | 42,7 | 19,7 | 27 | 0,98 | 179 |
| 07 | 29,3 | 3,68 | 239,2 | 1,71 | 7,98 | 42,7 | 19,7 | 27 | 0,98 | 134 |

В таблице I приведены экспериментальные данные, полученные на стенде ПФ-4, по критическим параметрам цилиндрических реакторов без замедлителя в активной зоне с различной толщиной замедляющего слоя из окиси бериллия в стальном отражателе. Приведены данные по критическим параметрам сборок с малым количеством окиси бериллия в активной зоне при наличии значительной толщины смягчающего слоя окиси бериллия в стальном отражателе. Во всех системах диаметр активной зоны равен 140 мм, общая толщина отражателя (стали и окиси бериллия) составляла 268 мм. Изменение толщины слоя окиси бериллия производилось за счет изменения толщины слоя стали. Пористость активной зоны и отражателя (объем, занятый воздухом) составаляла 11,4%. В смягчающем слое отражателя 12,8% объема было занято алюминием.

Из данных таблицы I видно, что даже в случае толстых замедляющих слоев в отражателе небольшое разбавление урана замедлителем приводит к существенному возрастанию критической массы вследствие увеличения утечки нейтронов из активной зоны. Это возрастание увеличивается при снижении толщины замедляющего слоя в отражателе. На стенде ПФ-4 проводились эксперименты по сравнению эффективности окиси бериллия ($\gamma=2{,}8$ г/см$^3$) и металлического бериллия ($\gamma=1{,}8$ г/см$^3$) в качестве внешних и внутренних замедлителей. Для приводимых в таблице сборок замена замедляющих слоев из окиси бериллия в отражателе на металлический бериллий одинаковой толщины не изменяет в пределах точности эксперимента

критические параметры системы. В активной зоне окись бериллия лишь незначительно хуже бериллия при равных объемах. Так, например, замена окиси бериллия на металлический бериллий в активной зоне сборки 07 увеличивает реактивность системы на 1,1% в К эфф, что эквивалентно уменьшению критической массы на 2,7%. При этом соотношение ядерных концентраций бериллия и урана-235 $\varrho_{Be}/\varrho_{U^5}=1{,}75$.

## Гетерогенные эффекты в промежуточных реакторах

Как правило, на стенде ПФ-4 исследовались системы, активные зоны которых физически можно было считать гомогенными. Однако, поскольку в опытах использовались урановые элементы различных толщин, специально исследовался вопрос о влиянии самоэкранирования урана на реактивность реактора. Одна из критических сборок с бериллиевым замедлителем и со средним отношением $\varrho_{Be}/\varrho_{U^5}=31$ была собрана таким образом, что центральная часть цилиндрической активной зоны представляла собой гетерогенную решетку с $\varrho_{Be}/\varrho_{U^5}=15{,}7$. Уран в этой части зоны был использован в толщинах d=20 мм (32 г/см²). В периферийной области активной зоны $\varrho_{Be}/\varrho_{U^5}=45$ и размещение урана в бериллии было практически гомогенным. Опыты по измерению плотности делений в ячейке показали, что в периферийной зоне уран практически не заэкранирован, в центральной же части активной зоны в центре урановой сборки из 4-х элементов толщиной по 5 мм каждый плотность делений падает примерно в два раза по сравнению с плотностью делений на границе этой сборки с бериллиевым замедлителем. Параллельно были проведены опыты по исследованию влияния 1 г урана в урановых элементах различных толщин на реактивность системы при помещении уранового образца как в центральную часть, так и в периферийную часть активной зоны. Опыты проводились с образцами, имеющими эффективную толщину уранового слоя от $2{,}3\cdot10^{-2}$ г/см² до 32 г/см².

Оказалось, что несмотря на значительную самоэкранировку делений в толстых слоях урана, влияние урана на реактивность практически одинаково для всех толщин уранового слоя в образце. Так, коэффициент экранировки, определенный как $f_э=\left(\frac{\Delta K}{K\,G_5}\right)_{ТЛ}\Big/\left(\frac{\Delta K}{K\,G_5}\right)_{ТН}$ (где индексы ТЛ — образец урана толщиной 32 г/см² и ТН — образец урана толщиной $2{,}3\cdot10^{-2}$ г/см²), оказался равным $1{,}10\pm0{,}05$ для центральной зоны реактора и $0{,}86\pm0{,}06$ для периферийной зоны.

Полученные результаты могут быть качественно объяснены с помощью известного соотношения:

$$\frac{\Delta K}{K}=\frac{\Delta_f F_L^+}{\Sigma_f}\left[\nu_f\frac{F_0^+}{F_L^+}A-\bar{\alpha}-1\right],$$

где $\frac{\Delta K}{K}$ — реактивность, вносимая делящимся образцом,

$\nu_f$ — число нейтронов, рождающихся в акте деления,

$\Delta f$ — число делений в образце,

$\Sigma f$ — полное число делений в реакторе,

$F^+_0$ — ценность нейтронов деления,

$F_L^+$ — ценность нейтронов, захватываемых ураном,

$\bar{\alpha}=\bar{\sigma}_\gamma/\bar{\sigma}_f$ — отношение сечений радиационного захвата и деления,

$A$ — коэффициент, учитывающий разницу между суммарной ценностью нейтронов, родившихся в результате захвата блоком нейтронов, пришедших из замедлителя и суммарной ценностью нейтронов, выходящих из блока в замедлитель.

Обычно, коэффициент А полагается равным 1 [6]. Однако, это справедливо лишь для тонких делящихся образцов. Если образец нельзя считать тонким, то коэффициент А можно записать в следующем виде:

$$A = 1 - p + \nu_f p \frac{\sigma_f}{\sigma_t} + p \frac{\sigma_{n'}}{\sigma_t} \cdot \frac{F_{n'}^{+}}{F_0^{+}} + p \frac{\sigma_n}{\sigma_t},$$

где $p$ — вероятность нейтрону деления претерпеть соударения с ядрами урана до выхода из уранового блока,

$\sigma_t$ — полное сечение взаимодействия с ураном для нейтронов деления,

$\sigma_n, \sigma_{n'}, \sigma_f$ — сечения деления, неупругого рассеяния и упругого рассеяния нейтронов деления соответственно,

$F^{+}_{n'}$ — ценность нейтронов деления, претерпевших неупругое соударение.

Таким образом, экранирование делений в толстых слоях урана может компенсироваться следующими тремя эффектами:

*а*) Как отмечается в работах [6], [7], при увеличении толщины делящегося образца, облучаемого резонансными нейтронами, имеет место уменьшения величины $\alpha$, что связано, по-видимому, с различной экранировкой радиационного и делительного сечений.

б) Значительная часть нейтронов деления, родившихся в толстых образцах урана-235, претерпевает неупругое столкновение с ядрами урана и выходит из уранового блока с более высокой ценностью, чем ценность нейтронов деления.

*в*) Размножение нейтронов деления в толстых урановых блоках, обусловленное высокой вероятностью нейтрону деления вызвать вторичное деление до выхода нейтрона из блока.

Все эти три эффекта могут привести к тому, что, концентрируя уран в реакторе в более толстых блоках, можно получить для определенных реакторов даже выигрыш в реактивности.

## Эффективность урана вблизи поглощающих стержней

Для большинства критических сборок стенда измерялось влияние на реактивность реактора (так называемые коэффициенты реактивности) различных материалов и, в первую очередь, компонент активной зоны. Особенный интерес представляет влияние на реактивность реактора горючего и зависимость коэффициента реактивности горючего от его места положения в активной зоне.

Знание такой зависимости существенно при решении вопросов, связанных с выгоранием горючего, вопросов рационального размещения горючего при осуществлении физического профилирования поля энерговыделения в реакторе и т.д.

На сборке с отношением $\varrho_{Be}/\varrho_{U^5} = 150$, проведены эксперименты по измерению коэффициентов реактивности горючего в окрестности поглощающих стержней реактора.

Поглощающий стержень из карбида бора с плотностью, равной 2,1 г/см$^3$ имел диаметр 19,4 мм. Высота поглощающего стержня была равна высоте активной зоны. Поглощающий стержень помещался на расстоянии 102 мм от оси реактора, и измерения проводились в точках, расположенных по дуге окружности диаметром около 200 мм.

Для определения эффективности урана были изготовлены два образца длиной, равной высоте активной зоны. Один образец — бериллиевый, другой — уран-бериллиевый с отношением ядерных концентраций $\varrho_{Be}/\varrho_{U^5} = 150$ (обогащение урана изотопом 235—90%).

Эффективность урана определялась по изменению критического положения регулятора реактора при замене уран-бериллиевого образца на бериллиевый.

Реактор при этом работал на постоянном уровне мощности, равном примерно 0,1 ватта.

Результаты измерений коэффициентов реактивности урана в окрестности поглощающего стержня приведены на фиг. 1 (верхняя кривая).

Из фиг. 1 видно, что эффективность урана возрастает при приближении к поглощающему стержню. Как известно (см. [8]), влияние какого-либо образца, помещаемого в реактор на реактивность определяется поглощающими, рассеивающими и замедляющими свойствами вещества образца, а также сечением деления, если вещество образца — делящееся. В случае поглощения и деления, изменение реактивности, кроме того, пропорционально потоку нейтронов и их ценности.

$$\left(\frac{\Delta K}{K}\right)_{\gamma,\mathrm{f}} = \mathrm{const} \int_0^\infty F(E)\,\sigma_\mathrm{f}(E)\,[\nu_\mathrm{f} F_0^+ - (1+\alpha) F^+(E)]\,\mathrm{d}E\,,$$

где $F(E)$ и $F^+(E)$ — поток и ценность нейтронов ($F^+{}_0$ — ценность нейтронов спектра деления),

$\nu_\mathrm{f}$ — число нейтронов, рождающихся в акте деления,

$\alpha$ — отношение сечений радиационного захвата и деления.

Изменение реактивности в результате рассеяния пропорционального градиенту потока:

$$\left(\frac{\Delta K}{K}\right)_\mathrm{n} = \mathrm{const} \int_0^\infty \frac{\partial F}{\partial \tau} F^+ \sigma_\mathrm{n}\,\mathrm{d}E\,.$$

Таким образом, увеличение коэффициента реактивности урана при приближении к поглощающему стержню может происходить за счет увеличения потока нейтронов, появления градиента потока и изменения ценности нейтронов в результате деления.

Измерение нейтронного поля, проведенное с помощью камеры деления, показывает, что поток нейтронов падает при приближении к поглощающему стержню примерно на 15% (см. фиг. 2).

Наличие градиента потока у поглощающего стержня действительно приводит к увеличению реактивности реактора при помещении образца вблизи стержня, однако измерения с образцом свинца (сечение рассеяния которого близко к сечению рассеяния урана) показывает, что это увеличение на два порядка меньше по сравнению с ураном (см. фиг. 1).

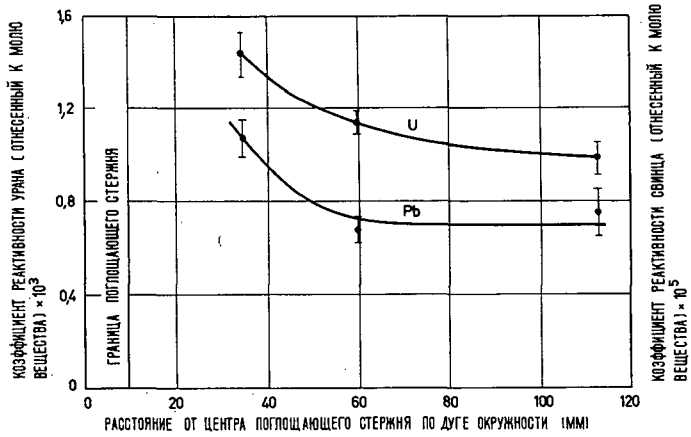


Фиг. 1
Значения коэффициентов реактивности урана и свинца в окрестности поглощающего стержня.

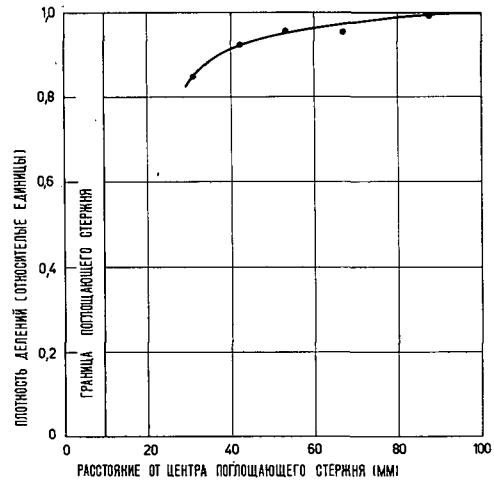


Фиг. 2
Распределение плотности делений в окрестности поглощающего стержня.

Увеличение коэффициента реактивности урана за счет изменения ценности нейтронов можно объяснить следующим образом. Уран при делении поглощает, главным образом, медленные нейтроны, а генерирует быстрые. Вблизи поглощающего стержня ценность медленных нейтронов низкая, так как они имеют большую вероятность быть захваченными бором. Нейтроны деления, прежде чем земедлятся до малых энергий, успевают уйти далеко от поглощающего стержня, где вероятность быть поглощенным без деления меньше. Таким образом, деление урана вблизи поглощающего стержня происходит на „обреченных“ нейтронах, большая часть которых все равно поглотилась бы в боре и была бы потеряна для цепной реакции.

**Компенсирующая способность стержней из различных материалов**

На сборке с отношением $\varrho_{Be}/\varrho_{U^5} = 150$ методом компенсации измеряемой реактивности регулирующим стержнем реактора, были проведены измерения с образцами сильно поглощающих веществ на предмет сравнения их компенсирующих способностей.

Измерения проводились в центральной части сборки с цилиндрическими образцами различных диаметров. Результаты измерений приведены в таблице II, причем значения компенсирующей способности исследованных веществ отнесены к компенсирующей способности прессованного карбида бора (плотностью 2,1 г/см³) того же диаметра и высоты.

Таблица II

**КОМПЕНСИРУЮЩАЯ СПОСОБНОСТЬ РАЗЛИЧНЫХ ВЕЩЕСТВ ДЛЯ СБОРКИ С $S_{Be}/S_{Z^5} = 150$**

| №№ пп | Материал стержня | Диаметр (мм) | $\frac{\left(\frac{\Delta K}{K}\right)_x}{\left(\frac{\Delta K}{K}\right)_{B_4C}}$ |
|---|---|---|---|
| 1 | Карбид бора плотностью 2,1 г/см³ | — | 1 |
| 2 | Иридий металлический | 13,6 | 0,90 |
| 3 | Порошок карбида бора плотностью 1,0÷1,1 г/см³ | 8 | 0,75 |
| 4 | Порошок карбида бора плотностью 1,0÷1,1 г/см³ | 19,4 | 0,75 |
| 5 | Набор резонансных поглотителей* | 12,0 | 0,67 |
| 6 | Тантал металлический | 19,4 | 0,59 |
| 7 | Тантал металлический | 8 | 0,41 |
| 8 | Гафний металлический | 7 | 0,54 |
| 9 | Порошок окиси рения, плотностью 1,0÷1,1 г/см³ | 19,4 | 0,53 |
| 10 | Порошок окиси рения, плотностью 1,0÷1,1 г/см³ | 7 | 0,40 |
| 11 | Кобальт металлический | 12 | 0,23 |
| 12 | Карбид бора с танталом** | 19,4 | 0,60 |

* Набор представляет собой коаксиальные цилиндры порошка окиси самария (диаметр 7 мм), серебра (толщина стенки 2 мм), тантала (толщина 0,2 мм), кобальта (толщина 0,2 мм) и вольфрама (толщина 0,1 мм).
** Образец представляет собой стержень из металлического тантала диаметром 12 мм, который окружен порошком карбида бора.

Из таблицы II видно, что замена карбида бора каким-либо ($n\ \gamma$)-поглотителем приводит к потере компенсирующей способности стержня. Единственным конкурентом карбиду бора (в данном спектре нейтронов) может быть иридий, компенсирующая способность которого лишь на 10% ниже компенсирующей способности прессованного карбида бора. Интерес могут также представлять наборы резонансных поглотителей, однако подбор материалов и их толщин в таком стержне требует дополнительного изучения.

В этом же спектре нейтронов были проведены измерения компенсирующей способности составных стержней, состоящих из поглотителя и замедлителя нейтронов. Компенсирующая способность такого составного стержня может увеличиться за счет более эффективного использования внутренних слоев этого стержня путем смягчения спектра нейтронов внутри стержня. Измерения, однако, показали (см. таблицу III), что ожидаемого выигрыша компенсирующей способности не наблюдается.

Результаты измерений компенсирующей способности составных поглощающих стержней приведены в таблице III. Наружный диаметр всех стержней был равен 19,4 мм. Компенсирующая способность стержня отнесена к компенсирующей способности порошка карбида бора (плотность 1,1 г/см$^3$) диаметром 19,4 мм и той же высоты, что и высота составного стержня.

ТАБЛИЦА III

**КОМПЕНСИРУЮЩАЯ СПОСОБНОСТЬ СОСТАВНЫХ ПОГЛОЩАЮЩИХ СТЕРЖНЕЙ ДЛЯ СБОРКИ С $\varrho_{Be}/\varrho_{U^5}=150$**

| №№ пп | Наружный цилиндр | | | Внутренний цилиндр | | $\frac{\left(\frac{\Delta K}{K}\right)_x}{\left(\frac{\Delta K}{K}\right)_{B_4C}}$ |
|---|---|---|---|---|---|---|
| | материал | диаметр (мм) | | материал | диаметр (мм) | |
| | | наружный | внутренний | | | |
| 1 | | — | — | Порошок карбида бора | 19,4 | 1 |
| 2 | Порошок карбида бора | 19,4 | 12 | Парафин | 12 | 0,95 |
| 3 | Порошок карбида бора | 19,4 | 12 | Бериллий | 10 | 0,73 |
| 4 | Кадмий | 19,4 | 17,4 | Парафин | 17,4 | 0,48 |

**Распределение потоков нейтронов различных энергий возле борного стержня и плотности захватов нейтронов внутри стержня**

На сборке с $\varrho_{Be}/\varrho_{U^5}=150$ по активации индикаторов из ванадия, индия, вольфрама и цинка было измерено пространственное распределение подкадмиевых нейтронов и нейтронов промежуточных энергий в окрестности поглощающего стержня из карбида бора*. Стержень имел плотность по бору 1,7 г/см$^3$, диаметр стержня 19,4 мм. Стержень отстоял на 204 мм от оси активной зоны. Распределения плотности нейтронов измерялись по дуге окружности с центром на оси активной зоны.

Индикаторы при активации помещались на середине высоты активной зоны. В качестве радиоактивных индикаторов использовались металлические фольги следующих толщин: ванадий — 450 мг/см$^2$, индий — 73 мг/см$^2$, вольфрам — 190 мг/см$^2$ и цинк — 280 мг/см$^2$. Индикаторы активировались в кадмиевых чехлах. Распределение подкадмиевых нейтронов получалось как разность активаций ванадия в кадмиевом чехле и без него.

У индия измерялась бета-активность с периодом полураспада 54 мин., обусловленная в основном захватом нейтронов с энергией, близкой к 1,46 эв. У вольфрама регистрировалась активность с периодом полураспада 24 часа, обусловленная, в основном, нейтронами с энергией близкой к 19 эв. У цинка регистрировалась активность с периодом полураспада 57 мин.; у соответствующего изотопа имеется резонанс в сечении захвата нейтронов при энергии 530 эв. Результаты измерений приведены в таблице 4 и на графике фиг. 3.

Форма распределений, полученных экспериментально, сравнивалась с расчетным нейтронным полем, полученным многогрупповым расчетом на методике, изложенной в [9]. Получено удовлетворительное согласие.

Распределение интенсивности поглощения нейтронов в боре по диаметру

* Измерения выполнены Ю. М. Шалашовым.

поглощающего стержня измерялось методом авторадиографии активированного ванадиевого диска. Диск, изготовленный из металлического ванадия толщиной 450 мг/см$^2$, имел диаметр равный диаметру поглощающего стержня (19,4 мм). Для активации он помещался на середине высоты актив-

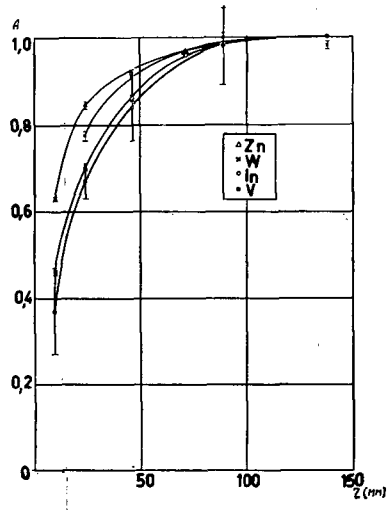


Фиг. 3
Распределение активности индикаторов (A) около поглощающего стержня.

ной зоны между двумя частями разрезанного поперек поглощающего стержня. После активации ванадиевый диск помещался для экспонирования на двустороннюю рентгеновскую пленку, закрытую светонепроницаемой бумагой. Проявленное изображение диска денситометрировалось. Зависимость плотности почернения изображения от активности индикатора была установлена в предварительных градуировочных опытах. Воспользовавшись этой зависимостью можно получить распределение активности по диаметру диска.

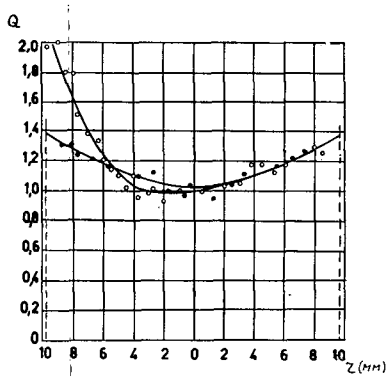


Фиг. 4
Распределение плотности поглощения нейтронов (Q) по диаметру поглощающего стержня.
○ — стержень вблизи от активной зоны
● — стержень вблизи отражателя

Энергетический ход эффективного сечения активации ванадия относительно близко следует ходу эффективного сечения поглощения нейтронов бором. Таким образом распределение активности ванадия по диаметру стержня дает представление о соответствующем распределении для бора.

Измерения проведены для двух положений стержня: вблизи оси активной зоны и вблизи отражателя.

Результаты измерений даны на графике фиг. 4. Краевой эффект, обусловленный конечной величиной геометрического разрешения, не позволяет получать распределение у края диска в пределах 1,5—2 мм. Кривые графика фиг. 4 экстраполированы в эту область. Для положения стержня вблизи отражателя в распределении плотности поглощения нейтронов наблюдается большой подъем со стороны отражателя. Подъем обусловлен существенным смягчением спектра нейтронов, возвращаемых отражателем.

Таблица IV

**АКТИВНОСТЬ РАЗЛИЧНЫХ ИНДИКАТОРОВ В ЗАВИСИМОСТИ ОТ РАССТОЯНИЯ ОТ БОРНОГО СТЕРЖНЯ**

| Индикатор | Расстояние от оси поглощающего стержня (мм) | Активность фольги (относительные единицы) |
|---|---|---|
| Ванадий (подкадмиевые нейтроны) | 10 | 0,37±0,10 |
| | 24 | 0,67±0,04 |
| | 46 | 0,84±0,08 |
| | 89 | 0,98±0,09 |
| | 138 | 1,00±0,10 |
| Индий | 10 | 0,461±0,005 |
| | 24 | 0,700±0,004 |
| | 46 | 0,860±0,005 |
| | 71 | 0,961±0,003 |
| | 138 | 1,000±0,003 |
| Вольфрам | 24 | 0,775±0,009 |
| | 46 | 0,913±0,007 |
| | 71 | 0,966±0,007 |
| | 89 | 1,000±0,007 |
| | 138 | 0,98 ±0,01 |
| Цинк | 10 | 0,631±0,004 |
| | 24 | 0,845±0,004 |
| | 46 | 0,915±0,004 |
| | 71 | 0,960±0,008 |
| | 138 | 1,000±0,004 |

## Компенсация избыточной реактивности с помощью поворотных цилиндров

В случае реакторов с большой утечкой нейтронов, какими являются реакторы, работающие на нейтронах промежуточных энергий, эффективным способом компенсации избыточной реактивности является изменение

утечки нейтронов из реактора путем изменения свойств отражателя по части поверхности активной зоны. Практически это осуществляется с помощью поворотных цилиндров, размещаемых на границе активной зоны и отражателя. В зависимости от конструкции отражателя могут рассматриваться различные типы компенсирующих поворотных цилиндров. Если бериллиевый слой отражателя достаточно толст, то цилиндр, диаметр которого равен или несколько больше толщины этого слоя, изготовленный из бериллия и имеющий по части дуги окружности покрытие из хорошего поглотителя нейтронов, например, из боросодержащего материала, позволит измерять реактивность системы путем поворота этого цилиндра вокруг своей оси. Если к поворотному цилиндру не предъявляется требований высокой компенсирующей способности, то в случае реакторов с составным отражателем, можно применить и составной поворотный цилиндр, в котором часть поперечного сечения занята бериллием, а другая материалом внешнего слоя составного отражателя.

На критической сборке с бериллиевым замедлителем, имевшей $\varrho_{Be}/\varrho_{U^5}=31$, проводились исследования сравнительной эффективности поворотных цилиндров различной конструкции. Активная зона сборки имела диаметр, равный 54 см, высоту 51 см. Боковой отражатель имел внутренний слой бериллия с эффективной толщиной 4 см (один ряд каналов стенда ПФ-4, заполненных бериллием) и внешний слой никеля толщиной 12,5 см. Торцевые отражатели имели внутренний бериллиевый слой толщиной 8 см и внешний никелевый слой толщиной 10 см.

Поворот компенсирующего цилиндра имитировался перестановкой каналов стенда ПФ-4, заполненных бериллием и никелем. Борное покрытие поворотного цилиндра имитировалось двумя стержнями из карбида бора с плотностью 2,1 г/см³, диаметром 8,4 мм. Стержни размещались вместо алюминиевых вытеснителей между каналами.

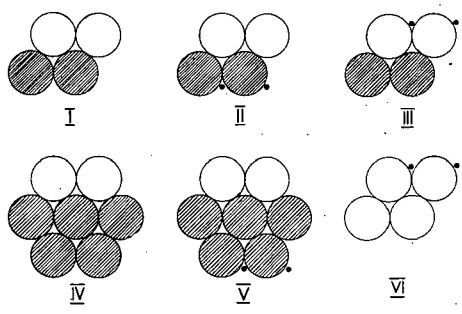


Фиг. 5
Макеты поворотных цилиндров
○ — канал, заполненный бериллием
⊕ — канал, заполненный никелем
● — стержень из карбида бора

Конструкция макетов поворотных цилиндров приведена на фиг. 5. Определенные экспериментом максимальные компенсирующие способности цилиндров (поворот на 180°) сведены в таблицу V.

ТАБЛИЦА V

**КОМПЕНСИРУЮЩАЯ СПОСОБНОСТЬ ПОВОРОТНЫХ ЦИЛИНДРОВ РАЗЛИЧНОЙ КОНСТРУКЦИИ**

| Тип цилиндра | I | II | III | IV | V | VI |
|---|---|---|---|---|---|---|
| Компенсирующая способность $\frac{\Delta K}{K}$ В % | 0,53 ±0,02 | 0,84 ±0,04 | 0,18 ±0,01 | 0,63 ±0,03 | 1,01 ±0,05 | 0,59 ±0,03 |

## Заключение

Приведенные в докладе экспериментальные данные имеют своей целью указать лишь на некоторые физические особенности промежуточных реакторов с бериллиевым замедлителем и, в первую очередь, на те из них, которым было уделено меньше внимания в работах, опубликованных ранее различными авторами (см., например [7]).

Показано принципиальное отличие во влиянии на критические параметры быстро-промежуточных систем внешнего и внутреннего замедления. Введение замедлителя во внутренние слои активной зоны приводит к увеличению критических объемов и загрузки ураном за счет возрастания утечки из активной зоны.

Интересными свойствами обладают гетерогенные промежуточные реакторы. Экспериментально показано, что эффект экранирования делений в толстых слоях урана, ведущий к снижению реактивности системы, может в значительной степени компенсироваться или даже перекрываться различными эффектами, положительно влияющими на реактивность.

Экспериментально обнаружен факт подъема эффективности урана-235 вблизи поглощающего стержня, что объясняется существенным возрастанием разности в ценностях нейтронов деления и нейтронов, захватываемых ураном.

Исследование показало, что наиболее эффективным материалом для поглощающих стержней промежуточного реактора является карбид бора. Довольно близко по эффективности к нему подходит металлический иридий.

Экспериментально показана возможность существенных перекосов в распределении захватов нейтронов, а следовательно и в энерговыделении, по диаметру борного стержня, размещенного вблизи бериллиевого отражателя, т.е. в области сильных градиентов нейтронных полей.

Измерения, проведенные с различными материалами компенсирующих поворотных цилиндров, показали, что достаточно эффективными являются составные цилиндры, как с поглотителем в виде карбида бора, так и без поглотителя. Действие последних обусловлено в основном разницей в отражающих свойствах различных материалов.

## ЛИТЕРАТУРА

[1] ЛЕЙПУНСКИЙ, А. И., КУЗНЕЦОВ, В. А. *и др.* Тяжеловодный физический реактор на эпитепловых нейтронах ПФ-2. Доклад на Венском семинаре по физике быстрых и промежуточных реакторов, 1961.

[2] МАРЧУК, Г. И., ИЛЯСОВА, Г. А. *и др.* Исследования критических параметров реакторных систем. Сборник статей. М., Госатомиздат, 1960, стр. 52.
[3] ПУПКО, В. Я., Физика и теплотехника реакторов. Приложение № 1 к журналу „Атомная энергия". М., Атомиздат, 1958, стр. 44.
[4] BUSSARD R. and DELAUER H., Nuclear Rocket Propulsion. Mc. Grav-Hill Book Co., N. J-Toronto-London (1958) p. 208.
[5] GROVER G., and PAXTON H. "Critical masses of oralloy assembly" *Nucleonics* **15** 6, (1957) 90.
[6] СТЮАРТ, Г., ГОФМАН, П., СТОРМ, М. Физические основы расчета реакторов на промежуточных нейтронах. Доклад № 2381 на 2-й международной конференции по мирному использованию атомной энергии. Сборник материалов конференции, т. 3.
[7] The Physics of Intermediate Spectrum Reactors. Ed. J. R. stehn, 1958.
[8] УСАЧЕВ, Л. Н., Уравнение для ценности нейтронов, кинетика реактора и теория возмущений. Сборник „Реакторостроение и теория реакторов", 1955.
[9] МАРЧУК, Г. И., Численные методы расчета ядерных реакторов. Атомиздат, 1958 г.

# II. 2. OTHER INTEGRAL EXPERIMENTS

# ÉTUDE DU FLUX DE NEUTRONS A L'ÉQUILIBRE DANS L'URANIUM NATUREL

J. L. CAMPAN, P. P. CLAUZON ET C. P. ZALESKI
CENTRE D'ÉTUDES NUCLÉAIRES DE SACLAY,
FRANCE

**Abstract — Résumé — Аннотация — Resumen**

**Research on neutron flux in equilibrium in natural uranium.** The results of measurements in a block of natural uranium are presented.

The detectors used are fission chambers, activation detectors and nuclear emulsions. The following details are given: (*a*) measurement methods in the energy range 1 keV — 3 MeV; (*b*) results of measurements of basic dimensions (diffusion length, asymptotic spectrum); (*c*) comparison with theoretical data obtained by calculations using the diffusion theory (check on validity of the theory, calculation methods and neutron constants used, etc.).

The spectrum measured may be described by the following experimental data:

| | |
|---|---|
| *Diffusion length* | 95.25 ± 0.5 |
| $\sigma_f$ 235/$\sigma_f$ 238 | 230 ± 10 |
| $\sigma_f$ 235/$\sigma$ Np 237 | 14 ± 0.5 |
| $\sigma_f$ 235/$\sigma_f$ 233 | 0.67 ± 0.003 |
| $\sigma_f$ 235/$\sigma_f$ 239 | 0.9 ± 0.05 |
| $\sigma_f$ 235/$\sigma$ In $_{(n,\gamma)}$ | 4.8 ± 0.1 |

**Etude du flux de neutrons à l'équilibre dans l'uranium naturel.** On présente les résultats de mesures effectuées dans un massif d'uranium naturel.

Les détecteurs utilisés sont des chambres à fission, des détecteurs d'activation et des émulsions nucléaires. Les auteurs exposent: *a*) les méthodes de mesures dans le domaine d'énergie de 1 keV à 3 MeV; *b*) les résultats de mesures de grandeurs fondamentales (longueur de diffusion, spectre asymptotique); *c*) la comparaison avec les valeurs théoriques obtenues par des calculs utilisant la théorie de la diffusion (contrôle de la validité de la théorie, des méthodes de calcul, des constantes neutroniques utilisées, etc.).

Le spectre mesuré peut être caractérisé par les valeurs expérimentales suivantes:

| | |
|---|---|
| *Longueur de diffusion* | 95,25 ± 0,5 |
| $\sigma_f$ 235/$\sigma_f$ 238 | 230 ± 10 |
| $\sigma_f$ 235/$\sigma$ Np 237 | 14 ± 0,5 |
| $\sigma_f$ 235/$\sigma_f$ 233 | 0,67 ± 0,003 |
| $\sigma_f$ 235/$\sigma_f$ 239 | 0,9 ± 0,05 |
| $\sigma_f$ 235/$\sigma$ (n, $\gamma$) In | 4,8 ± 0,1 |

**Изучение потока нейтронов в состоянии равновесия в природном уране.** В докладе излагаются результаты измерений, проведенных в блоке природного урана.

В качестве детекторов использовались камеры деления, активационные детекторы и эмульсионные ядерные детекторы. Авторы излагают: 1 — методы измерения в области энергий от 1 кэв до 3 Мэв; 2 — результаты измерения фундаментальных величин (диффузионная длина, асимптотический спектр); 3 — сравнение с теоретическими значениями, полученными в результате вычислений с использованием теории диффузии (проверка правильности теории, вычислительные методы, применявшиеся константы нейтронов и т.д.).

Измеренный спектр может характеризоваться следующими экспериментальными величинами:

| | |
|---|---|
| **Диффузионная длина** | 95,25 ± 0,5 |
| $\sigma_f$ 235/$\sigma_f$ 238 | 230 ± 10 |
| $\sigma_f$ 235/$\sigma$ Np 237 | 14 ± 0,5 |
| $\sigma_f$ 235/$\sigma_f$ 233 | 0,67 ± 0,003 |
| $\sigma_f$ 235/$\sigma_f$ 239 | 0,9 ± 0,05 |
| $\sigma_f$ 235/$\sigma_{(n,\gamma)}$ In | 4,8 ± 0,1 |

**Estudio del flujo neutrónico en equilibrio en el uranio natural.** Los autores dan a conocer los resultados de mediciones efectuadas en un bloque de uranio natural. Los detectores utilizados consisten en cámaras de fisión, detectores de activación y emulsiones nucleares. La memoria trata de: *a*) los métodos de medición aplicados en la gama de energías de 1 keV a 3 MeV; *b*) los resultados de las mediciones de ciertos parámetros fundamentales (longitud de dispersión, espectro asintótico); *c*) su comparación con los valores teóricos obtenidos por cálculo utilizando la teoría de la dispersión (comprobación de la validez de la teoría, de los métodos de cálculo, de las constantes neutrónicas empleadas, etc.).

El espectro medido se caracteriza por los siguientes valores experimentales:

| | |
|---|---|
| *Longitud de dispersión* | 95,25 ± 0,5 |
| $\sigma_f$ 235/$\sigma_f$ 238 | 230 ± 10 |
| $\sigma_f$ 235/$\sigma$ Np 237 | 14 ± 0,5 |
| $\sigma_f$ 235/$\sigma_f$ 233 | 0,67 ± 0,003 |
| $\sigma_f$ 235/$\sigma_f$ 239 | 0,9 ± 0,05 |
| $\sigma_f$ 235/$\sigma_{(n,\gamma)}$ In | 4,8 ± 0,1 |


## Introduction

*Objectifs.* Le but de l'expérience exponentielle rapide est l'étude de la propagation des neutrons dans un massif d'uranium naturel, à partir d'une source plane. Son intérêt est triple: *a*) mesure de grandeurs fondamentales caractérisant le phénomène: longueur de diffusion, spectre asymptotique; *b*) mise au point de méthodes de mesure dans le domaine d'énergie 1 keV—3 MeV; *c*) vérification de la validité des études théoriques menées parallèlement (méthodes de calcul, constantes neutroniques utilisées). Cette recherche expérimentale et théorique présente un intérêt certain pour les études de piles à neutrons rapides.

*Description sommaire.* Nous disposons pour cette étude d'un cube d'uranium naturel de 80 cm d'arête; monté dans la colonne diffusante de la pile EL2, il reçoit sur sa face avant un flux de neutrons thermiques (fig. 1). Les parois de la colonne diffusante sont tapissées de paraffine recouverte de cadmium. Il y a un espace libre autour du massif d'uranium. Un mur de paraffine est monté entre la face arrière du massif d'uranium et la porte en plomb de la colonne diffusante. Il est séparé de l'uranium par des feuilles de cadmium et de plastique boré. La succession des milieux dans le sens axial, c'est-à-dire perpendiculairement à la face avant du massif d'uranium, est illustrée sur la figure 2. Les conditions à la limite ne sont pas très nettes, et nous aurons à prendre des précautions quant à l'interprétation des résultats de mesure.

## 1. Etude théorique de la propagation des neutrons

### 1.1. Notion de spectre asymptotique

La face avant du massif d'uranium est soumise à un flux de neutrons thermiques. Ceux-ci provoquent la fission de l'uranium-235 et donnent naissance dans les premiers centimètres à un flux rapide. Le flux thermique s'atténue et devient

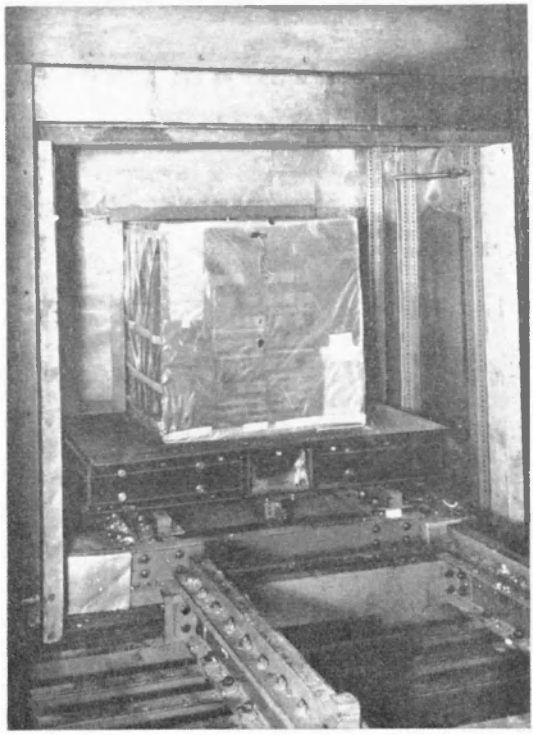

Figure 1
Vue du massif d'uranium en place dans la colonne thermique de EL2.

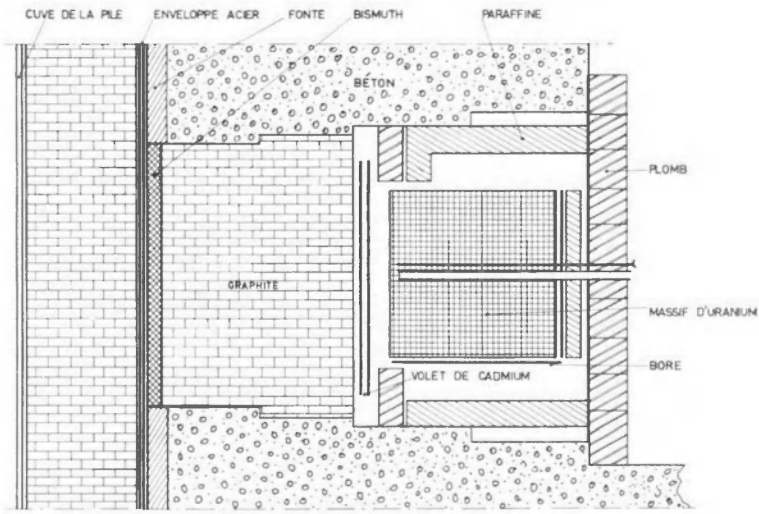


Figure 2
Schéma de mise en place du massif d'uranium.

rapidement négligeable. Le flux rapide, qui apparaît avec un spectre de fission, se propage en se dégradant en énergie sous l'effet des chocs inélastiques. Au contraire, par fissions, les neutrons lents tendent à donner naissance à des neutrons rapides. Il en résulte qu'au-delà d'une certaine distance de la source, la proportion des neutrons qui entrent dans chaque bande d'énergie $E$, $E+\mathrm{d}E$, soit directement par fission, soit par dégradation inélastique de neutrons de fission, tend à compenser ou à être compensée par la proportion des neutrons qui en sortent par dégradation inélastique, par capture ou par fission.

La répartition énergétique des neutrons tend à se stabiliser. Le spectre correspondant est appelé *spectre asymptotique* dans l'uranium naturel.

L'étude de la propagation des neutrons se ramène à la connaissance de la densité $\psi$ du flux des neutrons à toute énergie $E$, en tout point $r$ du massif, soit $\psi(E, r)$.

Dans un domaine où la distribution énergétique est stable (spectre asymptotique), $\psi(E, r)$ peut se mettre sous la forme d'un produit d'une fonction $\varphi(E)$ par une fonction $\chi(r)$, soit:

$$\psi(E, r) = \varphi(E)\,\chi(r).$$

### 1.2. Théorie de la propagation des neutrons

L'équation générale de la diffusion s'écrit:

$$-\mathrm{D}(E)\,\nabla^2\psi(E,r) + \left[\Sigma_{\mathrm{a}}(E) + \int \Sigma(E \to E')\,\mathrm{d}E'\right]\psi(E,r)$$
$$= \int \psi(E',r)\left[\nu\,\Sigma_{\mathrm{f}}(E')\,F(E) + \Sigma(E' \to E)\right]\mathrm{d}E'.$$

$F(E)$ caractérisant le spectre de fission,
$\Sigma_{\mathrm{a}}(E)$, $\Sigma_{\mathrm{f}}(E)$ étant les sections efficaces macroscopiques d'absorption et de fission,
$D(E)$ le coefficient de transport,
$\Sigma(E' \to E)$ la section efficace macroscopique différentielle de diffusion inélastique de l'énergie $E'$ à l'énergie $E$,
$\nu$ le nombre moyen de neutrons produits par fission.

Si l'on découpe l'échelle des énergies en $n$ intervalles $E_i$, $E_{i-1}$, on obtient:

$$-D_i\nabla^2\psi_i(r) + [\Sigma_{\mathrm{a}(i)} + \Sigma_{\mathrm{er}(i)}]\,\psi_i(r) = \Sigma_{\mathrm{er}(i-1)}\,\psi_{(i-1)}(r) + \sum_{j<i}\Sigma_{\mathrm{in}(j\to i)}\,\psi_j(r) +$$
$$+ F_i\sum \nu\,\Sigma_{\mathrm{f}(y)}\,\psi_j(r)\,\Delta E_j.$$

En incorporant dans l'absorption les fuites transversales, nous pouvons nous ramener à une dimension.

Nous avons résolu cette équation au moyen de deux codes à une dimension programmés à notre demande par le Service de calcul arithmétique: le code 48 $\Sigma$, où sont donnés comme conditions à la limite les flux à l'entrée et à la sortie, et le code 173 $\Sigma$, où sont donnés comme conditions à la limite les flux à l'entrée et les pentes des flux à la sortie.

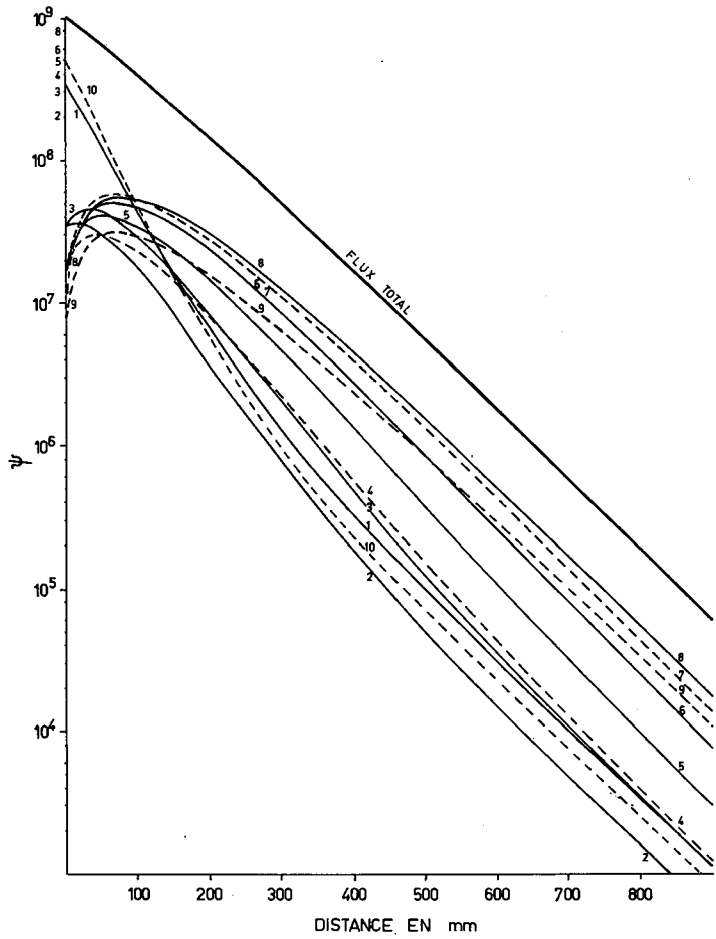


Figure 3
Calcul à dix groupes. Flux total et flux partiels.

## 1.3. Applications a l'uranium naturel

### 1.31. *Calcul du spectre asymptotique et de la longueur de diffusion*

L'équation de la diffusion peut se mettre sous la forme:

$$D_i \nabla^2 \psi_i(r) = \sum A_{ij} \psi_i(r)$$

si l'on utilise une théorie multigroupe.

L'hypothèse du spectre asymptotique se traduit par la relation:

$$\Delta^2 \psi_i(r) = k^2 \psi_i(r) \quad (\psi_i \text{ indépendant de } \psi_j)$$

d'où:

$$D_i k^2 \psi_i(r) = \sum A_{ij} \psi_j(r) .$$

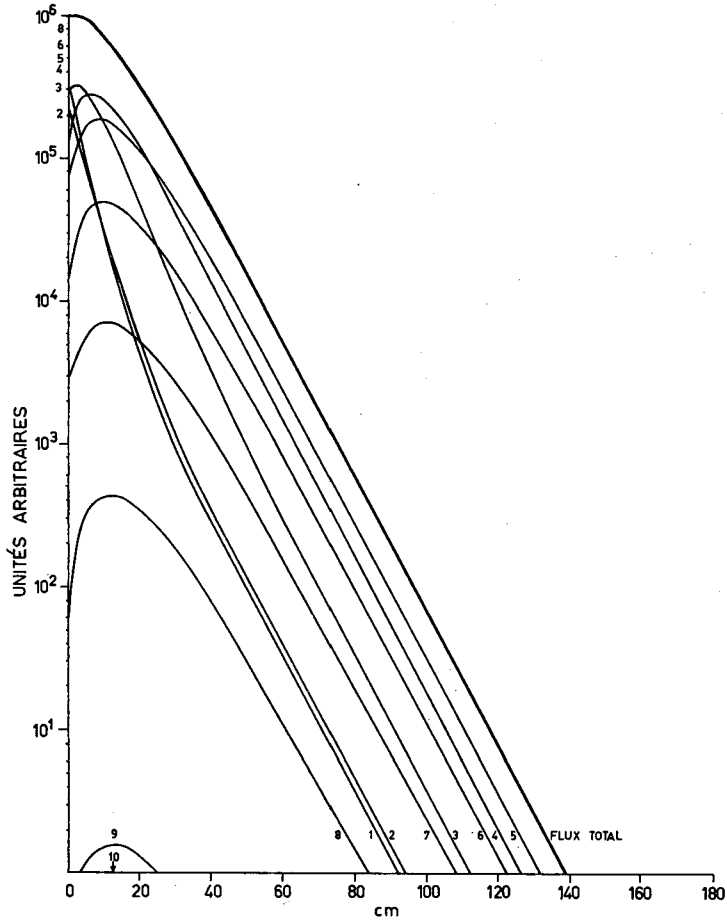


Figure 4
Propagation des flux (dix groupes) dans le massif d'uranium naturel supposé infini (constantes de Kiehn). Code 48 $\Sigma$ (sans correction de laplacien) transversal.

Nous obtenons donc le système d'équations linéaires:

$$\sum_{j \neq i} \frac{A_{ij}}{D_i} \psi_j(r) + \left[\frac{A_{ij}}{D_i} - k^2\right] \psi_i(r) = 0 .$$

Le mode fondamental correspond à la solution du système qui décroît le plus lentement, c'est-à-dire à la plus petite valeur de $k^2$.

Ce calcul est donc relativement simple. Nous l'avons appliqué aux différents lots de constantes trouvés dans la littérature et qui ont été utilisés pour des calculs neutroniques des assemblages à neutrons rapides. Les longueurs de diffusion obtenues sont rassemblées dans le tableau I ($L^2 = 1/k^2$).

1.32. *Evolution du flux des neutrons dans l'uranium naturel*

Nous avons utilisé pour ce calcul les codes à une dimension cités plus haut [3].

Le premier code est limité à 10 groupes en énergie. Nous avons donc fait un lot de sections efficaces à 10 groupes à partir des constantes à 20 groupes citées ci-dessus et du spectre mesuré dans l'uranium naturel.

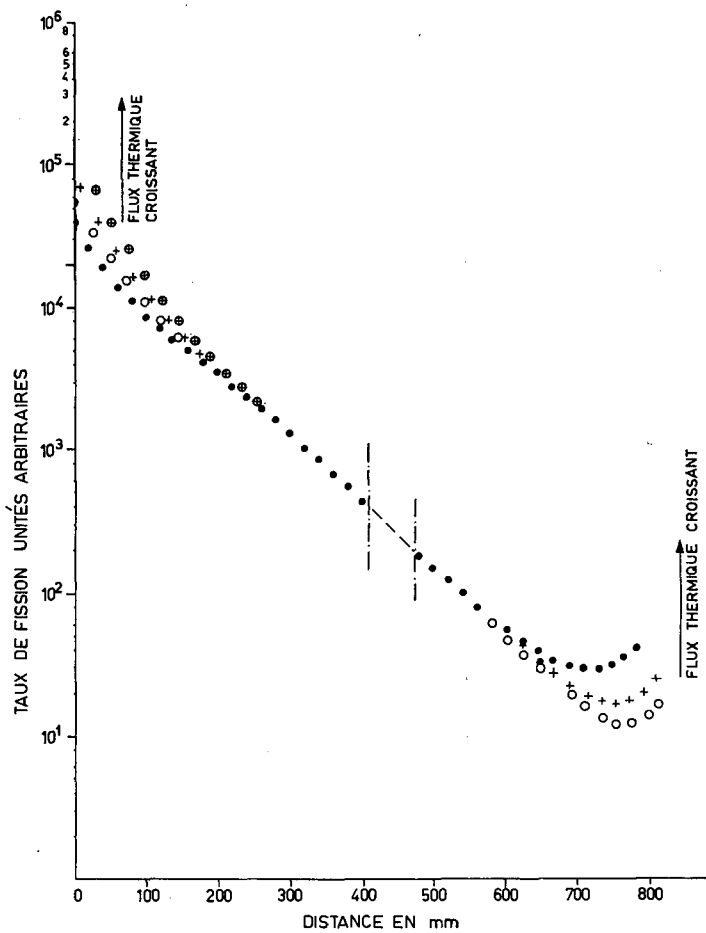


Figure 5
Influence des conditions aux limites sur la décroissance du flux total des neutrons.

La figure 3 nous montre l'évolution théorique du flux total et des flux partiels. On peut noter, dans ce cas de figure, que le flux ne paraît en équilibre qu'après 600 à 700 mm. La figure 4, où l'on montre les résultats obtenus avec les constantes de Los Alamos (Kiehn), semblent indiquer un équilibre vers 500 à 550 mm. Les imprécisions des constantes et des modes de calcul eux-mêmes font que l'on ne doit pas attacher une trop grande importance à ces discordances. Il nous paraît toutefois, en considérant l'ensemble des résultats, qu'en moyenne l'équilibre s'obtient vers 500 à 600 mm. Les indices de spectre calculés ne varient pratiquement plus au-delà de 500 mm.

Nous avons par ailleurs étudié l'influence des conditions aux limites; on doit noter en effet que le calcul n'en tient pas parfaitement compte. Nous avons supposé que le spectre des neutrons à l'entrée et à la sortie présente une composante thermique et une composante rapide (spectre de fission). En faisant varier la proportion de neutrons thermiques, nous avons obtenu les courbes de la figure 5,

TABLEAU I

**LONGUEURS DE DIFFUSION**

| Source de constantes | Référence | Nombre de groupes | Longueur de diffusion (mm) |
|---|---|---|---|
| Meneghetti | [4] | 10 | 97 |
| Loewenstein | [5] | 10 | 98 |
| Kiehn | [6] | 10 | 88 |
| Avery | [7] | 13 | 74 |
| ANL | [8] | 20 | 95,8 |

qui nous montrent que l'influence des conditions aux limites ne se fait plus sentir au-delà de 300 mm de la face d'entrée et en deçà de 250 mm de la face de sortie.

1.33. *Influence du nombre de groupes d'énergie sur le flux de neutrons calculé*

Notre seule hypothèse, en dehors de la théorie de la diffusion et de la méthode mathématique utilisée pour la résoudre, réside dans le choix des sections efficaces moyennes. Un lot de sections efficaces s'obtient à partir de constantes différentielles et d'un spectre de neutrons sur lequel s'effectue la pondération.

Si l'on veut étendre la zone de validité de la théorie, il est nécessaire d'augmenter le nombre de groupes d'énergie. Nous estimons que les calculs à dix groupes ne sont représentatifs que de 250 à 650 mm. Cette zone de validité se réduit à la zone 400 mm, 550 mm lorsque le calcul est fait à deux groupes seulement.

## 2. Expérience

### 2.1. DESCRIPTION DU MONTAGE

Le montage du dispositif expérimental a été effectué dans la colonne diffusante de la pile EL2 à Saclay en septembre 1957.

L'ensemble est schématisé sur la figure 2.

La colonne diffusante comprenait quatre étages de graphite. Nous en avons enlevé deux, créant ainsi une cavité dans laquelle le massif d'uranium a été monté.

Au fond de la cavité, nous avons construit un mur de plomb de 10 cm d'épaisseur, en y ménageant une fenêtre dans laquelle s'encastre la face avant du massif (fig. 1). Elle peut être fermée par un volet de cadmium commandé de l'extérieur, qui permet d'irradier le massif selon les besoins.

Le massif a été construit sur une plaque d'acier recouverte d'une feuille de plastique boré et supportée par un chariot monté sur rail. Il est enveloppé d'une chemise en vinyle destinée à retenir les produits de fission. Il est constitué de Influence des conditions aux limites sur la décroissance du flux total des neutrons. 10 t d'uranium naturel sous la forme de briques de $4 \times 4 \times 20$ cm, assemblées en cubes de 80 cm de côté.

Le massif est percé de quatre canaux à section circulaire dont la disposition est indiquée sur la figure 6. Deux de ces canaux, dits axiaux, parce que parallèles à l'axe de la colonne diffusante donc à la direction de la propagation des neutrons, ne traversent pas complètement le massif. En effet, pour éviter le transport de neutrons thermiques issus de la pile, ces canaux s'arrêtent à 4 cm de la face avant, la dernière brique n'étant pas percée. L'un de ces canaux a 10 cm de diamètre,

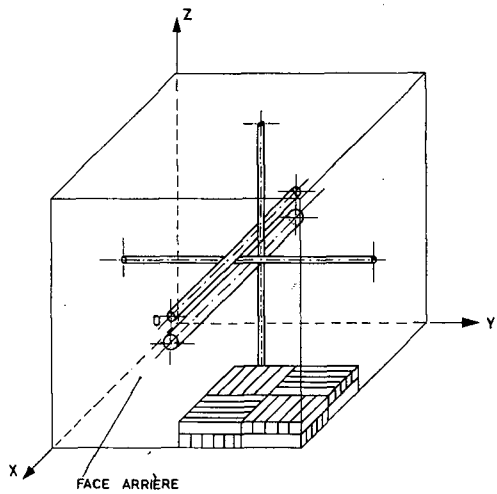


Figure 6
Montage du massif et disposition des canaux.

l'autre 30 mm; les deux autres canaux transversaux, l'un vertical, l'autre horizontal, ont un diamètre de 10 mm et traversent le massif de part en part. Pour assurer la continuité des canaux, toutes les briques d'uranium qui les supportent ont dû être usinées. Chaque canal est chemisé d'un tube d'aluminium destiné à faciliter l'introduction des appareils de mesure et à éviter leur pollution par les produits de fission.

Notons qu'il reste, entre les faces du massif et les protections en paraffine et cadmium blindant les parois de la cavité, un espace libre aménagé pour permettre l'implantation des mécanismes de manutention des détecteurs dans les deux canaux transversaux.

Nous avons dû, au cours des mesures, y déposer des matériaux, tels que paraffine ou plomb, pour vérifier si des neutrons réfléchis sur les parois de la colonne diffusante ne venaient pas perturber les mesures.

Derrière le massif, on trouvera successivement un mur de 7 cm d'épaisseur constitué par de la paraffine couverte de cadmium, la porte en plomb de la colonne diffusante (épaisseur 22 cm), puis un nouveau mur de paraffine de 45 cm d'épaisseur; enfin, un mur de béton, formant une enceinte accessible par une chicane, permet aux expérimentateurs d'approcher la sortie des canaux, le volet de cadmium étant fermé.

### 2.2. Mise en œuvre des détecteurs

Les caractéristiques de l'expérience et le faible niveau de flux dont nous disposions excluant les mesures en faisceau sorti, nous avons été conduits à n'utiliser que des détecteurs de petites dimensions susceptibles d'être introduits dans les canaux, dont les diamètres avaient été prévus assez petits pour que l'on puisse y négliger la variation du flux. Les détecteurs sont de trois types: détecteurs à activation, chambres à fission, émulsions nucléaires.

#### 2.21. *Détecteurs à activation*

Les détecteurs à activation se présentent sous la forme de petits disques. Afin de perturber le moins possible le flux des neutrons, les canaux sont emplis de billettes

d'uranium de longueurs diverses, entre lesquelles sont introduits les réacteurs, recouverts de minces feuilles d'aluminium destinées à éviter la pollution par les produits de fission (fig. 7). Les billettes ont ainsi un second but, qui est de définir

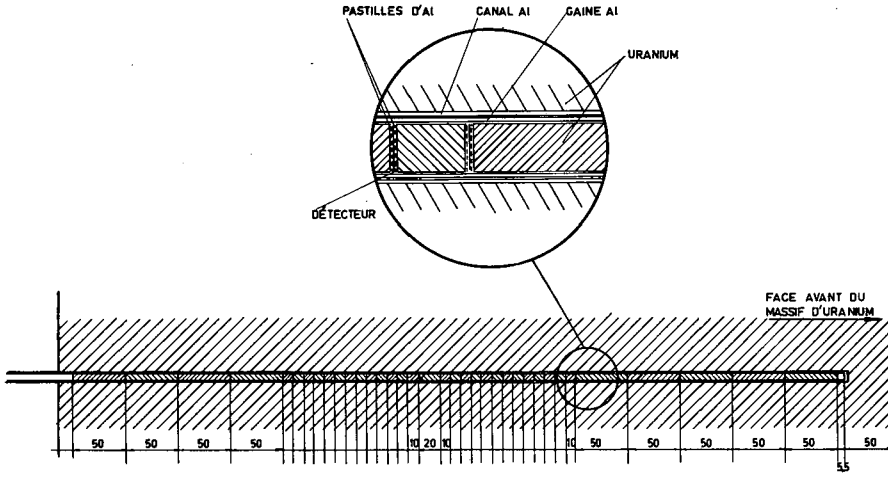


Figure 7
Schéma d'irradiation dans le petit canal axial.

avec précision la position des détecteurs à activation. Dans les canaux transversaux, les billettes d'uranium, montées sur un câble d'acier, sont introduites à l'aide d'un petit moteur électrique.

Après l'irradiation, dont la durée est de l'ordre de grandeur d'une période, l'activité est mesurée sur un ensemble de comptage comprenant huit photomultiplicateurs, sous lesquels les détecteurs sont permutés circulairement, afin de tenir compte des différences d'efficacité des diverses chaînes de comptage. D'autre part, les détecteurs, fabriqués en série, sont pesés et répartis en lots de même poids à 0,5% près. Nous n'introduirons pas de coefficients de détecteurs, mais, déterminant une distribution spatiale de flux à l'aide d'un grand nombre de points, nous évaluerons les incertitudes à partir de la dispersion des mesures [19].

2.22. *Chambres à fission*

Le mode opératoire est analogue à celui des détecteurs à activation. Dans les canaux transversaux, la chambre à fission est introduite à l'aide d'un câble d'acier

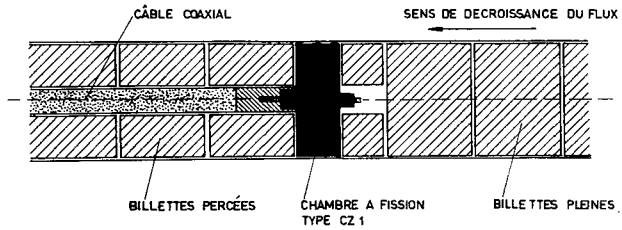


Figure 8
Schéma de disposition d'une chambre CZ 1 dans le canal axial de $\varnothing = 30$ mm.

mû par un moteur électrique. Dans le petit canal axial, elle est disposée à l'extrémité d'une canne rigide. Dans le grand canal axial ($\varnothing = 30$ mm) nous plaçons la chambre au milieu de billettes d'uranium (fig. 8) pour éviter les perturbations dues au transport des neutrons.

Les comptages étant de courte durée, nous utilisons une chambre moniteur, placée sur la face avant du massif et qui nous fournit directement une grandeur proportionnelle au flux intégré sur la durée de la mesure.

### 2.23. *Emulsions nucléaires*

L'émulsion nucléaire, enveloppée dans une feuille d'étain, est disposée dans une fente pratiquée dans une billette d'uranium. Celle-ci est ensuite introduite dans le grand canal axial entièrement rempli d'uranium. L'irradiation correspond à un flux intégré de $2 \cdot 10^{10}$ n/cm² (2 min à l'abscisse 380 mm).

## 2.3 Mesures de flux intégré

Si l'on prend les axes de références indiqués sur la figure 3, la théorie de la diffusion nous indique que, loin des frontières du massif d'uranium, le flux des neutrons a la forme:

$$\Psi(x\,y\,z) = \Psi \cos \frac{\pi}{l_y}(y - c) \cos \frac{\pi}{l_z}(z - c')\, e^{-\frac{x}{L}}$$

$l_y$ et $l_z$ représentant les dimensions extrapolées suivant les axes $Oy$ et $Oz$, $L$ la longueur de relaxation du flux suivant $Ox$.

La limite asymptotique de $L$ pour un bloc d'uranium dont les dimensions deviendraient infinies dans un demi-espace n'est autre que la longueur de diffusion $L_D$.

On peut remarquer que la formule ci-dessus ne fait pas intervenir la variable énergie, mais seulement la variable espace. Si donc la distribution énergétique du flux n'est pas en équilibre, on ne parviendra pas à déterminer $L$ et $L_D$.

Le dépouillement des mesures nous a montré que la décroissance du flux intégré par un détecteur $i$ avait grossièrement une allure exponentielle. On a donc été amenés à définir une longueur de relaxation apparente $L_i$.

Si nous utilisons des détecteurs $i$ dont les courbes de sections efficaces de capture en fonction de l'énergie sont très variées, et si l'on observe que les longueurs de relaxation apparentes $L_i$ sont égales, nous pourrons dire que la distribution énergétique des neutrons est en équilibre et nous écrirons:

$$L = \text{longueur de relaxation} = L_i.$$

Des définitions analogues introduisent les $(l_y)_i$ et $(l_z)_i$.

Le calcul des divers $L_i$, $(l_y)_i$ et $(l_z)_i$ a été fait à l'aide d'une méthode de moindres carrés décrite en [19].

Ces trois paramètres sont calculés dans la seule région où l'influence des conditions aux limites ne se fait pas sentir (entre 300 et 550 mm).

Les résultats des mesures faites avec divers détecteurs sont rassemblés dans le tableau II.

Nous constatons que les $L_i$ ne sont pas égaux, donc que la distribution énergétique du flux n'est pas en équilibre. Les neutrons les plus rapides décroissent plus vite que les neutrons plus lents du spectre.

TABLEAU II

**CALCUL DES DIVERS $L_i$, $(l_y)_i$, $(l_z)_i$**
**(millimètres)**

| Détecteurs | $i$ | $L_i$ | $\delta L_i$ | $(l_y)_i$ | $\delta(l_y)_i$ | $(l_z)_i$ | $\delta(l_z)_i$ |
|---|---|---|---|---|---|---|---|
| Phosphore (n, P) | 1 | 84,7 | 1,2 | — | — | — | — |
| Soufre | 2 | 83,6 | 0,5 | — | — | — | — |
| Thorium-232 | 3 | 83,5 | 1,5 | — | — | — | — |
| Uranium-238 | 4 | 84,3 | 0,5 | 1150 | 50 | 1175 | 50 |
| Neptunium-237 | 5 | 84 | 1 | — | — | — | — |
| U naturel | 6 | 90,4 | 0,7 | — | — | — | — |
| Indium | 7 | 90,6 | 0,15 | 1200 | 40 | — | — |
| Phosphore (n, γ) | 8 | 92,3 | 0,45 | — | — | — | — |
| Uranium-233 | 9 | 93 | 1 | — | — | — | — |
| Plutonium-239 | 10 | 93,8 | 0,1 | 1100 | 50 | 1125 | 50 |
| Manganèse | 11 | 94,1 | 1,3 | — | — | — | — |
| Or | 12 | 94,6 | 0,13 | 1150 | 50 | 1150 | 20 |
| Cuivre | 13 | 95,2 | 0,44 | — | — | — | — |
| Sodium | 14 | 95,3 | 0,9 | — | — | — | — |
| Uranium-235 | 15 | 95,5 | 0,2 | 1050 | 20 | 1100 | 20 |

## 2.4. EVOLUTION DU SPECTRE DES NEUTRONS LE LONG DE L'AXE DU MASSIF D'URANIUM:

### 2.41 *Exposé des méthodes de mesure et de dépouillement utilisées*

*a*) Détecteurs à activation et chambres à fission.

La réponse, en un point d'un détecteur de section efficace connue, nous fournit une information intégrée sur le spectre en ce point. Si nous disposons de plusieurs détecteurs dont les sections efficaces varient de façon sensiblement différente en fonction de l'énergie, nous disposerons d'autant d'informations sur le spectre, et nous pourrons approcher sa détermination dans le cadre d'une théorie multigroupe conduisant à la résolution d'un système linéaire.

Si l'on découpe l'axe des énergies en $l$ groupes $(E_j, E_{j-1})$ tels que:

$$0 = E_l < E_{l-1} < E_{l-2} \ldots < E_j < E_{j-1} < \ldots . < E_1 < E$$

et que, compte tenu du fait que:

$$n(r) = \frac{N}{A} \int_0^\infty \psi(E, r)\, \sigma(E)\, dE$$

où $n(r)$ = nombre de neutrons détectés par seconde au point $r$ par un détecteur de masse unité (N: nombre d'Avogadro, $A$: masse atomique de l'élément considéré), on introduise:

— la section efficace moyennée sur le spectre dans le groupe $j$:

$$\overline{\sigma_j(r)} = \frac{\int_{E_j}^{E_{j-1}} \psi(E, r)\, \sigma(E)\, dE}{\int_{E_j}^{E_{j-1}} \psi(E, r)\, dE}$$

— le flux de neutrons du groupe $j$:

$$\Psi_j(r) = \int_{E_j}^{E_{j-1}} \psi(E, r)\, \mathrm{d}E = \psi_j(r)\, \Delta E_j$$

où $\psi_j(r)$ est la densité de flux moyennée dans le groupe $j$ et $\Delta E_j = E_{j-1} - E_j$; $n(r)$ s'écrit alors:

$$n(r) = \frac{\mathrm{N}}{A} \sum_{j=1}^{j=l} \overline{\sigma_j(r)}\, \Psi_j(r)$$

$$n(r) = \frac{\mathrm{N}}{A} \sum_{j=1}^{j=l} \overline{\sigma_j(r)}\, \psi_j(r)\, \Delta E_j.$$

Cette méthode est décrite en [9], et nous l'avons appliquée à l'uranium naturel [10].

Mais la connaissance de $\overline{\sigma_j(r)}$ dépend de $\sigma(E)$, supposé connu, mais aussi du spectre cherché.

Pour tourner la difficulté [11], nous allons utiliser un découpage en énergie suffisamment fin pour que dans chaque intervalle le spectre soit assimilable à un segment de droite. L'erreur ainsi commise sera d'autant plus faible que le nombre et la précision des informations dont nous disposons seront plus grands.

Dans l'intervalle d'énergie $(E_j, E_{j-1})$, nous mettrons $\psi(E,r)$ sous la forme:

$$\psi(E,r) = \frac{1}{E_{j-1} - E_j} \left\{ \left[ \psi(E_{j-1}, r) - \psi(E_j, r) \right] E + \left[ E_{j-1}\, \psi(E_j, r) - E_j\, \psi(E_{j-1}, r) \right] \right\}$$

Nous choisirons $E$ de façon que $\psi(E, r)$ puisse être considéré comme nul.

Dans ces conditions $n(r)$ s'écrit:

$$n(r) = \frac{\mathrm{N}}{A} \sum_{j=1}^{j=l} \int_{E_j}^{E_{j-1}} \psi(E, r)\, \sigma(E)\, \mathrm{d}E$$

$$= \frac{\mathrm{N}}{A} \sum_{j=1}^{j=l+1} \frac{1}{E_{j-1} - E_j} \left\{ \left[ \psi(E_{j-1}, r) - \psi(E_j, r) \right] \int_{E_j}^{E_{j-1}} E\, \sigma(E)\, \mathrm{d}E \right.$$

$$\left. + \left[ E_{j-1}\, \psi(E_j, r) - E_j\, \psi(E_{j-1}, r) \right] \int_{E_j}^{E_{j-1}} \sigma(E)\, \mathrm{d}E \right\}$$

expression où s'introduisent les valeurs moyennes $(E\sigma)$ et $\sigma_j$ de $E\sigma(E)$ et $\sigma(E)$ dans l'intervalle $(E_j, E_{j-1})$.

Remarquons que ces quantités sont de simples moyennes arithmétiques indépendantes du spectre (donc du point $r$), et qu'elles peuvent être calculées à l'avance à partir des seules données de sections efficaces pour chaque détecteur [12].

A nombre égal d'informations, c'est-à-dire de groupes d'énergie, cette représentation du spectre par ligne brisée présente sur la représentation classique par une courbe en paliers l'avantage de permettre la pondération des sections efficaces sur le spectre à l'intérieur de chaque groupe d'énergie.

Nous obtenons:

$$n(r) = \frac{N}{A} \sum_{j=1}^{j=l} \{[\psi(E_{j-1}, r) - \psi(E, r)](E\sigma)_j + [E_{j-1}\psi(E_j, r) - E_j \psi(E_{j-1}, r)]\sigma_j\}$$

que nous pouvons écrire:

$$n(r) = \frac{N}{A} \sum_{j=1}^{j=l} \psi(E_j, r)\,[(E\sigma)_{j+1} - (E\sigma)_j + E_{j-1}\sigma_j - E_{j+1}\sigma_{j+1}]\,.$$

Si nous disposons des réponses de $l$ détecteurs, nous pouvons écrire $l$ équations analogues, qui formeront un système linéaire à $l$ inconnues $\psi(E_1, r), \ldots \psi(E_j, r), \ldots \psi(E_l, r)$, ordonnées des extrémités des segments représentant le spectre.

Dans le cadre de l'approximation utilisée, le flux total des neutrons au point $r$, défini comme:

$$\Psi(r) = \int_0^\infty \psi(E, r)\,\mathrm{d}E$$

s'écrira:

$$\psi(r) = \sum_{j=1}^{j=l} \frac{1}{2}\Big[\psi(E_{j-1}, r) + \psi E_j, r)\Big]\Delta E_j$$

ou:

$$\psi(r) = \sum_{j=1}^{j=l} \varphi(E_j, r)\,\frac{\Delta E_j + \Delta E_{j+1}}{2}$$

les flux par groupes ayant pour valeurs:

$$\psi_j(r) = \frac{1}{2}\Big[\psi(E_{j-1}, r) + \psi(E_j, \mathrm{r})\Big]\Delta E_j\,.$$

*Evaluation des incertitudes.*

Dans l'équation correspondant au détecteur $i$, appelons:

$b_j{}^i$ la quantité $\Big[(E\sigma)_{,+1} - (E\sigma)_j + E_{j-1}\sigma_j - E_{j+1}\sigma_{j+1}\Big]$

$N^i$ la quantité $\frac{A^i}{N} n^i(r)$

$\psi_j$ la quantité $\psi(E_j, r)$

Le système linéaire s'écrit:

$$\sum_{j=1}^{j=n} b_j{}^i \psi_j = N^i$$

soit:

$$\psi_i = \sum_{=1}^{i=n} B_i{}^j N^i$$

où la matrice $(B_i{}^j)$ est l'inverse de la matrice $(b_j{}^i)$.

TABLEAU III

**TAUX DE FISSION**

| Absc. (mm) | Chambre 561 | Chambre 761 | Chambre 861 | Chambre 961 |
|---|---|---|---|---|
| 120 | 1412000 ± 1% | 157067 ± 5% | 11724 ± 5% | 2000000 ± 5% |
| 150 | 720000 ± 1% | 100000 ± 5% | 7400 ± 5% | 1000000 ± 5% |
| 200 | 385000 ± 1% | 52470 ± 5% | 3590 ± 5% | 500000 ± 5% |
| 250 | 234000 ± 1% | 27000 ± 5% | 1700 ± 5% | 281000 ± 5% |
| 300 | 141775 ± 1% | 14000 ± 5% | 960 ± 5% | 160130 ± 5% |
| 350 | 85000 ± 1% | 7400 ± 5% | 460 ± 5% | 93000 ± 5% |
| 400 | 50000 ± 1% | 4050 ± 5% | 250 ± 5% | 54000 ± 5% |
| 450 | 30000 ± 1% | 2220 ± 5% | 140 ± 5% | 31000 ± 5% |
| 480 | 21600 ± 1% | 1580 ± 5% | 98 ± 5% | 22200 ± 5% |
| 500 | 17000 ± 1% | 1230 ± 5% | 77 ± 5% | 18000 ± 5% |
| 550 | 9600 ± 1% | 680 ± 5% | 45 ± 5% | 10130 ± 5% |
| 600 | 5450 ± 1% | 385 ± 5% | 26 ± 5% | 6050 ± 5% |
| 650 | 3130 ± 1% | 211 ± 5% | 16 ± 5% | 3600 ± 5% |
| 700 | 1900 ± 1% | 128 ± 5% | 10 ± 5% | 2200 ± 5% |
| 750 | 1185 ± 1% | 64 ± 5% | 6,35 ± 5% | 1325 ± 5% |
| 800 | 1000 ± 1% | 46 ± 5% | 4,4 ± 5% | 1200 ± 5% |

La loi de propagation des erreurs indépendantes nous conduit à:

$$\sigma^2 \psi_j = \sum_{i=1}^{i=n} (B_i^j)^2 (\sigma \mathrm{N}^i)^2 + \sum_{i=1}^{i=n} \sigma^2 B_i^j \mathrm{N}^{i^2}$$

qui s'écrit, en fonction de $\sigma^2{}_{b_k l}$, sous la forme:

$$\sigma^2 \varphi_j = \sum_{i=1}^{n} (B_i^j)^2 \sigma^2 \mathrm{N}_i + \sum_{ikl} \mathrm{N}^{i^2} (B_i^j)^2 (B_i^k)^2 \sigma_{b_k l}.$$

Même si l'évaluation de $\sigma^2{}_{b_k l}$ est difficile, le calcul des coefficients de la seconde sommation permet d'apprécier l'influence de l'incertitude des sections efficaces sur la précision de $\psi_j$.

*b*) Emulsions nucléaires.

Une seconde méthode utilise l'interaction (n, p) des neutrons sur les noyaux d'hydrogène d'une émulsion nucléaire.

Les noyaux d'hydrogène de la gélatine sont les noyaux cibles, les protons projetés par les neutrons rapides sont enregistrés dans l'émulsion.

La densité de flux de neutron $\psi(E)$ est liée au nombre de protons observés $r(E)$ par la relation [20]:

$$\psi(E) = -\frac{E}{[H]\, V \cdot \sigma_{(\mathrm{n,\,p})}(E)} \frac{\mathrm{d}\, r(E)}{\mathrm{d}\, E} \tag{1}$$

$[H]$ étant le nombre d'atomes d'hydrogène par centimètre cube de l'émulsion nucléaire, $V$ le volume dépouillé, $\sigma_{(n,\,p)}$ $(E)$ la section efficace d'interaction (n, p).

La limite inférieure de cette technique se situe vers 250 keV. Les possibilités de la méthode ont été décrites en [21].

TABLEAU IV

**RÉSULTATS POUR L'URANIUM NATUREL**

| Abscisse (mm) | $\psi_1$ | $\frac{\sigma_{\psi_1}}{\psi_1}$ (%) | $\psi_2$ | $\frac{\sigma_{\psi_2}}{\psi_2}$ (%) | $\psi_3$ | $\frac{\sigma_{\psi_3}}{\psi_3}$ (%) | $\psi_4$ | $\frac{\sigma_{\psi_4}}{\psi_4}$ (%) | $\psi_5$ | $\frac{\sigma_{\psi_5}}{\psi_5}$ % | $\psi_{tot.}$ | $\frac{\sigma_{\psi_{tot.}}}{\psi_{tot.}}$ (%) |
|---|---|---|---|---|---|---|---|---|---|---|---|---|
| 120 | 33 300 000 | ±6 | 13 100 000 | ±60 | 563 000 000 | ±15 | 83 000 000 | ±85 | — | — | 493 000 000 | ±25 |
| 150 | 21 000 000 | ±6 | 9 260 000 | ±50 | 259 000 000 | ±15 | 42 600 000 | ±85 | — | — | 244 000 000 | ±25 |
| 200 | 10 170 000 | ±6 | 7 020 000 | ±35 | 106 000 000 | ±15 | 25 100 000 | ±70 | — | — | 120 000 000 | ±25 |
| 250 | 4 800 000 | ±6 | 4 670 000 | ±25 | 45 100 000 | ±20 | 17 200 000 | ±60 | — | — | 67 000 000 | ±25 |
| 300 | 2 720 000 | ±6 | 1 900 000 | ±25 | 19 390 000 | ±30 | 11 600 000 | ±40 | 1 900 000 | 100 | 38 000 000 | ±25 |
| 350 | 1 291 000 | ±6 | 1 330 000 | ±25 | 9 180 000 | ±40 | 7 190 000 | ±50 | 2 700 000 | 95 | 22 000 000 | ±25 |
| 400 | 706 000 | ±6 | 745 000 | ±25 | 4 890 000 | ±40 | 4 300 000 | ±45 | 1 900 000 | 80 | 12 600 000 | ±25 |
| 450 | 395 000 | ±6 | 392 000 | ±25 | 1 736 000 | ±60 | 2 720 000 | ±40 | 1 870 000 | 45 | 7 130 000 | ±25 |
| 500 | 217 500 | ±6 | 219 000 | ±25 | 1 410 000 | ±60 | 1 510 000 | ±40 | 819 000 | 55 | 4 170 000 | ±25 |
| 550 | 127 500 | ±6 | 104 000 | ±30 | 778 000 | ±60 | 860 000 | ±45 | 476 000 | 60 | 2 350 000 | ±25 |
| 600 | 73 600 | ±6 | 54 100 | ±35 | 722 000 | ±50 | 465 000 | ±55 | 105 000 | 100 | 1 420 000 | ±25 |
| 650 | 45 500 | ±6 | 16 900 | ±60 | 541 000 | ±30 | 261 000 | ±50 | — | — | 853 000 | ±25 |
| 700 | 28 500 | ±6 | 8 170 | ±80 | 343 000 | ±30 | 157 000 | ±50 | — | — | 522 000 | ±25 |
| 750 | 18 150 | ±6 | — | — | 182 000 | ±35 | 105 000 | ±45 | — | — | 312 000 | ±25 |
| 800 | 12 600 | ±6 | — | — | 232 000 | ±25 | 82 000 | ±55 | — | — | 288 000 | ±25 |
| 850 | 9 000 | ±6 | — | — | 723 000 | ±15 | 137 000 | ±70 | — | — | 644 000 | ±25 |

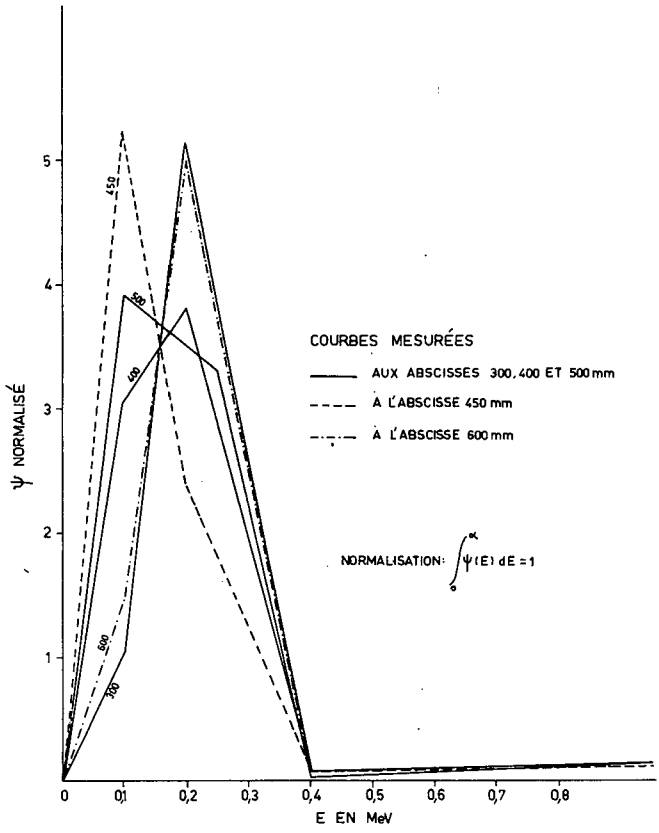


Figure 9
Evolution du spectre le long de l'axe.

On a choisi pour le dépouillement l'irradiation de durée 15 min. Ce dépouillement a été effectué par voie photographique [21]. Six mille traces environ ont été mesurées par point d'expérience. Les spectres expérimentaux sont exprimés en fonction des énergies des protons projetés par les neutrons dont on doit mesurer le spectre.

Le spectre des protons qu'il faut attendre à priori du spectre à l'équilibre a été calculé par la méthode de Monte-Carlo, en tenant compte des propriétés du choc proton-neutron, c'est-à-dire la section efficace et les conditions de conservation de l'énergie et d'isotropie de la diffusion dans le système du centre de masse. L'emploi de ces propriétés pour gouverner les nombres aléatoires choisis est équivalent à celui de la relation (1) dans un calcul analytique.

2.42 *Applications à l'uranium naturel*

Nous avons appliqué la méthode décrite en 2.41 *a* aux réponses de quatre chambres à fission: uranium-235, plutonium-239, neptunium-237 et uranium-238.

Le tableau III donne les taux de fission de ces chambres pour un gramme de détecteur et pour un flux de neutrons correspondant à une puissance de la pile EL2 de 2 MW (voir Tableau IV).

Les équations précédentes montrent que la précision que l'on obtient sur la détermination du spectre dépend du découpage en énergie utilisé. Le découpage en énergie qui semble nous donner la meilleure précision est: 0 — 100 — 200 — 400 — 1000 — 5000 keV.

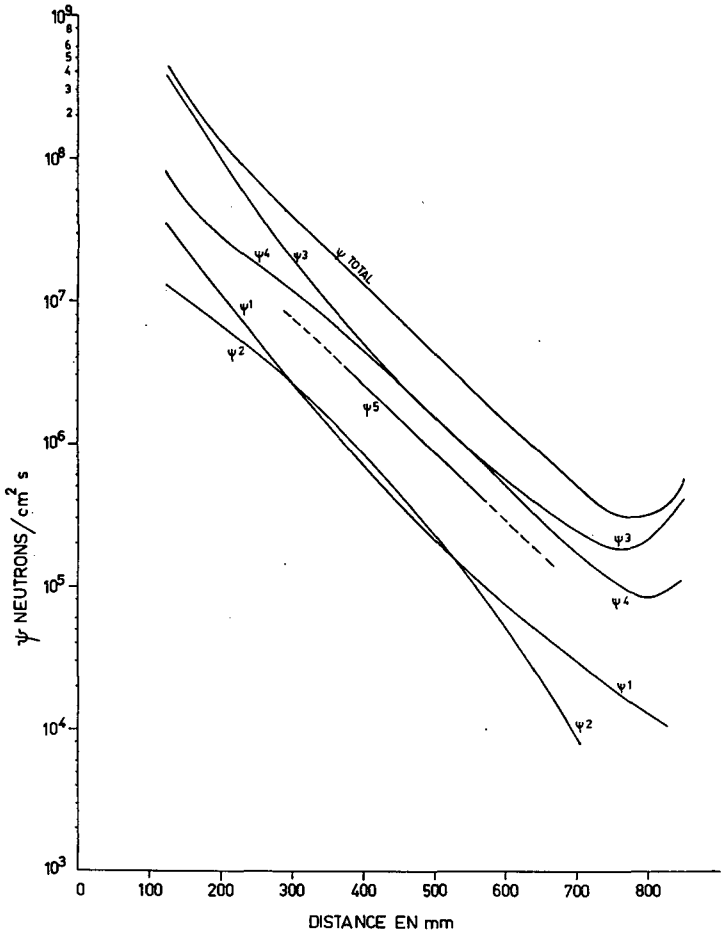


Figure 10
Distribution du flux total et des flux partiels.

Nous avons imposé au spectre de passer par l'origine et par le point d'abscisse 5000 keV et d'ordonnée nulle.

La figure 9 présente les spectres aux abscisses 300, 400, 450, 500 et 600 mm.

La figure 10 montre l'évolution des flux par groupe d'énergie le long de l'axe du massif, ainsi que le flux total.

Nous avons vérifié la méthode en recalculant à partir de ces résultats les réponses de l'uranium-233 et de l'indium et nous présentons sur les figures 11 et

12 les valeurs obtenues comparées à celles mesurées directement. L'accord est satisfaisant.

Nous avons appliqué la méthode des plaques nucléaires décrite en 2.41 *b*.

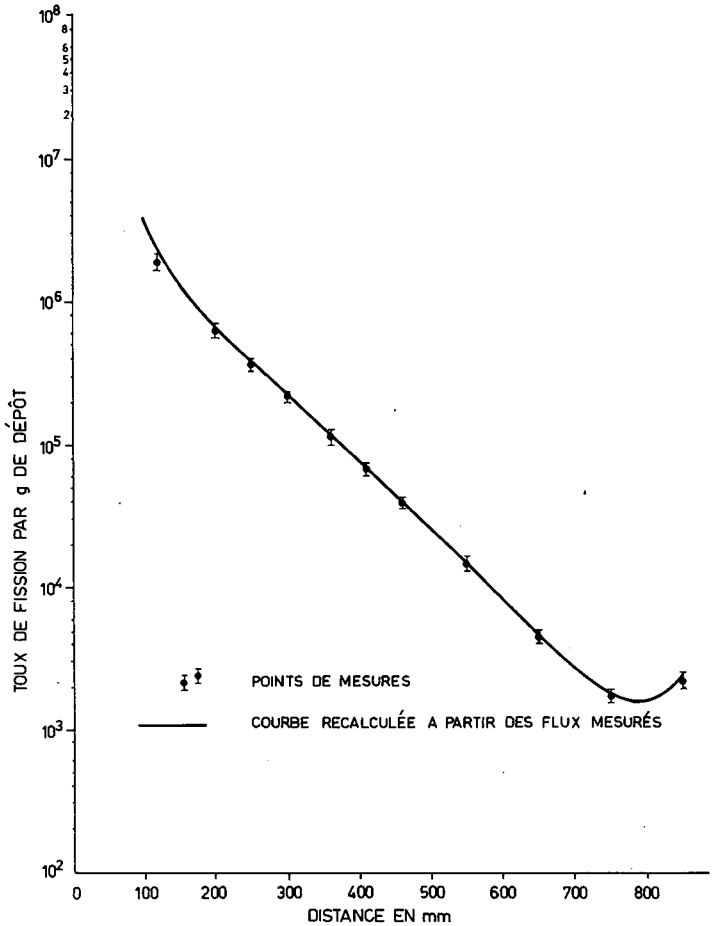


Figure 11
Distribution axiale de flux (uranium-233).

On a pu montrer qu'aux abscisses 280 et 380 la géométrie d'irradiation conduit à une répartition isotrope des traces dans l'émulsion. L'introduction de cette géométrie et de la relation parcours-énergie dans la méthode de Monte-Carlo permet de calculer pour le spectre à l'équilibre le spectre des longueurs projetées dans le plan de l'émulsion [21, 22].

Les figures 13 et 14 comparent le spectre calculé des longueurs projetées et les spectres expérimentaux.

La définition accrue de la méthode a permis de conserver un découpage supérieur aux vingt groupes du spectre calculé à partir des constantes ANL.

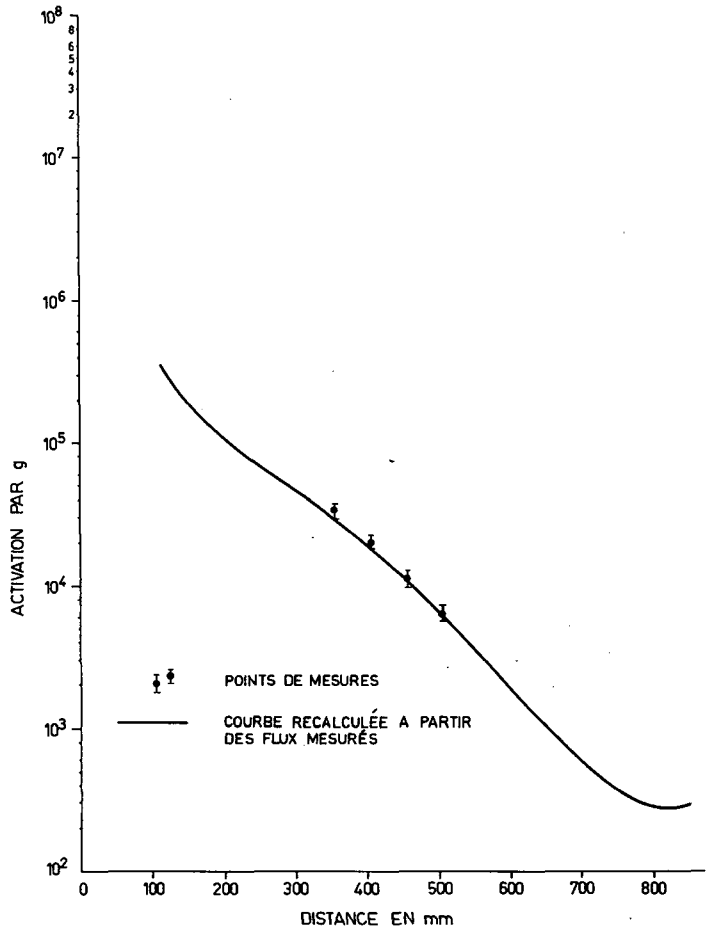


Figure 12
Distribution axiale de flux (indium).

## 3. Discussion des résultats obtenus

### 3.1. Influence des conditions aux limites - région d'équilibre du spectre

Les résultats précédents (voir également la figure 16) font apparaitre que, dans la région 420 — 520 mm, le spectre des neutrons évolue peu et que les distributions des flux partiels présentent pratiquement la même pente.

Les calculs multigroupes semblent montrer également que l'équilibre s'établit autour de ces valeurs.

La région définie plus haut est assez étroite; nous avons déterminé les pentes des divers flux intégrés par les détecteurs utilisés entre les abscisses 420 et 520 mm (voir tableau V).

TABLEAU V

**LONGUEURS DE RELAXATION APPARENTES POUR LES DIFFÉRENTS DÉTECTEURS**

| Détecteur | $L_i$ |
|---|---|
| $^{232}$Th | 88,2 |
| $^{233}$U | 91,2 |
| $^{235}$U | 90,2 |
| $^{237}$Np | 85,3 |
| $^{238}$U | 88,6 |
| $^{239}$Pu | 91,7 |
| Au (n, $\gamma$) | 90,5 |
| P (n, $\gamma$) | 89,7 |
| P (n, p) | 86,4 |
| S (n, p) | 86,9 |

Nous constatons que les écarts notés sous 2. 3 (voir tableau II) se sont nettement amoindris, mais n'en existent pas moins. En effet, la valeur moyenne de la longueur de relaxation pour les détecteurs à seuil est ici de 87,0 mm, et de 90,7 mm pour les détecteurs «thermiques».

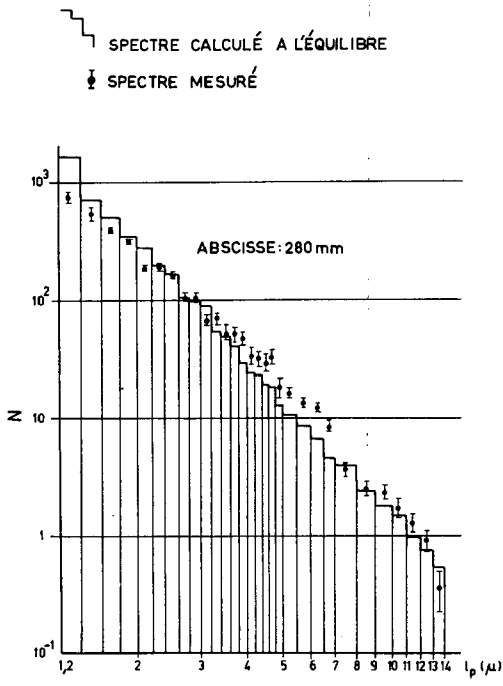


Figure 13
Histogramme des traces de protons de recul projetées dans le plan de l'émulsion nucléaire ($x = 280$ mm).

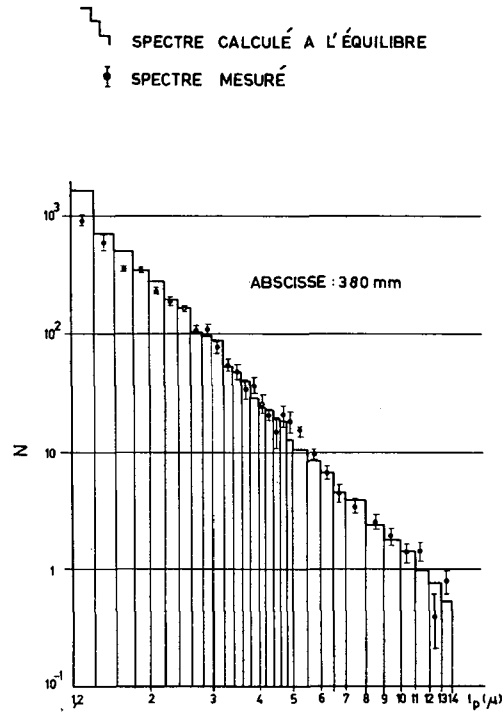


Figure 14
Histogramme des traces de protons de recul projetées dans le plan de l'émulsion nucléaire ($x = 380$ mm).

Si l'on admet une marge d'erreur confortable, on pourra estimer que le spectre est en équilibre. En fait, les mesures (détecteurs d'activation par exemple) sont reproductibles, et dans le stade actuel de nos études* nous ne pouvons dire que l'équilibre est atteint, bien que nous en soyons très proches.

Les grandeurs fondamentales que nous avons mesurées ne sont donc pas rigoureusement celles qui caractérisent le spectre des neutrons en équilibre dans l'uranium naturel. Nous pensons qu'elles en sont toutefois très voisines.

*Remarque.* Les derniers dépouillements d'émulsions nucléaires effectuées au Centre de Mol (Belgique) — Service de M. Beets — indiquent que le spectre au point d'abscisse 380 se confond avec le spectre calculé asymptotique, à partir de l'intervalle (1,8 — 2,0) μ des longueurs projetées des protons, tandis que le spectre à l'abscisse 280 est significativement différent, dans le sens d'un durcissement du spectre des neutrons. Au point d'abscisse 380, on peut donc admettre qu'au-delà de l'énergie neutronique 350 keV, le spectre des neutrons est identique au spectre calculé pour l'équilibre.

Nous avons, en outre, contrôlé que les conditions aux limites assez médiocres imposées au massif d'uranium n'ont pas d'influence dans la région centrale.

* Il est possible qu'une étude fine dans une région encore plus étroite que celle définie ici nous conduise à un résultat positif en ce qui concerne l'équilibre du spectre des neutrons.

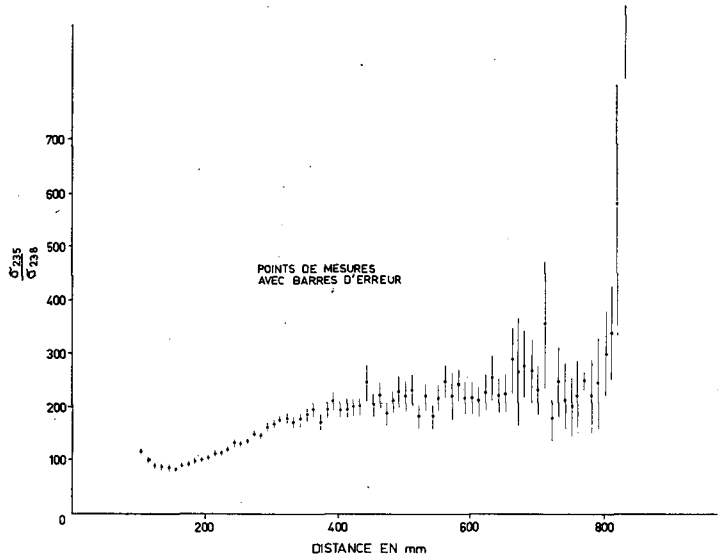


Figure 15
Evolution des rapports des sections efficaces moyennes de fission de l'uranium-235 et de l'uranium-238.

Nous avons rempli l'espace libre situé entre le massif et les parois de la colonne diffusante à l'aide de paraffine, puis de plomb. Nous n'avons constaté aucune différence dans la région centrale du massif d'uranium par rapport à nos premières mesures.

L'évolution du spectre telle que nous l'avons mise en évidence (fig. 9) s'explique parfaitement: à partir de la face avant du massif d'uranium, le spectre se dégrade peu à peu, du spectre de fission à celui de l'uranium naturel. Sur la face arrière, nous avons disposé de la paraffine, qui, thermalisant brutalement les neutrons, provoque dans l'uranium une augmentation du nombre des fissions et un durcissement du spectre. Le cadmium et le plastique boré que nous avions mis pour éviter ce phénomène semblent inefficaces pour le montage utilisé.

Les paramètres dont la valeur est donnée dans le paragraphe suivant ont été mesurés dans la région 420 — 520 mm.

### 3.2. Paramètres caractéristiques de l'uranium naturel

#### 3.21. *Longueur de diffusion mesurée*

Les mesures dans les canaux transversaux nous ont conduits aux dimensions extrapolées suivantes:

$$l_y \sim l_z \sim 1100 \pm 50 \text{ mm}.$$

L'évolution du flux total nous donne la longueur de relaxation dans la région (420 — 520 mm) où l'on est très voisin de l'équilibre ($L_i = 88{,}9$ mm).

Après les corrections dues aux fuites transversales, nous obtenons:

$$L_D = 95{,}25 \pm 0{,}5 \text{ mm}.$$

Ce paramètre est donné pour une densité de 18,8.

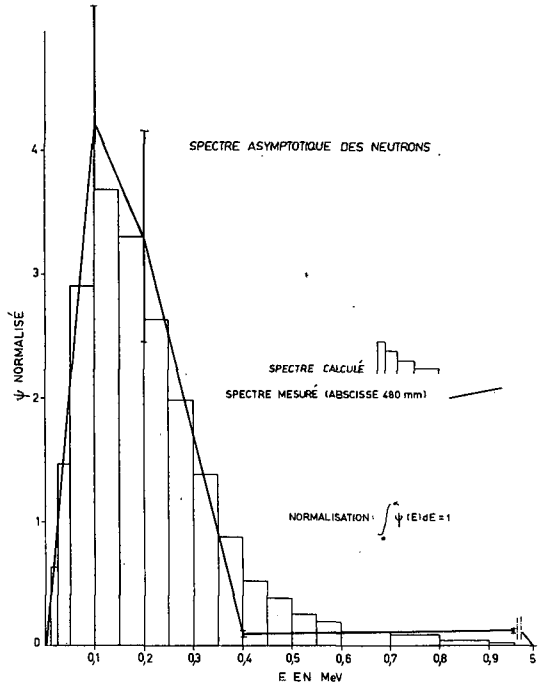


Figure 16
Spectre asymptotique des neutrons.

3.22. *Indices de spectre* (voir fig. 15)

Les valeurs suivantes ont été prises au point 480 mm:

$$\frac{\bar{\sigma}^{235}U}{\bar{\sigma}^{238}U} = 230 \pm 10 \qquad \frac{\bar{\sigma}^{235}U}{\bar{\sigma}^{237}Np} = 14 \pm 0{,}5$$

$$\frac{\bar{\sigma}^{235}U}{\bar{\sigma}^{233}U} = 0{,}67 \pm 0{,}003 \qquad \frac{\bar{\sigma}^{235}U}{\bar{\sigma}^{239}Pu} = 0{,}90 \pm 0{,}05$$

$$\frac{\bar{\sigma}^{235}U}{\bar{\sigma}\,In} = 4{,}8 \pm 0{,}1$$

3.23. *Spectre asymptotique*

Nous avons déterminé le spectre des neutrons au point d'abscisse 480 mm où le spectre est très voisin du spectre asymptotique.

Les résultats sont portés figure 16, comparés au spectre asymptotique calculé au moyen des sections efficaces à 20 groupes de l'ANL (Annexe III).

Nous constatons le bon accord des résultats expérimentaux et théoriques. Nous avons précisé la mesure au delà de 0,4 MeV à l'aide d'émulsions nucléaires et nous donnons les résultats figure 17.

En groupant les résultats des chambre à fission et des émulsions nucléaires, nous pouvons tracer le spectre de la figure 18.

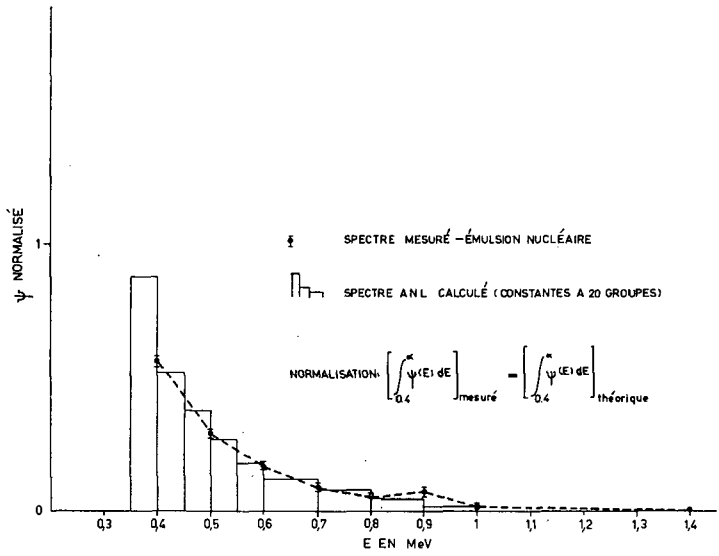


Figure 17
Spectre asymptotique des neutrons.

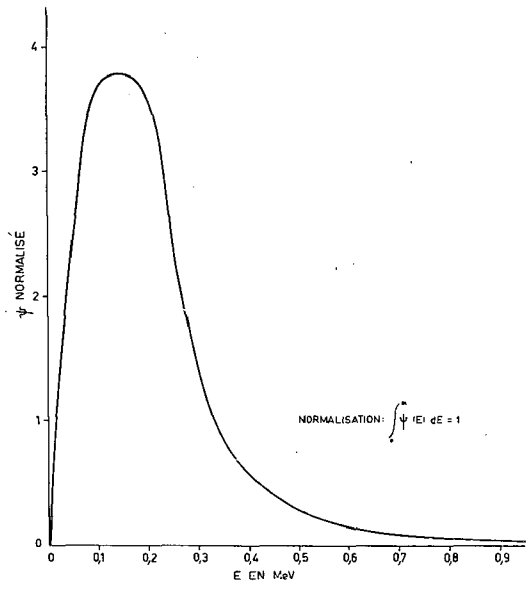


Figure 18
Spectre asymptotique de l'uranium naturel. Courbe expérimentale.

## 4. Comparaison des résultats théoriques et expérimentaux

### 4.1. Longueur de diffusion

Nous avons pu faire ici un calcul à 20 groupes (voir 1,31). La comparaison du résultat théorique, et de celui de la mesure est tout à fait satisfaisant:

$$L_{th} = 95{,}8 \text{ mm} \quad L_{exp} = 95{,}25 \text{ mm}$$

Nous avons cherché à chiffrer l'erreur commise sur ce paramètre lorsque l'on utilise un lot de sections efficaces à 10, 8, 5 ou 2 groupes, calculé à partir du lot à 20 groupes et du spectre expérimental des neutrons.

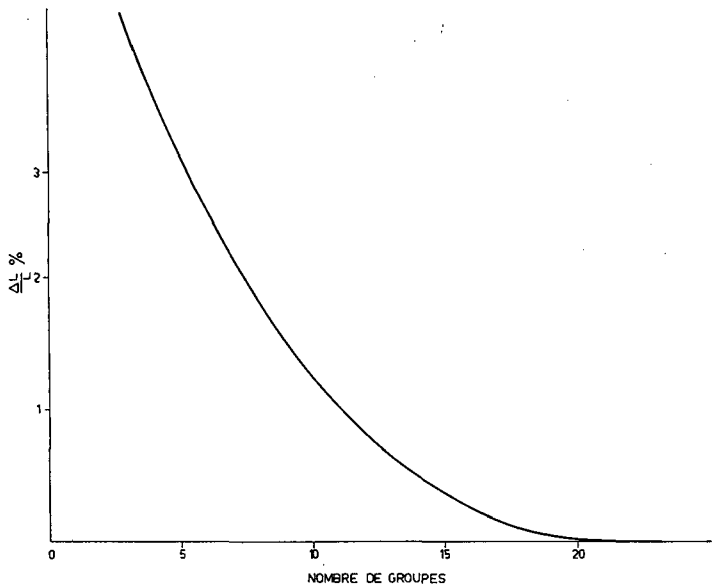


Figure 19
Erreur commise sur les valeurs calculées de la longueur de diffusion, en fonction du nombre de groupes d'énergie.

Nous avons pu ainsi tracer la courbe reproduite sur la figure 19. Nous voyons qu'un calcul à 10 groupes entraîne une erreur d'environ 1,2%, ce qui est raisonnable. Mais, dans un milieu comme l'uranium, il semble difficile de descendre au-dessous de 8 groupes en énergie; l'erreur commise serait alors supérieure à 2%.

### 4.2. Indice de spectre

Nous avons fait un tableau (tableau VI) comparant les résultats de nos mesures avec ceux des calculs faits avec une représentation mathématique plus ou moins valable, c'est-à-dire avec un nombre de groupes d'énergie plus ou moins grand.

TABLEAU VI

**INDICES DE SPECTRE**

| | Expérimental | 20 groupes | 10 groupes |
|---|---|---|---|
| $\sigma_f 5/\sigma_f 8$ | 230 ±10 | 220,7 | 191 |
| $\sigma_f 5/\sigma_f 7$ | 14 ± 0,5 | 15,4 | 12,6 |
| $\sigma_f 5/\sigma_f 3$ | 0,67 ± 0,003 | 0,63 | 0,63 |
| $\sigma_f 5/\sigma_f 9$ | 0,90 ± 0,05 | 0,92 | 0,90 |
| $\sigma_f 5/\sigma_{(n^{ln}, \gamma)}$ | 4,8 ± 0,1 | 5,2 | 5,3 |

Les divergences obtenues entre les résultats à 10 groupes et ceux à 20 groupes sont dues à l'étalement du spectre que nous constatons mieux sur le spectre lui-même.

### 4.3. SPECTRE ASYMPTOTIQUE

La même comparaison que pour les indices de spectre est faite sur la figure 20 pour les spectres asymptotiques expérimental et théorique à 20 et à 10 groupes en énergie. La figure 21 présente le spectre expérimental comparé à un spectre théorique à 5 groupes utilisant le même découpage en énergie.

Nous pouvons constater que lorsque l'on diminue le nombre de groupes d'énergie, le spectre des neutrons se trouve plus étalé sur l'échelle des énergies.

## Conclusion: bilan des mesures effectuées dans le monde sur l'uranium naturel

Nous avons rassemblé dans le tableau VII tous les résultats de mesures effectuées sur l'uranium naturel que nous avons pu trouver dans la littérature.

On peut noter un assez bon accord pour les indices de spectres, en particulier avec les résultats de Los Alamos (Pajarito). Par contre, l'accord est moins bon en ce qui concerne la longueur de diffusion, qui semble être un paramètre très sensible pour l'état d'équilibre.

Nous pensons que les buts que nous poursuivons ont été atteints bien que l'obtention de l'équilibre soit discutable. Toutefois, si une telle expérience était à reprendre, il serait souhaitable:

1. De pouvoir la monter de préférence loin de tout réflecteur afin d'améliorer les conditions aux limites (dispositif utilisé à Los Alamos) ou d'augmenter les dimensions du massif.

2. De disposer des conditions aux limites nettes et bien définies, dans le cas où il ne serait pas possible d'isoler le massif d'uranium, par exemple en l'enveloppant d'un massif d'acier; ce résultat était prévisible, mais nous nous attendions à une zone d'équilibre beaucoup plus nette avec le dispositif que nous avons utilisé.

Dans tous les cas, les méthodes de mesure développées ici sont parfaitement applicables; elles présentent l'avantage de déterminer de façon satisfaisante, bien qu'imparfaite, le spectre des neutrons, c'est-à-dire d'atteindre le flux des neutrons à différentes énergies, alors que généralement il était nécessaire de s'arrêter à la seule connaissance du flux intégré sur l'énergie par tel ou tel détecteur.

TABLEAU VII

**RÉCAPITULATION DES MESURES EFFECTUÉES SUR L'URANIUM NATUREL**

| Expérience | Référence | Principe de la mesure | Longueur de diffusion (mm) | $\frac{\sigma_f\ ^{235}U}{\sigma_f\ ^{238}U}$ | $\frac{\sigma_f\ ^{237}Np}{\sigma_f\ ^{238}U}$ | $\frac{\sigma_f\ ^{239}Pu}{\sigma_f\ ^{238}U}$ | $\frac{\sigma_f\ ^{235}U}{\sigma_f\ ^{233}U}$ | $\frac{\sigma_f\ ^{235}U}{\sigma_{n\gamma}\ In}$ |
|---|---|---|---|---|---|---|---|---|
| Saclay | — | Chambres à fission | | 230 ± 10 | 16,4 ± 1,2 | 256 ± 45 | 0,67 ± 0,003 | |
| | | Détecteurs à activation | 95,25 ± 0,5 | — | — | — | — | 4,8 ± 0,1 |
| Pajarito (Los Alamos) | [13] | Détecteurs à activation | 91,7 ± 1,8 | 238 ± 6 | 15 ± 2 | — | — | — |
| | | Radiochimie | — | 240 ± 12 | — | — | — | — |
| | | Chambres à fission | — | 243 ± 15 | 14,5 ± 0,1 | 250 ± 16 | — | — |
| Chicago | [14] | Chambres à fission | — | 200 | — | — | — | — |
| Oak Ridge | [15] | Détecteurs à activation | 96* | — | — | — | — | — |
| | | Chambres à fission | — | 336 | — | — | — | — |
| Argonne | [8] | Chambres à fission | 100 ± 12 | 363 ± 40 | — | — | — | — |
| | | Radiochimie | — | 220 | — | — | — | — |
| Pajarito | [16] | Détecteurs à activation | 131,8* 103,5* | 220 ± 22 | — | — | — | — |
| | | Radiochimie | — | 200 ± 10 | — | 228 ± 12 | — | — |
| | | Chambres à fission | — | 210 ± 10 | 15,9 ± 0,8 | — | — | — |
| URSS | [17] | Chambres à fission | — | 249 ± 20** | — | 230 ± *,** | — | — |

* La marge d'erreur n'est pas mentionnée.
** Valeurs données pour de l'U appauvri, corrigées pour l'U naturel.

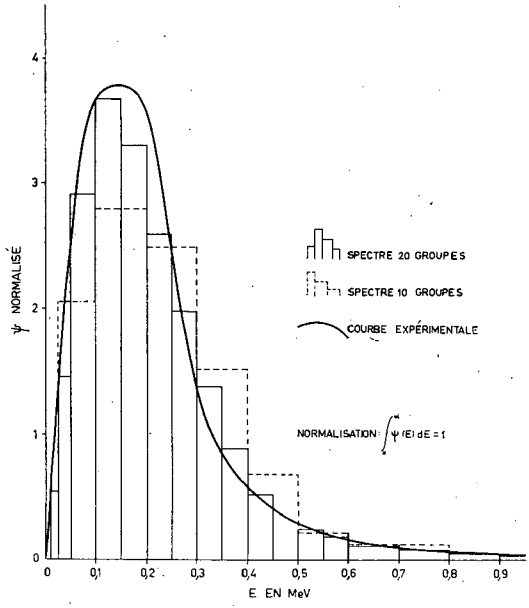


Figure 20
Comparaison des spectres théoriques à 20 et 10 groupes avec le spectre expérimental.

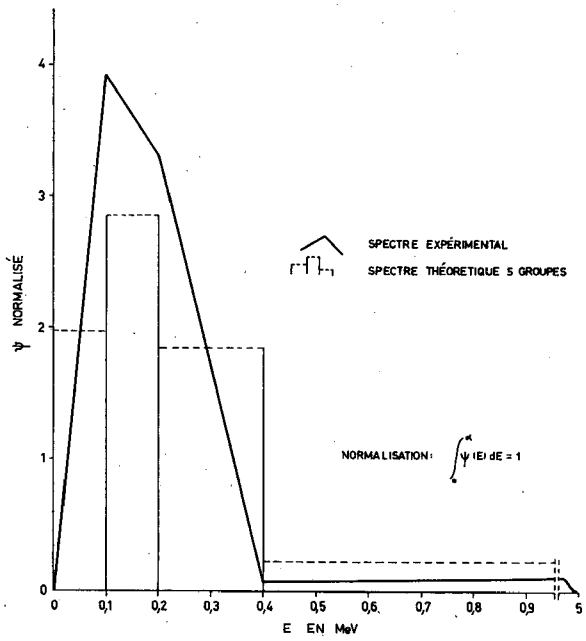


Figure 21
Spectre des neutrons au point d'abscisse 500 mm.

## RÉFÉRENCES

[1] CLAUZON, P. *et alii*, « Quelques résultats préliminaires des mesures faites sur un massif d'uranium naturel », Symposium de Harwell (1957).
[2] CAMPAN, J. L. *et alii*, «Expérience exponentielle rapide — Résultats préliminaires », note SNE n° 13.
[3] LAGO, B. *et alii*, « 48 $\Sigma$ — Calcul multigroupe de la propagation des flux neutroniques à travers des milieux multiplicateurs ou absorbants en géométrie plane », Section autonome de calcul arithmétique (DEP) n° 26, Groupe d'études de piles rapides (DRP) n° 60.129. — 173 $\Sigma$ (code à paraître).
[4] MENEGHETTI, D., HUMMEL, H. H. et LŒWENSTEIN, W. B., *Nucl. Sci. Engng* **3** (1958) 151—160.
[5] Reactor Physics Constants, ANL-5800, p. 417.
[6] KIEHN, R., Communication privée.
[7] AVERY, R., ANL-5492.
[8] MARTENS, F. H., ANL-5379.
[9] FISHER, G. J., Neutron Energy Spectrum Measurements in Unmoderated Assemblies, ANL.
[10] CAMPAN, J. L. *et alii*, «Etude expérimentale et théorique du spectre des neutrons dans un massif d'uranium naturel. Comparaison aux spectres calculés dans un réacteur rapide », Symposium de Risö (1960).
[11] BOILE, P. et CAMPAN, J. L., Mesures absolues à l'aide de chambres à fission dans un massif d'uranium naturel, Note interne CENS n° GEPR/59.35.
[12] GIACOMETTI, C., Programme Sigma-Aj. n° 2069/34, note interne SEPR/DRP/CENS n° R-275.
[13] CHEZEM, C. G., Neutron flux parameters of an uranium metal exponential experiment. Thesis submitted to Oregon State College.
[14] SNELL, A. H. *et alii*, Studies in a five ton metal pile, Rapport OR (1953).
[15] BROLLEY, J. R. *et alii*, Neutron multiplication in a massif of uranium metal, Rapport LA.
[16] NEVER, J. J. et STEWART, C. R., LA-2023.
[17] LEIPUNSKY, A. I. *et alii*, Proc. 2nd UN Int. Conf. PUAE **12** (1958) 3.
[18] Rapport CEA à paraître (expérience exponentielle rapide)
[19] BEETS, C. *et alii*. A paraître.
[20] ROSEN, L., *Nucleonics* **2** (1953) n° 7, p. 32 et n° 8, p. 38.
[21] BEETS, C., CEN, Bruxelles, R-1859.
[22] BEETS, C., CEN, Bruxelles, R-1351.

# FAST-NEUTRON SPECTRA BY THRESHOLD-DETECTOR ACTIVATION

O. W. Dietrich and J. Thomas
Atomenergikommissionen, Risø,
Denmark

## Abstract — Résumé — Аннотация — Resumen

**Fast-neutron spectra by threshold-detector activation.** Determination of fast-neutron spectra, by means of threshold detectors, has been under investigation.

A method, pointed out by Hartmann (1957), approximates the neutron flux by a linear combination of the response functions (cross-sections) of the detectors. Similar procedures can be made with simplified cross-sections (step-functions), as originally done by Hughes (1946), but assumption of the form of the spectrum is then required.

A new semi-empirical method is introduced in which the reactor spectrum is expressed as a product of the fission-neutron distribution and a parameter function that takes account of the deformation of the fission spectrum in the reactor to be expected theoretically.

Five threshold detectors have been activated in the DR-2 (Risø), and all interpretation methods are used and intercompared. The results show that, with this number of detectors, the semi-empirical method gives the most satisfactory information about the spectrum.

A drawback of the activation method is the few and, often, poorly known cross-sections.

**Détermination du spectre de neutrons rapides à l'aide de détecteurs à seuil.** Les auteurs ont cherché à déterminer le spectre de neutrons rapides à l'aide de détecteurs à seuil.

Une méthode, signalée par Hartmann (1957), permet d'obtenir une approximation du flux de neutrons par une combination linéaire des fonctions de réponse (sections efficaces) des détecteurs. On peut procéder de la même manière avec des sections efficaces simplifiées (fonction saut), comme l'avait fait initialement Hughes (1946), mais à la condition d'avoir une idée de la forme du spectre.

Les auteurs présentent une nouvelle méthode semi-empirique, dans laquelle le spectre du réacteur est exprimé comme le produit de la distribution des neutrons de fission par une fonction des paramètres qui tient compte de la déformation du spectre des neutrons de fission théoriquement prévue.

Les auteurs ont activé cinq détecteurs à seuil dans le DR-2 (à Risø); ils ont utilisé et comparé toutes les méthodes d'interprétation. Les résultats montrent qu'on obtient les meilleurs renseignements sur le spectre en utilisant la méthode semi-empirique avec ce nombre de détecteurs.

Un inconvénient de la méthode de l'activation tient à ce que l'on connaît peu de sections efficaces et qu'on les connaît souvent mal.

**Определение спектра быстрых нейтронов с помощью пороговых детекторов.** Проводилось исследование спектра быстрых нейтронов с помощью пороговых детекторов.

На основании указанного Хартманном в 1957 году метода проводится апроксимация нейтронного потока с помощью линейной комбинации ответных функций (поперечные сечения) детекторов. Аналогичные процедуры можно проделать с упрощенными поперечными сечениями (ступенчатые функции), как это первоначально было сделано Хьюзом в 1946 году, но в таком случае необходимо предположить форму спектра.

Вводится новый полуэмпирический метод, в котором спектр реактора выражается как продукт распределения нейтронов деления и как функция параметра, которая учитывает деформацию спектра деления в реакторе, предполагаемую на основе теоретических расчетов.

5 пороговых детекторов были активированы в датском реакторе DR-2 (Ризо), причем используются и сравниваются между собой все методы интерпретации. Результаты показывают, что с помощью такого числа детекторов полуэмпирический метод дает наиболее удовлетворительную информацию о спектре. Недостатком активационного метода является малое количество, к тому же часто слабоизученных поперечных сечений.

**Determinación de espectros de neutrones rápidos por activación de detectores de umbral.** Los autores han procurado determinar espectros de neutrones rápidos utilizando detectores de umbral.

El método propuesto por Hartmann (1957) permite obtener una aproximación del flujo neutrónico por combinación lineal de las funciones de respuesta (secciones eficaces) de los detectores. Se puede proceder del mismo modo con secciones eficaces simplificadas (funciones escalonadas), que es el método inicialmente empleado por Hughes (1946), pero para ello es necesario tener una idea de la forma del espectro.

Los autores describen un nuevo método semiempírico, en el que el espectro del reactor se expresa como el producto de la distribución de los neutrones de fisión y de una función de los parámetros en la que se tiene en cuenta la deformación del espectro de fisión en el reactor prevista teóricamente.

Los autores han activado 5 detectores de umbral en el reactor DR-2 (de Risø) y se han utilizado todos los métodos de interpretación, comparando sus resultados. Esos resultados demuestran que la información más satisfactoria sobre el espectro se obtiene utilizando el método semiempírico con el número de detectores indicado.

El método de activación presenta el inconveniente de que los datos sobre secciones eficaces que se poseen son escasos y, a menudo, carentes de precisión.

## Introduction

Activation measurements using threshold detectors offer the simplest means of obtaining data which can yield information on neutron spectra, especially inside a reactor. An important problem is the reduction of such data into a meaningful representation of the neutron spectrum.

In this report, two types of reduction methods are discussed: (*a*) methods in which an approximation to the flux spectrum is expressed as a linear combination of the cross-sections of the detectors, including methods with simplified cross-sections (such methods may be called mathematical methods), and (*b*) a semi-empirical method, in which the reactor spectrum is assumed to be a fission spectrum multiplied by a "hardening" function.

The discussion is based upon activation measurements using five threshold detectors, irradiated in a particular position in the core of the water-moderated reactor DR-2 (Risø).

## Threshold detectors

The conditions for the practical use of threshold detectors, including the knowledge of the cross-section functions, appeared to be fulfilled to a fair degree by the following five reactions:

$S^{32}$ (n, p) $P^{32}$
$P^{31}$ (n, p) $Si^{31}$
$Al^{27}$ (n, p) $Mg^{27}$
$Fe^{56}$ (n, p) $Mn^{56}$
$Al^{27}$ (n, $\alpha$) $Na^{24}$

The cross-section data for these reactions were taken from the compilation of HOWERTON [1] and the cross-section compilation BNL-325 [2]. The curves applied are depicted in Fig. 3.

As a check on the cross-section curves drawn, the average cross-sections in a fission spectrum, $\bar{\sigma}$, were calculated and compared with measured average cross-sections [3, 4] as shown in Table I. The deviations between calculated and measured average cross-sections are of about the same order of magnitude as the experimental uncertainties in the measurements of the differential cross-sections [1, 2].

TABLE I

**AVERAGE CROSS-SECTIONS IN A FISSION SPECTRUM**

*(millibarns)*

| | $S^{32}$ (n, p) | $P^{31}$ (n, p) | $Al^{27}$ (n, p) | $Fe^{56}$ (n, p) | $Al^{27}$ (n, $\alpha$) |
|---|---|---|---|---|---|
| $\bar{\sigma}$ calculated | 65.6 | 29.0 | 3.79 | 0.97 | 0.61 |
| $\bar{\sigma}$ measured (best value [4]) | 60 | 31 | 3.43 | 0.88<br>0.98 | 0.60 |

The activation integrals for the five detectors in the DR-2 flux were determined by using $4\pi$-$\beta$ and $4\pi\beta$-$\gamma$-coincidence counting. In the DR-2 records, the point of measurement is described as: Core no. 17, position D5 (element removed), centre, effect 1 MW.

The experimental uncertainties in the measurements are estimated at about 5%.

## Mathematical methods

Until recently, the use of threshold detectors was solely based upon the method of HUGHES (1946) [6].

Efforts have been made to reduce the dependence on simplified cross-sections and, in particular, on assumed flux distribution, which are necessary in the method of Hughes. This results in a method pointed out by HARTMANN (1957) [5], which is a generalization of Hughes' method, using the complete cross-section functions.

### EXPANSION WITH COMPLETE CROSS-SECTION FUNCTIONS

Following Hartmann, an approximation $\varphi'(E)$ to the real flux distribution $\varphi(E)$ is expanded in terms of a set of given functions $\psi_n(E)$:

$$\varphi'(E) = \sum_{n=1}^{K} a_n \psi_n(E) \tag{1}$$

where

$E$ = neutron energy (in MeV)
$a_n$ = expansion coefficient
$K$ = the total number of $\psi$ functions.

The criterion for determining $\varphi'(E)$, which forms the basis of the method, is the minimization of the mean square deviation

$$\varepsilon = \int (\varphi(E) - \varphi'(E))^2 \, dE \tag{2}$$

integrated over the expansion region.

Having in mind that the information concerning the neutron flux $\varphi(E)$, which is experimentally determined, are the activation integrals, $A_j$, defined by

$$A_j = \int_{E_{Tj}}^{\infty} \varphi(E) \, \sigma_j(E) \, dE \qquad (j = 1, \ldots, N) \tag{3}$$

where

$\sigma_j$ = the cross-section function for detector $j$
$E_{Tj}$ = the threshold energy for detector $j$
$N$ = the number of detectors

the minimization procedure is only possible if all the functions $\psi_n(E)$ are linear combinations of the cross-section functions for the detectors used in the spectral measurement.

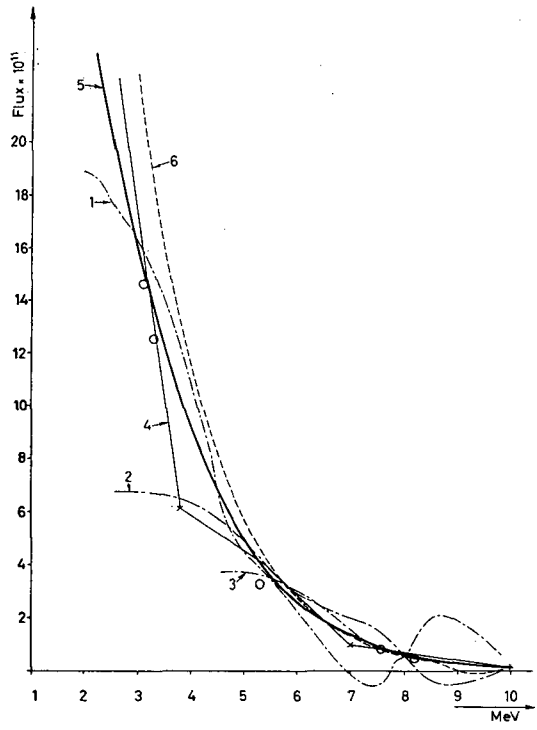


Fig. 1
Integral approximations to reactor spectrum.

Thus

$$\psi_n(E) = \sum_{j=1}^{N} q_{nj}\,\sigma_j(E) \quad (n=1, \ldots, K) \tag{4}$$

where $q_{nj}$ = expansion coefficient.

Naturally, $K$ is chosen equal to $N$, and thus—besides making the mean square deviation a minimum—the approximation $\varphi'(E)$ will be the only function of the form (1) which gives the correct calculated activities for the detectors.

Necessarily, the lower end of the approximation interval is the lowest threshold energy. The upper end may, for practical purposes, be stated at a finite energy.

Using four threshold detectors*, this procedure has been carried out, and the integral approximation

$$\int_E^{\infty} \varphi'(E)\,\mathrm{d}E \tag{5}$$

is drawn as curve number 1 in Fig. 1.

The smaller the interval over which the reactor spectrum $\varphi(E)$ is approximated, the more restricted the range will be in magnitude over which it varies. Since the criterion for determining $\varphi'(E)$ is minimum mean square deviation and not minimum mean square relative deviation**, the mean square deviation might be smaller in some region when the detectors with lowest threshold energy are eliminated, and therefore the lower energy of the approximation interval is increased. Certainly, at the same time the functions available to approximate $\varphi(E)$ decrease.

Curves 2 and 3 in Fig. 1 are integral approximations where the detectors $S^{32}$ (n, p) $P^{32}$ and $S^{32}$ (n, p) $P^{32} + Al^{27}$ (n, p) $Mg^{27}$, respectively, are eliminated.

STEP-FUNCTIONS FOR CROSS-SECTIONS

The analytical expressions for the coefficients $a_n$ in equation (1) take a simple form when the cross-sections beforehand are approximated by step-functions. It has been proposed to make this approximation in two ways:

(*a*) The approximation interval is divided into $N$ regions ($N$ = the number of detectors), and all the cross-sections and the unknown flux $\varphi(E)$ are averaged in each region.

Let $\sigma_{ji}$ denote the average cross-section for detector $j$, and $\varphi_i$ denote the average flux in region $i$.

Then the activation integrals, $A_j$, are approximated by the sum***

$$A_j = \sum_{i=1}^{N} \varphi_i \sigma_{ji} \quad (j = 1, \ldots, N). \tag{6}$$

This forms a set of linear equations which can be solved with regard to $\varphi_i$ ($i$ = 1, ..., N)****.

---

* $P^{31}$ (n, p) $Si^{31}$ has been omitted because the cross-section for this reaction is nearly proportional to the cross-section for the reaction $S^{32}$ (n, p) $P^{32}$.

** It is impossible to minimize the mean square relative deviation.

*** Only correct if $\sigma_{ji}$ is an average, weighted to the flux distribution.

**** The cross-section functions are assumed linearly independent.

This approximation $\varphi_i$ to $\varphi(E)$ will be a linear combination of some step-functions, which evidently are expressed in terms of the cross-sections. Since the approximation $\varphi_i$ is determined to give the correct activities, the mean square deviation is automatically minimized (see above) with the chosen regions.

The problem of minimization with regard to the choice of regions still exists.

Curve 4 in Fig. 1 is a step-function integral approximation worked out in this manner, using four detectors.

(*b*) A further approximation for the cross-sections can be obtained by using one-step functions. This simplification (originally introduced by Hughes) requires the knowledge of the flux distribution in some region over the threshold energies.

A reasonable guess for the flux spectrum is the fission-neutron distribution. Commonly, $E_{\text{eff}}$ denotes the step-energy for this simplified cross-section in the fission spectrum, and $\sigma_0$ denotes the step-height. These two quantities are calculated for the five detectors. The results are tabulated in Table II.

The circular points in Fig. 1 show the integral approximation by this method.

TABLE II

**ONE-STEP-FUNCTION CONSTANTS**

| | $S^{32}$ (n, p) | $P^{31}$ (n, p) | $Al^{27}$ (n, p) | $Fe^{56}$ (n, p) | $Al^{27}$ (n, $\alpha$) |
|---|---|---|---|---|---|
| $E_{\text{eff}}$ (MeV) | 3.3 | 3.1 | 5.4 | 7.6 | 8.2 |
| $\sigma_0$ (mb) | 354 | 141 | 88 | 115 | 113 |

## Semi-empirical methods

The methods mentioned in the preceding section were all based on the use of the experimental cross-sections for the threshold detectors as a basis for the flux determination. The two first methods relied solely on the shapes of the individual cross-section curves, the latter (historically the first), i.e. the method of Hughes, utilized also the knowledge of the fission spectrum.

In this section, we shall introduce a semi-empirical method, which relates calculated spectral shapes to the activation measurements. In general, we may state that, leaving the preceding methods, it is necessary to renounce the criterion of minimum mean square deviation. Instead, we use as a criterion for the best approximation: best correspondence between calculated and measured activities.

Previously, UTHE [7] has proposed a semi-empirical method in which he expands the approximation to $\varphi(E)$ in terms of functions which closely approximate the form of the expected neutron flux.

In the semi-empirical method here presented, the reactor spectrum is written as a product of a fission-neutron distribution and a one-parameter function, which takes account of the deformation of the fission spectrum in the reactor to be expected theoretically.

Thus,

$$\varphi(E) = \mathrm{f}\,(\alpha, E)\ S\,(E) \tag{7}$$

where

$S(E)$ = the fission neutron distribution

$\alpha$ = a parameter.

$f(\alpha, E)$ has been established from a simple type of removal theory, normally used in shielding calculations. The total reactor cross-section for neutrons is assumed to be a sum of a constant cross-section and an energy-dependent cross-section,

$$\Sigma_{\text{total}} = \Sigma_0 + \Sigma(E) . \tag{8}$$

In $\Sigma_0$ are included inelastic and absorption cross-sections for all materials in the reactor core except hydrogen, and $\Sigma(E)$ is simply the (n-p)-scattering cross-section.

Between 2 and 12 MeV, $\sigma_{\text{el}}$ (n-p) is well fitted by the function [8]

$$E^{-0.725}. \tag{9}$$

The removal theory is used in the sense that a neutron having once collided is lost for the fast spectrum. Considering the reactor core to be homogeneous and infinitely great, the spectrum will be

$$\varphi(E) = \frac{S(E)}{\Sigma_0 + \Sigma(E)} . \tag{10}$$

Therefore, the function $f(\alpha, E)$ is specified as

$$\frac{1}{1 + \alpha E^{-0.725}} \tag{11}$$

For varying $\alpha$, the activation integrals for the detectors are calculated. As a criterion for the best approximation, the minimized standard deviation between calculated activities divided by measured activities for the five detectors is used.

This standard deviation for varying $\alpha$ is depicted as a fully drawn curve in Fig. 2. As seen, the curve has a minimum of $\alpha = 11$. The integral approximation to $\varphi(E)$ for $\alpha = 11$ is shown as curve no. 5 in Fig. 1.

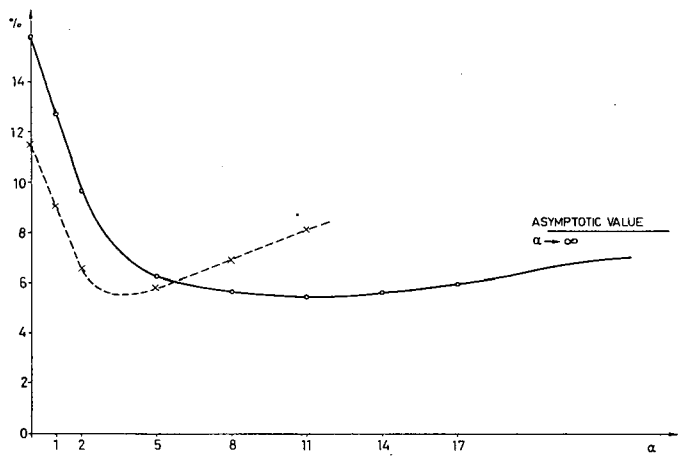


Fig. 2
Standard deviation between calculated and measured activities for the five threshold detectors used.

$\alpha$ has been calculated theoretically [9], and the result for homogeneous reactor core is 2.7. For water, the value is 10.4. The experimental facility is placed in a water lattice*, and the correctly calculated value is therefore expected to lie between the two values mentioned.

## Uncertainties

How the uncertainties originating from the cross-section curves propagate in the approximations has not been calculated for the following reasons: (*a*) the statements of uncertainties on different measured cross-sections are often disagreeing and therefore difficult to evaluate, and (*b*) the calculations would be tedious because the uncertainties vary with energy.

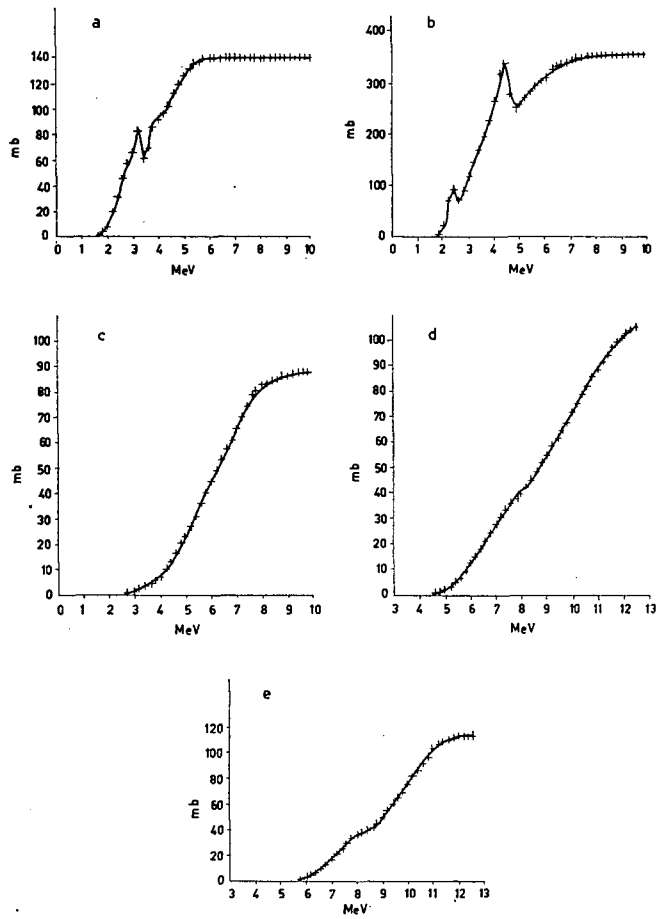


Fig. 3
Cross-sections for the threshold detectors. *a*: $P^{31}$ (n, p) $Si^{31}$ — *b*: $S^{32}$ (n, p) $P^{32}$ — *c*: $Al^{27}$ (n, p) $Mg^{27}$ — *d*: $Fe^{56}$ (n, p) $Mn^{56}$ — *e*: $Al^{27}$ (n, $\alpha$) $Na^{24}$.

* About 3.5 cm from U-Al plates in all horizontal directions.

The effects from uncertainties in the activation measurements, on the other hand, can be calculated in a relatively simple way. The results have different effects in the different methods.

*In the method of Hartmann*, only the maximum possible error has been calculated*. It appears to be a strongly oscillating function of energy. Especially in the higher end of the spectrum, the uncertainties are immense.

*In the method using the step-function approximation* for the cross-sections, the uncertainties still propagate in the spectrum approximation in a terrible manner. For instance, a 5% smaller activity measured for the $Al^{27}$ (n, p) $Mg^{27}$ reaction will cause a negative "flux" in the region from 3.8—5.4 MeV.

*In the method of Hughes*, each point (see Fig. 1) is encumbered with an uncertainty equal to the uncertainty in the measurement.

*For the semi-empirical method*, the propagation is a little more complicated with regard to the uncertainty in $\alpha$. Changes in the activities will modify the minimization curve in Fig. 2. It has been tried to attribute to each activity the maximal change. That is, 5% higher activities on the two detectors with lowest threshold energies, and 5% smaller activities on the two detectors with the highest threshold energies. The changed "standard deviation *versus* $\alpha$" is drawn as a stippled curve in Fig. 2. The minimum now lies at about 4. The form of the approximation is expected to vary slowly with $\alpha$ over the minimum region. The chosen changes in activities barely force $\alpha$ out of the very large minimum region, and therefore the uncertainty in $\alpha$ will be neglected. The activity uncertainties then only propagate in the normalization constant of the approximation. Here a 5% uncertainty in each measurement will give rise to an overall 2% uncertainty in the spectrum curve.

## Remarks

1. On Fig. 1 is drawn an integrated fission spectrum (curve 6), normalized to give the correct activity for the detector $Al^{27}$ (n, $\alpha$) $Na^{24}$. It is seen that the "hardening" of the spectrum is considerable: at about 3 MeV the measured differential flux is nearly one half of the undisturbed fission flux.

2. The method of Hartmann appears to be rather unsuitable for application. First, the strong oscillations are a disagreeable property, especially in the higher end of the spectrum where negative "fluxes" may occur**. This is due to the unsuitable shape of threshold cross-sections for approximating flux spectra. Furthermore, the method lacks a condition making the approximation positively definite. Finally, the uncertainties propagate in a disagreeable manner.

3. The step-function approximation must be rejected because the uncertainties propagate in a violent manner.

4. The method of Hughes seems to approximate quite well in spite of the rather rough assumptions required.

5. The semi-empirical method came out as the most satisfactory procedure. First, the minimum standard deviation between calculated activities divided by measured activities is of the same order of magnitude as the experimental uncertainties. Secondly, the properties of the physical quantity measured have been

* All uncertainties add up. The real uncertainty is unreasonably troublesome to calculate.

** Negative "fluxes" occur even with seven detectors as used in the computation by Hartmann.

taken into consideration (e.g. negative "fluxes" impossible). Thirdly, the uncertainties from the activity measurements propagate in an opportune manner.

6. The point at 5.4 MeV in Fig. 1, resulting from the method of Hughes, is evidently too low. The reason must be a too large cross-section curve for the reaction $Al^{27}$ (n, p) $Mg^{27}$. This agrees with the average cross-sections tabulated in Table I.

It is desirable that the cross-section curve for $Al^{27}$ (n, p) $Mg^{27}$ could be measured again. Altogether, the methods would gain in usefulness if more and better known cross-sections were available.

## ACKNOWLEDGEMENT

The authors wish to thank Prof. O. Kofoed-Hansen for valuable discussion and for supporting the work described in this report.

## REFERENCES

[1] HOWERTON, R. J., Tabulated Neutron Cross-Sections, Part 1. 0.001—14.5 MeV, UCRL-5226 (1958).
[2] HUGHES, D. J. and SCHWARTZ, R. B., Neutron Cross-Sections, BNL-325 (1958).
[3] ROCHLIN, R. S., *Nucleonics* **17** (1959) 55.
[4] MELLISH, C. E., "Threshold" Reaction Cross-Sections in Reactors, An Intercomparison, AERE/R-3251 (1960).
[5] HARTMANN, S. R., A Method for Determining Neutron Flux Spectra from Activation Measurements, WADC-Technical Report 57—375 (PB-131611) (1957).
[6] HUGHES, D. J., Pile Neutron Research, Addison-Wesley (1953).
[7] UTHE, P. M., Attainment of Neutron Flux-Spectra from Foil Activations, WADC-Technical Report 57-3 (1957).
[8] ROCKWELL, TH., Reactor Shielding Design Manual 3, Van Nostrand (1956).
[9] OLSEN, A., Private communication (Risø, 1960).

# PROPAGATION A LONGUE DISTANCE DE FLUX DE NEUTRONS DANS LES RÉACTEURS A NEUTRONS RAPIDES

A. Kania, R. Pasquet, P. Pépin, J. Rastoin et M. Solanes
Centre d'études nucléaires de Saclay,
France

**Abstract — Résumé — Аннотация — Resumen**

**Long-range neutron-flux propagation in fast reactors.** Methods for calculation of long-range neutron-flux transmission in fast reactors are first described. Then an attempt is made to determine the accuracy of the results obtained, taking into account the fact that the cross-sections are not known with certainty and that the calculation codes involve finite difference equations instead of differential analytic equations. The methods, when thus worked out in detail, are used to trace neutron-flux attenuation in mock-ups representing the RAPSODIE reactor shielding, and the results obtained by calculation are compared with experimental data.

**Propagation à longue distance de flux de neutrons dans les réacteurs à neutrons rapides.** On décrit en premier lieu les méthodes de calcul utilisées pour calculer la transmission à longue distance de flux neutroniques dans les réacteurs à neutrons rapides. On s'attache ensuite à définir la précision des résultats que l'on obtient en tenant compte des incertitudes sur la connaissance des sections efficaces et de ce que les codes de calcul traitent des équations aux différences finies au lieu d'équations analytiques différentielles. Les méthodes ainsi mises au point sont utilisées pour suivre l'atténuation de flux de neutrons dans des maquettes représentant la protection du réacteur RAPSODIE et les résultats obtenus par le calcul sont comparés à des mesures expérimentales.

**Распространение на большое расстояние потока нейтронов реакторов на быстрых нейтронах.** Прежде всего дается описание вычислительных методов, использовавшихся для расчета распространения на большое расстояние потока нейтронов в реакторах на быстрых нейтронах. Затем определяется точность полученных результатов с учетом погрешностей данных эффективных сечений и того, что вычислительные коды решают уравнения с конечными разностями вместо аналитических дифференциальных уравнений. Разработанные методы используются для того, чтобы проследить ослабление потока нейтронов в макетах, имитирующих защиту реактора РАПСОДИЯ, и результаты, полученные при помощи вычисления, сравниваются с экспериментальными измерениями.

**Propagación a larga distancia del flujo neutrónico en los reactores rápidos.** Los autores describen, en primer lugar, los procedimientos empleados para calcular la transmisión a larga distancia del flujo neutrónico en los reactores rápidos. Seguidamente definen la precisión de los resultados obtenidos teniendo en cuenta la incertidumbre en el conocimiento de las secciones eficaces y el hecho de que las claves de cómputo se refieren a ecuaciones de diferencias finitas en lugar de a ecuaciones analíticas diferenciales. Los citados procedimientos se utilizan para estudiar la atenuación del flujo de neutrones en maquetas representativas del blindaje del reactor RAPSODIE, y los resultados obtenidos por cálculo se comparan con los de las mediciones experimentales.

## Introduction

Le problème de la propagation du flux neutronique peut se poser d'une façon assez aiguë dans certains types de réacteurs rapides. La petitesse du cœur y donne en effet lieu à des fuites importantes de neutrons qui doivent ensuite être arrêtés dans les couches des protections où ils se manifestent par un dégagement de chaleur. Si on doit évacuer ce dernier par un système de refroidissement auxiliaire indépendant — ce qui sera peut-être le plus avantageux pour les piles rapides de puissance — il est nécessaire de définir avec précision la puissance calorifique dégagée, afin de ne pas avoir à construire des installations surdimensionnées: celles-ci ne sont pas souhaitables, non seulement d'un point de vue économique, mais aussi à cause des nombreuses canalisations supplémentaires qu'elles introduisent et qui rendent plus difficile le problème de la mise en place de la protection biologique.

Par ailleurs, l'absence de modérateur fait que les neutrons ont des énergies intermédiaires entre celles de la fission et du domaine thermique. De leur distribution spectrale en chaque point dépend l'activation du réfrigérant primaire (Na, NaK, etc.) qui baigne le cœur. Celle-ci joue un rôle important dans l'évaluation de la quantité de chaleur à évacuer par le système de refroidissement auxiliaire et dans les problèmes de protection biologique au niveau des échangeurs primaires.

Le problème de la propagation du flux à longue distance qui se pose, et qui se ramène à celui de la connaissance en chaque point du flux et de son spectre, peut être abordé soit théoriquement soit par des moyens expérimentaux. Nous décrivons dans ce mémoire les méthodes de calcul utilisées, en insistant sur les facteurs dont dépend leur précision, et nous leur comparons les résultats de mesures expérimentales effectuées sur des maquettes de certaines parties du réacteur RAPSODIE, grâce auxquelles la transmission dans le sodium et le fer a pu être étudiée.

## Méthodes de calcul

Les calculs ont été effectués à l'aide du code multigroupe, dont nous donnons en premier lieu quelques caractéristiques.

### Code de calcul utilisé

Nous avons utilisé un code de résolution multigroupe de l'équation de la diffusion, écrit à cet effet pour ordinateur Ferranti-Mercury par le Service de calcul électronique du Commissariat à l'énergie atomique [1]. L'équation traitée par le code en géométrie plane est:

$$D_i(k)\,\nabla^2\Phi_i(x) + \left[\Sigma_{\mathrm{a},i}(k) + \Sigma_{\mathrm{er},i}(k)\right]\Phi_i(x) = \Sigma_{\mathrm{er},i-1}(k)\,\Phi_{i-1}(x) + \\ + \sum_{j=1}^{j=i-1} \Sigma_{\mathrm{in},j\to 1}(k)\,\Phi_j(x)$$

dans laquelle:

$\Phi_i(x)$ est au point d'abscisse $x$ le flux dans le groupe d'énergie $i$,

$D_i(k)$ est le coefficient de diffusion du milieu $k$ considéré,

$\Sigma_{\mathrm{er},i}(k)$ et $\Sigma_{\mathrm{in},\,i\to 1}(k)$, sont respectivement dans le milieu $k$ les sections efficaces de transfert élastique du groupe $i$ au groupe $i+1$, de transfert inélastique du groupe $j$ au groupe $i$,

$\Sigma_{a,i}(k)$ est appelée section efficace d'absorption.

$$\Sigma_{a,i}(k) = \Sigma_{c,i}(k) + \Sigma_{in,i}(k)$$

relation dans laquelle $\Sigma_{c,i}(k)$ représente la capture parasite et où

$$\Sigma_{in,i}(k) = \sum_{j>i} \Sigma_{in,i\to j}(k).$$

Entre deux milieux consécutifs, il y a bien entendu continuité du flux et de courant. Les conditions aux limites sont, d'une part, la donnée des flux dans chaque groupe à la première face du premier milieu, et, d'autre part, une condition exprimant que le dernier milieu physique $k$ est suivi d'un milieu fictif $k+1$ semblable en tout au milieu $k$, à ceci près qu'il n'y a pas de transfert de neutrons d'un groupe d'énergie à un autre. Cette condition est:

$$\frac{d\Phi_i(X)}{dx} = \Phi_i(X)\sqrt{\frac{\Sigma_{a,i}(k) + \Sigma_{er,i}(k)}{D_i(k)}}$$

où $X$ est l'abscisse de la limite entre le milieu $k$ et $k+1$.

Le code permet d'effectuer des calculs à 50 groupes d'énergie au maximum, dans des ensembles plans ne comportant pas plus de 20 régions*. Il permet de plus d'obtenir les réponses de détecteurs infiniment minces qui ne perturberaient pas le flux à l'endroit où ils seraient placés, en calculant les quantités

$$R_l(x) = \sum_k \Sigma_{l,i}\Phi_i(x)$$

où $\Sigma_{l,i}$ représente dans le groupe $i$ la section de capture du détecteur $l$.

## Cas étudiés

Nous nous sommes essentiellement intéressés à l'étude de la transmission de flux tels qu'on peut les trouver à la sortie des couvertures de piles rapides, où les neutrons, à la suite de nombreux chocs qu'ils ont déjà subis depuis leur génération, ont une énergie moyenne de 100 keV. Les figures 1 et 2 représentent les spectres de neutrons à partir desquels toutes les études de transmission dans le sodium (fig. 1) et le fer (fig. 2) ont été faites.

Il s'ensuit que certaines des conclusions auxquelles nous aboutissons ne seraient peut-être pas transposables sans modification à des neutrons d'énergie moyenne beaucoup plus élevée.

L'emploi d'un code donne des résultats qui dépendent d'un certain nombre de facteurs dont nous voulons précisément étudier l'influence, et qui sont:

---

* En fait, le nombre de groupes, de régions, ne sont pas indépendants. Ils sont liés par la relation $KI^2 + 12K + IN + 6N - \frac{5Y}{2} - \frac{I2}{2} < 8{,}700$, où

| | |
|---|---|
| $I$ est le nombre maximal de groupes d'énergie | $I \leq 50$ |
| $K$ est le nombre maximal de régions | $K \leq 20$ |
| $N_k$ est le nombre maximal de points par région | $N_k \leq 100$ |
| $N = \sum_k N_K$ est le total de points | $N < 500.$ |

*a*) le pas d'intégration, *b*) le nombre de groupes, *c*) le remplacement des équations de la diffusion par des équations aux différences finies, et *d*) les valeurs des sections efficaces.

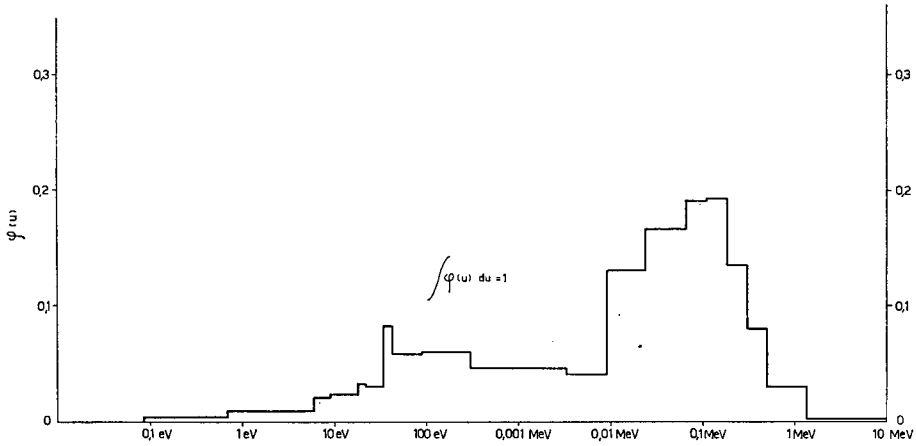


Figure 1
Spectre de neutrons utilisé pour l'étude de transmission dans le sodium.

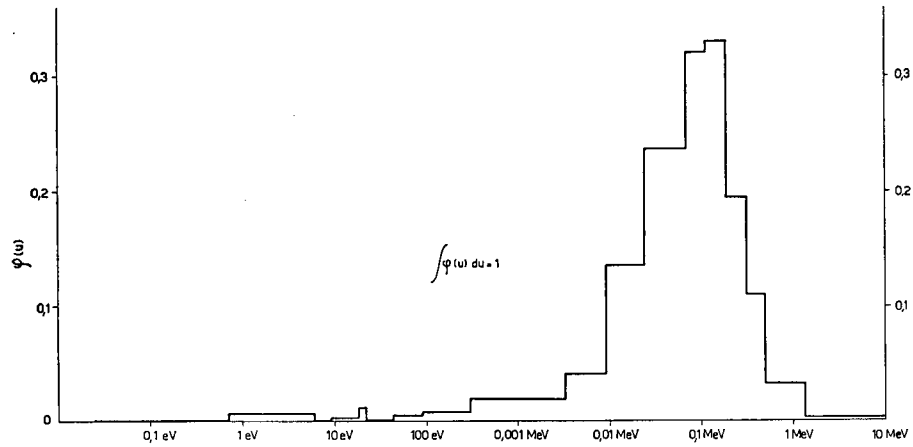


Figure 2
Spectre de neutrons utilisé pour l'étude de transmission dans le fer.

*Influence du pas d'intégration*

Puisque nous nous intéressons essentiellement aux neutrons d'énergie inférieure à 100 keV, nous utilisons un découpage fin au-dessous de cette limite, et nous prenons les sections efficaces correspondant à 20 groupes établies à partir d'un jeu provenant d'Atomics Power Development Associates (tableaux I et II). Plusieurs calculs de transmission dans un bloc plan semi-infini de sodium pur ont été faits, qui différaient entre eux uniquement par le pas d'intégration choisi. Les résultats de l'un d'entre eux sont portés sur la figure 3 où, à partir de

TABLEAU I

**DÉCOUPAGE EN ÉNERGIE ET SECTIONS EFFICACES MACROSCOPIQUES DU SODIUM**

| Numéro du groupe | Découpe en énergie | $Di$ (cm) | $\bar{\Sigma}_{a,i}$* (cm$^{-1}$) | $\Sigma_{er,\,i}$ (cm$^{-1}$) | $\Sigma_{in,\,i\to i+k}$ (cm$^{-1}$) | | | | | |
|---|---|---|---|---|---|---|---|---|---|---|
| | | | | | $k=1$ | $k=2$ | $k=3$ | $k=4$ | $k=5$ | $k=6$ |
| 1 | 10 —1,35 MeV | 6,96 | 0,0097 | 0,0024 | 0,0053 | 0,0010 | 0,0005 | 0,0003 | 0,0001 | 0 |
| 2 | 1,35—0,498 MeV | 4,35 | 0,0087 | 0,0044 | 0,0031 | 0,0006 | 0,0003 | 0,0002 | 0,0001 | — |
| 3 | 498 —302 keV | 4,64 | 0,0122 | 0,0122 | — | — | — | — | — | — |
| 4 | 302 —183 keV | 3,98 | 0,0143 | 0,0143 | — | — | — | — | — | — |
| 5 | 183 —111 keV | 4,64 | 0,0122 | 0,0122 | — | — | — | — | — | — |
| 6 | 111 —67,4 keV | 4,22 | 0,0135 | 0,0135 | — | — | — | — | — | — |
| 7 | 67,4—24,8 keV | 3,48 | 0,0082 | 0,0082 | — | — | — | — | — | — |
| 8 | 24,8—9,12 keV | 3,09 | 0,0092 | 0,0092 | — | — | — | — | — | — |
| 9 | 9,12—3,35 keV | 0,93 | 0,0310 | 0,0306 | — | — | — | — | — | — |
| 10 | 3,35—0,3 keV | 1,74 | 0,0086 | 0,0068 | — | — | — | — | — | — |
| 11 | 300 —90 eV | 4,64 | 0,0051 | 0,0050 | — | — | — | — | — | — |
| 12 | 90 —43 eV | 4,64 | 0,0085 | 0,0084 | — | — | — | — | — | — |
| 13 | 43 —34 eV | 4,64 | 0,0184 | 0,0179 | — | — | — | — | — | — |
| 14 | 34 —22 eV | 4,64 | 0,0182 | 0,0179 | — | — | — | — | — | — |
| 15 | 22 —18 eV | 4,64 | 0,0308 | 0,0304 | — | — | — | — | — | — |
| 16 | 18 —9 eV | 4,64 | 0,0090 | 0,0088 | — | — | — | — | — | — |
| 17 | 9 —6 eV | 4,64 | 0,0153 | 0,0148 | — | — | — | — | — | — |
| 18 | 6 —0,7 eV | 4,64 | 0,0038 | 0,0028 | — | — | — | — | — | — |
| 19 | 0,7—0,085 eV | 4,64 | 0,0059 | 0,0028 | — | — | — | — | — | — |
| 20 | 0,085 eV | 4,64 | 0,0083 | 0 | — | — | — | — | — | — |

* $\bar{\Sigma}_{a,\,i} = \Sigma_{a,\,i} + \Sigma_{er,\,i}$.

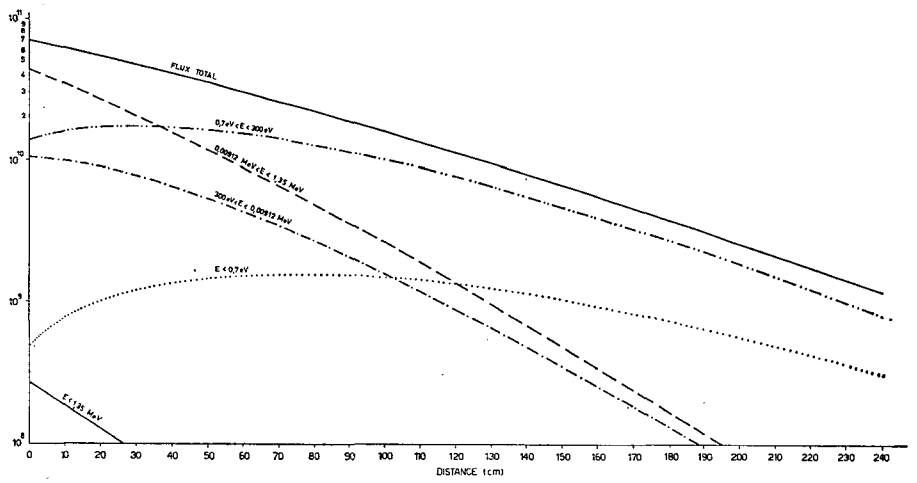


Figure 3
Transmission du flux neutronique dans le sodium. Cas type. Géométrie plane semi-infinie. 20 groupes. Pas d'intégration: 4 cm.

TABLEAU II

**SECTIONS EFFICACES MACROSCOPIQUES DU FER**

| Numéro du groupe $i$* | Di (cm) | $\Sigma_{a,\,i}$** (cm$^{-1}$) | $\Sigma_{er,\,i}$ (cm$^{-1}$) | $\Sigma_{in,\,i\to i+k}$ (cm$^{-1}$) | | | | | |
|---|---|---|---|---|---|---|---|---|---|
| | | | | $k=1$ | $k=2$ | $k=3$ | $k=4$ | $k=5$ | $k=6$ |
| 1 | 1,96 | 0,0627 | 0,0032 | 0,0419 | 0,0081 | 0,0045 | 0,0024 | 0,0012 | 0,0008 |
| 2 | 1,87 | 0,0313 | 0,0145 | 0,0031 | 0,0067 | 0,0035 | 0,0018 | 0,0013 | — |
| 3 | 1,23 | 0,0195 | 0,0193 | — | — | — | — | — | — |
| 4 | 1,23 | 0,0195 | 0,0193 | — | — | — | — | — | — |
| 5 | 1,23 | 0,0195 | 0,0193 | — | — | — | — | — | — |
| 6 | 1,12 | 0,0220 | 0,0211 | — | — | — | — | — | — |
| 7 | 1,31 | 0,0093 | 0,0091 | — | — | — | — | — | — |
| 8 | 1,31 | 0,0093 | 0,0091 | — | — | — | — | — | — |
| 9 | 0,562 | 0,0220 | 0,0212 | — | — | — | — | — | — |
| 10 | 0,479 | 0,0110 | 0,0103 | — | — | — | — | — | — |
| 11 | 0,351 | 0,0305 | 0,0279 | — | — | — | — | — | — |
| 12 | 0,348 | 0,0517 | 0,0466 | — | — | — | — | — | — |
| 13 | 0,348 | 0,1067 | 0,0999 | — | — | — | — | — | — |
| 14 | 0,348 | 0,1076 | 0,0999 | — | — | — | — | — | — |
| 15 | 0,348 | 0,1787 | 0,1694 | — | — | — | — | — | — |
| 16 | 0,348 | 0,0601 | 0,0490 | — | — | — | — | — | — |
| 17 | 0,348 | 0,0974 | 0,0822 | — | — | — | — | — | — |
| 18 | 0,348 | 0,0381 | 0,0155 | — | — | — | — | — | — |
| 19 | 0,342 | 0,0822 | 0,0155 | — | — | — | — | — | — |
| 20 | 0,320 | 0,1770 | 0 | — | — | — | — | — | — |

* Même découpage énergétique que pour le sodium (cf Tableau I).
** $\Sigma_{ai} = \Sigma_{ai} + \Sigma_{eri}$

20 groupes, on a regroupé les neutrons en cinq catégories afin de rendre le dessin lisible. On a suivi également en fonction de l'abscisse x dans le sodium les variations des sections efficaces de fission de $^{235}U$ et de $^{238}U$ moyennées par la relation

$$\bar{\sigma}_{f\,^{235}U}(x) = \frac{\sum_i \sigma_{f,\,i\,^{235}U}\,\Phi_i(x)}{\sum_i \Phi_i(x)} \quad \bar{\sigma}_{f^{238}U} = \frac{\sum_i \sigma_{f,\,i\,^{238}U}\,\Phi_i(x)}{\sum_i \Phi_i(x)}$$

dont les valeurs en chaque point sont des indices de la dureté du spectre.

Aussi longtemps que le pas varie dans des limites raisonnables, c'est-à-dire entre 1 et 10 cm, les résultats en sont peu affectés, ainsi que le montre le tableau III où l'on compare, pour différents pas, les flux et indices de spectre en deux points situés à 80 et 160 cm de l'entrée du bloc.

De même, une étude semblable bien qu'incomplète (le nombre de calculs effectués n'ayant pu à ce jour être aussi élevé qu'on l'aurait voulu) nous a montré que les résultats de transmission dans le fer dépendent peu du pas aussi longtemps qu'il est compris entre 10 et 5 cm.

*Influence du nombre de groupes*

Lorsque les sections efficaces présentent des résonances nombreuses, ce qui est toujours le cas en pratique, il est certain que le calcul pour en tenir compte doit être mené à l'aide d'un nombre de groupes très élevé, utilisant un découpage en énergie très fin. Dans ce cas, en effet, les équations des calculs multigroupes

TABLEAU III

**INFLUENCE DU PAS D'INTÉGRATION — TRANSMISSION DANS LE SODIUM ET LE FER**

| | $n$ (cm) | Pas (cm) | $\Phi_1$ | $\Phi_2$ | $\Phi_3$ | $\Phi_4$ | $\Phi_5$ | $\Phi_{tot}$ | $\sigma_f^{235}U$ (b) | $\sigma_f^{238}U$ (mb) |
|---|---|---|---|---|---|---|---|---|---|---|
| | Flux incident | Domaine d'énergie | 10—1,35 MeV | 1,35MeV—9,12keV | 9,12–0,3keV | 300—0,7 eV | <0,7 eV | — | — | — |
| SODIUM | | à l'entrée | $2{,}71\cdot10^{8}$ | $4{,}39\cdot10^{10}$ | $1{,}05\cdot10^{10}$ | $1{,}39\cdot10^{10}$ | $5{,}25\cdot10^{8}$ | $6{,}91\cdot10^{10}$ | 12 | 2,14 |
| SODIUM | 80 | 2 | $1{,}31\cdot10^{7}$ | $4{,}75\cdot10^{9}$ | $2{,}61\cdot10^{9}$ | $1{,}25\cdot10^{10}$ | $1{,}47\cdot10^{9}$ | $2{,}13\cdot10^{10}$ | 42,76 | 0,33 |
| SODIUM | | 5 | $1{,}31\cdot10^{7}$ | $4{,}77\cdot10^{9}$ | $2{,}63\cdot10^{9}$ | $1{,}25\cdot10^{10}$ | $1{,}54\cdot10^{9}$ | $2{,}15\cdot10^{10}$ | 43,14 | 0,33 |
| SODIUM | | 10 | $1{,}31\cdot10^{7}$ | $4{,}84\cdot10^{9}$ | $2{,}68\cdot10^{9}$ | $1{,}27\cdot10^{10}$ | $1{,}55\cdot10^{9}$ | $2{,}18\cdot10^{10}$ | 42,99 | 0,32 |
| FER | 140 | 2 | $6{,}82\cdot10^{5}$ | $3{,}37\cdot10^{8}$ | $2{,}54\cdot10^{8}$ | $3{,}84\cdot10^{9}$ | $9{,}14\cdot10^{8}$ | $5{,}35\cdot10^{9}$ | 75,25 | 0,069 |
| FER | | 5 | $6{,}82\cdot10^{5}$ | $3{,}40\cdot10^{8}$ | $2{,}56\cdot10^{8}$ | $3{,}87\cdot10^{9}$ | $9{,}24\cdot10^{8}$ | $5{,}39\cdot10^{9}$ | 75,28 | 0,068 |
| FER | | 10 | $6{,}82\cdot10^{5}$ | $3{,}49\cdot10^{8}$ | $2{,}66\cdot10^{8}$ | $3{,}96\cdot10^{9}$ | $9{,}40\cdot10^{8}$ | $5{,}52\cdot10^{9}$ | 75,00 | 0,067 |
| FER | Flux incident | à l'entrée | $1{,}68\cdot10^{11}$ | $2{,}08\cdot10^{13}$ | $2\cdot10^{2}$ | $3{,}6\cdot10^{11}$ | $3{,}9\cdot10^{10}$ | $2{,}34\cdot10^{13}$ | 3,09 | 3,9 |
| FER | 20 | 5 | $4{,}68\cdot10^{9}$ | $7{,}76\cdot10^{12}$ | $2{,}89\cdot10^{12}$ | $1{,}77\cdot10^{12}$ | $4{,}05\cdot10^{10}$ | $1{,}25\cdot10^{13}$ | 9,41 | 0,20 |
| FER | | 10 | $3{,}51\cdot10^{9}$ | $8{,}01\cdot10^{12}$ | $2{,}97\cdot10^{12}$ | $1{,}78\cdot10^{12}$ | $3{,}93\cdot10^{10}$ | $1{,}28\cdot10^{13}$ | 9,25 | 0,15 |
| FER | 80 | 5 | $1{,}05\cdot10^{5}$ | $1{,}70\cdot10^{11}$ | $1{,}67\cdot10^{11}$ | $1{,}32\cdot10^{11}$ | $3{,}80\cdot10^{9}$ | $4{,}73\cdot10^{11}$ | 16,46 | 0,000 012 |
| FER | | 10 | $0{,}93\cdot10^{5}$ | $1{,}90\cdot10^{11}$ | $1{,}92\cdot10^{11}$ | $1{,}61\cdot10^{11}$ | $5{,}01\cdot10^{9}$ | $5{,}49\cdot10^{11}$ | 17,29 | 0,000 09 |

se rapprochent des équations différentielles de la diffusion, et les sections efficaces de chacun des groupes sont presque indépendantes du spectre qui a servi à les calculer. Ce dernier point apparaît très clairement si on considère la définition d'une section efficace $\overline{\sigma}_i$ dans un groupe d'énergie $i$ dont les bornes sont $E_i$ et $E_{i-1}$

$$\overline{\sigma}_i = \frac{\int_{E_{i-1}}^{E_i} \sigma(E)\, \varphi(E)\, \mathrm{d}E}{\int_{E_{i-1}}^{E_i} \varphi(E)\, \mathrm{d}E}$$

Si $E_i - E_{i-1}$ est petit, c'est-à-dire si le découpage en énergie est fin, $\overline{\sigma}_i$ dépend peu de la densité de flux $\varphi(E)$ utilisée pour la pondération.

Une fois connus en divers points d'un milieu les flux et les spectres, qui auraient été auparavant calculés à l'aide d'un très grand nombre de groupes, on peut se demander si les mêmes résultats ne peuvent pas être obtenus à l'aide d'un nombre de groupes moindre. C'est ce que nous avons tenté de faire en essayant de reproduire par des calculs à 4 et 5 groupes des résultats de calculs à 20 groupes effectués sur la partie supérieure du réacteur RAPSODIE. Pour ces cas, le code utilisé était RASP [2], qui permet de traiter le problème en géométrie sphérique.

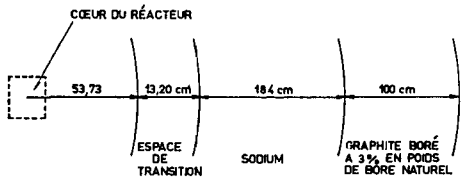


Figure 4
Schéma de la partie supérieure du réacteur RAPSODIE.
Composition en volume — Sodium, 20% — Acier inoxydable, 65% — Vide, 15%.

Le spectre des neutrons entrant dans l'espace de transition est fourni par des calculs de criticalité de la pile. Il correspond à la sortie des couvertures entourant le cœur.

Dans chaque milieu, on a calculé des sections efficaces moyennes à 4 et 5 groupes de neutrons par la relation de pondération

$$\sigma_I = \sum_j \frac{\sigma_j\, \Phi_j}{\sum_j \Phi_j}$$

où les flux $\Phi_j$ sont ceux obtenus par un calcul à 20 groupes en un point situé au milieu du sodium, et où le groupe $I$ du découpage à 4 ou 5 groupes couvre $j$ groupes du découpage à 20 groupes. Les limites du découpage à 4 et 5 groupes sont les mêmes que certaines bornes du découpage à 20 groupes, ainsi que le montre le tableau IV.

Les résultats sont portés sur la figure 5 où l'on a tracé les atténuations en ramenant à 4 groupes comparables les résultats des calculs à 20 et 5 groupes.

La proximité des courbes tracées permet de conclure, tout au moins dans le cas du sodium ci-dessus étudié, que l'on peut obtenir les mêmes résultats avec un nombre de groupes limité (4 par exemple), à condition que les constantes

TABLEAU IV

**COMPARAISON DU DÉCOUPAGE A 20, 5 ET 4 GROUPES**

| Domaine d'énergie | Numéro de groupe dans le découpage $i$ | | |
|---|---|---|---|
| | 20 groupes | 5 groupes | 4 groupes |
| 10—1,35 MeV | 1 | 1 | 1 |
| 1,35—0,498 MeV | 2 | 2 | 1 |
| 498—302 keV | 3 | 2 | 1 |
| 302—183 keV | 4 | 2 | 2 |
| 183—111 keV | 5 | 2 | 2 |
| 111—67,4 keV | 6 | 2 | 2 |
| 67,4—24,8 keV | 7 | 2 | 2 |
| 24,8—9,12 keV | 8 | 2 | 2 |
| 9,12—3,35 keV | 9 | 3 | 2 |
| 3,35—0,3 keV | 10 | 3 | 2 |
| 300—90 eV | 11 | 3 | 2 |
| 90—43 eV | 12 | 3 | 2 |
| 43—34 eV | 13 | 3 | 2 |
| 34—22 eV | 14 | 3 | 3 |
| 22—18 eV | 15 | 4 | 3 |
| 18—9 eV | 16 | 4 | 3 |
| 9—6 eV | 17 | 4 | 3 |
| 6—0,7 eV | 18 | 4 | 3 |
| 0,7—0,085 eV | 19 | 5 | 4 |
| <0,085 eV | 20 | 5 | 5 |

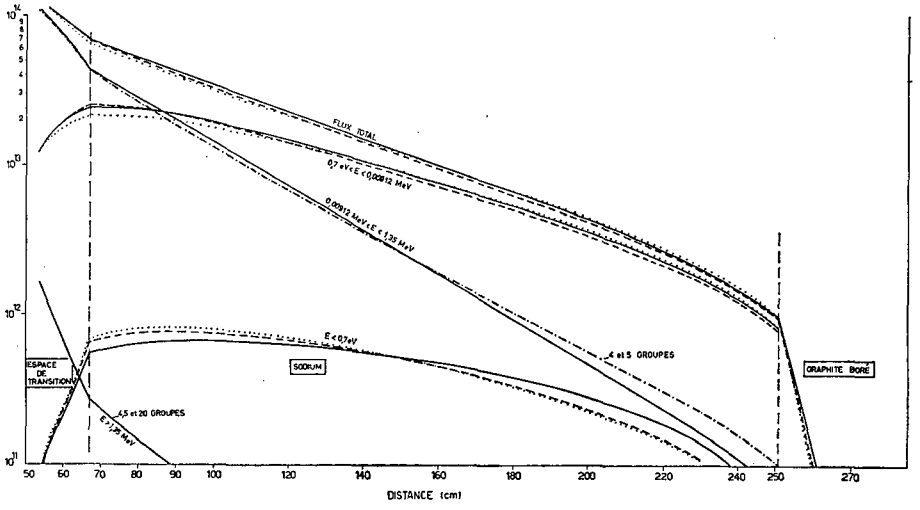


Figure 5

Transmission du flux dans le réacteur idéalisé RAPSODIE. Influence du nombre de groupes.

..... 4 groupes
- - - - - - - - 5 groupes
———— 20 groupes

(sections efficaces) utilisées soient bien représentatives du spectre et que ce dernier, qui a servi à les obtenir, ne varie pas trop rapidement à l'intérieur du milieu. Si le spectre se déforme de façon notable d'un point à un autre, il devient nécessaire de scinder, pour le calcul, le milieu physique en plusieurs milieux fictifs.

Nous voudrions insister sur le fait que, dans le cas que nous avons étudié ci-dessus, il n'est pas du tout certain que les 20 groupes utilisés soient en nombre suffisant — ni que leur découpage énergétique soit adéquat — pour que les calculs auxquels ils servent donnent des résultats suffisamment proches de la propagation physique. Des calculs à nombre de groupes plus élevé sont peut-être nécessaires, et seule la comparaison avec l'expérience peut permettre de préciser ce point.

*Comparaison des calculs multigroupes avec la solution analytique*

Entre les résultats des calculs multigroupes et ceux de la solution analytique du problème, il existe une légère différence, provenant de ce que le code de calcul remplace les équations différentielles de la diffusion par des équations aux différences finies. Nous avons donc comparé les résultats fournis en géométrie plane infinie par un calcul machine à 4 groupes dans le sodium, à ceux que donnent les équations de la diffusion qui, dans le cas d'un milieu non multiplicateur, se résolvent facilement à la main. On voit sur le tableau V que dans un bloc

TABLEAU V

**COMPARAISON DE LA SOLUTION ANALYTIQUE AUX CALCULS MULTIGROUPES VALEUR DU FLUX A 180 cm DE LA SOURCE**

| Groupes d'énergie | Flux à l'entrée | Flux à l'abscisse 180 | | |
|---|---|---|---|---|
| | | Calculs multi-groupes | Solution analytique | Différence (%) |
| 1 | $2{,}67 \cdot 10^{11}$ | $6{,}25 \cdot 10^{8}$ | $6{,}30 \cdot 10^{8}$ | —0,8 |
| 2 | $4{,}31 \cdot 10^{13}$ | $5{,}43 \cdot 10^{11}$ | $5{,}15 \cdot 10^{11}$ | +5,4 |
| 3 | $2{,}15 \cdot 10^{13}$ | $8{,}27 \cdot 10^{12}$ | $8{,}31 \cdot 10^{12}$ | —0,5 |
| 4 | $6{,}84 \cdot 10^{11}$ | $5{,}84 \cdot 10^{11}$ | $5{,}87 \cdot 10^{11}$ | —0,5 |

**Hypothèse de calcul: milieu plan semi-infini — constantes utilisées**

| Groupe | $Di$ (cm) | $\Sigma_c$ ($cm^{-1}$) | $\Sigma_c^2\ \Sigma_{er} + \Sigma_c$ ($cm^{-1}$) |
|---|---|---|---|
| 1 | 7,75 | $7 \cdot 10^{-6}$ | 0,0088 |
| 2 | 4,14 | $23 \cdot 10^{-6}$ | 0,0025 |
| 3 | 4,43 | $319 \cdot 10^{-6}$ | 0,00061 |
| 4 | 5,17 | $1474 \cdot 10^{-6}$ | 0,0074 |

semi-infini de sodium, et à 180 cm de l'entrée, c'est-à-dire après une atténuation de $10^2$ environ par rapport au flux d'entrée, les résultats sont tout à fait comparables, la différence n'atteignant que 5% dans un des groupes. On peut donc conclure que les erreurs introduites par l'emploi de différences finies des calculs multigroupes n'amènent que des erreurs négligeables.

TABLEAU VI

**TRANSMISSION DU FLUX DANS UN BLOC SEMI-INFINI DE SODIUM**

**Influence des variations des quotients $D\Sigma_a = D/[\Sigma_c + k(\Sigma_{er} + \Sigma_{in})]$**

| $x$ (cm) | $k$ | $\Phi_1$ | $\Phi_2$ | $\Phi_3$ | $\Phi_4$ | $\Phi_5$ | $\Phi_{total}$ | $\sigma_f^{235}U$ (b) | $\sigma_f^{238}U$ (mb) |
|---|---|---|---|---|---|---|---|---|---|
| Domaine d'énergie | | 10—1,35 MeV | 1,35 MeV—9,12 keV | 9,12—0,3 keV | 300—0,7 eV | 0,7—0 eV | — | — | — |
| Valeurs initiales ($x=0$) | | $2,68 \cdot 10^8$ | $4,31 \cdot 10^{10}$ | $1,04 \cdot 10^{10}$ | $1,36 \cdot 10^{10}$ | $4,84 \cdot 10^8$ | $6,79 \cdot 10^{10}$ | 12 | 2,14 |
| 80 | 0,5 | $3,25 \cdot 10^7$ | $9,93 \cdot 10^9$ | $1,31 \cdot 10^{10}$ | $1,92 \cdot 10^9$ | $0,63 \cdot 10^9$ | $2,56 \cdot 10^{10}$ | 26 | 0,69 |
| | 1 | $1,35 \cdot 10^7$ | $5,27 \cdot 10^9$ | $1,18 \cdot 10^{10}$ | $2,83 \cdot 10^9$ | $1,53 \cdot 10^9$ | $2,14 \cdot 10^{10}$ | 43 | 0,34 |
| | 1,5 | $0,70 \cdot 10^7$ | $3,03 \cdot 10^9$ | $0,96 \cdot 10^{10}$ | $3,01 \cdot 10^9$ | $2,22 \cdot 10^9$ | $1,78 \cdot 10^{10}$ | 61 | 0,21 |
| 160 | 0,5 | $3,93 \cdot 10^6$ | $1,63 \cdot 10^9$ | $4,94 \cdot 10^9$ | $1,27 \cdot 10^9$ | $4,43 \cdot 10^8$ | $8,30 \cdot 10^9$ | 41 | 0,25 |
| | 1 | $0,69 \cdot 10^6$ | $0,39 \cdot 10^9$ | $2,64 \cdot 10^9$ | $1,40 \cdot 10^9$ | $9,00 \cdot 10^8$ | $5,33 \cdot 10^9$ | 75 | 0,07 |
| | 1,5 | $0,18 \cdot 10^6$ | $0,11 \cdot 10^9$ | $1,31 \cdot 10^9$ | $1,03 \cdot 10^9$ | $9,99 \cdot 10^8$ | $3,46 \cdot 10^9$ | 112 | 0,03 |

TABLEAU VII

**TRANSMISSION DU FLUX DANS UN BLOC SEMI-INFINI DE FER**

**Influence des variations des quotients $D\overline{\Sigma}_a = D/[\Sigma_c + k(\Sigma_{er} + \Sigma_{in})]$**

| $x$ (cm) | $k$ | $\Phi_1$ | $\Phi_2$ | $\Phi_3$ | $\Phi_4$ | $\Phi_5$ | $\Phi_{total}$ | $\sigma_f^{235}U$ (b) | $\sigma_f^{238}U$ (mb) |
|---|---|---|---|---|---|---|---|---|---|
| Domaine d'énergie | | 10—1,35 MeV | 1,35 MeV—9,12 keV | 9,12—0,3 keV | 300—0,7 eV | 0,7—0 eV | — | — | — |
| Valeurs initiales ($x=0$) | | $1,68 \cdot 10^{11}$ | $2,08 \cdot 10^{13}$ | $2,00 \cdot 10^{12}$ | $3,6 \cdot 10^{11}$ | $3,9 \cdot 10^{10}$ | $2,34 \cdot 10^{13}$ | 3,09 | 3,9 |
| 20 | 0,5 | $13,3 \cdot 10^9$ | $1,13 \cdot 10^{13}$ | $2,91 \cdot 10^{12}$ | $0,59 \cdot 10^{11}$ | $0,60 \cdot 10^{10}$ | $1,43 \cdot 10^{13}$ | 5,7 | 0,50 |
| | 0,7 | $8,43 \cdot 10^9$ | $1,01 \cdot 10^{13}$ | $3,10 \cdot 10^{12}$ | $1,15 \cdot 10^{11}$ | $1,67 \cdot 10^{10}$ | $1,34 \cdot 10^{13}$ | 7,7 | 0,34 |
| | 1 | $4,68 \cdot 10^9$ | $0,88 \cdot 10^{13}$ | $3,41 \cdot 10^{12}$ | $2,01 \cdot 10^{11}$ | $3,76 \cdot 10^{10}$ | $1,25 \cdot 10^{13}$ | 8,9 | 0,21 |
| | 1,5 | $2,07 \cdot 10^9$ | $0,71 \cdot 10^{13}$ | $3,76 \cdot 10^{12}$ | $3,18 \cdot 10^{11}$ | $9,12 \cdot 10^{10}$ | $1,09 \cdot 10^{13}$ | 10,9 | 0,10 |
| 80 | 0,5 | $6,67 \cdot 10^6$ | $9,20 \cdot 10^{11}$ | $6,26 \cdot 10^{11}$ | $1,62 \cdot 10^{10}$ | $1,77 \cdot 10^9$ | $1,57 \cdot 10^{12}$ | 10 | 0,002 3 |
| | 0,7 | $1,06 \cdot 10^6$ | $4,98 \cdot 10^{11}$ | $4,23 \cdot 10^{11}$ | $1,98 \cdot 10^{10}$ | $2,47 \cdot 10^9$ | $0,95 \cdot 10^{12}$ | 13 | 0,000 6 |
| | 1 | $0,11 \cdot 10^6$ | $2,21 \cdot 10^{11}$ | $2,29 \cdot 10^{11}$ | $1,81 \cdot 10^{10}$ | $3,79 \cdot 10^9$ | $0,47 \cdot 10^{12}$ | 16 | 0,000 1 |
| | 1,5 | $0,004 \cdot 10^6$ | $0,68 \cdot 10^{11}$ | $0,88 \cdot 10^{11}$ | $1,12 \cdot 10^{10}$ | $3,40 \cdot 10^9$ | $0,17 \cdot 10^{12}$ | 21 | 0,000 01 |

*Influence des sections efficaces*

Les incertitudes sur les sections efficaces proviennent d'une part de la mauvaise connaissance des sections physiques $\sigma(E)$ et d'autre part de l'erreur systématique introduite par le moyennage qui permet d'obtenir à partir de spectres, supposés connus ou calculés, des sections $\sigma_i$ dans les groupes d'énergie par la relation

$$\sigma_i = \frac{\int \sigma(E)\,\varphi(E)\,\mathrm{d}E}{\int \varphi(E)\,\mathrm{d}E} = \frac{\int \sigma(u)\,\varphi(u)\,\mathrm{d}u}{\int \varphi(u)\,\mathrm{d}u}$$

où $\varphi(E)$ et $\varphi(u)$ sont les densités de flux évaluées en unité d'énergie ou de léthargie $u$ $[u = \log \frac{10^7}{E_{\mathrm{ev}}}]$.

Il est difficile d'évaluer l'incertitude globale d'un jeu de sections, car, pour un point donné, des sections peuvent, dans certains groupes, être sur-évaluées alors que d'autres sont sous-évaluées. Nous pensons néanmoins, d'une façon d'ailleurs un peu arbitraire, qu'un jeu donné peut être défini par une incertitude totale sur toutes ses sections de 50% environ en plus ou en moins. Comme ce sont surtout les quotients par le coefficient de diffusion des sections de transfert élastique et inélastique qui jouent un rôle prépondérant dans l'étude de la transmission des flux — les variations sur $\Sigma_c$ étant sans grande importance — nous avons modifié d'un facteur également arbitraire compris entre 0,5 et 1,5 les valeurs de $\Sigma_{er}/D$ et $\Sigma_{in}/D$ qui deviennent donc $k\,(\Sigma_{er}/D)$ et $k\,(\Sigma_{in}/D)$. Les tableaux VI et VII résument les calculs de transmission effectués à 20 groupes dans des blocs semi-infinis de fer et de sodium. On a groupé les neutrons en cinq catégories: $\Phi_1$, $\Phi_2$, $\Phi_3$, $\Phi_4$, $\Phi_5$, pour la commodité de lecture des résultats.

L'examen des tableaux VI et VII permet de conclure que les incertitudes sur les sections efficaces peuvent introduire des erreurs de l'ordre de 60% et 250% par rapport aux résultats calculés après une transmission de 160 cm dans le sodium et de 80 cm dans le fer.

D'une façon plus générale, on peut dire que ce sont les incertitudes sur les valeurs des sections efficaces et l'emploi d'un nombre de groupes peu élevé qui risquent de fausser les résultats des calculs multigroupes.

Nous nous proposons maintenant de comparer certains résultats expérimentaux de transmission dans le sodium aux calculs multigroupes afin de pouvoir définir d'une manière globale la précision de ces derniers.

## Comparaison avec les résultats expérimentaux

Des études de transmission de flux ont été effectuées dans des maquettes destinées à représenter certaines parties du réacteur RAPSODIE. Les expériences ont été montées à la sortie des colonnes thermiques du réacteur ZOE ou de la pile piscine TRITON, où une plaque mince d'uranium enrichi permet d'obtenir un courant de neutrons rapides qui pénètrent ensuite dans les maquettes étudiées. Celles-ci ont été construites dans des installations appelées NAIADE I et II, analogues aux « lid-tank facilities » classiques [3].

C'est surtout l'atténuation dans le sodium qui a été mesurée jusqu'à présent, soit que les bacs contenant ce dernier aient été placés directement derrière la plaque (fig. 5), soit qu'on ait entreposé entre celle-ci et le sodium de l'uranium naturel (fig. 6) ou de l'uranium et de l'acier (fig. 7).

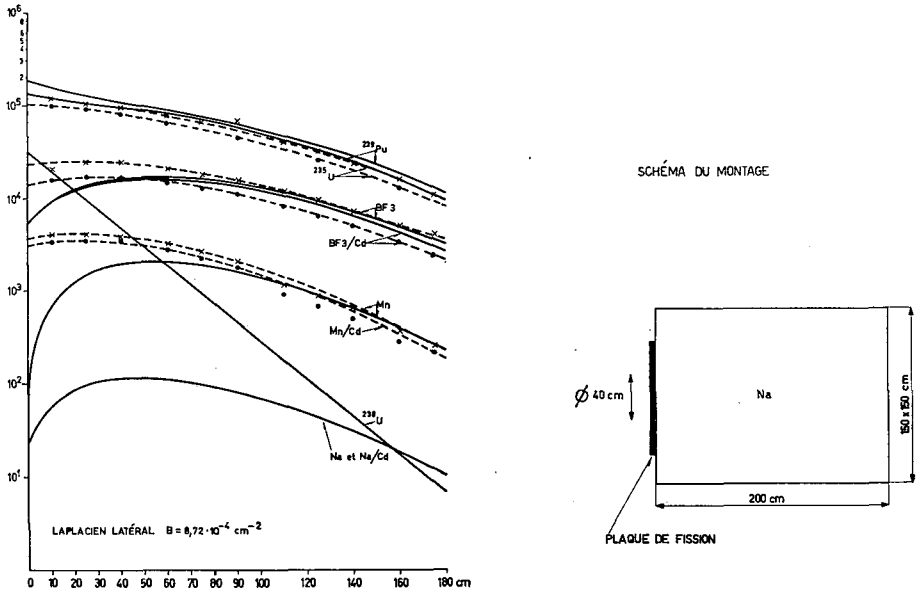


Figure 6
Transmission de neutrons dans le sodium. Réponse de détecteurs.
——————— Réponses calculées (20 groupes)
– – – – – – – – Resultats des mesures

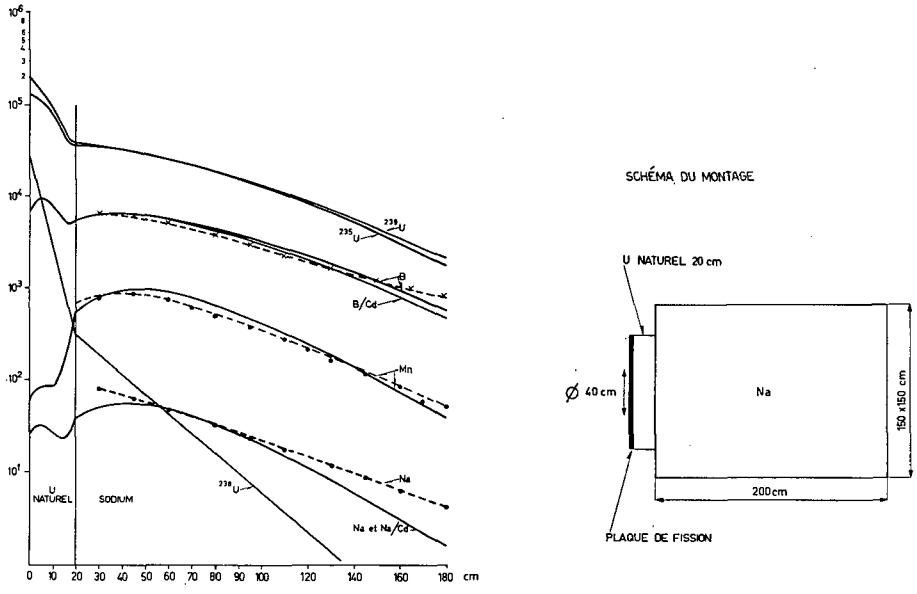


Figure 7
Transmission de neutrons dans le sodium. Réponses de détecteurs.
——————— Réponses calculées (20 groupes)
– – – – – – – – Résultats des mesures

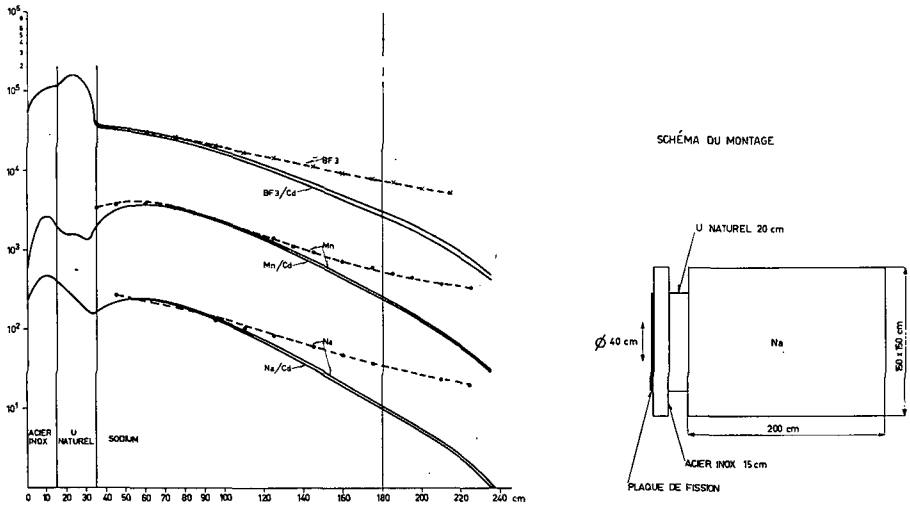


Figure 8
Transmission de neutrons dans le sodium. Réponses de détecteurs.
———————— *Réponses calculées (20 groupes)*
– – – – – – – – Résultats des mesures

Les appareils de mesure utilisés sont:

*a*) Des chambres d'ionisation à BF-3 nues ou sous cadmium;

*b*) Des chambres à fission avec dépôts de $^{235}U$, $^{238}U$ et $^{239}Pu$;

*c*) Des détecteurs d'activation tels que le manganèse, le manganèse sous cadmium, le sodium, le sodium sous cadmium, l'indium, et l'indium sous cadmium.

La précision des comptages obtenus est évaluée à 1%.

Parallèlement à ces expériences, on a utilisé la méthode de calcul à 20 groupes pour déterminer l'atténuation du flux dans les maquettes et les réponses des divers détecteurs ou chambres. On a tenu compte des dimensions finies des maquettes en ajoutant un laplacien latéral aux sections de capture. Quant aux réponses calculées des appareils de mesure, elles sont proportionnelles aux quantités:

$$R = \sum_i \Sigma_i \Phi_i$$

où $\Sigma_i'$ représente suivant le cas la section efficace de capture ou de fission du matériau détecteur utilisé.

On est donc à même de pouvoir comparer (fig. 6 à 8) la forme des courbes expérimentales et calculées, c'est-à-dire le taux d'atténuation.

On remarque que l'accord est très mauvais (cf. particulièrement figure 6) en des points situés près de la plaque de fission. Nous pensons que ceci provient essentiellement:

*a*) De ce que les dimensions de cette dernière sont faibles (c'est un disque de 40 cm de diamètre alors que le code de calcul le suppose infini);

*b*) De ce que l'on se trouve près des limites géométriques du milieu où l'équation de la diffusion s'applique mal;

*c*) De ce que le code de calcul prend pour données initiales la valeur des flux dans chaque groupe alors que la plaque donne lieu, en fait, à un courant entrant de neutrons qui sont ensuite partiellement réfléchis.

Dès que l'on considère des points à l'intérieur du milieu, les courbes se rapprochent et l'accord tend à devenir meilleur. Elles s'écartent ensuite près des limites du bloc de sodium, où il y a des perturbations dont le calcul ne tient pas compte.

## Conclusion

Dans l'avenir, il sera nécessaire, afin d'obtenir un meilleur accord entre le calcul et l'expérience, d'une part d'utiliser un nombre de groupes plus élevé et de mieux tenir compte dans les codes des conditions aux limites tant de source que de réflecteur, et d'autre part de faire, dans les maquettes, des mesures avec des détecteurs plus nombreux, dont les résultats plus diversifiés permettraient de mieux définir le spectre et de mieux apprécier la précision des calculs de propagation de flux dont la connaissance, ainsi qu'il a été indiqué plus haut, peut être très importante pour certains types de piles rapides.

## RÉFÉRENCES

[1] Programme 173 — Spécifications à paraître.
[2] LINDE, S., Radiation shielding program for the Ferranti Mercury Computer, RASP (1960).
[3] DE VILLIERS, J. *et alii*, Proc. 2nd UN Int. Conf. PUAE 2 (1958) 237.

SM 18/86

# РАСПРОСТРАНЕНИЕ НЕЙТРОНОВ В НИКЕЛЕВОМ ЭКРАНЕ РЕАКТОРА НА БЫСТРЫХ НЕЙТРОНАХ

М. Н. НИКОЛАЕВ, В. И. ГОЛУБЕВ, А. А. АБАГЯН И М. Ю. ОРЛОВ
АКАДЕМИЯ НАУК СССР, МОСКВА,
СССР

**Abstract — Résumé — Аннотация — Resumen**

**Neutron propagation in the nickel screen of a fast reactor.** The present study is the continuation of a series of macroscopic experiments carried out on the BR-1 fast zero-power reactor in order to study neutron propagation in various materials. The purpose of these investigations was to check and refine the system of constants used in multi-group, fast-reactor calculations. The results of experiments carried out on the BR-1 reactor with uranium and copper screens were reported in 1958 at the Second International Conference on the Peaceful Uses of Atomic Energy in Geneva (Paper No. 2038). The present paper is devoted to a study of neutron propagation in nickel. This material was chosen because it is widely used in reactors, both as a construction material and as a screen material (in the BR-5 reactor, for example).

Nickel cross-sections, especially their resonance structure, have been too little studied in the elementary experiments. Accordingly, the multi-group system of constants for nickel, compiled on the basis of those experiments, needed further checking by macroscopic experiment.

The distribution of neutrons of various energies over the radius of the reactor's nickel screen was measured with an assembly of detectors of various energy sensitivities. The results obtained are compared in this paper with the results of the 18-group calculation carried out with a $P_1$ approximation. The comparison shows that the results of the experiment tally satisfactorily with the calculation.

**Distribution des neutrons sur l'écran de nickel d'un réacteur à neutrons rapides.** Le mémoire rend compte d'une série d'expériences macroscopiques destinées à étudier, dans le réacteur de puissance zéro à neutrons rapides BR-1, la distribution du flux de neutrons dans diverses substances. Ces recherches visent à vérifier et à préciser les systèmes de constantes utilisées pour les calculs multigroupes des réacteurs à neutrons rapides. Les résultats des expériences effectuées dans le réacteur BR-1 avec des couches fertiles d'uranium et de cuivre ont été signalés à la deuxième Conférence internationale sur l'utilisation de l'énergie atomique à des fins pacifiques (Genève, 1958, mémoire n° 2038). Le présent mémoire étudie la distribution du flux de neutrons dans le nickel. Le choix de cette matière s'explique par son application étendue dans les réacteurs, soit comme matériau de construction, soit comme élément constitutif de l'écran (par exemple, dans le réacteur BR-5).

Dans les expériences élémentaires, on n'a pas suffisamment étudié les sections efficaces du nickel, notamment leur structure de résonance. C'est pourquoi le système multigroupe de constantes établi pour le nickel sur la base de ces expériences avait besoin d'une vérification complémentaire par la méthode macroscopique.

Les distributions du flux de neutrons de diverses énergies selon le rayon de l'enveloppe de nickel du réacteur ont été mesurées à l'aide d'un ensemble de détecteurs ayant des sensibilités différentes selon l'énergie. Les distributions obtenues ont été comparées aux résultats d'un calcul à 18 groupes. Il ressort de cette comparaison que les résultats de l'expérience concordent assez bien avec les calculs.

**Распространение нейтронов в никелевом экране реактора на быстрых нейтронах.** Настоящая работа является продолжением цикла макроскопических экспериментов по изучению распространения нейтронов в различных веществах, выполняемого на быстром реакторе нулевой мощности БР-1. Целью этих исследований является проверка и уточнение систем констант, используемых при многогрупповых расчетах реакторов на быстрых нейтронах. Результаты экспериментов, выполненных на реакторе БР-1 с урановым и медным экранами, были доложены в 1958 году на 2-й Международной конференции по мирному использованию атомной энергии в Женеве (доклад № 2038). Настоящая работа посвящена изучению распространения нейтронов в никеле. Выбор этого материала определяется его широким применением в реакторостроении в качестве конструкционного материала или материала экрана (например в реакторе БР-5).

Сечения никеля, в частности их резонансная структура, недостаточно изучены в элементарных опытах. Поэтому составленная на основании этих опытов многогрупповая система констант для никеля нуждалась в дополнительной проверке в макроскопическом эксперименте.

Распределения нейтронов различных энергий по радиусу никелевого экрана реактора измерялись с помощью набора детекторов, обладающих различной энергетической чувствительностью. Полученные распределения сравниваются с результатами 18-группового расчета, выполненного в $P_1$—приближения. Сравнение показывает, что результаты эксперимента находятся в удовлетворительном согласии с расчетом.

**Propagación de neutrones en la pantalla de níquel de un reactor rápido.** El presente trabajo representa la continuación de un ciclo de experimentos macroscópicos sobre la propagación de los neutrones en diferentes sustancias, realizados en el reactor rápido de potencia cero BR-1. El objeto de dichos experimentos es verificar y afinar los valores de un sistema de constantes que se aplican en los cálculos de reactores rápidos según la teoría de los multigrupos. Los resultados de los experimentos llevados a cabo con blindajes de uranio y cobre en el reactor BR-1 se expusieron en la Segunda Conferencia Internacional de las Naciones Unidas sobre la Utilización de la Energía Atómica con fines pacíficos, celebrada en Ginebra en el año 1958 (memoria número 2038). En cambio, la presente memoria se refiere al estudio de la propagación de los neutrones en el níquel. Se eligió este material en atención a sus múltiples aplicaciones como elemento estructural y como material de blindaje en la construcción de reactores (en el reactor BR-5, por ejemplo).

Aún no se han estudiado suficientemente, en el terreno experimental, las secciones eficaces del níquel, especialmente en lo que se refiere a su estructura resonante. Por tal motivo, en el caso del níquel, fue preciso confirmar mediante experimentos macroscópicos la validez del sistema de constantes de la teoría de multigrupos, basada en dichos experimentos.

Con la ayuda de un juego de detectores, dotados de diferentes sensibilidades energéticas, se determinaron las distribuciones radiales de los neutrones con diferentes niveles energéticos, en el blindaje de níquel del reactor. Los valores de las distribuciones se cotejaron con los resultados de un cálculo basado en un método de 18 grupos, con una aproximación $P_1$. Según esta comparación, los resultados experimentales concuerdan satisfactoriamente con los alcanzados mediante el cálculo teórico.

## Введение

Настоящая работа является продолжением цикла макроскопических экспериментов по изучению распространения нейтронов в различных веществах, выполняемого на быстром реакторе нулевой мощности БР-1. Целью этих экспериментов является проверка и уточнение систем констант, используемых при многогрупповых расчетах реакторов на быстрых нейтронах.

Результаты экспериментов, выполненных на реакторе БР-1 с урановым и медным экранами, были опубликованы в работе [1]. Настоящая работа посвящена изучению распространения нейтронов в никеле. Выбор этого материала определяется его широким применением в реакторостроении в качестве конструкционного материала или материала экрана (например в реакторе БР-5 [2]). Кроме того, детальное исследование распространения нейтронов в никеле позволяет выяснить ряд общих закономерностей прохождения нейтронов через вещество, таких как, например, влияние структуры сечений на замедление нейтронов в резонансной области и другие подобные вопросы.

Сечения никеля, в частности их резонансная структура, недостаточно изучены в элементарных опытах. Поэтому составленная на основании этих опытов многогрупповая система констант для никеля нуждалась в дополнительной проверке в макроскопическом эксперименте. Попытка провести такую проверку была произведена при сравнении результатов расчета пространственно-энергетического распределения нейтронов в никелевом экране реактора БР-5 с экспериментальными данными [3]. Однако, сложность геометрии экрана этого реактора и наличие в нем значительного количества конструкционных материалов и теплоносителя не позволило произвести детальный анализ причин расхождения между результатами расчета и эксперимента.

В настоящей работе экран реактора имел сравнительно простую геометрию, легко поддающуюся расчету. Экран не содержал никаких конструкционных материалов, что существенно облегчало интерпретацию результатов.

## Реактор и экспериментальная методика

Конструкция реактора была описана в работе [1]. В изучавшемся варианте экран реактора (рис. 1) был составлен из никелевых блочков диаметром 47 мм, плотно уложенных в дюралевом баке, имевшем форму шестигранной

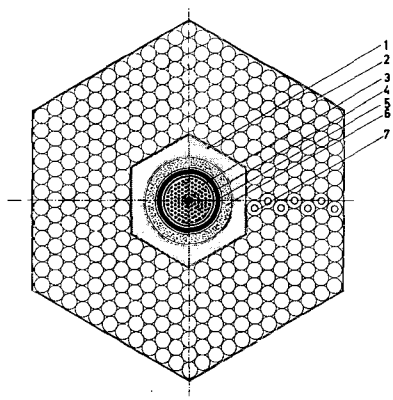


Рис. 1
Схематический разрез реактора.
1 — никелевый шестигранник; 2 — Никелевые блочки; 3 — Активная зона; 4, 5 — Органы регулирования; 6 — Урановое кольцо; 7 — Измерительные каналы.

призмы со стороной 57,5 см и высотой 70 см. Зазоры между блочками составляли 13 % по объему. В качестве первого слоя никелевого экрана служил сплошной шестигранник из никеля со стороной 21 см.

Спектр нейтронов в активных зонах больших реакторов, в частности, в активной зоне реактора БР-5, существенно мягче спектра концентрированной активной зоны реактора БР-1. Для того, чтобы приблизить спектр нейтронов, входящих в никелевый экран нашего реактора, к спектру активной зоны реактора БР-5, между никелевым экраном и активной зоной было помещено кольцо из обедненного урана толщиной 35 мм.

Измерение пространственно-энергетических распределений производилось в вертикальных измерительных каналах реактора с помощью набора детекторов, обладавших различной энергетической чувствительностью. В качестве таких детекторов использовались реакции деления $Pu^{239}$, $U^{235}$, $Th^{232}$, радиационного захвата нейтронов в $Au^{197}$, $J^{127}$, $Mn^{55}$, $Na^{23}$, $Cu^{65}$, $Cu^{63}$; реакции $P^{31}$ (n, p), $Si^{28}$ (n, p) и $B^{10}$ (n, $\alpha$).

Были также измерены распределения потоков нейтронов с энергиями, соответствующими 1-м резонансам $Au^{197}$ (4,9 эв), $Mn^{55}$ (337 эв) и $Na^{23}$ (2850 эв).

Вклад резонансных нейтронов в полную активность тонкого золотого индикатора определялся методом резонансной экранировки [4]. С этой целью производилось облучение тонких золотых индикаторов, окруженных золотыми фильтрами. Толщина фильтров (6,25 мг/см$^2$) была подобрана таким образом, что они в значительной степени поглощали нейтроны, соответствующие энергии 1-го резонанса, но являлись почти прозрачными для нейтронов других энергий. Таким образом, разность в активностях золотых индикаторов, облученных в фильтрах и без них, была пропорциональна потоку резонансных нейтронов.

На мягких спектрах, устанавливающихся в никелевом экране, активность натриевых индикаторов практически полностью обусловлена вкладом 1-го резонанса и вкладом от области более медленных нейтронов, где сечение захвата подчиняется закону $1/v$. Последний может быть определен с помощью детектора, обладающего чувствительностью, пропорциональной $1/v$. В нашем случае таким детектором являлась ионизационная камера со слоем $B^{10}$. Распределение потока резонансных нейтронов с энергией 2850 эв получалось как разность распределения, полученного с помощью натриевых индикаторов и соответствующим образом нормированного распределения, снятого с помощью борной камеры. При этом влияние эффективностей детекторов исключалось путем обычной процедуры калибровки детекторов в стандартном потоке тепловых нейтронов.

Таким же методом было измерено распределение потока нейтронов с энергией, соответствующей энергии первого резонанса марганца. Естественно, применение указанной методики оправдано только в том случае, если вклад второго и следующего за ним резонансов в активность индикаторов мал. Такие условия осуществлялись лишь на расстоянии нескольких пробегов от границы с урановым кольцом, поэтому определение потоков резонансных нейтронов методом вычитания „вклада $1/v$“ производилось только вдали от этой границы.

Все использовавшиеся индикаторы были достаточно тонкими; поправки на резонансную блокировку нейтронного потока в индикаторах составляли не более нескольких процентов.

**Расчет пространственно-энергетических распределений**

Было выполнено два варианта расчета реактора. В первом варианте производилось вычисление потоков нейтронов во всем реакторе, включая активную зону. В этом расчете нейтроны с энергией выше 1,4 мэв были разбиты на несколько групп, что позволяло рассчитать различия в распределениях, снятых с помощью имевшихся в нашем распоряжении пороговых детекторов. Распределение потоков нейтронов этих групп рассчитывалось в $P_3$—приближении. Оказалось, однако, что между результатами этого расчета и экспериментальными данными имеются существенные расхождения. Хотя и расчетные и экспериментальные данные могли быть с удовлетворительной точностью представлены формулой

$$N(r) \sim \frac{1}{r} e^{-r/L}$$

величины $L$ (длины релаксации), полученные экспериментальным и расчетным путем, отличались между собой на 8—12%. Для устранения этого расхождения требуется уточнение величин групповых параметров для нейтронов верхних групп, которое в настоящее время производится. Неточность вычисления потоков нейтронов верхних групп привела к ошибкам и в пространственных распределениях более медленных нейтронов.

Для того, чтобы иметь возможность независимой проверки групповых параметров в нижних энергетических группах был произведен 18-групповой расчет пространственно-энергетического распределения нейтронов в никелевом экране, в котором в качестве источников нейтронов использовалось экспериментальное распределение нейтронов верхней группы, измеренное с помощью камеры деления со слоем $Th^{232}$. Расчет производился в $P_1$—приближении в предположении о сферической симметрии реактора. На внутренней границе никелевого экрана требовалось равенство потоков нейтронов всех энергетических групп потокам, полученным в 1-м варианте расчета. Использованная при расчете 18-групповая система констант для никеля дана в таблице I.

Энергетическая зависимость чувствительностей использованных детекторов определялась путем усреднения всех имевшихся в нашем распоряжении данных о сечениях соответствующих реакций. В тех областях энергий, где экспериментальные данные о сечениях отсутствовали, сечения вычислялись на основании имеющихся сведений о резонансных параметрах.

Групповые сечения детекторов получались путем усреднения сечений по спектру бесконечной среды из никеля, $\Phi \infty (E)$:

$$\Phi_\infty(E) \sim \frac{1}{\Sigma_t(E) \cdot E} \cdot \varphi(E)$$

где $\varphi(E)$ — вероятность избежать резонансного захвата при замедлении в никеле до энергии $E$.

**Результаты измерений. Сравнение с расчетом**

Результаты измерения распределений различных реакций в никелевом экране реактора БР-1 представлены на рис. 2. Там же приведены распределения этих реакций, полученные в описанном выше 18-групповом расчете.

Таблица I

**18 — ГРУППОВАЯ СИСТЕМА КОНСТАНТ ДЛЯ НИКЕЛЯ***

| № группы, $i$ | 1 | 2 | 3 | 4 | 5 | 6 | 7 | 8 | 9 | 10 | 11 | 12 | 13 | 14 | 15 | 16 | 17 | 18 |
|---|---|---|---|---|---|---|---|---|---|---|---|---|---|---|---|---|---|---|
| $\Delta E$ | ∞ — 1,4Мэв | 1,4— —0,7 | 0,7— —0,4 | 0,4— —0,2 | 0,2— —0,1 | 100 кэв 47 кэв | 47— —22 | 22— —10 | 10— —1,8 | 1,8— —0,4 | 400 эв 150 эв | 150— —50 | 50— —20 | 20— —7,4 | 7,4— —2,7 | 2,7— —1,0 | 1,0— —0,3 | тепловые |
| $\sigma_{tr}$ | 2,3 | 2,6 | 3,3 | 4,4 | 6,8 | 9,0 | 9,2 | 27,0 | 18,69 | 15,10 | 16,79 | 17,06 | 17,42 | 17,51 | 17,64 | 17,87 | 18,24 | 22,3 |
| $\sigma_{сам}$ | 0,74 | 0,14 | 0,22 | 0,18 | 0,24 | 0,32 | 0,35 | 0,73 | 0,367 | 0,346 | 0,576 | 0,584 | 0,595 | 0,595 | 0,595 | 0,595 | 0,595 | 0 |
| $\sigma_c$ | 0,002 | 0,008 | 0,010 | 0,010 | 0,012 | 0,015 | 0,025 | 0,040 | 0,011 | 0,025 | 0,046 | 0,077 | 0,127 | 0,210 | 0,346 | 0,570 | 0,939 | ** |
| $\sigma_{i\to i+1}$ | 0,37 | 0,14 | 0,22 | 0,18 | 0,24 | 0,32 | 0,35 | 0,73 | 0,367 | 0,346 | 0,576 | 0,584 | 0,595 | 0,595 | 0,595 | 0,595 | 0,595 | — |
| $\sigma_{i\to i+2}$ | 0,13 | 0 | 0 | 0 | 0 | 0 | 0 | 0 | 0 | 0 | 0 | 0 | 0 | 0 | 0 | 0 | — | — |
| $\sigma_{i\to i+3}$ | 0,11 | 0 | 0 | 0 | 0 | 0 | 0 | 0 | 0 | 0 | 0 | 0 | 0 | 0 | 0 | — | — | — |
| $\sigma_{i\to i+4}$ | 0,08 | 0 | 0 | 0 | 0 | 0 | 0 | 0 | 0 | 0 | 0 | 0 | 0 | 0 | — | — | — | — |
| $\sigma_{i\to i+5}$ | 0,03 | 0 | 0 | 0 | 0 | 0 | 0 | 0 | 0 | 0 | 0 | 0 | 0 | — | — | — | — | — |
| $\sigma_{i\to i+6}$ | 0,01 | 0 | 0 | 0 | 0 | 0 | 0 | 0 | 0 | 0 | 0 | 0 | — | — | — | — | — | — |
| $\sigma_{i\to i+7}$ | 0,01 | 0 | 0 | 0 | 0 | 0 | 0 | 0 | 0 | 0 | 0 | — | — | — | — | — | — | — |

* Все сечения даны в барнах.
** Сечение зависит от температуры тепловых нейтронов.

Как видно из рисунка, формы всех расчетных распределений очень близки к полученным на опыте. Расчетные распределения реакций $U^{235}$ (n, f), $Pu^{239}$ (n, f), $Au^{197}$ (n, $\gamma$) и $Cu^{63}$ (n, $\gamma$) почти совпадают с экспериментальными и по абсолютной величине. В случае же других реакций расчеты и экспериментальные данные согласуются хуже. Так расчетные распределения реакций $J^{127}$ (n, $\gamma$) и $Cu^{65}$ (n, $\gamma$) лежат в 1,5 раза ниже, а распределения реакций $Mn^{55}$ (n, $\gamma$) и $Na^{23}$ (n, $\gamma$) соответственно в 1,6 и 1,3 раза выше экспериментальных точек.

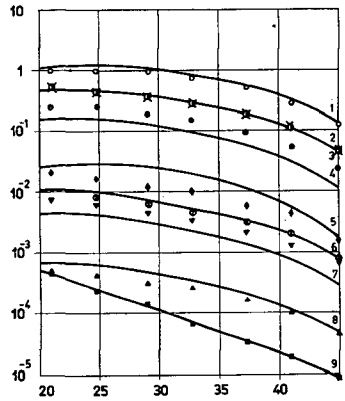


Рис. 2

Распределения реакций в никелевом экране. Кривые рассчитаны в $P_1$ — приближении многогрупповым методом. Экспериментальные данные представлены точками.

| *№ кривой* | *Символ* | *Реакция* |
|---|---|---|
| 1. | ◐ | $Au^{197}$ ($n$, $\gamma$) |
| 2. | ○ | $U^{235}$ ($n$, f) |
| 3. | × | $Pu^{239}$ ($n$, f) |
| 4. | ● | $J^{127}$ ($n$, $\gamma$) |
| 5. | ◆ | $Mn^{55}$ ($n$, $\gamma$) |
| 6. | ⊗ | $Cu^{63}$ ($n$, $\gamma$) |
| 7. | ▼ | $Cu^{65}$ ($n$, $\gamma$) |
| 8. | ▲ | $Na^{23}$ ($n$, $\gamma$) |
| 9. | ■ | $Th^{232}$ ($n$, f) |

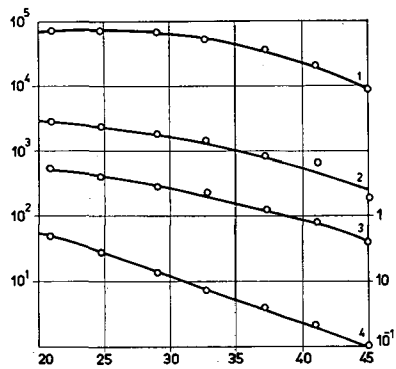


Рис. 3

Распределения потоков нейтронов различных энергий в никелевом экране.
1 — Поток нейтронов с энергией 4,9 эв; 2 — Поток нейтронов с энергией 337 эв; 3 — Поток нейтронов с энергией 2850 эв; 4 — Поток нейтронов с энергией 1,4 Мэв.

Указанные расхождения не могут быть объяснены неточностями расчета пространственно-энергетических распределений. Действительно, характеры энергетической зависимости сечений реакций $Mn^{55}$ (n, $\gamma$) и $Cu^{65}$ (n, $\gamma$), например, в интересующей нас области энергий весьма близки друг к другу. Однако, расчетные распределения этих реакций отклоняются от экспериментальных данных в разные стороны и, следовательно, расхождения не могут быть устранены путем измерения расчетного спектра. Изложенные соображения заставляют придти к выводу о том, что различие между экспериментальными и расчетными распределениями указанных выше реакций обусловлено неточностью использованных сечений детекторов.

В самом деле, точность, с которой известны резонансные параметры этих реакций, не позволяет надеяться на совпадение экспериментальных и расчетных данных с точностью лучшей 30—40 %.

Сечения реакций деления $Pu^{239}$ и $U^{235}$ и радиационного захвата нейтронов в $Au^{197}$ известны со значительно большей степенью точности, чем сечения остальных реакций. Совпадение экспериментальных и расчетных распределений этих реакций указывают на то, что расчет удовлетворительно описывает ту часть спектра нейтронов, к которой эти детекторы наиболее чувствительны (т.е. в области ниже нескольких кэв).

На рисунке 3 приведены распределения потоков нейтронов с энергиями 4,9, 337, 2850 эв и 1,4 мэв, измеренные с помощью резонансных индикаторов и камеры деления с $Th^{232}$.

Градуировка потоков на единицу мощности реактора была произведена путем сравнения эффективностей детекторов с эффективностью камеры деления с $Pu^{239}$, которой измерялся интеграл числа делений в активной зоне. Сравнение эффективностей производилось в стандартном потоке тепловых нейтронов.

На рис. 4 приведена гистограмма спектра нейтронов на расстоянии 29 см от центра реактора, полученная в результате 18-группового расчета. Точки на этом рисунке представляют экспериментальные данные. Как видно из рисунка, между расчетным и экспериментальным спектрами наблюдается удовлетворительное согласие.

Из рисунка 3 можно видеть, что начиная с расстояний 30 см от центра реактора отношения потоков нейтронов с энергиями 2850, 337 и 4,9 эв со-

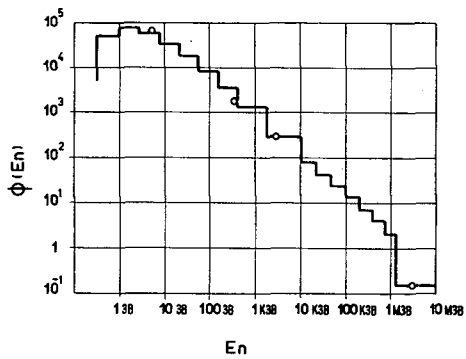


Рис. 4

Сравнение экспериментальных данных о потоках нейтронов различных энергий с расчетной гистограммой нейтронного спектра на расстоянии 29 см от центра реактора.

храняются постоянными. Неизменность формы мягкой области нейтронного спектра обусловлена тем обстоятельством, что замедление нейтронов в никеле в области 1-х резонансов и при более низких энергиях происходит значительно быстрее, чем замедление в резонансной области. Длина замедления быстрых нейтронов до энергии 10 кэв оказывается существенно больше, чем длина миграции нейтронов с энергией 10 эв. Поэтому при рассмотрении замедления нейтронов в области ниже нескольких килоэлектронвольт источники с хорошим приближением можно считать равномерно распределенными в пространстве. Спектр нейтронов в этом случае должен быть близок к равновесному спектру среды [1] и описываться формулой (1).

Расчеты показали, что в области энергий ниже 1-го резонанса никеля отклонения экспериментального спектра от равновесного находятся в пределах экспериментальных погрешностей.

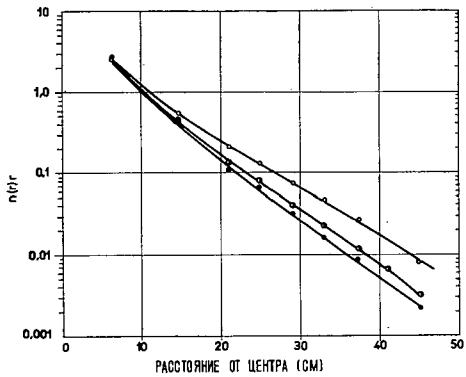


Рис. 5

Распределения потоков нейтронов, измеренные с помощью пороговых реакций.

1. ○ $Th^{232}$ (n, f)
2. ◐ $P^{31}$ (n, p)
3. ● $Si^{28}$ (n, p)

Распределения потоков, полученных с помощью пороговых индикаторов, представлены на рис. 5. Как видно из рисунка, длина релаксации нейтронов тем меньше, чем выше порог детектора. Следовательно, в никеле происходит непрерывное смягчение жесткой части спектра нейтронов. Длины релаксации, определенные по наклону кривых распределений использовавшихся нами пороговых реакций, приведены в таблице II.

Таблица II

**ДЛИНЫ РЕЛАКСАЦИИ БЫСТРЫХ НЕЙТРОНОВ В НИКЕЛЕ**

| Детектор | Порог (Мэв) | Длина релаксации (см) |
|---|---|---|
| $Th^{232}$ (n, f) | 1,5 | 7,9±0,2 |
| $P^{31}$ (n, p) | 2,5 | 6,6±0,2 |
| $Si^{28}$ (n, p) | 6,1 | 6,0±0,2 |

**Заключение**

Разумное согласие между расчетными и экспериментальными распределениями различных реакций заставляет думать, что в использованной нами многогрупповой системе констант для никеля параметры по крайней мере нижних групп выбраны правильно.

В области энергий от нескольких десятков кэв до 1 Мэв анализ спектра нейтронов не мог быть произведен на основании результатов, описанных выше экспериментов, поскольку в этой спектральной области лежала лишь небольшая доля нейтронов. Однако, полученные в настоящей работе данные свидетельствуют о том, что групповые параметры для нейтронов средних групп в целом правильно описывают замедление нейтронов в резонансной области, т.к. в противном случае согласия в формах расчетных и экспериментальных распределений медленных нейтронов не наблюдалось бы.

Более детальная проверка правильности констант в области энергий выше 10 кэв может быть осуществлена путем изучения пространственно-энергетических распределений нейтронов в среде из никеля с добавкой какого-либо поглотителя. Спектры нейтронов в этом случае были бы жестче и активация детекторов происходила бы в значительной мере и под действием нейтронов, лежащих в резонансной области.

Несмотря на то, что произведенная в настоящей работе проверка многогрупповой системы констант для никеля не является полной, она показала, что использовавшаяся система констант удовлетворительно описывает распространение нейтронов в чистом никеле. Поскольку эта система констант несущественно отличается от использованной при расчете реактора БР-5 [3], можно думать, что причиной отмеченных в указанной работе расхождений между расчетными и экспериментальными распределениями является неучет геометрических особенностей реактора БР-5.

## ЛИТЕРАТУРА

[1] Атомная энергия т.5, стр. 277 (1958)
[2] ЛЕЙПУНСКИЙ, А. И. *и др.* „Экспериментальные реакторы на быстрых нейтронах в СССР“ докл. № 2129 Женева 1958.
[3] НИКОЛАЕВ, М. Н. *и др.* „Измерения распределений нейтронных потоков в реакторе БР-5т. Отчет“ ФИ ГУИАЭ 1960.
[4] ГОЛУБЕВ, В. И. *и др.* „Использование резонансных индикаторов для исследования нейтронных спектров.“ *Атомная энергия* (в печати).

# II. 3. THEORETICAL CORRELATIONS

SM—18/77

# INTEGRAL PHYSICS DATA FOR FAST-REACTOR DESIGN*

W. B. LOEWENSTEIN AND D. MENEGHETTI
ARGONNE NATIONAL LABORATORY, ARGONNE, ILL.,
UNITED STATES OF AMERICA

**Abstract — Résumé — Аннотация — Resumen**

**Integral physics data for fast-reactor design.** The recent compilation of the section on fast-reactor physics for the forthcoming second edition of "Reactor Physics Constants" has necessitated a survey of the available experimental integral data. The choice of fast-reactor-physics integral data to be included in the compilation was based upon two criteria besides availability: (*a*) the data arise from relatively simple systems which lend themselves to simple theoretical analyses; and (*b*) complicated systems representing prototypes or mock-ups having general interest in terms of fast-power reactors.

The first criterion was decided upon so as to list integral data for those systems of most general utility for the verification of cross-section parameters and calculational procedures. The second criterion is based upon presentation of current data on actual fast power breeder reactor systems. These are too complicated for simple theoretical analysis. They demonstrate the complexity of the actual reactor versus the more idealized and easily analysed critical experiment.

Integral physics data for reactor design refer to measurements on reactor systems, critical or otherwise, of the various reactor physics quantities of practical and/or theoretical importance. These characterize and lead to an understanding of the system. The measurements are represented by critical mass, core shape factor, detector ratios, neutron spectra, material replacement experiments, reflector savings, neutron lifetime, Rossi-$\alpha$, and similar quantities.

These data are reviewed and the range of applicability is described. Limitations of experimental and analytical results are shown to exist in certain spectral and criticality analyses. Experimental and analytical investigations are suggested for future work. These will tend to narrow the gap between theory and experiment on "known" systems. They also include investigations to "firm up" the physics of large conceptual, fast power-breeder reactor systems.

**Données de physique intégrale intervenant dans les études de réacteur à neutrons rapides.** La compilation récente du chapitre sur la physique des réacteurs à neutrons rapides dans la préparation de la deuxième édition de «Reactor Physics Constants» a entraîné une récapitulation des résultats disponibles des mesures expérimentales globales. Le choix des données intégrales connues relatives à la physique des réacteurs à neutrons rapides à faire figurer dans cette compilation a été fait en fonction de deux critères: *a*) informations recueillies à partir de réacteurs relativement simples et qui se prêtent à des analyses théoriques simples, et *b*) informations recueillies à partir de réacteurs complexes, représentant des prototypes ou des maquettes, et qui offrent un intérêt général pour les réacteurs de puissance à neutrons rapides.

Le premier critère a pour objet de donner une énumération des informations concernant les systèmes les plus couramment utilisés pour vérifier les paramètres des sections efficaces et les méthodes de calcul. Le deuxième critère est fondé sur la représentation des informations courantes concernant les réacteurs à surgénération,

* Work performed under the auspices of the United States Atomic Energy Commission.

à neutrons rapides, existant. Ces informations sont trop compliquées pour qu'il soit possible de procéder à leur égard à des analyses théoriques simples. Elles prouvent la complexité du réacteur réel, par rapport à l'expérience critique plus schématique et plus facile à analyser.

Les données intégrales intervenant dans les calculs de réacteurs sont les résultats des mesures faites, sur des types de réacteurs critiques ou non, des diverses grandeurs de la physique des reacteurs qui présentent un intérêt pratique et/ou théorique. Elles caractérisent le type de réacteur et aident à sa compréhension. Les mesures portent sur la masse critique, le facteur forme du cœur, les pourcentages de détection, les spectres des neutrons, les expériences de substitution de matériaux, le gain réflecteur, le temps de vie des neutrons, l'$\alpha$ de Rossi et sur d'autres grandeurs similaires.

Les auteurs examinent ces données et décrivent leurs domaines d'application. Ils montrent que dans certaines analyses de spectre et d'état critique, les résultats expérimentaux et analytiques sont limités. Ils font des suggestions sur l'orientation des recherches expérimentales et analytiques à venir. Elles combleraient le fossé entre la théorie et l'expérience qui existe dans les systèmes «connus». Ces propositions comprennent également des suggestions en vue de «consolider» la physique de modèles théoriques de grands réacteurs surgénérateurs à neutrons rapides.

**Интегральные физические данные для расчетов реакторов на быстрых нейтронах.** Для составленного недавно раздела о физике реакторов на быстрых нейтронах, который должен войти в выпускаемое второе издание „Постоянные физики реакторов", потребовалось собрать материал по имеющимся экспериментальным интегральным данным. При включении в составленный раздел интегральных данных о физике реакторов на быстрых нейтронах, помимо факта их наличия, за основу были взяты два критерия: 1. эти данные получены из относительно простых систем, которые позволяют проводить простые теоретические анализы; 2. сложные системы, которые являются прототипами или моделями, представляют основной интерес для энергетических быстрых реакторов.

Первый критерий был принят для того, чтобы дать перечень интегральных данных таких систем, имеющих очень общее применение для проверки параметров сечения и методов расчетов. Второй критерий дает имеющиеся данные по фактическим энергетическим реакторам-размножителям на быстрых нейтронах. Эти системы слишком сложны для проведения простого теоретического анализа. Они свидетельствуют о сложности фактического реактора по сравнению с более идеализированным и легко анализируемым критическим опытом.

Интегральные физические данные для расчета реактора получены в результате проведенных на реакторных системах критических или некритических измерений, различных величин реакторной физики, имеющих практическое и теоретическое значения, или то или другое значение. Они характеризуют и позволяют понять систему. Даны измерения критической массы, коэффициента формы активной зоны, коэффициентов детекторов, спектров нейтронов, опытов с заменой материала, отражательной добавки, времени жизни нейтронов, Rossi-$\alpha$ и подобных характеристик и величин.

В докладе рассматриваются эти данные и описываются области их применения. Показано, что существуют ограничения и в экспериментальных и в аналитических результатах при анализах спектра и критичности системы.

Даны наметки будущих экспериментальных и аналитических исследований. Эти исследования помогут уменьшить разрыв между теорией и опытом для „известных" систем. Намечаются также исследования по „подкреплению" данных физики крупных энергетических реакторов-размножителей на быстрых нейтронах.

**Datos físicos integrales para el diseño de reactores rápidos.** La preparación del capítulo dedicado a la física de los reactores rápidos, en la segunda edición de la publicación «Reactor Physics Constants» que aparecerá en breve, exigió la recopilación de los datos disponibles sobre experimentos integrales. La elección de los datos integrales de física de los reactores rápidos que se ha de incluir en esa sección se basó

en los dos criterios siguientes: *a*) que los datos provengan de sistemas relativamente simples que se presten para un análisis teórico sencillo; y *b*) que se trate de sistemas complejos que representan prototipos o maquetas que ofrecen interés general para el estudio de los reactores de potencia rápidos.

Se fijó el primer criterio con la intención de registrar los datos integrales de aquellos sistemas que tienen una utilidad más general en la verificación de los parámetros y los procedimientos de cálculo de las secciones eficaces. El segundo criterio se basa en la presentación de los datos corrientes sobre sistemas reales de reactores de potencia reproductores rápidos. Estos son demasiado complicados para permitir un análisis teórico sencillo. Constituyen una demostración de la complejidad del reactor real si se compara con la instalación crítica de experimentación más esquemática y más fácil de analizar.

Los datos físicos integrales que intrevienen en el diseño de reactores constituyen el resultado de mediciones efectuadas en conjuntos críticos o subcríticos, de las diversas magnitudes físicas que presentan interés práctico y/o teórico. Esas magnitudes físicas caracterizan al sistema y permiten comprenderlo. Las mediciones mencionadas se refieren a la masa crítica, el factor de forma del cuerpo, las razones de detección, los espectros neutrónicos, los experimentos de sustitución de materiales, la economía del reflector, la vida de los neutrones, el $\alpha$ de Rossi y otras magnitudes análogas.

Los autores examinan estos datos y definen su campo de aplicación. Demuestran que existen límites de validez para los resultados experimentales y analíticos en ciertos estudios espectrales y de criticidad. Proponen algunas investigaciones experimentales y analíticas que podrían constituir el objeto de futuros trabajos y que contribuirían a colmar la laguna entre la teoría y la experimentación en los sistemas «conocidos». Al mismo tiempo, entre dichas investigaciones sugeridas se incluyen algunas tendientes a asentar sobre bases más firmes la física de los modelos de reactores de potencia reproductores rápidos.

## Introduction

Integral physics-data for reactor design refer to measurements on reactor systems, critical or otherwise, of the various reactor-physics quantities of practical and/or theoretical importance. These characterize and lead to an understanding of the system. The measurements include critical mass, shape factor, detector ratios, neutron spectra, material-replacement experiments, reflector savings, neutron lifetime, Rossi-$\alpha$ and similar quantities. These data are useful towards an understanding of the various reactor systems. Calculational procedures and cross-section parameters may be tested by comparison of calculated integral quantities with corresponding experimental quantities. From the practical viewpoint, the reliability of similar calculations for predicting properties of projected systems may be estimated. Integral comparisons between theory and experiment often point out inadequacies in cross-section data and/or in calculational procedures. Such comparisons tend to point out those areas requiring further experimental or analytical investigation.

Recent compilation of the section on fast-reactor physics for the forthcoming second edition of "Reactor Physics Constants" [1] has necessitated a survey of the available experimental integral data. The choice of information in fast-reactor physics integral data to be included in the compulation was, besides availability, based upon two criteria: that the data arise either from (*i*) relatively simple systems which lend themselves to simple theoretical analyses; or from (*ii*) complicated systems representing prototypes or mock-ups having general interest in terms of fast power reactors.

The first criterion was decided upon so as to list integral data for those systems of most general utility for the verification of cross-section parameters and calculational procedures. The second criterion is based upon presentation of current data on actual fast power-breeder reactor systems. These are too complicated for simple theoretical analysis. They demonstrate the complexity of the actual reactor *versus* the more idealized and easily analysed clean-geometry critical experiment.

Experimental information on fast-neutron systems is inadequate for a complete empirical understanding of fast-neutron physics. Such experimental information is not even adequate for predicting empirically the criticality of the many types of fast-neutron system currently being studied for various applications. This shortage of all-inclusive information has placed a premium on analytical techniques. Neutron cross-sections of pure materials as a function of neutron energy have been extensively investigated. These are then used in a multi-group transport or diffusion-theory formalism for comparison with measured integral reactor observables. To date, the agreement between theory and experiment is such that the analyst is quite cautious about predicting the neutronics of fast-neutron systems which have not been experimentally investigated. "Experimental investigation" does not imply here a mock-up of the conceptual system but does require an experimental investigation of a system "similar" to that of interest. "Similarity" implies that critical mass, core, reflector and spectral properties are generally like those of the conceptual system.

The major reason for the limitation on the type and number of critical experiments may be attributed to the limitation on the amounts of fissionable material available for such studies. The largest reported $U^{235}$ critical masses are between 580 and 700 kg. Reported critical masses utilizing Pu in any form have not exceeded 50 kg, while those utilizing $U^{233}$ have not yet gone critical without the addition of appreciable amounts of $U^{235}$. This experimental state of affairs is in stark contrast with the critical-mass requirements of the large central-station fast power-breeder reactor systems requiring up to 1000 kg of Pu or 1500 kg of $U^{235}$. Extrapolation of information from the known, relatively small, fast critical systems to the large conceptual systems leaves considerable uncertainty about the neutronics of the latter. To this end, a large amount of analytical effort is devoted to the means of inferring systematically the characteristics of the large assemblies from experiments on small systems. The latter may contain a region having the composition and spectrum of the conceptual system.

The understanding of the detailed reactivity and spectral behaviour of the systems which have been studied experimentally is also not complete. For example, multi-group techniques do not generally predict the measured $\sigma_c^{U^{238}}/\sigma_f^{U^{235}}$, important for determining the conversion ratio of a $U^{235}$-fuelled system. Similarly, it is difficult to infer properly the temperature and power coefficients of reactor systems from a zero-power critical experiment. Indirect experiments by replacing materials in the reactor core or reflector have given some insight into such problems but satisfactory precision on agreement between theory and experiment is, in general, not to be found. Agreement can, in all cases, be individually "forced" for a particular system. This latter approach not only loses generality, but also introduces uncertainty in the system prediction, for it is not always clear that the experiment is "correct" and/or applicable.

The limitations described form then a basis for a review of existing fast-neutron system data. Certainly, there is a great deal of information, much of it almost repetitive. There is sufficient general information that one can confidently predict

most of the necessary physics parameters of core volumes up to 200 l. Information becomes more limited in the 200- to 500-l core-size and is virtually non-existent beyond that size.

## 1. Critical-mass, core and reflector studies

The neutronics of fast-neutron systems centre about critical assemblies or reactors. The general nature of these is described before citing the detailed measurements performed on them. Most of the systems are relatively simple and thus amenable to calculation in spherical geometry by the use of shape factors* and corrections for heterogeneity and irregular boundaries.

### Pu- AND $U^{233}$-FUELLED SYSTEMS

Plutonium- and $U^{233}$-fuelled fast critical assemblies are reported by both the Los Alamos Scientific Laboratory (LASL) and the University of California Radiation Laboratory (UCRL).

High-density $\delta$-phase spherical plutonium cores are reported by LASL [2]. The unreflected (Jezebel) and the natural-uranium-reflected (Popsy) systems are basic. Criticality, spectrum and reactivity effects have been studied in detail.

Criticality only has been obtained for some Be-reflected high-density $\alpha$-phase [3] spherical plutonium cores at UCRL. Several $\delta$-phase spherical plutonium cores reflected by various thicknesses of carbon and beryllium are reported by the same group [4].

Critical reflector thicknesses for $U^{233}$ and $Pu^{239}$ spherical high-density cores are reported by LASL [5]. Reflectors include enriched (93%) uranium, natural uranium, Be, and tungsten-alloy (91.3 wt.% W). These are the only critical experiments utilizing up to 10 kg $U^{233}$. It is from such integral data, when correlated with calculations, that an unreflected sphere of $U^{233}$ is expected to be critical with about 16 kg $U^{233}$.

Critical masses of a cylindrical, unreflected Pu core and of a series of cylindrical, diluted, unreflected Pu cores having nominal Pu : diluent ratios of 2 : 1 have been reported [6] with depleted uranium, steel, Th, Al and air as diluents. Similar cylindrical systems with diluted cores but reflected with 19 cm natural uranium or with 19 cm thorium are also reported for fuel : diluent ratios of 1 : 1, 2 : 1 and 1 : 2.

These data are reported as measured. Serious analyses of these experiments would require some understanding of the inhomogeneity effects [7]. The basic assembly consists of stacks of $\sim$0.34-cm-thick Pu plates separated by diluent plates with $\sim$0.32, 0.64 and 1.27 cm thickness. All of the cores have a 15.1-cm diameter. The range of the core height to diameter ($L/D$) is fairly large ($0.23 \leq L/D \leq 2.82$) and many of these results are subject to appreciable shape-factor correction[1] for simple analysis in spherical geometry. These data do form a basis for the analysis of diluting plutonium with a representative coolant, structural and fertile materials of interest to reactor design. They are very useful towards the determination or verification of high-energy constants in a multi-group scheme.

---

* The shape factor is defined as the ratio of the spherical critical-mass of the system with similar core composition and reflector parameters to the critical mass of a given assembly.

## Highly enriched $U^{235}$ systems in optimum geometry

Among the most extensively studied fast-neutron critical systems are the bare (Godiva) [8] and natural-uranium-reflected (Topsy) assemblies from LASL [8, 9, 10, 11]. The spherical cores consist of high-density highly enriched ($\sim$93.5%) uranium. These, like the Jezebel and Popsy assemblies cited above, have yielded much information on criticality, spectrum and material replacement (reactivity effects) characteristic of extremely hard fast-neutron spectra. The Godiva assembly has also been subjected to a series of super prompt-critical bursts [12].

High-density enriched-uranium ($\sim$93.5%) cores have been studied at LASL with a multitude of reflectors of various thicknesses [11, 13]. While some of these experiments were performed in cylindrical geometry, all are reported in spherical geometry after suitable shape-factor corrections are applied. Reflectors include natural uranium, graphite, water, heavy water, paraffin, beryllium, beryllium oxide, tungsten, tungsten carbide, copper, nickel, aluminium, aluminium oxide, iron, zinc, thorium, titanium and magnesium.

These data are basic to nuclear-safety analyses. They can be helpful towards the determination of high-energy cross-section parameters for the reflector materials as used in multi-group analyses.

## Uranium cores of various enrichments and dilutions

A variety of critical-mass data for cores of various enrichments of $U^{235}$ in uranium and cores with diluents of structural, moderator and coolant materials have been reported by LASL and Argonne National Laboratory (ANL). The LASL Jemima [8, 14, 15] assemblies are stacks of interspersed plates of high-density highly enriched and natural uranium. Three bare Jemima assemblies have $U^{235}$ volume-fractions of about 53%, 37% and 29% with corresponding $L/D$ ratios of 0.58, 1.0 and 1.8 respectively. The single reflected Jemima assembly has about 16% $U^{235}$ by volume and is reflected by 7.62 cm of natural uranium. These data will require inhomogeneity corrections for comparison with homogeneous reactor calculations. The thicknesses of constituent plates in these assemblies are 0.6 cm and 0.8 cm for natural and enriched uranium, respectively. For example, the $\sim$29% enriched-uranium assembly consists of stacks, each containing one enriched and three natural-uranium plates. The distance between successive enriched uranium plates is 1.8 cm. The effect of inhomogeneity may be quite pronounced since it extends across the diameter of the core.

The ZPR-III assemblies [7] consist of thin rectangular plates of the basic constituent materials placed into core drawers of a two-half honeycomb machine. The assemblies are generally cylindrical cores, with $L/D$ ratios chosen to require the minimum of shape-factor corrections. There are two spherical systems. The assemblies are reflected by thick, high-density reflectors containing about 83.4 vol.% depleted uranium and 9 vol.% stainless steel. The ZPR-III assemblies include the following core compositions:

1. $U^{235}$, $U^{238}$, stainless steel, and aluminium containing 5 to 14 vol. % $U^{235}$, 1 to 38% $U^{238}$, 12 to 28% stainless steel and 19 to 43% aluminium [7, 16, 17].
2. $U^{235}$ highly diluted with $U^{238}$, including nominal $U^{238}/U^{235}$ ratios from 5 to 10 [16, 17].
3. $U^{235}$ diluted with graphite representing nominal graphite/$U^{235}$ volume ratios from 2 to 7 [7, 16, 17].

4. An assembly containing 43 vol. % aluminium and 9% stainless steel as diluent and an assembly containing 80 vol. % stainless steel as diluent, both fuelled with about 9.3 vol. % $U^{235}$ [16, 17].

5. Two oxide assemblies, fuelled with 5 to 6% $U^{235}$ and 9 to 10% $U^{238}$, having sufficient oxygen content in $Al_2O_3$ to provide O/U atomic ratios of about 2 and 1. The structural material is represented by about 25% stainless steel and the coolant by about 24% total aluminium content [16].

6. A sodium-containing assembly fuelled with ~9 vol. % $U^{235}$, 64% stainless steel and 16% sodium [16].

7. A core which mocks up the composition of a carbide-fuelled fast reactor (~5 vol. % $U^{235}$, 10% C, 25% aluminium) [16].

A wide variety of core sizes, compositions, neutron spectra and critical masses is represented by these particular assemblies. They pose a real test for analytical techniques and multi-group constants. These data must also be corrected for inhomogeneity when desiring a precision comparison between theory and experiment. Some of these systems approach compositions of idealized fast reactors designed to operate with a heat-removal system. Critical mass, spectral properties, neutron lifetime (by Rossi-$\alpha$) and selected material replacement experiments are reported for each system. Some systems have been subjected to more intensive experimental investigation. This variation of effort generally represents the type and number of material-replacement experiments performed on the system. Some assemblies stimulated only material-replacement experiments at the centre of the core, while on others material-replacement experiments were performed throughout the core and reflector. In addition, a number of EBR-II-size systems [7], containing about 14 vol. % $U^{235}$, 16% $U^{238}$, 31.5% Al and 12% stainless steel, were investigated on ZPR-III to determine the effect of low-density radial, axial and central blankets.

### Extreme geometry critical experiments

A number of critical configurations with high and low ratios of core height to core diameter were investigated at LASL and ANL. The latter (ANL) included rectangular core geometry [7]. These assemblies include two core compositions, one similar to that of EBR-II, while the other is a fairly dense core with ${}_NU^{238}/{}_NU^{235} \approx 3$. Both core systems are reflected with a high-density (~83 vol. %) depleted uranium reflector. Such data are basic to the construction of shape-factor curves [1]. The ratio of core height to diameter ($L/D$) varied from 0.2 to 2.2 for the EBR-II-size systems.

Another series of experiments basic to the construction of shape-factor curves are the LASL assemblies of highly enriched high-density uranium cores reflected by various thicknesses of natural uranium, graphite and water [10, 11, 18]. The ratios of core height to diameter are from 0.3 to 1.9, 0.2 to 3.0 and 0.2 to 3.5 for the water, graphite and natural-uranium reflectors respectively.

Special critical experiments in extreme geometry (very high or very low $L/D$) are reported by LASL with highly enriched, high-density uranium and plutonium with various thicknesses of natural uranium, graphite, $H_2O$, Be and polyethylene reflectors [19]. Critical-mass studies using 46% enriched uranium and having low $L/D$ ratios have been carried out at Aldermaston [20] for unreflected and reflected flat cylinders. Natural uranium, graphite, graphite and borated graphite, aluminium and steel are the reflectors studied to obtain experimental information about the consequences of fast-reactor core melt-down.

A series of critical experiments is reported from LASL [11] showing the influence of both internal and external reflectors for annular, high-density, highly enriched uranium cores. The reflectors are natural uranium polyethylene, graphite, and natural uranium in polyethylene. An assembly without inner reflector is also reported. The core heights are from 12.7 to 17.8 cm and the inner and outer core diameters are 15 and 31 cm respectively.

SPECIFIC REACTOR SYSTEMS

A number of fast-reactor critical experiments have been performed which do not lend themselves readily to criticality calculations in simple geometry. In most cases these have been performed to obtain design information for a specific reactor system. Others were investigated to obtain the effect of perturbing the idealized simple system by introducing structural plenum regions, etc., such as may be required for actual reactor design.

Typical of the critical experiments yielding design data for reactor construction are the results from ZEUS [21] which yielded detailed physics design parameters for the UKAEA fast reactor. Four distinct $U^{235}$-fuelled core assemblies were investigated. The cylindrical ZEUS cores have a radial reflector different from that in the axial direction. The various assemblies ranged in critical mass from 190 kg to 210 kg $U^{235}$. One of the assemblies was designed to yield information on the behaviour of systems containing ceramic fuel elements. The natural-uranium pieces in the core were largely replaced by graphite. In this way, a U:C atomic ratio of 2:3 was achieved which contains sufficient moderator to enable estimates of an actual ceramic fuel.

Engineering mock-ups of the Experimental Breeder Reactor-II (EBR-II) on ZPR-III have included a detailed mock-up with all the geometric and compositional asymmetries due to the presence of control- and safety-rods as well as the structural plena and non-uniform reflectors [7]. Many of the reactivity experiments were performed on a "clean core" mock-up which had a uniform core composition by eliminating detailed representation of control and safety mechanisms. The uniform core containing about 14 vol. % $U^{235}$, 16% $U^{238}$, 26.5% Al and 19% steel had a 36-cm height and $\sim$23-cm radius. The radial reflector consisted of three similar annular regions. Axially the core was reflected by structural gaps containing aluminium and stainless steel together with void, and in turn reflected by a mixture of aluminium, stainless steel, depleted uranium and void. The partial substitution of sodium for aluminium in both core and inner portions of the reflector region enabled an estimate of both incremental and total sodium-worth in the actual EBR-II. The inhomogeneity effects were found to be quite small in this mock-up on ZPR-III. An interesting experiment determined the neutron attenuation of flux through the core, the breeder blanket and into the neutron shield [22]. This experiment served to determine the instrument-response of neutron-flux monitoring equipment located in the neutron shield. Several neutron-shield configurations were investigated for optimum instrument-response. A similar effort determined the required strength of an Sb-Be neutron source to insure adequate count rates during reactor start-up. A series of detailed material-replacement experiments with $U^{235}$, $U^{238}$, Na and stainless steel were performed throughout the reactor core and reflector and are being used for an understanding of the power kinetics of the system. Experiments were performed to determine the reactivity worth of various control mechanisms, including motion of fuel, poison ($B_4{}^{10}C$) or both. These studies also yielded a calibrated oscillator rod [22].

Engineering mock-ups of the Enrico Fermi Fast Breeder Reactor (EFFBR) have also been carried out on ZPR-III [16, 23]. The "clean" core mock-up is a system with a core radius of 40 cm and a height of 76 cm containing approximately 6 vol. % $U^{235}$, 19% $U^{238}$, 25% Al, 14% SS, 5% Mo, and 4% Zr surrounded by axial and radial blanket regions of $U^{238}$ containing various volume-fractions of aluminium and stainless steel to simulate coolant and structural materials. The general experimental programme was similar to that on the EBR-II mock-up. Some experiments were of a more limited nature principally because of limited amounts of material available for macroscopic material-replacement experiments. An actual engineering mock-up including channels for the $B_4C$ control and safety mechanisms served to evaluate the reactivity worth of control, safety and oscillator sub-assemblies.

The Los Alamos Molten Plutonium Reactor (LAMPRE) mock-up experiments were conducted at LASL [24] to yield design information similar to that described for the EBR-II and Fermi reactors. The LAMPRE critical mass is about 22 kg Pu. LAMPRE is primarily a test for the feasibility of using molten Pu as a reactor fuel.

Two EBR-I mock-ups were conducted on ZPR-III [7]. These are the EBR-I Mark-II and Mark-III core mock-ups. The small core-size and geometric asymmetries in reflecting regions make these mock-ups of doubtful general utility other than in a qualitative sense.

The USSR has reported experiments on several reactors [25]. The BR-I zero-power reactor has a small Pu-fuelled reactor with either a depleted uranium or a copper reflector. Reported investigations on this facility were confined to criticality, cross-sections and flux-distribution phenomena.

The UKAEA ZEPHYR [21, 26] facility, also fuelled with a small Pu core, was used for basic reactor cross-section and reactivity studies. The attenuation of neutrons in both a thorium and a natural-uranium reflector was investigated.

In addition to the zero-power fast-reactor mock-ups, there is some physics information available from actual fast-reactor operation at power and/or temperature. Such results are currently limited to those obtained from:

1. The LASL fast reactor (Clementine). This is a Hg-cooled and Pu-fuelled system [27].
2. The ANL EBR-I. Three cores (Marks I, II and III) have yielded physics information on the basic reactor statics as well as an extended amount of data pertaining to reactor kinetics [28, 29, 30].
3. The USSR BR-2 reactor [25] is a Hg-cooled Pu-fuelled fast reactor, similar in size to the BR-1 experiment, with a uranium reflector.
4. The USSR Br-5 reactor [31] is fuelled with plutonium oxide near the centre of a small core surrounded by uranium molybdenum-alloy elements at the core periphery. This reactor is reported to have operated around 5 MW.
5. The UKAEA fast reactor (Dounreay) [32] has gone critical and been subjected to some low-power operation. Temperature effects upon reactivity have been measured.
6. Both the EBR-II [33] and the Fermi [34] reactors are expected to be placed into preliminary operational stages during 1961.

Critical experiments of interest because they involve coupling of fast and thermal fissioning regions to form a composite system are exemplified by the coupled fast-thermal power-breeder critical experiment [35] on ZPR-III and the ZPR-V critical assembly [36]. In the former, an internal fast core region is surrounded radially by an inner natural-uranium blanket and axially by a depleted low-density ura-

nium blanket. The radial blanket is then surrounded by a Be moderator region, followed by a depleted high-density uranium blanket surrounding the entire system. The ZPR-V reactor consisted of a central fast core region separated from an outer annular, water-moderated, $U^{235}$-fuelled region by a blanket of natural uranium. Of special interest are the integral data on the detector responses through the different regions and on the division of reactivity. Similar experiments have been reported by the UKAEA on the ZEPHYR reactor [21]. There the main reflector was replaced by graphite to provide a limited amount of neutron moderation for low-energy reactions in the inner uranium reflector surrounding the small Pu core. The USSR BR-3 experiment [25] is also a small coupled system. Thermalization is accomplished by use of a closely spaced uranium-water lattice surrounding a solid uranium region which reflects a small plutonium-fuelled core. The core is essentially that of the BR-1 reactor.

## 2. Integral data on core mock-up inhomogeneities

A series of experiments to estimate the effect of using finite fuel-plate thicknesses upon reactivity have been performed on various ZPR-III fast assemblies [7, 16]. These experiments determine the sensitivity of a given composition system to various fuel-plate thicknesses. In general, changes in reactivity have been determined which were due to the use of highly enriched $U^{235}$ fuel plates of 0.64 cm, 0.32 cm or 0.16 cm thickness. With increased heterogeneity (i.e. thicker fuel plates) an increase in reactivity was observed for the fast systems studied. These inhomogeneity studies suggest that corrections for this effect must be applied to either calculated or measured results for precision comparison between theory and experiment.

## 3. Spectral studies and detector ratios

Currently there is little experimental information on the characteristic neutron spectra of individual fast-neutron systems. Direct measurements of leakage spectra from Godiva and Jezebel [37], the unreflected, high-density, highly enriched uranium and plutonium cores, have been reported. A beam of neutrons was extracted from the EBR-I core for spectral studies [30]. All three of these experiments use the nuclear emulsion technique while low-energy neutrons from the EBR-I spectrum were detected with a cloud chamber. Proton-recoil emulsions were exposed in ZPR-V [36] as well as some ZPR-III assemblies. The latter results have not been reported mainly because data analysis is not complete.

Most of the experimental spectral data for fast-neutron systems must be inferred from measured detector ratios, activation cross-sections and neutron lifetime.

For instance, a measurement of $\bar{\sigma}_f\ U^{238}/\bar{\sigma}_f\ U^{235}$ allows an estimate of the fraction of the neutron flux above the $U^{238}$ fission-threshold ($\sim$1.4 MeV). Similarly, a measurement of $\bar{\sigma}_f\ U^{234}/\bar{\sigma}_f\ U^{235}$ can be used to determine the fraction of neutrons above the fission threshold of $U^{234}$ ($\sim$0.5 MeV). Also $\bar{\sigma}_{n,\gamma}\ U^{238}/\bar{\sigma}_f\ U^{235}$ is important towards a determination of the conversion ratio of a system fuelled with enriched uranium. A comparison of measured with predicted detector ratios from multigroup neutron-flux solutions gives a measure of the adequacy of a cross-section parameter set. Such comparison may suggest improvements or point out possible inconsistencies. Central detector-ratio data for systems whose spectral properties may be readily calculated are generally the basis for such comparisons.

Detector ratios for high-density uranium and plutonium systems (the LASL Godiva, Jezebel and Jemima) [2, 8, 14, 38] include $\bar{\sigma}_f U^{235}/\bar{\sigma}_f U^{238}$, $\bar{\sigma}_f Np^{237}/\bar{\sigma}_f U^{238}$, $\bar{\sigma}_f Pu^{239}/\bar{\sigma}_f U^{235}$, $\bar{\sigma}_f U^{234}/\bar{\sigma}_f U^{235}$, $\bar{\sigma}_f U^{233}/\bar{\sigma}_f U^{235}$ and $\bar{\sigma}_{n,\gamma} U^{238}/\bar{\sigma}_f U^{238}$. The reported values, particularly for $\bar{\sigma}_f U^{235}/\bar{\sigma}_f U^{238}$, are obtained by a variety of experimental techniques which do not always give the same quantity. In most cases the experimental differences are about the same as the difference between theory and average experimental values.

Detector ratios at the core centres for essentially all of the ZPR-III assemblies [7, 16, 17] have been obtained. In most cases these include: $\bar{\sigma}_f U^{238}/\bar{\sigma}_f U^{235}$, $\bar{\sigma}_f U^{234}/\bar{\sigma}_f U^{235}$, $\bar{\sigma}_f Pu^{239}/\bar{\sigma}_f U^{235}$, $\bar{\sigma}_f U^{233}/\bar{\sigma}_f U^{235}$, $\bar{\sigma}_f Pu^{240}/\bar{\sigma}_f U^{235}$ and $\bar{\sigma}_{n,\gamma} U^{238}/\bar{\sigma}_f U^{235}$.

Such data have been extensively studied by comparing them with predictions by multi-group diffusion theory and SNG calculations [8, 15, 39, 40]. In general it is possible to obtain fair agreement between measured and predicted values. Certain disturbing trends are observed when the required precision of comparison between theory and experiment is narrowed. Predicted values for $\bar{\sigma}_{n,\gamma} U^{238}/\bar{\sigma}_f U^{235}$ always appear to exceed measured values, often by as much as 20%. The predicted values of $\bar{\sigma}_f U^{238}/\bar{\sigma}_f U^{235}$ tend to be less than measured for the LASL Godiva, Jezebel, Popsy, Topsy and Jemima systems. The predicted values of the same quantity always tend to exceed measured ANL ZPR-III results. A consistent trend appears in comparing predicted with measured values for $\bar{\sigma}_f Np^{237}/\bar{\sigma}_f U^{238}$ or $\bar{\sigma}_f U^{234}/\bar{\sigma}_f U^{235}$. The former are usually under-predicted while the latter are over-predicted (by as much as 15%). In general it appears that the predicted multi-group neutron spectra tend to be more energetic than measured spectra. This conclusion is even more firmly established when comparing predicted with measured neutron lifetime (by the Rossi-$\alpha$ technique).

Integral out-of-pile measurements of threshold detector responses, with and without a spherical shell of the material to be studied separating the neutron source from the detector, permit the determination of the effective cross-sections averaged over the energy region above the detector threshold [41, 42, 43]. The experimental arrangement consists of a neutron source placed some distance from the shell, and the detector placed at the centre of the shell. Averaged cross-sections for fission-spectrum neutrons above the fission threshold of $U^{238}$ ($\sim$1.4 MeV) and above the fission threshold of $Np^{237}$ ($\sim$0.5 MeV) for uranium and various non-fissionable materials are available. The averaged cross-sections are $\bar{\sigma}_f$, $\bar{\sigma}_{tr}$ and $\bar{\sigma}_{in}$, where $\bar{\sigma}_{in}$ includes all processes other than fission for removal of neutrons from energies above the threshold. The average cross-section for fission of $U^{238}$ has been determined by LEACHMAN and SCHMITT [44].

Activation cross-sections have also been measured in fission [45], Godiva [46], Jezebel [46], ZEUS [21], ZEPHYR [21] and BR-1 [25] spectra for a large number of elements.

Integral measurements of the capture-to-fission ratio ($\alpha$) for both $U^{235}$ and $Pu^{239}$ are reported as a function of position in EBR-I [47]. The measurements were made through the core and the inner and outer blankets by mass-spectrometric techniques.

## 4. Uranium equilibrium-spectrum data

The degradation of neutron energies in a fast reactor is largely due to inelastic scattering. In a dilute fast system (large $U^{238}$ to $U^{235}$ atomic ratio) the neutron spectrum is then primarily determined by a fission spectrum distribution modified

by inelastic scattering in $U^{238}$. Measurements of average cross-sections and of diffusion length in a natural-uranium equilibrium spectrum are thus very useful for a comparison with corresponding calculated values to test the $U^{238}$ group cross-section parameters, especially the inelastic scattering matrix. The experiments generally consist in measuring the energy-dependence and spatial-dependence of various detectors at positions within a large block of natural uranium. One face of the block is fed by neutrons diffusing from a neutron source such as a reactor. The neutrons diffusing into the block cause fission and give rise to a fast-neutron source at a short distance into the block.

In addition, the presence of natural-uranium blankets in numerous reactor systems has enabled measurements of spectra and detector responses at positions, within the blankets, at which an equilibrium spectrum is approached.

Early experiments were performed at the Oak Ridge National Laboratory (ORNL). Recently measurements have been performed in France, at ANL [48] and at LASL [49]. In addition, measurements on depleted uranium have been made in the USSR [25]. The various reported values of diffusion length and detector responses have recently been summarized by CHEZEM [49].

## 5. Material-replacement measurements

A variety of material-replacement experiments in various fast-neutron systems have been reported. Significant systematic investigations include replacement data for the high-density Jezebel, Godiva, Topsy and a nickel-reflected Godiva assemblies [50]. Small samples of materials were substituted throughout core and reflector, where appropriate, to give fairly complete reactivity information as a function of radial position. About 60 distinct isotopes or materials were used in these investigations, some on all four assemblies.

Results of material-replacement experiments at the core centre and core boundary for numerous ZPR-III assemblies have been obtained [7, 16, 17] on a large assortment of materials including the fission-product mock-up materials (Physicum I and II) [7].

Results of material-replacement experiments uniformly distributed throughout the core of the EBR-II and Fermi mock-ups as well as other systems on ZPR-III have also been obtained.

Material-replacement data are often reported in either cent/mole or inhours/kg. (A cent is 1/100 of a dollar, the dollar being the amount of reactivity required to bring a system from delayed to prompt critical. An inhour is the amount of reactivity which will give a stable period of 3600 s.) Generally, material-replacement data become useful upon conversion of the relative-reactivity measurements in terms of reactor period or control-mechanism movement to absolute reactivity. This can be accomplished by assigning a conversion, based largely on theory, between reactor period and absolute reactivity, for example the number of inhours per % $\Delta k/k$. Most fast systems have a non-negligible number of $U^{238}$ fissions. Since the delayed-neutron fraction of $U^{238}$ is greater than either that of $U^{235}$ or $Pu^{239}$, the specification of this conversion, depending also on the importance of delayed *versus* prompt neutrons, becomes an important calculated quantity. Such calculated or estimated values are required to interpret experimental period measurements to absolute reactivity used by the reactor analyst.

The method of conversion described above is by no means unique. Since the conversion requires at least some analytical results, it is possible to choose almost

any reactor parameter that may be predicted with a minimum uncertainty. UKAEA results are usually normalized with respect to the reactivity worth of a sample of Pu at the centre of the core.

Material-replacement data including small sample and macroscopic regional substitution experiments are extremely useful for certain analytical techniques. Small sample substitution can be used to generate spectrum-averaged perturbation cross-sections. Large and small sample substitutions can be used to obtain information about the effect of perturbing a critical reactor. The most interesting such perturbations are either power- or temperature-induced. In a qualitative as well as semi-quantitative sense, such experiments can do much to narrow the scope of theoretical investigations on conceptual systems.

## 6. Integral data for fast-reactor dynamics

Zero- or low-power fast-reactor kinetics below prompt critical are principally determined by the delayed neutrons. Kinetic behaviour above prompt critical is principally determined by the prompt-neutron lifetime.

The influence of fertile fissions on the zero-power kinetics is generally important in a fast power-breeder reactor because of the large quantities of $U^{238}$, Th or $Pu^{240}$ both in the core and breeder blanket reflector. The evaluation of the effective delayed-neutron fraction of the system considers both the spatial distribution of the $U^{238}$ or fertile fissions [7, 8], which differs from that of the fuel ($U^{233}$, $U^{235}$ or $Pu^{239}$) fissions, as well as the different delayed-neutron characteristics of the fuel and fertile materials. Because of the importance of relating the measurements in inhours or cent/mole to reactivity in $\Delta k/k$, the evaluated and/or estimated inhours per per cent reactivity values for various ZPR-III assemblies have been reported [7]. Similar conversion formulae have been obtained for most of the LASL elementary critical experiments [8].

The importance of relating inhours to reactor period has stimulated investigation on the variation of this relationship as a function of the fast-neutron spectrum or the reactor system. This analytical investigation showed that the "inhour curve" is relatively invariant in the range of periods used for making measurements (30—200 s).

The prompt-neutron lifetime has been measured in many systems by various methods. The frequently used Rossi-$\alpha$ method gives the ratio of the overall lifetime of the system and the effective delayed-neutron fraction. The $1/v$ poison method is based upon a determination of the loss of reactivity associated with the insertion of a 1/v absorber uniformly into the system. A review paper [51] describes and compares the various methods [52, 53]. Rossi-$\alpha$ values for the LASL high-density, high-enrichment Pu and U systems and for the Jemima assemblies have been reported [8, 52]. Rossi-$\alpha$ values have been measured for a large number of ZPR-III fast assemblies [7, 53]. The experimental values together with calculated and/or estimated values of delayed-neutron fraction then allow prompt-neutron lifetimes to be determined. The prompt-neutron lifetime is a fairly sensitive "spectral index" of the reactor neutron spectrum.

Experimental information pertaining to the power kinetics of fast-neutron systems is limited to those reactors which have operated on nuclear heat over a large power range. Systematic experimental investigations have been reported for Godiva neutron pulses [12] and for extended periods of operation with EBR-I [28]. The Godiva-I assembly is one of the simplest and most thoroughly investi-

gated spherical critical systems. Godiva-II, the successor to Godiva-I, is a cylindrical reactor but has most of the Godiva-I properties and behaviour. Godiva-I was subjected to a series of self-limiting bursts. Each burst was initiated by a step-change in reactivity. Following the retirement of Godiva-I, after an accidental burst which damaged the reactor, Godiva-II was designed specifically for the reliable production of super-prompt-critical fission bursts. By empirical analysis of a series of Godiva-I bursts various relationships related to the period of the initial excess reactivity have been reported such as: total number of fissions in burst, maximum fission rate, temperature rise, and burst width as a function of excess reactivity above prompt critical. The relations were based on experiments ranging from 1 to 30 cents above prompt critical. (A cent $=0.01$ dollar $\approx 6.6\times$ $\times 10^{-3}\%\ \Delta k/k$.) Initial reactor periods before shut-down coefficients became operative ranged from $3.8\times10^{-2}$ s to $1.2\times10^{-5}$ s [54, 55, 56, 57].

Extended periods of power operation with EBR-I, Mark-I, II and III cores have yielded experimental information on fast power-reactor kinetics and stability [28, 30]. The appearance of a large resonance in the power transfer function and the occurrence of spontaneous oscillations under certain operating conditions on the Mark-II core have stimulated a large analytical effort on the EBR-I core loadings. Summaries of recent experimental and analytical work are given in Ref. [28, 29]. Some analytical models for EBR-I, Mark-II and Mark-III are described in Ref. [29, 58, 59, 60, 61]. The non-linear aspects of such studies are treated in Ref. [62].

The knowledge of the prompt temperature-coefficient of reactivity for fast reactors is of great importance because of its role in the safety of these systems. One component of the prompt temperature-coefficient is due to the Doppler effect which arises from a change in the relative velocity distribution of the neutrons and nuclei following a change in temperature. Doppler-broadening of the cross-section resonances leads to a lessening of flux depletion at these same resonances with a consequent increase in interaction rate. The positive component of a change in the reactivity is due to an increase in the fission rate of $U^{233}$, $U^{235}$, $Pu^{239}$ and $Pu^{241}$ as a result of the Doppler effect. The negative component of a change in reactivity is primarily due to the increase in the neutron-capture rate of Th, $U^{238}$ and $Pu^{240}$, as well as the thermally fissile isotopes just mentioned. The magnitude and sign of the net Doppler coefficient of reactivity is a function of the relative densities of fissionable and fertile materials, the neutron spectrum and the operating temperature of the reactor.

The Doppler temperature coefficient is a difficult quantity to calculate accurately for fast reactors because of the uncertainty of the resonance parameters and level-distribution of fissionable and fertile materials in the tens and hundreds of kilovolt energy region. A number of theoretical estimates of the coefficient for metal-fuelled fast reactors has been made using nuclear theory and low-energy resonance data [63, 64, 65, 66, 67]. Doppler reactivity effects have also been calculated for some large dilute $PuO_2$-$UO_2$-fuelled fast reactors [68, 69]. These analyses indicate that a fast oxide breeder reactor may have a Doppler coefficient of $-1.0\times10^{-5}\ \Delta k/k$ °C at 900°C. Two experiments have been done to measure the Doppler coefficient. The first experiment attempted to measure the Doppler effect of $U^{235}$ in a highly enriched EBR-I mock-up in ZPR-III [70]. A helix made of $U^{235}$ was electrically thermal-cycled between 50°C and 170°C and the change in reactivity was determined using pile oscillator techniques. Because of the uncertainties introduced into the experiment by expansion of the uranium upon

heating, the experiment yielded an upper limit of $0.83 \times 10^{-8}\ \Delta k/k$ °C for the Doppler effect of the 506-g $U^{235}$ sample at an average temperature of 106°C. Extrapolating this value of the Doppler effect to the entire critical mass of the reactor, one estimates the Doppler coefficient to be no greater than $1.6 \times 10^{-6}\ \Delta k/k$°C at 20°C for the EBR-I reactor.

The second measurement of the Doppler effect in a fast reactor was by oscillatory heating of natural-uranium and enriched-uranium (93% $U^{235}$) samples in the central channel of ZEUS [71]. The sample was surrounded by material having a $U^{238}/U^{235}$ ratio of 1.63. The accuracy of these experiments was also limited by the corrections necessary for the thermal-expansion effect of the sample. A small negative temperature coefficient corresponding to increased capture in $U^{238}$ with increasing temperature was reported.

The Doppler temperature coefficient for the entire ZEUS reactor was reported zero within experimental error. An upper limit for the magnitude of the Doppler coefficient, either positive or negative, was placed at $1 \times 10^{-6}$ per °C for the ZEUS reactor.

## 7. Calculational and theoretical information included in the RPCC

A limited amount of information of a calculational and theoretical nature has been included in the RPCC (Reactor Physics Constants Compilation). Foremost is the inclusion of a number of representative multi-group cross-sections [39, 40, 45, 72]. The primary motivation for including particular sets of constants is the versatility afforded by their combined use. Also included are few-group constants.

The calculated bucklings of $U^{235}$-$U^{238}$, $Pu^{239}$-$U^{238}$, $U^{233}$-Th, $Pu^{239}$-Th and $Pu^{239}$-$Pu^{240}$ mixtures as a function of the enrichment of the primary fissionable material in the mixture have been included because of possible general interest.

The results of extrapolation-distance and reflector-savings calculations for bare high-density uranium systems and for such systems surrounded by thick natural-uranium reflectors have been given. Results of calculations of extrapolation distances and reflector savings for some dilute systems are also included. This information is intended for semi-quantitative use. It is really a function of the reactor system and multi-group constants used for the calculations.

There is a section with comments on computational methods as applied to fast-reactor physics calculations [73, 74, 75, 76, 77, 78, 79, 80, 81]. This commentary re-emphasizes the point that "large" few-region reactor systems can be analytically treated with diffusion theory.

## 8. Suggested future experiments and experimental programmes

A review of existing experimental information serves to emphasize those areas where information is inadequate for either empirical analysis or systematic comparison with predicted physics parameters. The inability of theory to predict certain neutronic constants also implies additional experiments, either verifications of the reliability of existing data or new investigations to extend the current realm of experimental understanding.

In the planning of an experimental programme it must be recognized that it should, to a large extent, be stimulated by analytical investigations. It is very difficult to recommend a complete outline of experiments and programmes which should be pursued without knowing the future fast-reactor design requirements.

However, certain experimental requirements are self-evident although they are by no means all-inclusive.

Several relatively small fast reactors are to be fuelled with plutonium. The amount of plutonium per unit core volume will be sufficient to have some effect on the reactor spectrum. It is clearly necessary that the physics of plutonium-fuelled fast reactors might be the subject of a fairly short-range experimental programme. Such investigation would certainly have to include some critical experiments dealing with appreciable quantities of $Pu^{240}$.

The conceptual large central-station fast power-breeder reactor (core volume $>800$ l) is fuelled either with plutonium or uranium-233. No direct experimental information pertaining to these systems exists. There is, then, the question of what experimental information can be obtained on the neutronics of these conceptual systems. The approach may take one or all of several courses, in the performance of:

1. Some Pu-fuelled critical experiments requiring between 500—1000 kg Pu. These could include cores with metal, oxide or carbide "fuel".

2. $U^{235}$-fuelled critical experiments requiring between 800 and 1500 kg $U^{235}$. These reactors would be identical to those in (1) except that the ratio of fertile to fissile atoms in the core is smaller than in the Pu-fuelled system.

3. Exponential experiments with core compositions described in (1) and/or (2). The experience with fast exponential experiments has not been completely satisfactory. This technique may be made more reliable by increasing the size of the exponential column.

4. "Zoned" critical experiments, which may determine some of the required physics data on spectrum and criticality. These experiments are essentially critical exponential experiments. The region or composition of interest is assembled and maintains a fraction of the reactivity of the system. Criticality is achieved with either an internal or an external "driver" having, at least near the boundary of the region of interest, a spectrum similar to that expected in the composition to be studied. Portions of the driver far removed from the composition to be studied are merely a source of neutrons and can have a thermal-, epithermal- or fast-neutron spectrum. The ZPR-V experiments are an approach to this problem. However, insufficient reactivity in the fast system, coupled with a problem of neutron transmission through natural uranium, made the analysis of these experiments difficult. It may be necessary that facilities of this type operate on none, or very few, thermal neutrons.

The use of either zoned critical experiments or exponential experiments will require analytical verification of the feasibility of such an approach. Further, it is recommended that parallel efforts be carried out; one by use of, say, zoned experiments and the other through the direct critical experiment. Such experimental verification would suggest the framework of reliability of the indirect and less expensive approach towards the measurement of interesting reactor parameters.

The experimental scope and understanding of fast-neutron systems can be extended by the performance of a number of elementary critical experiments involving very few, preferably only two or three, materials. For instance, three assemblies have been investigated at ZPR-III that fall directly into this category. Each core contains about 10 vol. % $U^{235}$, the remaining core volume being occupied by either graphite, stainless steel or aluminium respectively. Each system is reflected by high-density depleted uranium. These experiments should be extended

to more degraded neutron spectra by systematically reducing the $U^{235}$ content per unit core volume. Such experiments have been performed with $U^{238}$ core diluent at both ZPR-III and LASL and are extremely useful for analytical studies with $U^{235}$ and $U^{238}$. Other materials of interest to fast-reactor design (such as sodium, molybdenum, niobium and zirconium) would be of considerable interest for few-material critical experiments.

The application of fast reactors in space technology when weight and size are to be minimized is the basis for an entirely new area of critical experiments. It is likely that such reactors will not have a thick uranium reflector. A thin reflector might be typical. Furthermore, the essentially bare core may contain no fertile materials. Most experimentally investigated cores contain sizeable amounts of fertile materials. In certain applications, the core may be quite "leaky" to reactor spectrum neutrons and there is virtually no experimental information about streaming effects in fast-neutron systems.

Existing shape-factor data should be extended to larger systems. Experimental results currently include the small, high-density highly-enriched uranium cores reflected by natural uranium, graphite and water. In addition there are some shape-factor data on EBR-II-size systems in high-density uranium reflectors also. Analytical time, effort and speculation can be reduced by experimentally investigating core shape factors of 500—800 l cores. It will be particularly important to investigate the effect of reflector density and non-uniformity along with the basic shape-factor results. Furthermore, the optimization of certain reflector regions (axial in current reactor designs) will require experimental verification. Optimum fuel-alloy burn-up will determine axial blanket alloy removal. Analytical and experimental efforts should be devoted to enhancing fertile fissions and plutonium production in the axial reflector.

The problem of fast-reactor control should receive considerable attention in the near future. It is apparent that currently designed moving fuel-control mechanisms increase in size roughly with reactor core-size. There is a high penalty in either thermal performance or expense with increasingly larger segments of movable fuel. The use of movable poison ($B_4{}^{10}C$) in a fast reactor presents some problems of mechanical design. It is appropriate to review this situation both analytically and experimentally. Schemes of moderator or moderator-and-poison control may offer promise.

The work leading to the development of techniques for measuring fast-neutron spectra in a differential way (as a function of neutron energy) should be revitalized. More spectral measurements, perhaps using nuclear emulsions, over an extended neutron energy range are required. As agreement between theory and experiment improves on criticality, the detailed spectral data become important for the next step in calculational improvement.

Experiments on heterogeneity effects for cylindrical fuel-rods in coolant and structural matrices will be of inteerst. Similarly, reactivity effects due to voids, and holes in core and reflector regions, have not been systematically investigated.

The analytical predictions of a positive sodium temperature coefficient for large reactors must be experimentally verified. A direct experiment of this effect would require at least 700—800 kg $U^{235}$ in a core with strongly absorbent "structural" material along with either sodium or an aluminium mock-up of the coolant material.

The importance of the Doppler coefficient of reactivity for large fast power-breeder reactors cannot be over-estimated. Experimental data are needed to verify

or reject theoretical predictions. The prompt Doppler coefficient of reactivity in a dilute reactor (large ratio of $N$ fertile/$N$ fissile) may be sufficiently negative to override the less prompt positive coolant void coefficient. Furthermore, in a dilute ceramic-fuelled fast reactor, where there is little if any expansion of fuel, the Doppler coefficient may be the only source of prompt negative reactivity feedback.

Importance measurements, by inserting small sources throughout a reactor, will yield useful information both as a function of position and neutron energy.

It is expected that as the number and types of critical experiments grow, there will be increasing attention paid to measurements pertaining to reactor kinetics.

## REFERENCES

[1] Reactor physics constants, ANL-5800 (1958).
[2] JARVIS, G. A. *et al.*, Two plutonium-metal critical assemblies, *Nucl. Sci. and Engng* **8** 6 (1960) 525.
[3] RALSTON, H. R., Critical parameters of spherical systems of alpha-phase plutonium reflected by beryllium, UCRL-5349 (1958).
[4] KLOVERSTROM, F., Spherical and cylindrical plutonium critical masses, UCRL-4957 (1957).
[5] PLASSMAN, E. A. and WOOD, D. P., Critical reflector thicknesses for spherical $U^{233}$ and $Pu^{239}$ systems, *Nucl. Sci. and Engng* **8** 6 (1960) 615.
[6] WOOD, D., BEYERS, C. and OSBORN, L., Critical masses of cylinders of plutonium diluted with other metals, *Nucl. Sci. and Engng* **8** 6 (1960) 578.
[7] LONG, J. K. *et al.*, Fast neutron power reactor studies with ZPR-III, Proc. 2nd UN Int. Conf. PUAE **12** (1958) 119.
[8] HANSON, G. E., Properties of elementary fast neutron critical assemblies, Proc. 2nd UN Int. Conf. PUAE **12** (1958) 84.
[9] JOSEPHSON, V., PAINE, R. W., Jr. and WOODWARD, L. L., Oralloy shape factor measurements, LA-1155 (1950).
[10] MALARY, E. C., Oralloy cylindrical shape factor and critical mass measurements in graphite, paraffin, and water tampers, LA-1305 (1951).
[11] PAXTON, H. C., Critical data for nuclear safety guides, LAMS-2415 (1960).
[12] WIMETT, T. F. and ORNDOFF, J. D., Applications of Godiva-II neutron pulses, Proc. 2nd UN Int. Conf. PUAE **10** (1958) 449.
[13] GRAVES, G. A. and PAXTON, H. C., Critical masses of oralloy assemblies, *Nucleonics* **15**, 6 (1957) 90.
[14] PAXTON, H. C. *et al.*, Bare critical assemblies of oralloy at intermediate concentrations of $U^{235}$, LA-1671 (1954).
[15] ROACH, W. H., Computational survey of idealized fast breeder reactors, *Nucl. Sci. and Engng* **8** 6 (1960) 621.
[16] Unpublished ZPR-III Data; private communication.
[17] KEENEY, W. P., and LONG, J. K., Dilute fast critical experiments in ZPR-III, *Trans. Amer. nucl. Soc.* **3** 2 (1960) 327.
[18] PAXTON, H. C. and GRAVES, G. A., Critical masses of fissionable metals as basic nuclear safety data, LA-1958 (1956).
[19] HANSEN, G., PAXTON, H. and WOOD, D., Critical plutonium and enriched-uranium-metal cylinders of extreme shape, *Nucl. Sci. and Engng* **8** 6 (1960) 570.
[20] DOMINEY, J. R., LANE, R. C. and THOMAS, A. F., Critical mass studies with slabs of 46% enriched uranium, NR/A-1/61 (1961).
[21] SMITH, R. D. and SANDERS, J. E., Experimental work with zero energy fast reactors, Proc. 2nd UN Int. Conf. PUAE **12** (1958) 89.
[22] Idaho Division Report, ANL-6301 (1960).
[23] ALEXANDERSON, E. L., GARELIS, E. and NIMS, J. B., Critical experiment calculation for the Enrico Fermi reactor, *Trans. Amer. nucl. Soc.* **1** 2 (1958) 98.
[24] BARKMANN, H. G. *et al.*, Preliminary critical experiments on a mockup of the Los Alamos molten plutonium reactor, LA-2142 (1957).
[25] LEIPUNSKY, A. I. *et al.*, Studies in the physics of fast neutron reactors, Proc. 2nd UN Int. Conf. PUAE **12** (1958) 3.

[26] HOLMES, J. E. R. *et al.*, Experimental studies on fast neutron reactors at A. E. R. E., Proc. UN Int. Conf. PUAE **5** (1956) 331.
[27] JURNEY, E. T. *et al.*, The Los Alamos fast plutonium reactor, LA-1679 (1954).
[28] THALGOTT, F. W. *et al.*, Stability studies on EBR-I, Proc. 2nd UN Int. Conf. PUAE **12** (1958) 242; SMITH, R. R. *et al.*, Instability studies with EBR-I Mark-III, ANL-6266 (1960).
[29] Proceedings of the Conference on Transfer Function Measurement and Reactor Stability Analysis, ANL-6205 (1960): SMITH, R. R., Recent EBR-I stability studies, p. 232, STORRER, F., Analysis of the power feedback relations in fast reactors, p. 251, OKRENT, D. and HUMMEL, H. H., Kinetics studies on EBR-I and EBR-II, p. 269.
[30] LICHTENBERGER, H. V. *et al.*, Operating experience and experimental results obtained from a NaK cooled fast reactor, Proc. UN Int. Conf. PUAE **3** (1956) 345.
[31] LEIPUNSKY, A. I. *et al.*, Experimental fast reactors, Proc. 2nd UN Int. Conf. PUAE **9** (1958) 348.
[32] CARTWRIGHT, H. and TATLOCK, J., The Dounreay fast reactor—basic problems in design, Proc. 2nd UN Int. Conf. PUAE **9** (1958) 316.
[33] KOCH, L. J. *et al.*, Construction design of EBR-II: an integrated unmoderated nuclear power plant, Proc. 2nd UN Int. Conf. PUAE **9** (1958) 323.
[34] AMOROSI, A. and YEVICK, G., An appraisal of the Enrico Fermi reactor, Proc. 2nd UN Int. Conf. PUAE **9** (1958) 358.
[35] AVERY, R. *et al.*, Coupled fast-thermal power breeder critical experiment, Proc. 2nd UN Int. Conf. PUAE **12** (1958) 151.
[36] HUMMEL, H. H. *et al.*, Experimental and theoretical studies of the coupled fast-thermal system ZPR-V, Proc. 2nd UN Int. Conf. PUAE **12** (1958) 166.
[37] STEWART, L., Leakage neutron spectrum from a bare $Pu^{239}$ critical assembly, *Nucl. Sci. and Engng* **8** 6 (1960) 595.
[38] NEUER, J. J. *et al.*, Preliminary survey of uranium metal exponential column, LA-2023 (decl. April 2, 1957).
[39] YIFTAH, S., OKRENT, D. and MOLDAUER, P., Fast Reactor Cross Sections —A Study Leading to a Sixteen Group Set, Pergamon Press, New York (1960).
[40] LOEWENSTEIN, W. B. and OKRENT, D., The Physics of fast power reactors, Proc. 2nd UN Int. Conf. PUAE **12** (1958) 16.
[41] BETHE, H. A., The reciprocity theorem in neutron scattering, LA-1428 (1952).
[42] BETHE, H. A., BEYSTER, J. R. and CARTER, R. E., Inelastic cross sections for fission spectrum neutrons, LA-1429 (1955).
[43] CARTER, R. E. and BEYSTER, J. R., Inelastic collision sections for fission spectrum neutrons, *Phys. Rev.* **90** 2 (1953) 389.
[44] LEACHMAN, R. B. and SCHMITT, H. W., Average fission cross section of $U^{238}$ for fission neutrons, LA-1624 (1953).
[45] HUGHES, D. J., GARTH, R. C. and LEVIN, J. S., Fast neutron cross sections and nuclear level density, *Phys. Rev.* **91** 6 (1953) 1423.
[46] BEYERS, C. C., Cross sections of various materials in the Godiva and Jezebel critical assemblies, *Nucl. Sci. and Engng* **8** 6 (1960) 608.
[47] KAFALAS, P., LEVENSON, M. and STEVENS, C. M., Determination of the ratio of capture to fission cross sections in EBR-I, *Nucl. Sci. and Engng* **2** 5 (1957) 657.
[48] BEYER, F. C. *et al.*, The fast exponential experiments, Proc. UN Int. Conf. PUAE **5** (1956) 347.
[49] CHEZEM, C. G., A uranium exponential experiment, *Nucl. Sci. and Engng* **8** 6 (1960) 652.
[50] ENGLE, L. B., HANSON, G. E. and PAXTON, H. C., Reactivity contributions of various materials in Topsy, Godvia and Jezebel, *Nucl. Sci. and Engng* **8** 6 (1960) 543.
[51] BENGSTON, J., Determination of prompt neutron decay constants of multiplying systems, Proc. 2nd UN Int. Conf. PUAE **12** (1958) 63.
[52] ORNDOFF, J. D., Prompt neutron periods of metal critical assemblies *Nucl. Sci. and Engng* **2** 4 (1957) 450.
[53] BRUNSON, G. S. *et al.*, Measuring the prompt period of a reactor, *Nucleonics* **15** 11 (1957) 132.
[54] HANSEN, G. E., Burst characteristics associated with the slow assembly of

fissionable materials, LA-1441 (1952).
[55] FUCHS, K., Efficiency for very slow assembly, LA-596 (1946).
[56] BRITTAN, R. O., Some problems in the safety of fast reactors, ANL-5577 (1956).
[57] STRATTON, W. R., COLVIN, T. H. and LAZARUS, R. B., Analysis of prompt excursions in simple systems and idealized fast reactors, Proc. 2nd UN Int. Conf. PUAE **12** (1958) 196.
[58] CARTER, J. C., SPARKS, D. W. and TESSIER, J. H., The internal feedback of EBR-I Mark-III *Nucl. Sci. and Engng* **8** 4 (1960) 326; CARTER, J. C., SPARKS, D. W. and TESSIER, J. H., The internal feedback of EBR-I Mark-III, ANL-6124 (February, 1960).
[59] BETHE, H. A., Reactor safety and oscillator tests, APDA-117 (1956).
[60] KINCHIN, G. H., The instability of fast reactors, AERE RP/M83 (1956).
[61] ACKROYD, R. T. *et al.*, Stability considerations in the design of fast reactors, Proc. 2nd UN Int. Conf. PUAE **12** (1958) 230.
[62] SANDMEIER, H. A., Nonlinear treatment of large perturbation in power reactor stability, *Nucl. Sci. and Engng* **6** 2 (1959) 85; SANDMEIER, H. A., The kinetics and stability of fast reactors with special considerations of non-linearities, ANL-6014 (1959).
[63] GOERTZEL, G., An estimation of Doppler effect in intermediate and fast neutron reactors, Proc. UN Int. Conf. PUAE **5** (1956) 472.
[64] FESHBACH, G., GOERTZEL, G. and YAMAUCHI, H., Estimation of Doppler effect in fast reactors, *Nucl. Sci. and Engng* **1** 1 (1956) 4.
[65] LANE, A. M., LYNN, J. E. and STOREY, J. S., An estimation of the Doppler effect in fast reactors, AERE T/M 137 (1956).
[66] BETHE, H. A., On the Doppler effect in fast reactors, APDA-119 (1957).
[67] NICHOLSON, R. B., The Doppler effect in fast neutron reactors, APDA-139 (1960).
[68] GREEBLER, P., HUTCHINS, B. A. and SUEOKA, J. R., Calculation of Doppler coefficient and other safety parameters for a large fast oxyde reactor, GEAP-3646 (1961).
[69] GREEBLER, P. and HUTCHINS, B. A., Calculation of Doppler reactivity effects in a $PuO_2$-$UO_2$ fueled fast reactor, *Trans. Amer. nucl. Soc.* **4** 1 (1961).
[70] KATO, W. Y. and BUTLER, D. K., Measurement of the Doppler temperature effect in an EBR-I type assembly, *Nucl. Sci. and Engng* **5** 5 (1959) 320; ANL-5809 (1958).
[71] BAKER, A. R. and JAQUES, T. A. J., A measurement of the contribution of the Doppler effect to the temperature coefficient of reactivity in a fast reactor, AERE R/M 168 (1958).
[72] HANSEN, G. E. and ROACH, W. H., Sixteen group cross sections, Los Alamos Scientific Laboratory Internal Report, N-2-753, Revision 1 (1960).
]73] CARLSON, B. G., Solution of the transport equation by $S_N$ approximations, LA-1891 (1955).
[74] CARLSON, B. G., WENDROFF, B. and BELL, B. I., Solution of the transport equation by the $S_N$ method, Proc. 2nd UN Int. Conf. PUAE **16** (1958) 535.
[75] CARLSON, B. G. *et al.*, The DSN and TDC neutron transport codes, LAMS-2346 (1960).
[76] CARLSON, B. G., Solution of the transport equation by $S_N$ approximations, LA-1599 (1953).
[77] CODD, J., SHEPHERD, L. R. and TAIT, J. H., The Physics of Fast Reactors, Progress in Nuclear Energy, McGraw-Hill Book Co., Inc., New York (1956), Series I: Physics and Mathematics, 264.
[78] FRANKEL, S. and NELSON, E., Methods of treatment of displacement integral equations, AECD-3497 (1953).
[79] MELVIN, H. M., A method of calculating the critical dimensions of spherically symmetrical reactors: Part II. systems with a finite tamper, AERE T/R-587 (1950).
[80] DAVISON, B., Neutron Transport Theory, Clarendon Press, Oxford (1957).
[81] OKRENT, D., AVERY, R. and HUMMEL, H. H., A survey of the theoretical and experimental aspects of fast reactor physics, Proc. UN Int. Conf. PUAE **5** (1956) 347.

SM—18/51

# THE CORRELATION OF INTEGRAL EXPERIMENTS AND HIGH-ENERGY CROSS-SECTIONS

J. CHERNICK, H. C. HONECK, P. MICHAEL, S. O. MOORE AND G. SRIKANTIAH
BROOKHAVEN NATIONAL LABORATORY, UPTON, N.Y.,
UNITED STATES OF AMERICA

**Abstract — Résumé — Аннотация — Resumen**

**The correlation of integral experiments and high-energy cross-sections.** Recent work on the correlation of integral experiments and high-energy cross-sections is discussed. The importance of integral data where cross-section measurements are inadequate is pointed out.

The sensitivity of estimates of fast fission of $U^{238}$ to inelastic cross-sections and energy degradation in the MeV energy range is shown by comparison of integral data with Monte Carlo calculations. It is shown that the Snell experiment is a sensitive index to the absolute values of inelastic cross-sections above 1.4 MeV. The results of attempts by the Brookhaven Cross-Section Evaluation Group to reconcile measurements of inelastic cross-sections of $U^{238}$ are given.

Other areas where integral data and critical experiments can be used to reduce computational uncertainties are the fast effect in beryllium, and $\eta$ of $U^{233}$ at intermediate energies. Critical experiments can reduce the present uncertainty in Be (n, 2n) cross-sections and in intermediate energy values of $\eta_{23}$.

**Corrélation entre les expériences intégrales et les sections efficaces à haute énergie.** Les auteurs analysent les travaux récents sur la corrélation entre les expériences intégrales et les sections efficaces à haute énergie. Ils font ressortir l'importance des données intégrales lorsque les mesures des sections efficaces sont insuffisantes.

Ils montrent que les prévisions concernant la fission rapide de $^{238}U$ dépendent étroitement de la précision des sections efficaces de diffusion inélastique et de la dégradation de l'énergie dans la gamme d'énergie de l'ordre du mégaélectronvolt, en comparant des données intégrales aux résultats des calculs par la méthode de Monte-Carlo. Ils montrent aussi que l'expérience de Snell constitue un indice sensible de la valeur des sections efficaces de diffusion inélastique au-delà de 1,4 MeV. Ils exposent les résultats des tentatives faites par le Groupe d'évaluation des sections efficaces de Brookhaven pour concilier les mesures des sections efficaces de diffusion inélastique de $^{238}U$.

Il existe d'autres domaines où les données intégrales et les expériences critiques peuvent permettre de réduire les incertitudes des calculs: l'effet de fission rapide dans le béryllium et la mesure de $\eta$ de $^{233}U$ à des énergies intermédiaires. Des expériences critiques peuvent réduire l'incertitude des valeurs des sections efficaces Be (n, 2 n) et des valeurs de $\eta_{23}$ pour des énergies intermédiaires.

**Корреляция интегральных экспериментов и поперечных сечений при высоких энергиях.** Обсуждается последняя работа о корреляции интегральных экспериментов и поперечных сечений при высоких энергиях. Указывается на важность интегральных данных в тех случаях, когда измерения поперечного сечения являются недостаточными.

Чувствительность оценок быстрого деления урана-238 в отношении сечения неупругого рассеяния и уменьшения энергии в диапазоне мегаэлектронвольтных энергий показывается сравнением интегральных данных с расчетами Монте Карло. Обнаруживается, что эксперимент Снелла является чувствительным индексом для абсолютных величин сечения неупругого рассеяния для энергий выше 1,4 мегаэлектронвольта. Даются результаты попыток Брукхейвенской группы по оценке поперечных сечений согласовать измерения сечения неупругого процесса урана-238.

Другими областями, где могут быть использованы интегральные данные и критические опыты, чтобы уменьшить вычислительные неточности, быстрый эффект в бериллии и $\eta$ урана-233 для промежуточных энергий. Подобным же образом критические опыты могут уменьшить нынешнюю неточность в поперечном сечении реакции Be (n, 2 n) и в значениях величины $\eta_{23}$ для промежуточных энергий.

**Correlación entre experimentos integrales y secciones eficaces a energías elevadas.** Los autores examinan los trabajos más recientes sobre la correlación entre los experimentos integrales y las secciones eficaces a energías elevadas. Señalan la importancia de contar con datos integrales en los casos en que las mediciones de las secciones eficaces no son satisfactorias.

Comparando los datos integrales con los resultados de los cálculos basados en el método de Monte Carlo, los autores ponen de manifiesto la influencia de las secciones eficaces de dispersión inelástica y la degradación de la energía en la gama de los megaelectrón-voltio sobre las estimaciones de la fisión del $^{238}U$ por neutrones rápidos. Demuestran que el experimento de Snell es un índice sensible de los valores absolutos de las secciones eficaces de dispersión inelástica por encima de los 1,4 MeV. Exponen los resultados alcanzados por el Grupo de evaluación de secciones eficaces, del laboratorio de Brookhaven en su intento de conciliar los resultados de las mediciones de las secciones de dispersión inelástica del $^{238}U$.

Otras cuestiones en que pueden usarse los datos integrales y los experimentos críticos para disminuir la incertidumbre del cómputo son: el efecto de fisión rápida en el berilio y la medición del $\eta$ para el $^{233}U$ a energías intermedias. Los experimentos críticos permiten disminuir la incertidumbre en los valores de la secciones eficaces correspondientes a la reacción Be (n, 2n) y en los valores de $\eta_{23}$ para energías intermedias.

## Introduction

The importance of accurate integral or critical experiments is becoming more widely appreciated in areas where the basic cross-section data are incomplete or persistently discrepant. A good example is the accuracy of recent determinations of the thermal value of eta for $U^{235}$ and $U^{233}$ by manganese-bath integral experiments and by aqueous critical experiments at the Oak Ridge National Laboratory (ORNL).

We should like to point out here some problem areas, of continued interest to us at the Brookhaven National Laboratory (BNL), where accurate integral and critical experiments can be used to supplement the presently inadequate knowledge of high-energy cross-sections.

## The fast effect in uranium

The importance of fast fission in $U^{238}$ for thermal as well as fast reactors need not be repeated here. However, as pointed out at the 1955 Geneva Conference [1], the main barrier to accurate calculations of the fast effect is the absence of adequate data on inelastic cross-sections of $U^{238}$ at energies above its fission threshold.

The improvement in measurements of high-energy inelastic cross-sections has been very slow. As discussed by CRANBERG [2], the available sphere-transmission data do not yield clear-cut results. The introduction of time-of-flight techniques has, however, improved our knowledge of the low-energy-level structure and the cross-sections for excitation of these levels. A tentative assignment of these

cross-sections for $U^{238}$, based on the data of Bachelor, Cranberg and Levin, R. B. Day and A. B. Smith, by S. Oleksa Moore of the Brookhaven Sigma Center is shown in Table I. Cross-section assignments to levels between 1.4 and 2 MeV are more uncertain and two alternate sets differing by about 0.6 b are shown. Above 2 MeV, the lower set has been joined to HOWERTON's estimates [3] of the inelastic cross-sections, the higher set to those of MANDEVILLE and KAVANAGH [4]. At these energies, energy losses in inelastic collisions must still be treated by a statistical model with a neutron temperature of about $0.20\,E_n^{1/2}$, with $E_n$ the neutron energy in MeV.

The ratio $\delta_{28}$ of $U^{238}$ to $U^{235}$ fissions in water-moderated, slightly enriched uranium and uranium oxide lattices has been measured at the Brookhaven and Bettis Laboratories respectively. Monte Carlo calculations by RIEF [5] based on Mandeville's cross-sections were found to be in reasonable agreement with these measurements. However, the data given in Table I indicates that Mandeville and Kavanagh over-estimate the importance of the 44-keV level at energies above the $U^{238}$ fission threshold. In Fig. 1, calculations of $\delta_{28}$ for single

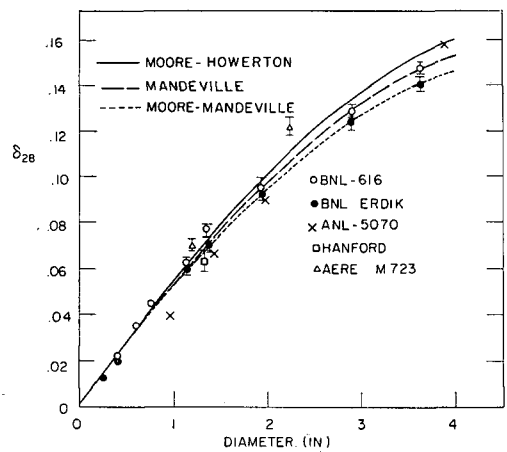


Fig. 1
Fast-fission ratio, $\delta_{28}$, for single natural-uranium rod in graphite.

uranium rods in a uniform thermal-neutron bath in graphite are compared with experimental data from various laboratories. The BNL and Harwell data have adequate precision and follow the general trend of the theoretical curves but apparently suffer from normalization difficulties. Thus the difference in the two sets of BNL results shown is due solely to two different calibration curves, (BNL-616, Price *et al.*, BNL-4715, Erdik) for the relative decay rates of $U^{238}$ and $U^{235}$ fission products in catcher foils as measured by a beta-counter. The problems of data calibration need to be resolved before integral data of this type can be used more effectively.

## The Snell experiment

The ratio of $U^{238}$ to $U^{235}$ fissions measured in a massive block of uranium is a sensitive index of $U^{238}$ inelastic cross-sections. The most recent of these

TABLE I

**CROSS-SECTION FOR EXCITATION OF ENERGY LEVELS IN $U^{238}$**
**(barns)**

| Level energy / $E_n$ (MeV) | 0.044 (MeV) | 0.147 (MeV) | 0.308 (MeV) | 0.654 (MeV) | 0.710 (MeV) | 0.728 (MeV) | 0.900 (MeV) | 1.010 (MeV) | 1.080 (MeV) | 1.210 (MeV) | 1.430 (MeV) | Moore-Howerton | | Moore-Mandeville | |
|---|---|---|---|---|---|---|---|---|---|---|---|---|---|---|---|
| | | | | | | | | | | | | 1.43—2.00 (MeV) | $\sigma_t$ (b) | 1.43—2.00 (MeV) | $\sigma_t$ (b) |
| 0.25 | 1.28 | 0.08 | 0 | 0 | 0 | 0 | 0 | 0 | 0 | 0 | 0 | 0 | 1.36 | 0 | 1.36 |
| 0.55 | 1.49 | 0.29 | 0.13 | 0 | 0 | 0 | 0 | 0 | 0 | 0 | 0 | 0 | 1.91 | 0 | 1.91 |
| 0.75 | 1.22 | 0.45 | 0.12 | 0.05 | 0.07 | 0 | 0 | 0 | 0 | 0 | 0 | 0 | 1.91 | 0 | 1.91 |
| 1.00 | 0.76 | 0.62 | 0.09 | 0.18 | 0.29 | 0.07 | 0.18 | 0 | 0 | 0 | 0 | 0 | 2.19 | 0 | 2.19 |
| 1.25 | 0.19 | 0.58 | 0.04 | 0.24 | 0.40 | 0.09 | 0.55 | 0.22 | 0.08 | 0.01 | 0 | 0 | 2.40 | 0 | 2.40 |
| 1.50 | 0 | 0.42 | 0 | 0.23 | 0.31 | 0.09 | 0.59 | 0.31 | 0.10 | 0.07 | 0.04 | 0 | 2.16 | 0.52 | 2.68 |
| 1.75 | 0 | 0.22 | 0 | 0.18 | 0.20 | 0.07 | 0.54 | 0.33 | 0.09 | 0.08 | 0.07 | 0.50 | 2.28 | 1.00 | 2.78 |
| 1.89 | 0 | 0.10 | 0 | 0.15 | 0.15 | 0.06 | 0.51 | 0.33 | 0.08 | 0.07 | 0.07 | 0.78 | 2.30 | 1.38 | 2.90 |
| 2.00 | 0 | 0 | 0 | 0.12 | 0.11 | 0.05 | 0.47 | 0.34 | 0.08 | 0.06 | 0.07 | 1.00 | 2.30 | 1.70 | 3.00 |

experiments [6] yields a value of $\delta_{\text{Snell}} = 0.582 \pm 0.017$ for natural uranium against older measurements [7] of 0.42. Chezem's result has been confirmed by preliminary measurements at Saclay [8].

In addition to the fast effect, the relaxation lengths measured in Snell experiments yield data on the buckling of low-enrichment uranium blocks. Calculations carried out at BNL indicate that the relaxation length approaches its asymptotic value in a large slab more slowly than does the fast-fission factor and the experimenter may therefore easily over-estimate its value. As suggested by WEINBERG and WIGNER [7], this tendency would account for the large relaxation lengths measured in the blanket of fast reactors.

TABLE II

**THE FAST FISSION FACTOR FOR NATURAL URANIUM**

| | $\delta_{\text{Snell}}$ | Relaxation length (cm) | Buckling ($\text{cm}^{-2}$) | $\delta_{28}$ | $\frac{\delta_{\text{Snell}}}{\delta_{28}}$ | "$L^2$" |
|---|---|---|---|---|---|---|
| Diffusion theory | | | | | | |
| Yiftah | 0.613 | 8.82 | —0.0129 | 0.444 | 1.381 | 21 |
| Moore-Mandeville | 0.411 | 7.89 | —0.0161 | 0.320 | 1.284 | 14 |
| Moore-Howerton | 0.528 | 8.06 | —0.0154 | 0.386 | 1.367 | 17 |
| Transport theory | | | | | | |
| Transport approx. Yiftah, $\bar{\mu}$ "standard" | 0.613 | 9.38 | —0.0114 | 0.449 | 1.365 | 23 |
| $\bar{\mu} \equiv 0$ | 0.570 | 8.30 | —0.0145 | 0.449 | 1.269 | 15 |
| Moore-Mandeville, $\bar{\mu}$ "standard" | 0.412 | 8.19 | —0.0149 | 0.319 | 1.292 | 15 |
| $\bar{\mu} \equiv 0$ | 0.389 | 7.44 | —0.0181 | 0.319 | 1.219 | 10 |
| Moore-Howerton, $\bar{\mu}$ "standard" | 0.528 | 8.36 | —0.0143 | 0.383 | 1.379 | 19 |
| $\bar{\mu} \equiv 0$ | 0.480 | 7.54 | —0.0176 | 0.383 | 1.253 | 11 |
| Chezem (expt.) | 0.582 ±0.017 | 9.17 ±0.18 | — — | — — | — — | — — |
| Weinberg and Wigner | 0.42 | 9.6 | —0.0109 | 0.37 | 1.15 | 12 |

Chezem's data are compared with theoretical calculations in Table II. In addition to the Moore-Mandeville and Moore-Howerton cross-sections, calculations have been carried out on the basis of the cross-section estimates of YIFTAH *et al.* [9]. In addition to $\delta_{\text{Snell}}$, the value of $\delta_{28}$ corresponding to zero-buckling has been calculated.

Diffusion theory results are shown toward the top of the table. The transport approximation with Yiftah's values of $\bar{\mu}$ was used in all these calculations. If energy degradation in elastic collisions is neglected and the transport approximation is used, the exact asymptotic solution of transport theory is given by:

$$\Phi_i = \frac{a_i}{1 - \Sigma_{\mathrm{eff}_i} a_i} \left\{ \sum_{j=1}^{i=1} \Sigma_{\mathrm{in}} (j \to i) \Phi_j + \chi_i \sum_{j=1}^{i\max} (\nu\Sigma_{\mathrm{f}})_j \Phi_j \right\}$$

where

$$a_i = \frac{1}{2\varkappa} \ln \left( \frac{\Sigma_{\mathrm{tr}_i} + \varkappa}{\Sigma_{\mathrm{tr}_i} - \varkappa} \right),$$

$$\Sigma_{\mathrm{tr}_i} = \Sigma_{\mathrm{in}_i} + \Sigma_{\mathrm{f}_i} + \Sigma_{\mathrm{c}_i} + \Sigma_{\mathrm{el}_i} (1 - \bar{\mu}_i) ,$$

$$\Sigma_{\mathrm{eff}_i} = \Sigma_{\mathrm{el}_i} (1 - \bar{\mu}_i) ,$$

and $\varkappa^2$ is the negative buckling of the block, $\chi$ is the energy-distribution of fission neutrons, and the source is normalized such that $\Sigma (\nu\Sigma_{\mathrm{f}})_j \Phi_j = 1$.

The results of the calculation are also given in Table II. It may be noted that the values of $\delta$ are unchanged by the use of transport theory, but there is a significant increase in the value of the relaxation length. It is also clear that low values of inelastic cross-sections are required at energies above the $U^{238}$ fission threshold in order to force agreement with Chezem's data. Yiftah's data are presently in the best agreement with Chezem's results.

The large values of $\delta_{\mathrm{Snell}}/\delta_{28}$ are surprising. Weinberg and Wigner [7] have suggested a value of $(1 + B^2L^2)^{-1} \approx 1.15$ based on one-velocity estimates of $U^{238}$ cross-sections. Values of "$L^2$" required are shown in the last column of the table and are considerably larger than 12 cm$^2$. Because of the sensitivity of the calculation of the reactor-buckling to exact transport effects, higher order transport-theory estimates are currently being carried out at BNL.

The minimum $U^{235}$ enrichment required for criticality in an infinite block of uranium has been reported as 5.4 at. % [10]. Our present calculations yield 5.5%, 6.1% and 6.5% for the Yiftah, Moore-Howerton and Moore-Mandeville cross-sections. The corresponding values of $\delta_{28}$ at these enrichments are reduced slightly to 0.420, 0.360 and 0.303.

## The fast effect in beryllium

There exists a sizable fast effect in beryllium due to the predominance of the (n, 2n) over the (n, $\alpha$) reaction for fission-energy neutrons. Although a serious discrepancy existed until recently between the (n, 2n) cross-section data of Fischer [11] and of Marion, Levin and Cranberg [12], estimates of the fast effect by Moore and Chernick, by Häfele, by Goldstein and by Rief average to a value of $\varepsilon_{\mathrm{Be}} = 1.075 \pm 0.020$. On the other hand, Aline, Novak and Wolfe [13] have maintained that a range of values from 1.03 to 1.19 was possible on the basis of the latter data. The recent results of Cranberg and Levin are in better agreement with those of Fischer; they would tend to increase estimates of $\varepsilon$ slightly. It is doubtful whether anyone would any longer seriously maintain that $\varepsilon$ could be as large as 1.19.

Good estimates of the fast effect in beryllium can also be obtained from critical experiments on thermal, nearly homogeneous $U^{235}$, Be critical experiments. A facility for such experiments in which "room effects" are minimized has just been completed at the Brookhaven National Laboratory.

Although a number of beryllium-moderated critical experiments have been carried out at various laboratories, in the USSR, at Saclay, at the Knolls Atomic Power Laboratory (KAPL) and other laboratories in the United States, we know

of only one critical experiment, denoted as CA-18 at ORNL [14], which approximates the stated requirements. The nuclear data available at the time these experiments were carried out were inadequate for accurate calculations of criticality. In view of the improvement in the cross-section data for both beryllium and $U^{235}$, we recently recalculated the multiplication factor of this assembly and our tentative estimate of 1.015 exceeds the experimental value of 1.002 by about 1%. Since the calculated value of $\varepsilon = 1.070$ for this assembly, it is felt that the CA-18 experiment pins down the fast effect in beryllium to about the accuracy of the cross-section data.

The theoretical estimates could be improved by comparison with more thorough experimental programmes of this type. Thus the thermal absorption cross-section of the beryllium in the CA-18 stack was not measured, although a change in cross-section from the assumed 9 mb to 10 mb would result in a decrease in multiplication factor of 0.4%. Only one old, doubtful age-measurement exists for beryllium, although our calculations yield a $\delta k$ of 4.1% between the assumptions of isotropic and non-isotropic scattering. Experimental measurements of the effect of heterogeneity on such assemblies would be useful, since these could include the effects of thermal and resonance self-shielding of the uranium foils as well as the anisotropy of the thermal-diffusion length. Our multi-group calculations indicate a $\delta k$ of 2.9% for self-shielding effects in CA-18, of which only 1% is contributed by resonance neutron self-shielding. While differences in $k$ between bare and extrapolated dimensions of small assemblies such as CA-18 are important, both the experimental flux distributions and calculations indicate that the effects of the aluminium-grid reflector and other structures increase $k$ by only 1.1%. As previously mentioned, the thermal value of eta for $U^{235}$ is now reliable. Intermediate energy values of eta are less reliable, but our multi-group calculations for CA-18 show that a change in the average eta for $U^{235}$ from 1.7 to 1.8 results in only a small change in $k$. The sensitivity to intermediate-energy eta-values is much more pronounced in less-thermal critical assemblies such as CA-1 [14].

**The energy variation of eta for uranium-233**

The variation of eta of $U^{233}$ with energy is very important in breeder reactors based on the thorium-$U^{233}$ cycle. A definitive value of $\eta_{23} = 2.295 \pm 0.015$ in a well-thermalized spectrum has only recently been obtained. In Fig. 2, values of $\eta_{23}$ are shown over the range from 2—11 eV. The points are calculations based on good resolution total, fission and scattering cross-sections measurements, with no attempt to make the data more consistent by changes in the energy scales of the various experiments. In Fig. 3, we have repeated earlier calculations [15] of the average value of eta in a reactor spectrum. The eta-values are somewhat increased by the recent increase in the thermal value of $\eta_{23}$.

More direct measurements of eta are also shown in Fig. 2. The resolution of these experiments is, however, not good and there are serious discrepancies, for example, between the results reported by YAETER *et al.* [16] and by Moore, Miller and Simpson. The significance of these discrepancies is shown in Fig. 3. While the differences in average eta-values are small for highly thermal or fast reactors, they are extremely serious for reactors in which a considerable fraction of the fissions occurs at intermediate energies.

In view of the difficulties of obtaining reliable eta-measurements at energies above a few eV, it would appear that well-planned programmes of $U^{233}$ critical

experiments are needed. The AETR programme, emphasizing the high-energy end of the neutron spectrum, is at present underway at Atomics International. A programme of water-lattice experiments with $U^{233}$-enriched, thorium-oxide rods has been undertaken by the experimental reactor physics group under Kouts at the Brookhaven National Laboratory. As $U^{233}$ becomes more readily available

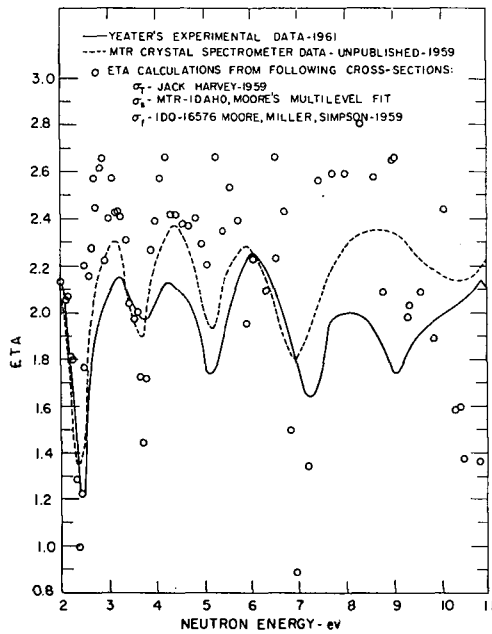


Fig. 2
Dependence of $\eta$ of $U^{233}$ on neutron spectrum.

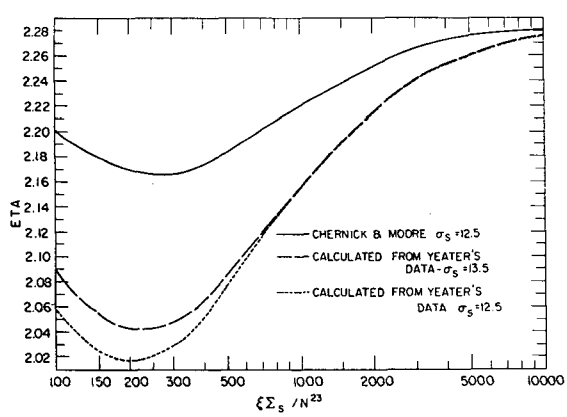


Fig. 3
Eta plotted against neutron energy for $U^{233}$.
($\sigma_S$ calculated in b)

for critical experiments, and as its handling problems are resolved, the adequacy of nuclear-physics data for $U^{233}$-fuelled reactors should rapidly approach parity with that for $U^{235}$-fuelled reactors.

## REFERENCES


[1] CHERNICK, J., Proc. UN Int. Conf. PUAE **5** (1955) 215.
[2] CRANBERG, L., Proc. Conf. Physics of Breeding, ANL-6122 (1959) 51. Also LA-2177 (1959).
[3] HOWERTON, R. J., UCRL-5351, I Pt II (1958).
[4] MANDEVILLE, C. E. and KAVANAGH, D. L., CWR-4028 (1958).
[5] RIEF, H., *Nucl. Sci. and Engng* **10** (1961) 83.
[6] CHEZEM, C. G., *Nucl, Sci. and Engng* 8 (1960) 652.
[7] WEINBERG, A. M. and WIGNER, E. P., The Physical Theory of Neutron Chain Reactors, Ch XX, U. of Chicago Press, Chicago, Illinois (1958).
[8] CAMPAN, J. L., CLAUZON, P., KIRCHNER, B., RIBON, P. et ZALESKI, C. P., Report SNE No. 13 (1958).
[9] YIFTAH, S., OKRENT, D. and MOLDAUER, P. A., Fast Reactor Cross Sections, Pergamon Press (1960).
[10] NEUER, J. J. and STEWART, C. B., LA-2023 (1956).
[11] FISCHER, G. J., *Phys. Rev.* **108** (1957) 99.
[12] MARION, J. B., LEVIN, J. S. and CRANBERG, L., Univ. of Maryland Physics Dept., Technical Report No. 124 (1958).
[13] ALINE, P. G., NOVAK, P. E. and WOLFE, B., *Nucl. Sci. and Engng* **7** (1960) 392.
[14] ZIMMERMAN, E. L., ORNL-2201 (1958).
[15] CHERNICK J. and OLEKSA MOORE, S., *Nucl. Sci. and Engng* **6** (1959) 537.
[16] YAETER, M. L., HOCKENBURY, R. W. and FULLWOOD, R. R., *Nucl. Sci. and Engng* **9** (1961) 105.

SM 18/53

# STATUS OF COMPUTATIONAL AND EXPERIMENTAL CORRELATIONS FOR LOS ALAMOS FAST-NEUTRON CRITICAL ASSEMBLIES*

G. E. HANSEN**

LOS ALAMOS SCIENTIFIC LABORATORY, UNIVERSITY OF CALIFORNIA,
LOS ALAMOS, N. MEX.,
UNITED STATES OF AMERICA

**Abstract — Résumé — Аннотация — Resumen**

**Status of computational and experimental correlations for Los Alamos fast-neutron critical assemblies.** New assemblies and improved measuring techniques call for periodic review of the status of computation *vs.* experiment. It is appropriate to emphasize neutron-spectral characterizations because of the particularly elusive problems associated with absolute spectral-index measurement and the need for checks of computation beyond simple critical size.

The ever-improving spectral-index measurements in conjunction with increasing precision, both of microscopic data for detector and assembly materials and of computational techniques, produce a gradual clarification of the characteristics of a family of fast-neutron critical assemblies. This family now includes unreflected and thick-uranium-reflected $U^{233}$ in spherical geometry.

Direct correlations among the experimental data will be presented to indicate the *a priori* possibilities for successful correlations with computation. Sensitivity of computed spectra and critical sizes to neutron-transport models (transport and linear approximations) and arithmetic approximations (finite angular segmentations and multi-group representations) will be presented for several typical assemblies to help establish the necessary computational detail. Comparisons between experiment and prediction will include, in addition to spectral indices and critical sizes, neutron lifetimes and delayed-neutron fractions.

**Corrélation entre les calculs et les expériences sur les ensembles critiques à neutrons rapides de Los Alamos.** Du fait de la mise en service de nouveaux réacteurs et de l'amélioration des méthodes de mesure, il est nécessaire de faire périodiquement la corrélation des expériences et des calculs. Il est utile d'insister sur les caractérisations de spectres de neutrons à cause des problèmes particulièrement délicats que pose la mesure absolue de l'indice spectral et de la nécessité de vérifier les calculs au-delà des simples dimensions critiques.

Les mesures constamment améliorées de l'indice spectral, associées à la précision croissante des données microscopiques relatives aux matériaux utilisés dans les détecteurs et les réacteurs ainsi qu'à celle des méthodes de calcul, permettent de connaître de mieux en mieux les caractéristiques d'une classe d'ensembles critiques à neutrons rapides. Cette classe comprend maintenant des montages à $^{233}U$, en géométrie sphérique, sans réflecteur ou avec un réflecteur constitué d'une couche épaisse d'uranium.

L'auteur présente des corrélations directes parmi les données expérimentales, pour montrer qu'il existe à priori la possibilité de bonnes corrélations avec les résultats des calculs. La sensibilité des spectres calculés et des dimensions critiques aux mo-

* Work performed under the auspices of the United States Atomic Energy Commission.

** Reporting on work done by D. Barton, W. Bernard, J. Grundl, G. Jarvis, J. Orndoff, H. Paxton, W. Roach and A. Usner of the critical assemblies group, and C. Browne, G. Knoblock and L. Smith of the radiochemistry group.

dèles de transport neutronique (approximations du transport et hypothèse de linéarité) et aux approximations arithmétiques (hypothèse de la segmentation angulaire et représentations multigroupes) est présentée pour divers ensembles critiques afin d'aider à établir les détails des calculs indispensables. La comparaison entre l'expérience et les prévisions porte sur les indices spectraux et les dimensions critiques, les durées de vie des neutrons et les rapports relatifs aux neutrons retardés.

**Состояние вычислительных и экспериментальных корреляций для Лос-Аламосской критической системы на быстрых нейтронах.** Новые системы и улучшенная измерительная техника предусматривают периодический пересмотр состояния вычислений в зависимости от эксперимента. Следует подчеркнуть важность нейтронно-спектральных характеристик из-за особенно трудноразрешимых проблем, связанных с абсолютным измерением спектральных индексов и необходимостью проверок вычислений сверх простого критического размера.

Постоянное улучшение измерения спектральных индексов вместе с увеличением точности как микроскопических данных для детектора и материалов сборок, так и вычислительной техники, приводит к постепенному прояснению характеристик группы критических систем на быстрых нейтронах. Эта группа сейчас включает активные зоны с $U^{233}$ без отражателя и с толстым урановым отражателем.

Прямая корреляция среди экспериментальных данных будет представлена с целью указать предшествующие возможности для успешных корреляций с вычислением. Будет представлена чувствительность вычисленного спектра и критических размеров к различным моделям переноса нейтронов (транспортные и линейные приближения) и арифметическим приближениям (ограниченные угловые сегментации и многогрупповые представления) для нескольких типичных систем, чтобы помочь установить необходимые расчетные детали. Сравнения между экспериментом и вычисленными данными будут включать также в дополнение к спектральным индексам и критическим размерам, время жизни нейтронов и доли запаздывающих нейтронов.

**Conjuntos críticos de neutrones rápidos de Los Alamos; correlación entre resultados calculados y experimentales.** La puesta en servicio de nuevos conjuntos críticos y el perfeccionamiento de los métodos de medición exigen una revisión periódica de la correlación entre los resultados calculados y los experimentales. Dados los problemas particularmente delicados que plantea la medición de índices espectrales absolutos y dada también la necesidad de comprobar los cálculos más allá de las simples dimensiones críticas, conviene hacer hincapié en las caracterizaciones de los espectros neutrónicos.

El continuo perfeccionamiento de las mediciones de índices espectrales, unido a la creciente precisión de los datos microscópicos relativos a los materiales utilizados en los conjuntos críticos y en los detectores así como la de los métodos de cálculo contribuyen a un mejor conocimiento de las características de un grupo de conjuntos críticos de neutrones rápidos. Este grupo comprende actualmente los conjuntos de $^{233}U$ en geometría esférica sin reflector o con un reflector constituído por una espesa capa de uranio.

El autor expondrá correlaciones directas entre los datos experimentales, para indicar que existe *a priori* la posibilidad de alcanzar correlaciones satisfactorias con los datos calculados. También presentará, para diversos conjuntos típicos y a fin de establecer los detalles de cálculo necesarios la sensitividad de los espectros calculados y de los tamaños críticos a los modelos de transporte neutrónico (aproximaciones de transporte e hipótesis de proporcionalidad) y a las aproximaciones aritméticas (hipótesis de la segmentación angular finita y representaciones de grupos múltiples). Las comparaciones entre los resultados experimentales y las evaluaciones se refieren a los índices espectrales y a los tamaños críticos, así como a los períodos de semidesintegración y a las razones correspondientes a los neutrones retardados.

## Introduction

The critical assemblies to be discussed in this report are restricted to bare and thick normal uranium-reflected metal spheres of $U^{233}$, $U^{235}$, and $Pu^{239}$. The principal emphasis will be on the neutron spectral indices for their inferences of inelastic scattering properties of these highly fissionable isotopes. Data from the plutonium and enriched uranium assemblies have appeared in several reports [1 — 6] and we shall repeat here much of what is perhaps already familiar. Section 1 presents the spectral index data and a selection of average values. Section 2 outlines the computational basis and illustrates some of its limitations. Section 3 then gives the computational and experimental correlations.

## 1. Spectral index data

Table I-A summarizes, as of 1954, the spectral index data for the Godiva (bare $U^{235}$) and Topsy (thick uranium-reflected $U^{235}$) central fluxes. At that time, the $\sigma_f(U^{238})/\sigma_f(U^{235})$ and $\sigma_f(Np^{237})/\sigma_f(U^{235})$ fission ratios established the

TABLE I

**SPECTRAL INDEX DATA**

**(A) Summary to 1954 for Godiva and Topsy central spectra**

| Index | Thermal $U^{235}$ fission neutron spectrum | Godiva | Topsy | Reference key |
|---|---|---|---|---|
| $\sigma_f(U^{235})/\sigma_f(U^{238})$ | 3.94 | 6.1 | 6.83 | (*a*) |
| | 3.33 | 5.94 | 6.67 | (*b*) |
| | — | 6.59 | 7.36 | (*c*) |
| | — | 6.18 | 6.63 | (*d*) |
| | — | 6.54 | 6.88 | (*e*) |
| $\sigma_f(U^{234})/\sigma_f(U^{238})$ | 4.25 | 5.0 | 5.15 | (*a*) |
| $\sigma_f(Np^{237})/\sigma_f(U^{238})$ | 4.08 | 4.8 | 5.02 | (*a*) |
| | 4.36 | 5.21 | 5.24 | (*b*) |
| | — | — | 5.18 | (*d*) |
| | — | 5.10 | — | (*e*) |
| $\sigma_f(U^{236})/\sigma_f(U^{238})$ | 1.58 | 1.8 | 1.95 | (*a*) |
| $\sigma_f(Pu^{239})/\sigma_f(U^{235})$ | 1.54 | 1.43 | 1.44 | (*a*) |
| | | 1.48 | ~1.55 | (*d*) |
| $\sigma_f(U^{233})/\sigma_f(U^{235})$ | 1.65 | 1.7 | 1.63 | (*a*) |
| $\sigma_f(Th^{232})/\sigma_f(U^{238})$ | — | (0.234 ±0.005)* | | (*d*) |
| $\sigma_{n,\,2n}(U^{238})/\sigma_f(U^{238})$ | — | 0.044 | 0.047 | (*d*) |
| $\sigma_{n,\,2n}(Th^{232})/\sigma_f(Th^{232})$ | — | (0.206 ±0.006)* | | (*d*) |
| $\sigma_{n,\,\gamma}(U^{238})/\sigma_f(U^{238})$ | — | 0.47 | 0.53 | (*d*) |
| $\sigma_{n,\,p}(S)/\sigma_f(U^{238})$ | — | 0.24 | 0.24 | (*f*) |
| $\sigma_{n,\,\gamma}(Au)/\sigma_f(U^{235})$ | — | 0.115 | 0.147 | (*f*) |
| | — | 0.094 | 0.107 | (*g*) |
| $\sigma_{n,\,\alpha}(Li^6)/\sigma_f(U^{235})$ | — | — | 0.436 ±0.013 | (*h*) |
| $\sigma_f(Np^{237})/\sigma_f(U^{235})$ | 1.03 | 0.79 | 0.76 | (*a*) |
| | 1.31 | 0.88 | 0.786 | (*b*) |
| | — | — | 0.781 | (*d*) |
| | — | 0.78 | — | (*e*) |

*Cont. following page*

TABLE I, cont.

**(B) Summary post-1954 central spectral indices****

| Index | $U^{235}$ | U-refl. $U^{235}$ | $U^{233}$ | U-refl. $U^{233}$ | $Pu^{239}$ | U-refl. $Pu^{239}$ | Reference key |
|---|---|---|---|---|---|---|---|
| $\sigma_f(U^{235})/\sigma_f(U^{238})$ | $x$ | $1.119x$ | $0.773x$ | $0.880x$ | $0.776x$ | — | $(c),(i)$ |
| | $x$ | $1.122x$ | — | — | $0.769x$ | — | $(b)$ |
| | 6.4 | 6.6 | 4.6 | — | — | — | $(j)$ |
| | — | — | — | — | — | 5.4 | $(d)$ |
| $\sigma_f(Np^{237})/\sigma_f(U^{235})$ | $y$ | $0.903y$ | $1.187y$ | $1.068y$ | $1.152y$ | — | $(c)$ |
| | $y$ | $0.896y$ | — | — | $1.188y$ | — | $(b)$ |
| $\sigma_f(Pu^{239})/\sigma_f(U^{235})$ | $z$ | $0.983z$ | — | — | $1.047z$ | — | $(c)$ |
| | 1.42 | — | — | — | — | — | $(j)$ |
| $\sigma_f(U^{233})/\sigma_f(U^{235})$ | $z$ | $1.002z'$ | — | — | $0.990z'$ | — | $(c)$ |
| $\sigma_c(U^{238})/\sigma_f(U^{238})$ | $0.47_6$ | — | — | — | — | — | $(j)$ |

Reference key: (*a*) Fission chambers—L. Lowry.
(*b*) Fission chambers—J. Grundl.
(*c*) Quadruple fission chambers—G. Jarvis.
(*d*) Radiochemistry—J. Sattizahn.
(*e*) Total γ-activity—G. Linenberger.
(*f*) β-γ counting—G. Linenberger.
(*g*) β-γ counting—C. Byers.
(*h*) Radiochemistry—R. Olcott.
(*i*) Quadruple fission chambers—D. Barton.
(*j*) Radiochemistry—C. Browne, G. Knoblock, L. Smith.

* These values hold at every internal point of the Godiva and Topsy assemblies.

** The column $U^{235}$ designates a bare enriched uranium [≡ Oy (~93.8% $U^{235}$)] sphere physically identified with Godiva I or II; the column U-reflected $U^{235}$ designates an ~8 inch natural uranium-reflected enriched uranium sphere physically identified with Topsy or Oy-Flattop; the column $Pu^{239}$ designates a bare δ-phase plutonium sphere—Jezebel; the column U-reflected $Pu^{239}$ designates an ~8 inch natural uranium-reflected δ-phase plutonium sphere physically identified with Popsy; $U^{233}$ designates a bare "23" (~98.1% $U^{233}$) sphere—"23" Jezebel; and U-reflected $U^{233}$ designates an ~8 inch natural uranium-reflected sphere—"23"-Flattop.

two $U^{235}$ inelastic parameters: (*a*) inelastic scattering cross-section from above to below the $U^{238}$ fission threshold and (*b*) inelastic scattering cross-section from above to below the $Np^{237}$ fission threshold, to be in the vicinity of 1.5 and 0.7 b respectively for an incident fission neutron spectrum source. The remaining indices gave surprisingly little additional information: either the indices were too similar to the above two ratios [e.g. $\sigma_f(U^{234})/\sigma_f(U^{235})$, $\sigma_f(U^{236})/\sigma_f(U^{235})$ and $\sigma_{n,\gamma}(U^{238})/\sigma_f(U^{238})$] or the neutron-energy-response characteristics were too uncertain [e.g. $\sigma_{n,\gamma}(Au)/\sigma_f(U^{235})$ and $\sigma_{n,p}(S)/\sigma_f(U^{235})$]. Regardless of absolute values, the independence of $\sigma_f(Th^{232})/\sigma_f(U^{238})$ and $\sigma_{n,2n}(Th^{232})/\sigma_f(Th^{232})$ ratios to position in the Topsy core and reflector implied a spectrum of supra $U^{238}$ threshold neutrons insensitive to the considerable differences in non-elastic scattering processes between $U^{235}$ and $U^{238}$: GRUNDL and USNER [1] later showed this spectrum, specifically for above the $P^{31}(n, p)$ threshold, to be the same as the corresponding segment of the fission neutron spectrum.

With the construction of the plutonium and $U^{233}$ assemblies, spectral index measurements have been made primarily with those few neutron-detectors whose response functions were thought best known. Table I-B completes the spectral-index data summary. The accurate intercomparisons among the different assemblies help considerably in establishing average index values. Nevertheless the final selection is subjective as it cannot be entirely divorced from prior aware-

ness of computed values. The author takes full blame for the particular choice given in Table II — namely, $\sigma_f(U^{235})/\sigma_f(U^{238})=6.4$ for Godiva and $\sigma_f(Np^{237})/\sigma_f(U^{235})=0.78$ for Topsy. From these two assignments and the multiple-fission-chamber intercomparisons of Table I-B follow all other $\sigma_f(U^{235})/\sigma_f(U^{238})$ and $\sigma_f(Np^{237})/\sigma_f(U^{235})$ absolute values (save for the U-reflected Pu system where multiple chamber measurements have not yet been made) including $\sigma_f(Np^{237})/\sigma_f(U^{238})=5.6$ for Topsy as contrasted to a value of $\sim 5.2$ suggested by Table I-A. If one weighted the available Topsy and Godiva data equally, he would obtain $\sigma_f(U^{235})/\sigma_f(U^{238})$ and $\sigma_f(Np^{237})/\sigma_f(U^{235})$ average values about 2% less than our selections. For inferences on inelastic scattering, however, it is essential to know the fractional changes in index values between the fission-neutron-spectrum source and the assembly neutron spectra. Because of difficulties with preparation of a pure fission-neutron spectrum, the data for $\sigma_f(U^{235})/\sigma_f(U^{238})$ and $\sigma_f(Np^{237})/\sigma_f(U^{238})$ listed under the second column of Table I-A are rather uncertain; nevertheless, the values are respectively lower than the 4.16 and 4.58 expected on the basis of the presumed known fission-neutron spectrum and fission cross-sections. Although this mild discrepancy may equally well be attributed to detector-ratio bias or fission cross-section bias, we have essentially attributed it to the former in the index values listed in Table II.

TABLE II

**SELECTED SPECTRAL INDICES**

**Average values**

| Index | $U^{235}$ | U-refl. $U^{235}$ | $U^{233}$ | U-refl. $U^{233}$ | $Pu^{239}$ | U-refl. $Pu^{239}$ |
|---|---|---|---|---|---|---|
| $\sigma_f(U^{235})\sigma_f(U^{238})$ | 6.4 | $7.1_6$ | $4.9_5$ | $5.6_3$ | $4.9_7$ | 5.4 |
| $\sigma_f(Np^{237})/\sigma_f(U^{235})$ | $0.86_4$ | 0.78 | $1.02_6$ | $0.92_3$ | $0.99_6$ | — |
| $\sigma_f(U^{233})/\sigma_f(U^{235})$ | 1.63 | 1.63 | — | — | 1.61 | — |
| $\sigma_f(Pu^{239})/\sigma_f(U^{235})$ | 1.42 | 1.40 | — | — | 1.49 | — |
| $\sigma_{n,\gamma}(U^{238})/\sigma_f(U^{238})$ | $0.47_6$ | 0.53 | — | — | — | — |

## 2. Computational basis

As a basis for neutronic computations, we have chosen the Carlson $S_n$ method with $S_4$ and transport approximations and with six energy-groups (two below the $Np^{237}$ fission threshold and two above the $U^{238}$ fission threshold) where the group cross-sections are defined in principle through fission neutron-spectrum weighting. The transformation of available cross-section data into this six-group representation is not particularly relevant here; we test the $U^{233}$, $U^{235}$, $U^{238}$ and $Pu^{239}$ sets given in [5] as purportedly being of this form: call this set $X$. We know *a priori* that the flux spectrum in, for example, a bare $U^{233}$ assembly is softer than the virgin fission-neutron spectrum primarily because of inelastic scattering, that the cross-section data for this process are quite uncertain, and that the spectral-index data should permit an improved description. First, a question naturally arises regarding errors in predicted quantities arising from the fixed computational basis itself and not connected with cross-section errors or uncertainties.

TABLE III

**APPROXIMATE ERRORS PRODUCED BY FISSION NEUTRON SPECTRUM WEIGHTING IN DEFINITION OF SIX GROUP CONSTANTS**

**(Including six-group detector specifications)**

| Computed quantity \ Spectrum | Oy (93.5% $U^{235}$) | Oy (37.5% $U^{235}$) | Oy ($16^1/_4$% $U^{235}$) | Oy (~6% $U^{235}$) |
|---|---|---|---|---|
| Reproduction No. | —0.4% | —0.9% | —0.9% | —0.3% |
| Lifetime | —0.6% | —0.8% | —1.2% | —1.2% |
| $\sigma_f(U^{235})/\sigma_f(U^{238})$ | —1.4% | —2.0% | —3.3% | —4.6% |
| $\sigma_f(Np^{237})/\sigma_f(U^{235})$ | 1.9% | 4.8% | 8.4% | 15 % |

The $S_4$ and transport approximations are primarily approximations on the spatial transport of neutrons and thus adversely affect computations of radial flux traverses and criticality (through improper computation of leakage probability). CARLSON and BELL [7] have made a systematic study of the criticality bias of $S_4$: their results imply, for our undiluted metal $U^{233}$, $U^{235}$ and $Pu^{239}$ spherical assemblies, that $S_4$ computed reproduction numbers are ~0.8% to 1.0% higher than the exact ($S_\infty$) values. Comparison between $S_4$ computed reproduction numbers for a bare $U^{235}$ sphere with and without transport approximation indicates that this latter approximation contributes an additional +0.2%. Of perhaps more interest are the errors introduced by fission-neutron-spectrum

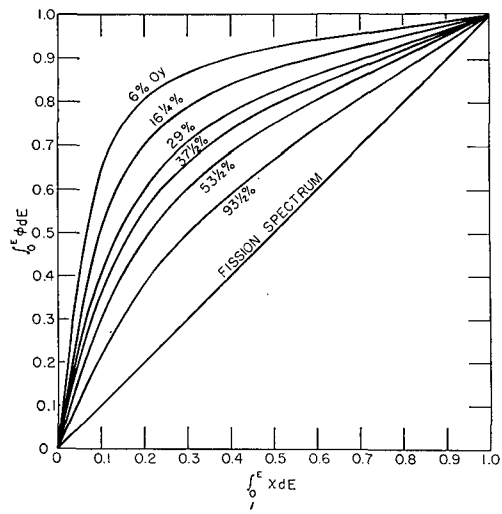


Fig. 1

A graphical portrayal of the flux spectra expected for several typial enriched uranium assemblies (the Jemima series). This report is restricted to spectra similar to that of $93^1/_2$% $U^{235}$, where fission-neutron spectrum weighting of multi-group cross-sections introduces no serious bias either in computation of spectra or, more pertinently, in computation of energy-sensitive detector responses to these spectra.

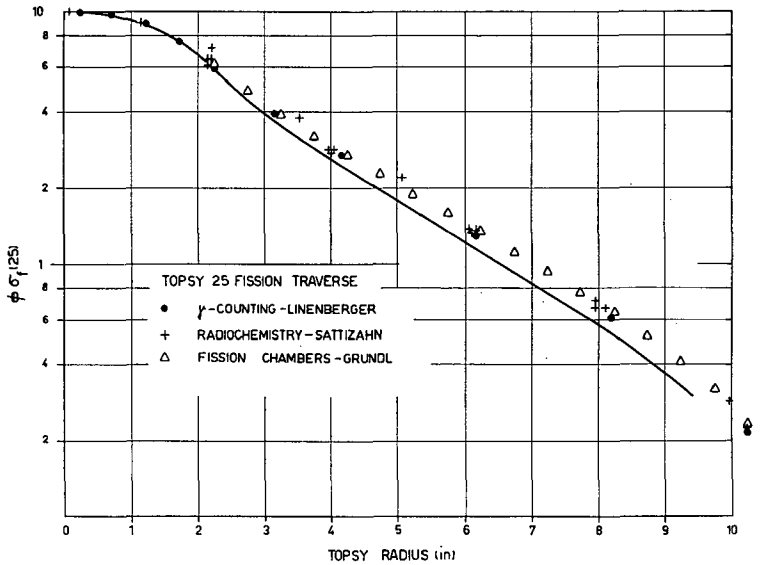


Fig. 2
Radial flux traverse in Topsy as seen by $U^{235}$ fission detectors. The solid curve represents the behaviour predicted on the basis of $S_4$ with transport approximation and six-group cross-sections of Ref. [5].

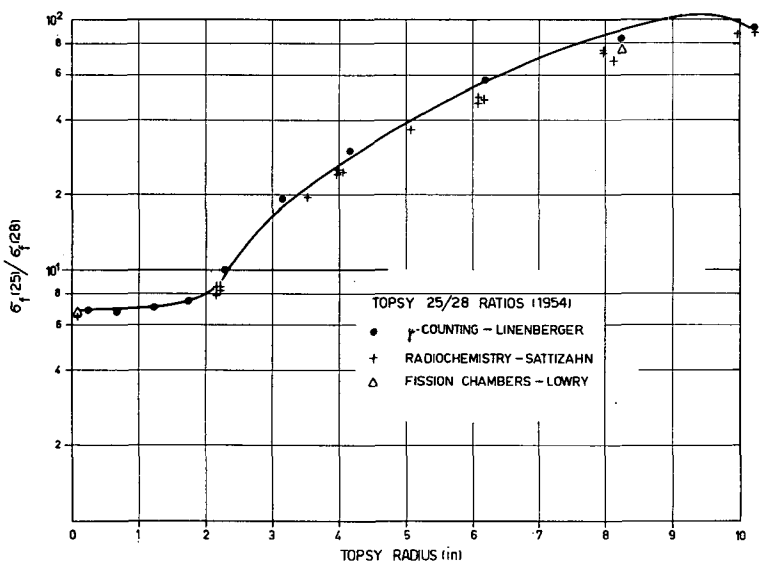


Fig. 3
Radial $\sigma_f(U^{235})/\sigma_f(U^{238})$ fission cross-section ratio traverses in Topsy. The solid curve is the predicted behaviour (see caption Fig. 1).

weighting rather than flux weighting of cross-section data to produce multigroup parameters. To illustrate errors arising from this part of our computational basis, we have chosen the fast-neutron spectra of Fig. 1 which apply closely to bare uranium systems of the indicated $U^{235}$ concentrations. Table III indicates corresponding errors in criticality (reproduction number), prompt-neutron lifetime, and the spectral indices $\sigma_f(U^{235})/\sigma_f(U^{238})$ and $\sigma_f(Np^{237})/\sigma_f(U^{235})$. It may be noted that the large errors introduced in computed $\sigma_f(Np^{237})/\sigma_f(U^{235})$ values for the diluted $U^{235}$ systems arise not in computation of spectra but in computation of the $Np^{237}$ detector-responses to these spectra. Figs. 2 and 3 compare two observed and computed radial traverse functions for the Topsy assembly where the radius-dependent neutron spectrum covers the gamut of spectra pictured in Fig. 1. All in all, the computational basis appears adequate for prediction of criticality, neutron lifetime, and central spectral indices of the critical systems under present consideration.

Since publication of the six-group cross-section sets of reference [5], the literature has introduced presumably more precise measurements of the $Np^{237}$ fission cross-section [8] and $U^{238}$ radiative capture cross-section [9], these data being represented in our six-group form in [3] (this reference also includes a similar representation of the $Pu^{240}$ fission cross-section of which we shall make use in the last section). We employ the recent $Np^{237}$ data for predictions of $Np^{237}$ detector-responses; however, to preserve the integrity of set $X$, the recent $\sigma_{n,\gamma}(U^{238})$ data are used only for a few computations of $\sigma_{n,\gamma}(U^{238}/\sigma_f(U^{238})$ ratios, the parenthesized values in Table IV, to illustrate their implications, for example on neutron economy in mixed $U^{235}$—$U^{238}$ systems.

## 3. Computational and experimental correlations

Although the central theme of this status report concerns the implications of spectral-index data for inelastic scattering properties of $U^{233}$, $U^{235}$ and $Pu^{239}$, the critical sizes and neutron lifetimes are also included in observed *versus* set-$X$-computed quantities listed in Table IV. The critical masses of the $U^{233}$ assemblies were determined in the same fashion as those of the entirely analogous $Pu^{239}$ assemblies [2], i.e. corrections for surface coatings, asphericity, etc., established through reactivity-coefficient data. The neutron lifetimes are given by the ratio of effective delayed-neutron fraction and delayed-critical Rossi-$\alpha$ [11], the effective delayed-neutron fraction being inferred from observation of the delayed to prompt critical surface mass increment (e.g., $\Delta m/m = 0.01060 \pm 0.00012$ for bare $U^{233}$).

For the two inelastic scattering parameters of fissionable isotope $x$ which may be obtained from the observed $\sigma_f(U^{235})/\sigma_f(U^{238})$ and $\sigma_f(Np^{237})/\sigma_f(U^{235})$, we choose in line with small sphere transmission experiments [12]

$$\overset{28}{\sigma}_{in}(x) \equiv \frac{\int \chi(E)\,\sigma^{in}(x, E \to E')\,[\sigma_f(U^{238}, E) - \sigma_f(U^{238}, E')]\,dE\,dE'}{\int \chi(E)\,\sigma_f(U^{238}, E)\,dE}$$

$$\overset{37}{\sigma}_{in}(x) \equiv \frac{\int \chi(E)\,\sigma^{in}(x, E \to E')\,[\sigma_f(Np^{237}, E) - \sigma_f(Np^{237}, E')]\,dE\,dE'}{\int \chi(E)\,\sigma_f(Np^{237}, E)\,dE}$$

TABLE IV

**COMPUTATIONAL AND EXPERIMENTAL CORRELATIONS**

| Parameter | $U^{235}$ | U-refl. $U^{235}$ | $U^{233}$ | U-refl. $U^{233}$ | $Pu^{239}$ | U-refl. $Pu^{239}$ |
|---|---|---|---|---|---|---|
| $\sigma_f(U^{235})/\sigma_f(U^{238})$ | | | | | | |
| obs. | 6.4 | $7.1_6$ | $4.9_5$ | $5.6_3$ | $4.9_7$ | 5.4 |
| comp. | 6.42 | 6.98 | 5.13 | 5.69 | 5.39 | 6.16 |
| $\sigma_f(Np^{237})/\sigma_f(U^{235})$ | | | | | | |
| obs. | 0.864 | 0.78 | 1.026 | $0.92_3$ | $0.99_6$ | — |
| comp. | 0.869 | 0.811 | 0.978 | 0.909 | 0.949 | 0.859 |
| $\sigma_f(Pu^{239})/\sigma_f(U^{235})$ | | | | | | |
| obs. | — | — | — | — | — | — |
| comp. | 1.403 | 1.384 | 1.441 | 1.418 | 1.437 | 1.398 |
| $\sigma_f(U^{233})/\sigma_f(U^{235})$ | | | | | | |
| obs. | — | — | — | — | — | — |
| comp. | 1.536 | 1.536 | 1.530 | 1.532 | 1.531 | 1.532 |
| $\sigma_c(U^{238})/\sigma_f(U^{238})$ | | | | | | |
| obs. | — | — | — | — | — | — |
| comp. | 0.543 (0.475) | 0.612 (0.531) | 0.391 (0.349) | 0.458 (0.404) | 0.423 (0.374) | 0.517 (0.452) |
| Critical mass* (kg core) obs. | $52.0_4$ | $17.4_1$ | 16.1 | — | $16.2_8$ | $5.7_9$ |
| comp. | 51.6 | 16.7 | 16.0 | 5.6 | 16.1 | 5.5 |
| Effective delayed-neutron fraction obs.** | $0.0065_9$ | — | $0.0029_0$ | — | $0.0019_3$ | — |
| comp.*** | $0.0069_1$ | — | $0.0028_7$ | — | $0.0019_9$ | — |
| Rossi-$\alpha$ at delayed critical (per $\mu$s) obs. | —1.10 | — | —1.00 | — | —0.65 | — |
| comp. | —1.22 | — | — | — | $-0.63_7$ | — |

* Specifically the computed and observed critical masses refer to the following idealized systems:
$U^{235}$ ≡ a critical sphere of Oy (93.8% $U^{235}$) at $\varrho$ (Oy) = 18.75 g/cm³.
U-refl. $U^{235}$ ≡ a critical sphere of Oy (94.1% $U^{235}$) at $\varrho$ (Oy) = 18.7 g/cm³ and close reflected with $8^1/_2$ in of normal uranium at $\varrho$ (U) = 18.8 g/cm³.
$U^{233}$ ≡ a critical sphere of "23" (98.1% $U^{233}$) at $\varrho$ ("23") = 18.6 g/cm³.
U-refl. $U^{233}$ ≡ a critical sphere of "23" (98.1% $U^{233}$) at $\varrho$ ("23") = 18.6 g/cm³ and close reflected with $7^1/_2$ in of normal uranium at $\varrho$ (U) = 18.9 g/cm³.
$Pu^{239}$ ≡ a critical sphere of Pu (95 $^1/_2$% $Pu^{239}$) at $\varrho$ (Pu) = 15.66 g/cm³ [2].
U-refl. $Pu^{239}$ ≡ a critical sphere of Pu ($98^1/_2$% $Pu^{239}$) at $\varrho$ (Pu) = 15.63 g/cm³ and close reflected with $9^1/_2$ in of normal uranium at $\varrho$ (U) = 18.8 g/cm³ [2].

** The direct observation is the surface mass increment between delayed and prompt critical. The $S_4$ computed reproduction number change for this mass increment is then identified with the effective delayed neutron fraction. This is a customary step leading to a computation of the Rossi-$\alpha$ at delayed critical. The step may be deleted when interest in the Rossi-$\alpha$ measurements is confined to implications of flux spectra for then observed derivatives of $\alpha$ with respect to surface mass permit interpretation without mention of delayed neutrons. The last row of Table IV effectively treats the Rossi-$\alpha$ in this fashion.

*** From the Keepin and Wimett [10] delayed-neutron fractions $\beta(U^{235}) = 0.0064_5$, $\beta(U^{238}) = 0.015{,}7$ $(U^{233}) = 0.0026_6$, $(Pu^{239}) = 0.00209$ and $(Pu^{240}) = 0.0025_7$ and relative effectiveness computations.

TABLE V

**INELASTIC SCATTERING CROSS-SECTIONS OF $U^{235}$, $U^{233}$ AND $Pu^{239}$ as implied by set X vs. those implied by observed spectral indices**

| | | $U^{235}$ | $U^{233}$ | $Pu^{239}$ |
|---|---|---|---|---|
| $\sigma^{28}$ in | Set $X$ | 1.46 | 1.07 | 1.07 |
| | Obs. | $1.5 \pm 0.1$ | $0.9 \pm 0.1$ | $0.6 \pm 0.2$* |
| $\sigma^{37}$ in | Set $X$ | 0.72 | 0.54 | 0.54 |
| | Obs. | $0.8 \pm 0.1$ | $0.4 \pm 0.1$ | $0.3 \pm 0.2$* |

* Based on the non-physical premise of the fission neutron spectrum for $Pu^{239}$ being the same as that for $U^{235}$. Re-analysis with the observed $Pu^{239}$ fission neutron spectrum [1] yields values of the two inelastic scattering cross-sections identical to those of $U^{233}$. Numbers following the $\pm$ symbol reflect changes in inelastic cross-section values accompanying $\sim 2^1/_2$% changes in spectral index values.

where $\varkappa(E)$ is the fission-neutron spectrum. Table V then lists the values of $\sigma_{in}^{28}$ $(\chi)$ and $\sigma_{in}^{37}$ $(x)$ implied by set $X$ together with those implied by the observed spectral indices of Table IV. This "implication" is via six-group computation and may be questioned for the case of $Pu^{239}$ where computation utilized the $U^{235}$ fission-neutron spectrum of set $X$ (see footnote to Table V). The "observed" inelastic cross-sections of $U^{235}$ and $Pu^{239}$ are generally in good agreement with the small sphere transmission measurements of BETHE *et al.* [12] and the differential inelastic-scattering measurements of CRANBERG [13]. STEWART's measurements [14] of the leakage spectrum of the bare $Pu^{239}$ assembly further substantiate the conclusions drawn from the central spectral-index data.

The disagreement between observed and computed Rossi-$\alpha$ values for the fast $U^{235}$ systems [5] remains a mystery.

The $\sigma_f(U^{233})/\sigma_f(U^{235})$ and $\sigma_f(Pu^{239})/\sigma_f(U^{235})$ ratios are not sensitive spectral indices and their primary function, together with reactivity-coefficient ratios of the same isotopes, is to check further general magnitudes of fission and neutron production cross-sections. In this connection, an earlier discrepancy [2] between the neutron-production cross-section of $Pu^{240}$ measured in Topsy and the similar cross-sections measured in Godiva and Jezebel has recently been resolved in favour of the Godiva and Jezebel measurements: in thick-U-reflected spherical geometry, critical masses of enriched uranium ($\sim$93.5% $U^{235}$) spherical shells surrounding 1.6 kg $\alpha$-phase Pu spheres of different $Pu^{240}$ content ($\sim$2 to $\sim$16%) established [15], for the central position, the equivalence 1 g $Pu^{240}$ $\sim$0.63 g $Pu^{239}$. With the same procedure as used in [3], this datum translates to $\bar{\nu}(Pu^{240}, 2\text{ MeV}) = 3.32 \pm 0.14$ neutrons emitted per $Pu^{240}$-fission induced by a 2 MeV neutron [15] as compared with the Godiva and Jezebel determined average value of $3.27 \pm 0.17$ [3].

## REFERENCES

[1] GRUNDL, J. and USNER, A., *Nucl. Sci. and Engng* **8** (1960) 598.
[2] JARVIS, G. A. *et al.*, *Nucl. Sci. and Engng* **8** (1960) 523.
[3] ENGLE, L. B., HANSEN, G. E. and PAXTON, H. C., *Nucl. Sci. and Engng* **8** (1960) 570.
[4] BYERS, C. C., *Nucl. Sci. and Engng* **8** (1960) 608.
[5] HANSEN, G. E., Proc. 2nd UN Int. Conf. PUAE **12** (1958) 84—88.
[6] WHITE, R. H., *Nucl. Sci. and Engng* **1** (1956) 53.
[7] CARLSON, B. G. and BELL, G. I., Proc. 2nd UN Int. Conf. PUAE **16** (1958) 535—549.
[8] MURRAY, R. B. and SCHMITT, H. W., *Phys. Rev.* **115** (1959) 1707.
[9] DIVEN, B. C., TERRELL, J. and HEMMENDINGER, A., *Phys. Rev.* **120** (1960) 556—569.
[10] KEEPIN, G. R., WIMETT, T. F. and ZEIGLER, R. K., *J. nucl. Energy* **6** (1957) 1.
[11] ORNDOFF, J. D., *Nucl. Sci. and Engng* **2** (1957) 450.
[12] BETHE, H. A., BEYSTER, J. R. and CARTER, R. E., LA-1939 del. (1955).
[13] CRANBERG, L., LA-2177 (1959).
[14] STEWART, L., *Nucl. Sci. and Engng* **8** (1960) 595.
[15] BARTON, D. M., BERNARD, W. and HANSEN, G. E., LAMS-2489 (1961).

# RECENT ADVANCES AND PROBLEMS IN THEORETICAL ANALYSES OF ZPR-III FAST CRITICAL ASSEMBLIES*

D. MENEGHETTI
Argonne National Laboratory, Argonne, Ill.,
United States of America

**Abstract — Résumé — Аннотация — Resumen**

**Recent advances and problems in theoretical analyses of ZPR-III fast critical assemblies.** Theoretical analyses of critical assemblies recently studied experimentally on the Argonne Zero Power Facility, ZPR-III, are compared with the measured data. Discrepancies between calculated and experimental values are examined, together with results from previous assemblies for systematic trends. Effects of modifications in the cross-sections and in the calculational procedures in reducing the discrepancies are discussed.

Calculation of reactivity changes, flux variations, and detector-response variations resulting from the heterogeneities caused by various intra-drawer configurations of fuel and diluent plates within the drawers of the critical assemblies are compared with experimental data. Transport methods for such thin slab cell configurations are compared. Improvements in the calculational methods for these cells are suggested; and, a simple multi-group approximation method, amenable to hand calculation, is described.

The sensitivities of reactivity and inhours as functions of asymptotic reactor period are examined for a range of fast-reactor compositions. Results of calculations of effective delayed-neutron fraction, inhours per cent $k_{\text{eff}}$, and prompt- and delayed-neutron worths are given for a series of fast assemblies.

**Progrès récents et problèmes concernant les études théoriques d'ensembles critiques à neutrons rapides du type ZPR-III.** L'auteur compare les études théoriques d'ensembles critiques dont l'étude expérimentale a été faite récemment avec le réacteur de puissance zéro d'Argonne (ZPR-III) aux données obtenues par mesures. Il étudie les écarts entre les valeurs calculées et les valeurs expérimentales, en se rapportant aux résultats obtenus sur d'autres ensembles, pour déceler les tendances systématiques. Il étudie dans quelle mesure des changements dans les valeurs des sections efficaces et dans les méthodes de calcul permettraient de diminuer ces écarts.

Les calculs des variations de la réactivité, du flux et de la réponse d'un détecteur dues à des hétérogénéités causées par diverses configurations du combustible et des plaques diluantes dans les tiroirs des ensembles critiques sont comparés aux données expérimentales. L'auteur compare aussi les méthodes de transport pour de telles configurations cellulaires à plaques minces. Il suggère des méthodes qui permettraient d'améliorer les calculs de ces cellules; il décrit encore une méthode simple d'approximation à plusieurs groupes, que l'on peut appliquer sans l'aide d'une calculatrice électronique.

L'auteur étudie les sensibilités de la réactivité et des «inhours» en fonction de la période asymptotique du réacteur pour toute une série de compositions de réacteurs à neutrons rapides. Les résultats des calculs de la fraction des neutrons retardés effective, les «inhours» pour cent et les valeurs des neutrons instantanés et retardés sont donnés pour une série d'ensembles critiques à neutrons rapides.

---

* Work done under the auspices of the United States Atomic Energy Commission.

**Последние успехи и проблемы в теоретическом анализе критических сборок на быстрых нейтронах типа ZPR-III.** Теоретический анализ критических сборок, недавно проверенный экспериментальным образом на аргоннском реакторе нулевой мощности ZPR-III, сравнивается с измеренными данными. Расхождения между вычисленными и экспериментальными значениями изучаются совместно с результатами, достигнутыми ранее на других сборках, для того, чтобы установить систематические отклонения. Обсуждается влияние модификаций в сечениях и в вычислительных методах на уменьшение расхождений.

Вычисления изменений реактивности, колебаний потока и колебаний показаний детектора в результате состояний гетерогенности, вызываемых различными внутрикассетными конфигурациями топлива и пластинок-разбавителей внутри кассет критических сборок, сравниваются с экспериментальными данными. Сравниваются транспортные методы для конфигураций такой тонкой плоской ячейки. В докладе предлагаются пути улучшения вычислительных методов для таких ячеек и описывается простой многогрупповой метод приближения, подходящий для немашинного вычисления.

Чувствительность реактивности и обратных часов как функций асимптотического периода реактора обсуждается для целого ряда композиций реакторов на быстрых нейтронах. Результаты вычислений эффективной доли запаздывающих нейтронов, обратных часов/процент „ценности" мгновенных и запаздывающих нейтронов даются для целого ряда сборок на быстрых нейтронах.

**Recientes adelantos y problemas en el análisis teórico de los conjuntos críticos de neutrones rápidos del tipo ZPR-III.** El autor compara los resultados del análisis teórico de conjuntos críticos, estudiados recientemente desde un punto de vista experimental mediante el reactor de potencia cero de Argonne (ZPR-III), con los datos obtenidos en la práctica. Examina las discrepancias entre los valores teóricos y los experimentales, así como los resultados obtenidos con otros conjuntos, a fin de deducir tendencias sistemáticas. Estudia en qué medida la modificación de los valores de las secciones eficaces y de los métodos de cálculo permitiría disminuir esas discrepancias.

Los valores calculados de las variaciones de reactividad, del flujo y de la respuesta del detector, resultantes de heterogeneidades causadas por diferentes configuraciones del combustible y de las placas diluyentes en los compartimientos de los conjuntos críticos se comparan con los datos experimentales. También se comparan los métodos de transporte para esas configuraciones celulares de placas delgadas. El autor sugiere introducir algunas mejoras de los procedimientos de cálculo de esas celdas y describe un método sencillo de aproximación en varios grupos, que no exige el empleo de máquinas calculadoras.

Examina la sensibilidad de la reactividad y de los «inhours» en función del período asintótico del reactor, para diferentes modelos rápidos. Expone los resultados del cálculo de la fracción efectiva de neutrones retardados, de los «inhours» por ciento y de los valores de los neutrones inmediatos y retardados, para distintos conjuntos de neutrones rápidos.

## General introduction

Theoretical analyses of fast critical assemblies experimentally studied on the Argonne Fast Critical Facility, ZPR-III [1], include such quantities as critical mass, flux spectrum, detector responses, prompt-neutron lifetime, delayed-neutron fraction, and material replacement. These calculations have suggested more intensive study on various theoretical aspects of fast-neutron reactor physics. Three recent studies are the effects of heterogeneities, sensitivity of reactivity-period relations to cross-sections and to composition, and the effects of resonance scattering on criticality calculations. The latter study is part of a continuing effort in the ZPR-III analytical programme to re-evaluate multi-group cross-sections as additional microscopic cross-section information and additional critical assembly data from different assemblies become available.

## Calculation of heterogeneity effects in ZPR-III fast assemblies

### Introduction

The mock-up of a fast-reactor system on the zero-power facility ZPR-III is usually carried out by using finite thicknesses of plates of, for example, enriched uranium, depleted uranium, stainless steel, aluminium, and graphite [1]. The number of such plates corresponding to the composition of interest are placed in some configuration relative to each other within each core drawer (Fig. 1).

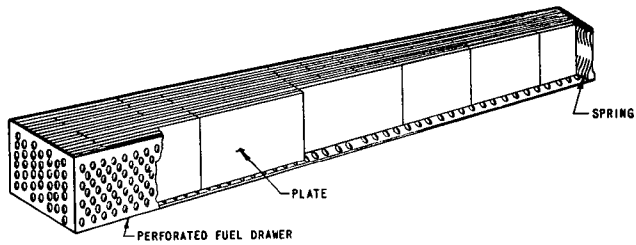


Fig. 1
Cut-away view of a core drawer showing positioning of plates in drawer.

The drawers are then inserted into the honeycomb arrays which form the two halves, one of which is movable, of the critical assembly machine. A horizontal cylindrical core thus consists of a repetition of an axially parallel, vertically aligned, configuration of the plates. Vertically, the plate configurations in all higher and lower drawers are in line and, except for the stainless-steel honeycomb structure and stainless-steel drawer bottoms, the geometry of the composite of plates is essentially a slab. It is of interest to ascertain the reactivity changes of such assemblies with variations in plate configuration as well as the deviations of reactivity from a homogeneous arrangement.

Calculated estimates of heterogeneity effects in various ZPR-III fast assemblies have been reported by previous investigators [1, 2]. The Carlson SNG-Code [3, 4] in $S_6$ approximation, with both 6- and 10-neutron energy groups, was used to obtain approximate solutions to the one-dimensional neutron transport equation. It has been observed both by these investigators [5] and by us that the use of the SNG-Code for these slab-cell calculations often led to unsymmetrical spatial flux distributions, although the cell configuration and composition distribution are symmetrical. Because of these observations and the need for a more detailed study of the calculation of heterogeneity effects, the present study was undertaken using the more recent Carlson Discrete $S_N$ Code (DSN) [6].

The results to be presented use the DSN-Code solutions to obtain the neutron spatial flux distributions, $U^{235}$- and $U^{238}$-fission detector responses, and multiplication constants for various plate configurations of three ZPR-III fast assemblies and a projected large $U^{235}$-fuelled fast assembly. The calculations were carried out in $S_4$, $S_8$, and $S_{16}$ approximations using three neutron energy groups having lower energy limits of 1.35 MeV, 9.12 keV and 1.0 keV. The three ZPR-III assemblies were similar in that they had two 0.32-cm thick plates of 93% enriched $U^{235}$ and 14 diluent plates, 0.32-cm thick, per core drawer. In the assemblies, the reflectors were 30-cm thick of high-density depleted uranium [1]. The cores differed in that the diluent was 99.8% depleted $U^{238}$, 63% density aluminium,

and graphite, respectively. (Assembly numbers are 22 (or 11), 23, and 14, respectively, where No. 22 is a reassembly of a previous [1] assembly numbered 11.) Perforations, approximately 0.95 cm in diameter, were used to reduce the aluminium plate density to 63% of its normal value. The experimental critical masses were 244 [7], 260 [7] and 136 [1] kg for the intra-drawer plate configurations in which the two enriched plates per core drawer were symmetrically separated by eight, eight and six diluent plates per drawer in the respective assemblies.

The intra-drawer plate configurations may be varied symmetrically by varying the separation distance between the two fuel plates. The calculated reactivity effects of such changes in configuration were compared with results of analogous experimental configuration changes obtained at the ZPR-III fast facility when all drawers of the fast core were so varied. In addition, the existence of a limited number of 0.16-cm enriched-fuel plates enables sectors of the cylindrical cores in the $U^{238}$ and aluminium diluent assemblies to be further unbunched so as to space the four 0.16-cm thick fuel plates by 1.28 cm of diluent. By extrapolation, the experimental reactivity change was obtained for a corresponding full core change which could be compared with results of calculations.

Analogous calculations are presented for a projected large $U^{235}$-fuelled fast assembly having a spherical critical mass of about 1000 kg, assuming a reflector savings of 20 cm. The average atomic densities of the core are:

$$N^{U^{235}} = 0.00172$$
$$N^{U^{238}} = 0.00626$$
$$N^{Fe} = 0.0207$$
$$N^{Al} = 0.0207$$

in units of $10^{24}$ atoms per cubic centimeter. In this assembly, all core materials other than those materials contained in the enriched-fuel plates are homogenized. The cell periodicity for this case is larger than the drawer periodicity, and the homogenized material is considered the diluent. The assumed thickness of diluent between equally spaced 0.32-cm thick fuel plates is 7.067 cm, and half as much between equally spaced 0.16-cm thick fuel plates.

A comparison of the convergence properties of solutions for a simplified two-region, one-energy group, repetitive slab cell having regional thicknesses and regional cross-sections representative of those encountered in some energy groups of the three-group DSN study are compared for DSN (N=2, 4, 8, 16), single-spherical harmonics PN (N=1, 3, ..., 11, 13) and double-spherical harmonics, DPN (N=1, 2, 3, 4, 5), solutions for the case of a spatially constant unit source density in the alternate regions of the cell. For such quasi-homogeneous cells, a simplified integral transport approximation method, amenable to hand calculation, is described. Application of the method to 3-energy group heterogeneity analyses for two fast systems having binary slab arrays of alternate fuel and diluent regions is presented.

## Procedure

A schematic drawing of the cross-sectional view of a ZPR-III basic cell is shown in Fig. 2 (left). The vertical outer regions, of iron, represent the composite of the stainless-steel box sides, the stainless-steel sides of the drawers located in the boxes, and the associated void spaces. The top and bottom iron regions represent the top and bottom stainless-steel of the box associated with each drawer, the stainless-steel bottom of the drawer, and associated void. The central region represents the plate region together with associated void. The following

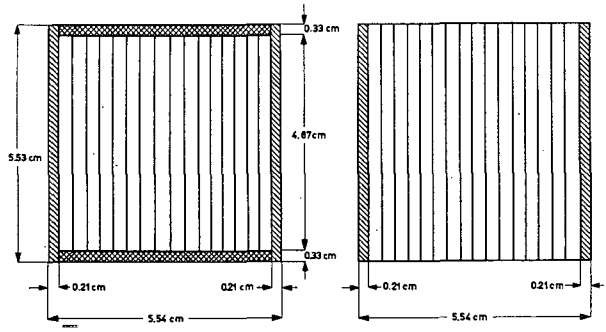


Fig. 2
Cross-section views of *left* ZPR-III basic cell and; *right* idealized slab cell.

changes were made to enable infinite slab geometry cell calculations with reflective boundary conditions to be applicable:

(*a*) The presence of stainless steel and void at top and bottom (Fig. 2 left) rather than plate material was accounted for by decreasing the atomic densities of the plates by 0.881 in the idealized cell (see Fig. 2 right). The iron displaced at the top and bottom of the plates was then accounted for by uniformly distributing that quantity of iron throughout the plate regions in the idealized slab geometry.

(*b*) As an assembly contains a finite repetition of cells in the direction transverse to the plates and also finite dimensions in the directions parallel to the plates, additional, spatially uniform group absorption cross-sections were assumed throughout the cell of the idealized slab-cell to account for the effect of neutron leakages upon the overall group flux levels relative to each other.

TABLE I

**THREE-GROUP FAST-NEUTRON CROSS-SECTIONS**
**(barns)**

| Group | | $U^{235}$ | $U^{238}$ | Fe | Al | C |
|---|---|---|---|---|---|---|
| I. $\chi_1 = 0.574$ 1.35 MeV → 10 MeV | $\nu_1$ | 2.65 | 2.8 | 0 | 0 | 0 |
| | $\nu_1\sigma_{f_1}$ | 3.445 | 1.484 | 0 | 0 | 0 |
| | $3\sigma_{tr_1}$ | 14.1 | 14.1 | 6.3 | 5.4 | 4.8 |
| | $\sigma_{a_1}$ | 2.8 | 2.67 | 0.7425 | 0.3803 | 0.28 |
| | $\sigma_{1\to 2}$ | 1.4 | 2.1 | 0.74 | 0.38 | 0.28 |
| II. $\chi_2 = 0.426$ 9.12 keV → 1.35 MeV | $\nu_2$ | 2.5 | 0 | 0 | 0 | 0 |
| | $\nu_2\sigma_{f_2}$ | 3.50 | 0 | 0 | 0 | 0 |
| | $3\sigma_{tr_2}$ | 18.0 | 21.0 | 8.7 | 9.0 | 10.7 |
| | $\sigma_{a_2}$ | 1.7 | 0.18 | 0.0082 | 0.0044 | 0.06 |
| | $\sigma_{2\to 3}$ | 0 | 0 | 0.0025 | 0.002 | 0.06 |
| III. $\chi_3 = 0$ 1 keV → 9.12 keV | $\nu_3$ | 2.50 | 0 | 0 | 0 | 0 |
| | $\nu_3\sigma_{f_3}$ | 15.0 | 0 | 0 | 0 | 0 |
| | $3\sigma_{tr_3}$ | 57.0 | 60.0 | 22.5 | 4.2 | 13.0 |
| | $\sigma_{a_3}$ | 9.0 | 0.8 | 0.015 | 0.006 | 0 |

$\sigma_{a_j} = \sigma_{f_{f_j}} + \sigma_{c_j} + \sigma_{j\to j+1}$

This leakage absorption was assumed to be $B^2/3\Sigma_{tr_j}$, the diffusion-theory group leakage term, where $B^2$ is the calculated material buckling of the homogenized core and $\Sigma_{tr_j}$ is the calculated group $j$ macroscopic transport cross-section of the homogenized core. The group leakage absorption cross-sections were assumed to be identical for a given core composition regardless of the particular configuration of the plates, because overall leakage from configurations of such thin-plate regions is more characteristic of average rather than regional compositions.

The 3-group fast-neutron cross-sections used are given in Table I. Group III, though used in this study, is not necessary for the non-carbon-containing assemblies, as very little of the reactivity of these systems is due to neutrons below Group II.

The atomic densities used in the various regions of the idealized slab-cell calculations are given in Table II.

TABLE II

**ATOMIC DENSITIES USED IN REGIONS OF THE SLAB CELLS**

| Cell regions | Atomic density* ($cm^{-3} \times 10^{-24}$) | | | | |
|---|---|---|---|---|---|
| | $U^{235}$ | $U^{238}$ | Fe | Al | C |
| Enriched (93%) $U^{235}$ plates | 0.0394 | 0.00296 | — | — | — |
| Depleted (99.8%) $U^{238}$ plates | 0.000085 | 0.0423 | — | — | — |
| 63% density aluminium plates | — | — | — | 0.0335 | — |
| Graphite plates | — | — | — | — | 0.06634 |
| Sides of box and drawer | — | — | 0.0512 | — | — |
| All plate regions** | — | — | 0.0042 | — | — |
| Homogenized diluent regions of the large metal system | 0.0000128 | 0.006407 | 0.02144 | 0.02162 | — |

* These are reduced densities to account for void, etc., in the slab idealization.

** Accounts for iron at top and bottom of the actual plates due to top and bottom of box and bottom of drawer by a uniform distribution throughout all plate regions.

The values used for material bucklings in computing the leakage-absorption terms in conjunction with homogenized core transport cross-sections were 0.005 $cm^{-2}$, 0.00303 $cm^{-2}$ and 0.0058 $cm^{-2}$, respectively, for the $U^{238}$, aluminium, and graphite diluent assemblies, and 0.0012 $cm^{-2}$ for the large metal system.

## RESULTS OF HETEROGENEITY CALCULATIONS BY DSN

The DSN-Code solutions in slab geometry for various configurations of each assembly were obtained in the $S_4$, $S_8$ and $S_{16}$ approximations. Mesh point intervals of 0.05 cm were generally employed, although in some cases smaller intervals were necessary in order to insure DSN-programme convergence of at least $\varepsilon = 3 \times 10^{-4}$ as defined in Ref. [6]. The relative values of the effective multiplication factors are shown in Figs. 3 and 4. The values of $k_{eff}$ for the homogeneous cell calculations are also shown (these differ slightly from unity because the material bucklings used for the leakage absorptions were not precisely the homogenized cell material bucklings). For these cells the calculated multiplication constants, for a given assembly cell configuration ,by $N = 4$, 8, and 16 approxi-

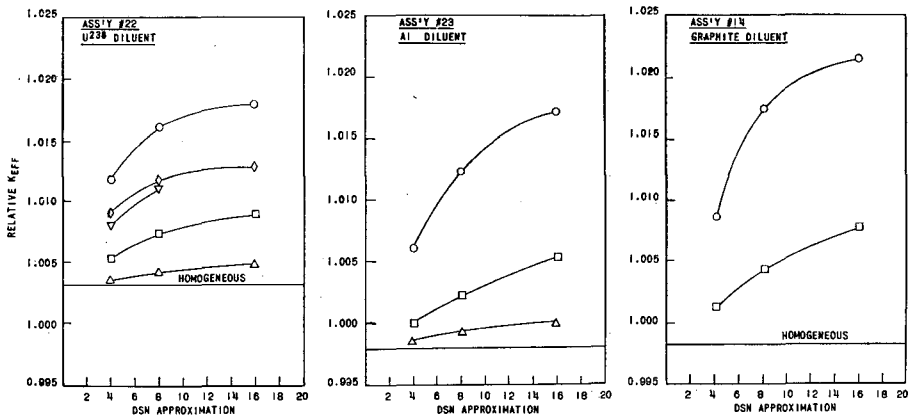


Fig. 3

Relative $k_{\text{eff}}$ values for various fuel-plate separations within core drawer cells of ZPR-III Assemblies Nos. 22 (or 11), 23 and 14 as calculated by DSN-Code.

Core-drawer compositions: two enriched uranium plates 0.32 cm thick and 14 diluent plates 0.32 cm thick.

○, 2 enriched plates adjacent at drawer centre; ◊, 0.64-cm separation between the two enriched plates; □, 2.56-cm separation between the two enriched plates; ▽, 2 enriched plates fully separated within drawer; △, 4 0.16-cm enriched plates separated by 1.28 cm of diluent.

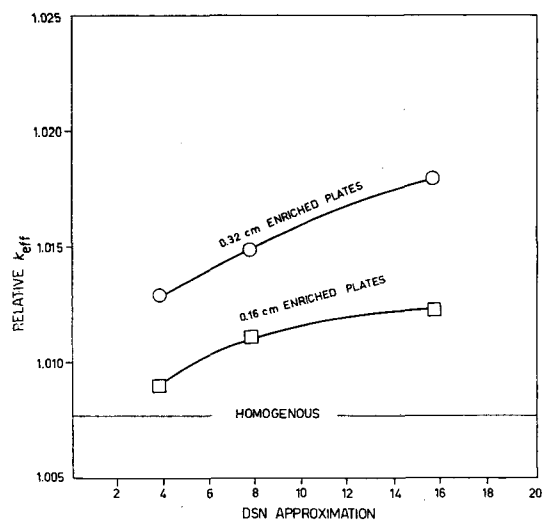


Fig. 4

Relative $k_{\text{eff}}$ for two fuel-plate thicknesses for a large (1000 kg critical mass) system as calculated by DSN-Code.

mations successively, increase such that the eigenvalues obtainable at $N=16$ are still generally far from the limiting values at large $N$. This especially leads to uncertainty if differences in $k_{\text{eff}}$ values from the homogeneous case are desired. For practical comparison of calculated $\Delta k_{\text{eff}}$ values between various plate configurations with corresponding experimental values, this limitation may not be as severe, because the $k_{\text{eff}}$-*versus*-$N$-approximation curves for the heterogeneous configurations generally tend to increase together and, in addition, the

TABLE III

**COMPARISON OF CALCULATED AND EXPERIMENTAL CHANGES IN $k_{eff}$ WITH CHANGES IN FUEL-PLATE CONFIGURATION**

| Assembly (primary diluent) | Plate configuration D = 0.32-cm diluent plate F = 0.32-cm fuel plate (F) = 0.16-cm fuel plate | Change in % $k_{eff}$ relative to standard* configuration | | |
|---|---|---|---|---|
| | | Calculated $S_{16}$ | Experimental (inhours)** | |
| 22 ($U^{238}$) | DDDDDDFDDFDDDDDD | 0.4% $k$ | 0.4% $k$ | (190.6 ih) |
| | DDDDDDDFFDDDDDDD | 0.9 | 0.9 | (415.3) |
| | D(F)DDDD(F)DDDD(F) DDDD(F)D | —0.4 | —0.4 | (—182.) |
| 23 (Al) | FDDDDDDDDDDDDDDF | 0.3*** | —0.2 | (—95.8) |
| | DDDDDDDFFDDDDDDD | 1.2 | 1.1 | (468.6) |
| | D(F)DDDD(F)DDDD(F) DDDD(F)D | —0.5 | —0.4 | (—160.) |
| 14 (Graphite) | DDDDDDDFFDDDDDDD | 1.4 | 1.3(5) | (424.) |

* DDDFDDDDDDDDFDDD for Assemblies 22 and 23.
DDDDFDDDDDDFDDDD for Assembly 14.
** Experimental inhour change obtained by ZPR-III Experimental Group [9]. Significant figures in % $k_{eff}$ based on the possible estimated uncertainty range in calculated values of inhours per percent.
*** Estimate of value at $S_{16}$ by extrapolation from calculated $S_4$ and $S_8$ values. See text for possible explanation of discrepancy between experiment and calculation for this configuration.

accuracy of the experimental $\Delta k_{eff}$ values is limited by uncertainty introduced in the auxiliary calculations for the conversion of inhours to per cent. Comparison of calculational values with the experimental values of changes in reactivity with changes in heterogeneity are given in Table III. The calculated values listed are obtained from the $S_{16}$ solutions, except when otherwise indicated. In general, the agreement is satisfactory. The case of the two 0.32-cm fuel plates separated by 14 plates of $U^{238}$ is, however, an exception, in that one would by the analyses as presented here expect an increase in reactivity over that for

TABLE IV

**DEVIATIONS IN PER CENT $k_{eff}$ FROM HOMOGENEOUS BY EXTRAPOLATION OF RELATIVE $k_{eff}$ *VERSUS* DSN APPROXIMATION**

| Assembly (primary diluent) \ Fuel-plate thickness | 0.64 cm | 0.32 cm | 0.16 cm |
|---|---|---|---|
| 22 ($U^{238}$) | a. 1.6 ±0.1* | b. 0.8 ±0.2 | c. 0.3 ±0.1 |
| 23 (Al) | a. 2.3 ±0.3 | b. 1.1 ±0.3 | c. 0.3 ±0.1 |
| 14 (Graphite) | a. 2.5 ±0.1 | d. 1.2 ±0.2 | — |
| Large metal (Al + Fe + $U^{238}$) | — | e. 1.3 ±0.2 | f. 0.5 ±0.1 |

* Errors in all cases represent only the estimated reliance of extrapolation to asymptotic.
[a]DDDDDDDFFDDDDDDD.
[b]DDDFDDDDDDDDFDDD.
[c]D(F)DDDD(F)DDDD(F)DDDD(F)D.
[d]DDDDFDDDDDDFDDDD.
[e]7.067 cm of homogenized diluent between equally spaced 0.32-cm enriched fuel plates.
[f]3.5335 cm of homogenized diluent between equally spaced 0.16-cm enriched fuel plates.

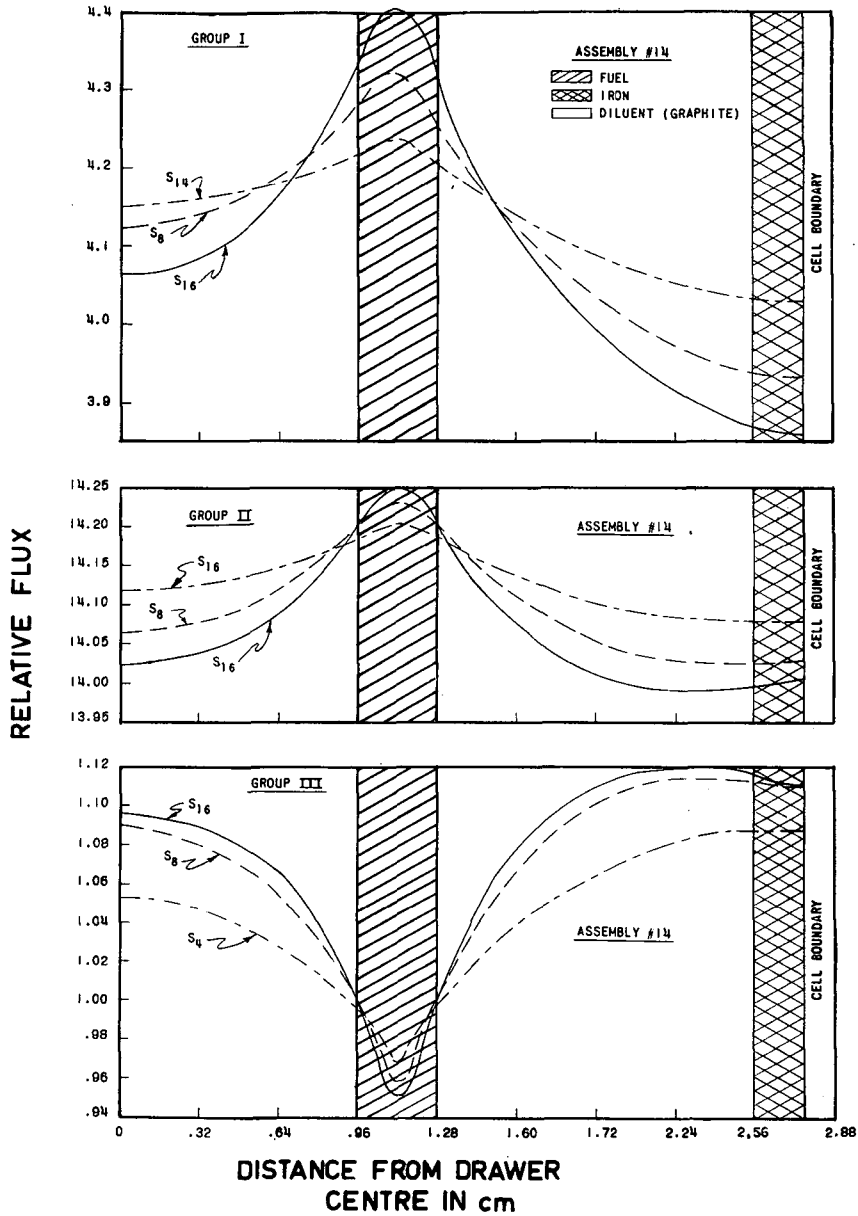


Fig. 5
Calculated group fluxes for Assembly-14 cell configuration having two 0.32-cm fuel plates separated by 1.92 cm of graphite diluent by DSN approximations. $N = 4, 8$ and 16.

the case of the two fuel plates separated by eight plates of $U^{238}$. The reason for the discrepancy may be the fact that, whereas as far as internal core regions are concerned, this fully separated configuration tends to bunch fuel plates

in adjacent drawers and hence to increase the reactivity; however, in the peripheral core drawers, the outer fuel plates do not have these closely neighbouring fuel plates and hence result in an overall reactivity decrease. This latter effect is not accounted for in the analyses.

Estimated deviations of heterogeneity from homogeneity by extrapolation of the $k_{\text{eff}}$-*versus*-DSN approximation are given in Table IV for plate configurations studied, which most closely approximate equally spaced fuel plates of 0.64-cm, 0.32-cm, and 0.16-cm thicknesses.

Comparison of $S_4$, $S_8$ and $S_{16}$ spatial distributions of the group fluxes are shown in Fig. 5 for the graphite diluent cell having fuel plates separated by 1.92 cm of diluent. Detailed fluxes, $U^{235}$-fission detector responses and $U^{238}$-fission detector responses as calculated for the various plate configurations of these cores are given in Ref. [8].

It is of interest to estimate to what extent a measurement of fission detector at a given position in a cell differs from that for the corresponding homogeneous cell, and to what extent the detector ratio of the average $U^{238}$-response divided by the average $U^{235}$-response across a heterogeneous cell differs from that for the corresponding homogeneous cell. The calculated maximum and minimum range of values for $U^{238}$- to $U^{235}$-fission detector ratios deviates from the calculated homogeneous ratios by the ranges shown in Fig. 6, depending upon the location of the detectors within the cell, i.e., whether at the peak, trough, or intermediate

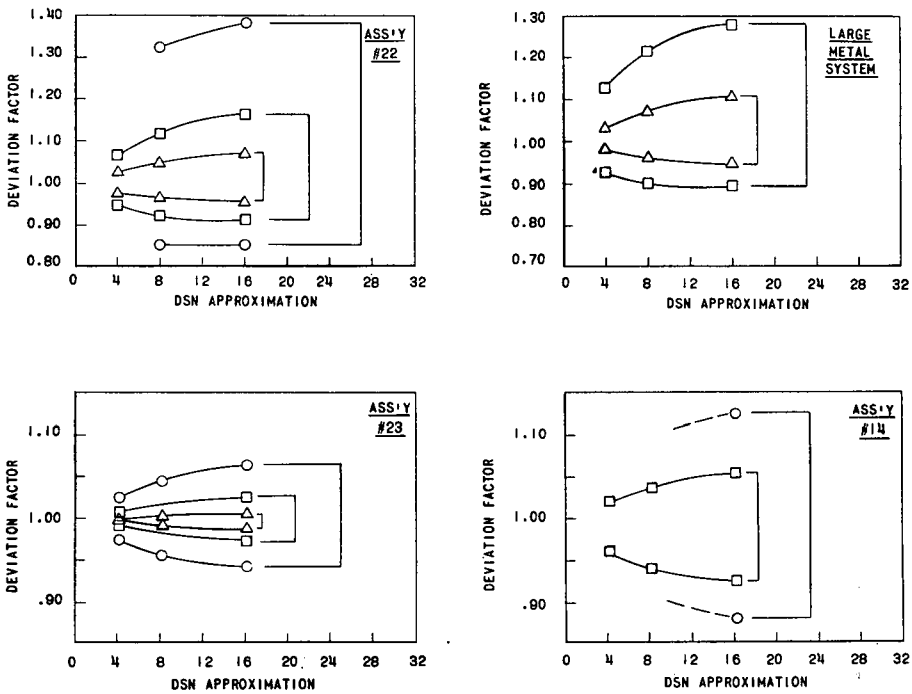


Fig. 6
Calculated intra-drawer range in deviation of $U^{238}$- to $U^{235}$-fission-detector ratios from homogeneous ratio for the ZPR-III Assemblies 22, 23 and 14, and for a large metal system.
Fuel thickness: ○, 0.64 cm; □, 0.32 cm; △, 0.16 cm

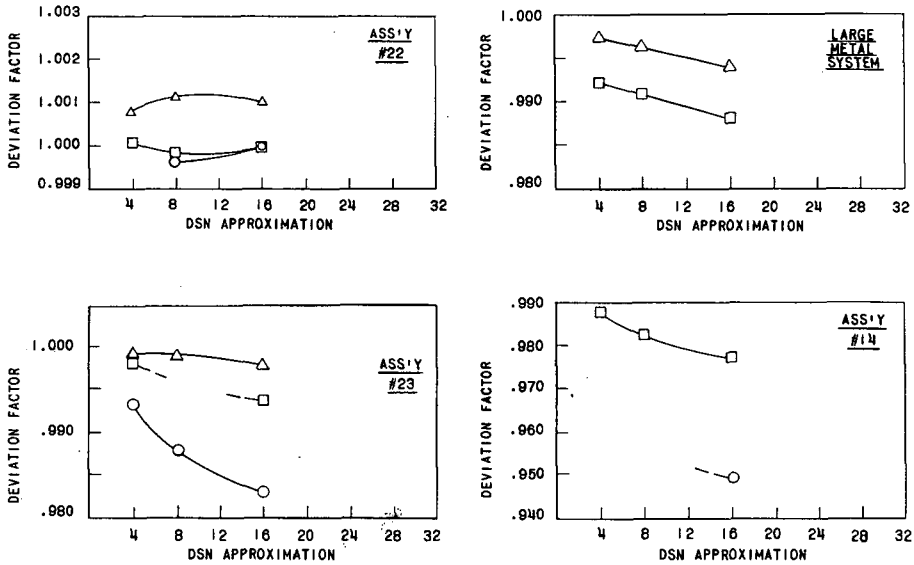


Fig. 7
Calculated deviations from homogeneous of spatial average $U^{238}$-fission-detector response to spatial average $U^{235}$-fission-detector response for ZPR-III Assemblies 22, 23 and 14, and for a large metal system.
Fuel thickness: ○, 0.64 cm; □, 0.32 cm; △, 0.16 cm

positions. The calculated deviations of the mean $U^{238}$-detector-response divided by the mean $U^{235}$-detector-response across the various cells relative to the corresponding homogeneous ratios are shown in Fig. 7. It should be noted that the latter deviations for the case of the assemblies having $U^{238}$-diluent are negligible, and the apparent deviations are greater than unity for the case of 0.16-cm thick fuel plates, due to limits of accuracy in the calculations.

### Comparison of DSN, PN, and DPN solutions for a binary cell

The necessity for many angular intervals (i.e., high $N$) in order to insure that eigenvalue and flux shape of such thin region slab-cells be sufficiently converged to the value and shape at $N \to \infty$ indicates that the neutrons travelling at very small oblique angles to the slab planes are very important in determining the flux shape. Thus a high-order approximation is required to characterize adequately the small tangential directions.

A simplified two-region, one-energy group, thin slab-cell having regional cross-sections of magnitudes representative of those encountered in some energy groups of the 3-group DSN heterogeneity study is analysed. DSN [6] ($N=2$, 4,8,16), Single-PN ($N=1, 3, \ldots, 11, 13$), and Double-PN ($N=1, 2, 3, 4, 5$) solutions are obtained for the case of a spatially constant unit-source density in one region and zero source in the second region. (These are not source iterative solutions as would be necessary for a heterogeneity calculation in an actual case; however, the main convergence features and comparisons of the methods are valid.)

The uncollided flux solutions are also obtained for comparison with the multiply-collided solutions. An integral transport solution for the uncollided flux showing the effects of successive neighbouring cell sources upon the overall solution is also calculated.

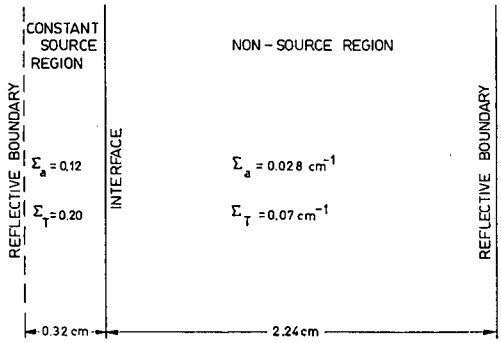


Fig. 8

Half-cell dimensions of thin cell and regional cross-sections.

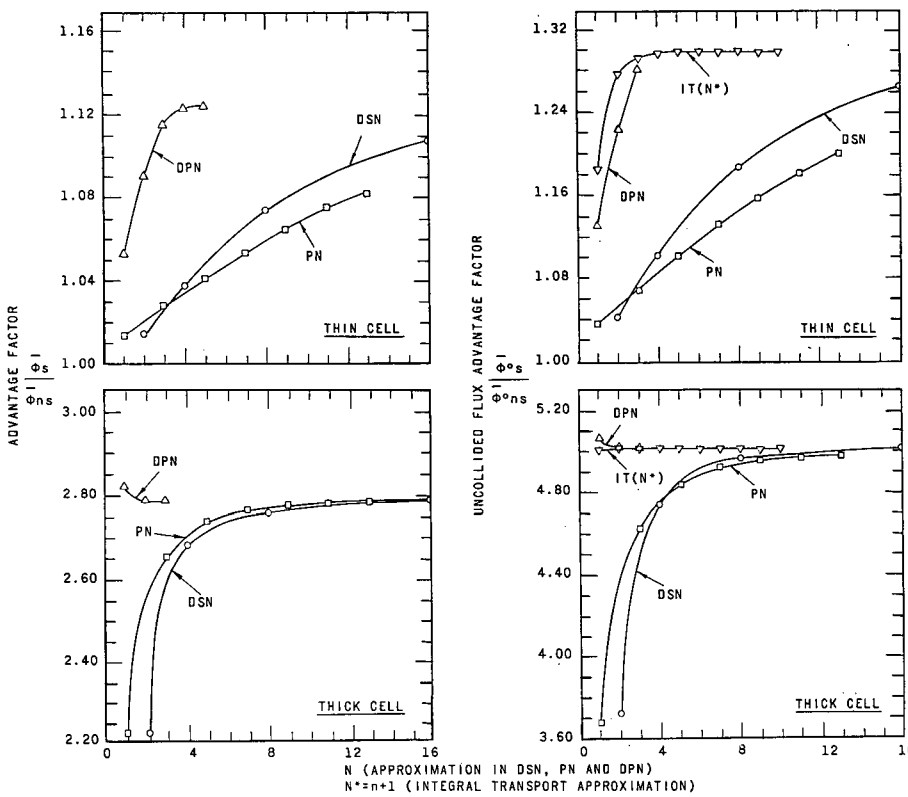


Fig. 9

Ratios of average flux in source region to average flux in non-source region for successive approximations by the various methods of solution for the thin and thick cells.

The dimensions of the half-cell and the macroscopic regional cross-sections are shown in Fig. 8. In the source region, the full regional thicknesses in absorption and total mean free paths are 0.0768 and 0.128, respectively. In the non-source region, the regional thicknesses in absorption and total mean free paths are 0.125 and 0.314, respectively.

In addition, to obtain a set of solutions which are more converged by all these methods, the regional thicknesses of the cell are increased to ten times the dimensions shown in Fig. 8 with identical macroscopic cross-sections retained.

The single-spherical-harmonics (PN) solutions are obtained by a programme [10] using as input the tabulated [11, 12] values of the determinantal roots $\nu_i$ and the functions $G_j(\nu_i)$. The double-spherical-harmonics (D PN) solutions are obtained using the Flip [13] programme and the RANCH [14] programme. The uncollided integral transport solution is also obtained by a programme [10].

The ratios of the average values of the flux in the source region to the average value of the flux in the non-source region are shown in Fig. 9 for successive approximations by the various methods of solution for the thin and thick cell. Only the DP-5 solution appears reasonably converged for the thin cell, whereas DS-16, P-13 and DP-2 give essentially converged identical advantage factors for the thick cell.

The uncollided flux advantage factors by DSN, PN and DPN as functions of solution approximations exhibit analogous convergence shapes to the preceding multiple collision results, except that the curves are displaced to larger advantage factor values. The results of the uncollided flux integral transport solutions show in this case that consideration of sources from about four to five neighbouring cells on both sides must be considered in order to give reasonably converged uncollided advantage factors. This is because sufficient neighbouring cells must be considered to account for the fate of the emitted source neutrons, especially those emitted in closely perpendicular directions (to the planes), which contribute largely to the overall flux level.

The uncollided fluxes are the solutions obtained by the various methods when the regional absorption cross-sections are increased so as to be equal to the regional total cross-sections.

Analogous calculations of the advantage factors for the uncollided flux by an integral transport solution in which the effects of successively more remote source regions upon the advantage factor are observable are also shown in Fig. 9 for the two cell sizes.

The spatial uncollided flux solutions for the thin cell for various nearest neighbour approximations are shown in Fig. 10. (The integral transport approximation refers to the number of neighbouring source regions considered in the calculations in the following sense. The $n=0$ refers to the uncollided flux in a source region due to neutrons arising from the sources in that region, and it refers to the uncollided flux in a non-source region due to neutrons originating in the adjacent source regions on both sides of the non-source region. Similarly, the $n=1$ solution refers to uncollided flux in a source region due to neutrons from sources arising in that region and in the closest neighbouring source regions on both sides, and it refers to the uncollided flux in a non-source region due to neutrons originating in the first and second nearest source regions on both sides of the non-source regions.) Insofar as the flux shape is concerned, the integral method requires in this case at most one neighbouring cell to be considered.

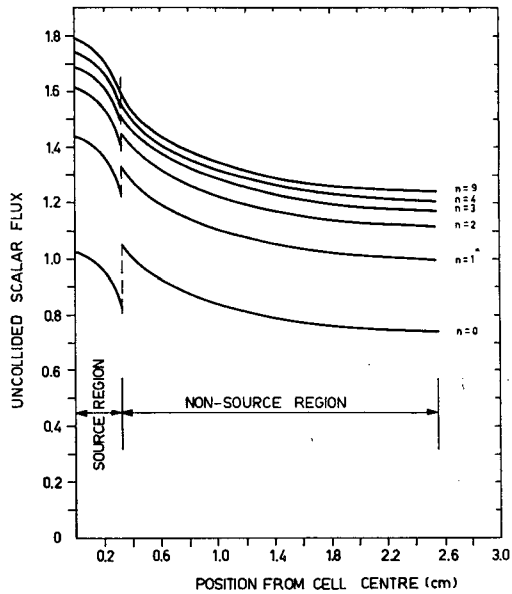


Fig. 10
Uncollided scalar-flux distributions showing effects of considering increased number of neighbouring cells.

The multiply collided and the uncollided vector fluxes at various positions by the DP-5 solution using double Gaussian quadrature are shown in Fig. 11. The angular spreads about $\mu=0$ in which the anisotropic component occurs are approximately the same in the two cases. The two sets of angular distributions differ essentially only by the increased magnitude of the isotropic flux level in the multiple collision case. This is because in this example the neutron sources (due to scattering) in the two regions are small relative to the applied source. Inclusion of the scattering source levels, based upon the homogeneous cell constant flux level, into the uncollided flux solution will result in more improved comparison with the anisotropic component of the multiply collided solution.

Comparison of the thin cell DSN, PN, and DPN solutions for approximations corresponding to equivalent numbers of discrete quadrature angles [15, 16], in the sense that PN is equivalent to single Gaussian quadrature solution having $N+1$ angles and DPN is equivalent to double Gaussian quadrature solution having $2(N+1)$ angles [17], shows that improved convergence is obtained by quadratures having finer characterization in the angular region about $\mu=0$.

Thus the greater effectivenesses of the DSN relative to the PN and of the DPN relative to the DSN are due to the increasingly more effective distributions of the small discrete directions in the region near $\mu=0$. For the case of the cell having regional thicknesses ten times as large the convergence rates by PN and DSN are quite similar, indicating that the differences of the quadratures are not important enough, i.e., the angular spread about $\mu=0$ which contributes to the anisotropic flux component is relatively large. The DPN results in this case converge from above, which suggests that the distributions of the discrete directions as demanded by double Gaussian quadrature are slightly too heavily distributed toward the $\mu=0$ region.

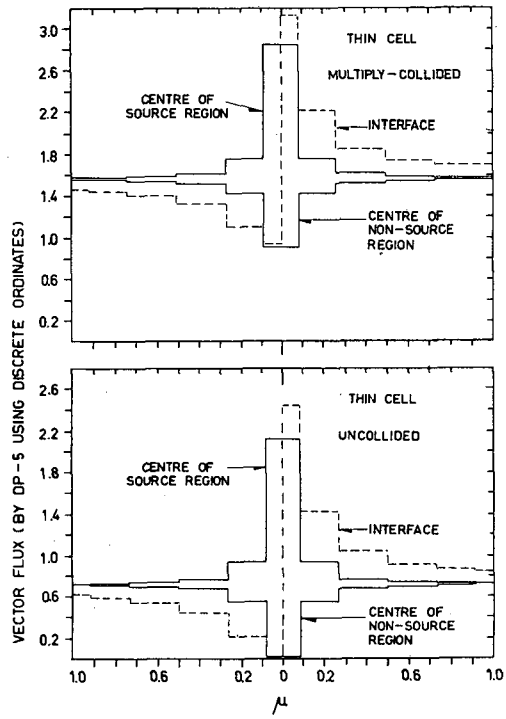


Fig. 11
Multiply collided and uncollided vector fluxes at various positions in the thin cell as obtained by a twelve-angle double Gaussian discrete ordinate calculation (equivalent to DP-5).

This suggests use of either a discrete ordinate method in which the discrete angles and weights of the quadrature are assigned so as to be effectively distributed, or an integral transport method in which the angular integration is accurately carried out.

## Simplified integral transport heterogeneity calculation for thin binary slab-cells

The above considerations suggest an approximate solution in which the spatial flux "shape" is obtained from an uncollided flux solution requiring consideration of sources from at most only a few nearest neighbour regions. The uncollided flux is considered to arise from "effective" flat regional source levels, which include the elastic-scattering sources as well as applied and fission sources, based upon the constant flux level of the equivalent homogeneous cell. The "level" of the uncollided flux shape is then adjusted by a constant flux term to satisfy the neutron-inventory requirement that total absorptions equal total actual sources (not including elastic-scattering sources) to obtain an approximation to the multiply collided flux distribution. If necessary, for more accuracy, a source iteration may be carried out using new effective flat regional sources based upon regional average flux values obtained. Detailed procedure and equations are given in Ref. [18].

The method has been applied to a three-group analysis for

$$\left(\frac{\Delta k_{\text{eff}}}{k_{\text{eff}}^{\text{homog.}}}\right)$$

for two fuel and diluent configurations, pertaining to the previously described "large metal system", consisting of 0.16-cm thick enriched-fuel plates separated by about 3.53 cm of diluent and 0.32-cm thick fuel plates separated by 7.06 cm of diluent. To allow direct comparisons of group-flux advantage factors with corresponding DS-16 results, the identical regional cross-sections and energy group are retained.

The separately calculated (non-source iterative) group advantage factors, $\bar{\varphi}_{j_{\text{fuel}}}/\bar{\varphi}_{j_{\text{diluent}}}$, are 1.17, 1.00 and 0.94 respectively with 0.16-cm fuel. Corresponding DS-16 factors (sources and three groups iterative) are 1.13, 1.00 and 0.93. DP-5 factors are 1.17 and 0.92 for groups 1 and 3 respectively. The group-3 factors do not affect the heterogeneity estimate, because the group-3 flux is negligible for this composition. For group 1, the predominant source region is the thin fuel plate region. The advantage factors are larger by the simplified integral transport approach and by DP-5 than by DS-16, in effect, because the latter has its minimum discrete ordinate at $|\mu| = 0.0626$, which is somewhat large to be encompassed within the region of predominant angular flux anisotropy for such a thin source region.

The value of $(k^{\text{hetero}} - k^{\text{homo}})/k^{\text{homo}}$ obtained is about $+0.006$, which may be compared with the DS-16 value of $+0.0043$. For the system, of equivalent composition, having 0.32-cm thick fuel plates separated by 7.06 cm of diluent, the values are $+$ 0.011 and $+$ 0.0100 respectively.

In the case of group 3, the predominant "source" region—because of neutron transfer from group 2 to group 3, is the diluent region whose group thickness is about one total mean free path, and the intervening absorption region (fuel plate) is a fraction of a mean free path. To obtain reasonably suitable uncollided flux "shape" convergence requires an $n=1$ nearest neighbour approximation, in contrast to an $n=0$ for the first two groups; however, in addition, the "shape" of the uncollided flux spatial distribution is not closely representative of the multiple collided "shape", so that the value 0.94 is larger than the DP-5 converged 0.92 value.

If heterogeneity cases are encountered for which the overall multiplication constant is too sensitive to the ratio of the average regional group fluxes for energy groups having such thick "effective" sources, subsequent collision sources must be considered. A division of the large "source" region into smaller subdivisions to insure that the assumption of constant regional "effective" sources do not affect the group advantage factor, to the extent of affecting the cell eigenvalue, may be necessary. In these instances, it would seem more advantageous to use the variational method [19] for these groups in conjunction with appropriately chosen trial functions for the diluent source region.

Thus the simplified integral transport approximation is most accurate and useful for thin cells having very thin predominant effective source regions. These cells are characteristic of fast-reactor critical assemblies fuelled by thin fuel plates, although the method may be useful for calculation of disadvantage factors in cases of thermal reactor cells having very thin water gaps.

## Effective delayed neutron fraction and inhour relation

### Introduction

A typical fast power reactor contains large quantities of $U^{238}$, both in the core and in the breeder blanket reflector. The neutron spectrum is such that a considerable fraction of the fissions occur in $U^{238}$.

The evaluation of quantities such as the effective delayed-neutron fraction of the system and the relation between reactivity and reactor period are complicated by the spatial distribution of the $U^{238}$-fissions, which differ from that of the fuel ($U^{235}$ or $Pu^{239}$) fissions, and by the delayed-neutron characteristics of $U^{238}$, which differ from that of the fuel.

The values of effective delayed-neutron fraction, prompt-neutron lifetime, and of worths of delayed and prompt neutrons have been calculated for a series of ZPR-III fast assemblies. The assemblies represent $U^{238}$ to $U^{235}$ atomic ratios in the range 1 to over 10. For comparisons the calculations were carried out using various multi-group cross-section sets.

The sensitivity of the reactivity *versus* asymptotic reactor period to both composition and to variations in multi-group cross-section parameters is of importance in the conversion of, for example, material replacement experiments in which the reactor periods are observed. Closely related to this is the sensitivity of conversion from inhours to reactivity. The sensitivities of these relations to composition and cross-sections have been studied for the range of $U^{238}/U^{235}$ atomic ratio from 1 to over 10.

### $\beta_{eff}$, $l_p$, and prompt- and delayed-neutron worths

The values of $\beta_{eff}$, $l_p$, and worths of prompt and delayed neutrons have been calculated for ZPR-III assemblies 6F, 9A, 22 (or 11), 24 and 25 using the core

Table V

**CORE AND REFLECTOR VOLUME FRACTIONS**

| Assembly | $V_f^{U^{235}}$ | $V_f^{U^{238}}$ | $V_f^{Fe}$ | $V_f^{Al}$ |
|---|---|---|---|---|
| 6F | 0.140 | 0.159 | 0.123 | 0.314 |
| 9A | 0.117 | 0.380 | 0.142 | 0.216 |
| 22 (or 11) | 0.0952 | 0.717 | 0.0915 | 0 |
| 24 | 0.0762 | 0.736 | 0.0915 | 0 |
| 25 | 0.0715 | 0.741 | 0.0915 | 0 |
| 30-cm blanket comp. | 0.0019 | 0.833 | 0.0731 | 0 |

compositions given in Table V. For comparison, analogous calculations were carried out using the following fast neutron cross-section sets:

(*a*) The 11-group set [20, 21] used largely in analysis of ZPR-III assemblies and having two groups above the $U^{238}$-fission threshold;

(*b*) The two 10-group sets [22] referred to as standard and revised, used in the analysis of the fast cores in ZPR-V, both having one group above the $U^{238}$-threshold, and differing in that the "revised" set incorporated more recent $U^{238}$ inelastic-scattering data.

The calculation of $\beta_{\text{eff}}$, $l_{\text{p}}$ and worths were carried out using a machine programme [10] which utilized as input the space- and energy-dependent flux and adjoint spherical geometry solutions for the reflected assemblies. The core region in each case has been treated as a single region, and the reflector as two regions. The first eight centimeters of reflector adjacent to the core are considered a separate region. This allows comparison of the separate $U^{238}$ -to $U^{235}$-ratio of fissions, and the various neutron worths to be obtained for the core, reflector region near the core, and outer region of the reflector in addition to values for the overall system.

The formulas used to obtain $\beta_{\text{eff}}$, $l_{\text{p}}$ and worths follow essentially the definitions as given by LONG *et al.* [1].

The fraction of the delayed neutrons, $\chi^{25}_{D_j}$ and $\chi^{28}_{D_j}$ respectively, emitted into energy group $j$ for the multi-group energy divisions of the 11-group cross-section set is given in Table VI. These values are based on the delayed-neutron abundances data of KEEPIN *et al.* [23], and the reported average energies of the delayed groups [20, 24]. The average number of delayed neutrons per $U^{235}$-fission, $(n/F)_{25}$, the average number of delayed neutrons per $U^{238}$-fission $(n/F)_{28}$, the average number of neutrons emitted per $U^{235}$-fission, $\bar{\nu}^{25}$, and the average number of neutrons emitted per $U^{238}$-fission, $\bar{\nu}^{28}$, are the values given by KEEPIN *et al.* [23].

The formulae for the case of two fissionable species ($U^{235}$ and $U^{238}$) for a system having multi-group flux and adjoint solutions $\varphi_i$ (r) and $\varphi_i^+$ (r) may be expressed in the forms:

$$\beta_{\text{eff}} = \frac{D}{D+P}$$

where

$$D = \frac{\left[\int \sum_{i=1}^{J} (\nu\,\Sigma_{\text{f}})_i^{25}\,\varphi_i\,\mathrm{d}V\right]\left[\int\left(\sum_{i=1}^{J}(\nu\,\Sigma_{\text{f}})_i^{25}\,\varphi_i\right)\left(\sum_{j=1}^{J}\chi^{25}_{D_j}\,\varphi_j{+}\right)\mathrm{d}V\right]\left(\frac{1}{\bar{\nu}^{25}}\right)\left(\frac{n}{F}\right)^{25}}{\left[\int\left(\sum_{i=1}^{J}(\nu\,\Sigma_{\text{f}})_i^{25}\,\varphi_i\right)\left(\sum_{j=1}^{J}\chi_j\,\varphi_j{+}\right)\mathrm{d}V\right]}$$

$$+\frac{\left[\int \sum_{i=1}^{J} (\nu\,\Sigma_{\text{f}})_i^{25}\,\varphi_i\,\mathrm{d}V\right]\left[\int\left(\sum_{i=1}^{J}(\nu\,\Sigma_{\text{f}})_i^{28}\,\varphi_i\right)\left(\sum_{j=1}^{J}\chi^{28}_{D_j}\,\varphi_j{+}\right)\mathrm{d}V\right]\left(\frac{1}{\bar{\nu}^{28}}\right)\left(\frac{n}{F}\right)^{28}}{\left[\int\left(\sum_{i=1}^{J}(\nu\,\Sigma_{\text{f}})_i^{25}\,\varphi_i\right)\left(\sum_{j=1}^{J}\chi_j\,\varphi_j{+}\right)\mathrm{d}V\right]}\,.$$

and where

$$P = \frac{\left[\int \sum_{i=1}^{J} (\nu\,\Sigma_{\text{f}})_i^{25}\,\varphi_i\,\mathrm{d}V\right]\left[\bar{\nu}^{25} - \left(\frac{n}{F}\right)^{25}\right]}{\bar{\nu}^{25}}$$

$$+\frac{\left[\int \sum_{i=1}^{J} (\nu\,\Sigma_{\text{f}})_i^{25}\,\varphi_i\,\mathrm{d}V\right]\left[\int\left(\sum_{i=1}^{J}(\nu\,\Sigma_{\text{f}})_i^{28}\,\varphi_i\right)\left(\sum_{j=1}^{J}\chi_j\,\varphi_j{+}\right)\mathrm{d}V\right]\left[\bar{\nu}^{28} - \left(\frac{n}{F}\right)^{28}\right]}{\left[\int\left(\sum_{i=1}^{J}(\nu\,\Sigma_{\text{f}})_i^{25}\,\varphi_i\right)\left(\sum_{j=1}^{J}\chi\,\varphi_j{+}\right)\mathrm{d}V\right]\left[\bar{\nu}^{28}\right]}\,.$$

TABLE VI

**MULTI-GROUP DISTRIBUTION OF DELAYED FISSION NEUTRONS***

**$(n/F)^{25} = 0.0165$; $(n/F)^{28} = 0.0412$; $\bar{\nu}^{25} = 2.56$; $\bar{\nu}^{28} = 2.62$**

| $E_i$ lower (MeV) | Group, $j$ | $\chi D_j^{25}$ | $\chi D_j^{28}$ |
|---|---|---|---|
| 2.25 | 1 | 0 | 0 |
| 1.35 | 2 | 0 | 0 |
| 0.825 | 3 | 0 | 0 |
| 0.500 | 4 | 0 | 0 |
| 0.300 | 5 | 0.962 | 0.987 |
| 0.180 | 6 | 0.038 | 0.013 |
| 0.110 | 7 | 0 | 0 |
| 0.067 | 8 | 0 | 0 |
| 0.025 | 9 | 0 | 0 |
| 0.0091 | 10 | 0 | 0 |
| 0 | 11 | 0 | 0 |

* Based upon data of KEEPIN *et al.* [23] and GOLDSTEIN [20, 24].

$$l_p = \frac{\int\left(\sum_{i=1}^{J} \frac{\varphi_i \varphi_i^+}{v_i}\right) \mathrm{d}V}{\int\left(\sum_{i=1}^{J} (\nu\,\Sigma_f)_i^{25}\,\varphi_i\right)\left(\sum_{j=1}^{J} \chi_j\,\varphi_j^+\right)\mathrm{d}V + \int\left(\sum_{i=1}^{J} (\nu\,\Sigma_f)_i^{28}\,\varphi_i\right)\left(\sum_{j=1}^{J} \chi_j\,\varphi_j^+\right)\mathrm{d}V}.$$

All integrals in the above expressions are over the entire reactor volume.

All integrals in the following expressions are over the volume regions separately or/and over the entire reactor volume:

$$\frac{\text{Number of } U^{238} \text{ fissions}}{\text{Number of } U^{235} \text{ fissions}} = \frac{\int \sum_{i=1}^{J} \Sigma_{f_i}^{28}\,\varphi_i\,\mathrm{d}V}{\int \sum_{i=1}^{J} \Sigma_{f_i}^{25}\,\varphi_i\,\mathrm{d}V}.$$

$$\frac{W_D^{28}}{W_P^{25}} = \frac{\left[\int\left(\sum_{i=1}^{J} (\nu\,\Sigma_f)_i^{28}\,\varphi_i\right)\left(\sum_{j=1}^{J} \chi_{D_j}^{28}\,\varphi_j^+\right)\mathrm{d}V\right]\left[\int \sum_{i=1} (\nu\,\Sigma_f)_i^{25}\,\varphi_i\,\mathrm{d}V\right]}{\left[\int\left(\sum_{i=1}^{J} (\nu\,\Sigma_f)_i^{25}\,\varphi_i\right)\left(\sum_{j=1}^{J} \chi_j\,\varphi_j^+\right)\mathrm{d}V\right]\left[\int \sum_{i=1}^{J} (\nu\,\Sigma_f)_i^{28}\,\varphi_i\,\mathrm{d}V\right]}.$$

$$\frac{W_D^{25}}{W_P^{25}} = \frac{\left[\int\left(\sum_{i=1}^{J} (\nu\,\Sigma_f)_i^{25}\,\varphi_i\right)\left(\sum_{j=1}^{J} \chi_{D_j}^{25}\,\varphi_j^+\right)\mathrm{d}V\right]}{\left[\int\left(\sum_{i=1}^{J} (\nu\,\Sigma_f)_i^{25}\,\varphi_i\right)\left(\sum_{j=1}^{J} \chi_j^{25}\,\varphi_j^+\right)\mathrm{d}V\right]}.$$

$$\frac{W_P^{28}}{W_P^{25}} = \frac{\left[\int\left(\sum_{i=1}^{J}(\nu\,\Sigma_f)_i^{28}\varphi_i\right)\left(\sum_{j=1}^{J}\chi_j\,\varphi_j^+\right)\mathrm{d}\,V\right]\left[\int\sum_{i=1}^{J}(\nu\,\Sigma_f)_i^{25}\varphi_i\,\mathrm{d}\,V\right]}{\left[\int\left(\sum_{i=1}^{J}(\nu\,\Sigma_f)_i^{25}\varphi_i\right)\left(\sum_{j=1}^{J}\chi_j\,\varphi_j^+\right)\mathrm{d}\,V\right]\left[\int\sum_{i=1}^{J}(\nu\,\Sigma_f)_i^{28}\varphi_i\,\mathrm{d}\,V\right]}.$$

Results of the calculations are summarized in Table VII. Included are also experimental values [1, 25] of Rossi-$\alpha$. Values for assemblies 6F, 9A, and 11 have also been previously reported [1] for the overall (core and reflector) volume using the 11-group set. Although the $\beta_{\mathrm{eff}}$ values for a given assembly differ somewhat for the various cross-section sets used, the differences are relatively small. Similarly, with increasing $U^{238}$-dilution, the $\beta_{\mathrm{eff}}$ values do not vary much. It is interesting to note, however, that the trend at higher dilutions is for a decrease in the $\beta_{\mathrm{eff}}$ values. In general, the calculated Rossi-$\alpha$ values are smaller than the experimental values, suggesting that the calculated spectra may not be sufficiently degraded.

## Reactivity and inhour relations

The reactivities *versus* asymptotic period for assemblies 6F, 9A, 22 (11), and 25 have been calculated with a step reactivity programme [26] using the Keepin *et al.* [23] delayed-group abundances, $a_i^{25}$ and $a_i^{28}$, and decay periods, $\lambda_i^{25}$ and $\lambda_i^{28}$, of $U^{235}$ and $U^{238}$, corrected to the adjoint-weighted effective delayed-neutron yields from $U^{235}$ to $U^{238}$. The adjoint weighted quantities $D^{25}$ and $D^{28}$ were obtained from the $\beta_{\mathrm{eff}}$-programme [10]. The flux and adjoints used are from diffusion-theory, spherical-geometry solutions for the assemblies using the 10-group standard cross-section set.

The form of the reactivity *versus* asymptotic period used is

$$\varrho \cong \sum_{i=1}^{6}\frac{\beta_i^{25}}{1+\lambda_i^{25}\,T} + \sum_{i=1}^{6}\frac{\beta_i^{28}}{1+\lambda_i^{28}\,T}$$

with $\beta_i^{25} = \beta_{\mathrm{eff}}\,C^{25}a_i^{25}$ where $\beta_{\mathrm{eff}}$ is the effective neutron delayed fraction, and $a_i^{25}$ is the fraction of the delayed neutrons from a $U^{235}$-fission which is emitted in delayed group $i$ and having decay constant $\lambda_i^{25}$.

$$C^{25} = \frac{D^{25}}{D^{25} + D^{28}}$$

where $D^{25}$ is the effective delayed-neutron yield from $U^{235}$-fission per $U^{235}$-fission and $D^{28}$ is the effective delayed-neutron yield from $U^{238}$-fission per $U^{235}$-fission

$$\beta_i^{28} = \beta_{\mathrm{eff}}\,C^{28}a_i^{28}$$

with analogous definitions. The $C^{25}$ and $C^{28}$ values are listed in Table VIII.

The calculated reactivity-*versus*-period relations for the assemblies are shown in Fig. 12. Variations in cross-section parameters are also expected to show up as a similar shift in the curves.

To estimate the possible error due to use of common delayed-group constants $\lambda_i$ for $U^{235}$ and $U^{238}$, assembly 22 (11) calculations were also carried out using the $\lambda_i$ of $U^{235}$ for both species and also the $\lambda_i$ of $U^{238}$ for both species. This comparison is shown in Fig. 13.

TABLE VII

**CALCULATED $\beta_{eff}$, $l_p$ AND DELAYED AND PROMPT WORTHS for ZPR-III Assemblies 6 F, 9 A, 22 (or 11), 24 and 25**

| Assembly | a. $\frac{\int \Phi \Sigma_f^{28} dV}{\int \Phi \Sigma_f^{25} dV}$ | b. $\frac{W_P^{28}}{W_P^{25}}$ | c. $\frac{W_D^{28}}{W_P^{25}}$ | d. $\frac{W_D^{25}}{W_P^{25}}$ | $\beta_{eff}$ | $l_p \times 10^8$ (s) | $\alpha = \frac{\beta_{eff}}{l_p}$ (calc.) | e. $\alpha_{exp}$ |
|---|---|---|---|---|---|---|---|---|
| **6F** | | | | | | | | |
| 10-group std. | | | | | | | | |
| Total | 0.26 | 0.64 | 0.57 | 0.95 | 0.00735 | 6.48 | $1.35 \times 10^5$ | $0.985 \times 10^5$ |
| Reg. 1 | 0.08 | 1.02 | 0.97 | 0.95 | | | | |
| Reg. 2 | 13.64 | 1.08 | 0.90 | 0.83 | | | | |
| Reg. 3 | 3.96 | 1.25 | 0.925 | 0.73 | | | | |
| 10-group rev. | | | | | | | | |
| Total | 0.27 | 0.63 | 0.56 | 0.95 | 0.00734 | 6.57 | $1.12 \times 10^5$ | — |
| Reg. 1 | 0.08 | 1.02 | 0.97 | 0.95 | | | | |
| Reg. 2 | 13.70 | 1.08 | 0.89 | 0.81 | | | | |
| Reg. 3 | 4.13 | 1.24 | 0.87 | 0.69 | | | | |
| 11-group | | | | | | | | |
| Total | 0.26 | 0.64 | 0.58 | 0.98 | 0.00746 | 7.79 | $0.96 \times 10^5$ | — |
| Reg. 1 | 0.07 | 1.02 | 1.00 | 0.98 | | | | |
| Reg. 2 | 11.06 | 1.09 | 0.94 | 0.85 | | | | |
| Reg. 3 | 2.79 | 1.28 | 0.97 | 0.74 | | | | |
| **9A** | | | | | | | | |
| 10-group std. | | | | | | | | |
| Total | 0.34 | 0.76 | 0.66 | 0.90 | 0.00753 | 6.00 | $1.25 \times 10^5$ | — |
| Reg. 1 | 0.19 | 1.02 | 0.92 | 0.90 | | | | |
| Reg. 2 | 12.09 | 1.07 | 0.86 | 0.79 | | | | |
| Reg. 3 | 3.33 | 1.325 | 0.96 | 0.71 | | | | |
| 10-group rev. | | | | | | | | |
| Total | 0.31 | 0.75 | 0.65 | 0.90 | 0.00739 | 6.39 | $1.16 \times 10^5$ | — |
| Reg. 1 | 0.17 | 1.02 | 0.92 | 0.90 | | | | |
| Reg. 2 | 10.79 | 1.07 | 0.85 | 0.78 | | | | |
| Reg. 3 | 3.54 | 1.22 | 0.83 | 0.67 | | | | |
| **22 (or 11)** | | | | | | | | |
| 10-group std. | | | | | | | | |
| Total | 0.38 | 0.88 | 0.72 | 0.825 | 0.00734 | 5.68 | $1.29 \times 10^5$ | $1.04 \times 10^5$ |
| Reg. 1 | 0.30 | 1.02 | 0.84 | 0.825 | | | | |
| Reg. 2 | 7.98 | 1.07 | 0.81 | 0.74 | | | | |
| Reg. 3 | 2.65 | 1.21 | 0.845 | 0.69 | | | | |

*Cont. following page*

TABLE VII, cont.

| Assembly | a. $\frac{\int \Phi \Sigma_f^{28} dV}{\int \Phi \Sigma_f^{25} dV}$ | b. $\frac{W_P^{28}}{W_P^{25}}$ | c. $\frac{W_D^{28}}{W_P^{25}}$ | d. $\frac{W_D^{28}}{W_P^{25}}$ | $\beta_{eff}$ | $l_p \times 10^8$ (s) | $\alpha = \frac{\beta_{eff}}{l_p}$ (calc.) | e. $\alpha_{exp}$ |
|---|---|---|---|---|---|---|---|---|
| 10-group rev. | | | | | | | | |
| Total | 0.38 | 0.88 | 0.71 | 0.82 | 0.00731 | 5.77 | $1.27 \times 10^5$ | — |
| Reg. 1 | 0.305 | 1.02 | 0.84 | 0.82 | | | | |
| 10-group rev. | | | | | | | | |
| Reg. 2 | 8.23 | 1.07 | 0.79 | 0.73 | | | | |
| Reg. 3 | 2.91 | 1.20 | 0.775 | 0.64 | | | | |
| 11-group | | | | | | | | |
| Total | 0.32 | 0.895 | 0.765 | 0.86 | 0.00734 | 6.49 | $1.13 \times 10^5$ | — |
| Reg. 1 | 0.26 | 1.02 | 0.88 | 0.86 | | | | |
| Reg. 2 | 6.43 | 1.08 | 0.855 | 0.78 | | | | |
| Reg. 3 | 1.89 | 1.23 | 0.89 | 0.705 | | | | |
| **24** | | | | | | | | |
| 10-group std. | | | | | | | | |
| Total | 0.42 | 0.89 | 0.71 | 0.81 | 0.00734 | 6.53 | $1.12 \times 10^5$ | $0.851 \times 10^5$ |
| Reg. 1 | 0.34 | 1.01 | 0.815 | 0.81 | | | | |
| Reg. 2 | 7.75 | 1.08 | 0.81 | 0.74 | | | | |
| Reg. 3 | 2.45 | 1.19 | 0.81 | 0.67 | | | | |
| 10-group rev. | | | | | | | | |
| Total | 0.42 | 0.89 | 0.70 | 0.795 | 0.00726 | 6.64 | $1.09 \times 10^5$ | — |
| Reg. 1 | 0.35 | 1.01 | 0.81 | 0.795 | | | | |
| Reg. 2 | 8.06 | 1.08 | 0.78 | 0.71 | | | | |
| Reg. 3 | 2.73 | 1.18 | 0.74 | 0.62 | | | | |
| 11-group | | | | | | | | |
| Total | 0.35 | 0.90 | 0.75 | 0.84 | 0.00731 | 7.57 | $0.966 \times 10^5$ | — |
| Reg. 1 | 0.29 | 1.01 | 0.85 | 0.84 | | | | |
| Reg. 2 | 6.35 | 1.10 | 0.855 | 0.77 | | | | |
| Reg. 3 | 1.75 | 1.215 | 0.85 | 0.69 | | | | |
| **25** | | | | | | | | |
| 10-group std. | | | | | | | | |
| Total | 0.39 | 0.93 | 0.74 | 0.80 | 0.00726 | 6.67 | $1.09 \times 10^5$ | $0.91 \times 10^5$ |
| Reg. 1 | 0.34 | 1.02 | 0.815 | 0.80 | | | | |
| Reg. 2 | 6.69 | 1.06 | 0.78 | 0.73 | | | | |
| Reg. 3 | 2.34 | 1.19 | 0.81 | 0.67 | | | | |
| 10-group rev. | | | | | | | | |
| Total | 0.40 | 0.925 | 0.73 | 0.79 | 0.00718 | 6.77 | $1.06 \times 10^5$ | — |
| Reg. 1 | 0.35 | 1.015 | 0.80 | 0.79 | | | | |
| Reg. 2 | 7.05 | 1.06 | 0.75 | 0.70 | | | | |
| Reg. 3 | 2.63 | 1.175 | 0.74 | 0.615 | | | | |
| 11-group | | | | | | | | |
| Total | 0.33 | 0.94 | 0.78 | 0.83 | 0.00725 | 7.69 | $0.943 \times 10^5$ | — |
| Reg. 1 | 0.30 | 1.02 | 0.85 | 0.83 | | | | |
| Reg. 2 | 5.42 | 1.07 | 0.82 | 0.76 | | | | |
| Reg. 3 | 1.68 | 1.21 | 0.86 | 0.69 | | | | |

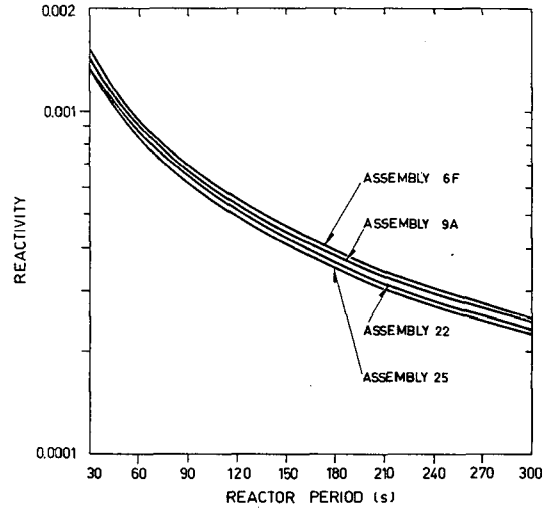


Fig. 12
Calculated reactivity as a function of period for various ZPR-III assemblies.

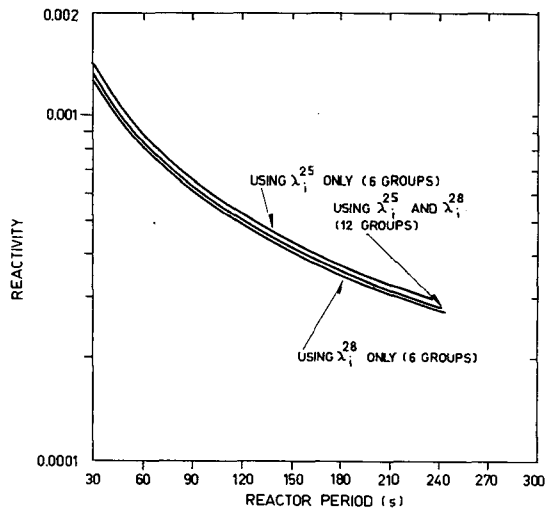


Fig. 13
Sensitivity of calculated reactivity as a function of period for ZPR-III Assembly 22 (or 11) to use of separate delay-neutron decay constants for $U^{235}$ and $U^{238}$.

---

Key to Table VII

a. Number of $U^{238}$-fission per $U^{235}$-fission.
b. Worth of a prompt $U^{238}$-fission neutron relative to the worth of a prompt $U^{235}$-fission neutron.
c. Worth of a delayed $U^{238}$-fission neutron relative to the worth of a prompt $U^{352}$-fission neutron.
d. Worth of a delayed $U^{235}$-fission neutron relative to the worth of a prompt $U^{235}$-fission neutron.
e. Ref. [1], except $\alpha_{exp}$ Ass'y 24 and 25 from Ref. [25].

TABLE VIII

**$C^{28}$ AND $C^{25}$ VALUES* FOR ASSEMBLIES 6F, 9A, 22 (11) AND 25**

| Assembly | $C^{28}$ | $C^{25}$ |
|---|---|---|
| 6 F | 0.28 | 0.72 |
| 9 A | 0.38 | 0.62 |
| 22 (11) | 0.45 | 0.55 |
| 25 | 0.47 | 0.53 |

* *Based upon 10-group standard set.*

The number of inhours per per-cent-reactivity has been calculated for the assemblies using the three sets of cross-sections and are given in Table IX. It is noted that this conversion factor is sensitive to cross-sections as well as the composition. The use of separate decay constants, $\lambda_i^{25}$ and $\lambda_i^{28}$, result in about 5 to 12 inhours per per-cent greater values than the use of $U^{235}$ decay constants for both species.

TABLE IX

**CALCULATED INHOURS PER PER-CENT REACTIVITY FOR ZPR-III ASSEMBLIES 6F, 9A, 22 (11), 24 AND 25, USING VARIOUS CROSS-SECTION SETS**

| Assembly | 10-group std. | 10-group rev. | 11-group |
|---|---|---|---|
| 6 F | 438 | 439 | 430 |
| | (432) | (433) | (425) |
| 9 A | 448 | 451 | |
| | (440) | (444) | |
| 22 or 11 | 475 | 479 | 467 |
| | (465) | (468) | (458) |
| 24 | 482 | 488 | 474 |
| | (471) | (477) | (464) |
| 25 | 486 | 492.5 | 478 |
| | (474.5) | (481) | (468) |

Note. Values in brackets are based on using the 6-group decay constants, $\lambda_i^{25}$, of $U^{235}$ for both $U^{235}$ and $U^{238}$.

Using the inhour per per-cent values and the reactivity relations given in Fig. 12, the inhour-versus-asymptotic-period relation shown in Fig. 14 was obtained. The inhours-*versus*-period relation shows dependence upon composition only for periods shorter than about 50 s for these assemblies. The insensitivity to cross-sections and composition in the period range in which many physics measurements are made emphasizes the practicality of inhours and similarly normalized quantities as units for stating experimental reactivity values.

## Effect of resonance-scattering on some ZPR-III criticality calculations

### INTRODUCTION

Numerous fast-neutron multi-group cross-section parameters have been used for the analyses of the ZPR-III fast critical assemblies [1, 20, 21]. These have generally ranged from about 10- to 16- energy groups. As the successive assemblies

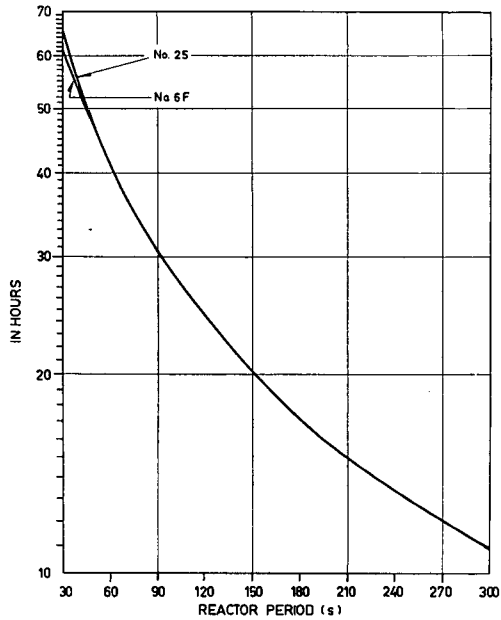


Fig. 14
Calculated inhours as a function of period.

have been studied, comparison with experimental results have shown that a seemingly adequate cross-section set for a large range of previous assemblies does not enable subsequent assemblies to be adequately predicted. For example, the 11-group cross-section set [20, 21] used for much of the ZPR-III analyses, which provided a good fit to the moderately dilute assemblies, has been found to overpredict the critical mass of assemblies No. 24 and 25 by about 30%. (Assemblies 24 and 25 contain nominal $U^{238}/U^{235}$ atomic ratios of about 9.5 and 10.4 respectively, and have corrected experimental critical masses of about 490 kg and 620 kg respectively.)

In the recent 16-group fast-reactor cross-section set of YIFTAH *et al.* [27], an effort was made to explain and document all choices and assumptions made. This enables an analyst to assess the present reliability of the constants and readily make suitably assessed modifications as new microscopic data and/or improved calculational procedures are employed.

Perusal of the calculated and corrected experimental masses listed by Yiftah *et al.* [27] indicates that the listed calculated critical masses are underpredicted by about —6 to —17%. Furthermore, those calculated assemblies listed containing appreciable aluminium and/or stainless steel tend to be most in error on the side of overreactivity. By use of their "conservative" $U^{235}$ values for $\nu$, the predicted critical deviations from observed values range from about +2 to —11%.

Recent ZPR-III assemblies 23, 29, 30, 31 and 32, which contain large volume fractions of aluminium and/or stainless steel, have emphasized this aspect by the underprediction by about —19 to —26% of the critical masses using the cross-section set. These large overpredictions of reactivity in such systems, observed also with previous sets [21, 22], suggested that these excessive deviations might

in part be due to not having considered the detailed flux shapes within groups due to scattering resonances of, for example, aluminium and the components of stainless steel in the evaluation of group cross-section parameters.

In the present study, the contribution of these resonance effects toward improving the critical-mass predictions is ascertained by re-evaluation of the group transport and group elastic-transfer cross-sections using the recent ELMOE code [28, 29]. ELMOE is an IBM-704 code which, by using hundreds of neutron energy groups with the detailed elastic-scattering matrix for the resonance scatterers, carries out a fundamental mode analysis, thereby obtaining material buckling and the detailed fine structure flux dependence upon energy. The programme then re-evaluates the gross group cross-sections for transport and elastic transfer for an energy-group structure such as in the 16-group set. The ELMOE code carries out either P1 or consistent P1 solutions. In the present study, results of ELMOE P1 calculations were employed.

## Critical masses and core material bucklings

ZPR-III assemblies 23, 29, 30, 31 and 32 contain appreciable volume fractions of aluminium and/or stainless steel. These cylindrical assemblies have approximately the core composition given in Table X; these values were used in the

Table X

**CORE AND REFLECTOR COMPOSITIONS**
**(Volume fractions)**

| Ass'y No. | $U^{235}$ (0.048)* | $U^{238}$ (0.048) | Al (0.0603) | S.S.** | 0 (0.096) |
|---|---|---|---|---|---|
| 23 | 0.0942 | 0.0071 | 0.4473 | 0.0916 | 0 |
| 29 | 0.0497 | 0.0997 | 0.2438 | 0.2475 | 0.1446 |
| 30 | 0.0592 | 0.0906 | 0.2341 | 0.2460 | 0.0728 |
| 31 | 0.0581 | 0.0914 | 0.2349 | 0.2449 | 0 |
| 32 | 0.0942 | 0.0071 | 0 | 0.801 | 0 |
| Refl. | 0.0019 | 0.833 | 0 | 0.0731 | 0 |

* $N$—values in units of $10^{24}$ per cubic centimeter.
** Stainless steel (assuming ~71.3 at. % Fe, 8.5 at. % Ni, and 20.2 at. % Cr having $N$-values for pure elements of 0.0847, 0.0913, and 0.0801 respectively.

calculations. The reflector in all cases is about 30-cm thick, of depleted uranium. The critical-mass calculations were carried out in spherical geometry using the SNG transport code [3, 4] in $S_4$ approximation. The 16-group set without and with the ELMOE evaluated group cross-sections for transport and elastic transfer was used. Except where otherwise stated, the modified aluminium cross-sections for transport and elastic transfer employed are those based upon an ELMOE calculation for the aluminium-assembly 23. Similarly, except where otherwise stated, the modified stainless-steel cross-sections employed are those obtained by an ELMOE calculation of the steel-assembly 32. The error incurred in this simple volume-fraction weighting is evaluated for the assembly 31, which consists approximately of equal volumes of aluminium and stainless-steel resonance scattering materials. The cylindrical critical-masses were obtained by use of

estimated shape factors [20, 21]. The reported experimental critical masses were corrected for the effects of slab geometry plate heterogeneities either by auxiliary calculations or by estimates based on results [9] of heterogeneity experiments so as to represent homogeneous cores.

Material buckling calculations for the cores have also been calculated using both the 16-group cross-section set unmodified and modified by the re-evaluated transport and elastic-transfer cross-sections. This was done largely to determine to what extent the reactivity effect of a decrease in transport cross-section is, in these high-reflector-density systems, compensated for by an increase in reflector savings.

The error incurred by the hybrid use of corrected transport and elastic-transfer cross-sections of aluminium—as evaluated for a primarily aluminium-diluent system such as assembly 23—and of stainless-steel—as evaluated for a stainless-steel-diluent system such as assembly 32—as employed in criticality calculations of an assembly containing approximately equal amounts of aluminium and stainless-steel, such as assembly 31, as diluents has also been studied.

The factors by which the unmodified 16-group cross-sections for aluminium for transport and elastic transfer must be modified if the flux depletion due to resonance scattering is to be accounted for in the predominantly aluminium-diluent assembly 23, are listed in Table XI. Also listed are the factors by which the stainless-steel transport and elastic-removal cross-sections as computed using the 16-group set [27] are to be multiplied if the flux depletion due to resonance scattering is to be accounted for in the stainless-steel-diluent assembly No. 32.

The homogenized-group transport cross-sections of the core and group elastic transfer contributions of aluminium and stainless steel as determined by an

TABLE XI

**RATIO OF CORRECTED TO UNCORRECTED TRANSPORT AND ELASTIC TRANSFER CROSS-SECTIONS for aluminium in assembly 23 and for stainless steel in assembly 32**

| Energy group | Group lower energy (MeV) | Ratio | | | |
|---|---|---|---|---|---|
| | | Aluminium | | Stainless steel | |
| | | Transport | Elastic transfer | Transport | Elastic transfer |
| 1 | 3.668 | (1) | (1) | (1) | (1) |
| 2 | 2.225 | 0.83 | 1.11 | 0.86 | 0.81 |
| 3 | 1.35 | 0.95 | 1.25 | 0.97 | 1.14 |
| 4 | 0.825 | 0.85 | 1.02 | 0.91 | 1.03 |
| 5 | 0.5 | 0.945 | 1.11 | 0.95 | 1.11 |
| 6 | 0.3 | 0.94 | 1.02 | 0.86 | 0.78 |
| 7 | 0.18 | 0.76 | 0.93 | 0.94 | 1.03 |
| 8 | 0.11 | 0.61 | 0.84 | 0.84 | 0.99 |
| 9 | 0.67 | 0.475 | 0.61 | 0.64 | 0.80 |
| 10 | 0.0407 | 0.67 | 0.68 | 0.95 | 0.95 |
| 11 | 0.025 | 0.24 | 0.36 | 0.49 | 0.75 |
| 12 | 0.015 | 0.71 | ~0 | 0.67 | 0.73 |
| 13 | 0.0091 | 0.97 | 1.00 | 0.98 | 0.98 |
| 14 | 0.0055 | (1) | (1) | (1) | (1) |
| 15 | 0.0021 | (1) | (1) | (1) | (1) |
| 16 | 0.0005 | (1) | (1) | (1) | (1) |

TABLE XII

**RATIO OF EVALUATED HOMOGENIZED CORE TRANSPORT AND ELASTIC-TRANSFER CROSS-SECTIONS FOR ASSEMBLY 31 TO COMPOSITE EMPLOYING EVALUATED Al CROSS-SECTIONS FOR ASSEMBLY 23 AND STAINLESS STEEL FOR ASSEMBLY 32**

| Energy group | Group lower energy (MeV) | Ratio | |
|---|---|---|---|
| | | a. Transport | b. Elastic transfer |
| 1 | 3.668 | (1) | (1) |
| 2 | 2.225 | 1.00 | 0.97 |
| 3 | 1.35 | 1.00 | 0.97 |
| 4 | 0.825 | 1.01 | 1.01 |
| 5 | 0.5 | 1.01 | 1.02 |
| 6 | 0.3 | 1.04 | 1.035 |
| 7 | 0.18 | 1.06 | 1.04 |
| 8 | 0.11 | 1.11 | 1.09 |
| 9 | 0.67 | 1.08 | 1.06 |
| 10 | 0.0407 | 1.035 | 1.11 |
| 11 | 0.025 | 1.13 | 1.38 |
| 12 | 0.015 | 1.02 | 1.07 |
| 13 | 0.0091 | 1.00 | 0.92 |
| 14 | 0.0055 | (1) | (1) |
| 15 | 0.0021 | (1) | (1) |
| 16 | 0.0005 | (1) | (1) |

a. Includes $U^{235}$- and $U^{238}$-transport contributions.

b. Does not include $U^{235}$- and $U^{238}$-elastic-transfer contributions.

TABLE XIII

**RESONANCE CORRECTED AND UNCORRECTED CALCULATED CRITICAL MASSES (kg $U^{235}$ in core)**

| Experimental | | | Calculated critical masses [1] | | | | Calculated $(\Delta M/M)_{\text{core edge}}$ / $(\Delta k/k)$ |
|---|---|---|---|---|---|---|---|
| | | | Regular $\nu^{25}$ values | | Conservative $\nu^{25}$ values[2] | | |
| Assembly | Measured (Ref. [7, 9]) | Corrected[3] | Without resonance corrections | With resonance corrections | Without resonance corrections | With resonance corrections | |
| 23 | 258 | 271 | 219 | 233 | 241 | 257 | 5.1 |
| 29 | 422 | 449 | 352 | 386 | 369 | 404 | 4.3 |
| 30 | 395 | 422 | 326 | 353 | 345 | 374 | 4.5 |
| 31 | 463 | 494 | 387 | 417 (407)[4] | 414 | 447 (436)[4] | 5.5 |
| 32 | 227.5 | 239 | 176 | 197 | 188 | 210 | 4.5 |

[1] Assumes shape factors of 0.94 for sphere to cylinder.

[2] Extrapolated from the listed results, of the regular $\nu^{25}$, by comparative bare core calculations using "regular" and "conservative" $\nu^{25}$ values.

[3] Assumes 1% k heterogeneity effects in assemblies 23 and 32 and 1.5% k heterogeneity effects in assemblies 29, 30, 31.

[4] Using cross-sections obtained by ELMOE programme expressly for assembly 31.

ELMOE calculation for the assembly 31 core, which contains approximately equal parts of aluminium and stainless-steel as diluent, divided by the corresponding homogenized-group cross-sections as constructed by use of the composite of ELMOE-evaluated aluminium cross-sections for assembly 23 and ELMOE-evaluated stainless-steel cross-sections for assembly 32, are listed in Table XII.

Results of the critical-mass calculations for these reflected assemblies are given in Table XIII together with the experimental [7, 9] and heterogeneity-corrected experimental values. The calculated masses assuming the "conservative" $\nu^{25}$ values [27] were obtained by estimating the fractional increase in critical mass from comparative material-buckling calculations.

Results of corresponding material-buckling calculations (16 groups) are given in Table XIV. These were carried out using asymptotic transport leakage [30]. For both the critical mass and the buckling calculations, the values listed were obtained by use of the ELMOE cross-sections for aluminium as obtained for assembly 23, together with the ELMOE cross-sections for stainless steel as obtained for assembly 32. In addition, for those assemblies containing oxygen, the intra-group resonance-scattering effects of oxygen were not accounted for.

TABLE XIV

**RESONANCE CORRECTED AND UNCORRECTED CALCULATED $B$ VALUES ($B^2$ = MATERIAL BUCKLING) AND PER CENT CHANGES IN BARE CORE REACTIVITIES**

| Assembly | Regular $\nu^{25}$ values | | | Conservative $\nu^{25}$ values | |
|---|---|---|---|---|---|
| | $B$ (cm$^{-1}$) | | 1. | $B$ (cm$^{-1}$) | 2. |
| | Without resonance correction | With resonance correction | Per cent ($\Delta k/k$) | With resonance correction | Per cent ($\Delta k/k$) |
| 23 | 0.0590 | 0.0558 | —5.8% | 0.0548 | —2.0% |
| 29 | 0.0526 | 0.0502 | —3.8% | 0.0496 | —1.1% |
| 30 | 0.0536 | 0.0512 | —4.0% | 0.0505 | —1.3% |
| 31 | 0.0486 | 0.0464 | —4.2% | 0.0457 | —1.3% |
| | 0.0486 | (0.0472)[3] | —2.7% | | |
| 32 | 0.0746 | 0.0712 | —4.7% | 0.0702 | —1.5% |

[1] Relative to bare core calculated without resonance corrections and with regular $\nu^{25}$ values.
[2] Relative to bare core calculated with resonance corrections and with regular $\nu^{25}$ values.
[3] Using cross-sections obtained by ELMOE-programme expressly for assembly 31.

These increases in calculated critical masses for assemblies 23, 31, and 32 due to consideration of the resonance-scattering effects correspond to reactivity decreases of about —1%, —0.7%, and —2% $k$ respectively. Corresponding decrease for assembly 31 using the composite cross-sections is about —1%. Thus the assembly-31 results obtained using the separately re-evaluated aluminium and stainless-steel cross-sections show that the composite of the stainless-steel and aluminium resonance structures are such that they lessen the overall resonance effect on critical-mass calculations. The reactivity decreases obtained for the bare cores by use of the ELMOE-corrected cross-sections are factors of 2 to 3 more than the reactivity decreases which may be deduced from the increases in the reflected critical masses. That this is due largely to the compensating effect of

the reflector saving, of the high-density reflector, increasing as the core leakage increases due to the cross-section changes for transport and elastic transfer is seen in Table XV. (The reflector savings values listed are the differences between the bare core radii obtained by the 16-group fundamental mode analysis using asymptotic transport leakage and by the critical core radii as obtained by the 16-group $S_4$ solutions.)

TABLE XV

**CALCULATED SPHERICAL REFLECTOR SAVINGS without and with resonance corrected cores (cm)**

| Assembly | Reflector saving[1] | |
|---|---|---|
| | Without resonance corrections | With resonance corrections |
| 23 | 22.9 | 24.4 |
| 29 | 15.8 | 17.3 |
| 30 | 18.3 | 19.8 |
| 31 | 21.6 | 23.6 (22.7)[2] |
| 32 | 13.4 | 14.8 |

[1] Difference of bare core fundamental mode calculation using asymptotic transport leakage and of reflected $S_4$-calculation.
[2] Using cross-sections obtained by ELMOE-programme expressly for assembly 31.

## Conclusions

For the aluminium-diluent assembly 23, the consideration of the resonance-scattering effects can be said to reduce the overprediction of reactivity to about the same range of overprediction as for assemblies [27] not containing appreciable aluminium and/or stainless steel. The overreactivity of the calculated assembly 23 is reduced to $+2.7\%$ $k$ and $+1.0\%$ $k$ respectively using the standard $\nu$ ($U^{235}$) and conservative $\nu$ ($U^{235}$) respectively. For comparison the uncorrected 16-group set gives $+3.8\%$ $k$ and $+2.2\%$ $k$ respectively.

The calculation of the stainless-steel assembly 32 has been improved by reduction of the reactivity error to $+3.8\%$ $k$ and $+2.7\%$ $k$ respectively using the two sets of $\nu$ ($U^{235}$). The predicted overreactivity is still, however, overly excessive in comparison with the calculated critical masses of assemblies not containing appreciable stainless steel. Similarly, the calculated overreactivity of assembly 31, containing about equal parts of aluminium and stainless steel, though reduced to $+3.2\%$ $k$ and $+2.1\%$ $k$ respectively, is still overly excessive, as are also assemblies 29 and 30 which in addition contain oxygen. It thus appears that the stainless-steel 16-group cross-sections are still too reactive (by about 1 or 2% $k$ in assembly 32). An increase in the average stainless-steel capture cross-section by about 40% in the energy groups between 9 keV and 1.35 MeV would reduce the assembly-32 reactivity by about 1% $k$.

The problem of the general underprediction of critical mass, aside from the stainless-steel overreactivity, appears to be due largely to the overreactivity of the $U^{235}$-group cross-sections. Thus *ad hoc* use of the "conservative $\nu$ ($U^{235}$)" values [27] improves agreement with experiment. These correspond to a $[d\bar{\nu}/dE]$

($U^{235}$) of about 0.1, with a normalization of 2.42 at thermal, over most of the energy range except above about 3.7 MeV, where the $\bar{\nu}$ ($U^{235}$) is taken to be 2.71. Recent measurements [31] of $\nu$ ($U^{235}$) suggest that a lowering of [$d\bar{\nu}/dE$] ($U^{235}$) is indeed indicated.

## ACKNOWLEDGEMENTS

The author wishes to acknowledge the kindness of Dr. H. H. Hummel and Mr. A. L. Rago for use of the ELMOE code, and Mr. G. J. Duffy for use of the exponential integral evaluating programme in advance of publications. The author wishes to thank Dr. R. Avery and Dr. H. H. Hummel for their interest and for valuable discussions on various aspects of the heterogeneity problem. The author is also indebted to Mr. M. F. Loomis for calculational assistance, and to Mr. C. A. Stevens for programming of the effective delayed-neutron and worth code.

## REFERENCES

[1] LONG, J. K. *et al.*, Proc. 2nd UN Int. Conf. PUAE **12** (1958) 119.
[2] LOEWENSTEIN, W. B. and OKRENT, D., American Nuclear Society Meeting (December 1956), Session 13, Paper 4.
[3] CARLSON, B. G. and BELL, G. I., Proc. 2nd UN Int. Conf. PUAE **16** (1958) 533.
[4] CARLSON, B. G., LA-1891 (1955).
[5] LOEWENSTEIN, W. B., Personal communication.
[6] CARLSON, B., LEE, C. and WORLTON, J., LAMS-2346 (1960).
[7] KEENEY, W. P. and LONG, J. K., *Trans. Amer. nucl. Soc.* **3** (1960) 327.
[8] MENEGHETTI, D. and LOOMIS, M. F., ANL-6218 (1960).
[9] LONG, J. K., Personal communication.
[10] MENEGHETTI, D., Unpublished.
[11] MARK, J. C., CRT-338 (1945, 1947).
[12] JEFFREY, A., *Math. Tab.* (*Wash.*) **13** (1959) 321.
[13] ANDERSON, B. L. *et al.*, WAPD-TM-134 (1959).
[14] HAGEMAN, L. A. and MANDEL, J. T., WAPD-TM-268 (1961).
[15] BAREISS, E. H., David Taylor Model Basin Report 1030 (1956).
[16] CARLSON, B., LA-2260 (1959).
[17] RICHTMYER, R. D., Difference Methods for Initial-Value Problems, Interscience Publishers, Inc., New York (1957) 121.
[18] MENEGHETTI, D., ANL-6345 (1961).
[19] BOHL, L. S., STEWART, J. C. and FRANCIS, N. C., *Nucl. Sci. and Engng* **4** (1958) 255.
[20] Reactor Physics Constants, ANL-5800 (1958) 24.
[21] LOEWENSTEIN, W. B. and OKRENT, D., Proc. 2nd UN Int. Conf. PUAE **12** (1958) 16.
[22] HUMMEL, H. H. *et al.*, Proc. 2nd UN Int. Conf. PUAE **12** (1958) 166.
[23] KEEPIN, G. R., WIMETT, T. F. and ZEIGLER, R. K., LA-2118 (1957).
[24] GOLDSTEIN, H., The Attenuation of Gamma Rays and Neutrons in Reactor Shields, Washington, D. C., Government Printing Office (1957) 40.
[25] BRUNSON, G. S., Personal communication.
[26] COHN, C. E. and TOPPEL, B. J., ANL-6134 (1960).
[27] YIFTAH, S., OKRENT, D. and MOLDAUER, P. A., Fast Reactor Cross Sections, Pergamon Press (1960).
[28] HUMMEL, H. H. and RAGO, A. L., *Trans. Amer. nucl. Soc* **3** (1960) 273.
[29] HUMMEL, H. H. and RAGO, A. L., *These proceedings*, vol. **I**, p. 231.
[30] OKRENT, D., AVERY, R. and HUMMEL, H. H., Proc. UN Int. Conf. PUAE **5** (1956) 347.
[31] SMITH, A. B., *These proceedings*, vol. **I**, p. 29.

INTERNATIONAL
ATOMIC ENERGY AGENCY,
VIENNA 1962

PRICE (A): North America US $9.00
Elsewhere: Sch 189,-
(54s.stg: NF 36; DM 31,50)